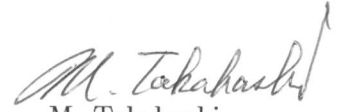# REAUSTENITISATION FROM BAINITE IN STEELS

By
Manabu Takahashi
Darwin College
Cambridge

A dissertation submitted for the degree of
Doctor of Philosophy,
at the University of Cambridge
September 1992

To my parents, my wife Yukimi and my daughter Mayuko

PREFACE

This dissertation is submitted for the degree of Doctor of Philosophy at the University of Cambridge. The work described was carried out under the supervision of Dr. H. K. D. H. Bhadeshia in the Department of Materials Science and Metallurgy between October 1987 and June 1989. Except where appropriately referenced, this work is, to my best knowledge, original and contains nothing which is the outcome of collaboration. This dissertation has not been submitted in whole or in part for a degree, diploma or other qualification. This dissertation does not exceed 60,000 words in length.

M. Takahashi

September 1992

i

ACKNOWLEDGMENTS

REAUSTENITISATION FROM BAINITE IN STEELS

Manabu TAKAHASHI

Darwin College

Department of Materials Science and Metallurgy

SUMMARY

A large number of industrial steel manufacturing and processing methods involve heating the alloy into a temperature regime where austenite is the stable phase. The characteristic and subsequent transformation of this austenite during cooling determine the final properties of the steel. The formation of austenite in steels has, therefore, been investigated both theoretically and using a variety of experimental methods. Since the general problem of austenite formation is very dependent on the initial microstructure, the work presented in this thesis concentrates on bainitic starting microstructures. Bainitic steels are at the forefront of new and exciting developments in steel technology.

The thesis begins with a literature review and critical assessment of the bainite reaction and of austenite formation. As a consequence, two interesting and unresolved problems relating to the bainitic transformation are first investigated. A quantitative model is developed which is shown to be capable of predicting the transition from upper to lower bainite. This has led to some unexpected predictions which explain a previously unnoticed phenomenon, that lower bainite does not occur in plain carbon steels containing less than about 0.3 wt.% carbon, and that upper bainite is not found when the carbon concentration exceeds about 0.4 wt.%. The second problem tackled relates to the kinetics of the bainite reaction. A model has been developed and applied to enable the prediction of time-temperature-transformation diagrams for the bainite reaction.

The studies on bainite are followed by experimental work on the growth of austenite from mixed microstructures of bainite and residual carbon enriched austenite. The need to nucleate austenite has been avoided by using this starting microstructure, although comparative experiments were also conducted on initial microstructures without any austenite. A detailed and completely new theory has been developed to enable the interpretation of the experimental data on austenite growth. The theory is based on the concept of local equilibrium at the transformation interface, involves multicomponent diffusion in both the parent and product phases, and makes predictions which are on the whole consistent with the experimental data. Non equilibrium growth is also featured in the form of paraequilibrium growth of austenite.

CONTENTS

NOMENCLATURE AND ABBREVIATIONS

Braces are used exclusively to denote functional relations; $D\{x\}$ thus implies that x is an argument of the function D. The bases of $\log\{x\}$ and $ln\{x\}$ are 10 and e respectively.

a_A^c	Activation of carbon at a point A in an isothermal section of the phase diagram
a	Starting thickness of a plate of bainitic ferrite
$a_{\gamma 0}, a_{\alpha 0}$	Lattice parameters of austenite and ferrite at ambient temperature as a function of chemical concentration
a_γ, a_α	Lattice parameters of austenite and ferrite at the reaction temperature before the reaction
a_γ^*	Lattice parameter of austenite at reaction temperature at any stage of the reaction
a_θ^3	Volume of cementite unit cell which is equal to $a_\theta b_\theta c_\theta$; a_θ, b_θ and c_θ are 4.51, 5.08 and 6.73 Å at ambient temperature respectively
Δa_m	Minimum detectable increase in austenite thickness
Ac_1	Temperature at which transformation from ferrite begins during heating
Ae_1	Boundary separating the α and $\alpha + \gamma$ phase fields
Ae_3	Boundary separating the γ and $\alpha + \gamma$ phase fields
Ae_3'	Paraequilibrium boundary separating the γ and $\alpha + \gamma$ phase fields
Ar_3	Temperature at which transformation from austenite begins during cooling
A_1	The ratio between $x_1^{\alpha\gamma}$ and $x_1^{\gamma\alpha}$
A_2	The ratio between $x_2^{\alpha\gamma}$ and $x_2^{\gamma\alpha}$
b	Coefficient of grain diameter in equation 1.27
bcc	Body centered cubic
B_S	Bainite-start temperature
B_1	Constant equal to $(x_2^{\gamma\alpha} - x_2^{\alpha\gamma})/(x_1^{\gamma\alpha} - x_1^{\alpha\gamma})$
B_2	The ratio between y_2^θ and $x_2^{\gamma\theta}$
c	Initial length of bainitic ferrite plate
C	Carbon
C_{N1-N4}	Constants in equations 5.2 - 5.4
CHT	Continuous-heating-transformation diagram
C_0	Constant in equation 5.32
d_i	Average diameter of i-th phase
D	Diffusivity of carbon in austenite, $D = D_{11}^\gamma$
$\overline{D}$	Weighted average diffusivity of carbon in austenite
$D_{ii}^{\gamma,\alpha}$	Diffusivity of i-th element in austenite or in ferrite ($i = 1$: carbon, $i = 2$: substitutional alloying element)
$D_{ij}^{\gamma,\alpha}$	Inter diffusion coefficient in austenite or in ferrite
D_B	Boundary diffusivity of a substitutional alloying element
fcc	Face centered cubic
g	Geometrical factor of pearlite equal to 0.72 in plain carbon steels
Δg_a^*	Activation energy of the interface process
$\Delta g^{\beta\alpha}$	Driving force for the transformation per atom
G_i	Free energy of each element, $i = 0, 1$ and 2 correspond to iron, carbon and the substitutional alloying element
$G_{\text{Fe}_3\text{C}}$	Free energy of cementite
$G_{\text{M}_3\text{C}}$	Free energy of M$_3$C type carbide
ΔG_m	Chemical free energy change accompanying the formation of 1 mole

	of nucleating phase in a large amount of matrix phase
ΔG_m^v	Maximum volume free energy change accompanying the formation of a nucleus in a large amount of matrix phase
$\Delta G^{\theta\alpha}$	Driving force for nucleation of cementite from ferrite
ΔG_1^θ	Activation energy for nucleation of cementite
ΔG_2^θ	Driving force for nucleation of cementite
$\Delta G_i^{0\alpha\rightarrow\gamma}$	Standard free energy change between α and γ for each element, $\mathrm{J\,mol}^{-1}$
h	Heating rate or alternatively Plank constant
H_i	Hardness of i-th phase
H_F	Hardness of tempered martensite just before the onset of recovery or coarsening of cementite particles
H_V	Micro-hardness of each phase
$H\{t\}$	Hardness of martensite at time t during tempering
$H\{D_{ii}\}$	Kinetic function
H_0	Initial hardness of martensite
$\Delta H\{t\}$	Change in hardness of martensite due to cementite precipitation during tempering
ΔH	Change in enthalpy between the parent and product phases
i	Iron ($i=0$), carbon ($i=1$) or substitutional alloying element X ($i=3$)
I	Nucleation rate per unit volume
J_i	Flux of carbon ($i=1$) or substitutional alloying element ($i=2$)
k	Boltzmann's constant
k_θ	Constant in equation 4.4
k_1, k_2	Constants in equation 4.11, or alternatively k_2 is the ratio between alloy concentrations and iron concentration
K	Boundary segregation coefficient which is the ratio between alloying element concentration in austenite near the boundary and that in the boundary
k_A, k_{A0}	Rate constants in an Avrami type equation
k_ϵ, k_p	Coefficients of ϵ_1 and l_p in the equation of the yield strength of martensite
k_θ	Constant in equation (4.4)
$k_{C\gamma}, k_{C\alpha}$	Constants of diffusion distance of carbon
$k_{X\gamma}, k_{X\alpha}$	Constants of diffusion distance of substitutional alloying element
K_P	Partition coefficient of substitutional alloying element between cementite and ferrite in pearlite
K_T	Constant equal to $4\pi\alpha_3^3 N_0\nu_1/3$ in equation 8.13
l_p	Average distance between a particle and its two or three nearest neighbours
l_α, l_γ	Diffusion distance of substitutional alloying element in ferrite and austenite
L_i	y coordinate of a point i in the temperature versus. relative length change diagram
L_i'	Temperature corrected x coordinate of a point i in the length change versus temperature diagram
L_S	Lower bainite-start temperature
L_α, L_γ	Diffusion distances of carbon in ferrite and austenite
$\Delta L/L$	Relative length change in dilatometry
ΔL_i	The maximum relative length change without the temperature correction
ΔL_m	The maximum relative length change with the temperature correction
$1/\overline{L}$	Number of intercepts of austenite/ferrite interface per unit length of test line
M_F	Martensite-finish temperature
M_S	Martensite-start temperature

n	Number of austenite plates per unit volume which can grow during reaustenitisation from mixtures of bainite and austenite, or alternatively time exponent of Avrami equation
n^e	Number of austenite particles in the starting microstructure
Δn	Decrease in the number of austenite particles which can grow due to impingement
N	Number of austenite particles
N_0	Initial nucleation site density for reaustenitisation from martensitic initial microstructure
N^v	Number of atoms per unit volume which are on dislocation lines
N_θ	Number of cementite particles at the completion of precipitation
NPLE	Negligible partitioning local equilibrium
p	Péclet number, or alternatively exponent constant in equations=5.1 and 5.4
P_i	An increment of incubation period spent in a small period of time Δt
PE	Paraequilibrium
PLE	Partitioning under local equilibrium
q	Increase in the half-thickness of austenite
Q	Effective activation energy for cementite precipitation
Q_B	Constant in equation 5.32
Q_0, Q'	Constants in equations 5.2 - 5.4
Q_1	Activation enthalpy for diffusion
r	Average cementite particle radius
r_C	Critical radius for growth at which the concentration difference in the matrix vanishes
r_ϕ	Radius of curvature at the advancing tip of the plate
r_0	Average cementite particle radius before the onset of Ostwald ripening
R	Universal gas constant
s, s_α, s_θ	Interlamellar spacing, respective thickness of ferrite and cementite lamellar
s_C	Critical spacing at which the growth rate becomes zero
S	Average carbon concentration in ferrite
S_0, T'	Constants in equations 5.2 - 5.4
S_{Ae_3}	Slope of the Ae_3 phase boundary
$S_{T_0'}$	Slope of the T_0' phase boundary
S_V	Effective austenite/ferrite interface area per unit volume
S_1, S_2	Functions of p as presented graphically in Trivedi's paper (ref. [46] in chapter 2), or alternatively S_1 is activation entropy for diffusion
Δs	Spike width of the substitutional alloying element in ferrite
t, t_i	Time
t_C	Time required for the carbon concentration in ferrite to drop to a specified level
t_d	Time required to decarburise a plate of bainitic ferrite
t_S	Time at which reaustenitisation starts on heating
t_ϵ	Time required to obtain a detectable amount of epsilon carbide in bainitic ferrite
t_θ	Time required to obtain a detectable amount of cementite precipitation in bainitic ferrite
Δt	Time interval spent by a sample at a temperature
T, T_i	Absolute temperature
T_b	Bainite or acicular ferrite transformation temperature
T_{ds}	Temperature at which the decomposition of residual austenite starts on continuous heating

T_A	Ambient temperature
T_E	Eutectoid temperature
T_S, T_F	Transformation-start and -finish temperatures during continuous heating
TTT	Time-temperature-transformation diagram
$T_{\gamma 1, \gamma 2}$	Reaustenitisation-start and 100% reaustenitisation-start temperatures for bainite + austenite initial microstructure
T_0	Temperature at which austenite and ferrite of the same composition have equal free energies
T_0'	Temperature at which austenite and ferrite (with a stored energy of $400\,\mathrm{J\,mol^{-1}}$) of the same composition have equal free energies
T_γ	Austenitising temperature
δT	Undercooling below the eutectoid temperature
ΔT	An increment of temperature during continuous heating
v	Growth rate of precipitate phase
v_d	Rate of carbon concentration dilution in austenite
v_B	Boundary diffusion controlled growth rate of pearlite
v_C	Velocity of a flat interface which is controlled by interface kinetics only
v_E	Edgewise growth rate of cementite plates
v_I	Growth rate of pearlite controlled by the interface process
v_V	Volume diffusion controlled growth rate of pearlite
v_θ	Volume of cementite
$\overline{V}$	Partial molar volume fraction of solvent in cementite
$V_{\alpha,\gamma,\theta}$	Volume fraction of ferrite, austenite and cementite at any stage of the reaction
$V_{\alpha'}$	Volume fraction of martensite
$V_{\alpha 0, \gamma 0, \theta 0}$	Initial volume fraction of ferrite, austenite and cementite
V_0	Initial volume fraction of a pre-existing austenite plate with the thickness a_0 and the length c_0
V_b^e	Maximum volume fraction of bainite obtained at a temperature
V_{cal}	Calculated volume fraction using T_0 concept
V_{opt}	Optically measured volume fraction
V_γ^F	Volume fraction of film type retained austenite
V_γ^B	Volume fraction of blocky type retained austenite
V_θ^e	Maximum volume fraction of cementite at a temperature
ΔV_γ	Increase in volume fraction of austenite
$w_{0,i}$	Iron-X interaction coefficients
x_i^{ab}	Iron ($i = 0$), carbon ($i = 1$) or the substitutional alloying element ($i = 2$) concentration in phase a at an interface between phases a and b which are in equilibrium or paraequilibrium
$x_i^{\alpha,\gamma,\theta}$	Iron ($i = 0$), carbon ($i = 1$) or the substitutional alloying element ($i = 2$) concentration in ferrite, austenite or cementite
$\overline{x}_i$	Average iron ($i = 0$), carbon ($i = 2$) or the substitutional alloying element ($i = 2$) concentration in the steel
$\overline{x}_i^{\alpha,\gamma,\theta}$	Average iron ($i = 0$), carbon ($i = 2$) or the substitutional alloying element ($i = 2$) concentration in ferrite, austenite or cementite
x_{Ae_3}	Carbon concentration given by the Ae_3 curve
$x_{Ae_3'}$	Carbon concentration given by the Ae_3' curve
x_{T_0}	Carbon concentration given by the T_0 curve
$x_{T_0'}$	Carbon concentration given by the T_0' curve
$x_1^{\alpha e}$	Equilibrium carbon concentration in ferrite

x_i^T	Carbon ($i = 1$) or the substitutional alloying element ($i = 2$) concentration on the transition line from PLE to NPLE regime in an isothermal section of the phase diagram
$\overline{x}_{i,j}$	Carbon ($i = 1$) or the substitutional alloying element ($i = 2$) concentration of the steel at the j-th iteration to obtain a PLE tie line (see Fig. 7.4 b)
$x_{i,j}^T$	Carbon ($i = 1$) or the substitutional alloying element ($i = 2$) concentration on the transition line from PLE to NPLE regime at the j-th iteration to obtain a PLE tie line (see Fig. 7.4 b)
X	Substitutional alloying element
y_i	Normalized i-th element concentration in cementite
Y	Mechanical property
z	Co-ordinate normal to transformation interface, or alternatively constant in equations 5.2-5.4
z^*	Position of interface along co-ordinate z
α	Ferrite
α'	Martensite
α_b	Bainitic ferrite
α_{lb}	Lower bainite
α_{ub}	Upper bainite
α_1	One dimensional parabolic thickening rate constant
α_3	Three dimensional parabolic rate constant
β	Aspect ratio of cementite plates, or alternatively parabolic lengthening rate constant which is assumed to be $3\alpha_1$ in the test
$\beta_{\alpha,\gamma,\theta}$	Thermal expansivities of ferrite, austenite and cementite
γ	Austenite
Γ_D	Capillarity constant
$\Gamma_i^{\alpha,\gamma}$	Activity coefficient of i-th element
δ	Boundary thickness
ϵ	Epsilon carbide
ϵ_1	Average transverse thickness of martensite cell structure
ϵ_{ij}	Wagner interaction parameters
η	η-carbide
$\eta_i^{\alpha,\gamma}$	Growth rate constants for i-th element in ferrite or austenite
θ	Cementite, or alternatively the maximum degree of reaction
μ_0	Interface kinetics coefficient at the top of the plate in equation 2.26
μ_i	Chemical potential of i-th element
μ_{Fe_3C}	Chemical potential of cementite
μ_{M_3C}	Chemical potential of M_3C carbide
ν	Characteristic frequency of the jump event of atoms at interfaces
ν_1	Rate constant in the nucleation function
ξ_e	Extended volume fraction of precipitating phase
$\xi\{t\}$	Volume fraction of precipitating phase at time t normalised by the maximum degree of the reaction
$\Delta\xi$	Increase in ξ
ρ	Dislocation density
σ	Either tensile or yield strength
σ_C	Solid solution strengthening effect of carbon on the intrinsic strength of martensite
σ_y	Yield strength of martensite

σ_0	Intrinsic strength of martensite
σ_0'	Residual strength equal to $(\sigma_0 - \sigma_C)$
$\sigma_{\alpha\alpha}, \sigma_{\alpha\beta}$	Interface energies per unit area between two matrix grains and between matrix and precipitating phase
$\Delta\sigma_y$	Change in yield strength of martensite
τ, τ_i	Incubation time prior to the formation of a detectable degree of transformation product
$\tau_f\{T\}$	Incubation time at temperature T for the C-curve representing a fraction f of the reaction
ϕ	Fraction of austenite in bainitic sheaf
Ω_0	Dimensionless supersaturation parameter

CHAPTER 1

REAUSTENITISATION IN STEELS

1.1 INTRODUCTION

A knowledge of the factors controlling the kinetics of austenite nucleation and growth is of interest both from a fundamental point of view, and because most commercial processes rely to some extent on heat treatments which cause the steel to revert into the austenitic condition.

The reverse transformation of low temperature (α) ferrite into austenite differs in many ways from the more usual case where the parent phase, which is stable at elevated temperatures, transforms on cooling below the equilibrium temperature. This is highlighted by an examination of the temperature dependence of kinetics for the two cases. The vast majority of transformations exhibit classical C-curve kinetic behaviour, in which the overall transformation rate goes through a peak as a function of supercooling below the equilibrium transformation temperature. This can be interpreted to be a consequence of two opposing effects; diffusion coefficients decrease with temperature, whereas the driving force for transformation increases as the undercooling increases. The kinetics of austenite growth from ferrite depend on the degree of *superheating* above an equilibrium transformation temperature. Both the diffusion coefficient and the driving force increase with superheating, so that the overall rate of transformation rises monotonically as the temperature is raised.

This in turn leads to several interesting effects. It is a common feature of normal reconstructive transformations, that they can be suppressed by rapidly cooling into a temperature regime where the rate of transformation becomes unreasonably small, when compared with the service life of the component concerned. Hence, austenite can in many steels (*e.g.,* 18/8 stainless steel) be retained by rapid cooling, even though it ceases to the thermodynamically stable phase at ambient temperature. It should be impossible to retain similarly the ferrite phase to high temperatures during a reaustenitisation experiment where only austenite is the stable phase at the elevated temperature, since atomic mobility always increases with temperature.

In steels which are lightly alloyed, rapid cooling from the austenite phase field does not always lead to the retention of the austenite. However, its decomposition may then be suppressed to very low temperatures so that any transformation cannot rely on substantial atomic mobility. The austenite may then decompose by a displacive mechanism, such as the martensitic transformation. During reverse transformation however, the temperatures involved are usually high enough to permit the rapid reconstructive transformation of austenite, and it is rare that the austenite grows by a martensitic mechanism from the ferrite.

In compendiums of time-temperature-transformation (TTT) diagrams for steel, the kinetics of austenite decomposition are usually presented as a function of alloy chemistry and the amount of austenite grain surface per unit volume (*i.e.* the austenite grain size). The number of variables to be considered when presenting similar data for the reverse transformation to austenite is much larger, since the initial microstructure can vary widely. It may consist of a mixture of any of the usual transformation products of austenite. The degree of sophistication with which it is necessary to specify the characteristics of the starting microstructure remains to be determined, but factors such as particle size, the distribution and chemistry of individual phases, homogeneity of the microstructure, the presence of nonmetallic inclusions, *etc.* should all be significant.

From an industrial point of view, any attempt at the estimation of microstructure of steels calls for a knowledge of the kinetics of reaustenitisation as a function of alloy chemistry, thermomechanical processing and the starting microstructure. Since such information is rarely available, there are few examples where the theory of phase transformations has been applied quantitatively towards the design or optimisation of commercial processes.

It is possible to think of many examples where detailed knowledge on the reaustenitisation process could be applied to considerable advantage. For example, one of the most difficult and widely used processes is that of welding, where unlike most commercial routes, an optimum microstructure is expected immediately after deposition from the liquid state, without the luxury of homogenisation or thermomechanical treatments after deposition. Furthermore, the welding process itself dissipates heat into the adjacent parent plates being joined, thereby influencing its microstructure, often in a detrimental manner. Any attempt at the estimation of microstructure in the fusion or heat-affected zones of such welds requires either a knowledge of, or a method of computing the TTT diagram for the transformation of a specified initial microstructure into austenite. It would be essential to have such information as a function of the chemistry of both the weld deposit and of the parent plate, since they are unlikely to have the same composition. A facility must also exist for converting the isothermal transformation diagrams into continuous-heating transformation (CHT) diagrams, since most industrial processes involve anisothermal heat-treatments. During welding, regions of the parent plate and of the fusion zones of multirun welds undergo transient temperature rises, which sometimes take the alloy into the $\alpha + \gamma$ phase field or beyond, causing profound changes in microstructure by the time the weld has cooled again to ambient temperature. In multirun welds, each region can be expected to undergo several such thermal cycles.

The purpose of this review is to collate and assess the work that has already been reported in the literature on reaustenitisation. However, an attempt is also made to use the opportunity to consider how the research can be extended in a systematic way, so as eventually to provide a framework for the estimation of microstructure in steels.

1.2 NUCLEATION OF AUSTENITE

The formation of austenite in steels is well established to be a nucleation and growth process [1]. The nucleation site, growth rate and morphology of the austenite that forms is sensitive to the initial microstructure, as well as the chemical composition and reaction temperature. As pointed out earlier, this contrasts with the decomposition reactions of austenite in steels, where the initial austenite grain size and chemical composition are usually the only important factors which need to be represented in *TTT* diagrams.

Much of the research on the role of the initial microstructure on the morphology of the austenite during growth, points towards two main types; in one case, the austenite is said to be "acicular", the term meaning needle-like, but implying a plate shape in three dimensions. Acicular austenite is often said to form intragranularly with respect to the prior austenite grain structure. The other common observation is of "globular" austenite in which the new phase seems to grow more or less isotropically, the nucleation sites often being the prior austenite grain boundaries. Most of these observations are based on reaustenitisation experiments in which the initial microstructures consisted of pearlite, martensite or mixtures of ferrite and carbide particles. There are very few data for initial microstructures which are completely ferritic or bainitic.

2

1.2.1 Initial Microstructure: Ferrite and Pearlite

Reaustenitisation beginning with a mixture of ferrite and pearlite is important in the production of dual phase steels which have a final microstructure of ferrite and about 20% martensite. These steels have a good combination of strength and uniform ductility, and find applications in the automobile industry.

When a fully pearlitic steel, or one containing pearlite and allotriomorphic ferrite is heated to induce reverse transformation, the austenite nucleates heterogeneously at the junctions between pearlite colonies [1], or at the interfaces between the grains of allotriomorphic ferrite and pearlite colony boundaries [1-5]. Garcia and DeArdo [3] studied the formation of austenite in a series of 1.5Mn wt.% steels which were annealed in and above the intercritical region; the intercritical region is the part of the phase diagram where mixtures of austenite and ferrite can be in thermodynamic equilibrium. The austenite was found to nucleate on cementite particles located on either pearlite colony boundaries or boundaries separating pearlite colonies and ferrite grains. A similar result was reported by Speich *et al.* [2] for austenite formation in eutectoid steels. This is in spite of the relatively large amount of inter-lamellar surfaces available within the pearlite colonies, which seem to be much less effective as sites for the nucleation of austenite [2]. Sharma *et al.* [6] have reported interlamellar spacings for pearlite in Fe-0.74C-0.4Cr wt.% alloy; using their data, we estimate that the interlamellar surface per unit volume is some 30–600 times larger than the amount of inter-pearlite-colony surface per unit volume. A full explanation of why the latter kind of surface is more effective in nucleating austenite is not yet available. It may be the case that the allotriomorphic ferrite/pearlite colony junctions, or junctions between pearlite colonies represent relatively high energy interfaces, in which case the free energy gained as such junctions are eliminated by the formation of nuclei would tend to proportionately reduce the activation free energy for nucleation. Of course, the activation free energy would have to be sufficiently small to overwhelm the higher site density associated with the inter-lamellar boundaries.

1.2.2 Initial Microstructure: Ferrite and Cementite

For an initial microstructure of a ferrite mixed with isolated cementite particles, the particles are usually located either at ferrite/ferrite grain boundaries or within ferrite grains. When low-carbon martensite is heavily tempered, the resulting cementite particles tend to locate at the ferrite/ferrite grain boundaries. However, if a martensitic specimen is tempered, cold worked and then recrystallised by tempering, then most of the cementite particles are dispersed in the ferrite matrix away from the ferrite/ferrite grain boundaries [2]. The effects of these different dispersions of cementite particles on the nucleation of austenite has been examined in many investigations [2-4,7]. Austenite is found to nucleate predominantly at junctions between cementite particles and ferrite/ferrite grain boundaries, rather than on the particles located within the ferrite grains. Speich *et al.* [2] suggested that this is because an additional surface free energy is available from the α/α grain boundary when austenite nucleates on a cementite particle located at such a boundary. It is however, difficult to guess which of the three different sites, *i.e.* $Fe_3C/\alpha/\alpha$ grain boundaries, grain edges and corners, is the most effective nucleation site for austenite, given uncertainties in the values of the interface energy terms for ferrite/carbide, austenite/carbide and ferrite/austenite boundaries. A knowledge of these interface energies as a function of crystallography and chemical composition is also required for a more complete description. Experimental data on three phase orientation relationships do not seem to be available.

3

If the ferrite grain size is very large, the density of sites available at $Fe_3C/\alpha/\alpha$ junctions can become very small compared with the density of cementite particles within the ferrite grains, and nucleation on the latter sites might be expected to dominate even though the activation energy is higher. Consistent with this, Lenel and Honeycombe [4] have reported the intragranularly nucleation of austenite when the initial ferrite grain size is very large.

1.2.3 Martensitic Initial Microstructure

The formation of austenite from an initially martensitic microstructure is of obvious relevance to high-strength steels, but also to dual phase steels with a microstructure which is a mixture of martensite and allotriomorphic ferrite. Martensite is in general a very unstable phase, especially so in iron alloys containing interstitials such as carbon or nitrogen. In such alloys, the heating that is necessary to induce the reverse transformation may first lead to a tempering of the martensite and eventually, to its decomposition into virtually carbon free ferrite and cementite or other carbide phases. The process of reaustenitisation from martensite in steels can therefore be complex, and there are interesting differences that arise when the iron alloy does not contain any interstitial alloying elements.

1.2.3.1 Martensite in steels

In experiments on reaustenitisation from martensite, the nucleation of austenite is found to occur preferentially at the prior austenite grain boundaries [8-10]. Intragranular nucleation with respect to the prior austenite grain boundaries, has been also reported, although it is not clear whether such nucleation has been confirmed using stereological analysis [11-13]

The effect of alloy chemistry on the nucleation site of austenite has been studied by Plichta and Aaronson [12] and Koo and Thomas [13]. Plichta and Aaronson [12] classified the sites in two groups. In ternary steels containing Mo or Cr, the main nucleation site was found to be the prior austenite grain boundaries. On the other hand, in ternary steels containing Mn, Ni, Cu, Si, Al or Co, the martensite plate boundaries were found to be the the predominant sites for the nucleation of austenite. There does not seem to be any explanation for this effect.

Martensite in steels tempers rather rapidly at elevated temperatures; carbon in iron even has significant mobility at ambient temperatures [14,15]. Hence, when reaustenitisation is carried out at high temperatures, the austenite forms from a spheroidised microstructure rather than from martensite proper [8]. Another factor to consider is the possible existence of retained austenite trapped between martensite laths, which may persist to the reaustenitisation temperature if the heating rate to that temperature is high enough to prevent its decomposition during heating [16]. Any retained austenite particles which survive to the reaustenitisation temperatures, can then grow, so that the nucleation of austenite is not required.

1.2.3.2 Martensite in interstitial-free iron alloys

The reverse transformation from martensite in interstitial-free alloys can be classified further into cases where the martensite behaves in a thermoelastic manner, and those in which the transformation tends to be less reversible. The lack of reversibility in the latter cases is usually attributed [17] to a loss of interface coherency during the growth of the martensite itself, due to any plastic accommodation effects accompanying the martensitic transformation. When the martensite is then heated, the plates do no shrink by the backwards movement of the austenite/martensite interface, but small plates of austenite grow by a displacive transformation mechanism within the martensitic regions. This was demonstrated by Kessler and Pitsch [18] using surface relief and light microscopy observations on an Fe-33Ni wt.% alloy. They also

4

showed that each martensite plate tends to transform into several different crystallographic variants of austenite, so that the original austenite grain structure is not reproduced. On the other hand, such a mechanism could be used to refine the austenite grain size, by repeated cycling between the M_F and T_F temperatures.

For the austenitic transformation discussed above, it is evident that the reverse displacive transformation of a single plate of austenite can lead to several orientations of austenite plates. This contrasts with thermoelastic martensites, which are usually found in ordered alloys, the ordering promoting crystallographic reversibility by making the reverse transformation path unique [17]. Consequently, a single crystal of martensite would then be expected to transform back to a unique orientation of austenite. The first thermoelastic ferrous martensite was reported by Dunne and Wayman [19,20] in ordered Fe-Pt alloys, which in the disordered condition showed nonthermoelastic behaviour with considerable hysteresis between the T_S and M_S temperatures.

The shape memory effect in thermoelastic martensites is a consequence of the reversibility of the martensite/austenite transformation. The martensite which forms when a single crystal of the parent phase is cooled, tends to grow as clusters of self-accommodating groups. Under the influence of stress, at temperatures below M_F, the glissile inter-variant interfaces are able to move in a way which accommodates the externally applied stress. Thus, some crystallographic variants of martensite grow at the expense of others. Under suitable conditions, a single orientation of martensite may be left, which when heated, converts back into the original single crystal of austenite [21]. The transformation back into the *original* single crystal of austenite is a consequence of the fact that there is in these alloys, a unique reverse correspondence between the martensite and austenite, even though there may be several forward lattice correspondences so that each austenite grain can transform into several martensite crystals [22]. These arguments can be extended to polycrystalline materials as well, although the details might be different [22].

1.2.4 Ferritic Initial Microstructure

Little work has been done on reaustenitisation of specimens which are fully ferritic, because of their extremely low hardenability. This makes it almost impossible to freeze the austenite microstructure to ambient temperature, even in the form of martensite. Speich *et al.* [2] studied the formation of austenite in a low carbon steel using a laser-pulse heating and a helium-water droplet spray technique, which is capable of achieving a heating rate of $\sim 10^6\,^\circ\mathrm{C\,s^{-1}}$ and a cooling rate of $\sim 10^5\,^\circ\mathrm{C\,s^{-1}}$. They showed that austenite initiated at the ferrite grain boundaries and during the quench to ambient temperature, each austenite grain transformed back to ferrite which had a much finer grain size when compared with the original ferritic microstructure.

1.2.5 Bainitic Initial Microstructure

The formation of austenite from bainitic microstructures such as bainite and acicular ferrite has been studied by Nehrenberg [23], Matsuda and Okamura [9], Law and Edmonds [10]. For a bainitic initial microstructure, Law and Edmonds [10] have reported that the nucleation of austenite occurs primarily at the prior austenite grain boundaries. This contrasts with a martensitic initial microstructure in the same steel, which exhibited the intragranular nucleation of austenite during isothermal reaustenitisation at high temperatures, although the *intragranular* nature of the nucleation was not established using stereological analysis.

5

The nucleation of austenite can, therefore, be usefully characterised by the nature of the heterogeneous nucleation site. When the initial microstructure is either a mixture of ferrite and cementite particles, or a mixture of ferrite and pearlite, the nucleation of austenite is found to occur predominantly at ferrite/ferrite grain boundaries. At these grain boundaries, there may be further preferential location of the nucleation site at positions where the boundaries have junctions with carbide particles. These carbides may consist of isolated spheroidised cementite, or of the edges of the pearlitic-cementite lamellar where they impinge on ferrite/ferrite boundaries. In pearlitic steels, sites where two colonies meet, giving rise to ferrite/ferrite grain boundaries (with cementite lamellar in contact), are also known to be favourable positions for the heterogeneous nucleation of austenite. It should be noted that when austenite forms from martensite in steels, tempering during heating to the Ac_1 temperature can make the reaustenitisation process identical to that for the ferrite and carbide starting microstructure. All these results emphasise the role of high energy ferrite/ferrite grain boundaries, whereas the lower energy boundaries, such as those between martensite plates within the the prior austenite grains do not seem to be as effective in nucleating austenite. It seems reasonable to assume that the grain boundaries resulting from the impingement of ferrite grains growing from two different adjacent austenite grains are likely to be of a higher energy, than those interfaces resulting from the tempering of martensite plates formed within a single austenite grain.

Direct or indirect measurements of the nucleation rate or the nucleation density have been carried out by Judd and Paxton [7], Dirnfeld *et al.* [24] and Roosz *et al.* [25]. Roosz *et al.* [25] measured the volume fraction of austenite formed in an eutectoid steel, and obtained a value four for the time exponent n in an application of the Avrami equation. By expressing theoretically the volume fraction and the amount of austenite/pearlite interfacial area per unit volume as a function of the nucleation rate and the growth rate, and by comparison with experimental data, they were able to determine the nucleation rate of austenite as a function of a superheating from the Ae_1 temperature. Consequently, the nucleation and the growth rates were found to be constant throughout the reaction.

Judd and Paxton [7] also measured the number of austenite particles formed from a mixture of ferrite and cementite particles, and showed that the nucleation rate of austenite was reasonably constant. They obtained the incubation periods for the reaction at different temperatures by extrapolating the linear relation between the number of nuclei and the holding time back to zero nuclei. Dirnfeld *et al.* [24] also reported the change in the number of austenite particles formed from a mixture of ferrite and cementite particles. Although the nucleation rate at the very early stage of the reaction seems to be constant at a particular temperature, it decreases with time when the volume fraction of austenite reaches about 0.2, because of site saturation.

1.3 GROWTH OF AUSTENITE

1.3.1 Ferrite–Pearlite Mixtures

Speich *et al.* [26] studied the formation of austenite from a mixture of ferrite and pearlite, and suggested that its growth could be divided into three stages. In the first stage, immediately after the nucleation of austenite at the ferrite-pearlite interface, the austenite grows into pearlite until the latter is completely consumed. The growth rate during this stage is assumed to be controlled by the rate of carbon diffusion in the austenite behind the advancing interface,

the diffusion path lying along the pearlite-austenite interface, and the diffusion distance being related to the inter-lamellar spacing of the pearlite. Because of the short diffusion distance, the growth rate during this step is expected to be rather high, with wider inter-lamellar spacings tending to reduce growth rate; wider spacings are also known to lower the nucleation rate of austenite [1]. When the dissolution of pearlite is complete, the austenite has a relatively high carbon concentration but is not in equilibrium with the remaining ferrite. Consequently, in the second stage, the austenite grows into the surrounding ferrite to achieve its equilibrium volume fraction as specified by the lever rule in the two phase region, at a rather slow growth rate, which at high temperatures is controlled by carbon diffusion in the austenite. In alloy steels the growth involves either paraequilibrium or negligible-partitioning-local equilibrium at the interface. At relatively low temperatures, substitutional elements are required thermodynamically to partition between the phases and growth may then occur under partitioning local equilibrium conditions. In any event, as the austenite grows into the ferrite, the extent of the diffusion field involved increases, causing the reaction to exhibit parabolic kinetics. Eventually, the diffusion fields of different austenite grains may interfere, leading to soft impingement; in this, the final stage, the growth rate is very slow indeed. The final stage may involve the homogenisation of substitutional alloying element gradients in the austenite and ferrite, and diffusion of such elements in austenite is particularly sluggish.

While the scheme described above is on the whole reasonable, Nemoto [27] has demonstrated, using hot-stage electron microscopy, that as the austenite grows into the colonies of pearlite, the lamellar of cementite may not dissolve completely at the advancing interface, but may be engulfed by the austenite to dissolve later, as time permits. The ferritic part of pearlite can therefore transform to austenite more rapidly when compared with pearlitic cementite. Cementite dissolution in the austenite after the cementite has been engulfed by the austenite has also been reported by Roberts and Mehl [1] and Nehrenberg [23].

1.3.2 Ferrite–Spheroidised Cementite Mixtures

When austenite nucleates at ferrite/ferrite grain boundaries in a mixed microstructure of ferrite and cementite particles, the allotriomorphs of austenite eventually engulf any carbides lying on the grain boundary [2]. Subsequent growth can occur only by carbon diffusion within the austenite envelope, from the position of the dissolving carbide to the advancing ferrite-austenite boundary [2,4,7]. The rate of dissolution of cementite particles during reaustenitisation has been investigated [7,28]. Judd and Paxton [7] assumed local equilibrium at all the interfaces, and calculated the volume fraction of austenite during isothermal reaustenitisation using experimentally determined incubation periods and a constant nucleation rate for the formation of austenite. They also claimed that some of the carbides begin to dissolve in the ferrite during the incubation period prior to austenite nucleation, thereby raising the carbon concentration of the ferrite close to the concentration given by the extrapolated metastable phase boundaries governing the equilibrium between ferrite and cementite. This leads to a reduction in the carbon concentration gradient within the ferrite to very low level, so that the flux of carbon from isolated particles within the ferrite, to any growing austenite must be very small indeed.

Hillert *et al.* [28] categorised the process of austenite formation from $\alpha + Fe_3C$ mixtures, where the cementite is in the form of spherical particles isolated in a matrix of ferrite, into five distinct regimes (Fig. 1.1). When the distance between particles of cementite is very large (as in low carbon steels), the dissolution of each particle, after becoming engulfed by austenite, will be controlled by the diffusion of carbon in the austenite shell (type 1). For more

realistic carbon concentrations, the distance between adjacent particles is not large enough to neglect any flux arising from carbon transport through the ferrite matrix from isolated cementite particles to austenite particles (type 2). This situation must become more prevalent when the nucleation rate of austenite is low. At sufficiently high carbon contents, an austenite grain containing an undissolved cementite particle may come into contact with neighbouring cementite particles before the dissolution of the original cementite particle is complete (type 3). If the carbon content is much higher than the critical value at the Ae_3 phase boundary, the austenite continues to grow with the cementite particles inside the shell being partially dissolved, and the dissolution continuing at some distance behind the austenite/ferrite interface, (type 4). At very high supersaturations, the formation of austenite can virtually reach completion without the dissolution of the cementite particles, with subsequent slow cementite dissolution occurring after the transformation of all the ferrite, (type 5). Hillert accounted for the effect of substitutional alloying elements on the carbon flux through the austenite shell and ferrite matrix assuming the local equilibrium at all the phase interfaces and linear gradients of chemical composition in the two phases, and obtained a good agreement with the experimental data.

1.3.3 Bainitic Ferrite–Austenite Mixtures

When an iron-carbon alloy is heated to a temperature within the $\alpha + \gamma$ phase field until equilibrium is established between allotriomorphic ferrite and austenite, a small rise or fall in temperature leads to the growth or dissolution respectively, of the austenite until the volume fractions once again satisfy the lever rule [29]. The transformation of austenite into allotriomorphic ferrite is in this sense reversible, and exhibits little or no hysteresis. On the other hand, for martensite in steels, there is a large difference between the M_S and the austenite-start temperature (T_S) recorded during heating. This is because the martensite tempers (or autotempers) and because its formation does some work in the form of irreversible plastic deformation. It is in this context that the results of reaustenitisation experiments on bainite can be interpreted.

If carbides precipitate from the austenite during the bainite reaction then a considerable hysteresis is expected during reverse transformation which would require the renucleation of austenite. On the other hand, a large hysteresis effect is not expected if reverse transformation begins from an *equilibrium* mixture of just bainitic ferrite and austenite. Of course, if the bainite forms by diffusionless transformation and the excess carbon is rejected into the residual austenite subsequent to transformation, then the reaction would cease before an equilibrium mixture of ferrite and austenite is reached, so that an increase in temperature would not lead to an immediate reversal of transformation.

Recently, Yang [16], and Yang and Bhadeshia [30,31] have investigated the growth of austenite in bainite or acicular ferrite microstructures. † The reaustenitisation experiments involved the heating of mixtures of either bainitic ferrite and austenite or acicular ferrite and austenite, obtained by isothermal transformation below the B_S temperature. The starting microstructures thus already contained austenite, which grew during the reaustenitisation process.

The problem can be studied best in steels which transform to bainite without any precipitation of carbides. In these circumstances, the microstructure obtained by isothermal trans-

---

† Acicular ferrite is similar in transformation mechanism to bainite, but because the plates of acicular ferrite nucleate intragranularly on inclusions, the detailed morphology differs. Bainite sheaves consist of parallel platelets of bainitic ferrite, whereas clusters of acicular ferrite consist essentially of platelets radiating outwards from the "point" nucleation sites.

formation below B_S is a mixture of bainitic ferrite and carbon-enriched residual austenite. To study the reverse transformation, the mixture can be heated to an isothermal reaustenitisation temperature, so that the nucleation of austenite is unnecessary. Experiments like these have shown that the reaustenitisation occurs by a diffusional process, and have established clearly that there is indeed a large difference between the B_S and T_S temperatures. This is in spite of the fact the starting microstructure exists in a metastable $\alpha + \gamma$ phase field. Furthermore, the T_S temperature is found to correspond approximately to the Ae_3 temperature of the *residual austenite*. The degree of reaustenitisation increases from zero at the T_S temperature, to 100% at the austenite-finish or T_F temperature, which is the Ae_3 temperature of the alloy as a whole. It should be emphasised that if bainite was simply the product of equilibrium or paraequilibrium transformation like allotriomorphic ferrite, a rise in temperature above the isothermal bainite transformation temperature should lead to a reversal of reaction with little hysteresis.

The observed reaustenitisation behaviour can be understood on the basis of the following model [30,31]. In steels where carbide precipitation from austenite is relatively sluggish, the formation of bainite ceases prematurely during isothermal transformation as the residual austenite carbon concentration approaches the T_0' curve on the phase diagram. The stage at which reaction stops is when the carbon content of the residual austenite reaches the T_0' curve of the phase diagram (Fig. 1.2). It follows that the carbon concentration x_1^γ of the austenite when the formation of acicular ferrite ceases at T_b, is given by:

$$x_1^\gamma = x_{T_0'}\{T_b\} \tag{1.1}$$

as indicated by the point **a** Fig. 1.2. Furthermore, we note that:

$$x_{T_0'}\{T_b\} \ll x_{Ae_3}\{T_b\} \tag{1.2}$$

where $x_{Ae_3}\{T_i\}$ is marked **b** in Fig. 1.2.

Thus, although the formation of *bainite* ceases at T_i, because the carbon content of austenite is far less than the equilibrium concentration (*i.e.* $x_1^\gamma \ll x_{Ae_3}\{T_b\}$), the driving force for austenite to transform *reconstructively* to ferrite is still negative.

This remains the case until the temperature T is high enough (*i.e.* $T = T_S$) to satisfy the equation:

$$x_1^\gamma = x_{T_0'}\{T_b\} = x_{Ae_3}\{T_S\} \tag{1.3}$$

Hence, reaustenitisation will first occur at a temperature T_S, as indicated by the point **c** in Fig. 1.2, and as observed experimentally. This is a consequence of the mechanism of the bainite reaction, which does not allow the transformation to reach completion. If this were not the case, then the lever rule demands that the temperature need only be raised infinitesimally above T_b in order for the reverse $\alpha \rightarrow \gamma$ transformation to be thermodynamically possible.

The theory predicts that at any temperature T_γ greater than T_S, the $\alpha_b \rightarrow \gamma$ transformation should cease as soon as the residual austenite carbon concentration (initially $x_{T_0'}\{T_b\}$) reaches the Ae_3 curve, with

$$x_1^\gamma = x_{Ae_3}\{T_\gamma\} \tag{1.4}$$

The equilibrium volume fraction of austenite at the temperature T_γ, is then given by:

9

$$V_\gamma\{T_\gamma\} \simeq \overline{x}_1 / x_{Ae_3}\{T_\gamma\} \qquad (1.5)$$

assuming that the carbon concentration of ferrite is negligible and that $x_{Ae_3}\{T_\gamma\} > \overline{x}_1$. When $x_{Ae_3}\{T_\gamma\} = \overline{x}_1$, the alloy eventually becomes fully austenitic (point **d**, Fig. 1.2), and if this condition is satisfied at $T_\gamma = T_F$, then for all $T_\gamma > T_F$, the alloy transforms completely to austenite.

This model explains why the degree of $\alpha_b \rightarrow \gamma$ transformation increases from approximately zero at T_S (the Ae_3 temperature of the *residual austenite*) to 100% at T_F (the Ae_3 temperature of the alloy as a whole). The behaviour is a direct reflection of the fact that the composition of the residual austenite after the bainite reaction has ceased is far below equilibrium. This in turn provides further support for the incomplete reaction phenomenon and its implication that the growth of bainite is diffusionless. Finally, it should be noted that the model discussed above assumes that the carbon concentrations of both phases is uniform at all stages.

1.3.3.1 Kinetic theory: One-dimensional growth from a mixture of austenite and bainitic ferrite

When reaustenitisation is from a starting mixture of bainitic ferrite and austenite, the transformation kinetics are relatively easy to interpret since austenite nucleation need not be considered.

Since both bainite and acicular ferrite are in the form of thin plates, the movement of the planar austenite/ferrite interfaces can, during the early stages of reverse transformation, be modelled in terms of one-dimensional growth. For simplicity, it is assumed that growth is diffusion-controlled. All the redistribution of carbon must occur within the austenite during its growth, since the amount of carbon in the ferrite is negligible. Microanalysis experiments have demonstrated that the reaustenitisation process involves the reconstructive growth of austenite in the alloys studied by Yang and Bhadeshia [30,31], with substitutional elements partitioning between the austenite and ferrite [30,31]. The extent of substitutional solute partitioning is known to decrease with an increase in driving force (which in turn increases with T_γ). The microanalysis experiments reported were not of sufficient spatial resolution to identify the compositions at the transformation interface, but it is likely that local equilibrium exists at the interface for low T_γ with a tendency towards zero bulk partitioning, (*i.e.* negligible-partitioning local equilibrium or paraequilibrium [32-40], as T_γ increases to beyond the Ae_3 temperature of the alloy. This makes a full analysis impossible since it is not yet possible to determine theoretically, which of these infinite possibilities, between the limits of local equilibrium and paraequilibrium, the system chooses to adopt as a function of temperature. In other words, the compositions of the phases at the interface cannot as yet be deduced theoretically.

If local equilibrium is achieved at least approximately at the transformation interface, then the growth rate calculated assuming carbon diffusion-controlled motion of the γ/α interface, using the *equilibrium* carbon concentrations may give a good guide to the factors influencing the kinetics of transformation. This amounts to assuming that the effect of substitutional solute gradients in influencing the flux of carbon is zero [36]. There is a further implicit assumption that the tie-line (of the equilibrium phase diagram) which determines the interface compositions passes through the bulk composition of the alloy. This is unlikely in substitutionally alloyed steels [35,39], but may be a good approximation since the alloys considered here are dilute.

Finally, any effects due to soft impingement (overlap of diffusion fields) were not taken into account, since it is only the early stages of transformation that are considered in the present study. Hence, the austenite and ferrite are both in effect assumed to be semi-infinite in extent.

One-dimensional diffusion-controlled growth involves the parabolic thickening of layers of austenite. The increase in the half-thickness of austenite can therefore be described as (see for example, [40,41]):

$$q = \alpha_1 t^{1/2} \tag{1.6}$$

$$dq = 0.5\alpha_1 t^{-1/2} dt \tag{1.7}$$

where q is the *increase* in the half-thickness of the austenite layer, of starting thickness a, and α_1 is the one-dimensional parabolic thickening rate constant.

The geometry assumed for the thickening of austenite layers is based on the plate shape of bainite or acicular ferrite. If c is the largest dimension of a bainitic ferrite plate, idealised as a rectangular parallelepiped with sides of length a, b and c, with $c = b \gg a$, then when both of the sides of a ferrite plate are penetrated by the growing austenite, the total area of the γ/α interface which advances into the plate of ferrite is $2c^2$. This reduces the thickness of the plate by $\Delta a_m/2$ from either side. If the minimum detectable change in volume fraction is ΔV_γ, then it follows that:

$$\Delta V_\gamma = 2nc^2 \int_0^{\Delta a_m/2} dq \tag{1.8}$$

where n is the initial number of particles of austenite per unit volume, and Δa_m is the minimum detectable thickness increase.

On combining equations 1.7 and 1.8, we get:

$$\Delta V_\gamma = 2nc^2 \int_0^{\tau} 0.5\alpha_1 t^{-1/2} dt \tag{1.9}$$

where τ is the time taken for the minimum detectable transformation.
After integration, this becomes:

$$\Delta V_\gamma = 2\alpha_1 nc^2 \tau^{1/2} \tag{1.10}$$

so that

$$\tau = \left(\frac{\Delta V_\gamma}{2\alpha_1 nc^2} \right)^2 \tag{1.11}$$

However,

$$2nc^2 = S_V = 2/\overline{L}$$

so that

$$\tau = \left(\frac{\Delta V_\gamma}{\alpha_1 S_V} \right)^2 \tag{1.12}$$

where S_V is surface area of γ/α boundary per unit volume, and $1/\overline{L}$ is the number of intercepts of γ/α boundary per unit length of test line [42]. It is clear from equation 1.12, that the value of τ is dependent on not only the parabolic rate constant α_1 but also the surface area of γ/α interface per unit volume S_V for a specific amount of reaustenitisation.

For the same starting microstructure and a specific amount of transformation, τ decreases rapidly as the isothermal reaustenitisation temperature increases due to the increase in α_1. Equation 1.12 also indicates that the morphology of the starting microstructure will effect τ, because S_V must depend on the detailed nature of the initial microstructure. This explains the

11

different rates at which the $\alpha_b + \gamma$ and $\alpha_a + \gamma$ reaustenitise; the distribution of plates in an acicular ferrite microstructure is such that S_V is smaller than that of a bainitic microstructure, so that it reaustenitises at a slower rate. The analysis shows that for a specified amount of reaustenitisation, and a fixed initial microstructure,

$$\tau \propto \frac{1}{\alpha_1^2}. \tag{1.13}$$

1.3.3.2 Estimation of the Parabolic Thickening Rate Constant

The parabolic rate constant α_1 can be deduced by analogy with already existing theory for the $\gamma \to \alpha$ transformation [40,43,44]. Fig. 1.3 shows the carbon concentration profiles in α and γ before reaustenitisation and during austenite growth; the austenite must become more dilute in carbon as it grows, the rate of interface motion being determined by the diffusion of carbon in the austenite behind the interface. In Fig. 1.3, the $\overline{x}_1^\gamma$ is the carbon concentration in the austenite before the start of reaustenitisation; it is given by $\overline{x}_1^\gamma = x_{T_0'}$; for $T_b = 460\,^\circ\mathrm{C}$, $x_{T_0'} = 0.01235$ mole fraction of carbon (Fig. 1.3). In Fig. 1.3, the carbon concentration of γ at γ/α interface during reaustenitisation is $x_1^{\gamma\alpha}$, and the carbon concentration of γ far away from the interface remains $\overline{x}_1^\gamma$. It is assumed that the carbon concentration of α remains the same, $x_1^{\alpha\gamma}$, before and during reaustenitisation. The coordinate z is defined normal to γ/α interface.

During reaustenitisation the flux of carbon in the austenite, towards the γ/α interface, at the position of interface can be expressed as:

$$J = -D\{x_1^{\gamma\alpha}\}\left(\frac{\partial x_1^\gamma}{\partial z}\right) \tag{1.14}$$

where the use of braces implies a functional relationship, *i.e.* $D\{x_1^{\gamma\alpha}\}$ implies that the function D is evaluated at the concentration $x_1^{\gamma\alpha}$. The diffusion coefficient of carbon in austenite, D, is known to be strongly concentration dependent [45-49]. We assume that a weighted average diffusivity, $\overline{D}$, can adequately represent the effective diffusivity of carbon [50] in the concentration gradient; it is given by:

$$\overline{D} = \int\limits_{\overline{x}_1^\gamma}^{x_1^{\alpha\gamma}} D dx_1 / (x_1^{\alpha\gamma} - \overline{x}_1^\gamma) \tag{1.15}$$

The rate at which carbon concentration of austenite is diluted can then be written as:

$$v_d = v(\overline{x}_1 - x_1^{\alpha\gamma}) \tag{1.16}$$

where v is the velocity of interface.

Given that the position z^* of the interface along the coordinate z is defined by the equation:

$$z^* = \alpha_1 t^{1/2},$$

it follows that:

$$v = \frac{dz^*}{dt} = 0.5\alpha_1 t^{-1/2} \tag{1.17}$$

Combining equations 1.16 and 1.17, the rate at which carbon concentration of γ is diluted can be expressed as:

$$v_d = 0.5\alpha_1 t^{-1/2}(\overline{x}_1^\gamma - x_1^{\alpha\gamma}) \tag{1.18}$$

12

Conservation of mass at the interface requires that (i.e., combining equations 1.14 and 1.18):

$$0.5\alpha_1 t^{-1/2}(\overline{x}_1^\gamma - x_1^{\alpha\gamma}) = -\overline{D}\left.\frac{\partial x_1^\gamma}{\partial z^*}\right|_{z=z^*}.$$ (1.19)

The concentration gradient $\partial x_1^\gamma/\partial z^*$ in equation 1.19 is evaluated at the position of the interface, *i.e.* at $z = z^*$. Equation 1.19 simply states that the rate of dilution of the austenite, per unit of time, equals the carbon flux towards the γ/α interface. From Fick's laws, the differential equation for the matrix is given by:

$$\frac{\partial x_1^\gamma}{\partial t} = \frac{\partial\left(\overline{D}\frac{\partial x_1^\gamma}{\partial z}\right)}{\partial z}$$ (1.20)

subject to the boundary condition $x_1^\gamma = x_1^{\gamma\alpha}$ at $z = z\{t\}$, and $x_1^\gamma = \overline{x}_1^\gamma$ at $t = 0$, and equation 1.19. It can be solved [40,43,44,51] to give an implicit relation for α_1 as a solution of the form:

$$\Omega_0 = \frac{\overline{x}_1^\gamma - x_1^{\gamma\alpha}}{\overline{x}_1^\gamma - x_1^{\alpha\gamma}} = H\{\overline{D}\}$$ (1.21)

where

$$H\{\overline{D}\} = \left(\frac{0.25\pi}{\overline{D}}\right)^{0.5} \alpha_1 \left[\text{erfc}\left\{\frac{0.5\alpha_1}{\overline{D}^{0.5}}\right\}\right]\exp\left\{\frac{\alpha_1^2}{4\overline{D}}\right\}$$ (1.22)

Finally the parabolic rate constant α_1 can be calculated using equations 1.21 and 1.22 with the diffusivity calculated following Bhadeshia [49].

1.3.3.3 The Relation between the Parabolic Rate Constant and TTT Curves

Consistent with the theory discussed earlier, Fig. 1.4 and Fig. 1.5 [18] show that $\log\{\tau\}$ is found experimentally to be proportional to $\log\{\alpha_1^{-2}\}$, the linear correlations in all cases being extremely good. It is, however, noted that the slope, which is expected to be the unity from the theory discussed earlier [40,41], appears not to be equal to unity.

1.3.4 Reaustenitisation from Cementite and Bainitic Ferrite

The earliest reported work on reaustenitisation from bainite containing cementite seems to be that of Nehrenberg [23]; the morphology of austenite which grew from high-temperature transformation products, such as pearlite, was found to be more or less equiaxed in shape. On the other hand, the austenite particles formed by the transformation of martensite or bainite, was found to assume an "acicular" morphology. The acicular morphology seemed to be generated by the growth of austenite between bainite or martensite platelets (*i.e.* along plate boundaries). By contrast, later work on the reaustenitisation of a Fe-1V-0.2 wt.% carbon steel found that with martensite and bainite as the starting microstructure, the austenite forms predominantly at the prior austenite grain boundaries [10]. This latter study also indicated that the nucleation rate of austenite tends to increase in the order of martensite, bainite and allotriomorphic ferrite as the starting microstructures.

Whether the austenite grows in an equiaxed or an acicular morophology is of practical importance, not because of the detailed difference in morphology, but because in the latter case, the steel exhibits a *memory effect* in which the original austenite grain structure is regenerated (both with respect to shape and crystallography) when the reaustenitisation process is completed [52,53]. When the memory effect operates, the austenite grain structure cannot

be refined by repeated cycling into the austenite phase field followed by transformation. This can be a disadvantage in many commercial applications. The creep ductility of bainitic and martensitic steels of the type used in the power generation industry is improved by grain refinement [53]. † The memory effect prevents the achievement of a fine austenite grain structure even when the austenitising temperature used is relatively low.

The memory effect has been shown to be a direct consequence of the existence of retained austenite in the starting bainitic or martensitic microstructure [53]. The reaustenitisation heat treatment causes the films of austenite to grow, and those originating from the same prior austenite grain then coalesce to regenerate the prior austenite grain structure (Fig. 1.6). In these circumstances, the reaustenitisation process does not require the nucleation of new austenite grains, although if the superheating is large enough, then the nucleation of new grains may follow in addition to the growth of the retained austenite.

The memory effect vanishes if the bainitic microstructure is annealed at a sufficiently high temperature to remove the retained austenite, and then reheated into the austenite phase field (Fig. 1.6). Furthermore, the austenite then grows with a more or less equiaxed morphology. The austenite may also decompose during heating to the reaustenitisation temperature, so that slow heating from ambient temperature also destroys the memory effect. Very rapid heating to the reaustenitisation temperature can reduce the memory effect by inducing the nucleation of new austenite grains [53].

It is interesting to note that the memory effect does not exist when the starting microstructure is allotriomorphic ferrite [53]. This is probably because the ferrite allotriomorphs usually grow into both the adjacent austenite grains, thereby destroying the prior austenite grain structure. With martensite and bainite, the plate growth is entirely restricted to the grain in which they nucleate, so that there exist sharp discontinuities in crystallographic orientation at the position of the prior austenite grain boundaries. Indeed, it is for this reason that the prior austenite grain boundaries are good sites for the nucleation of new grains of austenite when the initial microstructure is bainitic or martensitic. If the steel contains residual impurities such as arsenic, phosphorus or tin, which tend to segregate to the prior austenite grain boundaries, then the memory effect is enhanced [53], presumably because the segregation reduces the grain boundary energy, thereby making heterogeneous nucleation less likely.

1.4 OVERALL TRANSFORMATION KINETICS

The overall transformation kinetics can be characterised by TTT (time temperature transformation) curves for different volume fractions of a phase formed by the transformation. Once TTT curves are obtained, it becomes possible to calculate the evolution of the transformation during any heat treatment assuming the additivity of the transformation, although this assumption is not generally correct as discussed later [41].

During decomposition process of austenite in steels, the driving force for the transformation increases when the reaction temperature is reduced. However, the mobility of atoms decreases with temperature. Therefore, the well known C-shaped TTT curves are obtained for this process (Fig. 1.7). In the case of reaustenitisation, on the other hand, both the driving force and the mobility of atoms increases with the reaction temperature. As the result, the time required for reverse transformation decreases monotonically with temperature (Fig. 1.7).

---

† Note that creep in these materials, for typical circumstances, is not controlled by grain boundary diffusion or sliding.

The volume fraction of austenite normalised by its equilibrium volume fraction, ξ, transformed during isothermal holding at a temperature T can be expressed by the Avrami type equation.

$$\xi\{t\} = 1 - \exp\{-k_A t^n\} \qquad (1.23)$$

As was pointed out by Christian [41], a kinetics investigation limited to the establishment of the value of n in the Avrami equation most appropriate to the assumed growth law, does not give sufficient information for the growth mechanism to be deduced. Nevertheless, this method is one of the shortest ways of obtaining information of the overall reaction. For investigating the overall transformation kinetics of austenite, attempts have been made at fitting the Avrami equation to extra data [2,24,25]. Speich *et al.* [2] have made optical microscopic measurements of the volume fraction of austenite in hypereutectoid steels transformed during isothermal holding at different reaction temperatures, and obtained a value of three for the power of time n in the Avrami equation. Rooz *et al.* [25] have also measured the volume fraction of austenite in an eutectoid steel, and declared that the slope was four instead of three. They have concluded from this n value and the optical studies which show that the austenite nuclei appear at the edges of the pearlite colonies, that reaustenitisation from pearlitic microstructures occurs at a constant growth rate and the constant nucleation rate without the occurrence of site saturation throughout the reaction [25]. In the case of the formation of austenite from a mixture of ferrite and spheroidised cementite particles, Dirnfeld *et al.* [24] reported that the slope n depends on the reaction temperature and changes in the vicinity of about 0.05 and 0.4 of volume fractions transformed. Although all these experiments seem to be valid for the particular system considered, they cannot directly be applied to other systems having different initial conditions and chemical compositions.

The constant k_A in equation (1.23) was studied in a special case where site saturation occurs [24]. The value k_A calculated for the grain boundary, edge and corner nucleations using the observed grain diameter and growth rate of austenite. The observed k_A value at 40% of transformation is almost constant which is close to the values of the grain boundary nucleation at a low temperature (*i.e.* 760 °C), the edge nucleation at medium temperatures (*i.e.* 780 °C and 800 °C) and the corner nucleation at a high temperature (*i.e.* 820 °C).

There have been several attempts to predict the formation of austenite theoretically [7,28, 54,55]. They all assume the existence of the local equilibrium at the interface between austenite and ferrite matrix. The calculations solve the diffusion equation either analytically or numerically. All of them, therefore, dealt with the growth rate of austenite into a ferrite matrix controlled either by the diffusion of carbon in austenite and/or ferrite or by the diffusion of both carbon and the substitutional alloying element in austenite and/or ferrite. Although they managed to calculate the growth rate of austenite in each case, it was necessary to assume or neglect the nucleation rate of austenite since there was no theory available. In the case of the formation of austenite from a mixture of ferrite and austenite, since the nucleation of austenite is essentially unnecessary, the calculation of the growth rate of austenite can be converted to the evolution of the reaction directly.

1.5 ANISOTHERMAL TRANSFORMATION

In a real heat treatment which involves reaustenitisation, the transformation does not take place isothermally but in a non-isothermal manner. As it is widely used for the calculation of the transformation process in a non-isothermal process from isothermal data such as a TTT curve,

the additivity of the transformation is usually assumed for the calculation of reaustenitisation during a non-isothermal heat treatment. However, as discussed by Christian [41], the additivity of the reaction is valid only when the reaction is isokinetic [56], in which the fraction transformed at a fixed temperature is dependent only on the time and on a single function of the temperature. In general, the reaction is not isokinetic because of the different temperature dependence of the growth rate and nucleation rate of the transforming phase. However, when the site saturation of the reaction is maintained at the early stage of the reaction, the reaction will be considered to be isokinetic and the additivity of the transformation can be used [41].

In the case of the formation of austenite from a mixture of ferrite and austenite, the nucleation of austenite is not necessary since austenite already exist before the onset of the reaction. The increase in volume fraction of austenite is then conducted by the growth of pre-existing austenite, and therefore the reaction can be treated as isokinetic allowing the use of the additivity of the reaction.

If $\tau\{T\}$ is the time taken to produce a fixed amount of transformation, an additive reaction implies that the total time t to reach a specified stage of the transformation is obtained [41] from

$$\int_0^t \frac{dt'}{\tau\{T\}} = 1$$

where T is now a function of time. The calculation can be done practically by replacing the non-isothermal integration by the summation of a set of sufficiently small steps of isothermal reactions.

1.5.1 Continuous Heating Transformation

The behaviour during continuous heating should be related to the isothermal transformation kinetics. For example, the continuous heating curve could be treated as a series of small isothermal steps, each occurring at a successively higher temperature, with a time interval t_i associated with each step (where i is the subscript identifying the step number). If the time necessary to reach a specified increment of transformation is written as τ_i for the isothermal transformation at temperature T_i, then the simplest approximation is to assume Scheil's rule [70]. In this, the specified increment of transformation is achieved during continuous heating when

$$\sum_{i=1}^n \frac{t_i}{\tau_i} = 1. \tag{1.24}$$

An application of this rule to the τ values listed in Table 1.1, for the $\alpha_a + \gamma$ starting microstructure, showed that during continuous heating $(0.06\,^{\circ}\mathrm{C\,s^{-1}})$ of that microstructure, reaustenitisation should begin at a temperature of $\cong 685\,^{\circ}\mathrm{C}$. It is however evident from Fig. 1.8 that for the same heating rate, the as-deposited welds begin to transform to austenite at a much lower temperature of about $630\,^{\circ}\mathrm{C}$.

Of course, the incubation time data of Table 1.1 refer to reaustenitisation from an initial microstructure generated by isothermal transformation to acicular ferrite or bainite at $460\,^{\circ}\mathrm{C}$. On the other hand, the primary weld microstructure arises during continuous cooling of the weld to ambient temperature. The carbon concentration x_1^{γ} of the austenite in the weld may then be approximated by $x_{T_0'}$ evaluated at the martensite-start M_S temperature of the alloy concerned. This is because the weld can be assumed to continue transforming to acicular ferrite until the M_S temperature is reached. Unfortunately, the composition of the residual austenite is expected

to change as acicular ferrite forms, so that its M_S temperature is not easy to evaluate, especially if the carbon is inhomogeneously distributed in the austenite [57-59]. Nonetheless, the values of $x_{T_0'}$ evaluated at the M_S temperature of the untransformed alloy must provide a lower limit to the carbon concentration of the residual austenite. Since this is larger than the corresponding value at $460\,^{\circ}$C, it is not surprising that the welds begin the reaustenitisation process at lower temperatures and at faster rates when compared with isothermal reaustenitisation in which the initial microstructure was generated by transformation at $460\,^{\circ}$C.

In fact, the rate at which the reaustenitisation-start temperature T_S is expected to decrease as the temperature T_b for the isothermal formation of acicular ferrite decreases, is given by

$$\frac{\partial T_S}{\partial T_b} = \frac{S_{T_0'}}{S_{Ae_3}}, \tag{1.25}$$

where $S_{T_0'}$ and S_{Ae_3} refer to the slopes of the T_0' and Ae_3 curves of the phase diagram respectively. For the alloy (Table 1.1), the ratio $S_{T_0'}/S_{Ae_3}$ is found to be 2.36 (Fig. 1.9) for the carbon concentration range $0 \rightarrow 0.04$ mole fraction on the phase diagram. Since the difference in $T_S \{0.06\,^{\circ}$C s$\}$ between the samples isothermally transformed at $460\,^{\circ}$C and the as-welded microstructure is $685 - 630\,^{\circ}$C, the *effective value* of T_b for the as-welded microstructure is estimated to be $436\,^{\circ}$C.

1.6 CRYSTALLOGRAPHY

There are few crystallographic studies on partially reaustenitised microstructures when compared with those on the microstructures obtained by the decomposition of austenite.

The orientation relationship between austenite formed during heating and ferrite matrix was studied by D'Yachenko and Fedorov [60] in a Fe-0.6C wt.% steel using X-ray diffraction at high temperatures. They observed a relation $(111)_{\gamma} \parallel (110)_{\alpha}$ when a quenched specimen was heated slowly. However there were no general features of the orientation relations when the specimens were annealed before the heat treatment, or when a higher heating rate was used, and grain refinement was observed in these cases. A consistent orientation relationship between austenite and the ferrite matrix has also been reported by other researchers. Fong and Glover [61] reported orientation relationships between austenite precipitates formed during nitriding in a Fe-1.93Mn wt.% steel, which were close to a Kurdjumov-Sachs (K-S). This observation was supported by Matsuda and Okamura [9], Koo and Thomas [13], Law and Edmonds [10] and Lenel and Honeycombe [4].

Matsuda and Okamura [9] showed that the acicular austenite grains formed in a martensitic initial microstructure nearly all had the same orientation, with a K-S orientation relationship between the austenite and the ferrite matrix. They concluded from the results that the mechanism of formation of acicular austenite is martensitic. However, it is known that this orientation relationship can also be obtained even for reconstructive transformation [40]. Hence different evidence such as surface relief will be required to confirm this conclusion.

Law and Edmonds [10] studied the crystallographic relationship between grain boundary nucleated austenite grains and adjacent ferrite grains. They found that austenite nodules were K-S related to the ferrite grains into which they did not grow but not with the ferrite grain into which they grew. However Lenel and Honeycombe [4] studied the orientation relationships between austenite and ferrite matrix in the case of the formation of austenite from a mixture of ferrite and pearlite, showing that the austenite can grow into one or both ferrite grains to

which the austenite grain was K-S or Nishiyama-Wasserman (N-W) related. Further studies are necessary to understand the direction of the growth of grain boundary nucleated austenite.

1.7 APPLICATIONS

There are many examples in which reaustenitisation plays an important role in the evolution of the ultimate microstructures, and thus the final mechanical properties of products.

1.7.1 Ferrite-Martensite Dual Phase Steels

Ferrite-martensite dual phase steel, which gives good strength-ductility combinations, is one of the major successful applications of heat treatment in the manufacture of steels [62]. Such steels are now used widely in the automobile industry and contribute to the major reduction in automobile weight achieved in the past two decades. This has been one of the most desirable targets in the automobile industry from not only an economical point of view after the oil crisis but an environmental point of view. There are two different approaches in the production of dual phase steels [63]. One of them involves a combination of the accelerated cooling and a slower cooling of austenite at around the ferrite transformation-start temperature, Ar_3, after hot rolling at rather low temperatures. This method provides as-hot-rolled dual phase steels which are cheaper than those produced after cold rolling followed by intercritical annealing at temperatures between Ae_1 and Ae_3. In this latter heat treatment, a certain volume fraction of austenite, which has been produced by the intercritical annealing, is surrounded by soft ferrite matrix; the austenite then transforms into martensite during a final quenching process. In both cases, the amount, hardness and distribution of martensite, and the ferrite grain size determine the ultimate mechanical properties of the dual phase steels. When a steel is annealed at an intercritical temperature, the amount, size, distribution and chemical concentration of austenite particles formed during the annealing are determined by the reaction temperature, holding time at the temperature and initial microstructure of the steel. In order to obtain the microstructure including an appropriate amount of austenite with its optimum size and distribution, one needs to select these conditions carefully.

1.7.2 Steels containing some Retained Austenite

Using a similar process as the production of dual phase steels, Sawai et al. [64] and Matsumura et al. [65,66] reported very high strength steels with an excellent ductility. These steel were reported to contain less than 25 % retained austenite. In high carbon steels, this phenomenon is known as transformation induced plasticity (TRIP after Zackay [67]). The heat treatment conducted here was more complicated than that to get the dual phase steel mentioned earlier. Steels are heated to an intercritical temperature for a short period (e.g. 1.5 min). The steels are then cooled down to a bainite transformation temperature followed by an isothermal holding at the temperature for less than 30 min, thus allowing bainite transformation at the temperature to be completed. The steels quenched after the bainite treatment have microstructures containing ferrite, bainite, martensite and retained austenite. In order to make austenite particles stable even at ambient temperature, bainite transformation process was added to the process for the production of conventional dual phase steels. In this process, not only are the prediction of the amount, size, distribution and chemical content of austenite particles formed during the intercritical annealing important, but also the bainite transformation following the intercritical annealing must be predicted. This low carbon retained austenite steel is expected to be used for automobiles.

1.7.3 Welding of Steels

Welding is, as well recognised, a complicated heat treatment of an inhomogeneous material. The welded part is usually divided into two different regions; the weld deposit, which is the melted region, and the heat affected zone, which may have been heated to various temperatures during welding. Especially in multirun welds, the layers deposited initially are reheated by the deposition of subsequent layers and experience a complicated thermal cycle which results in several modifications of microstructure. The weld deposit and heat affected zone sometimes can act the weakest part of toughness because of the coarse microstructure developed in these regions during welding. The fine microstructure which has been achieved by special technique such as a controlled rolling and an accelerated cooling, can be easily broken during welding. A theoretical model to predict the microstructure of weld deposits has been developed by Bhadeshia *et al.* [40]. However, the heat affected zone can contained regions of complete reaustenitisation, partially reaustenitisation, recrystallisation and tempering. Therefore the prediction of the reverse transformation is essential to complete the prediction of the microstructure of the heat affected zone.

1.7.4 Initial Austenite Grain Size

Obtaining a fine grain microstructure is known to be almost the only way of improving the toughness and ductility without sacrificing the strength of steels. It is for this purpose that micro-alloying and controlled-rolling technology have become so prominent in steel manufactures. In addition to this, there is no doubt that the initial austenite grain dimensions can affect the scale of the final microstructure in steels.

Even in the case of hot working, the larger the initial austenite grain diameter the larger the scale of final microstructure in those cases where the total reduction in thickness is not large. It is also useful to note that rapid heating and cooling techniques are used to get the fine microstructures [68]. After the completion of reverse transformation, austenite grows by reducing its total grain boundary energy, and the rate of growth depends on the metal's composition, the temperature and on the initial grain diameter (see for example [69]). Normal grain growth usually stops long before a metal has become converted into a single crystal and there is, in practice, a maximum attained grain size. The magnitude of this maximum grain size usually depends on the composition and the annealing temperature. When there exist dispersed particles in the specimen, a maximum grain size beyond which grains cannot be expected to grow is determined by the ratio of the mean radius and volume fraction of the particles (see for example [69]). Therefore the austenite grain diameter will be determined by the reverse transformation and the grain growth after the completion of the transformation. In the cases, where the initial austenite grain diameter can influence the scale of the final microstructure, not only reverse transformation kinetics but also grain growth mechanism after transformation is important and needs to be investigated.

1.8 TRANSFORMATION FROM AUSTENITE

The main aim of this work is to investigate the formation of austenite from different initial microstructures as a function of chemical composition and temperature. Since the reaustenitisation process is strongly affected by the initial conditions such as microstructure and chemical distribution, it is essential to understand the transformation from austenite to ferrite.

In this section, the Widmanstätten, bainitic, martensitic transformation and diffusional formation of ferrite are summarised. The key characteristics of phase transformations in steels

have been rationalised by Bhadeshia ([70], Table 1.2). When austenite is rapidly cooled to a very low temperature, there may not be enough time or atomic mobility to facilitate the diffusional formation of ferrite. Under the circumstance, Widmanstätten ferrite, bainite or martensite can form depending on a level of the under-cooling. In contrast, when specimens are cooled to a relatively high temperature below the Ae_3 temperature, the austenite phase can undergo complete reconstruction into the ferrite phase. Allotriomorphic ferrite, idiomorphic ferrite and pearlite are considered to be in this category.

1.8.1 Widmanstätten ferrite formation in steels

Widmanstätten ferrite can form at low under-coolings below the Ae_3 temperature where the driving force for transformation is small, so that the partitioning of carbon during transformation is thermodynamically necessary. The formation of Widmanstätten ferrite is accompanied by a change in the shape of the transformed region; the shape change due to a single wedge of Widmanstätten ferrite consists of two adjacent and opposing invariant-plane strain deformations which allow an elastically accommodated strain energy accompanying plate formation to be rather small, of the order of $50\,\mathrm{J\,mol^{-1}}$ [70]. These invariant-plane strain deformations imply the existence of an atomic correspondence between parent and product phases as far as the iron and substitutional solute atoms are concerned, although carbon atoms can diffuse during the growth. When Widmanstätten ferrite nucleates from grain boundary allotriomorphs of ferrite, it is called a "Widmanstätten ferrite side-plate" but when it nucleates directly from austenite grains, it is referred to as a "Widmanstätten ferrite primary side-plate". The growth rate of Widmanstätten ferrite has been reported to be in a good agreement with the calculated edgewise growth of a plate or a needle. The growth of Widmanstätten ferrite is controlled by the carbon diffusion in the matrix ahead of the moving interface.

1.8.2 Bainite transformation in steels

The bainite transformation has been summarised recently by Christian *et al.* [71] and Bhadeshia [70]. Bainite forms from austenite in steels in a temperature between that in which pearlite is produced and the martensitic transformation. Although the pearlitic and bainitic transformation temperature ranges overlap each other in low alloy steels, and this makes the interpretation of microstructure and kinetics difficult, two separate C-curves can be detected in medium alloy steels in the isothermal time-temperature-transformation (TTT) diagrams. The upper C-curve represents the time taken for the initiation of diffusional transformations whereas the lower C-curve for the initiation of the Widmanstätten ferrite or bainite transformation which are considered to be conducted by a shear mechanism rather then a diffusional mechanism.

The lower C-curve usually exhibits the flat top corresponding to the bainite-start temperature B_S, and this relates to the nature of bainite transformation in steels. The bainite transformation exhibits the classical kinetics of nucleation and growth, but ceases well before the completion of the decomposition of residual austenite has occurred. The volume fraction of bainite isothermally transformed is a function of the reaction temperature, and increases with decreasing reaction temperature. The point which corresponds to 0% transformation can define the B_S temperature. The termination of bainite transformation occurs when the carbon content of residual austenite reaches the value where ferrite, whose free energy is raised by a stored energy term associated with the strain of the transformation, and austenite of identical composition have the same free energy [70]; this is called the incomplete reaction phenomenon.

Unlike the products of diffusional transformation, a platelet in a sheaf grows to a limiting

size which is typically about $10\,\mu m$ long with a thickness of about $0.2\,\mu m$. The bainite transformation causes a change in the shape [70] of the transformed region, which is known to be an invariant-plane strain. In the invariant-plane strain shape change, an atomic correspondence between the parent and product phases exists at least for the iron and substitutional alloying elements. As a consequence of the shape deformation, which is identical for each platelet within a sheaf, bainitic ferrite has a stored energy of about $400\,J\,mol^{-1}$ [72]. The platelets within a sheaf have a small spread of orientations so that where they impinge on one another only "low angle" boundaries are formed. At relatively high temperatures where bainite forms, any excess carbon in ferrite can rapidly partition into the residual austenite since the diffusivity of carbon at the temperatures is high when it is compared to the rate of carbide precipitation from a supersaturated ferrite. At lower temperatures, on the other hand, the carbide precipitation can occur prior to the partitioning of carbon atoms from the supersaturated ferrite into the surrounding untransformed austenite.

Bainite is usually classified into upper bainite and lower bainite. The difference of these phases is the existence of cementite particles within the ferrite matrix in the case of lower bainite but not in the case of upper bainite. Both upper and lower bainite tend to form as aggregates (sheaves) of small lenticular platelets of ferrite separated by regions of austenite, martensite and/or cementite. When the time to decarburise the ferrite is small relative to the time required to relieve the carbon supersaturation by the precipitation of carbides within the ferrite, then upper bainite is obtained; otherwise, lower bainite forms [73].

The orientation relationship between bainitic ferrite and austenite is close to either the Kurdjumov-Sachs or the Nishiyama-Wassermann orientation relationships. Though the relative orientations of the cementite and austenite is not known, the ferrite and cementite are relatively oriented in a variant of the Bagaryatskii relationship commonly observed for the precipitation of cementite in tempered martensite or quench-aged ferrite [74].

1.8.3 Martensitic transformation in steels

Martensitic transformation has been studied initially because of its technological importance in the hardening of steels and recently because of its special characteristic of shape memory. Martensitic transformations have recently been summarised by Nishiyama [75,76]. The martensite transformation is a phase transformation that occurs by the cooperative atomic movements without any diffusion of atoms. The time taken to form a martensite crystal in steels is in some cases said to be of the order of 10^{-7} sec. A necessary condition for the occurrence of martensitic transformation is that the free energy of martensite be lower than that of austenite [76]. Moreover, since additional energy, such as that due to surface energy and transformation strain energy, is necessary for the transformation to take place, the difference between the free energies of austenite and martensite must exceed the required additional energy. Therefore the austenite to martensite transformation cannot occur until the specimen is cooled to a particular temperature below the value where the free energy difference between austenite and martensite is zero. This temperature is called martensite-start temperature M_S, and varies with the chemical composition of steels.

It is well known that martensite crystals produced in an austenite crystal have definite crystallographic relations to those of the untransformed part of the austenite crystal, which are designated the Kurdjumov-Sachs or Nishiyama-Wassarmann orientation relationships.

1.8.4 Reconstructive formation of ferrite in steels

The reconstructive transformation of austenite to ferrite in steels has been summarised by Bhadeshia [77]. When transformation is controlled totally by diffusion in the matrix ahead of the interface, a reasonable approximation for the growth of ferrite is that the compositions of the phases in contact at the interface are in equilibrium; this is referred to as local equilibrium at the interface. The diffusional formation of ferrite in Fe-X-C (X indicates a substitutional alloying element) alloys can be governed by a variety of possible growth modes [77], because of the large difference in the diffusivities of carbon and substitutional atoms in austenite.

At a low supersaturation, considerable partitioning and long-range diffusion of substitutional alloying elements can occur, so that the driving force for carbon diffusion will be reduced to a level which allows the substitutional element flux to keep pace with the carbon flux at the interface. This state is called the partitioning under local equilibrium (or PLE) [39]. However at higher supersaturations, the partitioning of substitutional atoms can be negligible, so that it causes a very large gradient of the substitutional element at the interface, which increases the driving force for X diffusion in austenite and allows the flux of X to keep up with the long range diffusion of carbon in austenite. In this situation, the diffusion of substitutional atoms is limited to an extremely short range. This state is referred to as the negligible partitioning under local equilibrium (or NPLE) [39]. In contrast to the two equilibrium states where the local equilibrium exists at the interfaces and both carbon and substitutional element diffuse during transformation, there exists a state where the local equilibrium cannot be satisfied at the interfaces because of the rapid reaction. In this case, at very high supersaturations, the diffusion of substitutional atoms can be completely negligible and the two adjoining phases have identical X/Fe atom ratio, even though carbon atoms diffuse during the reaction keeping the chemical potential identical in both the phases at the interface. Therefore, the rate of the reaction is controlled by the diffusion of carbon in the austenite. This state is designated as paraequilibrium [32].

1.9 PREDICTION OF MICROSTRUCTURE IN STEELS

Theories of phase transformations can be effectively used in the prediction of the microstructure of steels. In turn, these could be applied to the design of new alloys or new processes. Although all of the kinetics of phase transformations in steels have not yet been established, even partial knowledge of the phase transformations can be applied to this purpose.

1.9.1 Microstructure prediction in welding

Welding is a process where an extended range of temperature is experienced by a material used in the process. Therefore there are various different reactions happen during welding such as reaustenitisation, melting, solidification, delta ferrite to austenite transformation, formation of ferrite from austenite and dissolution and formation of various kinds of precipitations. In addition to this, a repeated heat input in a multi-run welding makes the problem more complicated. The phases formed in a deposition during cooling may be heated again by the subsequent deposition on it, which may make the position experience additional phase transformations and leads to a completely different microstructure from the beginning.

Bhadeshia and his coworkers [40] have reported a model to predict the microstructure of a weld deposit from the alloy chemistry and thermal history of the deposition.

The model consists of the TTT curve prediction and the kinetics calculation of phase transformations from austenite. They assumed the initial austenite microstructure as a columnar

which is usually observed in solidification. The growth of ferrite allotriomorph at austenite grain boundaries is calculated by first evaluating the one-dimensional parabolic thickening controlled by carbon diffusion in austenite. The paraequilibrium is assumed in the calculation. When the temperature reaches the W_S temperature, which can be calculated from the alloy chemistry, the formation of Widmanstätten ferrite takes place. Since Widmanstätten ferrite can grow through the whole grain, hard impingement, which is an impingement by a structural contact of two adjacent growing phases, is expected to occur. They took into account of the effect and added the formation of acicular ferrite, which is well known as a phase which improves the toughness of the weld, within the austenite grains. Since the model is based on thermodynamics, they managed to take into account the effect of alloy additions on the microstructural development during the heat cycle such as Si, Mn, Ni, Mo, Cr, V. Although the TTT calculation model does not deal with the effect of the initial dimension of austenite grains, the subject has been recently tackled by Reed and Bhadeshia [78] with a model for predicting heat cycles which is experienced by any part of a weld during multirun welding from welding conditions and the weld geometry.

1.9.2 Microstructure prediction of hot worked steels

Computer control systems has been widely used in hot working processes mainly to control the sizes and shapes of products. However, there has been a growing demand for numerical models which make it possible to predict mechanical properties of hot worked steels via the prediction of microstructural development during and after hot working. This sort of model is desired not only from the industrial point of view but also from its fertile theoretical interest. Once a model is obtained, it could be used and contribute to a remarkable reduction in the amount of mechanical testing carried out to guarantee the properties of products, to an extension of the possibility of producing various levels of mechanical properties out of a steel using a wide range of production conditions which may lead a new concept of an alloy design in industries, and to a decrease in time on research and development by providing a flexible simulation model on computers.

When one intends to predict a microstructural development of hot worked steels, one may consider the effect of hot working; in other words the effect of defects introduced by the hot working, on phase transformations which occur on cooling after the hot working and determine the ultimate microstructure in the products. Especially when it is essential to obtain a very fine grain structure in the final stage of the production in order to maintain a high toughness or ductility without tolerating its strength, a combination of hot working at relatively low temperatures of austenite single phase region, and rapid cooling after the hot working has been commonly used; this is referred as the controlled rolling technique. In this case, the transformation occurs from work-hardened austenite which is very different from that from undeformed austenite in terms of the overall reaction rate.

A phenomenological study on microstructural development of austenite associated with hot working led to the construction of an empirical model which deals with recrystallisation, recovery and grain growth processes of austenite (for example [79]). Sellars [79] collated the knowledge on recrystallisation and grain growth of austenite and proposed an empirical model which can calculate dynamically the development of austenitic microstructure during and after hot working. The change in the austenitic microstructure during and after hot working in a austenite single phase region consists of two phenomenologically different recrystallisation processes as well as the grain growth and recovery.

Recrystallisation which occurs during hot working is called the dynamic recrystallisation. The minimum required strain for the onset of the dynamic recrystallisation is a function of strain rate, temperature, initial austenite grain size and alloy chemistry. The larger the initial grain size, the lower the hot working temperature and the larger the strain rate of the working, the larger is the strain required for the onset of the dynamic recrystallisation. In addition to this, the minimum required strain for the onset of the dynamic recrystallisation is increased by additions of alloying elements such as niobium and titanium. The average grain diameter of recrystallised grains relates only on the strain rate and reaction temperature but not on the strain nor on the initial austenite grain diameter.

When a hot worked steel which has not recrystallised dynamically, is held at a high temperature after the hot working, the static recrystallisation may take place. In this case, the minimum required strain for the onset of the static recrystallisation is dependent on the initial austenite grain size, reaction temperature and alloying compositions but not on the strain rate. The average grain diameter of statically recrysatallised grains is determined only by the initial austenite grain diameter and strain but not by the reaction temperature nor the strain rate.

Therefore static recrystallisation is believed to play an important role in the case of high speed hot workings such as continuous hot rolling processes whereas the dynamic recrystallisation in low speed hot workings such as thick plate hot rolling processes.

Dynamic recovery occurs on hot working and determines the final dislocation density at the end of the hot working. The higher the strain rate and the lower the reaction temperature, the higher the dislocation density. The static recovery, on the other hand, occurs after the hot working by a diffusion of atoms.

Considering all of these factors as well as the grain growth of austenite, one can predict the microstructure of austenite before the onset of phase transformations during cooling after hot working as a function of hot working conditions such as temperature, time, strain and strain rate, and chemical compositions of steels. An example of the calculation flow chart can be seen in Fig. 1.10.

When hot working is carried out at a temperature at which work-hardened austenite can recrystallise in a short period, the initial austenite microstructure of phase transformations during the following cooling process does not differ significantly from that of the reheated austenite despite the fact that the average grain diameter of austenite is finer in the former case than in the later case. In the case, therefore, phase transformation could be considered independently from the hot working except the effect of the initial austenite grain diameter, which can be taken into account as the difference in the nucleation site density. However, when a hot working is conducted at lower temperatures, partially recrystallised or unrecrystallised austenite microstructures is expected to dominate the microstructure before the temperature of the steel reaches the point at which the formation of ferrite can occur. It has been well established that finer microstructure can be obtained in the case than the cases with hot working at higher temperatures. Because the controlled rolling technique has been very important from industrial point of view, the effect of hot working at lower temperatures on phase transformation has been studied although most of this work is empirical.

Umemoto *et al.* [80] studied the formation of pearlite from work-hardened austenite and managed to model the effect of hot working on the pearlite formation. The effect of hot working consists of three factors when a steel was hot worked at a temperature where no recrystallisation was observed, which are; 1) an increase in the austenite grain surface area per unit volume due

to an elongation of austenite grains, 2) an increase in the nucleation rate per unit area of austenite grain surface, and 3) an formation of additional nucleation sites such as deformation bands and deformed twin boundaries. They considered the effect of the elongation of austenite grains from geometrical calculation; *i.e.* a spherical austenite grain becomes an ellipsoid after rolling. The effect of the increase in the nucleation rate per unit area and the increase in the additional nucleation sites (deformation bands) were assumed to be proportional, respectively, to the true strain and a square of the true strain based on previous experimental results [81,82]. Using experimentally obtained constants for these factors, they compared the effect of the three factors mentioned above on the acceleration of the formation of pearlite. When the austenite grain diameter is relatively small (less than 100 μm), the acceleration of the formation of pearlite is mainly due to the increase in the nucleation rate per unit area of austenite grain surface. When the initial austenite grain diameter is larger, on the other hand, the formation of additional nucleation site rather than austenite grain surface becomes dominant [81,82].

Numerical models which deal with the hot working and cooling process have been reported independently [83,84,85]. They adopted the Avrami type expressions for the kinetics of the formation of ferrite, pearlite and bainite, and independently obtained coefficients in the expression by a least square fitting to the experimental data. Once one can calculate the microstructure such as volume fraction, strength and diameter of each phases, mechanical properties can then be predictable through an empirical relations between microstructure and the mechanical properties. The relationship between microstructure and mechanical properties in multi-phase steels are, however, less understood. Even for a dual phase structure, a full stress-strain curve (S-S curve) is not reproducible from S-S curves of each phases. Empirically observed relations which have been checked to have good correlations to experiment have a form as follows.

$$Y = f\{V_i, H_i, d_i\} \tag{1.26}$$

where Y is a mechanical property and V_i, H_i and d_i are respectively volume fraction, hardness and diameter of i-th phase. It is rather well known that the strength of a ferritic steel can be expressed by the form, namely;

$$\sigma = \sigma_0 + \sum\{a_i V_i H_i\} + b d_\alpha^{-1/2} \tag{1.27}$$

where σ is either tensile or yield strength, d_α average ferrite grain diameter, and σ_0, a_i and b are constants to be determined from experiments.

Esaka *et al.* [83] have extended the idea to ductilities of steels without any justification, and succeeded in expressing the mechanical properties of hot worked steels with various kind of microstructure including ferrite, acicular ferrite, pearlite, bainite and martensite from chemical content of the steel, hot working conditions and cooling conditions.

Although all of the models are not physically based, it must be emphasised that the accumulated knowledge of recrystallisation and phase transformation in steels is now at a stage of being applied to predict the ultimate microstructure obtained by heat treatment and thermo-mechanical treatment. The work has not, however, been extended to processes including reverse transformation which may become important either when the initial microstructure plays an important role for the development of the final microstructure or when full or partial reverse transformation is introduced during the process.

1.10 SUMMARY

It appears that in practice, austenite grows by a reconstructive transformation mechanism because diffusion rates are significant at the elevated temperatures where the reaction normally occurs. The exception to this is iron based shape memory alloys, and cases involving remarkably large heating rates.

The reconstructive growth process may involve a variety of conditions at the transformation front, including paraequilibrium, local equilibrium and a variety of intermediate states. Which of these operates in practice is a challenging subject for research.

There is very little known about the nucleation mechanism of austenite, apart from some general data on the types of nucleation sites as a function of the starting microstructure. However, a first approximation in the derivation of overall transformation kinetics might be to ignore nucleation on the grounds that it is likely to be rapid at high temperatures. There are interesting features of the overall transformation kinetics; both the driving force and diffusivities increase with superheat, making austenite formation distinct from the usual C-curve kinetics of classical TTT diagrams. In fact, the formation of austenite should always become easier as the degree of superheating is increased.

REFERENCES

1. R. A. Roberts and R. F. Mehl: *Trans. ASM*, 1943, **31, 613.**

2. G. R. Speich and A. Szirmae: *Trans. TMS-AIME*, 1969, **245, 1063.**

3. C. I. Garcia and A. J. DeArdo: *Metall. Trans.*, 1981, **12A, 521.**

4. U. R. Lenel and R. W. K. Honeycombe: *Metal Science*, 1984a **18, 201.**

5. X-L. Cai, A. J. Garratt-R and W. S. Owen: *Metall. Trans.*, 1985, **16A, 543.**

6. R. C. Sharma, G. R. Purdy and J. S.Kirkaldy: *Metall. Trans.*, 1979 **10A, 1129.**

7. R. R. Judd and H. W. Paxton: *TMS AIME*, 1968, **242, 206.**

8. M. Baeyertz: *Trans. ASM*, 1942, **30, 458.**

9. S. Matsuda and Y. Okamura: *Trans. ISIJ*, 1974a, **14, 363.**

10. N. C. Law and D. V. Edmonds: *Metall. Trans.*, 1980, **11A, 33.**

11. S. Kinoshita and T. Ueda: *Tetsu-to-Hagane*, 1973, **59, 55.**

12. M. R. Plichita and H. I. Aaronson: *Metall. Trans.*, 1974, **5, 2611.**

13. J-Y. Koo and G. Thomas: *Metall. Trans.*, 1977, **18A, 525.**

14. P. G. Winchell and M. Cohen: *Trans. ASM*, 1962, **55, 347.**

15. P. G. Winchell and M. Cohen: *Electron Microscopy and Strength of Crystals, Interscience, New York,* 1963, 995.

16. J-R. Yang: *Ph. D. Thesis, University of Cambridge* 1988.

17. C. M. Wayman: *Proceedings of ICOMAT 89.,* 1989.

18. H. Kessler and W. Pitsch: *Acta Metall,* 1965, **13, 871.**

19. D. Dunne and C. M. Wayman: *Metall. Trans.*, 1973a, **4, 137.**

20. D. Dunne and C. M. Wayman: *Metall. Trans.*, 1973b, **4, 147.**

21. C. M. Wayman: *"Phase Transformations", York Conference, Institute of Metals, London,* 1979, **1,** IV 1.

22. C. M. Wayman: *"Phase Transformations in Solids", ed. T. Tsakalakos, Materials Research Society, North Holland,* 1983, **21,** 657.

23. A. E. Nehrenberg: *Trans. AIME J. of Metals,* 1950, **188,** 162.

24. S. F. Dirnfeld, B. M. Korevaar and F. B. Spijker: *Metall. Trans.,* 1976, **15,** 1437.

25. A. Roosz, Z. Gacsi and E. G. Fuchs: *Acta Metall.,* 1983, **31,** 509.

26. G. R. Speich, V. A. Demarest and R. L. Miller: *Metall. Trans.,* 1981, **12,** 1419.

27. M. Nemoto: *Metall. Trans.,* 1977, **18A,** 431.

28. M. Hillert, K. Nilsson and L-E. Törndahl: *JISI,* 1971, **209,** 49.

29. J. W. Christian: *"The Theory of Transformations in Metals and Alloys",* Part 1, 2nd. ed., *Pergamon Press, Oxford,* 1988.

30. J-R. Yang and H. K. D. H. Bhadeshia: *"Welding Metallurgy of Structural Steels",* TMS-AIME, *Warrendale, Ohio,* ed. J. Y. Koo, 1987, 549.

31. J-R. Yang and H. K. D. H. Bhadeshia: *"Phase Transformations 87",* The Institute of Metals, *London,* ed. G. W. Lorimer, 1988, 203.

32. A. Hultgren: *Jernkontorets Ann.,* 1951, **135,** 403.

33. E. Rudberg: *Jernkontorets Ann.,* 1952, **136,** 91.

34. M. Hillert: *Jernkontorets Ann.,* 1952, **136,** 25.

35. M. Hillert: *Internal Report, Swedish Institute of Metals Research.* 1953.

36. J. S. Kirkaldy: *Canad. J. Phys.,* 1958, **36,** 907.

37. G. R. Purdy, D. H. Weichert and J. S. Kirkaldy: *Trans. Met. Soc. A. I. M. E.,* 1964, **230,** 1025.

38. H. I. Aaronson, H. A. Domian and G. M. Pound: *Trans. Met. Soc. A. I. M. E.,* 1966, **236,** 768.

39. D. E. Coates: *Metall. Trans.,* 1973, **4,** 2313.

40. H. K. D. H. Bhadeshia, L-E. Svensson and B. Gretoft: *Acta Metall.,* 1985, **33,** 1271.

41. J. W. Christian: *"The Theory of Transformations in Metals and Alloys",* Part 1, 2nd. ed., *Pergamon Press, Oxford,* 1988.

42. R. T. DeHoff and F. N. Rhines, eds.: *"Quantitative Microscopy", McGraw-Hill Book Company, New York.* 1968,

43. C. Zener: *J. App. Phys.,* 1949, **20,** 950.

44. C. A. Dubé: *Ph.D. Thesis, Carnegie Inst. of Tech.* 1948.

45. R. P. Smith: *J. Amer. Chem. Soc.,* 1946, **68,** 1163.

46. C. Wells, W. Batz and R. F. Mehl: *Trans. Met. Soc. A. I. M. E.,* 1950, **188,** 533.

47. R. H. Siller and R. B. McLellan: *Trans. Met. Soc. A. I. M. E.,* 1969, **245,** 697.

48. R. H. Siller and R. B. McLellan: *Metall. Trans.,* 1970, **1,** 985.

49. H. K. D. H. Bhadeshia: *Metal Science,* 1981, **15,** 477.

50. R. Trivedi and G. M. Pound: *J. Appl. Phys.,* 1967, **38,** 3569.

51. C. Atkinson: *Acta Metall.,* 1967, **15,** 1207.

52. V. D. Sadovskii: *C. E. Trans.,* 1956. 7648.

53. S. T. Kimmins and D. J. Gooch: *Metal Science* 1983, **17,** 519.

54. A. D. Roming and R. Salzbrenner: *"Solid-Solid Transformation '81",* ed. H. I. Aaronson, *AIME,* 1981, 849.

55. J. Ågren: *Mat. Sci. and Eng.,* 1982, **55,** 135.

56. Avrami, M.: *J. Chem. Phys.,* 1939, **7,** 1103.

57. A. Schrader and F. Wever: *Arch Eisenhuttenwesen,* 1952, **23,** 489.

58. S. J. Matas and R. F. Hehemann: *Trans. Met. Soc. A. I. M. E.,* 1961, **221,** 179.

59. H. K. D. H. Bhadeshia and A. R. Waugh: *Acta Metall.*, 1982, **30**, 775.

60. S. S. D'Yachenko and G. V. Fedorov: *Fiz. Metal. Metalloved.*, 1964, **18**, 73.

61. H. S. Fong and S. G. Glover: *Trans. JIM*, 1975, **16**, 115.

62. S. Hayami and T. Furukawa: *Proc. of "Microalloying '75", Union Carbide Corp., New York*, 1975, 56.

63. S. Hayami, T. Furukawa, H. Gondoh and H. Takechi: *"Formable HSLA and Dual Phase Steels", ed. A. T. Davenport, The Metall. Society of AIME*, 1979, 167.

64. I. Sawai, A. Ueda and E. Kamisaka: *Tetsu-to-Hagane*, 1985, S1292.

65. O. Matsumura, Y. Sakuma and H. Takechi: *Trans. ISIJ*, 1987, **27**, 570.

66. O. Matsumura, Y. Sakuma and H. Takechi: *Scripta Metall.*, 1987, **21**, 1301.

67. V. F. Zackay, E. R. Parker, D. Fahr and R. Busch: *Trans. ASM*, 1967, **60**, 252.

68. R. A. Grange: *Trans. ASM*, 1966, **59**, 26.

69. Cotterill, P. and Mould, P. R.: *"Recrystallization and grain growth in metals", Surrey University Press, London.* 1976.

70. H. K. D. H. Bhadeshia: *"Phase Transformation '87", G. W. Lorimer ed., Institute of Metals, London*, 1988, 309.

71. J. W. Christian and D. V. Edmonds: *"Phase transformation in Ferrous Alloys", A. R. Marder and J. I. Goldstein ed., The Metall. Soc. of AIME*, 1983, 293.

72. H. K. D. H. Bhadeshia: *Acta Metall.*, 1981, **29**, 1117.

73. S. J. Matas and R. F. Hehemann: *Trans. AIME*, 1961, **221**, 179.

74. H. K. D. H. Bhadeshia and J. W. Christian: *Metall. Trans. A*, 1990, **21A**, 767.

75. Z. Nishiyama: *"Some Old and New Views of the Nature of Martensites", Proc. of 1st. JIM Int. Symp. on New Aspects of Martensitic Transformation, Kobe, Japan*, 1976, 1.

76. Z. Nishiyama: *"Martensitic Transformation", ed. M. E. Fine*, 1978.

77. H. K. D. H. Bhadeshia: *"Diffusional Formation of Ferrite in Iron and its Alloys", Progress in Materials Science*, 1986, **29**, 321.

78. R. C. Reed and H. K. D. H. Bhadeshia: *Proc. Int. Conf. on "Trends in Welding Research"*, 1990.

79. C. M. Sellars: *Sheffield Int. Conf. on "Hot working and Processes"*, 1979, **7**, 3.

80. M. Umemoto, H. Ohtsuka and I. Tamura: *Trans. ISIJ*, 1983, **23**, 775.

81. I. Kozasu, C. Ouchi, T. Sampei and T. Okita: *Proc. of "Micro Alloying '75", Union Carbide Corp., New York*, 1975, 100.

82. K. Esaka, J. Wakita, M. Takahashi, O. Kawano and S. Harada: *Seitetsu-Kenkyu*, 1988, **321**, 92.

83. Y. Saito: *Tetsu-to-Hagane*, 1988, **74**, 609.

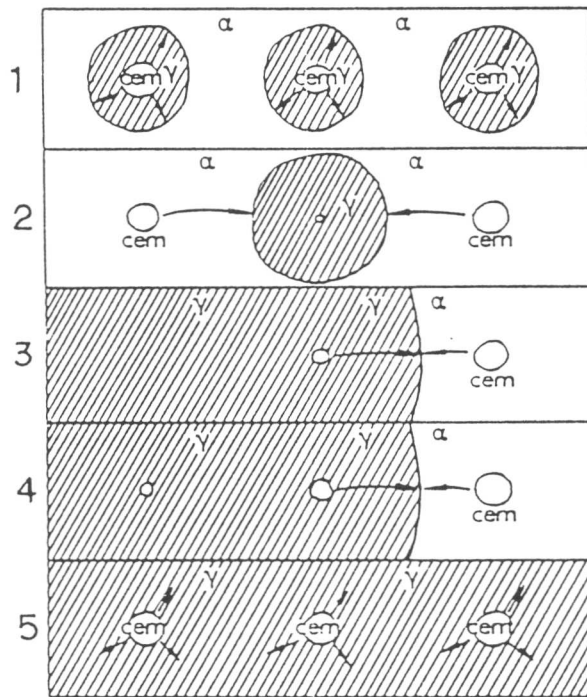84. M. Suehiro, K. Sato, Y. Tsukano, H. Yada, T. Senuma and Y. Matsumura: *Trans. ISIJ*, 1987, **27**, 438.

Fig. 1.1 Different mechanisms of dissolution of cementite during the formation of austenite from the mixture of ferrite and spheroidised carbide [28].
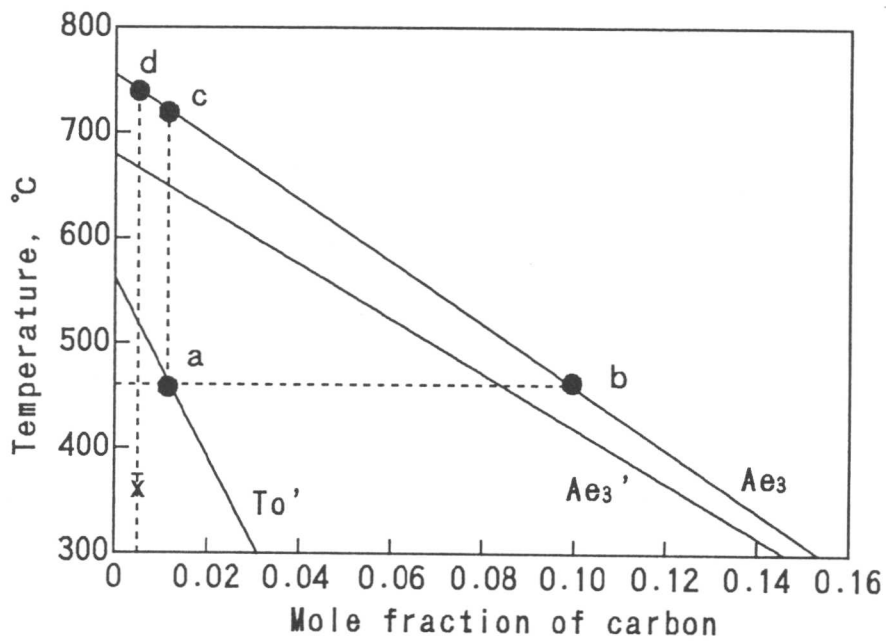

Fig. 1.2 Calculated phase diagram showing the Ae_3, Ae'_3 and T'_0 curves for a Fe-0.27Si-1.84Mn-2.48Ni-0.20Mo wt.% alloy.
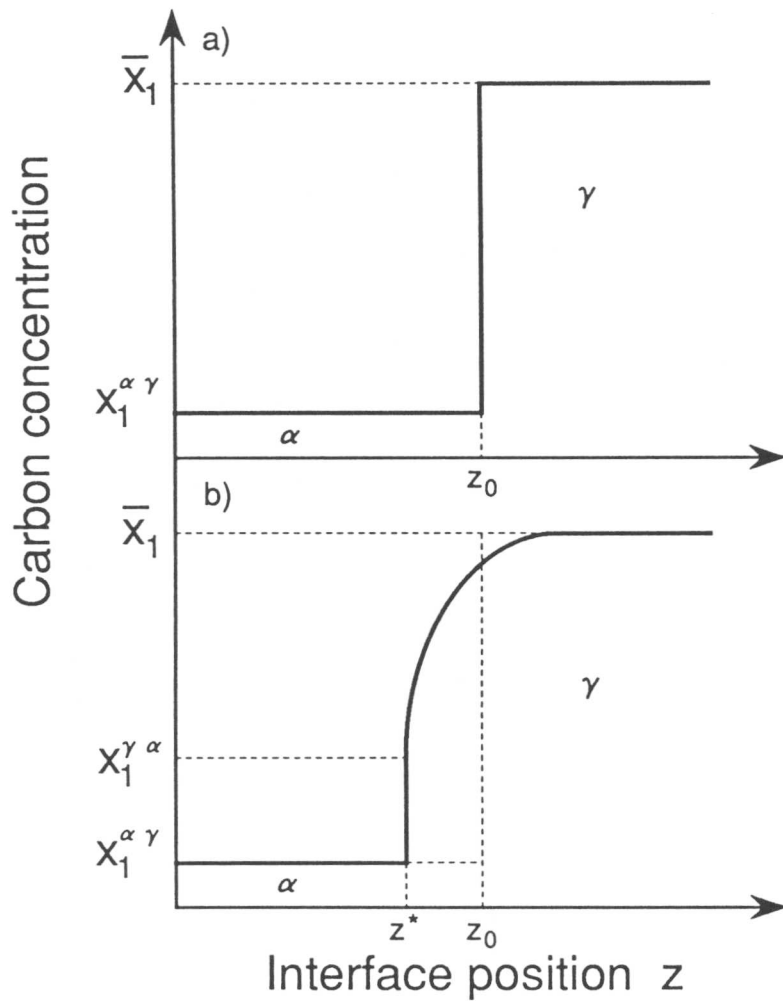
Fig. 1.3 Schematic illustration of the carbon concentration profile (a) before and (b) during reausteni-tisation. The interface position z^* is defined normal to the interface. $\overline{x_1}$ is the initial carbon concentration in austenite, $x_1^{\gamma\alpha}$ and $x_1^{\alpha\gamma}$ are carbon concentration in ferrite and austenite at the interface which are in equilibrium.
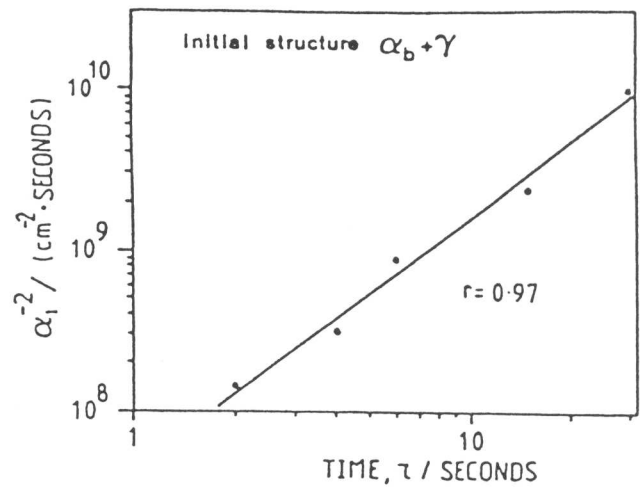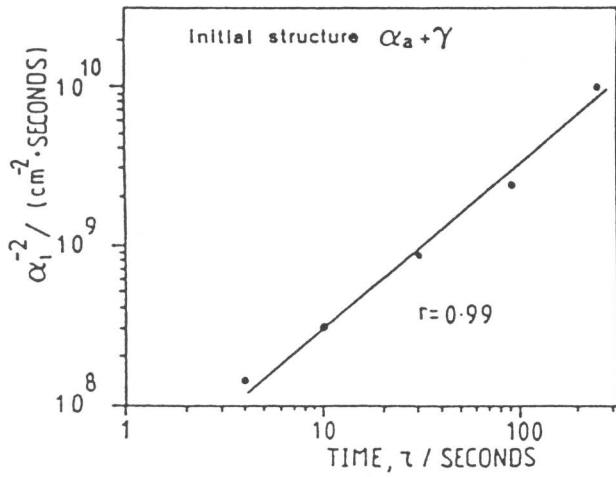
Fig. 1.4 Relation between the time taken for the smallest detectable amount of reaustenitisation and α_1^{-2} (a) in the case of an acicular ferrite + austenite initial microstructure and (b) a bainite + austenite initial microstructure.
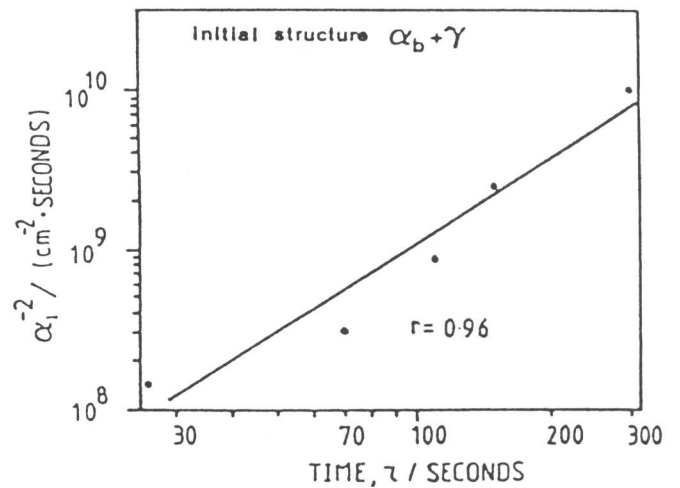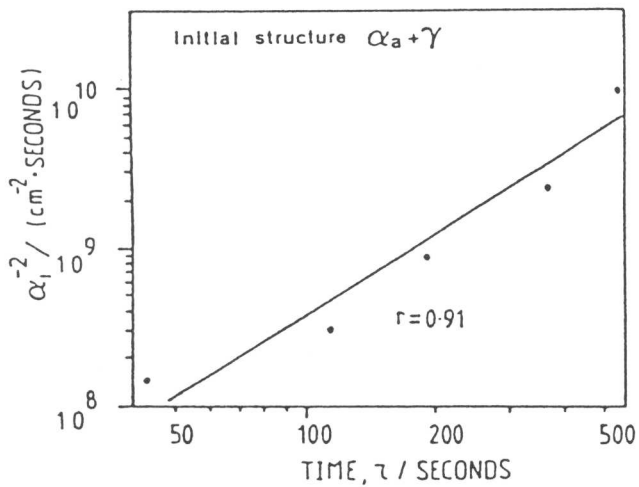
Fig. 1.5 Relation between the time taken for 0.05 volume fraction of reaustenitisation and α_1^{-2} (a) in the case of an acicular ferrite + austenite initial microstructure and (b) a bainite + austenite initial microstructure.

31

a)

b)

A α
γ
α
γ
α

Bainitic ferrite + austenite

A α
γ
α
γ
α

Bainitic ferrite + austenite

B

θ

θ

Ferrite + cementite (tempered)

C

γ
α
γ
α

Growth of austenite layers

C

θ

γ

Nucleation and growth
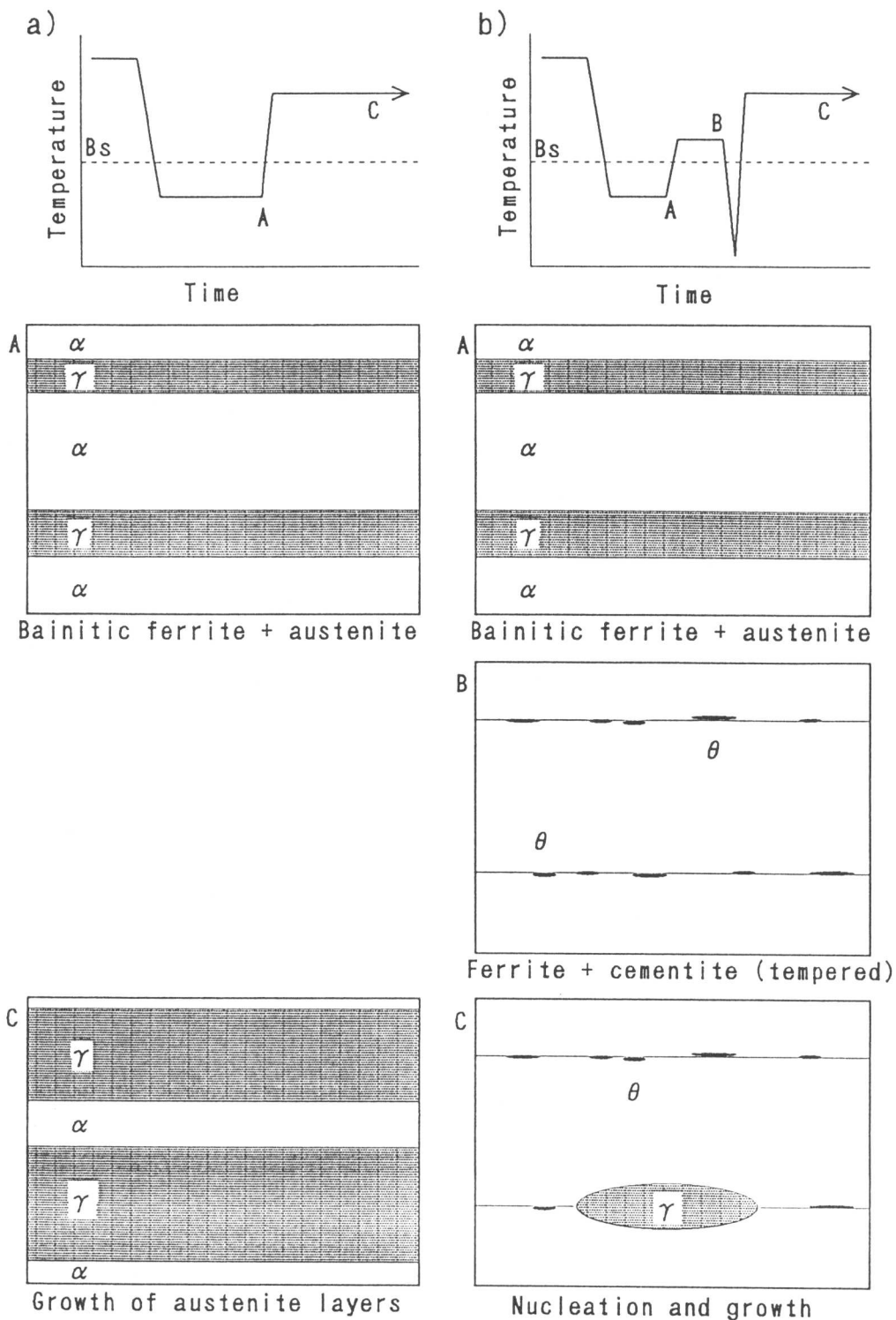
Fig. 1.6 Illustrations of the formation of austenite from two different starting microstructures. (a) A mixture of bainitic ferrite and austenite is generated by isothermal transformation at a temperature below B_S. When this microstructure is reheated to an elevated temperature, the growth of preexisting austenite occurs. (b) The mixture of bainitic ferrite and austenite is tempered at an intermediate temperature to remove any austenite left untransformed after the bainite transformation. Reheating to an elevated temperature then requires the austenite to nucleate before it can grow.
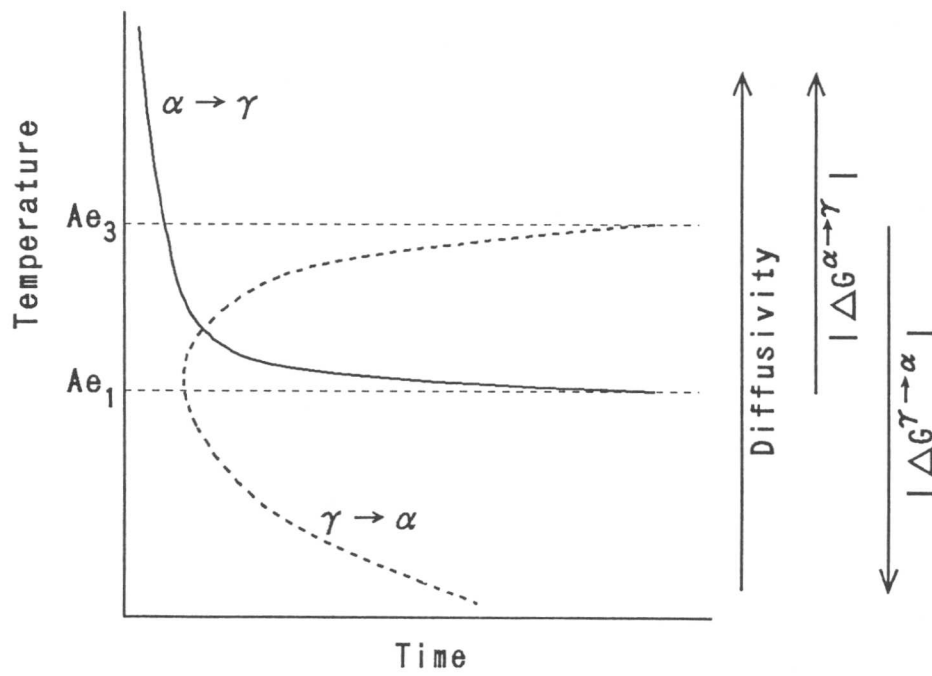
Fig. 1.7 TTT curves for $\gamma \to \alpha$ and $\alpha \to \gamma$.
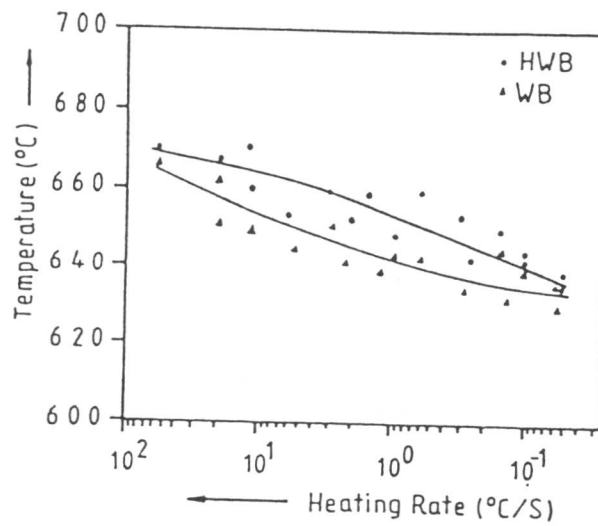
Fig. 1.8 Reaustenitisation-start temperature during continuous heating in the steel in Table 1.1 (HWB) with an as deposited weld microstructure.

Table 1.1 Time taken for the smallest detectable amount of reaustenitisation from a mixture of acicular ferrite and austenite.

C	Si	Mn	Ni	Mo	Cr	V	Ti	Nb
0.060	0.27	1.84	2.48	0.20	0.05	0.01	0.02	0.01

Temperature, °C	Time, seconds
680	250
690	90
700	30
710	10
720	5
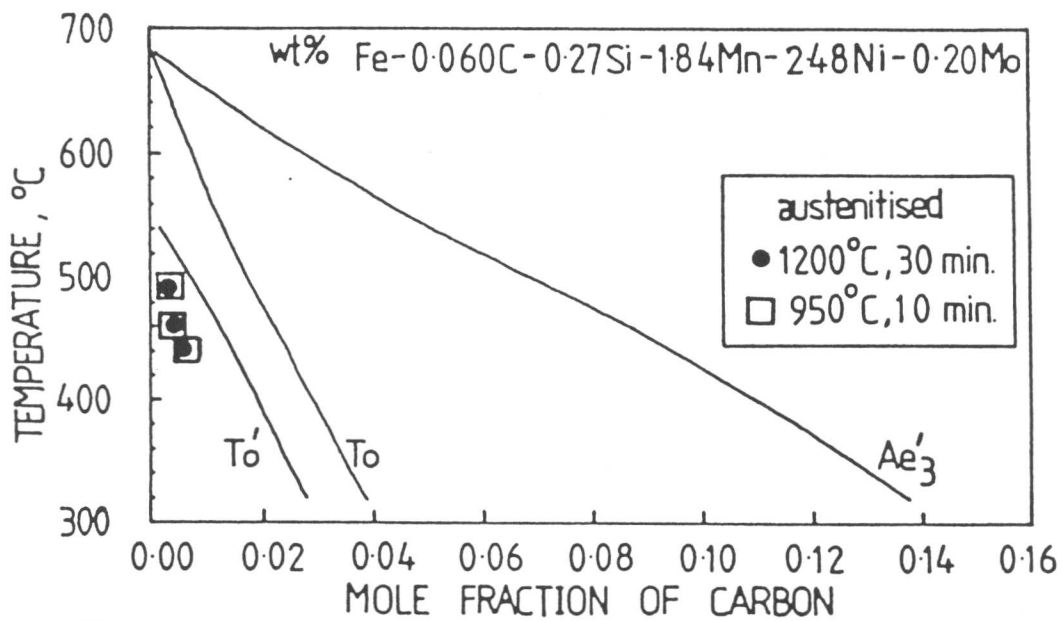
Fig. 1.9 Calculated phase diagram of the steel in Table 1.1

Table 1.2 Key characteristics of transformations in steels [70]. α' is martensite, α_{lb} is lower bainite, α_{ub} is upper bainite, α_a is acicular ferrite, α_W is Widmanstätten ferrite, α if allotriomorphic ferrite, P is pearlite, and X denotes substitutional alloying elements. Comments on each characteristics are ($=$) consistent, ($\neq$) inconsistent and ($\otimes$) only sometimes consistent with transformation.

| Comment	α'	α_{lb}	α_{ub}	α_a	α_w	α	α_i	P
Nucleation and growth reaction	$=$	$=$	$=$	$=$	$=$	$=$	$=$	$=$
Plate morphology	$=$	$=$	$=$	$=$	$=$	$\neq$	$\neq$	$\neq$
IPS shape change with shear component	$=$	$=$	$=$	$=$	$=$	$\neq$	$\neq$	$\neq$
Diffusionless nucleation	$=$	$\neq$	$\neq$	$\neq$	$\neq$	$\neq$	$\neq$	$\neq$
Only carbon diffuses during nucleation	$\neq$	$=$	$=$	$=$	$=$	$\neq$	$\neq$	$\neq$
Reconstructive diffusion during nucleation	$\neq$	$\neq$	$\neq$	$\neq$	$\neq$	$=$	$=$	$=$
Often nucleates intragranularly on defects	$=$	$\neq$	$\neq$	$=$	$\neq$	$\neq$	$=$	$\neq$
Diffusionless growth	$=$	$=$	$=$	$=$	$\neq$	$\neq$	$\neq$	$\neq$
Reconstructive diffusion during growth	$\neq$	$\neq$	$\neq$	$\neq$	$\neq$	$=$	$=$	$=$
Atomic correspondence (all atoms) during growth	$=$	$=$	$=$	$=$	$\neq$	$\neq$	$\neq$	$\neq$
Atomic correspondence, during growth, for atoms in substitutional sites	$=$	$=$	$=$	$=$	$=$	$\neq$	$\neq$	$\neq$
Bulk redistribution of X atoms during growth	$\neq$	$\neq$	$\neq$	$\neq$	$\neq$	$\otimes$	$\otimes$	$\otimes$
Local equilibrium at interface during growth	$\neq$	$\neq$	$\neq$	$\neq$	$\neq$	$\otimes$	$\otimes$	$\otimes$
Local paraequilibrium at interface during growth	$\neq$	$\neq$	$\neq$	$\neq$	$=$	$\otimes$	$\otimes$	$\neq$
Diffusion of carbon during transformation	$\neq$	$\neq$	$\neq$	$\neq$	$=$	$=$	$=$	$=$
Carbon diffusion-controlled growth	$\neq$	$\neq$	$\neq$	$\neq$	$=$	$\otimes$	$\otimes$	$\otimes$
Cooperative growth of ferrite and cementite	$\neq$	$\neq$	$\neq$	$\neq$	$\neq$	$\neq$	$\neq$	$=$
High dislocation density	$=$	$=$	$=$	$=$	$\otimes$	$\neq$	$\neq$	$\neq$
Incomplete-reaction phenomenon	$\neq$	$=$	$=$	$=$	$\neq$	$\neq$	$\neq$	$\neq$
Necessarily has a glissile interface	$=$	$=$	$=$	$=$	$=$	$\neq$	$\neq$	$\neq$
Always has an orientation within the Bain region	$=$	$=$	$=$	$=$	$=$	$\neq$	$\neq$	$\neq$
Grows across austenite grain boundaries	$\neq$	$\neq$	$\neq$	$\neq$	$\neq$	$=$	$=$	$=$
High interface mobility at low temperatures	$=$	$=$	$=$	$=$	$=$	$\neq$	$\neq$	$\neq$
Displacive transformation mechanism	$=$	$=$	$=$	$=$	$=$	$\neq$	$\neq$	$\neq$
Reconstructive transformation mechanism	$\neq$	$\neq$	$\neq$	$\neq$	$\neq$	$=$	$=$	$=$

Reheating condition

Conditions of RM →

Initial grain size of FM

Conditions of FM →

Calculation of coefficients
$\left\{\begin{array}{l}\text{recovery} : k, \tau_k \\ \text{static rex: } S, \tau_s \\ \text{dynamic rex: } m, \varepsilon_s, \varepsilon_c \\ \text{grain growth: } K, A\end{array}\right.$

Recrystallization

$1-f_D$ $1-f_D-f_s$ f_N

f_c f_s f_N

(dynamic rex.)   (static rex.)   (non rex.)

$\left[\begin{array}{l}f_D=1-\exp\{-(\dfrac{\varepsilon-\varepsilon_c}{\varepsilon_s-\varepsilon})^m\} \\ d_D=DZ^{-0.155}\end{array}\right.$ $\left[\begin{array}{l}f_s=1-\exp\{-(\dfrac{t}{\tau_s})^s\} \\ d_s=C\cdot do^n\ \varepsilon^{-\ell}\end{array}\right.$ $\left[\begin{array}{l}f_N=1-f_D-f_s \\ d_N=do\cdot\exp(-\varepsilon/4)\end{array}\right.$

(grain growth)   (grain growth)

Calculation of average grain size
Calculation of residual strain
$\left[\begin{array}{l}\bar{d}=1\left/\left(\dfrac{f_D}{d_{dyn.}^2}+\dfrac{f_s}{d_{st.}^2}+\dfrac{f_N}{d_{non.}^2}\right)^{1/2}\right. \\ \triangle\varepsilon=(f_D\cdot\varepsilon_c+f_N\cdot\varepsilon)\cdot\exp\{-(\dfrac{t}{\tau_k})^k\}\end{array}\right.$
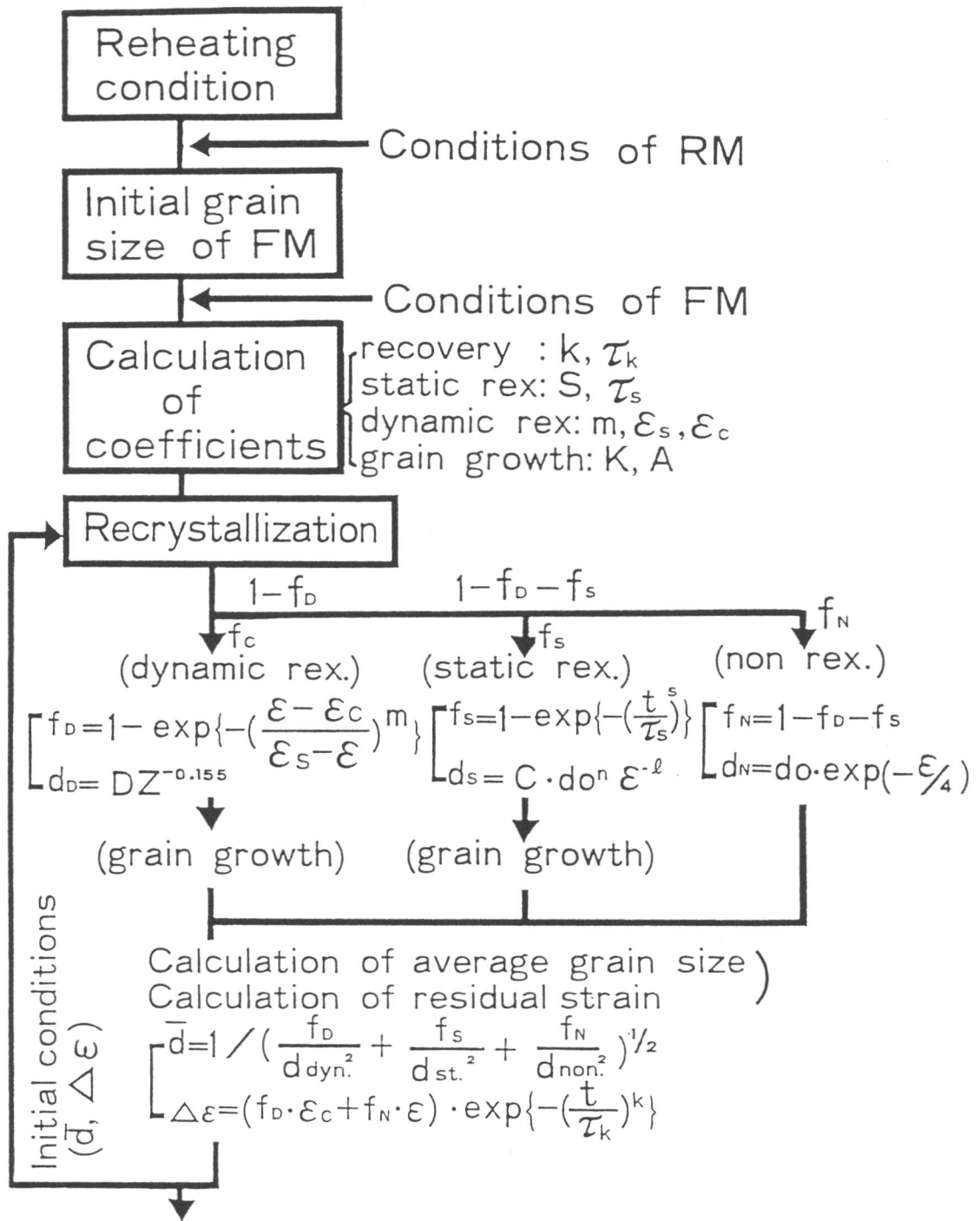
Initial conditions $(\bar{d}, \triangle\varepsilon)$

Fig. 1.10 Flow chart for the calculation of microstructural development of austenite during and after hot working.

A MODEL FOR THE TRANSITION FROM UPPER TO LOWER BAINITE

2.1 INTRODUCTION

Bainite can be regarded as a non-lamellar mixture of ferrite and carbides, but within this broad description, it is possible to identify two classical morphologies, traditionally called upper and lower bainite (see for example, [1-4]). Lower bainite is obtained usually by transformation at lower temperatures, although both phases can sometimes be found in the same microstructure. Both upper and lower bainite tend to form as aggregates (sheaves) of small platelets or laths (sub-units) of ferrite. The essential difference between upper and lower bainite is with respect to the carbide precipitates. In upper bainite, the bainitic ferrite is free of precipitation, any carbides growing from the regions of carbon-enriched residual austenite which are trapped between the sub-units of ferrite. By contrast, lower bainitic ferrite contains a fine dispersion of plate-like carbides (*e.g.*, ϵ-carbide or cementite) within the bainitic ferrite plates.

The transition between upper and lower bainite is generally believed to occur over a narrow range of temperatures. There are circumstances where both phases can form simultaneously during isothermal transformation near the transition temperature [5]. The first clear indication of the mechanism of the transition emerged from the work of Matas and Hehemann [6], whose experiments on several steels (containing 0.38-1.0 wt.% C) indicated a narrow transition temperature range centered around 350 °C, irrespective of steel composition. They suggested that the difference between upper and lower bainite is related to the kinetics of carbide precipitation from ferrite. In their model, both upper and lower bainite form with a supersaturation of carbon, but with the former, almost all of the excess carbon is rejected into the residual austenite; with lower bainite, carbon precipitates rapidly in the supersaturated ferrite, so that the amount that diffuses into the residual austenite is reduced. The relatively constant transition temperature was explained by suggesting that ϵ-carbide will, for some reason, not precipitate from ferrite at temperatures above $\sim 350\,°C$. The ϵ-carbide was envisaged as a precursor to the formation of cementite.

While the Matas and Hehemann model is intuitively reasonable, their belief that the transition temperature, L_S, is constant for all steels is not consistent with other experimental results [5,7-10]. The transition temperature can be as high as 500 °C and is found to vary with the carbon concentration. The model also requires the carbide in lower bainite to be ϵ-carbide, which might then convert to cementite on further tempering. Later work has shown that it is possible to obtain lower bainite containing the appropriate cementite particles, without any ϵ-carbide as a precursor [11]. Franetovic *et al.* [12,13] have also reported lower bainite containing η-carbide (Fe_2C) in a high-silicon cast iron and there is no reason to suppose that precipitation temperature and behaviour of η-carbide should be similar to that of ϵ-carbide. It is also difficult to explain why ϵ-carbide should not precipitate from ferrite at temperatures above 350 °C.

Pickering [5] found that L_S rises initially and then decreases to $\sim 350\,°C$, becoming independent of the carbon concentration beyond ~ 0.8 wt.%C. His explanation of the transition is essentially the same as that of Matas and Hehemann [6], that the transition to lower bainite occurs when the rate of carbon diffusion from ferrite is slow, so that the carbides have an opportunity to precipitate. The model does not, however, account for any changes in the kinetics of

carbide precipitation as a function of carbon concentration. Similar results have been obtained for more heavily alloyed steels, where the peak in the experimental transition curve is found to shift to lower carbon concentrations [8]. Pickering suggested that for high carbon steels (where the transition was claimed to be insensitive to carbon concentration), the cementite precipitates directly from the austenite, as its carbon concentration x_1^γ exceeds the concentration $x_1^{\gamma\theta}$ which is given by the extrapolated $\gamma/(\gamma + Fe_3C)$ phase boundary; this does not explain the formation of carbides within the bainitic ferrite.

To summarise, a plausible model for the transition from upper to lower bainite could be constructed from the assumption that there is no fundamental difference in transformation mechanism between these two forms of bainite, if the bainitic ferrite is, when it forms, super-saturated with carbon. The excess carbon may partition eventually into the residual austenite or precipitate from the ferrite in the form of carbides. If the latter process is dominant, then lower bainite is obtained. Upper bainite is obtained only when the carbon partitions relatively rapidly into the residual austenite, before the carbides have an opportunity of precipitate. This essentially amounts to the Matas and Hehemann model [6], but without the constraint that the transition temperature is limited to a narrow temperature range around 350 °C. The model is illustrated schematically in Fig. 2.1. The purpose of this chapter is to test as far as is possible, the quantitative form of the hypothesis summarised above, and to assess any predictions in the context of available experimental data. The work utilises recent results on the theory for the time required to decarburise supersaturated ferrite; cementite precipitation kinetics are treated approximately using information from martensite tempering data.

2.2 TIME REQUIRED TO DECARBURISE SUPERSATURATED FERRITE

If it is assumed that the diffusivity of carbon in ferrite is very high when compared with that in austenite, and that local paraequilibrium is established during the partitioning of carbon between the austenite and ferrite, then the time t_d required to decarburise a supersaturated bainitic ferrite plate of thickness w is given by [4]:

$$t_d = \frac{a^2 \pi (\overline{x}_1 - x_1^{\alpha\gamma})^2}{16 \overline{D} (x_1^{\gamma\alpha} - \overline{x}_1)} \tag{2.1}$$

where $\overline{x}_1$ is the average carbon concentration in the steel as a whole. $x_1^{\alpha\gamma}$ and $x_1^{\gamma\alpha}$ are the carbon concentrations in ferrite and austenite respectively, when the two phases are in paraequilibrium. The diffusivity D of carbon in austenite is very sensitive to the carbon concentration [14-17]. Hence, when dealing with concentration gradients, it is necessary to consider instead a weighted average diffusivity [18], $\overline{D}$, given by

$$\overline{D} = \int\limits_{\overline{x}_1}^{x_1^{\gamma\alpha}} \frac{D \, dx}{(x_1^{\gamma\alpha} - \overline{x}_1)}. \tag{2.2}$$

This procedure is valid strictly for the situation where the concentration profile does not change with time, but is recognised to be a good approximation for non-steady state conditions, as exist during the partitioning of carbon from the supersaturated ferrite. In the present work, D was calculated as discussed in [19].

The calculated kinetics of partitioning are illustrated for three steels with different carbon concentrations with calculated [20,21] martensite-start (M_S) and bainite-start (B_S) tempera-tures, in Fig. 2.2. The calculations assume that $a = 0.2 \, \mu m$, and this is the approximation used

throughout this work. For each steel, the time t_d goes through a minimum as a function of transformation temperature. The minimum arises because the diffusion coefficient of carbon decreases with temperature (leading to an increase in t_d), while at the same time, the amount of carbon that the austenite can tolerate, $x_1^{\gamma\alpha}$, rises with falling temperature; $x_1^{\gamma\alpha}$ was calculated as in [22]. The decarburisation time also increases as the average carbon concentration of the steel rises; given that an increase in carbon concentration should accelerate the precipitation of carbides in the ferrite, it should lead to an increase in L_S, as reported by Pickering [5] and Llopis and Parker [8] for low carbon concentrations.

2.3 TIME FOR THE PRECIPITATION OF CEMENTITE

Information on the kinetics of the cementite precipitation from supersaturated ferrite is not available in sufficient depth to enable the first principles calculation of the volume fraction of cementite as a function of time, temperature and chemical composition. An attempt is made here to derive the overall kinetics of cementite precipitation using published data [23,24] on hardness changes observed during the initial stages of isothermal tempering of martensite.

2.3.1 An Empirical Method

When martensite contains an excess concentration of carbon in solid solution, the carbon will tend to precipitate in the form of carbides during tempering. Prolonged annealing can also lead to recovery, recrystallisation and the coarsening of cementite precipitates. For the present purposes, it is consequently important to focus on the early stages tempering, which should represent solely, the effects of precipitation from supersaturated ferrite.

Speich [23] reported that the change in hardness of martensite in plain carbon steels after an hour of tempering at temperatures above $320\,^{\circ}$C, includes significant contributions from recovery, recrystallisation and coarsening of cementite particles (Fig. 2.3). Hence, the data representing hardness changes during tempering below $320\,^{\circ}$C were utilised to obtain a function which expresses the change in the volume fraction of cementite precipitation as a function of time and temperature. An Avrami type equation [25] was used for the purpose:

$$\xi\{t\} = 1 - \exp\{-k_A t^n\} \tag{2.3}$$

where $\xi\{t\}$ is the volume fraction of cementite normalised by its equilibrium volume fraction at the reaction temperature, t is the time, and k_A and n are rate constants determined from the experimental data. It is assumed that $\xi\{t\}$ is related at any time t to the hardness of the martensite, $H\{t\}$ as follows,

$$\xi\{t\} = \frac{H_0 - H\{t\}}{H_0 - H_F}. \tag{2.4}$$

H_0 is the hardness of the as-quenched virgin martensite, H_F is its hardness when all the carbon has precipitated, but before any significant recovery, recrystallisation or coarsening has occurred. Implicit in this relation is the assumption that the amount of carbon precipitated is linearly related to the change in hardness during the early stages of tempering.

Using the values of hardness for plain carbon martensite tempered for 1 hour at 320° C, reported by Speich [23], H_F was expressed empirically as a function of the initial hardness and average carbon concentration $\overline{x}_1^{\alpha}$ (mole fraction), as follows:

$$H_F = H_0(1 - 1.731\,\overline{x}_1^{\alpha\,0.34}) \tag{2.5}$$

39

This equation is valid for plain carbon steels containing less than 0.4 wt.% carbon ($\bar{x}_1^\alpha < 0.0186$), the value of H_F becoming constant thereafter. The hardness H_0 of plain carbon martensite before tempering can be also be deduced from the data reported by Speich [23]:

$$H_0 = 1267\,\bar{x}_1^{\alpha\ 0.9} + 240 \tag{2.6}$$

where the hardness of martensite in pure iron is 240 Hv [24]. This equation reflects empirically, the hardness of virgin martensite in plain carbon steels as a function of carbon in solid solution; there is however, evidence to suggest that the effect of carbon tends to saturate, so that H_0 should not exceed a maximum value of about 800 Hv irrespective of carbon concentration [26]. Consequently, the maximum value of H_0 permitted in the present analysis is taken to be 800 Hv.

2.3.2 An Independent Calculation

There are more elaborate theories available for the change in the strength of low-carbon martensite due to the precipitation of cementite, so that the difference $(H_0 - H_F)$ can be evaluated independently from the empirical approach discussed above. The change can be expressed in terms of the decrease in solid solution strengthening as carbon is absorbed during the growth of cementite, and an increase in strength as the cementite particles precipitation harden the martensite. Thus, the yield strength of martensite, σ_y, is expressed as a combination of the intrinsic yield strength, the effect of the dislocation cell structure, and precipitation hardening by cementite [27]:

$$\sigma_y = \sigma_0 + k_\epsilon \epsilon_1^{-1} + k_p l_p^{-1} \ , \ \text{MPa} \tag{2.7}$$

where σ_0 is the intrinsic strength of martensite, ϵ_1 is the average transverse thickness of the cell structure, and l_p is the average distance between a particle and its two or three nearest neighbours. The latter is given by $l_p = 1.18r(\frac{2\pi}{3V_\theta})$, where r is the average particle radius measured in m, and V_θ is volume fraction of the particles. k_ϵ and k_p are constants, with $k_p = 0.519V_\theta^{1/2}$, MPa m^{-1}. The value of k_ϵ is not relevant for the present work since it is the *changes* in hardness prior to recovery that are of interest.

The intrinsic strength of martensite can be factorised into the solid solution strengthening effect of carbon, σ_c, and the residual strength σ_0':

$$\sigma_0 = \sigma_0' + \sigma_c \tag{2.8}$$

From the work of Speich and Warlimont [28],

$$\sigma_c = 8 \times 10^3 \bar{x}_1^{\ 1/2} \ , \ \text{MPa.} \tag{2.9}$$

Since the hardness $H\{t\}$ relates to the yield strength as follows [28],

$$\sigma_y = 2.59H\{t\} - 78.20 \ , \ \text{MPa,}$$

the change in hardness of martensite due to cementite precipitation can be written

$$-\Delta HV = -0.3865\Delta\sigma_y \tag{2.10}$$

40

where $\Delta\sigma_y$ is the change in yield strength (measured in units of MPa), due to cementite precipitation in the early stages of tempering. Equations to calculate the number of cementite particles and its volume fraction will be given in a later section. The calculated hardness changes of martensite in 0.1, 0.2 and 0.4 wt.% carbon steel, in terms of the decrease in solute carbon and the increase in cementite precipitates, are shown in Fig. 2.4. Although the relation between hardness and the amount of the precipitation (thus the decrease in solute carbon) is not linear, the predicted changes in hardness are remarkably consistent with those indicated by Speich [23] (Fig. 2.5).

2.3.3 Parameters for the Avrami Equation

The tempering data can now be used to obtain the parameters of the Avrami relation given in equation 2.3. For the case where martensite is tempered for one hour, the rate constant k can be calculated using the relationship:

$$k_A = -\ln\{1 - \xi\{1\,\mathrm{hr}\}\} \quad (\mathrm{hours})^{-n} \tag{2.11}$$

where $\xi\{1\,\mathrm{hr}\} = (H_0 - H\{1\,\mathrm{hr}\})/(H_0 - H_F)$. The calculated k values for different tempering temperatures for data from Speich [23] could then be used to express k as a function of temperature:

$$k_A = k_{A0}\exp\{-\frac{Q}{RT}\} \tag{2.12}$$

giving $k_{A0} = 4.07 \times 10^4 \bar{x}_1^{0.635}$ hours^{-n}, $Q = 33598$ J mol^{-1}. R is the universal gas constant.

The time exponent n in the Avrami equation can be obtained by plotting $\log\ln\{1/(1 - \xi\{t\})\}$ against $\log\{t\}$. The data reported by Speich [23], which show the changes in hardness during the tempering of martensite in 0.18 and 0.097 wt.% carbon steels, were used and n was found to be 0.62. It follows that

$$\xi\{t\} = 1 - \exp\{-4.07 \times 10^4 \bar{x}_1^{0.635} t^{0.62}\}. \tag{2.13}$$

This equation can be used to estimate the time necessary to obtain a specified degree of transformation as a function of temperature and the carbon concentration of the steel.

The formation of cementite is known to be exceptionally slow in steels containing large amounts of silicon. Bhadeshia and Edmonds [26] measured the change in hardness of martensite by tempering in Fe-0.43C-2.0Si-3.0Mn (wt.%) system at different temperatures. Although their data are not extensive enough to reveal all the constants needed in the Avrami equation, k_{A0} was, for that steel, evaluated by assuming that Q and n are the same as for the plain carbon steels considered previously:

$$k_A = 550\exp\{-33589/RT\}\,, \quad \mathrm{hours}^{-n}. \tag{2.14}$$

2.3.4 Calibration for t_θ

The method used to estimate the upper to lower bainite transition temperature, involves a comparison of the time t_d required to decarburise a plate of ferrite, with the time interval t_θ necessary to obtain a "detectable" amount of cementite precipitation in the ferrite. If $t_d \ll t_\theta$ then it may be assumed that upper bainite is obtained, and vice versa (Fig. 2.6). Of course, t_θ is a function of ξ, and instead of choosing a detectable value of ξ in an arbitrary way, the value was fixed by comparison with experimental data on L_S. The Fe-0.43C-2.0Si-3.0Mn (wt.%)

41

system is ideal for this purpose since the B_S, M_S and L_S temperatures are well characterised [20]. Calculated values of t_d and t_θ (the latter for $\xi = 0.01$, 0.02 and 0.05) are plotted, together with B_S, M_S and L_S temperatures in Fig. 2.7. As expected, the t_d curves exhibit minima, while t_θ was, over the temperature range of interest, found to increase as the reaction temperature decreased. For temperatures below the calculated B_S temperatures, where it is possible for bainite to grow, any intersections between the t_d and t_θ curves are of relevance to the location of the transition temperatures. L_S is defined as the highest temperature at which $t_\theta < t_d$. On comparing the t_θ and t_d curves for the Fe-0.43C-2.0Si-3.0Mn wt.% alloy, it was found that the experimental L_S of around 320 °C could be predicted fairly accurately is the "detectable" volume fraction of cementite is set as $\xi = 0.01$. Consequently, for all subsequent calculations, the L_S temperature is defined by the point where $t_\theta\{\xi = 0.01\} < t_d$.

The reason why it is necessary to consider only a very small amount of precipitation (1%) to explain the onset of lower bainite may be that the relation between the hardness and the amount of carbon atom used up for the precipitation is not linear (Fig. 2.3); thus, the calculated 1% precipitation may in reality correspond to a larger degree of precipitation. The time for decarburisation may also be increased by soft-impingement of the diffusion fields of neighbouring sub-units of bainitic ferrite in a sheaf of bainite. The partitioning of carbon may also be retarded by the precipitation of carbides within the ferrite, since the net flux towards the austenite/ferrite interface would be reduced.

The calculated t_d and t_θ for plain carbon steels with carbon concentrations of 0.1, 0.2, 0.3, 0.4 and 0.5 wt.% are shown in Fig. 2.8 as a function of reaction temperature. As expected, the higher the carbon concentration the longer is the time required to decarburise the plates. On the other hand, the driving force for cementite precipitation increases with carbon supersaturation, so that t_θ is found to decrease with $\overline{x}_1$. The calculated M_S and B_S temperatures are also plotted in the Fig. 2.4.

The calculated L_S temperatures are plotted against the carbon content of steels in Fig. 2.9. According to the calculations, lower bainite should not be observed in plain carbon steels with carbon concentrations less than 0.32 wt.%. Furthermore, only lower bainite (*i.e.* no upper bainite) should be found in steels with carbon content more than 0.4 wt.%. Steels containing between 0.32 and 0.4 wt.% of carbon should exhibit both both upper and lower bainite, depending on the reaction temperatures. Finally, it should be noted that at low temperatures where t_θ and t_d both become very large, the times required for precipitation or redistribution of carbon exceed that to complete transformation, consistent with the fact that untempered martensite can be obtained at temperatures near M_S, with the degree of autotempering of the martensite decreasing as M_S is reduced.

2.4 DISCUSSION

2.4.1 Comparison between calculated and observed L_S temperatures

The general behaviour indicated by the calculations for plain carbon steels, is found to be that observed experimentally. Some very recent interesting work by Oka and Okamoto [10] (Fig. 2.10) proves that there is no upper bainite in plain carbon steels with more than 0.8 wt.% of carbon; the only bainite observed was classical lower bainite at all temperatures above the M_S temperature. This is consistent with the present calculations.

Ohmori and Honeycombe [29], in a study of plain carbon steels, showed that during isothermal transformation above the M_S temperature, only upper bainite could be obtained in samples

containing less than 0.4C wt.% (Fig. 2.11). This is consistent with the calculations presented earlier, although their observation that upper bainite can be obtained in steels with a carbon concentration up to ~ 0.85C wt.% is not consistent with the theory, nor with the data reported by Oka and Okamoto [10]. Their diagram additionally indicates a constant L_S temperature of around $350\,^{\circ}$C, which is also inconsistent with the theory and with the Oka and Okamoto results. These particular discrepancies and contradictory experimental results cannot be explained at this moment, and further research is called for. Although their published diagram [29] is based on experimental data, the actual data points are not presented and it is therefore difficult to assess the validity of some of the boundaries illustrated.

The change in the transition temperature from upper to lower bainite has also been reported by Pickering [5] and Llopis and Parker [8] for a variety of alloyed steels. Their observations (Fig. 2.12) show that the L_S temperature increases with carbon concentration in lower carbon region and then goes through a maximum value as the carbon concentration is increased further. After the maximum, L_S is found to stabilise at a constant value. This tendency is quite consistent with the present calculations, although the reported constant value of L_S at higher carbon concentrations is not. A possible explanation arises from the fact that the calculated B_S temperatures [21] for the alloys concerned turns out to be in very good agreement with L_S temperatures reported by Pickering [5] for carbon concentrations above 0.4 wt.%. The implication is that the high carbon data become consistent with the work of Oka and Okamoto, if it is assumed that no upper bainite is obtained in those steels, the so called transition temperature corresponding to the B_S temperature. Furthermore, if we focus on Pickering's data (excluding some of the other points he plotted from unspecified published research), then the L_S plateau shown in Fig. 2.12 may simply be an artifact of plotting since a smooth sloping curve can be fitted through all the high carbon data.

According to the present calculations, only lower bainite is expected in steels with more than 0.32 wt.% of bulk carbon content. However, the calculations are for ferrite plates whose carbon concentration is initially identical to that of bulk alloy, since the model assumes that bainite growth is diffusionless, with carbon redistribution occurring after the growth event. As a consequence of the redistribution, which is expected to be substantial when t_d is smaller than t_θ, there is an enrichment in the carbon concentration of residual austenite as the bainite transformation proceeds. Consequently, any bainite which forms from enriched austenite will itself have a higher than bulk concentration of carbon. This leads to the possibility of the transformation beginning with the growth of upper bainite, but with the enriched austenite then decomposing to lower bainite at the later stages of transformation. There is then a real possibility of obtaining a mixture of upper and lower bainite in steels containing less than 0.32 wt.% carbon, especially if carbide precipitation from the austenite is relatively sluggish, and therefore does not act to relieve any carbon enrichment in the austenite.

The maximum carbon concentration that can be tolerated in residual austenite before the bainite reaction ceases is expressed approximately by the T_0' curve [3,4,22]. Therefore if the carbon concentration in residual austenite at the T_0' curve (*i.e.* $x_{T_0'}$) is greater than 0.32 wt.%, lower bainite can be expected to form during the later stages of reaction. However, the formation of cementite from the residual austenite also becomes possible if $x_{T_0'} > x_1^{\gamma\theta}$, where $x_1^{\gamma\theta}$ is a point on the $\gamma/(\gamma + \theta)$ phase boundary (calculated as in [30,31]), since the austenite will then be supersaturated with respect to the cementite. The fact that a curve showing the carbon concentration in austenite which is in equilibrium with cementite in plain carbon steels

crosses the T_0' curve at 0.4 wt.% of carbon concentration (560 °C), leads to the identification of three regimes for bainite on the Fe–C phase diagram (Fig. 2.13). In steels with more than 0.4 wt.% of the initial bulk carbon content (region B), lower bainite is to be expected from the earliest stages of transformation. For steels whose composition lies in region A, lower bainite is expected to be absent during isothermal transformation at all temperatures above M_S, and this behaviour is valid for any stage of transformation since the austenite cannot be supersaturated with cementite as far as regime A is concerned. The behaviour in the region marked C should be more complex. The residual austenite for these steels (region C) may at some stage of transformation contain enough carbon to precipitate cementite. If the kinetics of cementite precipitation from austenite are rapid, then lower bainite may not be obtained in steels with an average carbon concentration less than 0.32 wt.%, but otherwise, a mixed microstructure of upper and lower bainite might arise.

2.4.2 Comparison with the tempering of martensite

In the present model for the upper to lower bainite transition, the microstructure of lower bainite in effect arises due to the "autotempering" of supersaturated plates of bainitic ferrite. The lower bainite should consequently exhibit many of the characteristics of tempered martensite. When high-carbon martensite is tempered, the first carbide to form is usually a transition carbide such as ϵ−carbide, which is replaced eventually by the thermodynamically more stable cementite. Similarly, when lower bainite forms in high carbon steels, ϵ−carbide forms first, and transforms subsequently into cementite during prolonged holding at the isothermal transformation temperature [6].

The chances of obtaining ϵ−carbide (instead of cementite) in lower bainite increase as the transformation temperature is reduced for the same steel (see Table II, [6]). As the transformation temperature is reduced, and the time required to decarburise a supersaturated plate of bainite increases, a high carbon concentration can persist in the ferritic matrix for a time period long enough to allow the formation of ϵ−carbide, which does not form if the carbon concentration is less than about 0.25wt.%, [32]. This effect also explains the result that a medium carbon Fe-0.43C-3Mn-2Si wt.% steel transforms to lower bainite containing cementite particles [33], although when quenched to martensite, gives ϵ-carbide on tempering [26] Some of the carbon is in the former case, lost to the austenite by diffusion, thereby preventing the formation of ϵ−carbide.

The ideas discussed here can in principle be predicted using the present model. Fig. 2.14 illustrates calculation for a Fe-0.6C wt% alloy, for transformation temperatures where only lower bainite is obtained. The continuous curves represent the time required for the carbon concentration in the bainitic ferrite to drop to a specified level, and the vertical line represents the time t_C taken for this concentration to reach 0.25 wt.%, the level below which ϵ−carbide should not form [32]. The bainitic ferrite is assumed to have an initial carbon concentration of 0.6 wt.%. The curves are calculated using equation 2.1, but by replacing $x_1^{\alpha\gamma}$ with x_1^{α}, which represents the amount of carbon in the bainitic ferrite at any instant of time, with $x_1^{\alpha\gamma} \leq x_1^{\alpha} \leq \overline{x}_1$. The dashed curves are schematic, and represent the time (t_ϵ) required to precipitate a detectable volume fraction of ϵ−carbide; there is as yet no theory which can predict these curves, nor are there suitable experimental data which can be used to estimate the curves empirically. Although the curves are schematic, their form is based on the corresponding curves for cementite, as used in the earlier analysis. If $t_\epsilon < t_C$, then the lower bainite should contain ϵ−carbide rather than cementite, and vice versa. It is evident that it is possible to envisage circumstances

where a lowering of the transformation temperature can lead to a transition from lower bainite containing cementite, to lower bainite containing ϵ−carbide. A similar diagram could be used to rationalise the observation that in a medium carbon steel, the lower bainite is found to contain cementite, while the tempering of martensite in the same steel leads to ϵ−carbide formation.

2.4.3 Other Differences between Upper and Lower Bainite

The fact that lower bainite forms at a higher undercooling below B_S when compared with upper bainite has other implications. Sub-unit growth during the bainite transformation ceases when the interface is blocked by plastic accommodation induced defects [34]. For a given defect density, lower-bainite sub-units should be longer than those of upper bainite, since the driving force for transformation increases with undercooling. At lower transformation temperatures the matrix is able to support higher strains without plastic deformation so that the defect density *in the matrix* itself would be lower. Step quenching experiments in which an alloy is first partially transformed to lower bainite and then up-quenched into the upper bainite transformation range are consistent with this since they show that the growth of lower bainite ceases following the up-quench [35]. This also appears to be the case when specimens partially transformed to lower bainite experience an increase in temperature within the lower bainite transformation range [36].

2.5 CONCLUSIONS

A model, based on an idea by Matas and Hehemann, has been developed to enable the estimation of the temperature at which the upper bainite reaction gives way to the formation of lower bainite. The model involves a comparison between the times required to decarburise supersaturated ferrite plates with the time required to precipitate cementite within the plates. If the decarburisation process dominates, upper bainite is predicted whereas relatively rapid carbide precipitation within the ferrite leads to the formation of lower bainite.

Some of the predictions of the theory are in agreement with reported experimental data. Consistent with the results of Ohmori and Honeycombe, it is found that lower bainite cannot form in plain carbon steels containing less than ~ 0.3 wt.% carbon. Upper bainite is predicted to be absent in plain carbon steels containing more than 0.4 wt.% carbon; this is in agreement with the results of Oka and Okamoto, although contradictory results have been reported by Ohmori and Honeycombe, who were able to obtain both upper and lower bainite in high carbon Fe-C alloys. The maximum in the curve of transition temperature versus carbon concentration, reported by Pickering and Llopis & Parker is also consistent with the theory.

To summarise, more experimental work is needed to verify some of the detailed predictions of the model, and to resolve some of the discrepancies between experimental data reported in the literature. More work is also needed from a theoretical point of view, to develop fully the kinetics of cementite precipitation from supersaturated ferrite, and to couple the processes of cementite precipitation with the simultaneous redistribution of carbon into the residual austenite. In the mean time, the current model seems to provide a rational basis for the transition temperature.

APPENDIX
- Further Modelling of the Kinetics of Cementite Precipitation in Ferrite -

In this section, we consider alternative models for the kinetics of cementite precipitation in ferrite, with the aim of examining the possibility of more fundamental theory compared with the rather empirical martensite tempering data based methods used earlier. Such models could be useful in taking account of alloying element effects on the kinetics of cementite precipitation from supersaturated ferrite, and hence permit an easy extension of the transition work to alloy steels.

It is assumed here that the growth of cementite platelets is controlled by the diffusion of carbon in the supersaturated ferrite, and that it involves the one-dimensional advance of interfaces parallel to the habit plane of each cementite particle. A one-dimensional parabolic thickening rate constant (α_1) for this process can be calculated using the following equation [25]:

$$\frac{\overline{x}_1 - x_1^{\alpha\theta}}{x_1^{\theta\alpha} - x_1^{\alpha\theta}} = \sqrt{\frac{\pi}{4D_{11}^\alpha}} \alpha_1 \exp\left\{\frac{\alpha_1^2}{4D_{11}^\alpha}\right\}\left[1 - \text{erf}\left\{\frac{\alpha_1}{\sqrt{4D_{11}^\alpha}}\right\}\right] \tag{2.15}$$

where $x_1^{\theta\alpha}$ and $x_1^{\alpha\theta}$ are the equilibrium carbon concentrations in cementite and ferrite respectively, at the interface between cementite and ferrite, and D_{11}^α is the diffusion coefficient of carbon in ferrite [37].

The lengthening rate of the "allotriomorphs" of cementite is correspondingly given by a rate constant with is taken to be $\alpha_3 \simeq 3 \times \alpha_1$; this seems somewhat arbitrary, but gives a similar aspect ratio to that obtained for allotriomorphic ferrite [38]. The volume of a cementite plate, v_θ, is then given approximately by:

$$\begin{aligned} v_\theta &= (\alpha_1 t^{1/2})(\alpha_3 t^{1/2})(\alpha_3 t^{1/2}) \\ &= 9\alpha_1^3 t^{3/2} \end{aligned} \tag{2.16}$$

Venugopalan and Kirkaldy [39] reported the average grain size of cementite r_0 before the onset of the Ostwald ripening, as a function of tempering temperature of martensite.

$$r_0^3 = (2.26 - 6.4 \times 10^{-3}T + 4.6 \times 10^{-6}T^2)V_\theta \times 10^{-3} \tag{2.17}$$

where V_θ is the volume fraction of cementite, T is the tempering temperature in K, and r_0 is the average grain size of the cementite particles in μm. The number of cementite particles per unit volume (N_θ) can therefore be described by

$$N_\theta = \frac{V_\theta^e}{\frac{4}{3}\pi r_0^3} \tag{2.18}$$

where V_θ^e is the maximum volume fraction of cementite obtained at the temperature concerned, and can be calculated from the initial carbon concentration in the ferrite $\overline{x}_1$ (mole fraction) by $V_\theta^e \simeq 1.0065\frac{4\overline{x}_1}{1-4\overline{x}_1}$, taking account of the difference in ferrite and cementite densities in respect of the unit cell.

Assuming now, that there is initially a number V_θ of sites available for the growth of cementite, and that no new sites are formed subsequently, the precipitation process can be described simply in terms of the growth of cementite. Thus, using the extended volume method

46

of Avrami to take account of impingement between growing particles, the volume fraction of cementite normalised by the maximum volume fraction V_θ^e is expressed by

$$\xi = 1 - \exp\{-\xi_e\} \tag{2.19}$$

where ξ_e is an extended fraction, given by

$$\xi_e = 9V_\theta \alpha_1^3 t^{3/2}/V_\theta^e \tag{2.20}$$

For cases where it may not be justified to start the transformation from a fixed number of growth centres, it is necessary to have some kind of a nucleation rate function. If it is assumed that nucleation always occurs heterogeneously on dislocations, the nucleation rate per unit volume, I, on dislocations can be written as follows [25,40]:

$$I = (N^v)^{1/3} \rho \frac{RT}{h} \exp\left\{ -\frac{\Delta G_1^\theta + \Delta G_2^\theta}{RT} \right\} \tag{2.21}$$

where h is the Planck constant, N^v the number of atoms per unit volume which are on dislocation lines, ΔG_1^θ the activation free energy of nucleus formation on a dislocation, and ΔG_2^θ the activation energy for the transfer of atoms across the nucleus/matrix interface. ρ is the dislocation density.

Therefore the volume fraction of cementite normalised by the maximum volume fraction of cementite is in these circumstances expressed by:

$$\xi\{t\} = 1 - \exp\{-\xi_e\}$$

with

$$\xi_e = \frac{1}{V_\theta^e} I(9\alpha_1^3) \int_0^t (t - \tau)^{3/2} d\tau = \frac{18}{5} \frac{I\alpha_1^3}{V_\theta^e} t^{5/2} \tag{2.22}$$

where τ is the incubation period.

The activation energy for nucleation, ΔG_1^θ, should decrease as the inverse square of the driving force for nucleation of cementite from ferrite:

$$\Delta G_1^\theta \propto (\Delta G^{\theta\alpha})^{-2}, \tag{2.23}$$

so that ΔG_1^θ should tend to become small relative to ΔG_2^θ at high carbon supersaturations. In such circumstances, ΔG_1^θ may be ignored and the nucleation rate may be expected to decrease with undercooling. This is consistent with the data from the empirical analysis discussed earlier, where it is found that t_θ increases monotonically with a decrease in temperature, rather than showing a C-curve behaviour. Consequently, it seems justified to ignore the ΔG_1^θ term for the present analysis, where it is assumed that $\Delta G_1^\theta \ll \Delta G_2^\theta$. The value of ΔG_2^θ is not known, but the activation energy for the self diffusion in ferromagnetic iron is 240 kJ mol^{-1} [41], and since the α/θ interface has a relatively high energy, ΔG_1^θ is expected to be less than 240 kJ mol^{-1}. In order to "derive" its value, an attempt was made to match the values of N_θ obtained as discussed earlier, with the number of particles per unit volume, to be expected using the nucleation function in equation 2.21.

Assuming that the dislocations all lie along $< 111 >$ directions, $N^v = \rho/[\frac{\sqrt{3}}{2} \times 2.8664 \times 10^{-10}]$. The dislocation density in bainitic ferrite formed at different temperatures has been

47

measured by Smith [42] and Fondekar *et al.* [43]. Because these data are not on their own adequate to obtain an expression of the dislocation density as a function of the reaction temperature, similar data for martensite, reported by Kehoe and Kelly [44], were included in the analysis, to yield the following empirical relation for the dislocation density in ferrite (Fig. 2.15):

$$\log \rho = 9.28480 + \frac{6880.73}{T} - \frac{1780360}{T^2} \tag{2.24}$$

where ρ is the dislocation density in m^{-2}, and T is the reaction temperature in K. For the martensite, the transformation temperature was taken to be the M_S temperature. Although dislocation densities of martensite measured by Norström [45] are also plotted in the figure, those data were not used in deriving the above expression because of uncertainties in the method used to assess the thickness of the thin foil samples used. The curve plotted in Fig. 2.14 does not therefore take account of these data.

To find the most appropriate value of ΔG_2^θ, the number of particles per unit volume N_θ at the completion of precipitation was calculated as follows:

$$N_\theta = \int\limits_0^\infty I[1 - \xi\{t\}]\, dt \tag{2.25}$$

and Fig. 2.16 shows that a reasonable fit with the empirical data of Venugopalan and Kirkaldy [39] could be obtained by setting $\Delta G_2^\theta = 190$ kJ mol^{-1}. This was the value used in all subsequent calculations.

Another possibility of the calculation of the volume fraction of cementite is based on the theory of diffusion-controlled growth of plate shaped particles [46]. The edgewise growth of a precipitate plate from a matrix which is initially at a uniform solute concentration $\bar{x}_1$, can be obtained from following equation.

$$\Omega_0 = \sqrt{\pi p}\, e^p\, \text{erfc}\, \sqrt{p}\left[1 + \frac{v_E}{v_C}\Omega_0 S_1 p + \frac{r_C}{r_\phi}\Omega_0 S_2 p\right] \tag{2.26}$$

with

$$p = \frac{v_E r_\phi}{2 D_{11}^\alpha}$$

$$r_C = \frac{x_1^{\alpha\theta}\Gamma_D}{x_1^{\alpha\theta} - \bar{x}_1}$$

$$v_C = \mu_0(x_1^{\alpha\theta} - \bar{x}_1)$$

$$\Omega_0 = \frac{x_1^{\alpha\gamma} - \bar{x}_1}{x_1^{\alpha\gamma} - x_1^{\theta\alpha}}$$

where v_C is the velocity of a flat interface which is controlled by interface kinetics only, r_ϕ is the radius of curvature at the advancing tip of the plate, r_C is the critical radius for growth at which the concentration difference in the matrix vanishes in absence of the interface kinetics, and v_E is the edgewise growth rate of the plate. The functions S_1 and S_2 have been presented graphically in [46]. The terms $x_1^{\alpha\theta}, x_1^{\theta\alpha}$ are the carbon concentrations at the interface in ferrite and in cementite, Γ_D is the capillarity constant, given by

$$\Gamma_D = \frac{\sigma_{\alpha\theta}\overline{V}}{(x_1^{\alpha\theta} - \bar{x}_1)RT}$$

where $\sigma_{\alpha\theta}$ is the α/θ interfacial free energy per unit area, $\overline{V}$ is the molar volume of cementite, and D_{11}^{α} is the diffusivity of carbon in ferrite.

If a disc shape is assumed for a cementite plate, whose height and radius are respectively c_{θ} and r, the volume v_{θ} per cementite plate is

$$v_{\theta} = \pi r^2 c_{\theta} = \frac{\pi}{\beta} r^3 = \frac{\pi}{\beta}(V t)^3 \tag{2.27}$$

where β is an aspect ratio of cementite plates. Therefore, using the extended volume method of Avrami, the volume fraction of cementite normalised by the maximum volume fraction of cementite V_{θ}^{e} is found to be

$$\xi\{t\} = 1 - \exp\{-\xi_e\} \tag{2.28}$$

where

$$\xi_e = N_{\theta}\frac{\pi}{\beta}(V t)^3/V_{\theta}^{e} \tag{2.29}$$

and N_{θ} is the number of cementite particles per unit volume.

In Fig. 2.17, the calculated times required for $\xi = 0.05$ of cementite precipitation in a Fe-0.4C wt.% in terms of only the parabolic growth, the combination of nucleation and parabolic growth, and plate growth are compared with the calculated times using the empirical methods used earlier. The calculations used $\sigma_{\alpha\theta} = 0.7\text{J m}^{-2}$ [47], $x_1^{\theta\alpha} = 0.25$, and the equilibrium carbon concentration in ferrite as presented in [48]. The aspect ratio β in the plate growth model is assumed either to be three, which is to consistent to the parabolic growth model, or fifteen, which was as observed approximately in Fe-0.43C-2.0Si-3.0Mn wt.% .

It is evident that the models based on parabolic thickening both indicate much faster transformation kinetics relative to the empirical results, although the result from the nucleation and growth model approaches the empirical result at lower temperatures. The plate growth model, while differing in an absolute sense from the empirical data, gives a similar trend as a function of temperature. It could in principle be adapted (for example, by reducing the number of nucleation sites available per unit length of dislocation line) to better fit the experimental data. An appropriate selection of the nucleation function for cementite precipitation, and the use of the plate growth theory could, therefore, give closure with the empirical result and allow the estimation of the lower bainite transformation temperature in alloyed steels as well as in plain carbon steels. However, it is essential to investigate the early stages of the cementite precipitation in detail before any further modifications to the theory for the transition. Note also that the models ignore any precursor reactions such as the precipitation of $\epsilon-$carbide, which may influence the overall kinetics of cementite formation.

REFERENCES

1. R. F. Mehl: *"Hardenability of Alloy Steels"*, A. S. M., Ohio, 1939, 1.

2. R. F. Hehemann: *"Phase Transformations"*, 1970, 397.

3. J. W. Christian and D. V. Edmonds: *"Phase Transformations in Ferrous Alloys"*, eds. A. R. Marder and J. I. Goldstein, A. S. M., Ohio, 1984, 293.

4. H. K. D. H. Bhadeshia: *"Phase Transformations '87"*, ed. G. W. Lorimer, Institute of Metals, London, 1988, 309.

5. F. B. Pickering: *Transformation and Hardenability in Steels*, Climax Molybdenum Co, Ann Arbor, 1967, 109.

6. S. J. Matas and R. F. Hehemann: *Trans. AIME,* 1961, **221,** 179.

7. S. Matsuda: *Tetsu-to-Hagane,* 1970, **56,** 1428.

8. A. M. Llopis, referred to in E. R. Parker: *Metall. Trans.,* 1977, **8A,** 1025.

9. H. K. D. H. Bhadeshia: *Acta Metall.,* 1980, **28,** 1103.

10. M. Oka and H. Okamoto: *Proc. Int. Conf. Martensitic Transformations '86, The Japan Institute of Metals,* 1986, 271.

11. H. K. D. H. Bhadeshia and D. V. Edmonds: *Metal Science,* 1979, **13,** 325.

12. V. Franetovic, A. K. Sachdev and E. F. Ryntz: *Metallography,* 1987, **20,** 15.

13. V. Franetovic, M. M. Shec and E. F. Ryntz: *Materials Science and Engineering,* 1987, **96,** 231.

14. R. P. Smith: *Acta Metall.,* 1953, **1,** 578.

15. C. Wells, W. Batz and R. F. Mehl: *Trans. Met. Soc. A. I. M. E.,* 1950, **188,** 533.

16. R. H. Siller and R. B. McLellan: *Trans. Met. Soc. A. I. M. E.,* 1969, **245,** 697.

17. R. H. Siller and R. B. McLellan: *Metall. Trans.,* 1970, **1,** 985.

18. R. Trivedi and G. M. Pound: *J. Appl. Phys.,* 1967, **38,** 3569.

19. H. K. D. H. Bhadeshia: *Metal Science,* 1981, **15,** 477.

20. H. K. D. H. Bhadeshia and D. V. Edmonds: *Acta Metall.,* 1980, **28,** 1265.

21. H. K. D. H. Bhadeshia: *Metal Science,* 1981, **15,** 178.

22. H. K. D. H. Bhadeshia: *Acta Metall.,* 1981, **29,** 1117.

23. G. R. Speich: *Trans. AIME,* 1969, **245,** 2553.

24. W. C. Leslie: *McGraw-Hill, Inc, New York, USA.,* 1981.

25. J. W. Christian: *"The Theory of Transformations in Metals and Alloys", 2nd edition, Part 1, Pergamon Press, Oxford,* 1975.

26. H. K. D. H. Bhadeshia and D. V. Edmonds: *Metal Science,* 1983, **17,** 411.

27. J. Daigne, M. Guttmann, and J. P. Naylor: *Materials Science and Engineering,* 1982, **56,** 1.

28. G. R. Speich and H. Warlimont: *JISI, April,* 1968, 385.

29. Y. Ohmori and R. W. K. Honeycombe: *Trans. ISIJ,* 1971, **11,** 1160.

30. C. Zener: *Trans. AIME,* 1969, **169,** 513.

31. W. A. West: *Trans. AIME,* 1969, **169,** 535.

32. C. S. Roberts, B. L. Averbach and M. Cohen: *Trans. A. S. M.,* 1957, **45,** 576.

33. H. K. D. H. Bhadeshia and D. V. Edmonds: *Metal Science,* 1979, **13,** 325.

34. H. K. D. H. Bhadeshia and D. V. Edmonds: *Metall. Trans. A,* 1979, **10A,** 895.

35. R. H. Goodenow and R. F. Hehemann: *Trans. AIME,* 1965, **233,** 1777.

36. J. S. White and W. Owen: *J. I. S. I.,* 1961, **197,** 241.

37. R. B. McLellan, M. L. Rudee and T. Ishibachi: *Trans. Met. Soc. A. I. M. E.,* 1965, **233,** 1938.

38. J. R. Bradley and H. I. Aaronson: *Metall. Trans. A,* 1977, **8A,** 317.

39. D. Venugopalan and J. S. Kirkaldy: *Hardenability Concept with Applications to Steel, ed D. V. Doane and J. S. Kirkaldy,* 1978, 249.

40. J. W. Cahn: *Acta Metall.,* 1956, **4,** 572.

41. J. Fridberg, L. -E. Törndahl and M. Hillert: *Jernkont. Ann.,* 1969, **153,** 263.

42. G. M. Smith: *Ph. D. Thesis, University of Cambridge,* 1984.

43. M. K. Fondekar, A. M. Rao and A. K. Mallik: *Metall. Trans.,* 1970, **1,** 885.

44. M. Kehoe and P. W. Kelly: *Scripta Metall.,* 1970, **4,** 473.

45. L. -A. Norström: *Scandinavian Journal of Metall.,* 1976, **5,** 159.

46. R. Trivedi: *Metall. Trans.,* 1970, **1,** 921.

47. J. J. Kramer, G. M. Pound and R. F. Mehl: *Acta Metall.,* 1958, **6,** 763.
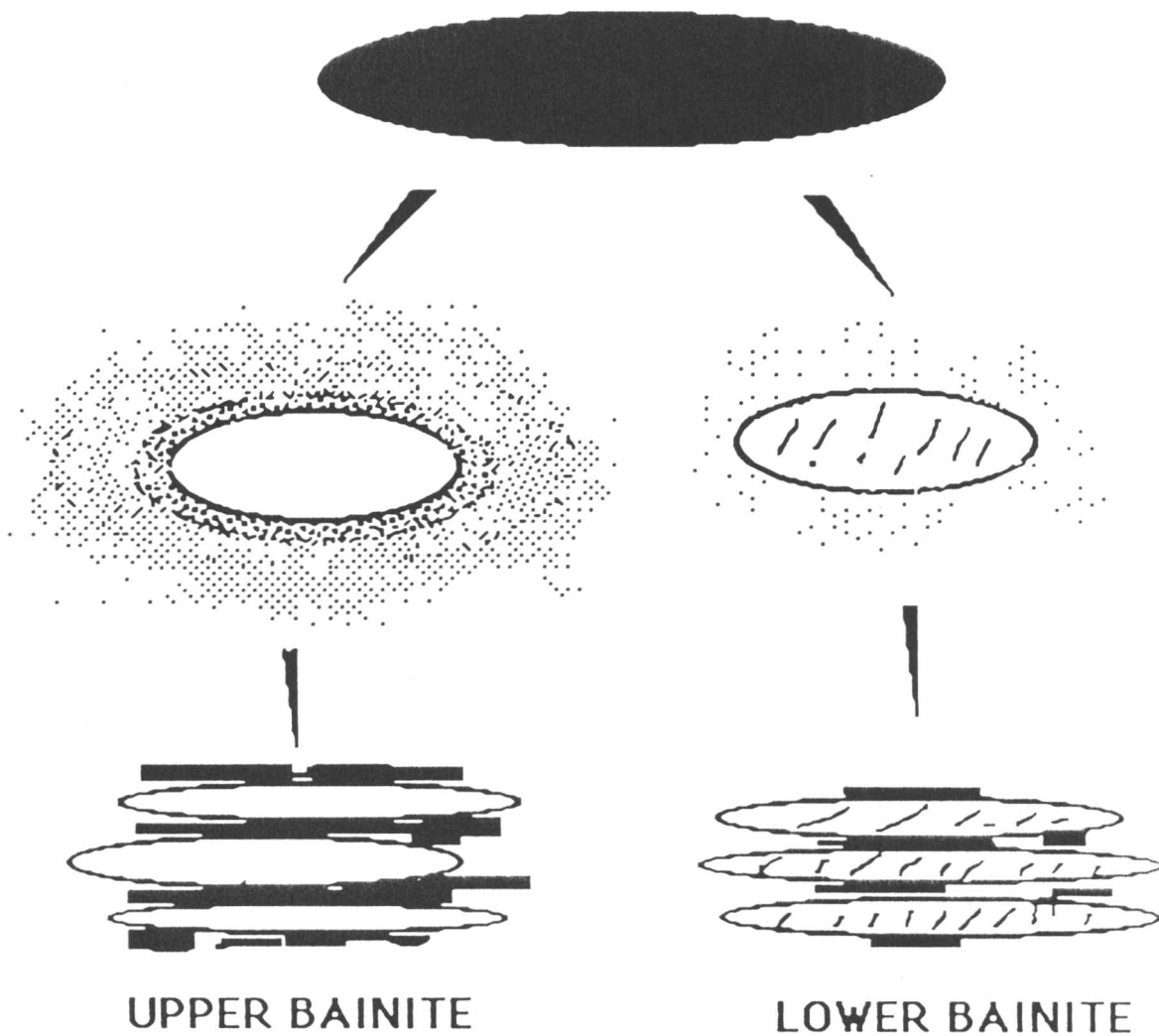
48. H. K. D. H. Bhadeshia: *Metal Science,* 1982, **16,** 167.

Fig. 2.1 Schematic illustration of the transition from upper to lower bainite. Lower bainite is obtained when the time required for excess carbon to partition from supersaturated ferrite into the residual austenite becomes large relative to the time required to precipitate cementite within the bainitic ferrite. Note that any carbon-enrichment of the residual austenite may eventually lead to the precipitation of further carbides, as illustrated above.
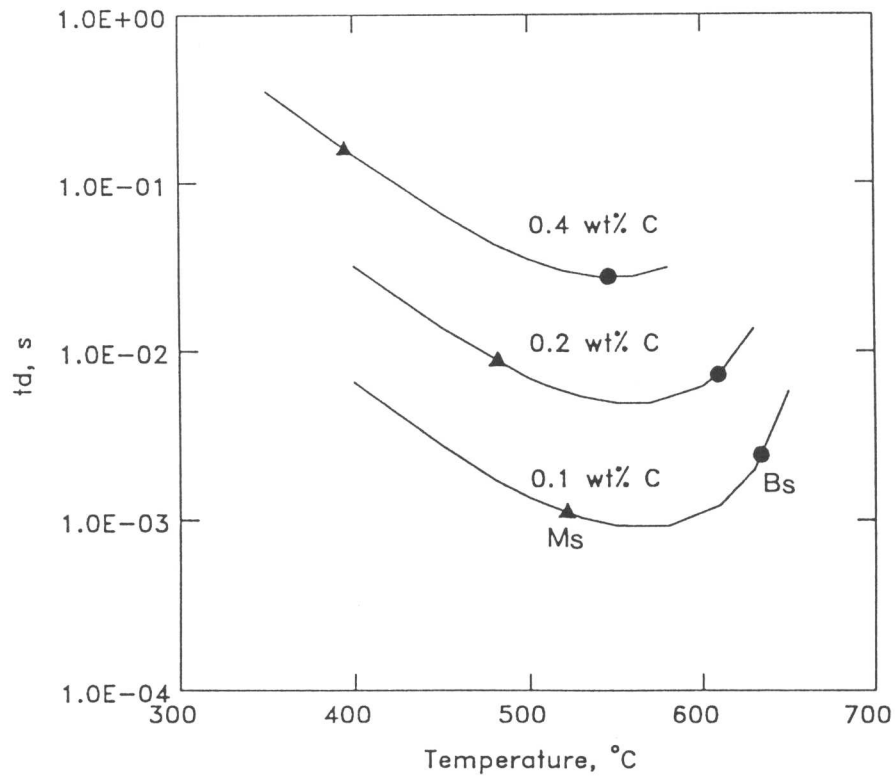
Fig. 2.2 Calculated time for the decarburisation of supersaturated ferrite plates (of thickness 0.2 μm) in plain carbon steels with 0.1, 0.2 and 0.4 wt.% carbon respectively. The calculated martensite-start and bainite-start temperatures are also indicated.
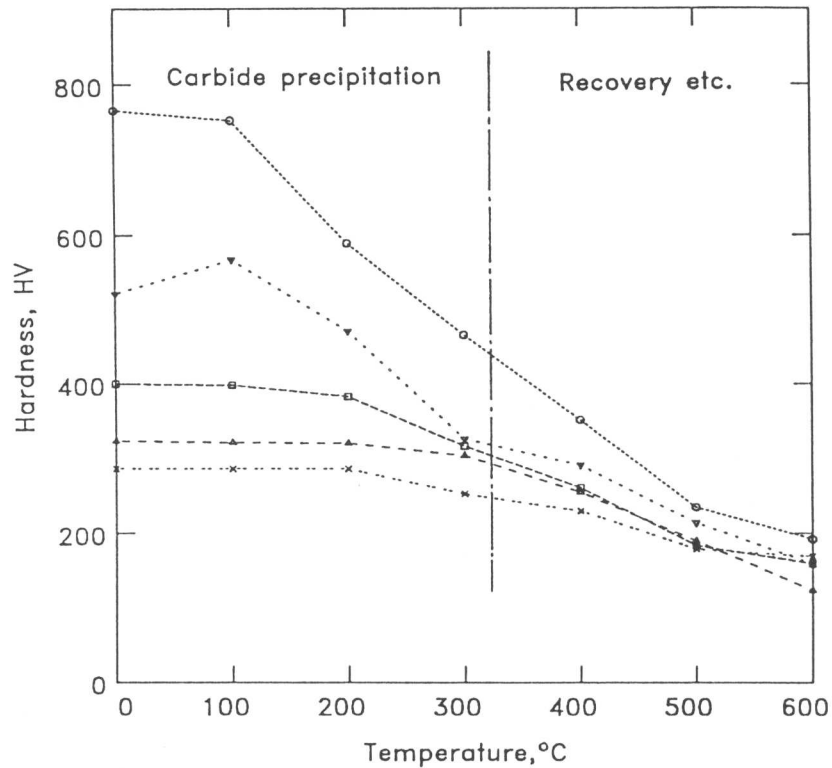
Fig. 2.3 Hardness curves for iron-carbon martensite samples which were tempered for 1 hour at the temperatures indicated; data due to Speich, [23]. The data to the left of the vertical line largely represent changes due to the precipitation of carbides, rather than recovery or coarsening processes.
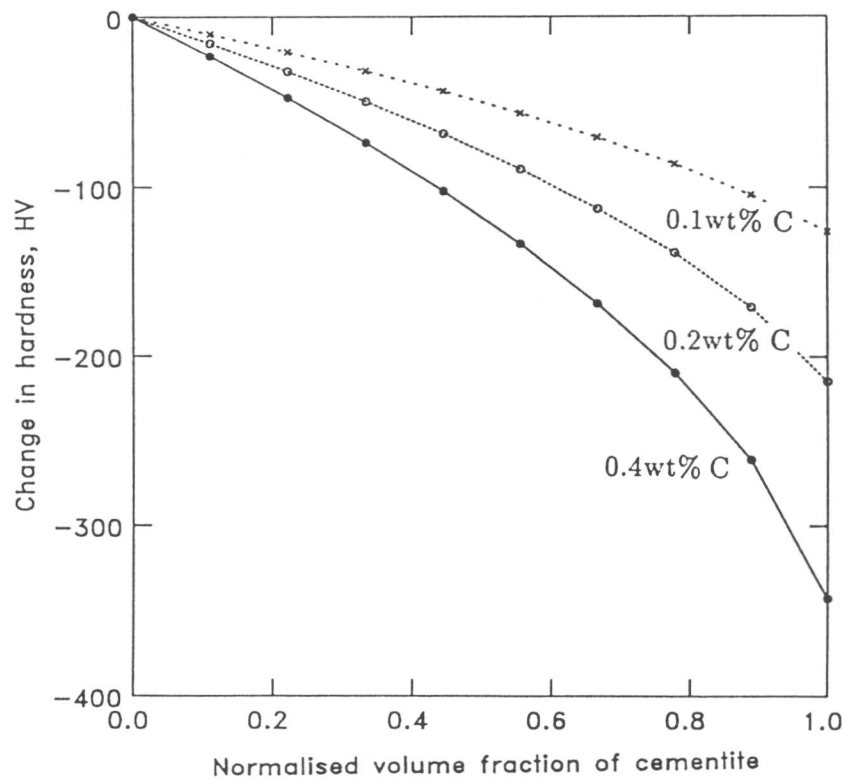
Fig. 2.4 Calculated changes in the hardness of martensite, due to cementite precipitation in 0.1, 0.2 and 0.4 wt.% plain carbon steels. Note that the horizontal axis represents the volume fraction of cementite normalised with respect to its equilibrium volume fraction.
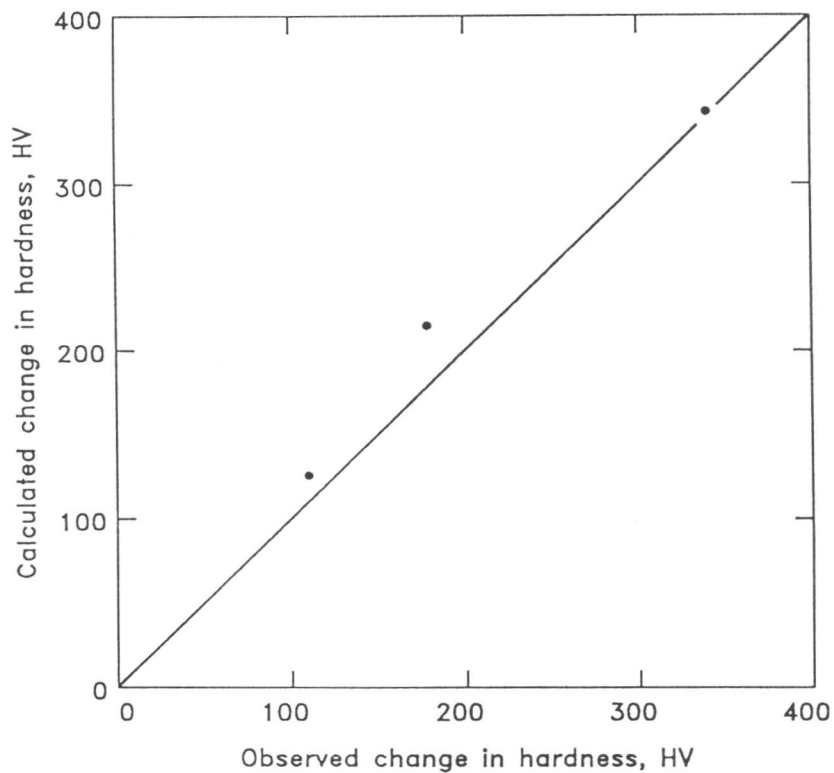
Fig. 2.5 Comparison of calculated changes in the hardness of plain carbon martensite, during tempering which leads to the precipitation of excess carbon in the form of cementite, with data reported by Speich [23].
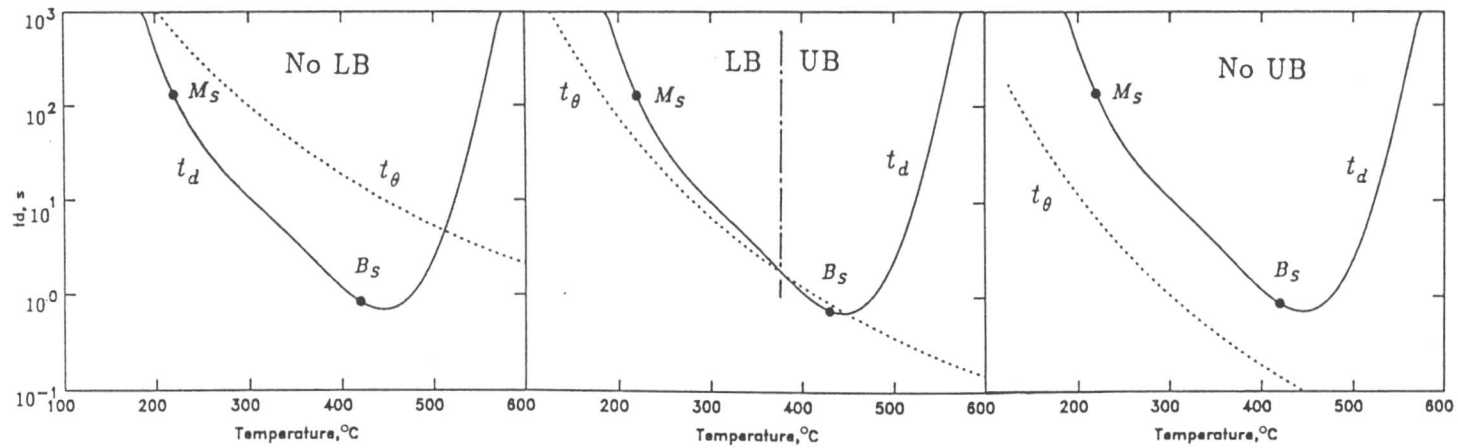
54

Fig. 2.6 Schematic illustration of how differences in the relative behaviours of the t_d and t_θ curves can lead to: (a) a steel which is incapable of transforming to lower bainite; (b) a steel which should under appropriate transformation conditions be able to transform to upper or lower bainite; (c) a steel in which bainitic transformation always leads to the formation of lower bainite. The abbreviations LB and UB refer to lower and upper bainite respectively.
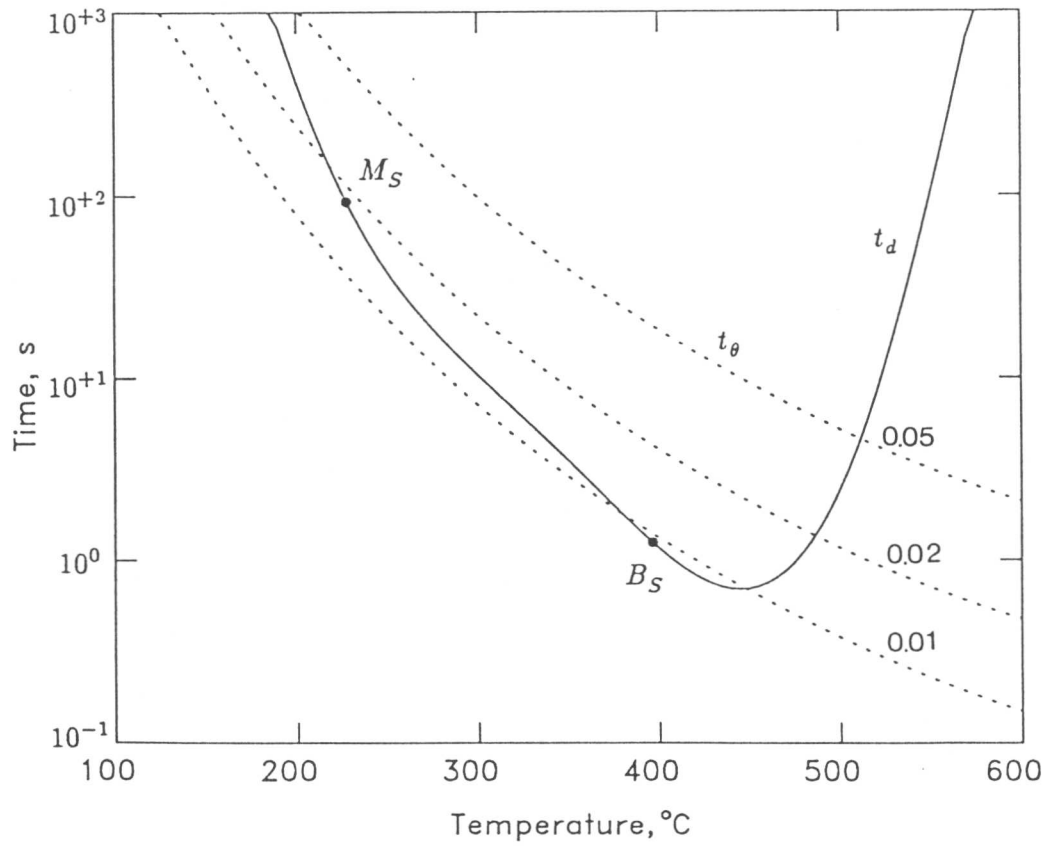
Fig. 2.7 Calculated decarburisation time (t_d : solid line) and the time required for cementite precipitation (t_θ : dashed line) as discussed in the text, for a Fe-0.43C-2.0Si-3.0Mn, wt.%, alloy. t_θ was calculated for 0.01, 0.02 and 0.05 of cementite precipitation.
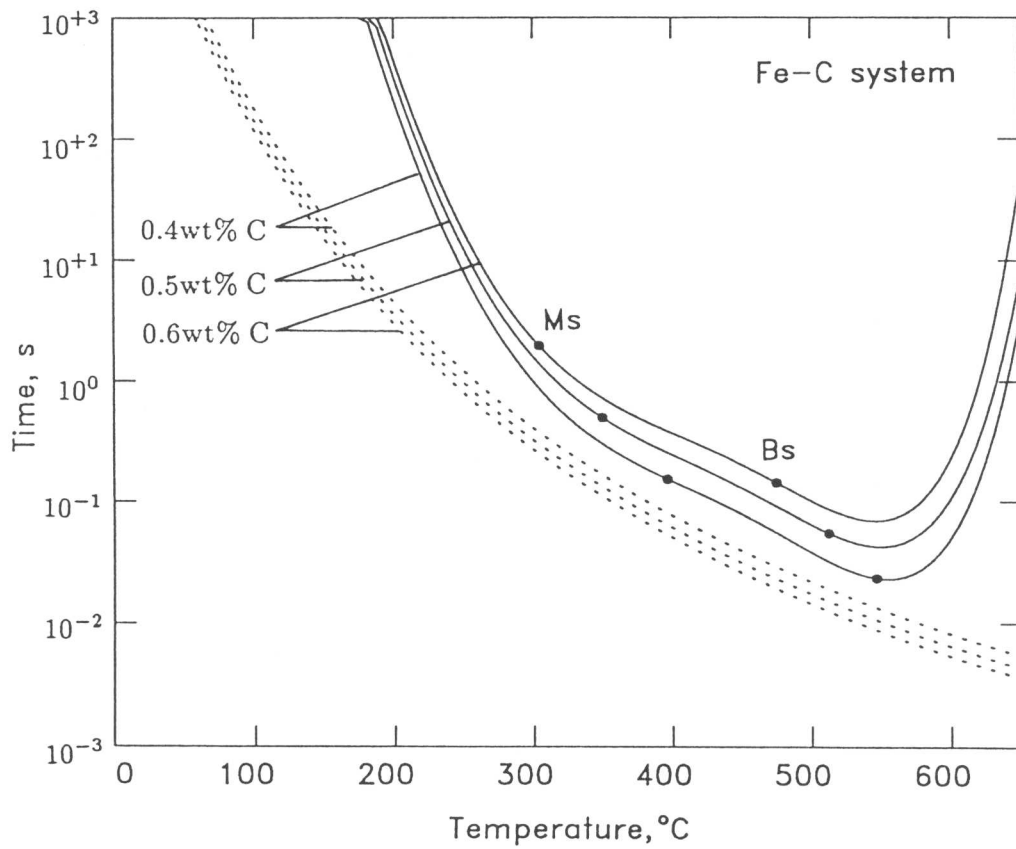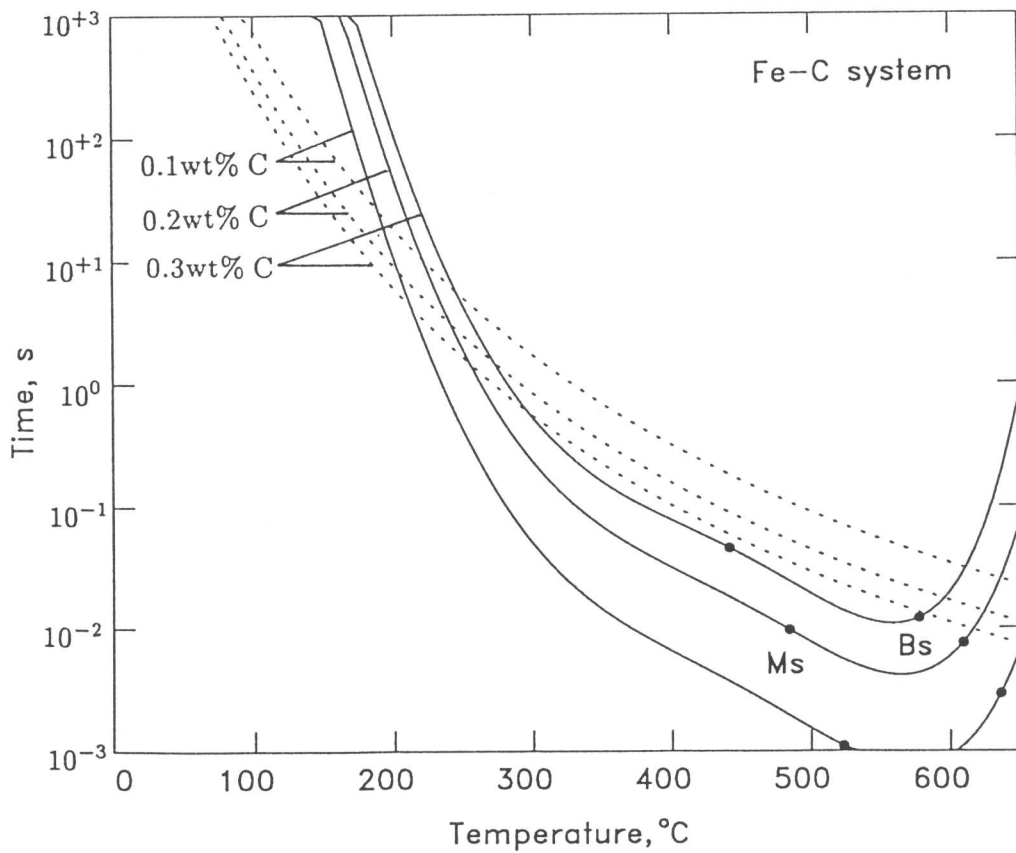
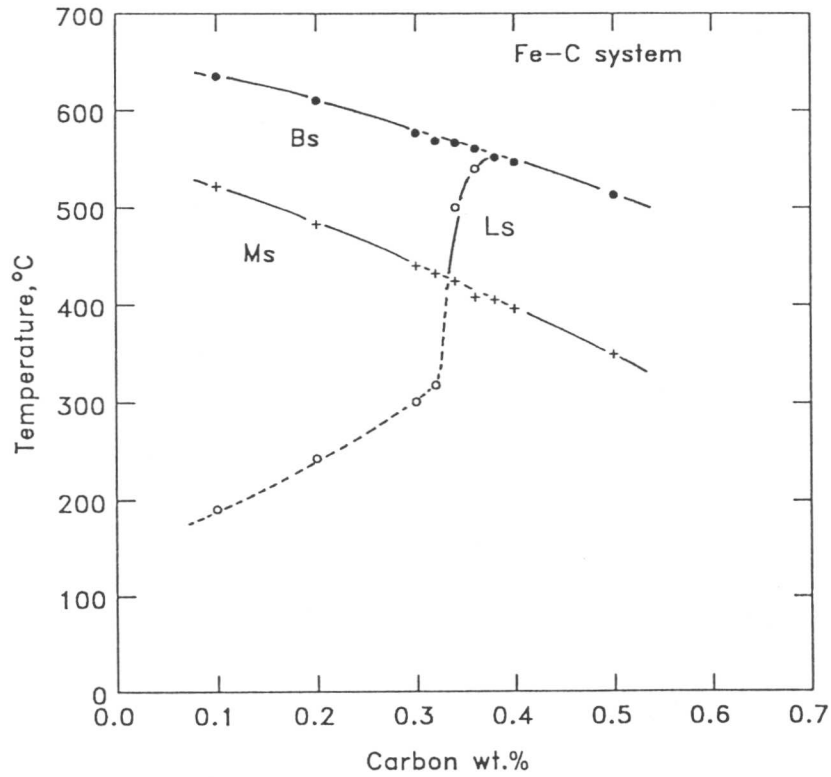Fig. 2.8 Calculated t_d and t_θ curves for plain carbon steels.

57

Fig. 2.9 Calculated lower bainite-start temperatures L_S for plain carbon steels, as a function of the transformation temperature. M_S and B_S are, respectively, the calculated martensite-start and bainite-start temperatures.
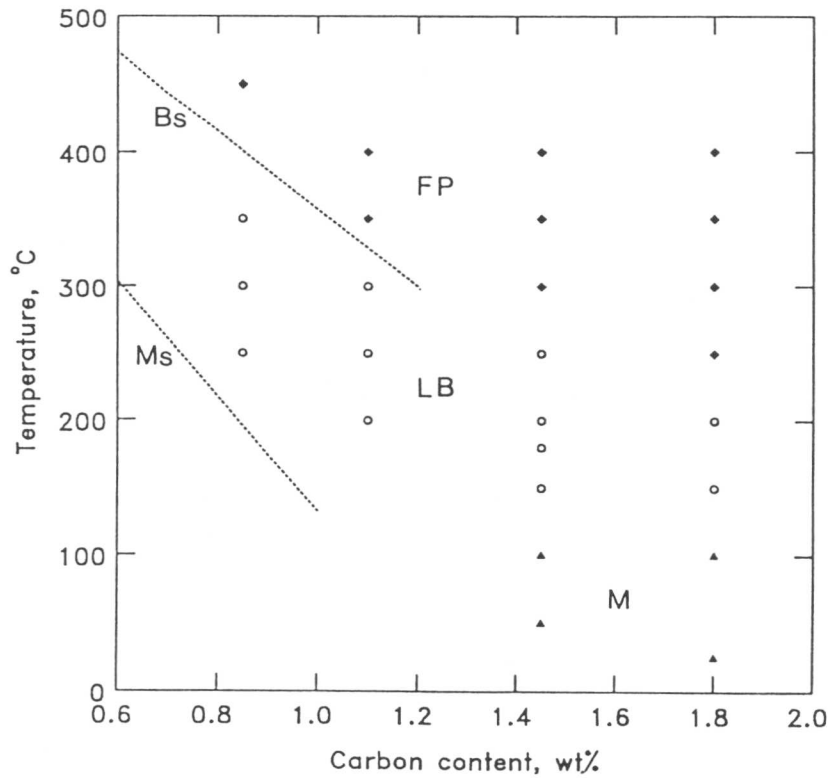

Fig. 2.10 Experimental data (Oka and Okamoto, [10]) illustrating the temperatures at which fine nodules of pearlite (FP), classical lower bainite (LB) and martensite (M) were obtained by isothermal transformation of plain carbon steels. The lines represent our calculated bainite-start and martensite-start temperatures.
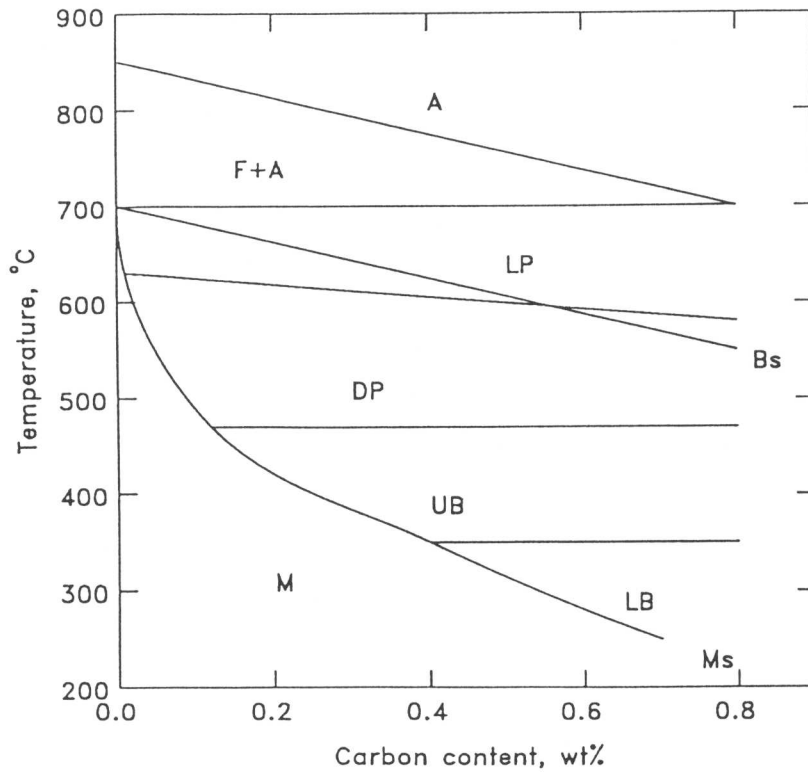
Fig. 2.11 The effect of carbon concentration on the temperature range where each microstructure is formed, after Ohmori and Honeycombe [29]. (A : austenite, F : ferrite, LP : lamellar pearlite, DP : degenerate pearlite, UB : upper bainite, LB : lower bainite, M : martensite, B_S : bainite-start temperature, M_S : martensite-start temperature.)
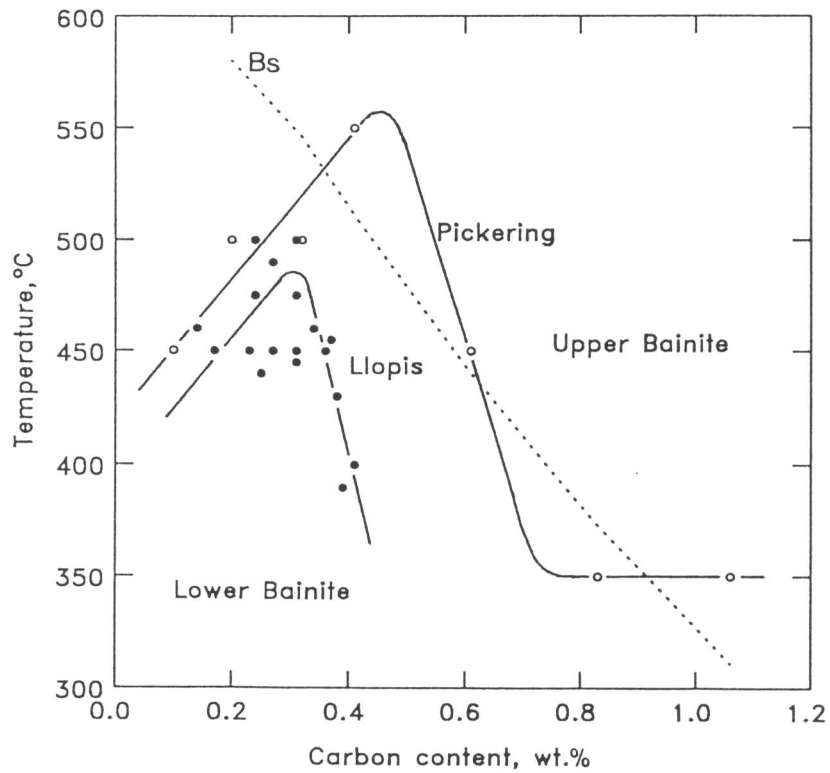

Fig. 2.12 Effect of carbon concentration on the temperature of change from upper to lower bainite, in alloy steels. After Pickering, [5], and Llopis and Parker, [8]. The dashed line represents our values of calculated bainite-start temperatures.

59

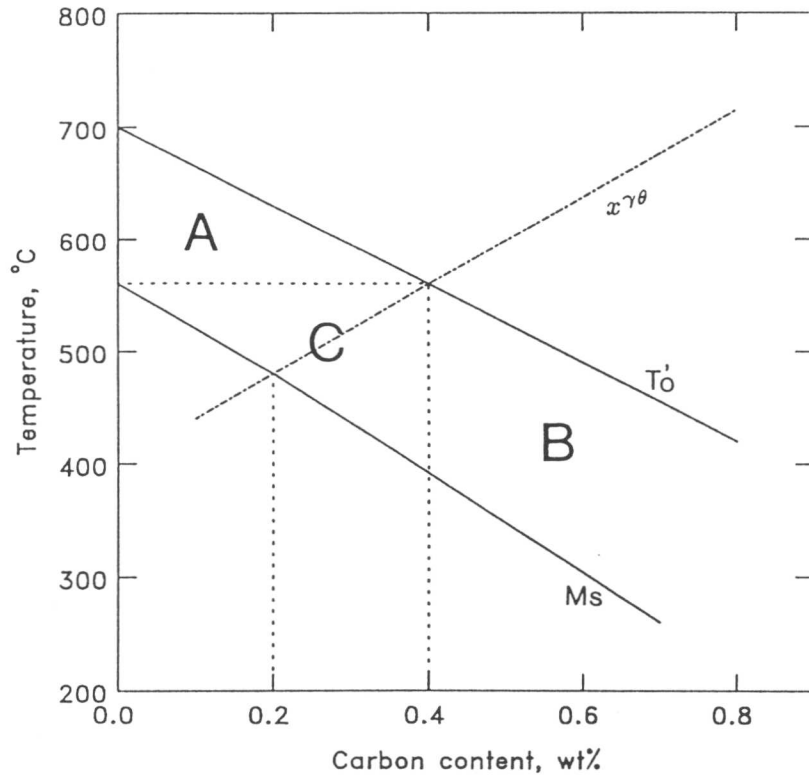Fig. 2.13 Identification of regimes (**A**, **B**, **C**) in which the progress of isothermal transformation can lead to changes in the nature of the transformation product. The line marked $x_1^{\gamma\theta}$ is the calculated $\gamma/(\gamma + Fe_3C)$ phase boundary.
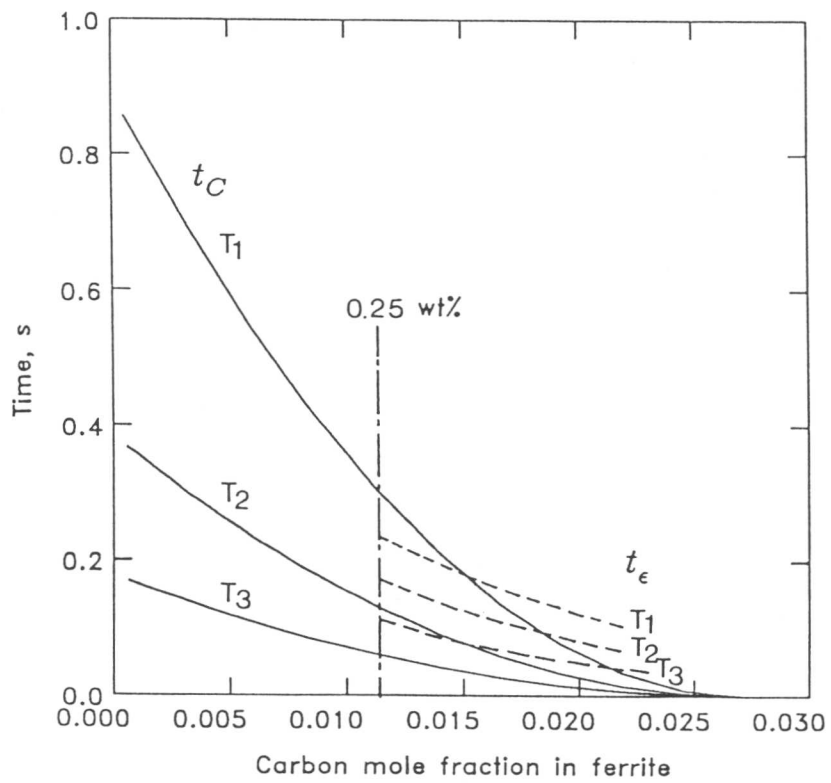

Fig. 2.14 Illustration of a possible explanation for the transition from lower bainite containing epsilon carbide, to lower bainite containing cementite
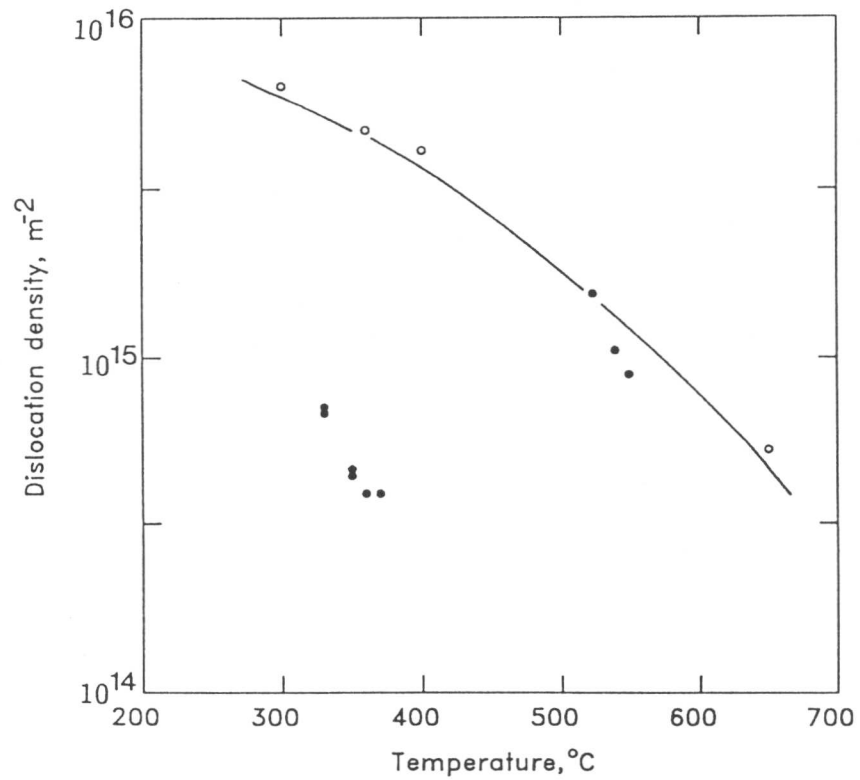
Fig. 2.15 Changes in the dislocation density of bainitic ferrite (open circles) and martensite (solid circles) as a function of the reaction temperature. The cluster of points that lie below the curve are due to Norström [45]. The other data are due to Smith [42], Fondekar *et al.* [43], and Kehoe and Kelly [44].
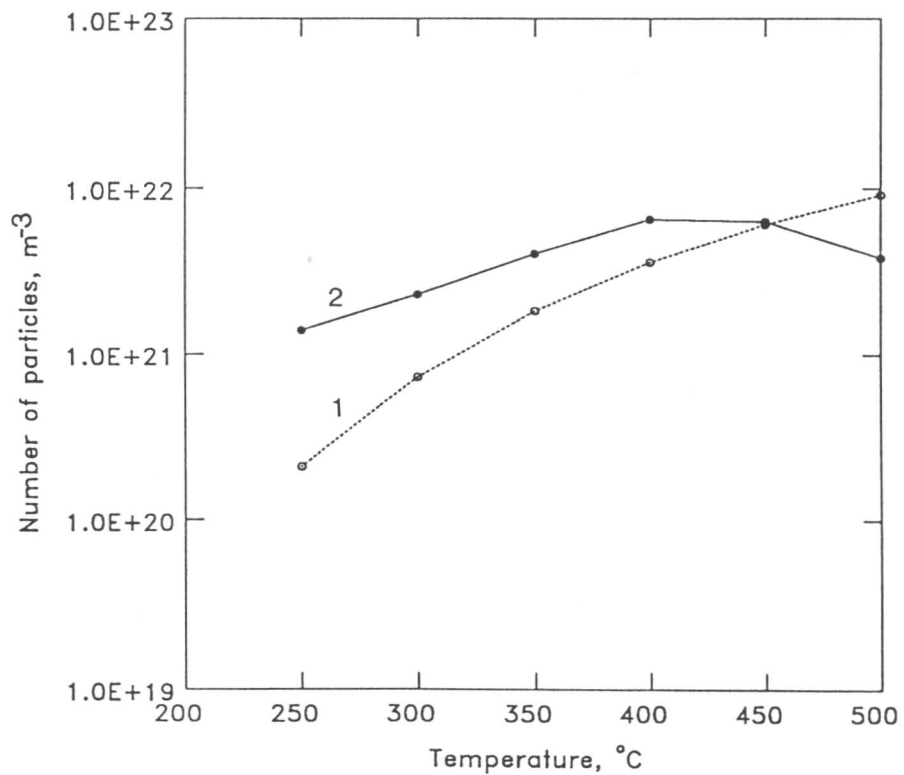
Fig. 2.16 Calculated number of cementite particles at the completion of precipitation N_θ (line 1) compared with the values (line 2) estimated from the empirical data of Venugopalan and Kirkaldy [39].
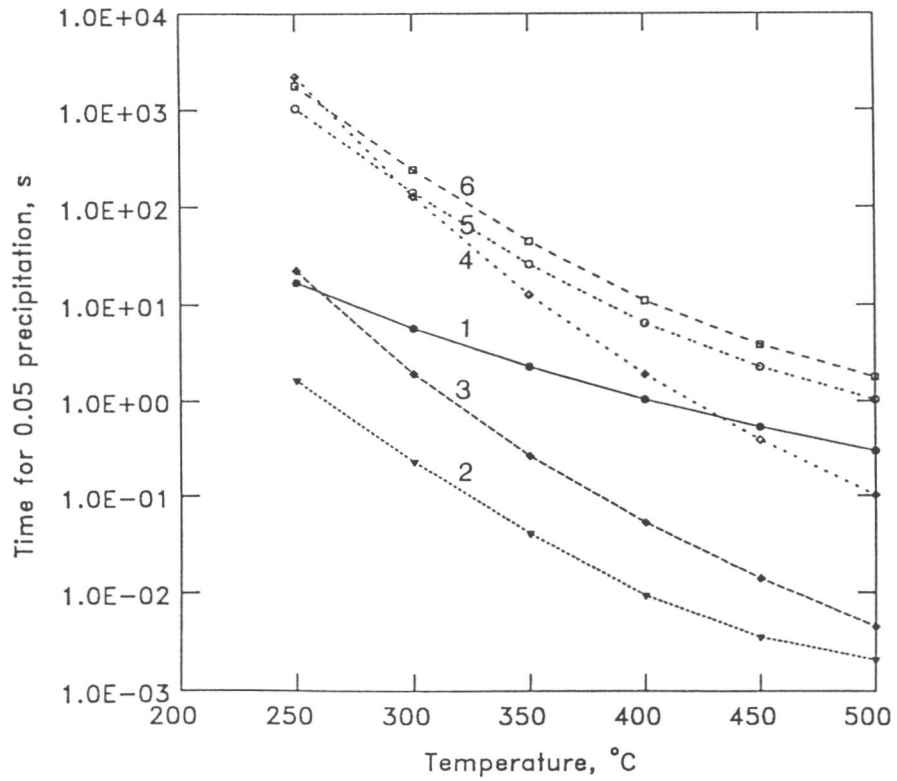
Fig. 2.17 Time for $\xi = 0.05$ cementite precipitation calculated from an empirical method (line 1), a parabolic growth model (line 2), a nucleation and parabolic growth model with $\Delta G_2^\theta = 190$ $J\,mol^{-1}$ (line 3) and with $\Delta G_2^\theta = 240$ $J\,mol^{-1}$ (line 4), and a plate growth model with the aspect ratio of 3 (line 5) and 15 (line 6) discussed in the text, as a function of the reaction temperature.

A MODEL FOR THE MICROSTRUCTURE OF SOME ADVANCED BAINITIC STEELS

3.1 INTRODUCTION

Bainitic steels are now at the forefront of some potentially exciting developments in the steel industry, especially when the steels are destined for high-technology applications [1-15]. This, combined with recent advances in phase transformations theory, provides a unique opportunity for the development of fundamental alloy design procedures which could be used in the optimisation of candidate steels before they are fully commercialised.

In discussing bainitic steels, it is necessary to distinguish between two microstructural classes of bainitic steels. Although bainite is generally recognised to be a non-lamellar mixture of ferrite and carbides, the carbide precipitation reaction often lags behind the growth of bainitic ferrite, the time lag sometimes being so long that carbides are simply not found in the microstructure obtained by transformation within the bainite temperature range – the microstructure then consists of just bainitic ferrite and carbon-enriched residual austenite (together with any martensite which might form as the residual austenite is cooled to ambient temperature) [16-18]. A large number of bainitic alloys are used in a condition where carbides are not found in the microstructure, and this forms one of the classes of bainitic steels; the other is the more conventional microstructure in which carbide particles are found between the bainitic ferrite platelets, and in the case of lower bainite, within the platelets as well. The theoretical problem which is the aim of the present work, is also therefore two fold: to predict mixed microstructures of bainitic ferrite, austenite and martensite, and to predict those containing mostly mixtures of bainitic ferrite and carbides. The complete problem is in fact quite formidable (Fig. 3.1) and only some aspects of it are addressed in this chapter.

3.2 CARBIDE-FREE BAINITIC STEELS

It is an experimental fact that in steels where other reactions do not interfere (or occur simultaneously) with the growth of bainitic ferrite, the maximum volume fraction of ferrite that forms on prolonged holding at the isothermal transformation temperature is far below that expected on the basis of equilibrium or paraequilibrium transformation [19-22]. The important characteristic of this *incomplete reaction phenomenon* is that the reaction stops well before the austenite achieves its paraequilibrium carbon concentration as given by the Ae'_3 curve on the phase diagram [17,18]. In fact, it stops when the carbon concentration of the residual austenite approaches the T_0 curve, which describes the locus of all points on the phase diagram where austenite and ferrite of the same chemical composition have identical free energies. For bainite, whose growth is accompanied by an invariant-plane strain shape deformation, the strain energy of transformation is about $400\,\mathrm{J\,mol^{-1}}$ [23], and the T_0 curve as modified to account for this stored energy is called the T'_0 curve.

A transformation in which carbon partitions during growth, and in which the mechanism of transformation is reconstructive (so that the product phase is not limited by austenite grain boundaries, and can grow to any size), can continue until the austenite achieves its equilibrium or paraequilibrium composition. Such a mechanism cannot therefore explain the observations

described above. On the other hand, the incomplete reaction phenomenon can be understood if it is assumed that the bainitic ferrite grows without diffusion, with the carbon being partitioned into the residual austenite immediately after the growth event. As the austenite becomes progressively enriched with carbon, a stage is eventually reached when it is thermodynamically impossible for further bainite to grow by diffusionless transformation. At this point, the composition of the austenite is given by the T_0' curve of the phase diagram. This also explains why the degree of transformation to bainite is zero at the bainite-start (B_S) temperature and increases with undercooling below B_S. The T_0' curve has a negative slope on a temperature/carbon concentration plot; the austenite can therefore tolerate more carbon as the temperature is reduced, before diffusionless transformation becomes impossible. The T_0 and T_0' curves are in fact only slightly different in carbon concentration, and given that the carbon is often inhomogeneously distributed in the residual austenite [24-27], it is a reasonable assumption to neglect the strain energy term in estimating the austenite composition when isothermal bainitic ferrite growth ceases.

3.2.1 Thermodynamics

As emphasised above, the incomplete reaction phenomenon can only be assessed quantitatively in steels where other reactions do not overlap with the formation of bainitic ferrite. These steels must obviously have a large enough bainitic hardenability and in addition should contain elements such as Al, Si, or Cr which retard the precipitation of cementite [28-33]. Many commercial alloys satisfy these conditions: ultrahigh-strength alloys such as "300M" steel, austempered ductile cast irons, forging steels, bainitic dual phase steels, *etc.* In all cases, their microstructures should consist of mixtures of bainitic ferrite, retained austenite and martensite.

An established method of estimating the limiting volume fractions in such microstructures is based on the T_0 concept [18]. This assumes that isothermal reaction is permitted for a time period t_C which is long enough to permit the volume fraction of bainitic ferrite to reach its limiting value. The effect of kinetic limitations is considered later.

The microstructure after isothermal transformation (at T_b) in the upper bainite transformation range followed by cooling to ambient temperature (T_A) consists of bainitic ferrite, carbon-enriched retained austenite and untempered martensite which forms during cooling from $T_b \rightarrow T_A$. At T_b, the bainite reaction will cease when the carbon concentration of the residual austenite (x_1^γ) approaches the T_0 curve:

$$x_1^\gamma \rightarrow x_{T_0} \qquad (3.1)$$

If the small difference in density between the ferrite and austenite is ignored, then the maximum volume fraction of bainitic ferrite (*i.e.* V_b^e) is given by a lever rule applied to the Ae_1' and T_0 curves:

$$V_b^e = (x_{T_0} - \bar{x}_1)/(x_{T_0} - x_1^{\alpha\gamma} - S) \qquad (3.2)$$

where $x_1^{\alpha\gamma}$ is the paraequilibrium carbon concentration of the bainitic ferrite, $\bar{x}_1$ the average carbon concentration of the alloys and S is the amount of carbon which is tied up as carbides within the bainitic ferrite.

On cooling the sample to ambient temperature, some of the residual austenite may transform to martensite with the remainder being retained. The martensite-start temperature (M_S)

of the residual austenite can be estimated by assuming that its carbon concentration is x_{T_0}, so that the amount of martensite ($V_{\alpha'}$) that forms is given by [34]:

$$V_{\alpha'} = (1 - V_b^e)[1 - \exp\{-0.011(M_S - T_A)\}] \qquad (3.3)$$

Note that when dealing with upper bainite, the method permits the calculation of the volume fractions of all the phases and also their detailed chemical compositions. There is unfortunately, no method for predicting S, so that similar calculations for lower bainite are not yet possible. The method also assumes that the partitioned carbon is distributed homogeneously within the residual austenite. No account is taken of the fact that many industrial alloys are chemically heterogeneous.

Some new published data are available for comparison against the T_0 criterion. The lattice parameters of austenite retained in Fe-0.2C-1.5Si wt.% alloys containing varying concentrations of manganese have been measured using X-ray diffraction by Usui *et al.* [35]. Since carbon in solid solution causes an expansion of the austenite lattice parameter, these data can be used to deduce the carbon concentration of the retained austenite. Taking the relationship between the lattice parameter and x_1^γ to be given by [36]:

$$a_{\gamma 0} = 0.3573 + 0.00075 x_1^\gamma , \quad \text{nm} \qquad (3.4)$$

It is found that the calculated compositions of the retained austenite agree well with the calculated T_0 curves (Fig. 3.2), and the effect of manganese is also well represented by the thermodynamically calculated T_0 curves.

3.2.2 Kinetics

Many industrial heat-treatments involve isothermal transformation for time periods less than those required to allow the bainite reaction to reach completion. It is often the case that the heat-treatment utilised is not isothermal. The thermodynamic approach described above fails in both of these circumstances. To correctly treat such cases, it is necessary to be able to predict the appropriate time-temperature-transformation (TTT) and continuous-cooling-transformation diagrams for bainite.

Bhadeshia has presented a method [37], based on Russell's expression for incubation time during nucleation [38,39], for estimating the TTT diagram of multicomponent steels. The TTT diagram is considered to consist essentially of two 'C'-curves, the high temperature curve representing reconstructive reactions such as allotriomorphic ferrite and pearlite, the lower temperature curve representing displacive transformations such as Widmanstätten ferrite and bainite. Most of the features of published TTT diagrams for steels can be understood via the different effects of alloying elements on these two C-curves. The original paper however, dealt with just a prediction of the incubation period prior to the onset of transformation at each temperature (*i.e.* the curves representing the initiation of a detectable degree of transformation). This is of course inadequate for the present requirements but the method can be adapted to predict the whole family of C-curves representing the progress of bainitic reaction in a particular steel, as described below.

In the original model, the incubation time τ for the beginning of transformation is given by:

$$\ln\{\tau(\Delta G_m)^p T^{-z}\} = (Q'/RT) + C_4 \qquad (3.5)$$

where p, z, Q' and C_4 are constants obtained by fitting to experimental data, ΔG_m represents the maximum driving force available for nucleation and τ represents the incubation time prior to the formation of a detectable degree of transformation product. As the bainite reaction proceeds beyond this initial stage, the austenite becomes enriched with carbon. The degree of enrichment can easily be calculated using the mass balance condition. In the present work, bainite C-curves representing further degrees of reaction are calculated by applying equation (3.5) to enriched austenite, with ΔG_m depending on the new composition of the austenite.

Scheil's rule [39] is then used to convert the TTT diagram into a CCT diagram. It is therefore assumed that the additivity principle applies to each of the C-curves in the TTT diagram, with the specified degree of transformation being achieved if

$$\int_0^t \Delta t / \tau_f\{T\} = 1 \qquad (3.6)$$

where $\tau_f\{T\}$ is the incubation time at temperature T for the C-curve representing a fraction f of reaction, Δt is the time interval spent by the sample at the temperature T, and t is the time defined to be zero above the bainite-start temperature.

Typical calculations, for a series of low alloy silicon-rich steels are presented in Fig. 3.3. Note that they do not allow for the formation of lower bainite, for the solidification-induced chemical segregation that is inevitably present in commercial alloys, the effects on inhomogeneous carbon distributions, etc. The calculations are in this sense, unrealistic, but the trends that they indicate should be correct.

3.3 CARBIDE PRECIPITATION FROM BAINITIC FRRITE

As discussed earlier, the growth of bainite is probably diffusionless, but any excess carbon in the supersaturated ferrite soon afterwards partitions into the residual austenite or precipitates within the bainitic ferrite in the form of carbides. When the process of carbon partitioning into the residual austenite is rapid relative to that of carbide precipitation, the transformation product is called "upper bainite", whereas "lower bainite" is obtained when some of the carbon supersaturation is relieved by precipitation within the bainitic ferrite.

The transition from upper to lower bainite can therefore be estimated by comparing the time t_d required to partition excess carbon into austenite, with the time t_C necessary to achieve a detectable degree of carbide precipitation within the ferrite [40]. The diffusion time is given by:

$$t_d \simeq \frac{a^2 \pi (\overline{x}_1 - x_1^{\alpha\gamma})^2}{16 \overline{D} (x_1^{\gamma\alpha} - \overline{x}_1)} \qquad (3.7)$$

where $\overline{x}_1$ is the average carbon concentration in the steel as a whole, $x_1^{\alpha\gamma}$ and $x_1^{\gamma\alpha}$ are the carbon concentrations in the ferrite and austenite which are in paraequilibrium, and $\overline{D}$ is a weighted average carbon diffusivity in austenite [41,42].

66

Although there is as yet no rigorous model capable of predicting the kinetics of carbide precipitation from supersaturated ferrite, it is possible to fit Avrami type relationships to martensite tempering data and estimate the time period t_C [43], and consequently, by comparing t_d and t_C, the upper to lower bainite transition temperature L_S. Using this method, it has been demonstrated that there is a maximum in L_S as a function of carbon concentration at around 0.4 wt.% carbon (Fig. 3.4) in Fe-C alloys. It is further predicted that in plain carbon steels, only upper bainite can be obtained before the onset of martensitic transformation, followed by a narrow range of carbon in which both upper and lower bainite are possible, and as the carbon concentration is increased (> 0.4 wt.% C), only lower bainite and martensite can be obtained during heat treatment at temperatures below that at which pearlite forms [43]. These predictions, together with the position of the peak and the shape of the transition curve are in fact consistent with published experimental data on plain carbon steels [43] (Fig. 3.5).

On applying this model [43] to experimental data on Fe-Mn-Mo-C alloys [44], without taking account of any effect of the substitutional alloying elements on carbide precipitation kinetics, good agreement between theory and experiment is once again obtained (Fig. 3.6).

3.4 CEMENTITE PRECIPITATION FROM SUPERSATURATED AUSTENITE

Austenite is supersaturated with respect to cementite (θ) precipitation when $x_1^\gamma > x_1^{\gamma\theta}$; for the bainite reaction, this means that $x_{T_0} > x_1^{\gamma\theta}$ since the growth of bainitic ferrite stops when x_1^γ reaches the value x_{T_0} given by the T_0 curve of the phase diagram. A consequence of the precipitation of cementite from austenite is that its carbon concentration drops below x_{T_0}, so that the growth of bainitic ferrite can continue to an extent larger than would be otherwise possible. It is therefore important to be able to predict the kinetics of cementite precipitation from the residual austenite, and the problem is one of nucleation and growth of cementite.

Assuming that the cementite forms by reconstructive transformation (the actual mechanism has yet to be established), the incubation time τ for nucleation can be estimated using Russell's model [37,38]. The incubation time should decrease as the magnitude of the maximum driving force for nucleation, ΔG_m, increases (see equation 3.4). Our calculations based on the assumption that the nuclei form with the equilibrium composition, indicate that the retardation of cementite precipitation by silicon cannot be related to the nucleation stage, since silicon is actually found to increase ΔG_m (Fig. 3.7).

3.4.1 Effect of Alloying Elements on Cementite Growth

The growth rate is here estimated using the theory of diffusion-controlled interfacial motion. Since the cementite particles found in bainitic microstructures are plate shaped and usually have large aspect ratios, it may be a good approximation to represent the formation of these plates using a one-dimensional parabolic thickening rate constant (α_1), so that the plates are essentially treated here as allotriomorphs. It is further assumed that any concentration gradients can be approximated as being constant (after Zener) and the problem is studied for ternary Fe-C-X alloys, where "X" denotes a substitutional solute; C and X are in the equations that follow, identified using the subscripts 1 and 2 respectively. When local equilibrium is assumed to exist at the transformation interface, it can be demonstrated using the methods of Kirkaldy and Coates [45,46] that the parabolic thickening rate constant can be obtained from the simultaneous solution of the following equations:

$$\alpha_1^2 = \overline{D}_{11}^\gamma \frac{(\overline{x}_1^\gamma - x_1^{\gamma\theta})^2}{(x_1^{\theta\gamma} - \overline{x}_1^\gamma)(x_1^{\theta\gamma} - x_1^{\gamma\theta})} + D_{12}^\gamma \frac{(\overline{x}_2^\gamma - x_2^{\gamma\theta})^2}{(x_2^{\theta\gamma} - \overline{x}_2^\gamma)(x_2^{\theta\gamma} - x_2^{\gamma\theta})} \qquad (3.8)$$

$$\alpha_1^2 = D_{22}^\gamma \frac{(\overline{x}_2^\gamma - x_2^{\gamma\theta})^2}{(x_2^{\theta\gamma} - \overline{x}_2^\gamma)(x_2^{\theta\gamma} - x_2^{\gamma\theta})}. \qquad (3.9)$$

where $\overline{x}_1^\gamma$ and $\overline{x}_2^\gamma$ represent the average composition of the austenite, and $x_{1,2}^{\theta\gamma}$ and $x_{1,2}^{\gamma\theta}$ the equilibrium compositions of the cementite and austenite respectively. $\overline{D}_{11}^\gamma$ is the weighted average diffusivity of carbon in the austenite, D_{12}^γ represents the dependence of the carbon flux in austenite on the concentration gradient of the substitutional solute, and D_{22}^γ the diffusivity of the substitutional solute in the austenite. The diffusion coefficient D_{12}^γ is given by

$$D_{12}^\gamma = D_{11}^\gamma \frac{\epsilon_{12} x_1^\gamma}{1 + \epsilon_{11} x_1^\gamma} \qquad (3.10)$$

where the ϵ terms are the Wagner interaction parameters which arise in dilute solid solution models, as discussed elsewhere [47]. It is assumed that the composition of the growing cementite is uniform everywhere.

It is also possible that the cementite grows with paraequilibrium, in which case the iron atom to substitutional solute atom ratio should be constant everywhere. The rate constant is then given by:

$$\alpha_1^2 = \overline{D}_{11}^\gamma \frac{(\overline{x}_1^\gamma - x_1^{\gamma\theta})^2}{(x_1^{\theta\gamma} - \overline{x}_1^\gamma)(x_1^{\theta\gamma} - x_1^{\gamma\theta})} \qquad (3.11)$$

Note that the concentration terms $x_1^{\theta\gamma}$ and $x_1^{\gamma\theta}$ now represent *paraequilibrium* rather than equilibrium compositions of the two phases.

Fig. 3.8 shows the results of growth rate calculations, carried out assuming paraequilibrium growth of cementite from austenite. It is evident that the growth of cementite is substantially retarded by silicon.

3.5 STABILITY OF AUSTENITE AND EFFECT ON PROPERTIES

The mixture of bainitic ferrite and austenite is in principle an ideal combination from many points of view [11-15]. Most modern high-strength steels are clean in the sense that they are largely free from nonmetallic inclusions. Those destined for critical applications are usually vacuum arc refined prior to fabrication and heat-treatment. As a consequence, it is the components of the intrinsic microstructure, such as particles of cementite, which are responsible for damage initiation. The upper bainitic ferrite and austenite mixture is however, free from cleavage and void nucleating cementite. The ferrite also has a very low interstitial content, since much of the excess carbon is partitioned into the residual austenite; the toughness of ferrite is known to deteriorate rapidly with an increasing concentration of carbon in solid solution.

The microstructure derives its strength from the ultrafine grain size which results from the displacive mechanism of ferrite growth, giving an effective grain size which is much less than $1 \, \mu$m. Such a small grain size cannot be achieved by any commercial process other than mechanical alloying (powder metallurgical process). A fine grain structure is an optimum method for improving strength since unlike most other strengthening mechanisms, the improvement in

strength is also accompanied by an improvement in toughness. The intimately dispersed and ductile *fcc* austenite films between the ferrite platelets can be expected at the very least to have a crack blunting effect, and could also make increase the work of fracture by undergoing martensitic transformation under the influence of the stress field of the propagating crack (*i.e.* the TRIP, or transformation induced plasticity effect [48,49]). The diffusivity of hydrogen in austenite is relatively sluggish [50], so that its presence can in some circumstances enhance stress corrosion resistance [51,52]. And all these potential benefits can be achieved by creating a duplex microstructure with the cheapest austenite stabiliser available, carbon, whose concentration in the austenite is enhanced during transformation, so that the average carbon concentration of the steel need not be large.

In spite of all these potential advantages, the bainitic ferrite/austenite microstructure has on many occasions failed to live up to its promise [11-15, 53], primarily because of the instability of relatively large or blocky regions of austenite which become trapped between sheaves of bainite. The blocks of austenite tend to transform to high-carbon, untempered martensite under the influence of small stresses and consequently have an embrittling effect. The films of austenite that are trapped between the platelets of ferrite in a sheaf are much more stable, partly because of their higher carbon concentration, and also because of the physical constraint to transformation due to the close proximity of plates in all directions.

If it is assumed that a fraction ϕ of a sheaf is consists of films of austenite, then it can be demonstrated that the ratio of the volume fractions of film and blocky austenite (prior to any martensitic transformation) is given by:

$$V_\gamma^F / V_\gamma^B = \phi V_\alpha / (V_\gamma - \phi V_\alpha) \qquad (3.12)$$

where V_γ^F and V_γ^B are the volume fractions of film and blocky type retained austenite respectively, and V_α and V_γ the total volume fractions of bainitic ferrite and residual austenite respectively. It is found experimentally that high strength and good toughness can be obtained by maintaining the above ratio to a value greater than 0.9 [11,12]. The question then arises as to the factors which control this ratio. There are in fact three different ways of minimising the volume fraction of blocky austenite, each involving an increase in the volume fraction of bainite.

Lowering the transformation temperature permits the bainite reaction to proceed to a greater extent but there is a limit to the minimum transformation temperature since the lower bainite and martensite reactions eventually set in. An increase in the extent of reaction can also be achieved by reducing the overall carbon concentration of the steel, so that the austenite reaches its limiting composition at a later stage of the reaction. The T_0 curves of the phase diagram, which determine the composition of the austenite at the point where the reaction stops, can also be shifted to higher carbon concentrations by altering the substitutional solute concentration of the steel. The effect on toughness in reducing the amount of blocky austenite is very pronounced, with large reductions in the impact transition temperatures as the ratio of film to blocky austenite is increased in the manner just described. Note that for a duplex $\alpha + \gamma$ microstructure, the strength actually increases as the fraction of bainitic ferrite increases, so that the better toughness is obtained without sacrificing strength. Typical compositions of high-strength steels which show good toughness are given in Table 3.1. Fig. 3.9 shows how the

mechanical properties compare with quenched and tempered steels. It is evident that in some cases, the properties match those obtained from much more expensive maraging steels.

Table 3.1 Chemical compositions (wt.%) of some successful alloys based on a mixed microstructure of bainitic ferrite and austenite.

	C	Si	Mn	Ni
	0.22	2.0	3.0	–
	0.40	2.0	–	4.0

The properties of these steels improve only slightly when tempered at temperatures not much higher than the transformation temperature at which the original bainite formed. However, annealing at elevated temperatures or prolonged periods at low temperatures can lead to the decomposition of the austenite into ferrite and carbides, with a simultaneous drop in strength and toughness, especially the upper shelf energy. The latter effect can be attributed directly to the void nucleating propensity of carbide particles in the tempered microstructure, as illustrated by the much smaller void size evident in the fracture surface of the tempered sample.

The mechanical property data on these high silicon steels, especially those steels designed using the phase transformation theory discussed earlier, look extremely promising. It is however, unlikely that the experimental steels represent the optimum compositions and further development work could lead to even better properties. It is also necessary to carry out a comprehensive assessment of properties such as stress corrosion resistance, fatigue etc.

3.5.1 Ductility

The influence of retained austenite on ductility has been studied mainly in steels containing a high silicon concentration, where cementite formation can be prevented, and consequently large quantities of carbon-enriched austenite can be retained. Ductility as measured by tensile elongation, reaches a peak (optimum) value as a function of the volume fraction of retained austenite, when the amount of austenite is varied by altering the volume fraction of isothermal transformation to bainite [54]. Furthermore, the uniform elongation behaves in a similar way to total elongation when plotted against the volume fraction of retained austenite. The difference between the uniform and total elongation decreases as the optimum volume fraction of retained austenite is reached; beyond the optimum value, tensile failure occurs before the necking instability so that the difference between uniform and total elongation vanishes.

It seems that the best elongation behaviour is observed when the retained austenite is present mainly in the form of films between the sub-units of bainite, rather than as blocky regions between the sheaves of bainite [54]. Hence, the optimum retained austenite content increases as the transformation temperature decreases, because the sub-unit thickness decreases, permitting more of the austenite to be in the film morphology for a given volume fraction of transformation to bainite. For the same reason, the elongation becomes less sensitive to retained austenite content as the transformation temperature is reduced. While mechanically

unstable austenite, i.e. the austenite which decomposes to deformation induced martensite, is recognised to cause a deterioration in toughness for bainitic steels [11,12,53], this is not the case for ductility, presumably because of the TRIP effect and the lower strain rates involved in conventional tensile tests.

It must be emphasised that all these results are very difficult to interpret quantitatively. Changes in retained austenite content cannot easily be made without altering other factors such as the tensile strength and the distribution of the austenite. For example, Miihkinen and Edmonds [14] have reported a monotonic increase in uniform and total ductility with retained austenite content. The latter was varied by altering the transformation temperature, so that the strength increased as the austenite content decreased.

3.6 SUMMARY

A start has been made on the complicated problem of predicting the microstructure of bainitic steels, by developing an approximate method of calculating the time-temperature-transformation diagram for the formation of bainite. There remain significant difficulties: future work will have to address the problem of chemical segregation, nonuniform distribution of carbon in any residual austenite, more complete models for carbide precipitation during bainitic transformation, and other problems highlighted in Fig. 3.1. It should nevertheless be possible to give good hints on the expected changes of microstructure and mechanical properties as alloy chemistry and thermal treatments are varied. Steady progress is also being made in evaluating the relationships between microstructure and mechanical properties, although more research is needed to establish these on a quantitative basis.

REFERENCES

1. O. Matsumura, Y. Sakuma and H. Takechi: *Trans. ISIJ*, 1987, **27,** 570.

2. O. Matsumura, Y. Sakuma and H. Takechi: *Scripta Metall.*, 1987, **21,** 1301.

3. S. Bandoh, O. Matsumura and Y. Sakuma: *Trans. ISIJ*, 1988, **28,** 569.

4. M. Imagumbai, R. Chijiiwa, N. Aikawa, M. Nagumo, H. Homma, S. Matsuda and H. Mimura: *"HSLA Steels: Metallurgy and Applications"*, eds. J. M. Gray, T. Ko, Z. Shouhua, W. Baorong and X. Xishan, ASM International, Ohio, 1985, 557.

5. K. Yamamoto, S. Matsuda, T. Haze, R. Chijiiwa and H. Mimura: *"Residual and Unspecified Elements in Steel"*, ASM International, Ohio, USA, 1987, 1.

6. R. Chijiiwa, H. Tamehiro, M. Hirai, H. Matsida and H. Mimura: *"Offshore Mechanics and Arctic Engineering Conference (OMAE)"*, Houston, Texas, 1988, 1.

7. K. Nishioka and H. Tamehiro: *"Microalloying '88: International Symposium on Applications of HSLA Steel"*, Chicago, Illinois, USA, September 1988, 1.

8. H. K. D. H. Bhadeshia: *"Steel Technology International"*, ed. P. H. Scholes, Sterling Publications International Ltd., London, 1989, 289.

9. Y. Tomita and K. Okabayashi: *Metall. Trans. A*, 1983, **14A,** 485.

10. Y. Tomita and K. Okabayashi: *Metall. Trans. A*, 1985, **16A** 73.

11. H. K. D. H. Bhadeshia and D. V. Edmonds: *Metal Science*, 1983, **17,** 411.

12. H. K. D. H. Bhadeshia and D. V. Edmonds: *Metal Science*, 1983, **17,** 420.

13. V. T. T. Miihkinen and D. V. Edmonds: *Materials Science and Technology*, 1987, **3,** 422.

71

14. V. T. T. Miihkinen and D. V. Edmonds: *Materials Science and Technology,* 1987, **3**, 432.

15. V. T. T. Miihkinen and D. V. Edmonds: *Materials Science and Technology,* 1987, **3**, 441.

16. R. F. Hehemann: *Phase Transformations,* ASM, Metals Park, OH, USA, 1970, 397.

17. J. W. Christian and D. V. Edmonds: *Int. Conf. on "Phase Transformations in Ferrous Alloys",* A. R. Marder and J. I. Goldstein eds., TMS–AIME, Warrendale, PA, USA, 1984, 293.

18. H. K. D. H. Bhadeshia and J. W. Christian: *Metall. Trans. A,* 1990, **21A**, 767.

19. A. Hultgren: *Trans. ASM,* 1947, **39**, 915.

20. A. Hultgren: *Jernkontorets Ann.* 1951, **135**, 403.

21. M. Hillert: *Jernkontorets Ann.* 1951, **135**, 25.

22. E. Rudberg: *Jernkontorets Ann.* 1952, **136**, 91.

23. H. K. D. H. Bhadeshia: *Acta Metall.,* 1981, **29**, 1117.

24. S. J. Matas and R. F. Hehemann: *Trans. TMS-AIME,* 1961, **221**, 179.

25. A. Schrader and F. Wever: *Arch. Eisenhüttenwesen,* 1952, **23**, 489.

26. H. K. D. H. Bhadeshia and A. R. Waugh: *Acta Metall.,* 1982, **30**, 775.

27. I. Stark, G. D. W. Smith and H. K. D. H. Bhadeshia: *Phase Transformations '87* G. W. Lorimer ed., Institute of Metals, London, 1988, 211.

28. E. C. Bain: *"Alloying Elements in Steel",* ASM, Cleaveland, OH, USA,, 1939.

29. W. S. Owen: *Trans. ASM,* 1954, **46**, 812.

30. J. Gordine and I. Codd: *JISI,* 1969, **207.1**, 461.

31. R. M. Hobbs, G. W. Lorimer, N. Ridley: *JISI,* 1972, **210.2**, 757.

32. A. G. Alten and P. Payson: *Trans. ASM,* 1953, **45**, 498.

33. E. E. Langer: *Metal Science Journal,* 1968, **2**, 59.

34. P. P. Koistinen and R. E. Marburger: *Acta Metall.,* 1959, **7**, 59.

35. N. Usui, K. Sugimoto, E. Nishida, M. Kobayashi and S. Hashimoto: *CAMP-ISIJ,* 1990, **3**, 2013.

36. H. K. D. H. Bhadeshia: *Metal Science* 1982, **16**, 159.

37. K. C. Russell: *Acta Metall.* 1968, **16**, 761.

38. K. C. Russell: *Acta Metall.,* 1969, **17**, 1123.

39. J. W. Christian: *"The Theory of Transformations in Metals and Alloys",* Part I, 2nd edition, Pergamon Press, Oxford, 1975.

40. H. K. D. H. Bhadeshia: *"Phase Transformation '87",* G. W. Lorimer ed., Institute of Metals, London, , 1988, 309.

41. R. H. Siller and R. B. McLellan: *Metall. Trans. A,* 1970, **1**, 985.

42. H. K. D. H. Bhadeshia: *Metal Science,* 1981, **15**, 477.

43. M. Takahashi and H. K. D. H. Bhadeshia: *Materials Science and Technology* 1990, **6**, 592.

44. F. B. Pickering: *"Transformation and hardenability in steels",* Ann Arbor, MI, Climax Molybdenum, 1967, 109.

45. J. S. Kirkaldy: *Canadian Journal of Physics,* 1958, **36**, 899.

46. D. E. Coates: *Metall. Trans.* 1972, **3**, 1203.

47. C. Wagner: *"Thermodynamics of Alloys",* Addison–Wesley, Reading, Massachusetts, USA, 1952, 53.

48. W. W. Gerberich, G. Thomas, E. R. Parker and V. F. Zackay: *2nd Int. Conf. "Strength of Metals and Alloys",* ASM, Metals Park, Ohio, USA, 1970, **3**, 894.

49. E. R. Parker and V. F. Zackay: *Engineering Fracture Mechanics,* 1975, **7,** 371.

50. J. H. Shively, R. F. Hehemann and A. R. Troiano: *Corrosion,* 1966, **22,** 253.

51. R. Kerr, F. Solana, I. M. Bernstein and A. W. Thompson: *Metall. Trans. A,* 1987, **18A** 1011.

52. F. Solana, C. Takamatate, I. M. Bernstein and A. W. Thompson: *Metall. Trans. A,* 1987, **18A,** 1023.

53. R. M. Horn and R. O. Ritchie: *Metall. Trans. A,* 1978, **9A,** 1039.

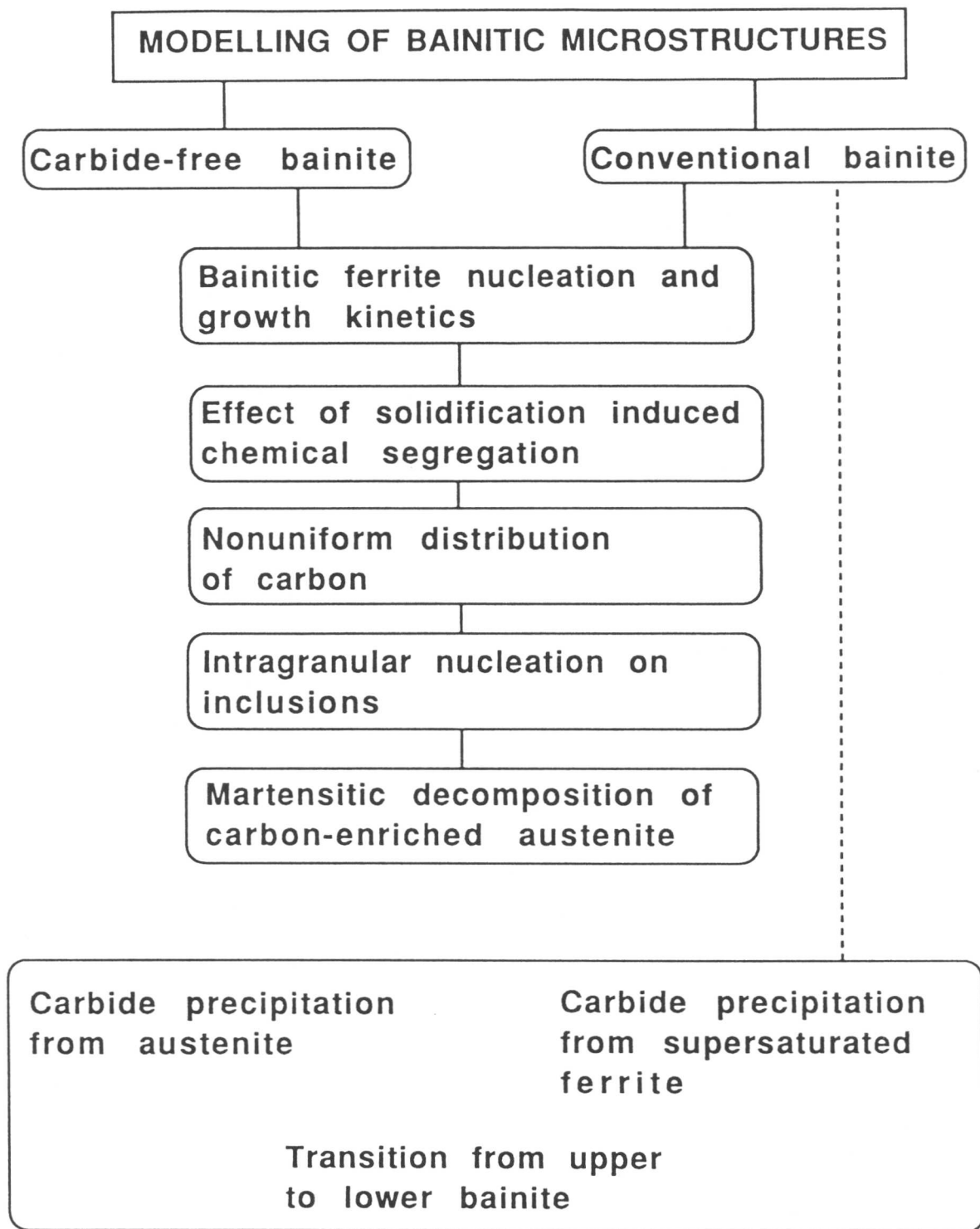54. B. P. J. Sandvik and H. P. Nevalainen: *Metals Technology,* 1981, **13,** 213.

Fig. 3.1 Flow chart summarising the aspects of transformation which need to be addressed in order to be able to generally predict the microstructure of bainitic steels.
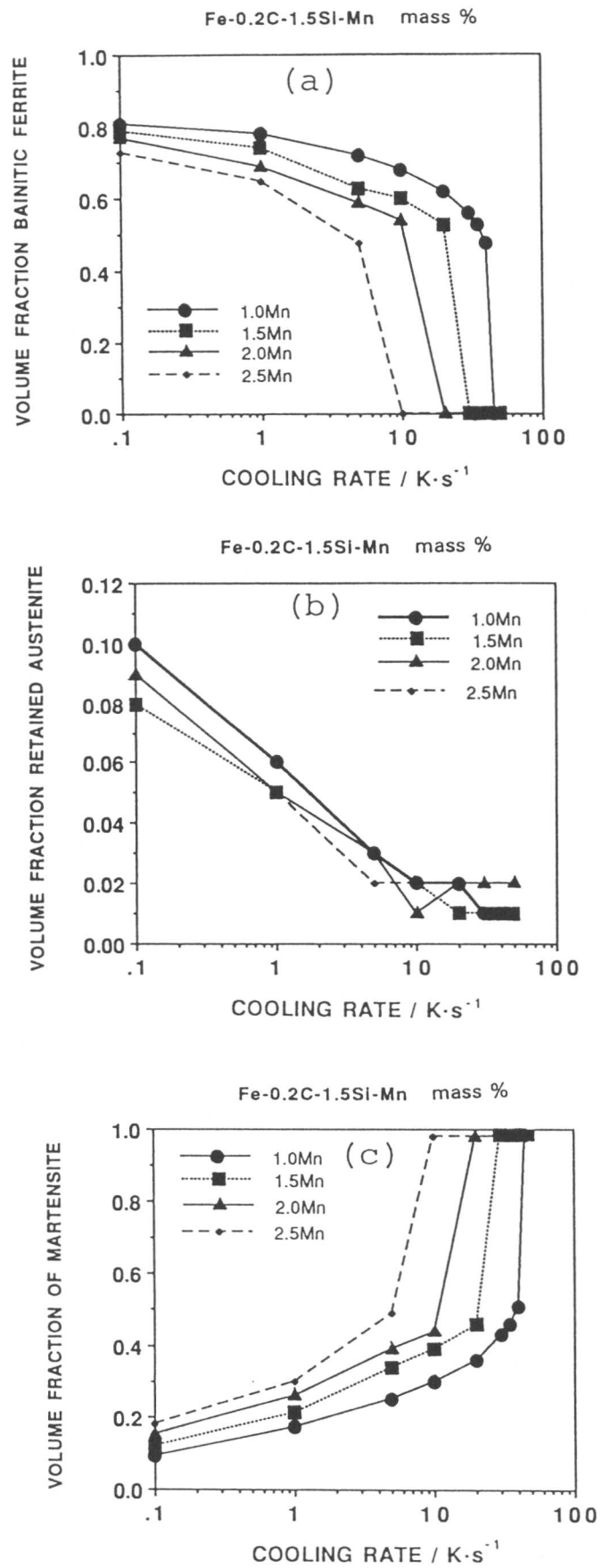
Fig. 3.3 Typical calculated microstructure for a series of Fe-Mn-Si-C alloys.
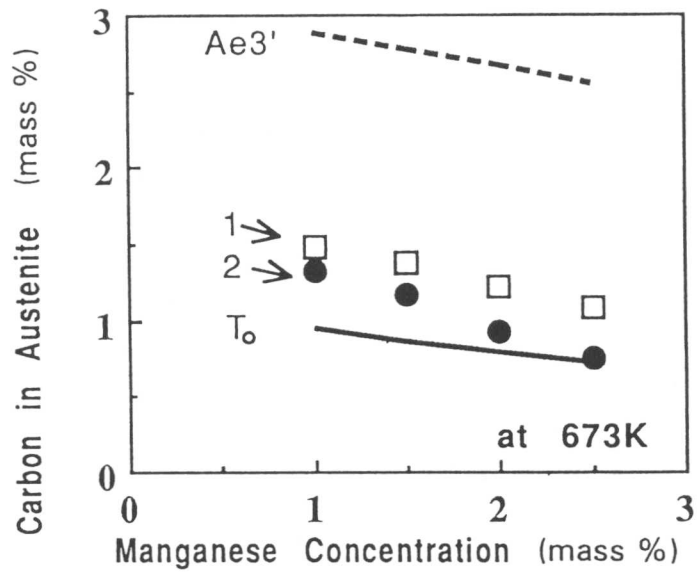
75

Fig. 3.2 An analysis of published data [35] on the carbon concentration of retained austenite in a mixed microstructure of bainitic ferrite, martensite and retained austenite. The calculations of the Ae_3' and T_0 curves were carried out as described in [11,12]. Usui *et al.* [35] measured the lattice parameter of austenite and used a relationship between the parameter and carbon concentration to deduce the data illustrated by curve 1. A better parameter/carbon relation is used here to generate curve 2. It is evident that there is good agreement of the austenite composition with that predicted by the T_o calculations.
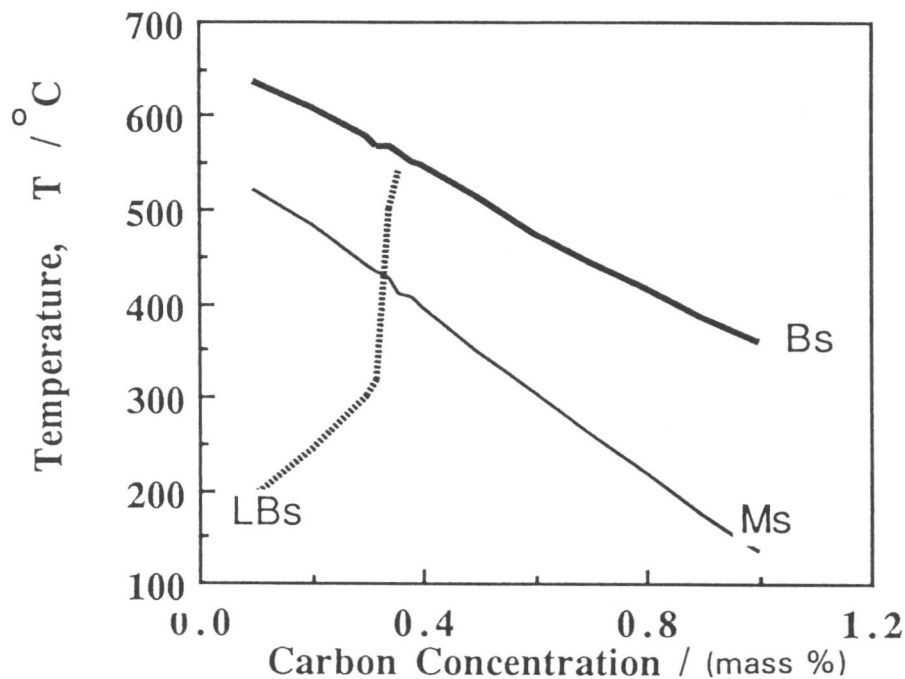
Fig. 3.4 Prediction of the upper to lower bainite transition temperature as a function of the carbon concentration for a series of plain carbon steels [43]. B_S, L_S and M_S represent the bainite-start, lower bainite-start and martensite-start temperatures. Both calculation and theory seem to indicate that only upper bainite is obtained with the carbon concentration for Fe-C alloys is less than about 0.4 wt.%, and only lower bainite when that concentration is exceeded.
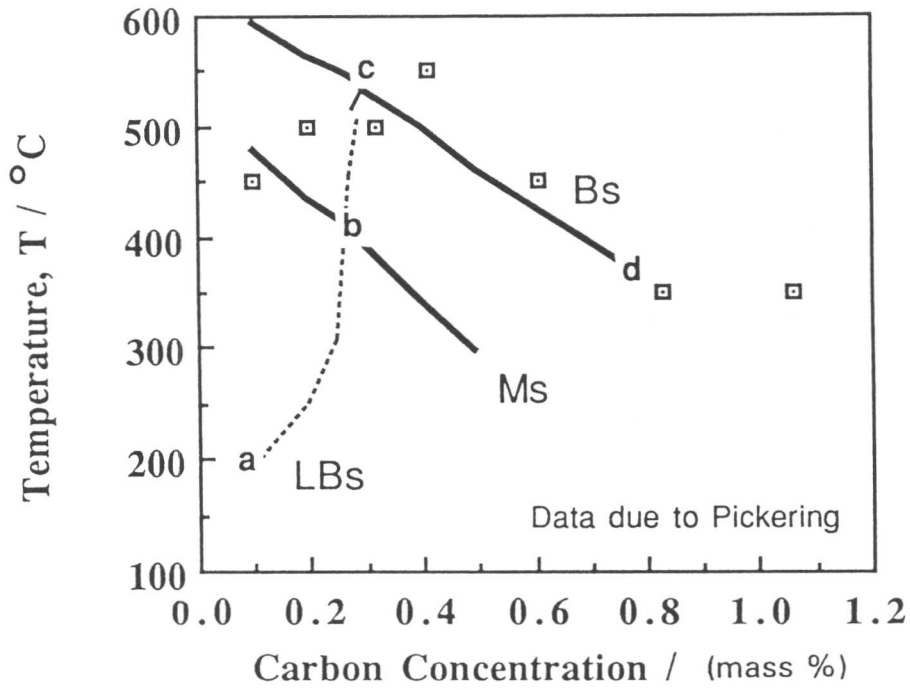
Fig. 3.5 Comparison between calculated and observed upper to lower bainite transition temperature in Fe-Mn-Mo-C alloys. Observed data (circle) is after Pickering [44]. On applying the model [43] to the data, the effect of substitutional alloying elements on carbide precipitation kinetics is not taken into account.
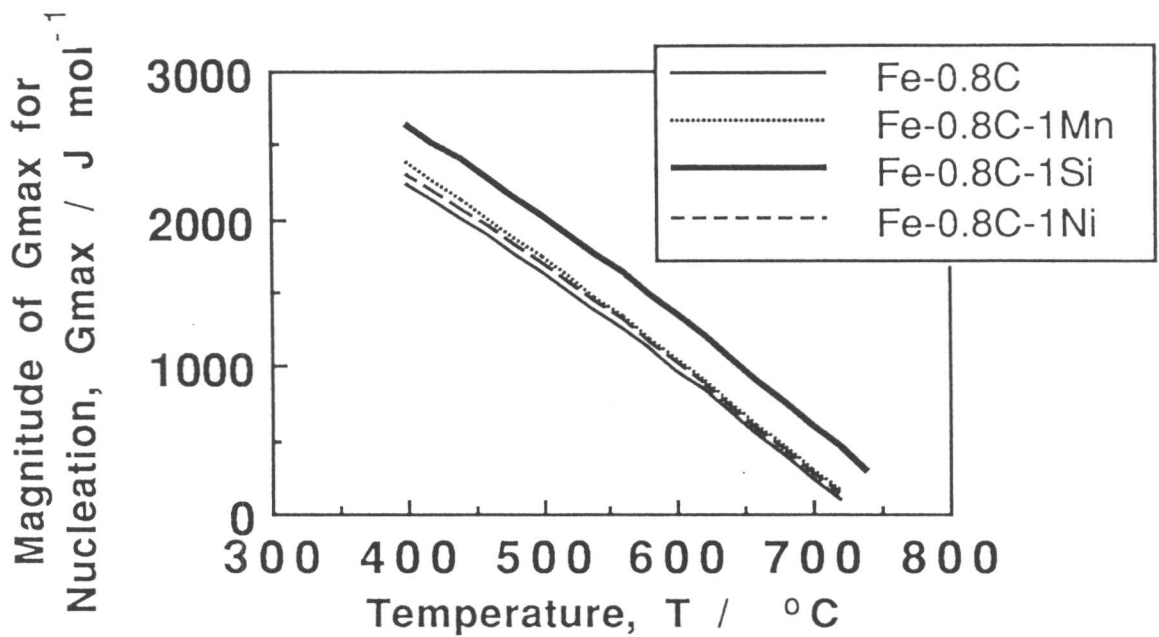
Fig. 3.6 Calculated maximum free energy change (G_{max}) due to the nucleation of cementite from austenite in Fe-0.8C-X wt.% ternary alloys, assuming that the cementite nuclei have the equilibrium composition.

77
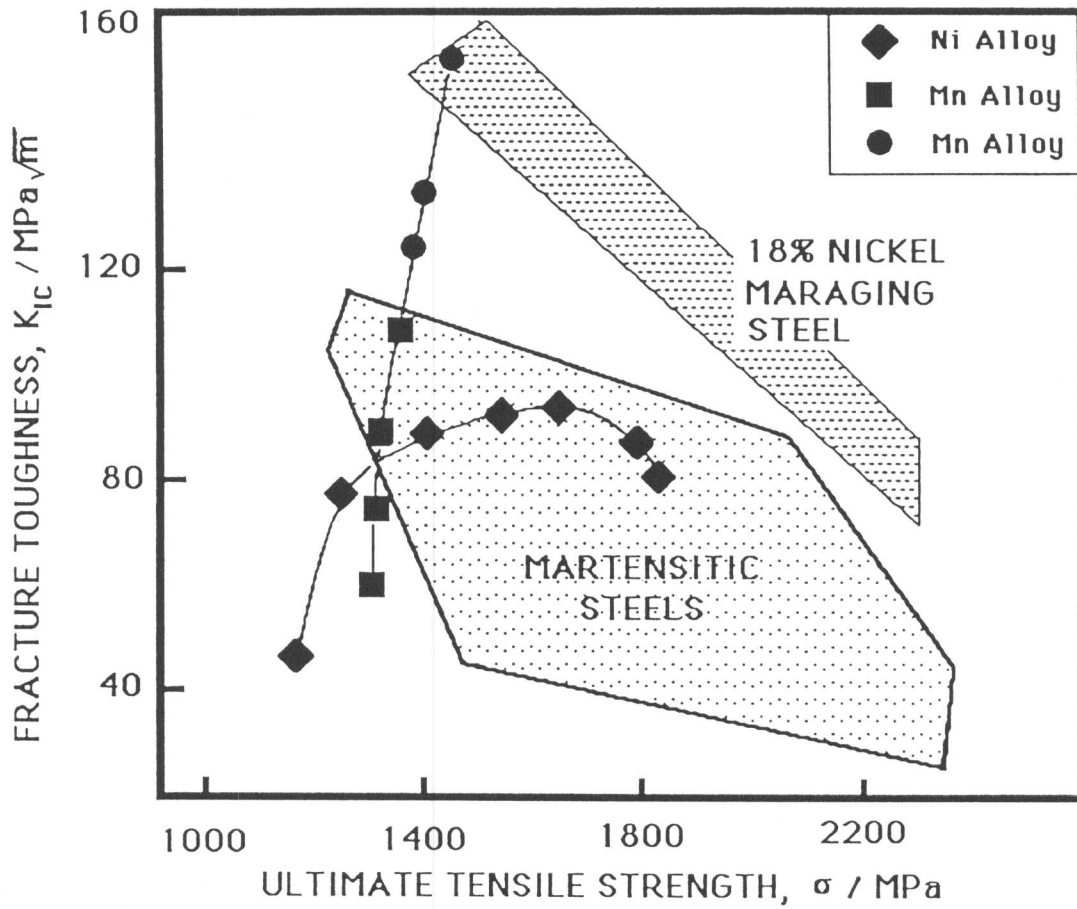
Fig. 3.8 Comparison of the mechanical properties of mixed microstructure of bainitic ferrite and austenite, versus those of quenched and tempered martensitic alloys [15].
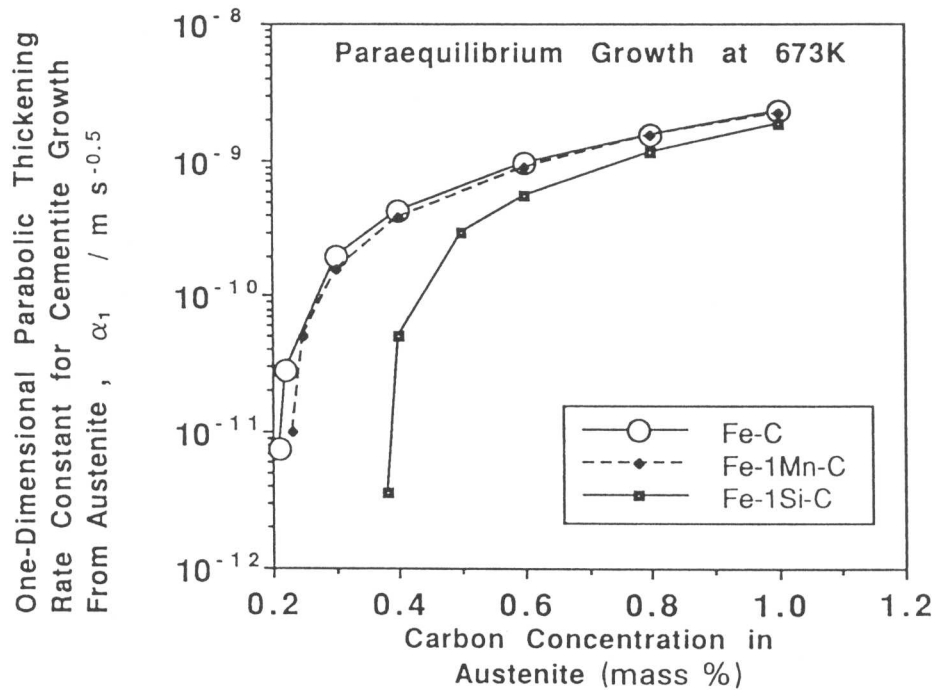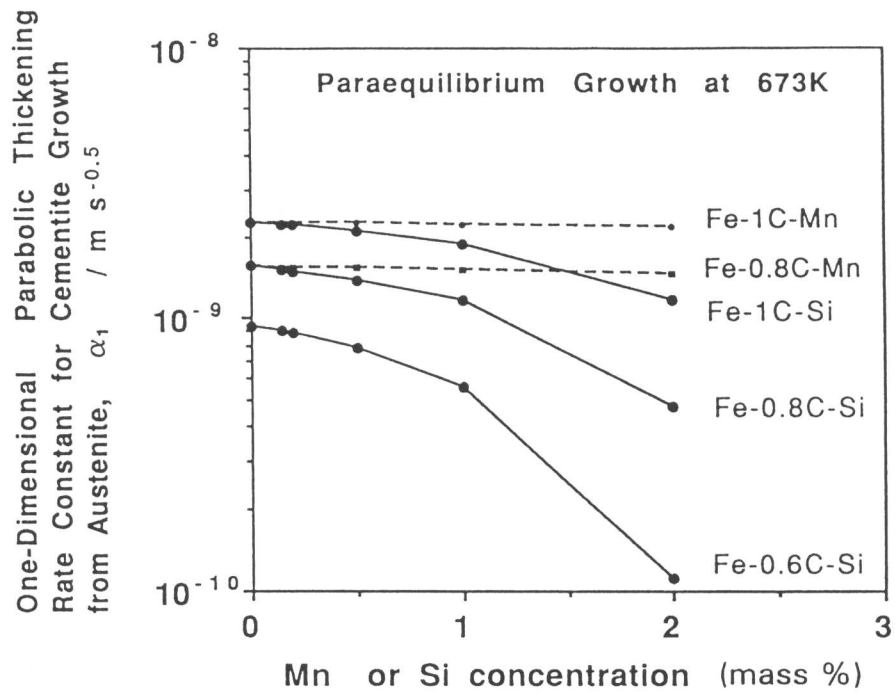
Fig. 3.7 Parabolic thickening rate constants for the paraequilibrium growth of cementite allotri-
omorphs from austenite.

CHAPTER 4

REAUSTENITISATION FROM A MIXTURE OF BAINITE AND AUSTENITE

4.1 INTRODUCTION

In this chapter, reaustenitisation from a mixture of ferrite and austenite is studied since it may then proceed only by the growth of pre-existing austenite. The nucleation of austenite may not therefore be a controlling factor. For this purpose, a mixture of bainitic ferrite and residual austenite was selected as the initial microstructure. Prior to reaustenitisation experiments from a mixture of bainitic ferrite and austenite, the bainite transformation itself was studied to better understand the mechanism of transformation. Fe-C-Cr and Fe-C-Si-Mn alloys were used for this purpose.

4.2 EXPERIMENTAL PROCEDURE

A Fe-0.30C-4.08Cr wt.% ternary alloy was used to study reaustenitisation from a mixture of a bainitic ferrite and austenite. The same material has been studied separately by Bhadeshia [1,2].

All dilatometry was performed on a Theta industries high speed dilatometer, which has a water cooled radio-frequency furnace of essentially zero thermal mass, since it is only the specimen which undergoes the programmed thermal cycle. The length transducer on the dilatometer was calibrated using a pure platinum specimen of known thermal expansion characteristics. The dilatometer has been specially interfaced with a BBC/Acorn microcomputer so that length, time and temperature information can be recorded at microsecond intervals during the heat cycle, and the data are stored on a floppy disc. The information is then transferred to a mainframe IBM3084 computer for further analysis. Specimens for dilatometry were machined in the form of 3 mm diameter rods with about 20 mm of length. To avoid surface nucleation and surface degradation, they were plated with nickel. This nickel plating process is in two stages; nickel striking and nickel plating. Striking was carried out in a solution made up of 250g nickel sulphate, 27 ml concentrated sulphic acid and distilled water, amounting to one litre in all, at $50\,^{\circ}$C with a current density of 7.75 mA mm^{-2} for three minutes. The plating solution consisted of 140g nickel sulphate, 140g anhydrous sodium sulphate, 15g ammonium chloride and 20g boric acid, was made up to one litre with distilled water. The plating was carried out at $50\,^{\circ}$C with a current density of 0.4 mA mm^{-2} for fifteen minutes. This two processes finally give a plate thickness of approximately 0.08 mm.

Isothermal and continuous heating reaustenitisation experiments from a mixture of bainitic ferrite and austenite have been carried out on the dilatometer. All specimens used in the experiments were heated at $1100\,^{\circ}$C for 30 min and quenched in water with ice, to get a martensitic microstructure prior to the actual heat treatments.

In order to obtain a mixture of bainite and austenite, specimens were reaustenitised at $1000\,^{\circ}$C for 10 min and quenched to selected bainite transformation temperatures, 420, 448, $472\,^{\circ}$C and held there for 30 min. The quenching from the reaustenitising temperature to the bainite transformation temperatures was conducted in the dilatometer using helium gas giving about $30\,^{\circ}$C s^{-1} of cooling rate between $800\,^{\circ}$C and $500\,^{\circ}$C, where the diffusional transformation of austenite was expected to occur. The calculated [3] time-temperature-transformation

(TTT) curve for the Fe-0.3C-4.08Cr wt.% alloy is shown in Fig. 4.1. According to this calculation, the equilibrium transformation temperature from austenite to ferrite Ae_3, paraequilibrium transformation temperature from austenite to ferrite Ae'_3, bainite-start temperature B_S and martensite-start temperature M_S are 781, 730, 492, 348 °C respectively. As it can be seen in the figure, the depressed diffusional C-curve (upper C-curve) makes the formation of bainite directly from austenite easy. In fact, no evidence of transformation during helium quenching was observed from the length change of the specimens on quenching to the bainite transformation temperatures.

Following to isothermal transformation to a mixture of bainite and residual austenite, the specimens were heated directly to isothermal reaustenitisation temperatures of interest without being cooled below the bainite transformation temperatures. Isothermal reaustenitisation experiments were carried out at temperatures between 720 °C and 820 °C with a rapid heating from the bainite transformation temperatures at around 500 °C s^{-1}. Continuous heating reaustenitisation experiments at heating rates between 0.1 and 11.0 °C s^{-1} were also carried out to study the formation of austenite on heating. We emphasize again that the reaustenitisation treatments were started directly from the bainite transformation temperatures after 30 min of isothermal holding without cooling below it (Fig. 4.2).

After the isothermal reaustenitisation at each reaction temperature, the specimens have been helium quenched to ambient temperature to freeze the completely or partially transformed austenite into untempered martensite for metallographic study and other experiments.

Prior to the experiments, all specimens were homogenised at 1250 °C for 3 days while sealed in quartz tubes containing a partial pressure of pure argon, and they were quenched into iced-water to get fully martensitic microstructure.

Optical microscopy was carried out on an Olympus microscope and photographs were taken by using an Olympus camera fitted to the microscope. Specimens were hot mounted in acrylic plastic, and ground on silicon carbide paper to a sufficient depth to remove any unrepresentative surface, and then mechanically ground down to 1200 grade emery paper and finally polished with 6 and 1 μm diamond pastes. Before optical microscopy, specimens were etched using 2% nital.

Microhardness measurements were done on a Leitz hardness measuring digital eyepiece with the option of Vickers hardness tester to which a computer-counter-printer is attached. Specimens were polished and etched by 2% nital before the measurements. The indentation load applied was selected either 0.0981 N or 98.1 N in each case.

Thin foil specimens were prepared for transmission electron microscopy from 0.25 mm thick discs slit from specimens used in the dilatometry. The discs were ground to about 0.04 mm by abrasion on 1200 grade emery paper and then electro-polished in a twin jet electro-polisher using a 5% perchloric acid, 25% glycerol and 70% ethanol mixture solution either at ambient temperature or at around 0 °C, and 50 V. The microscopy was conducted on either a Philips EM300 or a Philips EM400T transmission electron microscopes operated at 100 or 120 kV.

4.3 BAINITE TRANSFORMATION

Isothermal experiments were conducted to examine the nature of bainite transformation which is used to obtain the initial microstructure for reaustenitisation experiments. Fe-2.0Si-3.0Mn wt.% systems with four different carbon contents; 0.059, 0.12, 0.22 and 0.43 wt%, were studied as well as the Fe-0.3C-4.08Cr wt.% alloy.

4.3.1 Bainite transformation in the Fe-0.3C-4.08Cr wt.% alloy

Three bainite transformation temperatures were selected to obtain three different mixtures of bainite and residual austenite. The relative length changes during isothermal bainite transformation at these temperatures are shown in Fig. 4.3. It can be seen that 30 min of holding at each bainite transformation temperature is long enough to allow the specimen to stop reacting.

In interpreting the experimental data, it is usually assumed that the dimensional change observed during isothermal reaction is proportional to the volume fraction of transformation, and it is sometimes assumed that the point where dimensions cease to change represents a 100% of transformation. When reaction ceases before the parent phase has completely transformed, it is useful to be able to calculate the volume fraction of product phase that has been obtained. For the transformation of austenite (γ) into a mixture of bainitic ferrite and carbon-enriched austenite, Bhadeshia [3] has shown that the relative length change can be related to the volume fraction of ferrite (V_α) by the equation:

$$\frac{\Delta L}{L} = \frac{2V_\alpha a_\alpha^3 + (1 - V_\alpha)a_\gamma^{*3} - a_\gamma^3}{3a_\gamma^3} \tag{4.1}$$

with

$$a_\alpha = a_{\alpha 0}(1 + \beta_\alpha(T - 300))$$

$$a_\gamma = a_{\gamma 0}\{\overline{x}_1, x_i^\gamma\}[1 + \beta_\gamma(T - 300)]$$

$$a_\gamma^* = a_{\gamma 0}\{x_1^\gamma, x_i^\gamma\}[1 + \beta_\gamma(T - 300)]$$

where
$\frac{\Delta L}{L}$: length change due to transformation per unit length,

$\beta_{\alpha,\gamma}$: linear thermal expansion coefficients of ferrite and austenite respectively, K^{-1},

$\overline{x}_1$: average carbon content in the steel, mole fraction,

x_i^γ : alloy concentrations in austenite, mole fraction; i's denote different alloying element,

x_1^γ : carbon content of residual austenite at any stage of the reaction, mole fraction,

$a_{\gamma 0}$: lattice parameter of austenite at ambient temperature as a function of chemical concentrations in the austenite,

a_γ : lattice parameter of austenite at the reaction temperature before the reaction,

a_γ^* : lattice parameter of austenite at reaction temperature at any stage of the reaction,

$a_{\alpha 0}$: lattice parameter of ferrite at ambient temperature (300 K),

a_α : lattice parameter of ferrite at reaction temperature.

In equation (4.1), it is assumed that $\frac{\Delta L}{L}$ is a third of the relative volume change $\frac{\Delta V}{V}$; this is a very good approximation since the changes in density during transformations in steels are small. For the same reason, the implicit assumption that mass fractions are identical is also justified. If this last assumption is avoided, we obtain [4]:

$$\frac{\Delta L}{L} = \left\{1 + \frac{1}{a_\gamma^3}\left[\frac{2a_\alpha^3 a_\gamma^{*3}}{V_\alpha a_\gamma^{*3} + 2(1 - V_\alpha)a_\alpha^3} - a_\gamma^3\right]\right\}^{1/3} - 1 \tag{4.2}$$

However the difference between the results from equation (4.1) and (4.2) is found to be negligible. The factor of two in the numerator of equation (4.1) arises because the unit cell of ferrite contains two iron atoms whereas that of austenite has four.

Note that equation (4.1) can be used for all situations where austenite decomposes into a mixture of carbon-enriched residual austenite and ferrite, and furthermore, the ferrite may or may not be supersaturated with respect to carbon, since the effect of excess carbon is manifested in an alteration of the lattice parameter of the ferrite. Using a similar method, the following equation can be derived for the case where cementite precipitation occurs in conjunction with ferrite formation from austenite [4]:

$$\frac{\Delta L}{L} = \frac{2V_\alpha a_\alpha^3 + V_\theta a_\theta^3/3 + (1 - V_\alpha - V_\theta)a_\gamma^{*3} - a_\gamma^3}{3a_\gamma^3} \tag{4.3}$$

where

V_θ : volume fraction of cementite,

a_θ^3 : $a_\theta b_\theta c_\theta$,

$a_\theta, b_\theta, c_\theta$: lattice parameters of cementite, which are 4.51, 5.08 and 6.73 Å at ambient temperature respectively.

The volume fraction of cementite, where the total carbon content in ferrite including any cementite particles is S, can be obtained as follows assuming all carbon atoms in the ferritic matrix are locked in cementite:

$$V_\theta = \frac{1}{1 + k_\theta} \tag{4.4}$$

with

$$k_\theta = \frac{a_\alpha^3(1 - 3\frac{S}{x_0^\alpha})}{a_\theta^3 \frac{1}{2}\frac{S}{x_0^\alpha}}$$

where x_0^α is iron mole fraction in ferrite.

The dependence of the lattice parameter of austenite on alloying elements was reported by Ridley *et al.* [5] and Dyson and Holmes [6], giving,

$$a_{\gamma 0} = 3.573 + 0.0065\text{C} + 0.0010\text{Mn} - 0.0002\text{Ni} + 0.0006\text{Cr} + 0.0056\text{N} + 0.0028\text{Al}$$
$$- 0.0004\text{Co} + 0.0014\text{Cu} + 0.0053\text{Mo} + 0.0079\text{Nb} + 0.0032\text{Ti}$$
$$+ 0.0017\text{V} + 0.0057\text{W}$$

where chemical composition and $a_{\gamma 0}$ are measured in at% and Å respectively.

The carbon concentration of residual austenite x_1^γ is related to the volume fraction V_α of ferrite or ferrite and cementite transformed, and expressed by :

$$x_1^\gamma = \frac{\overline{x}_1 - V_\alpha S}{1 - V_\alpha} \tag{4.5}$$

Therefore the lattice parameter of austenite in the equations changes with the volume fraction of ferrite or ferrite and cementite.

Fig. 4.4 represents the relations between volume fractions transformed and corresponding relative length changes during transformation at 420 °C to ferrite with 0.03 wt.% carbon, to supersaturated ferrite with 0.2 wt.% carbon and to a mixture of carbon free ferrite and cementite with 0.2 wt.% of carbon locked in the transformed phases altogether respectively. In these

calculations, the expansion coefficients of ferrite and austenite are taken to be 1.1826×10^{-5} and $1.8431 \times 10^{-5} \mathrm{K}^{-1}$ [3], and the linear expansivity of cementite is assumed to be the same as that of ferrite. It is evident that the linearity between volume fraction of transformation products and corresponding relative length change is preserved, at least, up to 0.7 of the volume fraction.

It is emphasized however in equations (4.1), (4.2) and (4.3) that it is never justified that the maximum length change observed during isothermal transformation corresponds to the complete transformation of austenite [4]. Bainite transformation in steels is considered to be a good example of this. Although the growth of bainitic ferrite is displacive and diffusionless, carbon redistribution can occur *after* the reaction because bainite transformation usually takes place at higher temperatures where carbon atoms can still move very quickly. As a consequence, the carbon enrichment of residual austenite occurs. The following formation of bainitic ferrite occurs from the carbon-enriched residual austenite causing further enrichment of carbon in the residual austenite. When the carbon concentration in residual austenite reaches the T_0' curve (where ferrite, whose free energy has been raised by a stored energy term (400 $\mathrm{J\,mol^{-1}}$ [7]) associated with the transformation strain, and austenite of identical composition have the same free energy) further diffusionless formation of ferrite becomes thermodynamically impossible since it requires a positive free energy change as shown in Fig. 4.5: this is referred to as the incomplete reaction phenomenon. Therefore even when the reaction is observed to have stopped, carbon enriched austenite can still exist if other competing processes such as cementite precipitation directly from the carbon enriched austenite and reconstructive formation of ferrite, such as pearlite formation do not overlap the reaction. This can actually be seen in Fig. 4.6 where a relative length change during helium quenching after the completion of bainite transformation at 420 °C is presented. There is an expansion which corresponds to martensitic transformation of untransformed austenite at 420 °C on cooling.

The calculated carbon concentrations of residual austenite after 30 min of isothermal holding at 420, 448 and 472 °C in the Fe-0.3C-4.08Cr wt.% alloy were plotted in Fig. 4.7, where the calculated Ae_3, Ae_3', T_0 and T_0' curves were also drawn. The calculation of the Ae_3 curve is based on the work reported by Gilmour *et al.* [8] and Kirkaldy *et al.* [9], and the other values are calculated according to Bhadeshia's work [10]. The error bars correspond to the values of the carbon content of ferrite, S, between 0.03 and 0.2 wt.% [3]. The calculated carbon contents of residual austenite from the maximum relative length change during the isothermal bainite transformation are in good agreement with the T_0' curve. This shows that bainite transformation ceases well before the equilibrium condition is achieved, thus establishing that bainitic ferrite grows by a diffusionless transformation mechanism with carbon redistribution *after* the initial growth event.

The microstructure of a specimen which was helium quenched after 30 min of isothermal bainite transformation at the temperature consists of martensite, which was austenite before the helium quench, and some retained austenite and bainite (Fig. 4.8), as it was expected from the TTT curve of the material used (see Fig. 4.1) and its thermal history. Micro-hardness measurements show 802 Hv{10g} for martensite which is the white etched area in the picture and 550 Hv{10g} for bainite.

As it can be seen in a TEM micrograph of a specimen quenched after the termination of bainite transformation at 420 °C (Fig. 4.9), the initial microstructure shows a typical lower bainitic microstructure. An average thickness of the residual austenite films was about 0.04μm whereas

the average thickness of bainitic ferrite plates was found to be 0.3μm. The ferrite matrix (which is plate or lath in shape) contains cementite particles as it can be seen in the figure. As discussed in Chapter 2, the cementite particles in lower bainite are considered to have precipitated directly from carbon supersaturated bainitic ferrite. The cementite particles which can be seen within bainitic ferrite seem to have a very similar orientation as it can be seen in the TEM micrograph. It is usually said that cementite particles which precipitate from carbon supersaturated bainitic ferrite show a single variant; this can be seen in Fig. 4.9. This is sometimes taken as evidence of cementite precipitation at interfaces between bainitic ferrite and austenite matrix, instead of within the bainitic ferrite. It is not understood why cementite particles in lower bainite have a single variant. However, a multi-variant cementite precipitation is also observed in some cases although the possibility of a sectioning effect has not been assessed. Fig. 4.10 shows a TEM micrograph of the Fe-0.3C-4.08Cr wt.% alloy isothermally held at 478 °C for 23 days after austenitisation at 1000 °C. The microstructure is still a mixture of bainite and austenite, and the bainitic ferrite seems to contain multi-variant cementite precipitation.

4.3.2 Bainite transformation in Fe-2.0Si-3.0Mn system

In order to investigate the formation of ferrite without carbide, Fe-Si-Mn alloys with different levels of carbon content were examined. A Mn addition can suppress the upper (reconstructive) C-curve, and provides a remarkable difference in incubation periods for the displacive and reconstructive formation of ferrite below the B_S temperature. Since the solubility of Si in cementite is extremely small, a Si addition can retard remarkably the cementite precipitation from untransformed carbon enriched austenite. Therefore, the alloys are ideal for examining the formation of ferrite from austenite without any carbide precipitation throughout a wide range of reaction temperatures. The materials used in the present experiment were Fe-2.0Si-3.0Mn wt.% alloys with 0.059, 0.12, 0.22 and 0.43 wt% of carbon respectively. All specimens were homogenised at 1250 °C for 3 days prior to the experiments. After being heated to 950 °C for 10 min, specimens were helium quenched to and held at various ferrite formation temperatures for an extended period of time in the dilatometer which allows the specimens to complete the reaction. First the bainite transformation temperature for each alloy was selected as such to give the identical free energy change due to the transformation from austenite to ferrite: -615 J mol^{-1} calculated as discussed by Bhadeshia [11]. The bainite transformation temperatures used in the experiment were listed in Table 4.1 for each alloy with its bainite-start and martensite-start temperatures. In addition to these temperatures, a bainite transformation temperature, 270 °C for Fe-0.43C-2.0Si-3.0Mn wt.% alloy at which austenite is expected to transform to lower bainite instead of to upper bainite, and temperatures between 400 and 500 °C for the Fe-0.12C-2.0Si-3.0Mn wt.% alloy were used to examine the incomplete reaction phenomenon in bainite transformation.

The relative length changes obtained during the bainite transformation are shown in Fig. 4.11. It can be seen that the holding time is long enough to allow the reaction to cease during the isothermal holding at each reaction temperature. Typical TEM micrographs for upper and lower bainite obtained in the present experiments in the Fe-0.43C-2.0Si-3.0Mn wt.% alloy are shown in Fig. 4.12. The relative length changes were then converted to the volume fractions of ferrite transformed during the isothermal holding and the carbon concentrations in untransformed austenite using equation (4.1). The calculated results can be seen in Table 4.2. These calculated carbon concentrations at the end of the bainite transformation were plotted

Carbon content wt%	T_b, °C	B_S	M_S
0.059	495	545	422
0.12	470	515	388
0.22	435	475	337
0.43	350	398	227

Table 4.1: Bainite transformation temperature T_b for each alloy used in the experiment at which the free energy change due to ferrite transformation is identical; *i.e.* −615 J mol^{-1}. Calculated B_S, and M_S temperatures are also listed.

in a calculated phase diagram of Fe-2.0Si-3.0Mn wt.% system (Fig. 4.11). It can be clearly seen that the bainite transformation has terminated far before the residual austenite reaches its equilibrium in the system, and that the carbon concentrations in the residual austenite are close to the T_0' curve even in the case of lower bainite transformation at 270 °C in the Fe-0.43C-2.0Si-3.0Mn wt.% alloy. The calculated result for 270 °C in Table 4.2 did not take into account of cementite precipitation in ferrite. When the total carbon content in ferrite including any cementite is altered up to 0.2 wt.%, the calculated x_1^γ varies between 0.028 and 0.030 mole fraction.

Carbon content, wt%	T_b, °C	$\Delta L/L$	x_1^γ, mole fraction
0.059	495	0.00318	0.004
0.12	470	0.00334	0.010
0.22	435	0.00226	0.014
0.43	350	0.00343	0.035
0.43	270	0.00299	0.030

Table 4.2: Carbon concentration in residual austenite calculated by equation (4.1).

A TEM micrograph of a specimen which was allowed to transform partially to bainite at 350 °C shows that a bainite sheaf consists of many small units of bainitic ferrite plates which form side by side. An extension of bainite sheaf seems to stop at a prior austenite grain boundary or when it encounters one of the neighbouring bainite sheaves as can be seen in Fig. 4.13. Although it is not clear from the micrograph, the two bainite sheaves which touch may have started from different points in the same austenite grain, since an identical origin of the start of the extension of a bainite sheaf may have one direction of propagation.

Fig. 4.14 shows a lower bainite microstructure obtained at 270 °C. Untransformed austenite is trapped between two adjacent bainitic ferrite plates.

As clarified by isothermal bainite transformation experiments in the Fe-2.0Si-3.0Mn and Fe-0.3C-4.08Cr wt.% alloys, transformation stops when the average carbon concentration in austenite reaches the T_0 or the T_0' curves. This means that the microstructure at the completion of bainite transformation consists of bainitic ferrite and austenite as long as no additional reaction, such as cementite precipitation from untransformed austenite or pearlite formation, overlaps with the bainite reaction. Therefore a mixture of bainitic ferrite and austenite can be obtained easily for use as an initial microstructure for reaustenitisation experiments.

4.4 ISOTHERMAL REAUSTENITISATION FROM A MIXTURE OF BAINITE AND AUSTENITE

Isothermal reaustenitisation from a starting microstructure of bainitic ferrite and residual austenite was studied in the Fe-0.3C-4.08Cr wt.% alloy (heat cycle 3 in Fig 4.2). The nucleation of austenite is therefore unnecessary during reheating experiments thereby allowing growth effects to be studied in isolation.

4.4.1 Microstructural study

A bainite transformation temperature of 420 °C was used to obtain a mixture of bainite and austenite as the initial microstructure for the experiments.

Optical and transmission electron microscopy was carried out on specimens quenched after 30 min of isothermal reaustenitisation at different reaustenitisation temperatures. No transformation except martensitic transformation was detected during the helium quench to ambient temperature.

Optical micrographs of isothermally reaustenitised specimens are presented in Fig. 4.15. The white areas correspond to martensite, which was austenite at the reaction temperature, and the dark etched area is tempered bainite which remained untransformed during austenitisation. The volume fraction of austenite increases with the reaction temperature and reaches unity above 805 °C (Fig. 4.15). At a temperature slightly below 805° C, the martensitic microstructure shows traces of a residual bainitic microstructure indicating the existence of some chemical heterogeneity.

Although the volume fraction of austenite changes significantly with the reaction temperature, the morphology of the untransformed bainite does not show large differences. This suggests that reaustenitisation proceeds by the dissolution of the bainitic ferrite and there was no evidence of independent nucleation of austenite. The pre-existing austenite simply grows by the motion of the original α_b/γ interfaces as discussed by Yang and Bhadeshia [12-14].

A typical TEM micrograph of a specimen quenched after isothermal reaustenitisation is shown in Fig. 4.16. A bainitic structure still remains after 30 min of isothermal reaustenitisation at 781 °C. Since cementite is not stable at that temperature, the lower bainitic cementite precipitates have disappeared completely, and new precipitates, larger in size and located rather randomly in the tempered ferrite matrix were observed. These precipitates are expected under equilibrium conditions to be M_7C_3 chromium rich carbides confirmed by a convergent beam diffraction pattern (Fig. 4.17). Fig. 4.17 also shows that the average thickness of austenite is around $0.4\mu m$, which is far larger than that in the initial microstructure. This shows that the reaustenitisation progresses by the thickening of pre-existing austenite films at the expense of ferrite.

A TEM micrograph of a specimen reaustenitised at 778 °C is presented in Fig. 4.18. A grain boundary between the austenite and ferrite matrix can be seen in the micrograph. The dislocation density in the ferrite was found to be very low because it has been tempered at 778 °C for 30 min during the austenitisation heat treatment. The M_7C_3 precipitates were also found in the specimen. However, the size of the precipitates found in the tempered ferrite matrix was larger than those in austenite. The average particle size in the ferrite matrix was about $0.3\mu m$ compared to around $0.06\mu m$ in the austenite region. This may be understood as follows. Since the solubility of chromium in austenite is higher than that in ferrite, the particles which have precipitated in ferrite dissolved in austenite after being engulfed by the austenite. As a result, fine precipitates, which may have been dissolving during the reaction, but have not

had enough time to dissolve completely, can be found in the austenite. This is also supported by the fact that the advancing interface in Fig. 4.18 seems to have been growing towards the particles which locate in ferrite matrix. The same feature can be seen in Fig. 4.19 where no particles were observed in austenite whereas precipitates, about 0.2 μm in diameter, were found in ferrite.

The micro-hardness measurements (Fig. 4.20), show an increase in hardness with the reaction temperature. Since the hardness of martensite depends mainly on the carbon concentration, the hardness of martensite should be higher at a lower reaustenitisation temperature, where a higher carbon concentration in austenite is expected as long as there is no phase other than ferrite and austenite. There is, however, M_7C_3 carbide at these temperatures which may reduce the carbon concentration in austenite. As it is discussed in Chapter 6, the equilibrium carbon concentration in austenite decreases with superheat in the $\alpha + \gamma + M_7C_3$ region. In the $\gamma + M_7C_3$ region, on the other hand, the carbon concentration increases with temperature. Chromium concentration, however, increases monotonically with temperature. As a result, the hardenability of austenite seems to increase with austenitisation temperature.

4.4.2 Dilatometry

A contraction of specimens during reaustenitisation is expected to occur due to the difference in the density between austenite and ferrite. Typical relative length changes obtained during isothermal reaustenitisation are shown in Fig. 4.21.

In the case of high reaustenitisation temperatures, reaction starts during heating in spite of the high heating rate. Therefore in order to obtain the total degree of transformation at the reaction temperature, the relative length change should be corrected as follows [15]. Since the length change during up-quenching was recorded by the computer, the correction can be done easily as shown in Fig. 4.22. If there is no transformation during heating, the length of the specimen will vary approximately linearly with temperature due to the constant expansivity of the initial phase. Therefore the deviation from the straight line which corresponds to the linear thermal expansion of the initial microstructure must due to the transformation which occurred on heating. If the low temperature part of the curve is extrapolated to the reaction temperature, the vertical difference between the extrapolated line and the actual length change curve gives the true length change due to the transformation, as if no reaction had occurred during heating to the isothermal transformation temperature. As a result, the maximum relative length change due to the whole transformation should be ΔL_m instead of ΔL_i illustrated in the figure. This correction can be regarded as a temperature correction of the data. Consider a point i in a length versus temperature plot, with coordinates L_i and T_i. The contributions to the term L_i arises from thermal expansion and dimensional changes due to transformation during heating to the isothermal reaustenitisation temperature T_γ. We need to remove the effect of the transformation during heating to T_γ. This can be done by adding to L_i, the length increment associated with heating from T_i to T_γ, so that the corrected length L_i' is given by;

$$L_i' = L_i\{1 + \beta_i(T_\gamma - T_i)\} \qquad (4.6)$$

where β_i indicates the thermal expansivity of the initial microstructure obtained from the up-quenching part of the data. The corrected relative length changes for the data shown in Fig. 4.22 are plotted in Fig. 4.23. The maximum relative length change ΔL_m is also indicated in the figure. The relative length changes during isothermal reaustenitisation at

different reaction temperatures are compared in Fig. 4.24; these data have been temperature corrected using equation (4.6). At each reaction temperature, the relative length decreases rapidly at the beginning of the reaction. Then the reaction rate becomes sluggish and reaches a saturation value. Not only the maximum relative length change but also the reaction rate increases with reaction temperature. The maximum length changes ΔL_m due to the isothermal reaustenitisation at different reaction temperatures are plotted in Fig. 4.25. The ΔL_m increases with the reaction temperature and reaches the maximum value at around 790 °C.

Any further increase in the reaction temperature did not result in an increase in relative length change: a slight decrease in the relative length change is observed between 805 and 820 °C. This can be understood as follows. The relative length change due to the 100% transformation can be obtained as the difference in the mean atom spacing in ferrite and in austenite at the temperature: the mean atom spacing in austenite is smaller than that of in ferrite. However the thermal expansivity of austenite is larger than that of ferrite, the higher the reaction temperature the smaller the difference in the mean atom spacing is, hence the smaller relative length change due to the 100% transformation at the temperature is obtained (Fig. 4.26). While the maximum degree of the transformation increases with the reaction temperature, the relative length change due to the reaction increases until the reaction temperature is raised to the point above which the 100% reaustenitisation can occur. A further increase in the reaction temperature, however, causes the decrease in the relative length change due to the reaustenitisation because of the difference in the thermal expansivities of ferrite and austenite. Therefore the maximum in the relative length change is obtained at a certain temperature which corresponds to the Ae_3 temperature of the system.

Martensite transformation occurs during helium quenching after 30 min of isothermal reaustenitisation. The relative length changes during quenching are shown in Fig. 4.27. The higher temperature part in each graph shows a straight line corresponding to thermal contraction of the microstructure obtained at the end of the isothermal reaustenitisation. The relative length change due to transformation during quenching (Fig. 4.27 e) is due to martensitic transformation. Fig. 4.27 f shows that the relative length changes are almost the same at the reaction temperatures 805 °C and 815 °C corresponding to martensitic transformation from fully austenitic microstructures, consistent with the results discussed above.

4.4.3 Equilibrium study of the maximum degree of the reaction

As discussed by Yang and Bhadeshia [12,13], reaustenitisation from a mixture of austenite and bainite or acicular ferrite starts when the reaction temperature is raised to the Ae_3 temperature $T_{\gamma 1}$ of residual austenite in the initial microstructure, whose carbon concentration is given by the T_0' curve at the bainite or acicular ferrite transformation temperature. And partial reaustenitisation is expected to occur between $T_{\gamma 1}$ and $T_{\gamma 2}$ (the Ae_3 temperature of the steel).

The temperatures, $T_{\gamma 1}$, and $T_{\gamma 2}$, above which the completion of reaustenitisation occur in the Fe-0.3C-4.08Cr wt.% alloy can be then obtained from the phase diagram shown in Fig. 4.28. For the material used in the present experiment, the carbon content of residual austenite after the cessation of bainite transformation at 420 °C was calculated to be 0.00228 in mole fraction which is $x_{T_0'}$ at 420 °C. Paraequilibrium is assumed here for the calculation at 420 °C. The calculated Ae_3 temperatures of austenite with its carbon concentration identical to 0.00228 and the bulk carbon concentration are used to determine the temperatures $T_{\gamma 1}$ and $T_{\gamma 2}$. The temperature range of partial reaustenitisation was found to be between $T_{\gamma 1} = 751$ °C and $T_{\gamma 2} = 781°$ C. The equilibrium volume fraction of austenite at a temperature between these

two temperatures can be calculated from Ae_3 curve of the system as discussed earlier [12-14]. In the case where the carbon content of ferrite is not negligible, however, the volume fraction of austenite should also be a function of carbon concentration in ferrite transformed

$$V_\gamma\{T_\gamma\} = \frac{\bar{x}_1 - S}{x_{Ae_3}\{T_\gamma\} - S} \tag{4.7}$$

where S is carbon content of ferrite (the carbon may be in solution or in the form of precipitates in the ferrite). The calculated equilibrium volume fraction of austenite V_γ is listed in Table 4.3, where the value S has been assumed to be 0.2 wt%.

Temperature, °C	x_{Ae_3}, at.%	V_γ
750	2.30	0.33
755	2.16	0.38
760	2.01	0.42
765	1.86	0.48
770	1.72	0.57
775	1.57	0.70
780	1.42	0.91

Table 4.3: Equilibrium volume fractions of austenite at different temperatures calculated from equation (4.7)

To calculate the relative length change from the equilibrium volume fraction of austenite, three different reactions were assessed:

(1) $\alpha + \gamma(x_\gamma = x_{T_0'}) \longrightarrow \gamma(x_\gamma = x_{Ae_3}) + \alpha$

(2) $\alpha + \theta + \gamma(x_\gamma = x_{T_0'}) \longrightarrow \gamma(x_\gamma = x_{Ae_3}) + \alpha + \theta$

(3) $\alpha + \theta + \gamma(x_\gamma = x_{T_0'}) \longrightarrow \gamma(x_\gamma = x_{Ae_3}) + \alpha + \theta$ no dissolution of θ

In case (1), the starting microstructure assumed to be a mixture of ferrite (α), whose carbon content is negligibly small, and austenite (γ) whose carbon concentration can be determined by the T_0' curve at the bainite transformation temperature T_b, and the final structure of a lower quantity of ferrite and austenite with its carbon concentration is identical to that given by the Ae_3 curve at the reaustenitisation temperature. For case (2), the starting structure is assumed to be a mixture of ferrite with zero carbon content, cementite (θ) and austenite with its carbon content identical to the value at the T_0' curve. The final stage, in this case, is assumed to be a mixture of ferrite with zero carbon, cementite and austenite with the carbon content identical to the equilibrium value. The ratio of the volumes between ferrite and cementite is assumed to be the same during the reaction. In the last case, (3), the same initial structure as in the case (2) and a mixture of ferrite, cementite and austenite with the carbon content identical to the equilibrium value for the final structure are assumed. So that, in this case, no dissolution of cementite in austenite is assumed. The conversion of the equilibrium volume fraction of austenite into relative length change can be done using the following equations :
For case (1);

$$\frac{\Delta L}{L} = \frac{1}{3} \frac{a_\gamma^{*3}V_\gamma + 2a_\alpha^3(1 - V_\gamma) - a_\gamma^3 V_{\gamma 0} - 2a_\alpha^3(1 - V_{\gamma 0})}{a_\gamma^3 V_{\gamma 0} + 2a_\alpha^3(1 - V_{\gamma 0})} \tag{4.8}$$

For case (2);

$$\frac{\Delta L}{L} = \frac{1}{3} \frac{a_\gamma^{*3} V_\gamma + 2a_\alpha^3 (1 - V_\gamma)\frac{1 - V_\gamma - V_{\theta 0}}{1 - V_{\gamma 0}} + \frac{1}{3} a_\theta^3 (1 - V_\gamma)\frac{V_{\theta 0}}{1 - V_{\gamma 0}} - a_\gamma^3 V_{\gamma 0} - 2a_\alpha^3 (1 - V_{\gamma 0} - V_{\theta 0})}{a_\gamma^3 V_{\gamma 0} + 2a_\alpha^3 (1 - V_{\gamma 0} - V_{\theta 0}) + \frac{1}{3} a_\theta^3 V_{\theta 0}}$$

(4.9)

For case (3);

$$\frac{\Delta L}{L} = \frac{1}{3} \frac{a_\gamma^{*3} V_\gamma + 2a_\alpha^3 (1 - V_\gamma - V_{\theta 0}) - a_\gamma^3 V_{\gamma 0} - 2a_\alpha^3 (1 - V_{\gamma 0} - V_{\theta 0})}{a_\gamma^3 V_{\gamma 0} + 2a_\alpha^3 (1 - V_{\gamma 0} - V_{\theta 0}) + \frac{1}{3} a_\theta^3 V_{\theta 0}}$$

(4.10)

with

$$a_\alpha = a_{\alpha 0}(1 + \beta_\alpha (T - 25))$$
$$a_\gamma = a_{\gamma 0}(1 + \beta_\gamma (T - 25))$$
$$a_\gamma^* = a_{\gamma 0}^*(1 + l_\gamma (T - 25))$$

where

$V_{\gamma 0}$ = volume fraction of austenite in the initial microstructure,
V_γ = volume fraction of austenite at any stage of the reaction,
$V_{\theta 0}$ = volume fraction of cementite in the initial microstructure,

The volume fraction of cementite in the initial microstructure, where the average carbon content in ferrite including cementite particles is S, can be obtained as follows assuming all carbon atoms in ferrite are locked in as cementite particles:

$$V_{\theta 0} = \frac{1}{1 + k_\theta}(1 - V_{\gamma 0})$$

with

$$k_\theta = \frac{a_\alpha^3 (1 - 3\frac{S}{x_0^\alpha})}{a_\theta^3 \frac{1}{2} \frac{S}{x_0^\alpha}}.$$

The relative length change due to complete reaustenitisation at each temperature can be then calculated by setting $V_\gamma = 1$ in the equations.

The calculated relative length changes for each case are drawn in Fig. 4.29, where $a_\alpha = 2.866$ Å (after Bhadeshia [3]), $\beta_{\alpha,\gamma} = 1.244 \times 10^{-5}$, 2.065×10^{-5} K^{-1} (obtained in the present work from continuous heating experiments with the starting structure of martensite) and the same expression as the previous section for the thermal expansivity of austenite as a function of alloying element compositions was used. The thermal expansion coefficient of cementite was reported to increase with temperature [16]. Using data published by Stuart and Ridley [16] the expression of the mean linear expansion coefficient as a function of temperature was obtained as follows:

$$\beta_\theta = 5.4872 \times 10^{-6} + 3.6450 \times 10^{-9} T + 9.2833 \times 10^{-12} T^2$$

where T is temperature in °C. Although the data were available only up to 700 °C, this expression was assumed without any justification to be applicable at higher temperatures than

700° C. It may be worth noting that the thermal expansivity of cementite is very close to that of ferrite at temperatures where reaustenitisation occurs.

For cases (1) and (2), there are rather big discrepancies between the experimental data and calculated values. The value obtained for the maximum relative length change at around 800 °C differs significantly from that given by the two calculations. The calculated slope for the partially reaustenitised part, however, seems very similar to that obtained in the experiments although there is about 10 or 15 °C difference between the calculations and experimental results. The maximum relative length changes which correspond to full transformation into austenite; *i.e.* the cases reaustenitised at 805 and 815 °C, are well expressed by case (3), where the cementite is assumed not to dissolve in austenite. The slope for the region where the transformation to austenite is incomplete, on the other hand, does not agree with the experimental results. When the reaction temperature is very high, where alloy carbides are not thermodynamically stable, the dissolution of cementite (which has existed in the initial ferrite matrix) will occur after the completion of reaustenitisation as discussed by Hillert *et al.* [17]. Therefore, in this case, the relative length change due to the isothermal reaustenitisation can be calculated by equation (4.10). However, when the reaction temperature is not high enough for the effect of dissolution of cementite to be neglected, the calculation in case (3) should be modified. This might be one of the reasons that the slope of partially transformed part is not in good agreement with the data.

Another reason of the discrepancy could be due to the existence of alloy carbide precipitation at the reaction temperatures. The equilibrium phase diagram of a steel which has similar chemical composition; Fe-5 wt.% Cr, is shown in Fig. 4.30. The calculated equilibrium phase diagram for Fe-C-Cr ternary alloy [18] at different temperatures is also shown in Fig. 4.30. M_7C_3 is stable below about 820 °C both in the ferrite and in austenite phases. Thus, the theory which has been proposed by Yang and Bhadeshia [12-14] should be modified. The precipitation reduces the carbon content of austenite below the α/γ equilibrium carbon content, x_{Ae_3}, which is obtained assuming that there is no effect of precipitation on the equilibrium. Hence further transformation is expected to occur after the precipitation; transformation from austenite to ferrite might occur. When the reaction temperatures are not high enough, the precipitation can occur before or during the formation of austenite. In this case, the Ae_3 temperature should be calculated under the ferrite, austenite and alloy carbide three phase equilibrium condition. Although this calculation has not been tackled, the existence of stable precipitation will raise the Ae_3 temperature, so that the $T_{\gamma 1}$ and $T_{\gamma 2}$ temperatures will be calculated higher than in the absence of carbide precipitation. This may 0explain the difference between the theory and experimental data in the temperature range of partial reaustenitisation.

The calculated temperature range of partial reaustenitisation in the Fe-0.3C-4.08Cr wt.% system by the theory proposed by Yang and Bhadeshia [12-14] was between 751 °C and 781 °C and the value expected from the experimental results was, on the other hand, between 760° C and 795° C.

4.5 CONTINUOUS HEATING REAUSTENITISATION FROM A MIXTURE OF BAINITE AND AUSTENITE

Although isothermal study of transformation is always necessary to understand the kinetics of the reaction, heat-treatments in practice are rarely isothermal. Continuous heating reaustenitisation is therefore studied in this section.

4.5.1 Dilatometry

Experiments have been carried out on the specimens with three different starting mixtures of bainite and austenite. The relative length changes during continuous heating are shown in Fig. 4.31. The upper part of the figure shows changes in the relative length and temperature during heating as a function of time, and the lower part is the plot of the relative length change against temperature. It can be seen that the change in temperature of the specimen is controlled to give a constant heating rate throughout continuous heating up to $1000\,^{\circ}\mathrm{C}$ although a constant rate is of course not necessary in any fundamental sense. The transformation-start and -finish temperatures can be determined easily by plotting the relative length change against temperature as can be seen in Fig. 4.31. The lower temperature part of the relative length change curve shows a straight line corresponding to a linear thermal expansion of the starting microstructure (a mixture of bainite and austenite). The linear thermal expansion coefficient of the initial microstructure increases with the bainite transformation temperature (Fig. 4.32). When a lower bainite transformation temperature is selected, a specimen contains larger amount of austenite whose thermal expansion coefficient is larger than ferrite. The higher temperature part of the curve, on the other hand, is due to the linear thermal expansion of austenite since the specimen is then fully austenitic. Therefore the points where the actual relative length curve deviates from each straight lines give the transformation-start, T_S, and -finish, T_F, temperatures respectively.

The transformation-start and -finish temperatures determined from the relative length change during continuous heating at different heating rates are plotted in Fig. 4.33. Both increase with the heating rate. The effect of the initial austenite volume fraction and the carbon content of residual austenite, *i.e.* bainite transformation temperature, on the transformation-start and -finish temperatures can be also seen in the figure. When the heating rate is low, $1.1\,^{\circ}\mathrm{C\,s^{-1}}$, the higher the bainite transformation temperature the lower the transformation-start and -finish temperatures. At $5\,^{\circ}\mathrm{C\,s^{-1}}$ of heating rate, in contrast, this tendency has been inverted. The normalized austenite volume fraction transformed on heating was calculated from the relative length change (Fig. 4.34).

With relatively low heating rates, however, an expansion of the specimen before the onset of reaustenitisation has been detected (Fig.4.31). This expansion of specimen has been pointed out as the decomposition process of residual austenite by Yang [15]. Therefore the transformation-start temperatures which have been observed in low heating rates are not the proper T_C for the starting microstructure of the mixture of bainite and austenite obtained at each bainite transformation temperature. However the data obtained with higher heating rates can be treated as proper transformation-start and -finish temperatures, because no transformation of specimens has been observed before the start of reaustenitisation during continuous heating.

4.5.2 Decomposition of austenite during heating

As it has been discussed by Yang and Bhadeshia [12-14], the transformation-start temperature during continuous heating from a mixture of austenite and either bainite or acicular

ferrite is restricted by the carbon concentration of residual austenite just before the start of continuous heating directly from the bainite or acicular ferrite transformation temperatures. When the bainite or acicular ferrite transformation temperature is lower, the carbon content of residual austenite will be higher because of the negative slope of the T_0' curve. Higher bainite transformation temperatures give correspondingly higher reaustenitisation-start temperatures during continuous heating.

However, in the present experiments, the transformation-start temperature during the continuous heating at $1.1\,^{\circ}\mathrm{C}\,\mathrm{s}^{-1}$ is lower when the bainite transformation temperature T_b was higher. The situation corrects itself when the heating rate is raised to $5\,^{\circ}\mathrm{C}\,\mathrm{s}^{-1}$, with the order of the transformation-start temperature being in agreement with the theory. The reason for the disagreement at the low heating rate, is the decomposition of austenite during heating. For a heating rate of $1.1\,^{\circ}\mathrm{C}\,\mathrm{s}^{-1}$, austenite decomposition during heating was observed for all the bainite transformation temperatures used (420, 448 and $472\,^{\circ}\mathrm{C}$). For a heating rate of $5\,^{\circ}\mathrm{C}\,\mathrm{s}^{-1}$, in contrast, the decomposition of austenite could not be detected during heating.

The temperature at which the relative length change versus temperature first indicates the decomposition of austenite is designated T_{ds}. When heating rate was $1.1\,^{\circ}\mathrm{C}\,\mathrm{s}^{-1}$, the T_{ds} temperatures determined experimentally were found to be as shown in Fig. 4.35. T_{ds} is found to decrease with increasing T_b. This order can be understood as follows. When T_b is lower, the carbon concentration in residual austenite is higher because of the negative slope of the T_0' curve. Thus reconstructive formation of ferrite from the residual austenite becomes sluggish. This corresponds to to the fact that the upper C-curve in the TTT diagram is shifted to a longer time direction by increasing the carbon concentration in austenite. As a result, the lower the bainite transformation temperature, the higher the temperature at which a reconstructive formation of ferrite from the residual austenite on heating starts.

In order to investigate the decomposition process during continuous heating, a specimen was helium quenched from $730\,^{\circ}\mathrm{C}$ after heating at $1.1\,^{\circ}\mathrm{C}\,\mathrm{s}^{-1}$ after 30 min of isothermal bainite transformation at $448\,^{\circ}\mathrm{C}$. The microstructure of the specimen (Fig. 4.36) consists of three phases; white, black and a dark etched areas. The micro-hardness of the white areas correspond to that of martensite (austenite before quenching) at 753 Hv (10g). The dark etched areas are expected to be bainite, with a hardness of 444 Hv (10g). The hardness of the third phase was 400 Hv (10g), and a TEM micrograph confirmed (Fig. 4.37) that it is pearlite.

The volume fraction of pearlite formed by the decomposition of austenite during continuous heating can be calculated from the relative length change obtained in the experiments. A relative length change due to decomposition of residual austenite to pearlite during heating was expressed by:

$$\frac{\Delta L}{L} = \frac{1}{3}\frac{V_\gamma a_\gamma^{*3} + (1 - V_\gamma - V_\theta)2a_\alpha^3 + V_\theta \frac{1}{3}a_\theta^3 - V_{\gamma 0}a_\gamma^3 - (1 - V_{\gamma 0} - V_{\theta 0})2a_\alpha^3 - V_{\theta 0}\frac{1}{3}a_\theta^3}{V_{\gamma 0}a_\gamma^3 + (1 - V_{\gamma 0} - V_{\theta 0})2a_\alpha^3 + V_{\theta 0}\frac{1}{3}a_\theta^3} \quad (4.11)$$

with

$$V_{\theta 0} = \frac{1 - V_{\gamma 0}}{1 + k_1}$$

$$k_1 = \frac{a_\alpha^3(1 - 3\frac{S}{x_0^\alpha})}{a_\theta^3 \frac{1}{2}\frac{S}{x_0^\alpha}}$$

94

$$\Delta V_\gamma = \frac{V_{\gamma 0} - V_\gamma}{1 + k_2}$$

$$k_2 = \frac{a_\alpha^3 \left(1 - 3\frac{x_1^\gamma}{x_0^\gamma}\right)}{a_\theta^3 \frac{1}{2}\frac{x_1^\gamma}{x_0^\gamma}}$$

$$\Delta V_\theta = V_\theta - V_{\theta 0}.$$

The lattice parameters of austenite $a_{\gamma 1}$, $a_{\gamma 2}$, ferrite a_α, and cementite $a_\theta^3 = a_\theta b_\theta c_\theta$ were calculated as described earlier. The carbon content of austenite has been assumed to be constant during the decomposition process. The calculated volume fractions of austenite (now martensite), bainite and pearlite are listed in Table 4.4. The calculations are for the data obtained at $730\,^\circ$C. According to the calculated results, the volume fraction of pearlite is larger when the bainite transformation temperature was $448\,^\circ$C than both the cases of the transformations at 420 and $472\,^\circ$C. This can be understood as follows. When the bainite transformation temperature is lower, decomposition starts at a lower temperature. So a higher degree of decomposition may be expected than in the case of a higher bainite transformation temperatures giving a higher amount of *normalised* volume fraction of decomposition. It is, however, important to note that the initial amount of austenite which has the potential to decompose is smaller in lower bainite transformation temperatures. As a result, the amount of austenite which decomposes on heating to $730\,^\circ$C reaches a peak at the bainite transformation temperature.

Temperature, $^\circ$C	x_1^γ, at.%	$V_{\gamma 0}$	V_γ	$V_{\gamma 0} - V_\gamma$
420	2.4	0.30	0.03	0.27
448	1.6	0.67	0.08	0.59
472	1.4	0.94	0.59	0.35

Table 4.4: Calculated volume fractions of the phases obtained by the reaction.

Phase	V_{opt}	V_{cal}	Hv(10g)
Bainite	0.58	0.50	444
Martensite	0.24	0.23	753
Pearlite	0.18	0.27	400

Table 4.5: Volume fractions derived from dilatometry, of the specimen helium quenched during heating at $1.1\,^\circ$Cs^{-1}. Starting microstructure is obtained by bainite transformation at $445\,^\circ$C.

The volume fractions of the three phases observed in the specimen helium quenched from $730\,^\circ$C on heating at $1.1\,^\circ$Cs^{-1} after the 30 min of isothermal bainite transformation at 448° C can also be calculated from the relative length change obtained. The total relative length change due to the decomposition of austenite during heating was measured as 6.64×10^{-4}. The calculated volume fraction and carbon content of residual austenite after 30 min of isothermal bainite transformation, which showed 2.24×10^{-3} of relative length change, was 0.5 and 1.7 at.%

respectively. From these values, the volume fraction of pearlite transformed from austenite during heating was calculated (designated as V_{cal} in Table 4.5). The results of the quantitative optical measurements were also listed (designated as V_{opt} in Table 4.5). The dilatometric results are in reasonable agreement with the optically measured volume fraction of each phase.

4.6 CONCLUSIONS

Bainite transformation behaviour has been studied in a Fe-0.3C-4.08Cr wt.% alloy, and in a Fe-2.0Si-3.0Mn steel with 0.06, 0.12, 0.22 and 0.43 wt%C. Bainite transformation was confirmed to cease prematurely when the carbon concentration in the residual austenite reaches the T_0 or T_0' curve rather than the paraequilibrium concentration. This suggests that bainite transformation in steels proceeds by diffusionless growth of bainitic ferrite.

Bainite transformation was used to obtain mixtures of bainitic ferrite and austenite, so that the growth of austenite layers could be studied. The following results were obtained.

From isothermal reaustenitisation experiments:
1) Reaustenitisation does not start until the temperature is raised to the Ae_3 temperature of the austenite in the initial microstructure.
2) 100% reaustenitisation occurs at temperatures above the Ae_3 temperatures of the bulk carbon content.
3) The maximum relative length change due to 100% reaustenitisation shows a slight decrease with increasing temperature since the difference in thermal expansivities of ferrite and austenite decreases as the temperature is raised.
4) From an equilibrium analysis of the relative length change for reaustenitisation, the reaction at higher temperatures seems not to be accompanied by dissolution of cementite whereas some dissolution does occur at partial reaustenitisation temperatures.
5) Reaustenitisation seems to proceed by the thickening of pre-existing austenite in the starting microstructure.
6) M_7C_3 chromium rich carbide can be found after 30 min of isothermal reaustenitisation at temperatures below 815° C.

From continuous heating reaustenitisation experiments:
7) A lower reaustenitisation-start temperature was obtained for a lower bainite transformation temperature.
8) Decomposition of pre-existing austenite to pearlite occurs on heating when the heating rate is less than $5\,^{\circ}\mathrm{C\,s^{-1}}$.
9) The decomposition-start temperature can be understood by the TTT curves for the austenite in the initial microstructure.
10) This supports that the concept of the incomplete reaction phenomenon, which was also suggested by isothermal bainite transformation.

REFERENCES

1. H. K. D. H. Bhadeshia: *Acta Metall.,* 1980, **28,** 1103.

2. H. K. D. H. Bhadeshia: *Proc. Int. Conf. "Solid-Solid transformations",* 1981, 1041.

3. H. K. D. H. Bhadeshia: *Metal Science,* 1982, **16,** 159.

4. M. Takahashi and H. K. D. H. Bhadeshia: *J. of Materials Science Letter,* 1989, **8,** 477.

5. N. Ridley, H. Stuart and L. Zwell: *Trans. AIME,* 1969, **245,** 1834.

6. D. J. Dyson and B. Holmes: *JISI,* 1970, **May,** 469.

7. H. K. D. H. Bhadeshia: *Acta Metall.,* 1981, **29,** 1117.

8. J. G. Gilmour, G. R. Purdy and J. S. Kirkaldy: *Metall. Trans.,* 1972, **3,** 1455.

9. J. S. Kirkaldy, B. A. Thomson and E. A. Baganis: *"Hardenability Concepts with Applications to Steel", ed. D. V. Doane and J. S. Kirkaldy, AIME,* 1978, 82.

10. H. K. D. H. Bhadeshia and D. V. Edmonds: *Acta Metall.,* 1980, **28,** 1265.

11. H. K. D. H. Bhadeshia: *Metal Science,* 1980, **14,** 230.

12. J-R. Yang and H. K. D. H. Bhadeshia: *Proc. Int. Conf. on "Welding Metallurgy of Structural Steels", ed. J. Y. Koo, AIME, Warrendale, Pennsylvania,* 1987, 549.

13. J-R. Yang and H. K. D. H. Bhadeshia: *Proc. Int. Conf. "Phase Transformations '87", Institute of Metals, London, ed. G. W. Lorimer,* 1987b 203.

14. J-R. Yang and H. K. D. H. Bhadeshia: *Proc. Int. Conf. on "Welding Metall. of Structural Steels", ed. by J. Y. Koo, The Metall. Society of the AIME,* 1987, 549.

15. J-R. Yang: *Ph.D thesis in the University of Cambridge,* 1988.

16. H. Stuart and N. Ridley: *JISI,* 1966, **July,** 711.

17. M. Hillert, K. Nilsson and L-E. Törndahl: *JISI,* 1971, **209,** 49.

18. B. Uhrenius: *"Hardenability Concepts with Applications to Steel", ed. D. V. Doane and J. S. Kirkaldy, AIME,* 1978, 28.
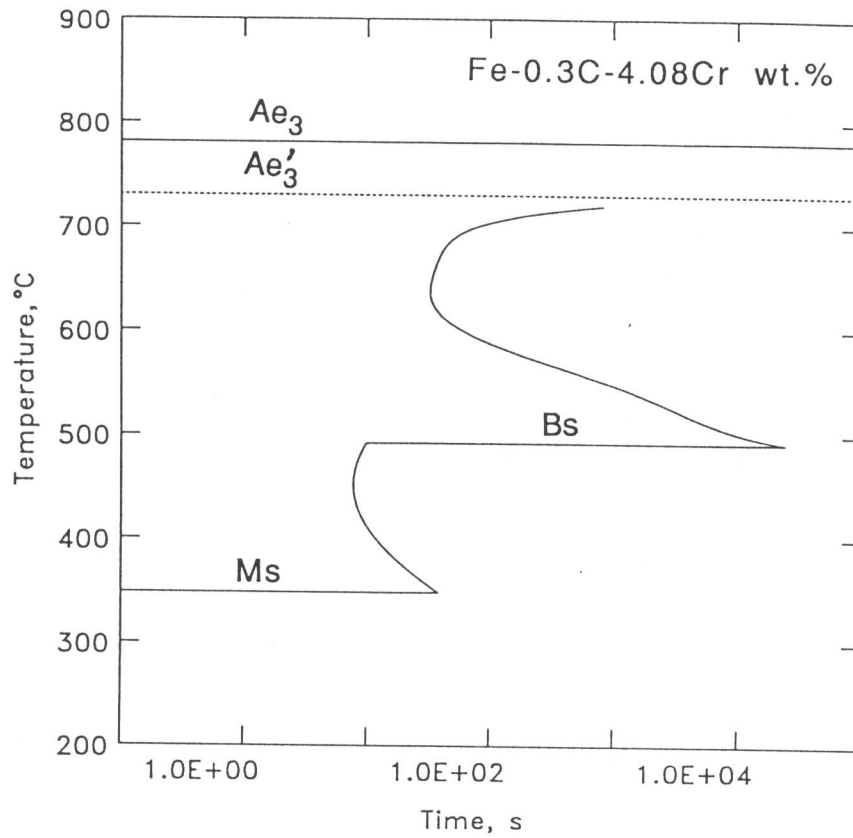
Fig .4.1 Calculated time-temperature-transformation curve for the material used in the experiments [3].
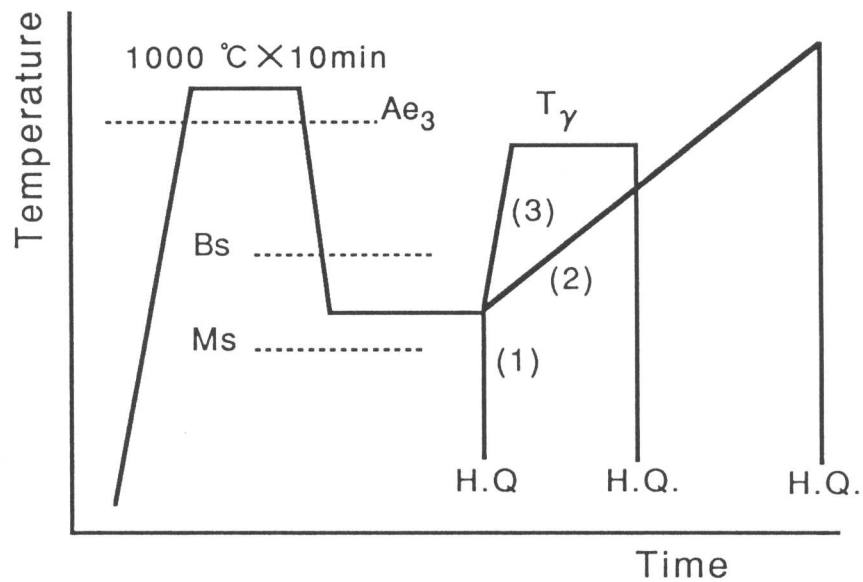

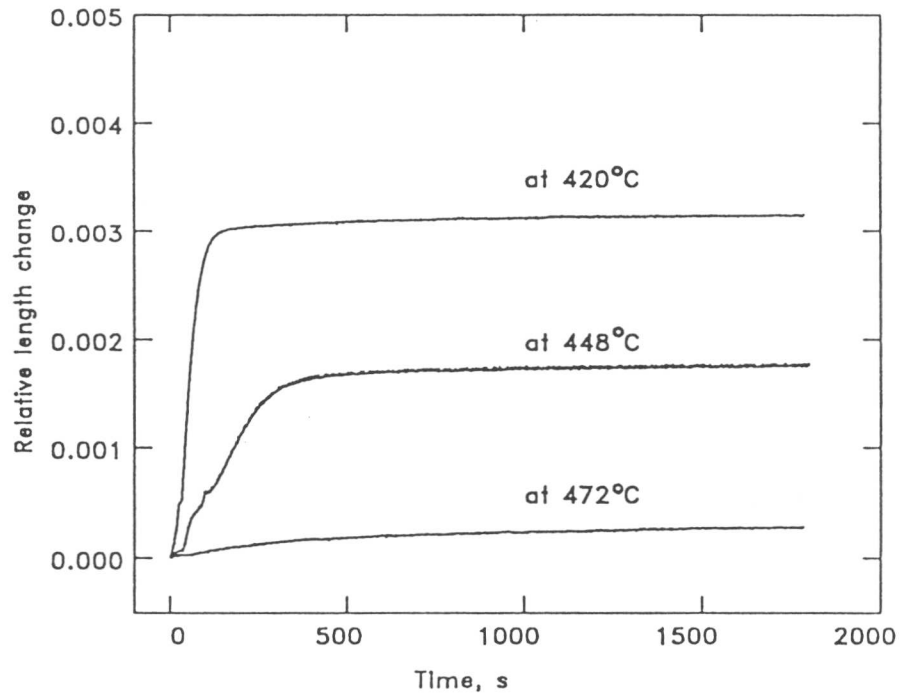Fig. 4.2 Schematic illustration of heat treatments.

Fig. 4.3 Relative length change during isothermal bainite transformation at 420°C, 448°C and 472°C after austenitisation at 1000°C for 10 min.
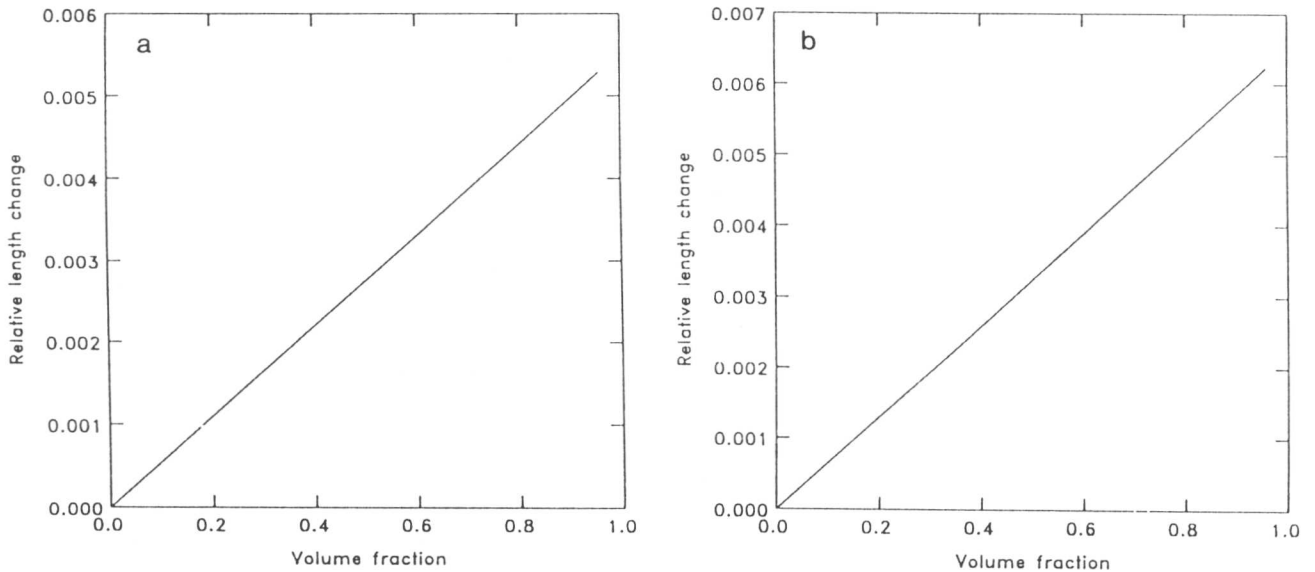

Fig. 4.4 Length change as a function of volume fraction of ferrite during isothermal transformation of austenite to ferrite which is supersaturated with 0.2 wt.% carbon (a), and to a mixture of ferrite and cementite (b) at 420°C [4].
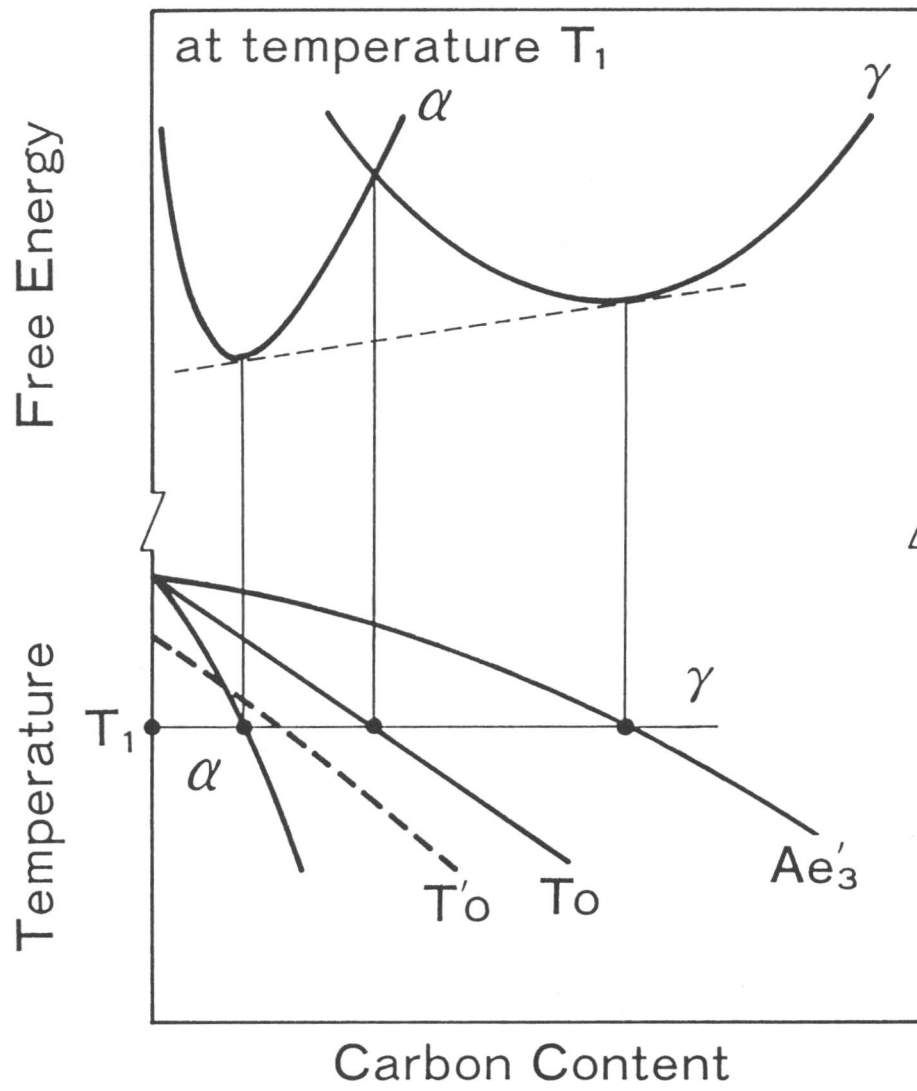
Fig. 4.5 Schematic illustration of the free energy curves of austenite and ferrite.
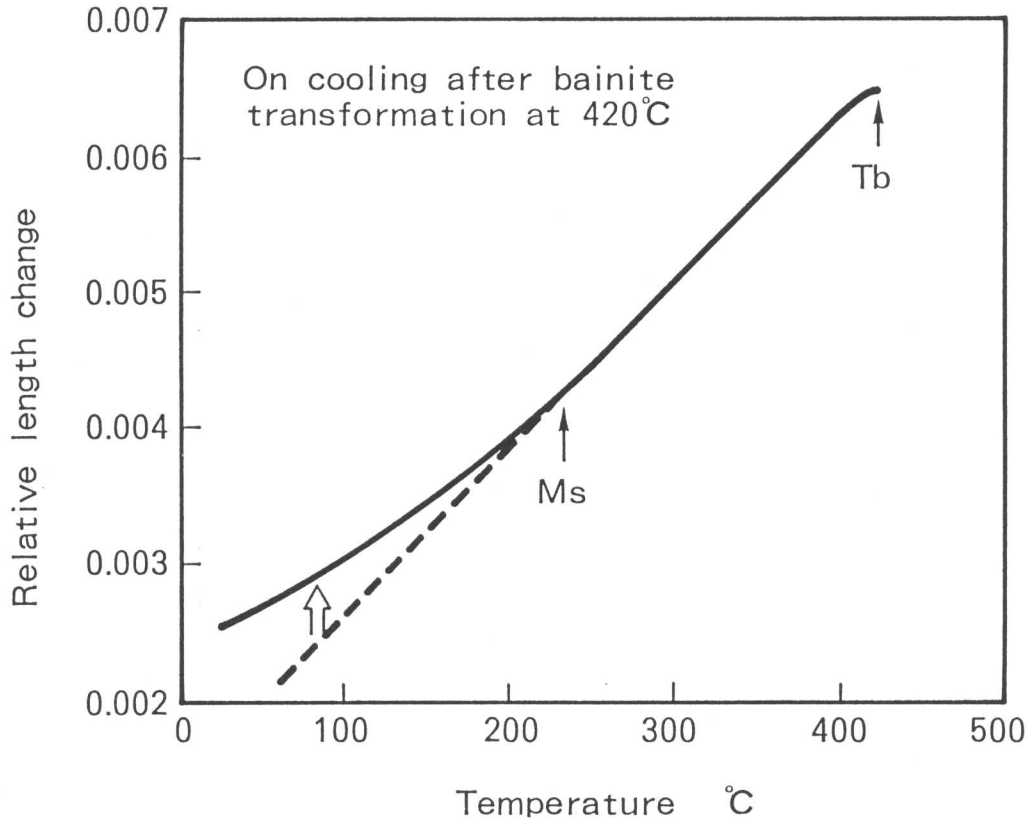
Fig. 4.6 Relative length change during helium quenching after the cessation of bainite transformation at 420 °C showing a martensitic transformation.
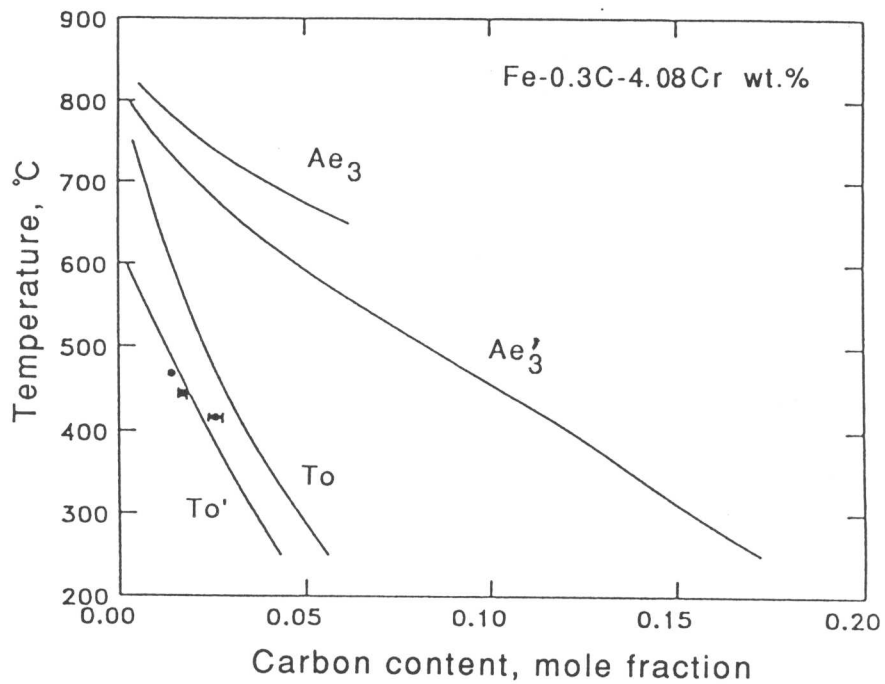
Fig. 4.7 Calculated phase diagram of the Fe-0.3C-4.08Cr wt.% alloy; plots correspond to the calculated carbon concentration of residual austenite after 30 min of isothermal bainite transformation at each reaction temperatures.

Fig. 4.8 Optical microstructure of a specimen helium quenched from 420 °C after bainite transformation.
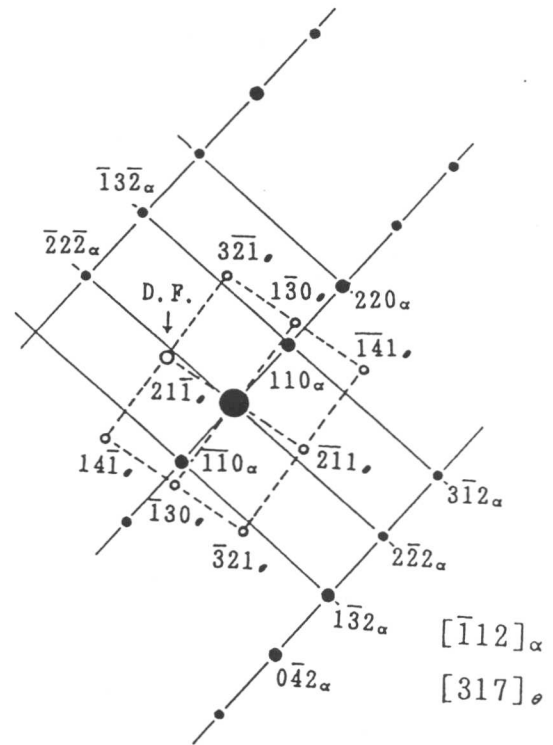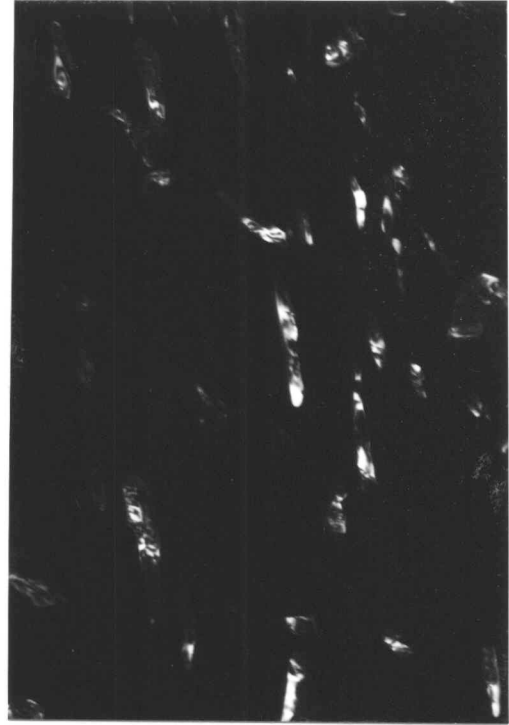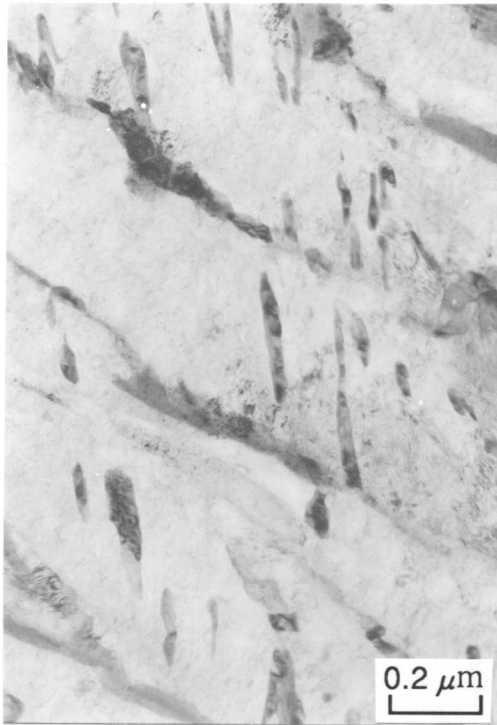
Fig. 4.9 TEM bright field image of the initial lower bainitic microstructure and a dark field image of cementite particles.

103

Fig. 4.10 TEM bright field image of lower bainite after 23 days of isothermal holding at 478 °C.
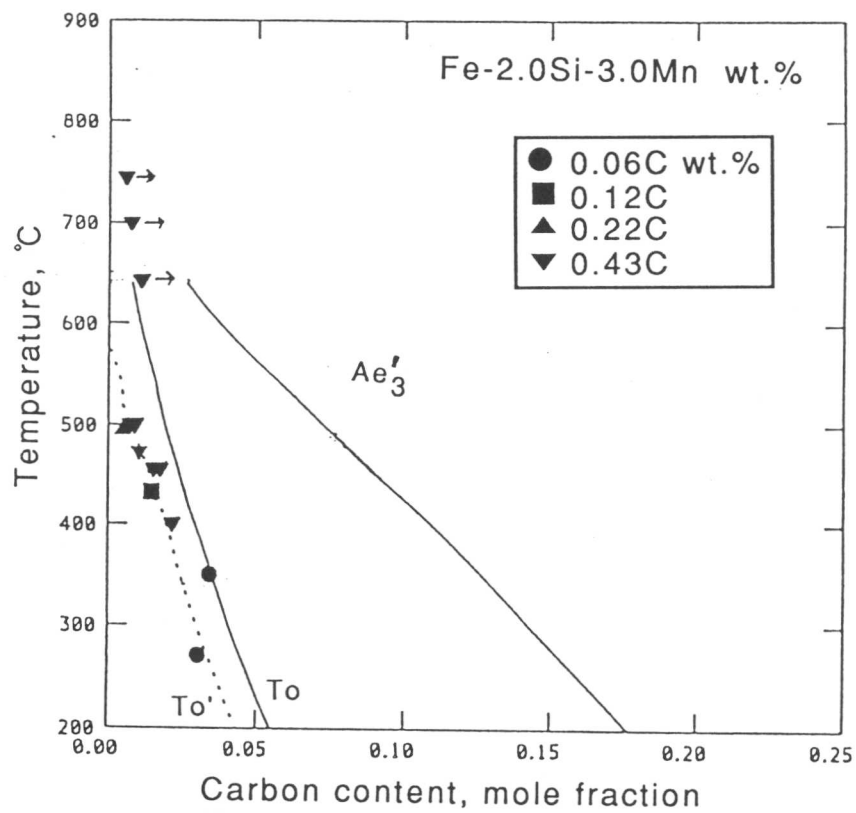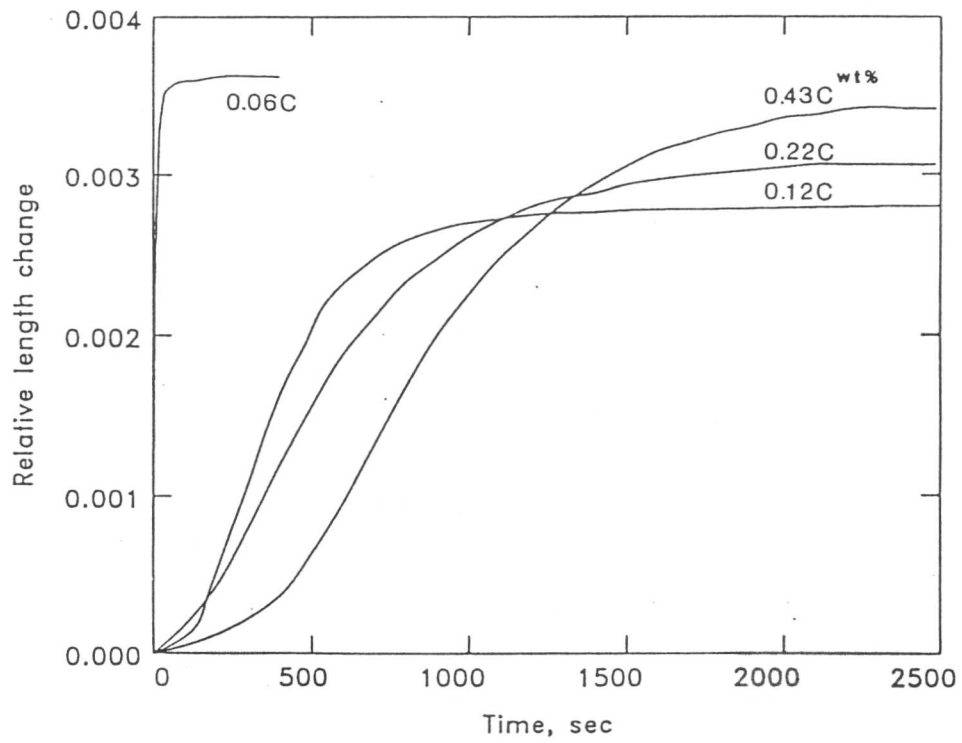
Fig. 4.11 Relative length change during isothermal bainite transformation at each reaction temperatures (a) and calculated phase diagram of the Fe-2.0Si-3.0Mn system with plots of calculated carbon concentration of residual austenite (b).
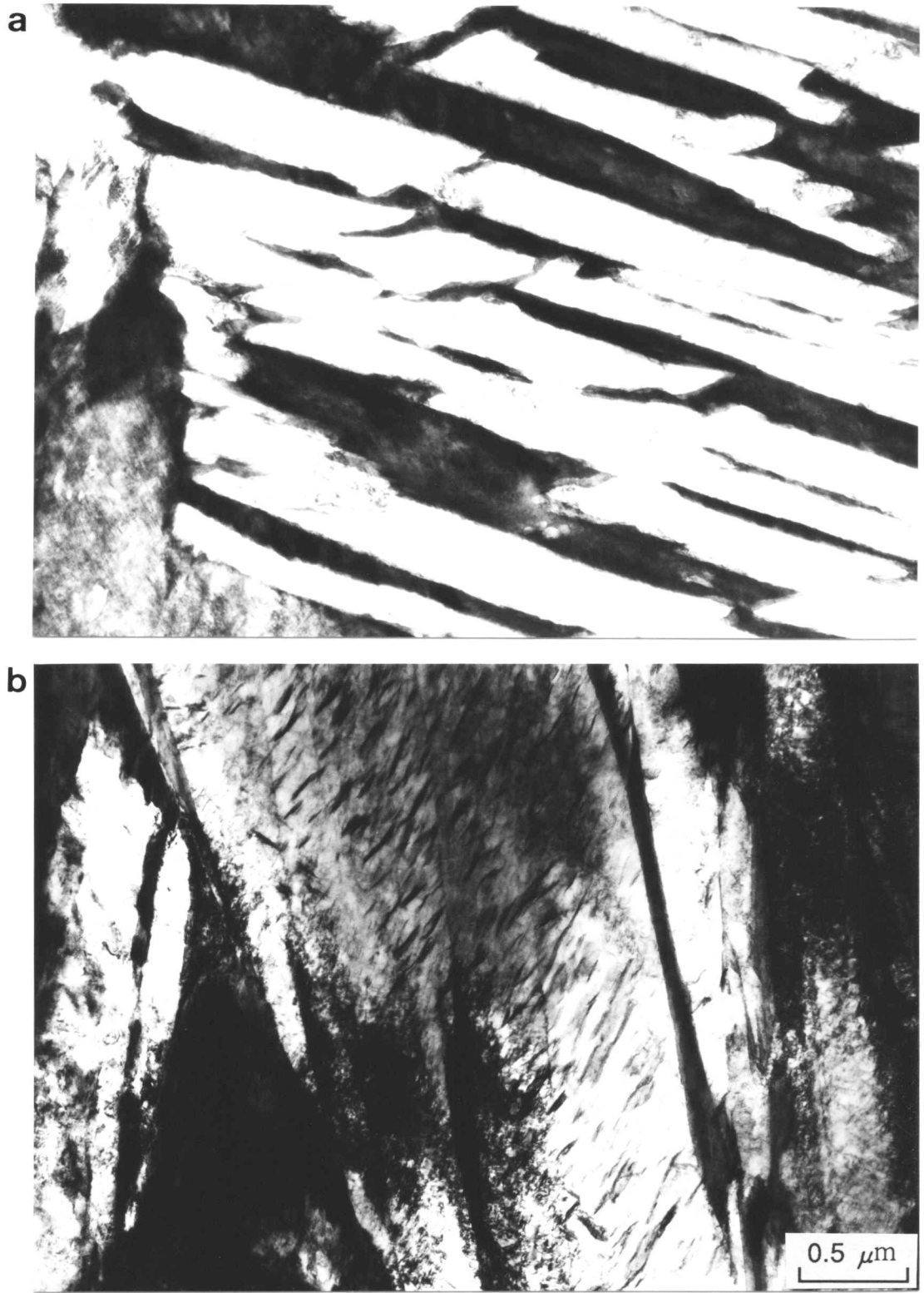
Fig. 4.12 Typical TEM micrographs of upper and lower bainite obtained in the Fe-0.43C-2.0Si-3.0Mn alloy at a) 350 °C and b) 270 °C respectively.
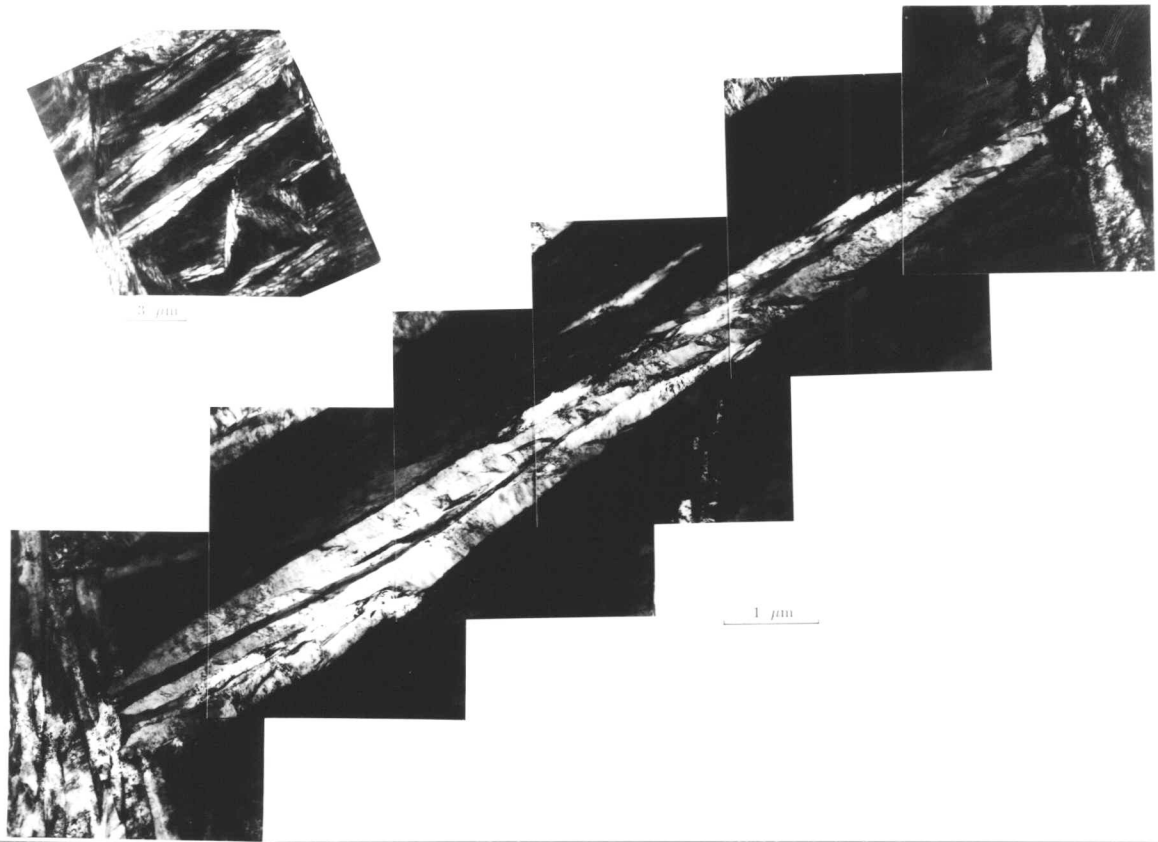
Fig. 4.13 TEM bright field image of upper bainite microstucture obtained at 350 °C in the Fe-0.43C-2.0Si-3.0Mn alloy.
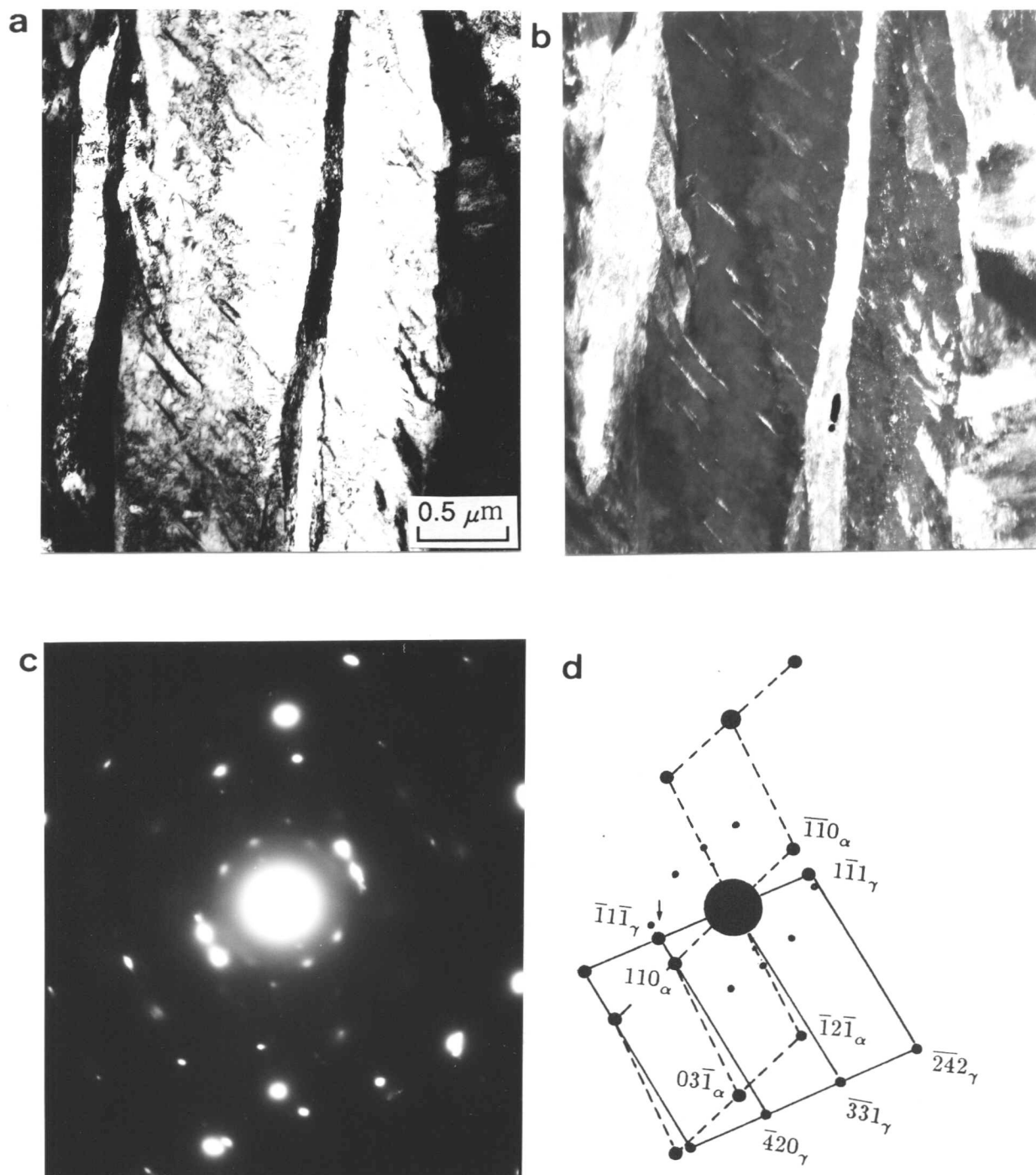
Fig. 4.14 (a) TEM bright field image of lower bainite obtained at 270 °C in the Fe-0.43C-2.0Si-3.0Mn alloy and (b) a dark field image of residual austenite trapped in between two adjacent bainitic ferrite plates. (c) is a selected area diffraction pattern.

a) Reaustenitised at 778 °C
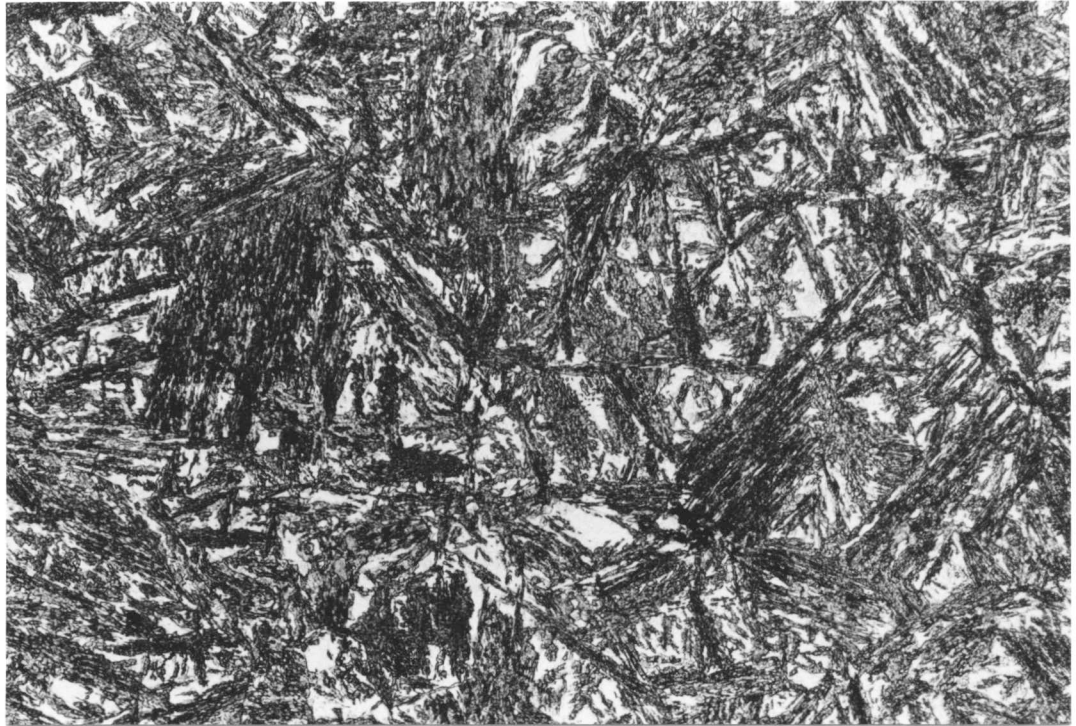
b) Reaustenitised at 785 °C

Fig. 4.15 Optical micrographs of isothermally reaustenitised specimens at a) 778 °C, b) 785 °C, c) 790 °C and d) 805 °C.

c) Reaustenitised at 790 °C

50 μm

d) Reaustenitised at 805 °C

20 μm
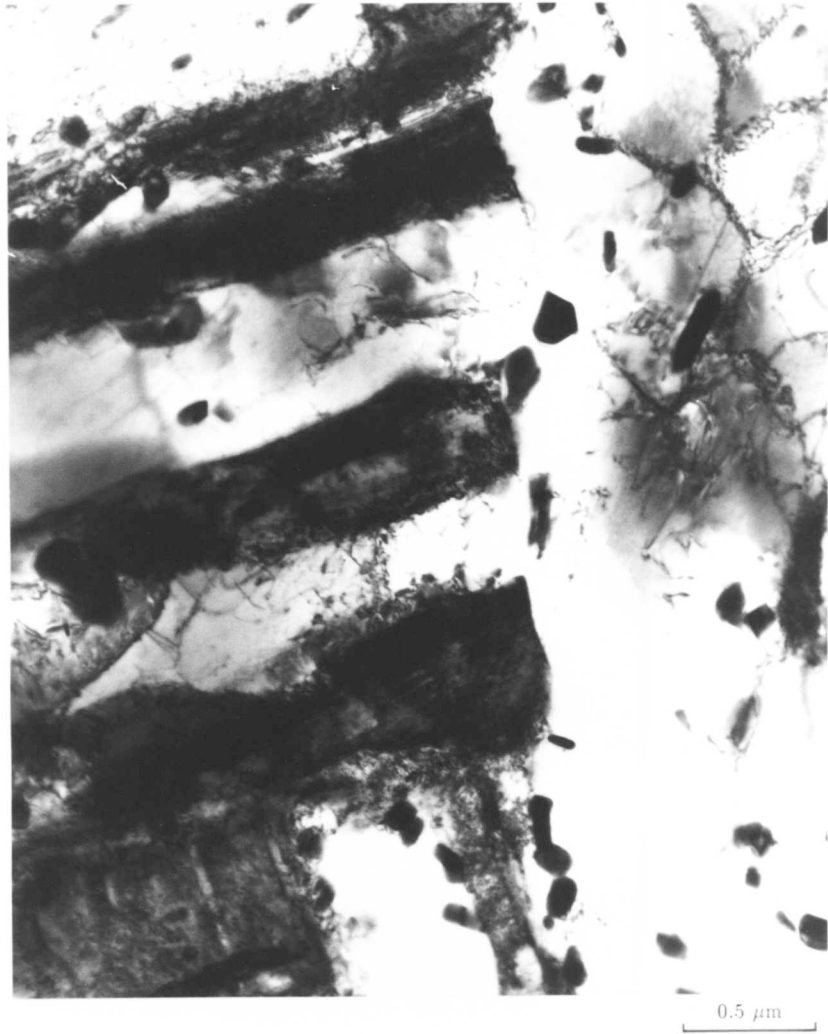
Fig. 4.16 TEM bright field image of a specimen quenched from 785 °C after 30 min of isothermal reaustenitisation at the temperature.
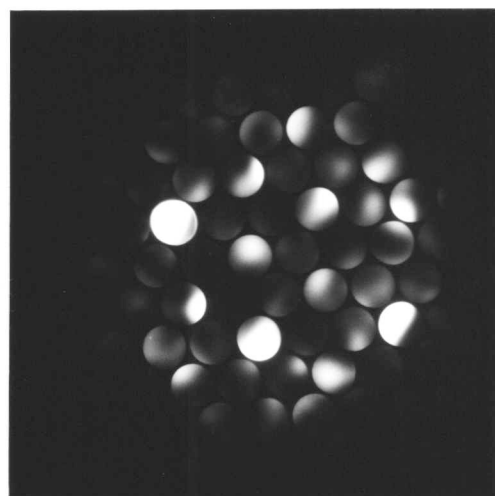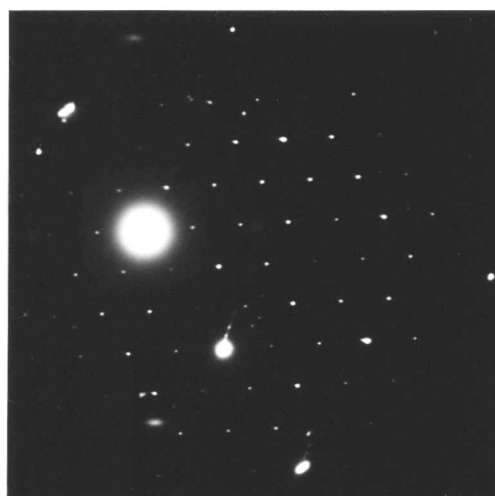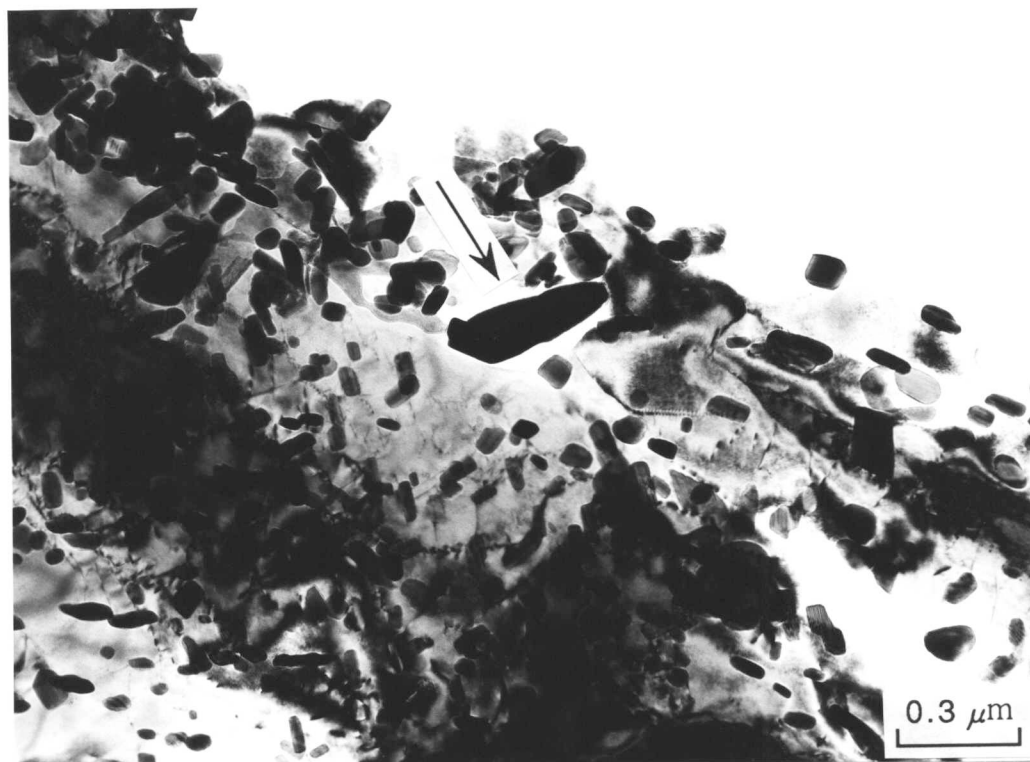
Fig. 4.17 TEM bright field image of precipitates with a selected area electron diffraction pattern and a convergent beam electron diffraction pattern of one of the particles.

Fig. 4.18 TEM bright field image of a specimen reaustenitised at 778 °C.
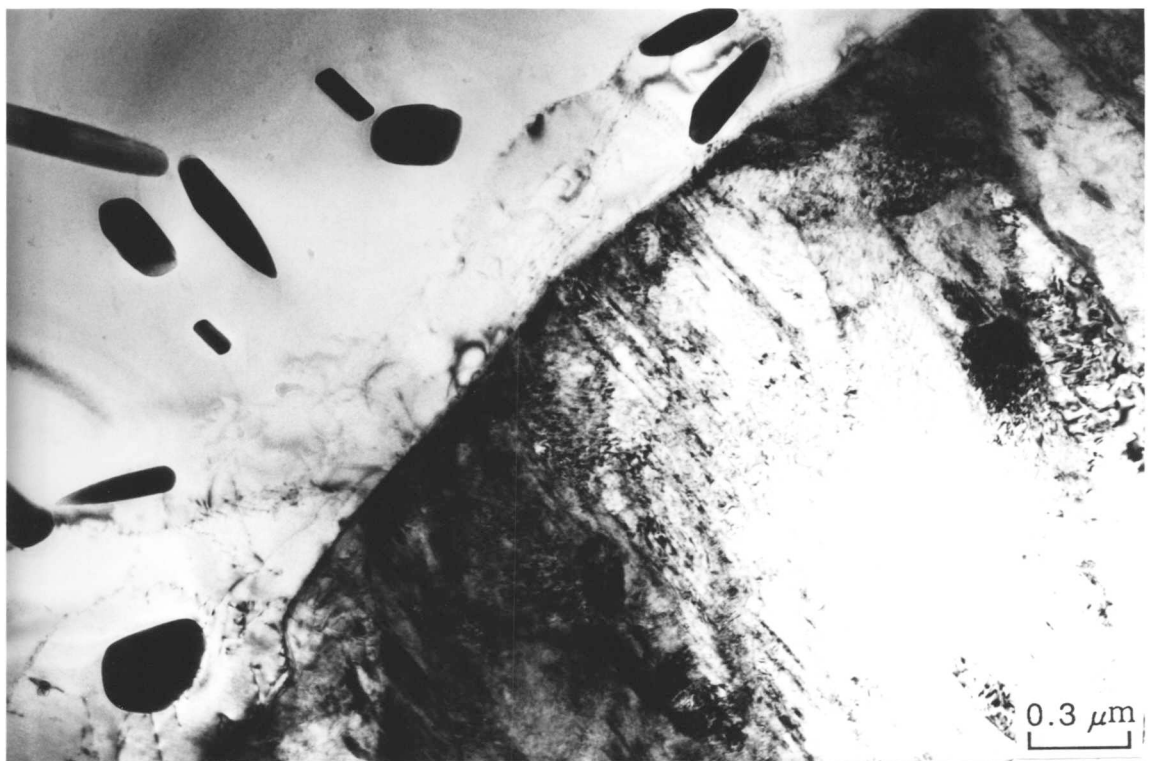
Fig. 4.19 TEM bright field image of a specimen reaustenitised at 778 °C.
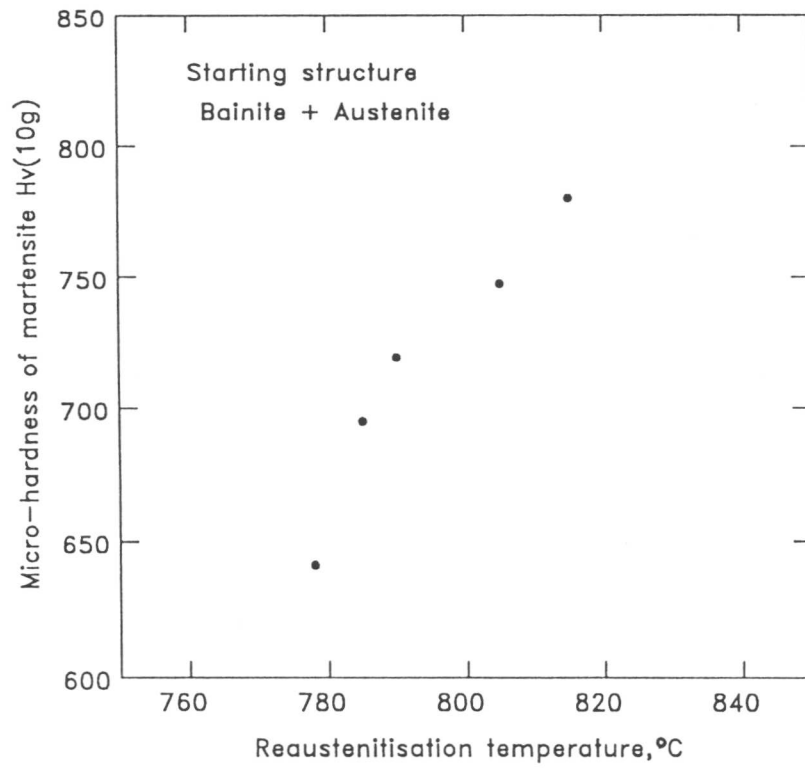
Fig. 4.20 Change in hardness of martensite with reaustenitisation temperature.
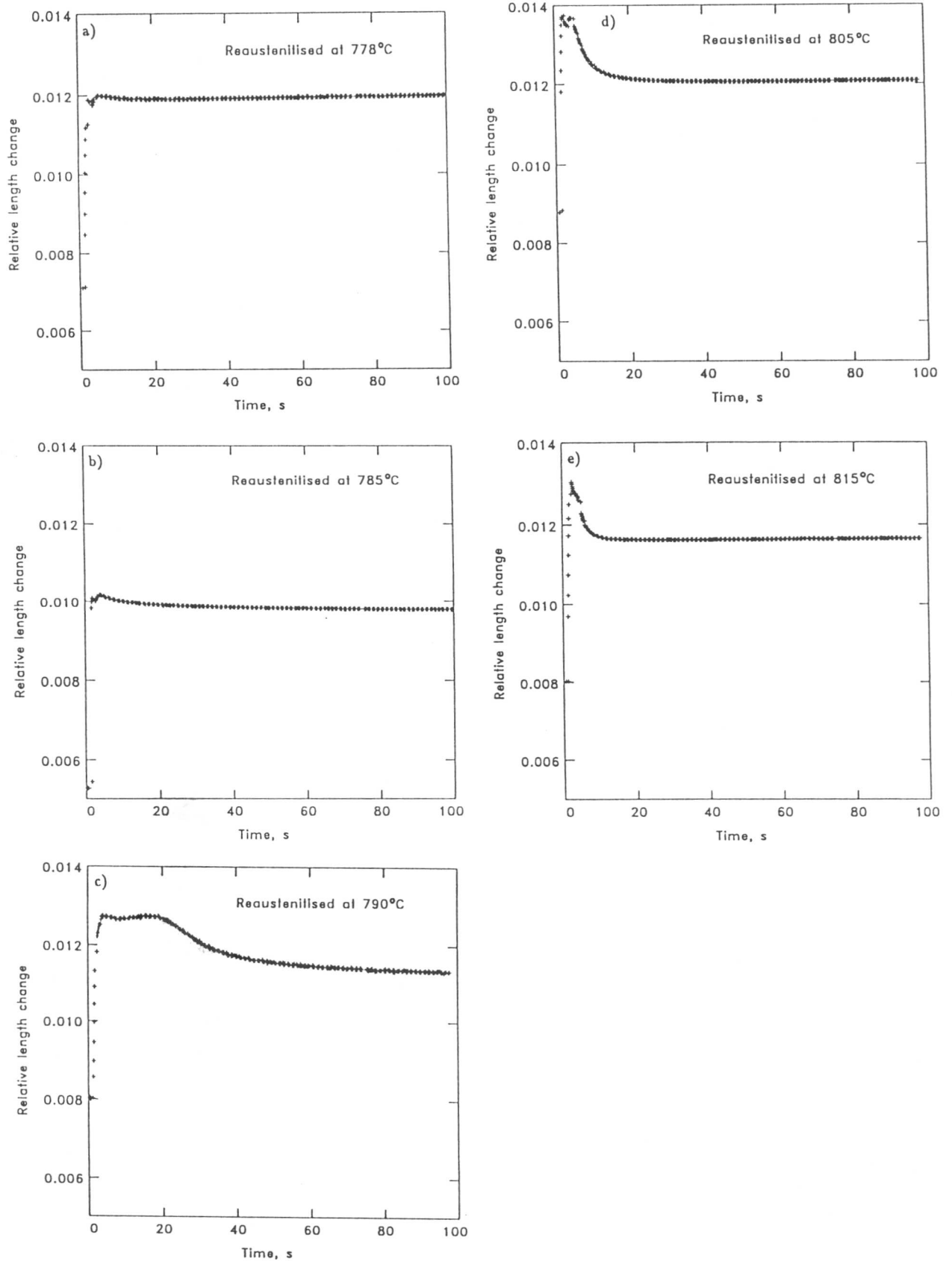
Fig. 4.21 Relative length changes during isothermal reaustenitisation from a mixture of bainite and austenite at a) 778 °C, b) 785 °C, c) 790 °C, d) 805 °C and e) 815 °C.

115
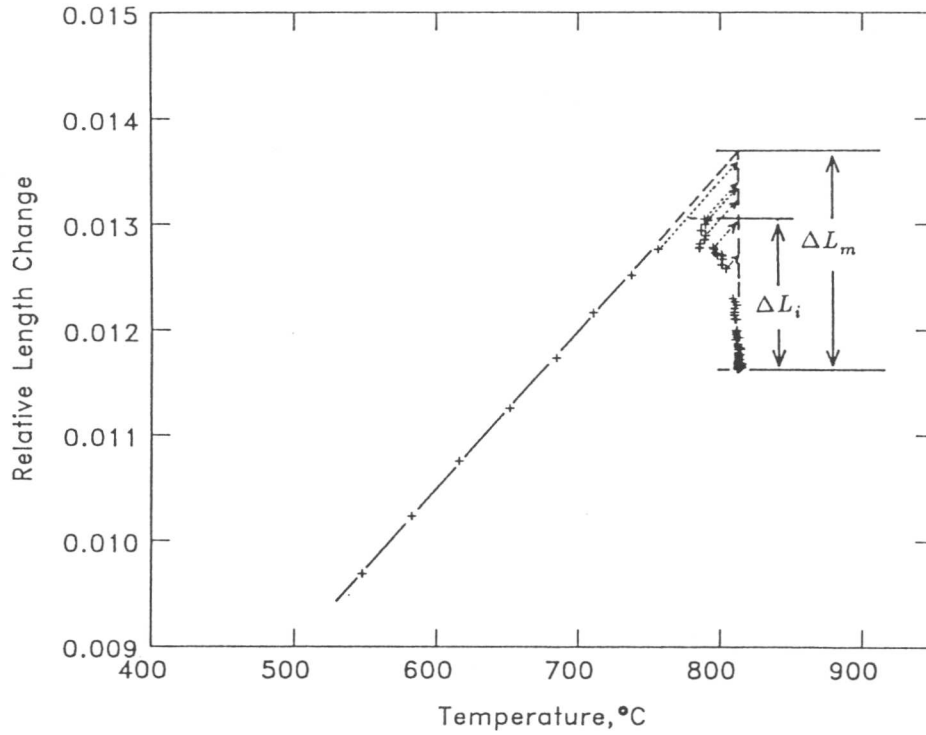
Fig. 4.22 Change in relative length during up-quenching and isothermal holding at 815 °C. A method of the temperature correction is illustrated in the figure.
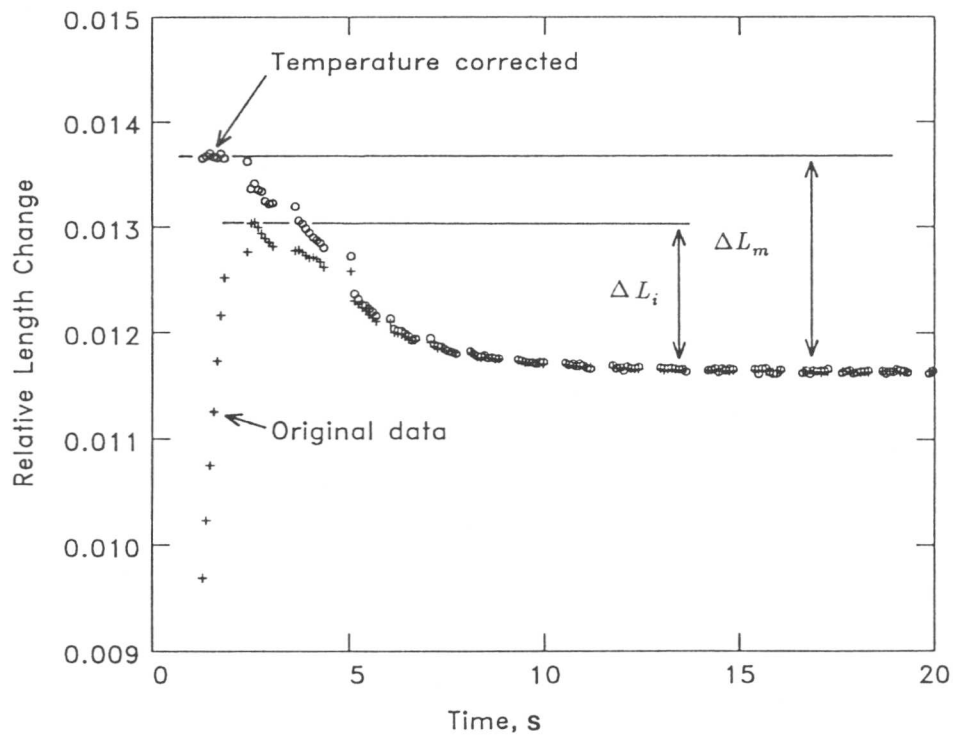
Fig. 4.23 Temperature corrected relative length change of the data in Fig. 4.22.
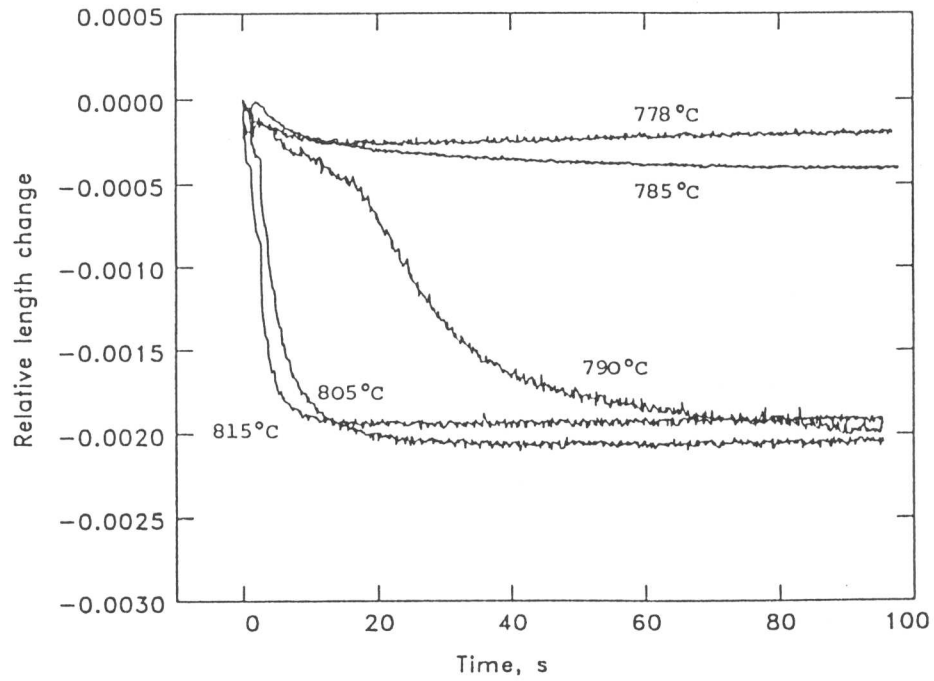
Fig. 4.24 Relative length changes during isothermal reaustenitisation from the mixture of bainite and austenite at different reaction temperatures.
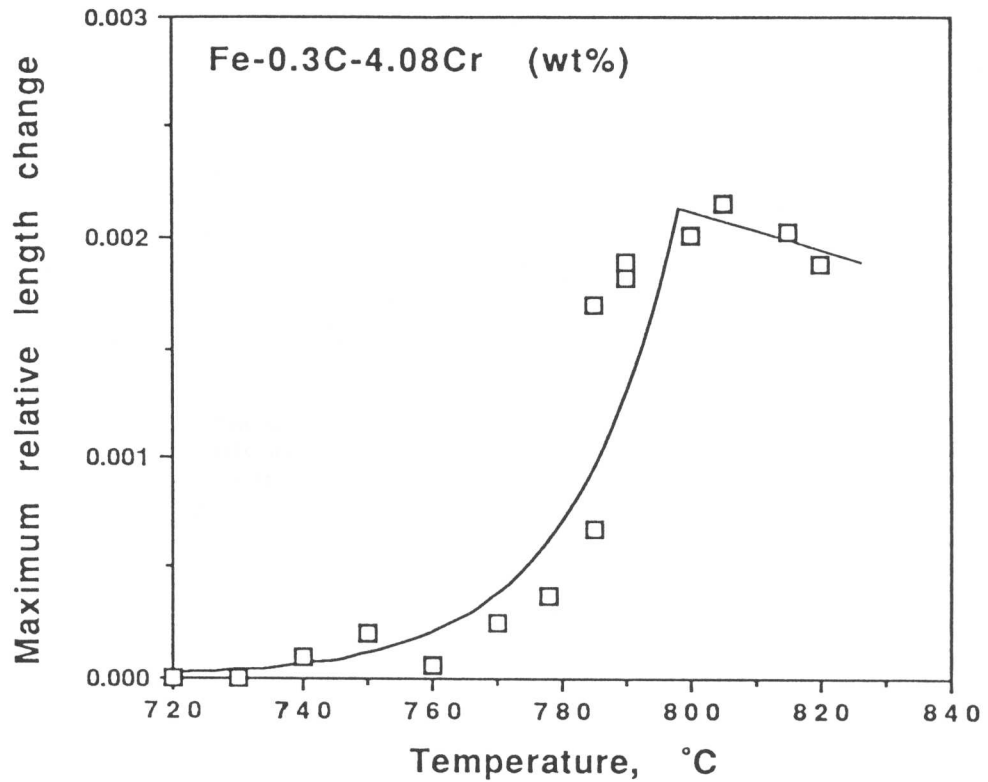
Fig. 4.25 Maximum relative length changes due to isothermal reaustenitisation from the mixture of bainite and austenite at different reaction temperatures.
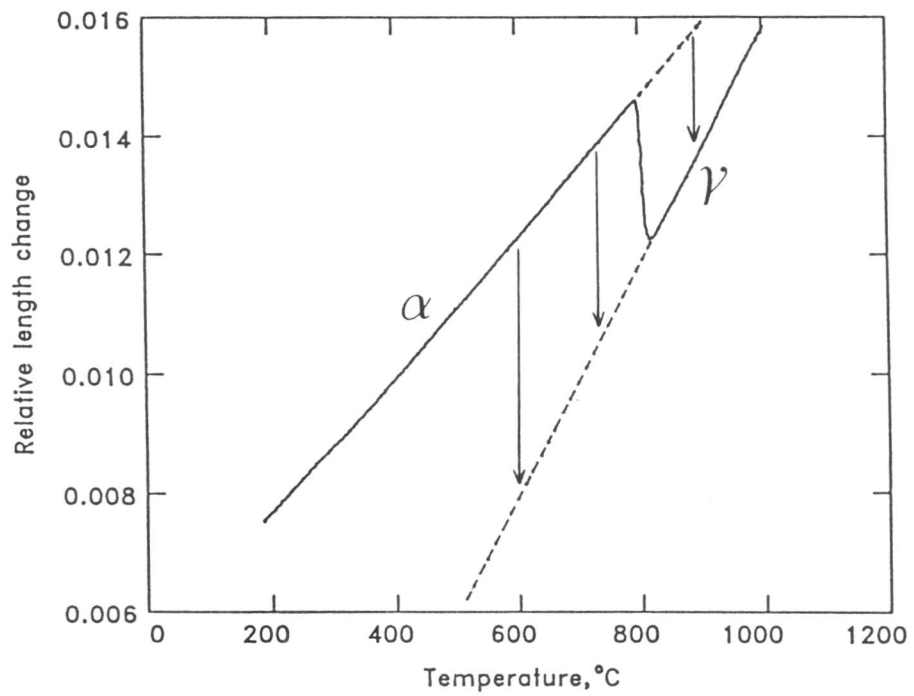
Fig. 4.26 Relative length change as a function of temperature during heating. Difference in thermal expansion coefficients of ferrite and austenite causes a change in the maximum relative length change due to 100 % of transformation.
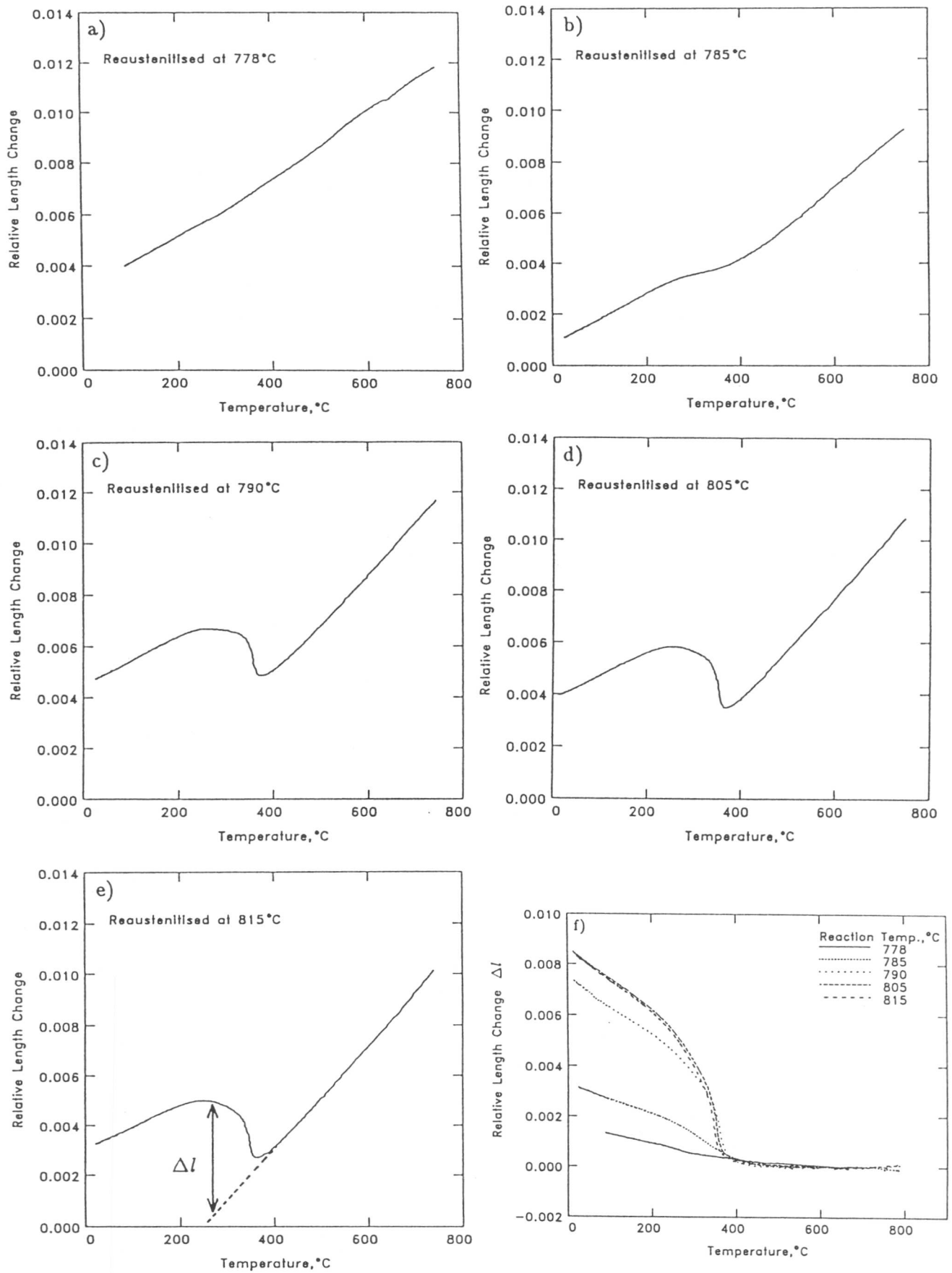
Fig. 4.27 Relative length changes during helium quenching after 30 min of isothermal reaustenitisation from the mixture of bainite and austenite at a) 778 °C, b) 785 °C, c) 790 °C d) 805 °C and e) 815 °C. Relative length changes Δl due to martensitic transformation are compared in f).

119
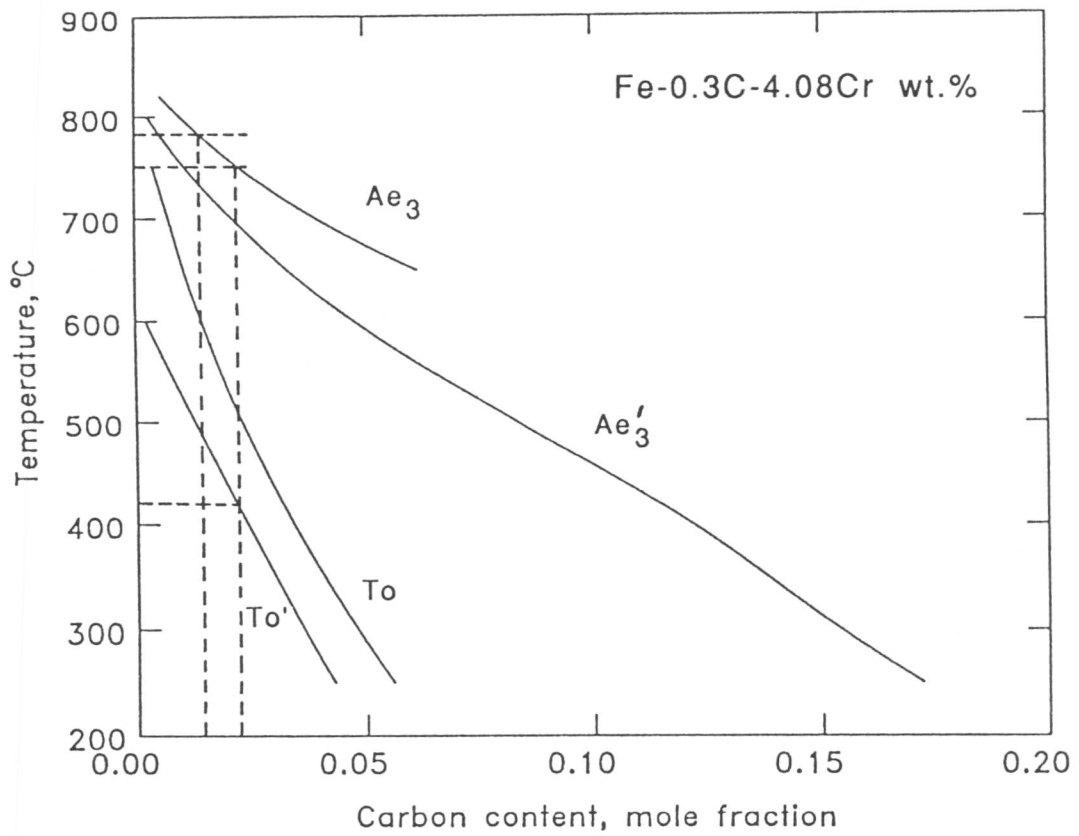
Fig. 4.28 Calculated phase diagram of the Fe-0.3C-4.08Cr alloy, which illustrates the partially reaustenitised temperature range.
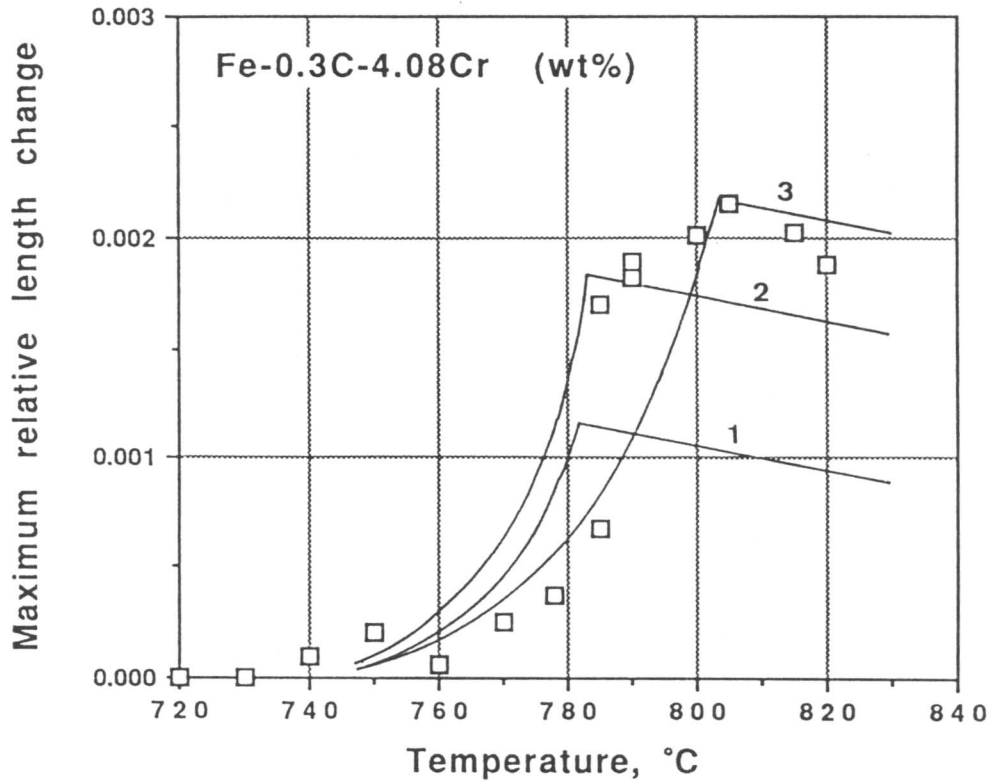
Fig. 4.29 Calculated maximum relative length changes for equilibrium isothermal reaustenitisation. Line 1 is calculated for case (1), line 2 for case (2) and line 3 for case (3). Plots are experimentally observed maximum relative length changes.
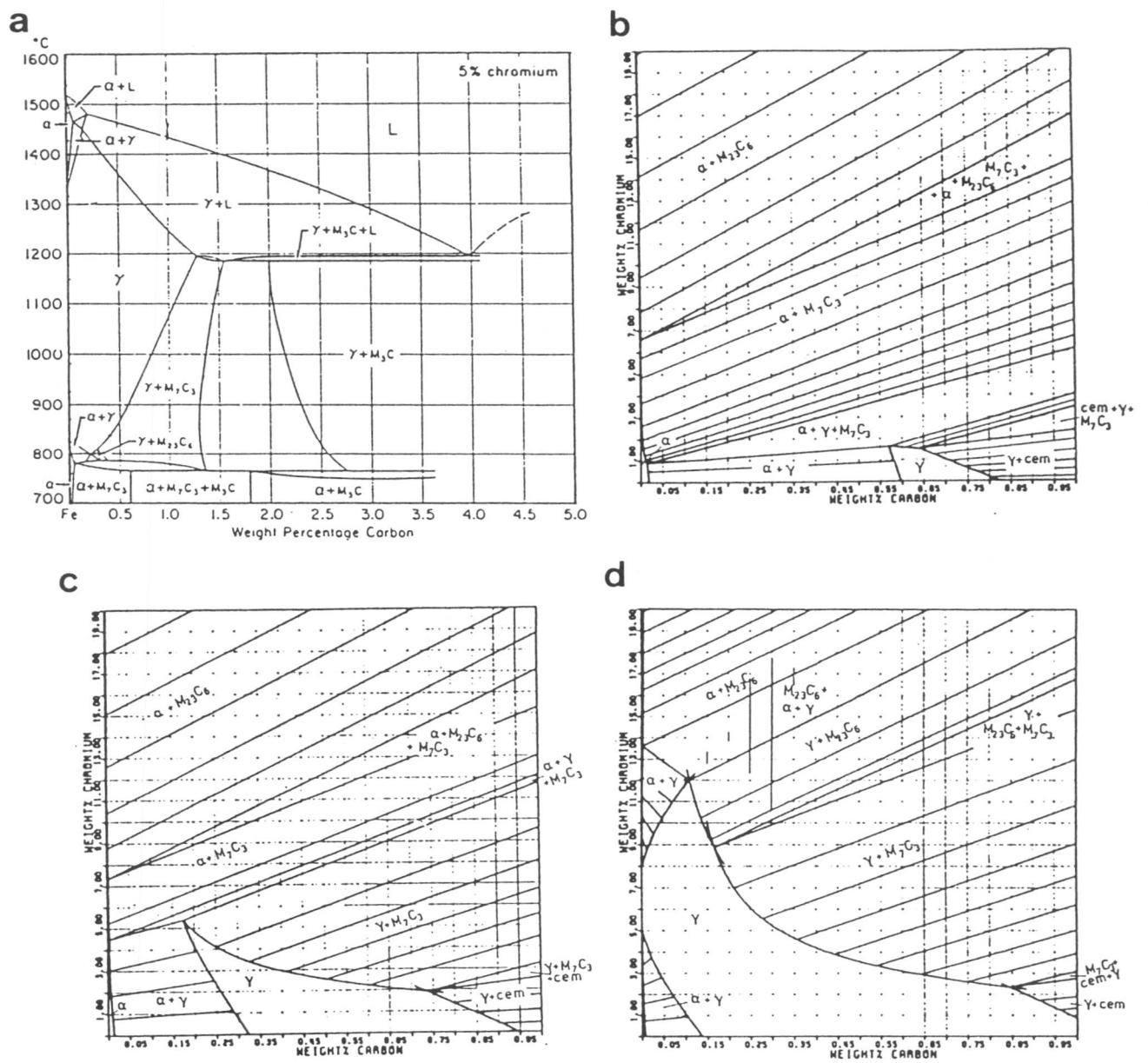
Fig. 4.30 (a) Equilibrium phase diagram of a Fe-5 wt.% Cr alloy (Metals Handbook) and calculated equilibrium phase diagrams for Fe-C-Cr ternary alloy at (b) 750 °C, (c) 800 °C and (d) 850 °C [18].

121
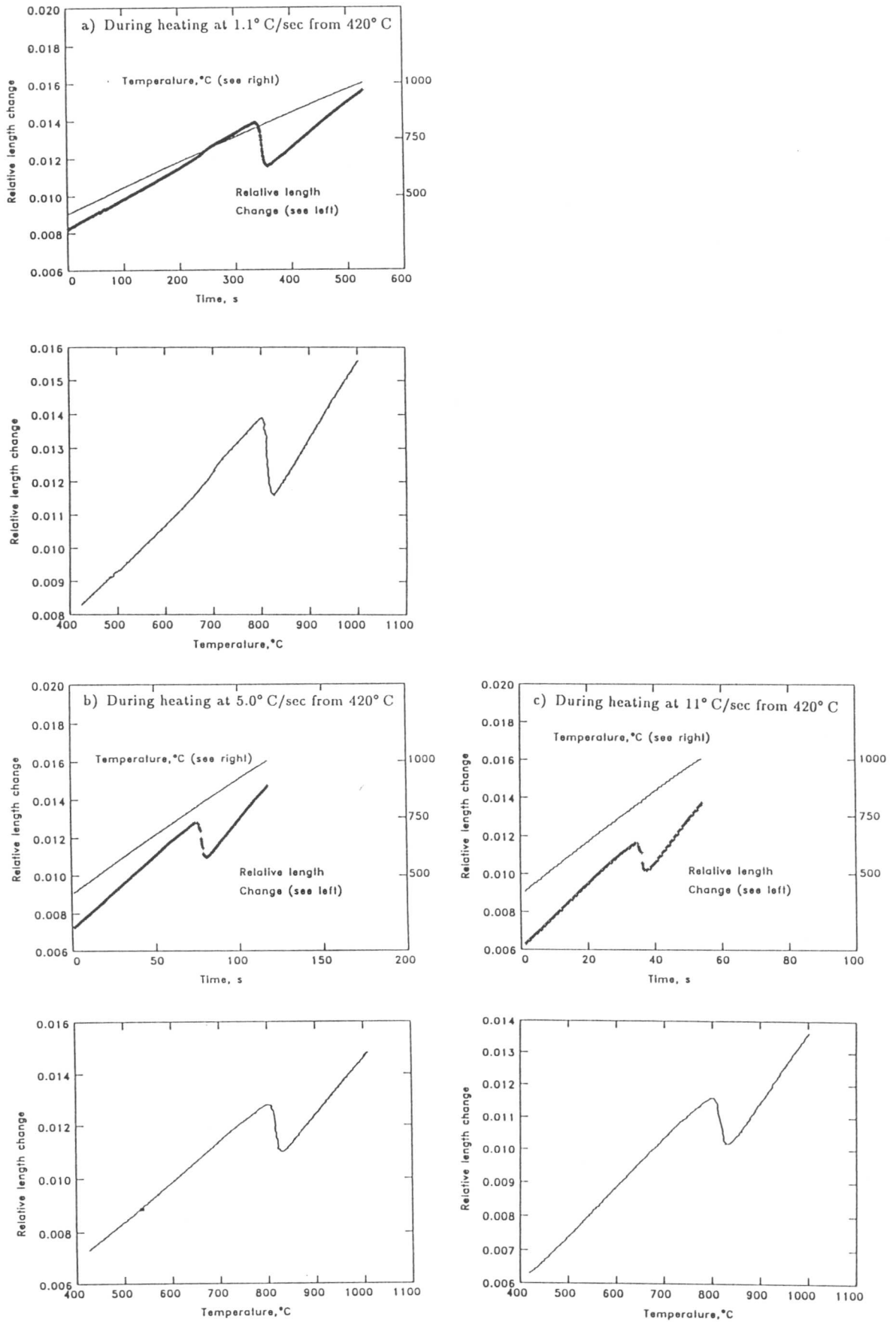
Fig. 4.31 Change in relative length and temperature during continuous heating reaustenitisation from the mixture of bainite and austenite at a) $1.1\,^{\circ}\mathrm{C\,s^{-1}}$ from $420\,^{\circ}\mathrm{C}$, b) $5.0\,^{\circ}\mathrm{C\,s^{-1}}$ from $420\,^{\circ}\mathrm{C}$, c) $11\,^{\circ}\mathrm{C\,s^{-1}}$ from $420\,^{\circ}\mathrm{C}$, d) $1.1\,^{\circ}\mathrm{C\,s^{-1}}$ from $448\,^{\circ}\mathrm{C}$, e) $5.0\,^{\circ}\mathrm{C\,s^{-1}}$ from $448\,^{\circ}\mathrm{C}$, f) $1.1\,^{\circ}\mathrm{C\,s^{-1}}$ from $472\,^{\circ}\mathrm{C}$ and g) $5.0\,^{\circ}\mathrm{C\,s^{-1}}$ from $472\,^{\circ}\mathrm{C}$.

122

d) During heating at 1.1° C/sec from 448° C

e) During heating at 5.0° C/sec from 448° C

f) During heating at 1.1° C/sec from 472° C

g) During heating at 5.0° C/sec from 472° C
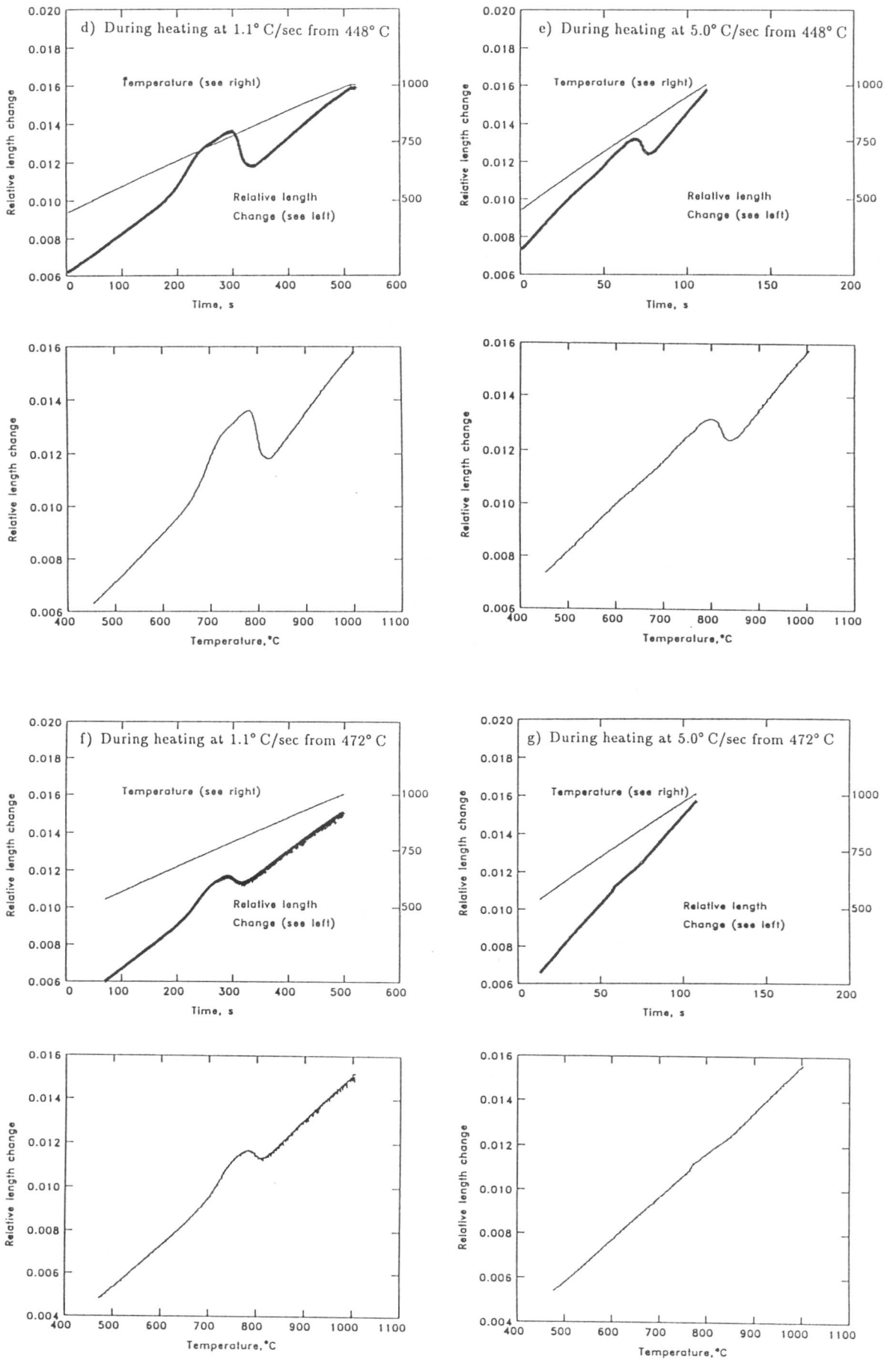
Fig. 4.31 (continued).
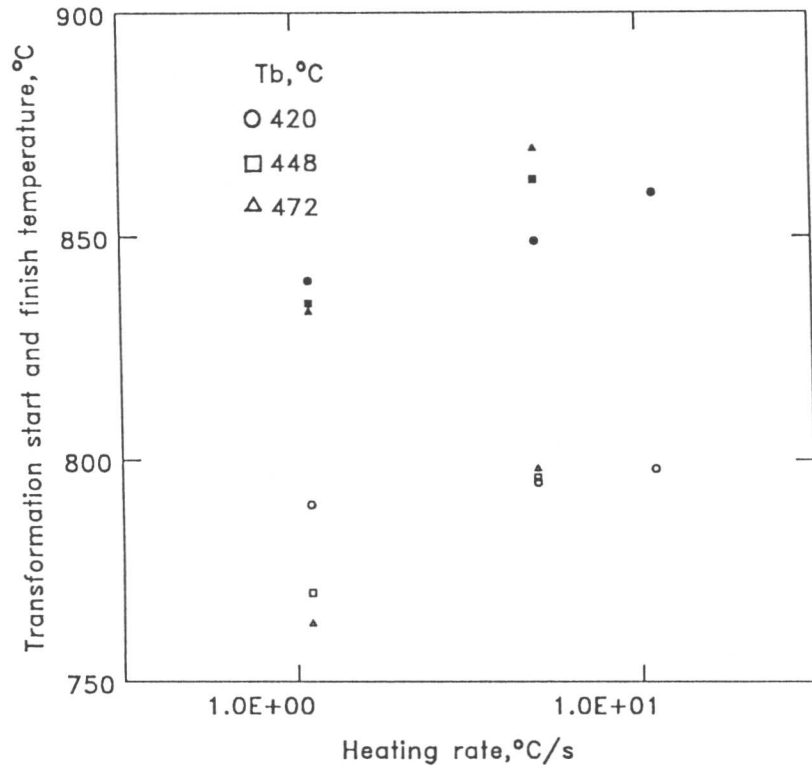
Fig. 4.32 Change in the thermal expansion coefficient of the initial microstructure of mixtures of bainite and austenite as a function of bainite transformation temperature.
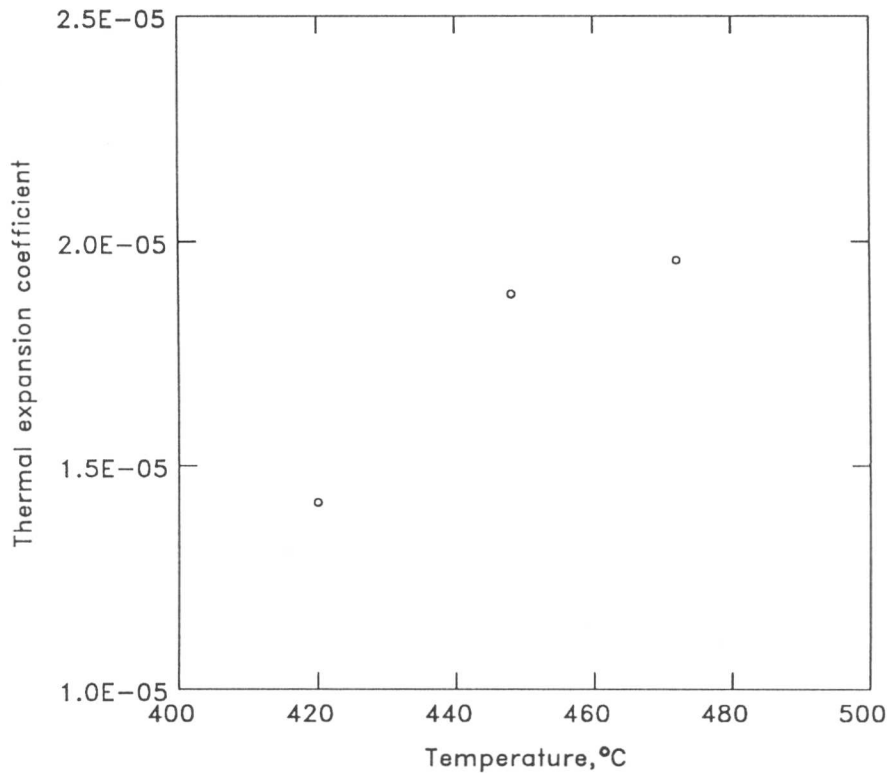
Fig. 4.33 Transformation-start (open) and -finish (solid) temperatures during continuous heating reaustenitisation from the mixtures of bainite and austenite obtained at T_b.

124
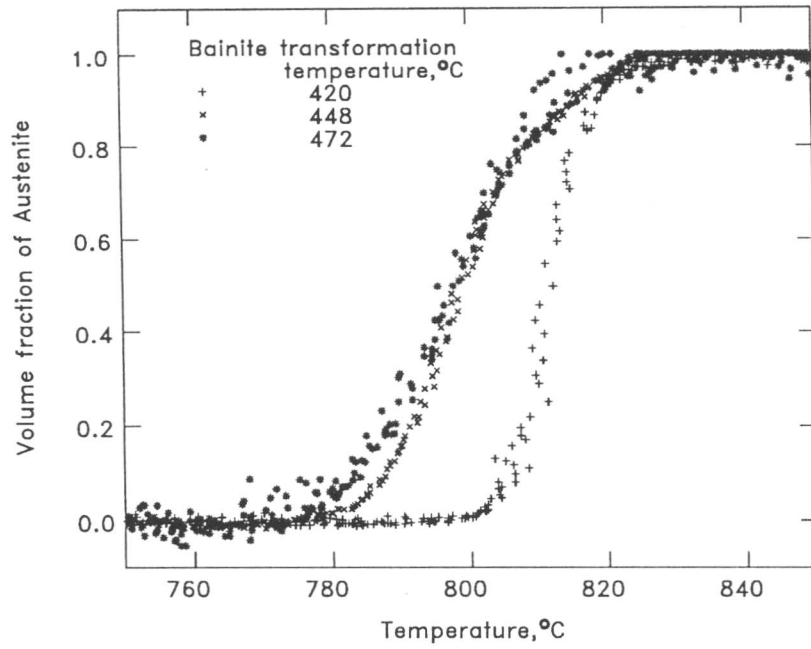
Fig. 4.34 Normalised volume fraction of austenite transformed on heating as a function of temperature.
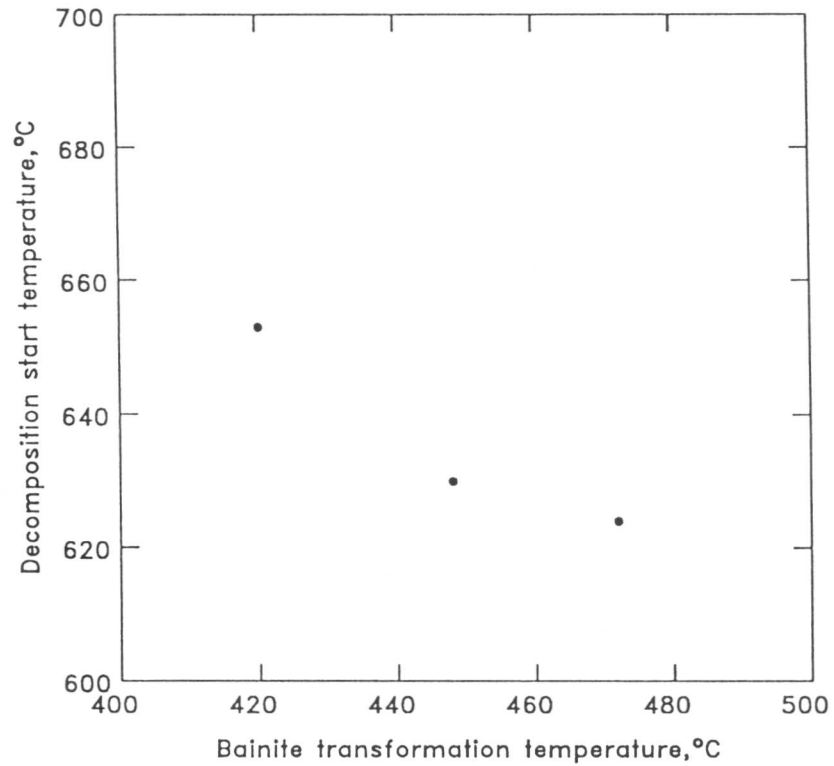
Fig. 4.35 Decomposition-start temperatures during continuous heating plotted against the bainite transformation temperature.

125
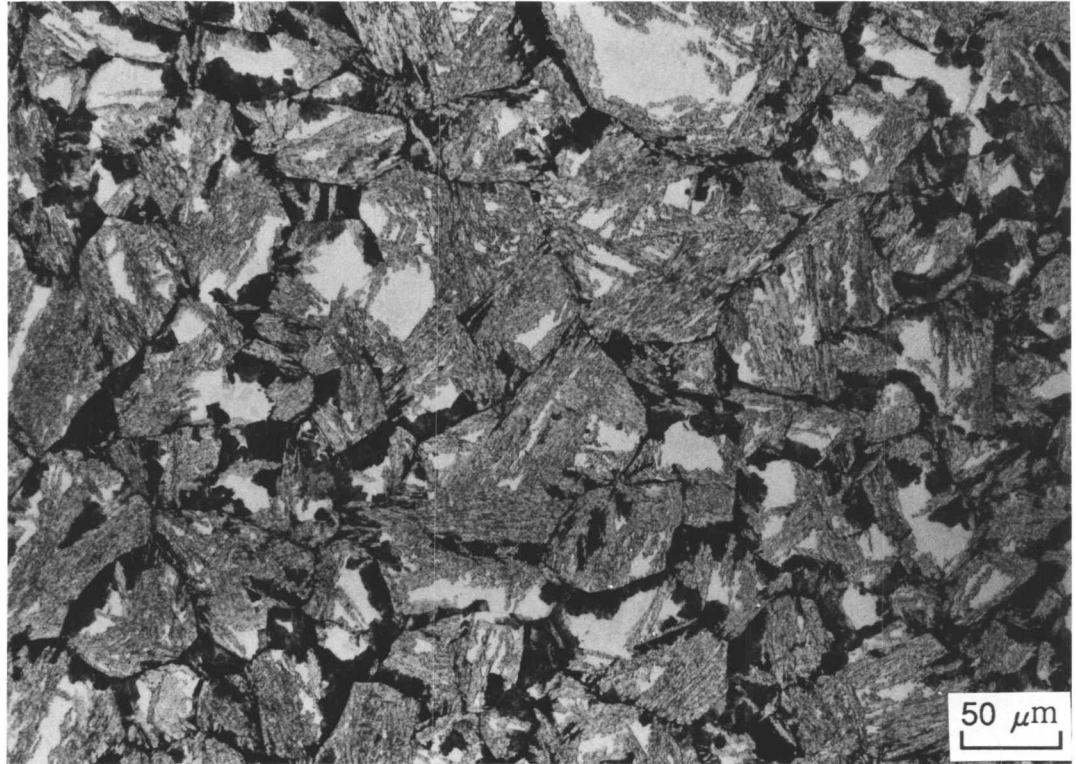
Fig. 4.36 Optical micrograph of a specimen helium quenched during the proceeding of decomposition of residual austenite on the way of the continuous heating reaustenitisation experiment at $1.1\,^{\circ}\mathrm{C\,s^{-1}}$ after 30 min of isothermal bainite transformation treatment at $445\,^{\circ}\mathrm{C}$.
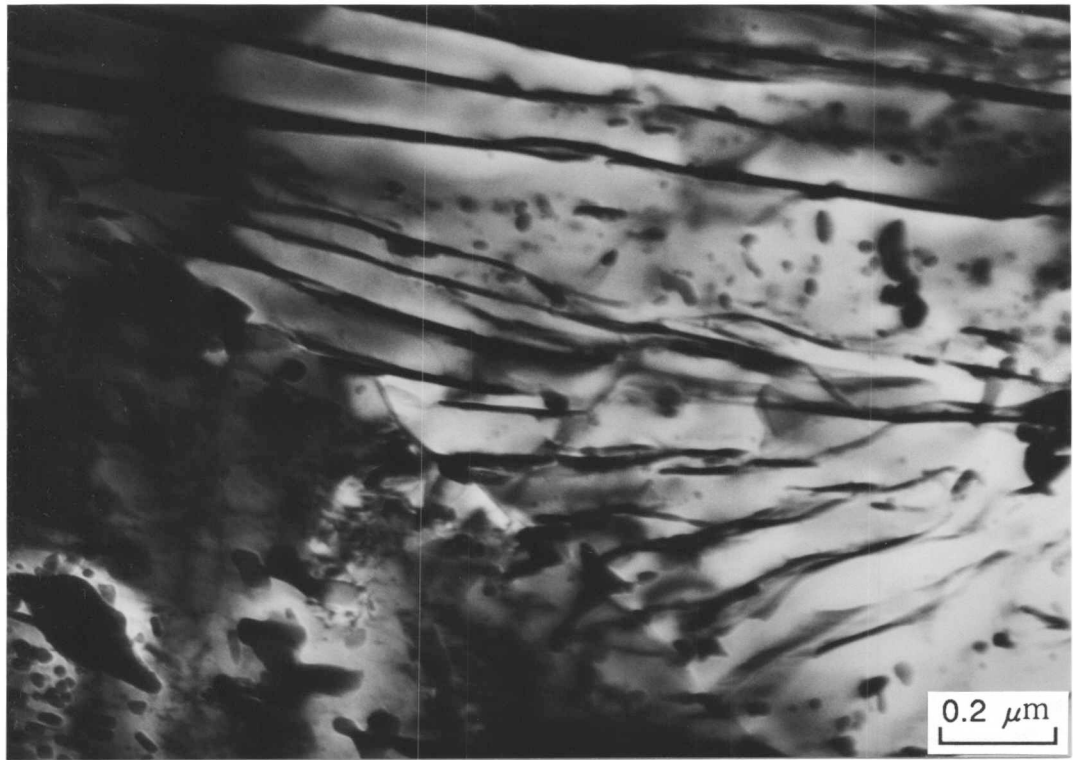
Fig. 4.37 TEM bright field image of the specimen in Fig. 4.36.

CHAPTER 5

PEARLITE TRANSFORMATION IN STEELS

5.1 INTRODUCTION

The reconstructive formation of pearlite in steels is studied in this chapter. Since the bainite transformation stops before equilibrium is achieved, the untransformed austenite can decompose to ferrite and cementite by a reconstructive mechanism. This may happen during a prolonged isothermal holding at a bainite transformation temperature and during heating after bainitic transformation. The later case can be found, for example, in multirun welding where the successive deposition of weld metal heats up the underlying layers.

5.2 DECOMPOSITION OF RESIDUAL AUSTENITE DURING HEATING

As discussed in the previous chapter, the austenite left untransformed after the completion of bainite transformation (*i.e.* residual austenite) decomposes to pearlite during slow heating. The decomposition-start temperature T_{ds} increases with the heating rate and no detectable decomposition of austenite occurs at higher heating rates (Fig. 5.1). The lower the bainite transformation temperature, the higher the decomposition-start temperature (Fig. 5.1).

An attempt to calculate the temperature T_{ds} at which the decomposition of residual austenite starts on heating, from an initial microstructure which is a mixture of bainitic ferrite and residual austenite, is made in this section.

The temperature T_{ds} for the reconstructive formation of ferrite from austenite on heating can be calculated by using the TTT curve for austenite which has the same chemical composition as the residual austenite. Scheil's rule may then be applicable for the calculation of the reconstructive formation of ferrite on heating, although there is no proof of that the reaction is isokinetic [1].

5.2.1 TTT curve calculation of untransformed austenite

Bainite transformation ceases prematurely when the carbon concentration of the residual austenite reaches the T_0' curve ($x_{T_0'}$), because the diffusionless formation of ferrite from austenite with its carbon content of more than $x_{T_0'}$ at a reaction temperature will cause a positive free energy change, which is thermodynamically impossible. However, since the $x_{T_0'}$ value is far less than the equilibrium carbon concentration of austenite, reconstructive transformations can occur even after the bainite reaction ceases. This decomposition may be expressed by the upper C-curve of the TTT diagram, which will be used here for the estimation of T_{ds}.

The calculation of TTT diagrams for the materials with different chemical compositions were carried out using a method reported by Bhadeshia [2]. He assumed an expression for incubation periods proposed by Russell [3], given by:

$$\tau \propto \frac{T}{(\Delta G_m^v)^p D} \tag{5.1}$$

where

T : absolute temperature,

D : an effective diffusion coefficient related to boundary or volume diffusion, depending on the coherency state of the nucleus concerned,

ΔG_m^v : the maximum volume free energy change accompanying the formation of a nucleus in a large amount of matrix phase,

p : an exponent whose magnitude is a function of the nature of the nucleus. Russell [3] obtained $p = 2$ for a coherent nucleus and $p = 3$ for an incoherent one.

On substituting an Arrhenius expression for diffusion coefficients:

$$D \propto \exp(S_1/R)\exp(-Q_1/RT) \tag{5.2}$$

where S_1 is the activation entropy for diffusion and Q_1 is the activation enthalpy for diffusion. Bhadeshia [2] obtained the following relation:

$$\ln[(\Delta G_m)^p \tau/T] = Q_1/(RT) + C_{N1} \tag{5.3}$$

where ΔG_m is the chemical free energy change accompanying the formation of one mole of nucleating phase in a large amount of matrix phase and C_{N1} is a constant. He then expressed Q_1 and S_1 as a function of temperature; $i.e.$ $Q_1 = Q_0 + C_{N2}(T-T')$ and $S_1 = S_0 + C_{N3}\ln(T-T')$, where S_0, Q_0, C_{N2}, C_{N3} and T' are constants, and finally obtained the following expression [2]:

$$\ln\left[\frac{\tau(\Delta G_m)^p}{T^z}\right] = \frac{Q'}{RT} + C_{N4} \tag{5.4}$$

with constants z, Q' and C_{N4}. By maximizing the correlation coefficient when the equation is compared with experimentally observed TTT curves, Bhadeshia [2] obtained $Q' = 0.2432 \times 10^{-6}$ J mol^{-1}, $C_{N4} = -0.0135$, $p = 5$ and $z = 20$ for shear transformation, and $Q' = 0.6031 \times 10^{-6}$ J mol^{-1}, $C_{N4} = -0.01905$, $p = 4$ and $z = 20$ for diffusional transformation respectively. These values were used to calculate the transformation-start temperature of austenite during heating in the present work.

The carbon content of residual austenite $x_1^\gamma\{T_b\}$ and the volume fraction of untransformed austenite V_γ have been calculated from the relative length change $\Delta L/L$ during isothermal bainite transformation at each temperature T_b using equation 4.1, and the results are listed in Table 5.1. The calculated TTT curves for the austenite which has the carbon concentration identical to each values listed in Table 5.1 can be seen in Fig. 5.2. The incubation periods for both diffusional and displacive transformations become large with lowering the bainite transformation temperature. The lower the bainite transformation temperature, the lower the B_S and M_S temperatures of the austenite because of an increase in carbon concentration in the untransformed austenite.

T_b, °C	$\Delta L/L$	$x_1^\gamma\{T_b\}$, at.%	V_γ
420	3.86×10^{-3}	2.4	0.299
448	1.76×10^{-3}	1.8	0.669
472	2.90×10^{-4}	1.4	0.944

Table 5.1: Volume fractions and carbon contents of residual austenite in the initial microstructure

5.2.2 Kinetic calculation of decomposition-start temperature

A point on an upper C-curve representing the minimum detectable reconstructive formation of ferrite at a temperature T_i is now designated as an incubation period $\tau\{T_i\}$. When ΔT refers to a small temperature step in a small time period Δt, $\frac{\Delta T}{\Delta t}$ gives a heating (or cooling) rate at a temperature. At a step between T_i to $T_i + \Delta T$, austenite spends a part of the incubation period ;

$$P_i = \frac{\Delta t}{\tau_i} \tag{5.5}$$

with

$$\tau_i = \frac{1}{2}(\tau\{T_i\} + \tau\{T_i + \Delta T\}).$$

When the summation of P_i becomes unity, the transformation is assumed to start. In order to calculate the position where the austenite is on the TTT diagram during heating after the completion of bainite transformation, the following equation is used (Fig. 5.3).

$$t_i\{T\} = \tau_i \sum_i P_i \tag{5.6}$$

where

$T \ : T_i + \frac{1}{2}\Delta T_i$

$t_i\{T\}$:instantaneous time on the TTT diagram at a temperature T on heating.

The calculations were carried out for continuous heating at constant rates between 0.01 and $10\,^{\circ}\mathrm{C\,s^{-1}}$, for three materials whose carbon contents are identical to the residual austenite left untransformed after the cessation of the bainite transformation at 420, 448 and 472 $^{\circ}$C in the Fe-0.3C-4.08Cr wt.% alloy respectively (Fig. 5.4). Since the formation of bainitic ferrite is thermodynamically impossible above the temperature at which the bainite treatment was conducted, and since the incubation period of reconstructive formation of ferrite at temperatures below the B_S temperature is usually extremely large, the calculation was started from the B_S temperature. In Fig. 5.5, the transformation-start temperatures for each material are drawn with the T_{ds} temperatures obtained in the present experiments. Each calculated transformation-start curve corresponding to the different carbon content increases linearly with heating rate at low heating rates, and rapidly increases at higher heating rates, reaching to the Ae'_3 temperature; above this heating rate, transformation is not expected to occur during heating. Although the calculation treats the austenite in isolation (*i.e.* ignore the presence of the bainitic ferrite), rather good agreement was obtained with experimental results (Fig. 5.5). The fact that almost no decomposition has been observed in the cases of the heating at more than $5\,^{\circ}\mathrm{C\,s^{-1}}$ is also explained as the austenite can be heated up above the Ae'_3 temperature without meeting the diffusional C-curve on heating (Fig. 5.5).

The fact that the change in the decomposition-start temperature of austenite during continuous heating can be understood by using the T_0 concept, is further evidence in support of the incomplete reaction phenomenon.

5.3 FORMATION OF PEARLITE BELOW THE B_S TEMPERATURE

Pearlite formation at very low temperatures may become important under circumstances where austenite is held at low temperatures for an extended period of time without being cooled

below the M_S temperature of the alloy. This may occur, for example, in the heat affected zone of a multirun weld or in the very slow cooling of hot rolled steel strip after coiling.

Bhadeshia [4,5] reported a diffusional perturbation of the interface between bainitic ferrite and residual austenite in the Fe-0.3C-4.08Cr wt.% alloy after an extended period of isothermal holding at 478 °C, just below the B_S temperature 492 °C of the alloy. The growth rate of the perturbation of the interface was found to be far slower than the calculated growth rate of ferrite controlled by the carbon diffusion [5]. Although bainite transformation ceases when the carbon concentration in residual austenite becomes $x_{T_0'}$, reconstructive transformation to ferrite is still possible since $x_{T_0'}$ is far smaller than the equilibrium carbon concentration of the austenite. A relative length change due to bainite transformation at 472 °C; which is very close to the reaction temperature used by Bhadeshia [5], in the Fe-0.3C-4.08Cr wt.% alloy can be seen in Fig. 4.3, showing that the bainite transformation completed within about 30 min of isothermal holding at the temperature.

Specimens with the identical alloy chemistry as [5] were heated to 1100 °C in a furnace and transfered to a different furnace at 478 °C. The specimens were then quenched into water after 300, 600, 241200 (67 hours), 576000 (160 hours), 1987200 (23 days), and 3715200 (43 days) seconds. The volume fraction of bainite increases with time and seems to remain constant beyond 30 min [5] as it can be seen in optical micrographs (Fig. 5.6). After 160 hours of isothermal holding, the formation of a new phase can be found at the austenite grain boundaries (Fig. 5.6). The new phase then grows into one of the austenite grains separated by the grain boundaries at which the nucleation takes place. From a TEM micrograph, one can see a lamellar structure of carbide and ferrite (Fig. 5.7). The structure and the temperature of the transformation suggest that the new phase is pearlite nucleated at the austenite grain boundaries.

The calculated upper C-curve which corresponds to reconstructive formation of austenite, was extrapolated to temperatures lower than the B_S temperature of the alloy. The extrapolated C-curve shows the time required to obtain the minimum detectable amount of reconstructive ferrite is about 150 hours, close to the value observed optically in the present work. This may mean that the austenite after the completion of bainite transformation behaves like an isolated austenite for reconstructive formation of ferrite.

The maximum thickness of pearlite at each holding time were measured and plotted in Fig. 5.8, giving the growth rate of pearlite in the alloy at 478 °C equal to about 1.0×10^{-9} cm s^{-1}.

5.4 GROWTH RATE OF PEARLITE

The pearlite discussed above seems to consist of a mixture of alloy carbide (M_7C_3) and ferrite as mentioned by Bhadeshia [5]. However, it is established that the formation of conventional pearlite can form at a temperature below the B_S temperature after the completion of bainite transformation [6]. Therefore it is important to investigate the formation of pearlite at very low temperatures as well as at temperatures close to the Ae_1 temperature. In this section, the growth theories of conventional pearlite which have been published so far are studied.

The formation of pearlite is expected to occur when austenite is cooled to temperatures at which both ferrite and cementite are thermodynamically stable. Pearlite is a lamellar mixture of iron and iron carbide which is very common constituent of a wide variety of steels contributing substantially to strength. As a result, it has been investigated intensively so far. The kinetics of pearlite transformation have been reviewed recently (for example [7,8]).

Pearlite transformation in steels is reconstructive and known to show a constant growth rate because the composition of untransformed matrix remains unchanged except near the transformation front [1]. The growth rate of pearlite is believed to be controlled by either volume diffusion of carbon [9,10] or by boundary diffusion of substitutional alloying element [11-13]. The two growth theories are summarized as follows.

When the growth rate of pearlite is controlled by the bulk diffusion of atoms in austenite ahead of the interface, the diffusion of carbon may play a more important role than that of substitutional alloying elements, since the diffusivity of the substitutional alloying elements in austenite is far smaller than that of carbon. As a result, the substitutional alloying elements may not diffuse a long distance during the reaction. Therefore the equilibrium condition which is maintained at the interface between austenite and pearlite may be either the negligible partitioning local equilibrium (NPLE) or paraequilibrium (PE). The growth rate of pearlite is expressed as follows [10]:

$$v_V = \frac{D}{g}\frac{s^2}{s_\alpha s_\theta}\frac{x_1^{\gamma\alpha} - x_1^{\gamma\theta}}{x_1^{\theta\gamma} - x_1^{\alpha\gamma}}\frac{1}{s}[1 - \frac{s_C}{s}] \tag{5.7}$$

where

v_V : volume diffusion controlled growth rate of pearlite,

D : volume diffusion coefficient for carbon in austenite,

g : geometric factor equal to 0.72 in plain carbon steels,

$x_1^{\gamma\alpha}$: carbon concentration at the γ/α interface in γ, under either local equilibrium or paraequilibrium with α,

$x_1^{\gamma\theta}$: carbon concentration at the γ/θ interface in γ, under either local equilibrium or paraequilibrium with θ,

$x_1^{\theta\gamma}$: carbon concentration at the θ/γ interface in θ, under either local equilibrium or paraequilibrium with γ,

$x_1^{\alpha\gamma}$: carbon concentration at the α/γ interface in α, under either local equilibrium or paraequilibrium with γ,

s : interlamellar spacing,

s_C : critical spacing at which the growth rate becomes zero,

s_α, s_θ : respective thickness of ferrite and cementite lamellar.

with the maximum velocity criterion, the relation between s and s_C can be obtained by setting the first derivative of equation (5.7) equal to zero, which leads to [9],

$$s = 2s_C \tag{5.8}$$

where

$$s_C = \frac{2\sigma_{\alpha\theta}T_E}{\Delta H \delta T} \tag{5.9}$$

with

$\sigma_{\alpha\theta}$: surface energy of ferrite/cementite interface,

ΔH : change in enthalpy between the parent and product phases,

T_E : eutectoid temperature,

δT : undercooling below the eutectoid temperature.

131

The critical spacing s_C can be compared to observed interlamellar spacing assuming the relation (5.8). Interlamellar spacings in Fe-C, Fe-C-Cr, Fe-Ni and Fe-C-Mn alloys [8,15-17] were used to obtain an empirical expression for the interlamellar spacing as a function of the temperature and the alloy contents. Using the data (Table 5.2), the following relation was obtained for Fe-C, Fe-C-Mn, Fe-C-Ni and Fe-C-Cr steels.

$$\log\{s\} = -2.2358 + 0.09863 \times \text{Mn} - 0.05427 \times \text{Cr} + 0.03367 \times \text{Ni} - \log\{\frac{T_E - T}{T_E}\} \qquad (5.10)$$

where s is measured in μm and Mn, Cr and Ni in wt.%. It is noted that an addition of Cr or Ni decreases the interlamellar spacing as it is observed in many other alloys, whereas a Mn addition causes an increase in the lamellar spacing. A comparison between observed and calculated interlamellar spacing can be seen in Fig. 5.9. The expression for the interlamellar spacing was applied to a material which contains both Mn and Cr. The observed and calculated interlamellar spacing of Fe-1.02Mn-1.05Cr wt.% alloy [18] are plotted in Fig. 5.10. The expression of interlamellar spacing obtained in the present work seems to represent experimental results very well even in alloys which contain both Mn and Cr.

Comparing equations (5.9) and (5.10) assuming the relation (5.8), the following relation should be maintained.

$$\log\{\frac{4\sigma_{\alpha\theta}}{\Delta H}\} = -2.2358 + 0.09863 \times \text{Mn} - 0.05427 \times \text{Cr} + 0.03367 \times \text{Ni}$$

If coefficients reported by Puls and Kirkaldy [7] are adopted, the left hand side becomes -2.404 in plain carbon steels which is very close to the value -2.236 obtained in the present analysis.

$\Delta H = 6.09 \times 10^9 \text{ erg cm}^{-3}$

$\sigma_{\alpha\theta} = 600 \text{ erg cm}^{-2}$

$T_E = 1000 \text{ K}$

It is, however, worth noting that using a more advanced theory proposed by Hashiguchi and Kirkaldy [19], the ratio s/s_C varies between 1 and 2.

When the partitioning of the substitutional alloying elements is substantial during the growth event of pearlite, boundary diffusion of the alloying elements may control the growth rate of pearlite, since the boundary diffusivity of the substitutional alloying elements may become comparable to the bulk diffusivity of carbon in austenite, and, as a result, a long range diffusion of the substitutional alloying elements may become possible during the reaction. The growth rate, in the case, is expressed as follows [13].

$$v_B = 12 K D_B \delta \frac{s^2}{s_\alpha s_\theta} \frac{(x_2^{\gamma\alpha} - x_2^{\gamma\theta})}{\overline{x}_2} \frac{1}{s^2} \left(1 - \frac{s_C}{s}\right) \qquad (5.11)$$

where

v_B : boundary diffusion controlled growth rate,

K : boundary segregation coefficient which is the ratio between alloying element concentration in austenite near the boundary and that in the boundary,

D_B : boundary diffusion coefficient of substitutional alloying element,

δ : thickness of the boundary,

$x_2^{\gamma\alpha}$: substitutional alloying element concentration at the γ/α interface in γ which is under either local equilibrium or paraequilibrium with θ,

$x_2^{\gamma\theta}$: substitutional alloying element concentration at the γ/θ interface in γ which is under either local equilibrium or paraequilibrium with θ,

$\overline{x}_2$: average substitutional alloying element concentration in the alloy concerned.

Sharma et al. [14] determined the factor $KD_B\delta$ for Cr steels with from 0.9 to 1.8 wt.% of Cr, giving:

$$KD_B\delta = 7.6 \times 10^{-8} \exp\left(-\frac{40350}{RT}\right) , \text{cm}^3\,\text{s}^{-1} . \qquad (5.12)$$

These models have been applied to calculate theoretically the growth rate of pearlite [7,14,20,21]. Although the calculated results show reasonable agreement with experimentally observed growth rates of pearlite in plain carbon steels [7], it seems to be more difficult to predict the growth rate of pearlite in alloyed steels. At higher temperatures, where lower supersaturations are expected to exist, boundary diffusion of the substitutional alloying element seems to control the growth of pearlite [7,14,21]. At higher supersaturations, on the other hand, the reaction seems to be controlled by volume diffusion under local equilibrium [14,19,22]. It is, however, worth pointing out that experimentally observed growth rate of pearlite tends to have the maximum velocity at a certain temperature. This was observed in Fe-C-Cr alloys [14,21], in Fe-C-Mn-Cr alloys [18], in Fe-C-Mn alloys [16,23] and Fe-C alloys [15,24], whereas the theoretical calculations have not succeeded in reproducing the position of the peak and the slope below the peak, except a work of Hashiguchi and Kirkaldy [19] who have combined volume and boundary diffusion controlled growth models and managed to obtain an excellent agreement with experimentally observed growth rates of pearlite in a Fe-C binary system, although they had to adopt a few adjustable parameters. Therefore it can be said that the calculation of the growth rate of pearlite at lower temperature is not yet established.

5.5 CALCULATION OF THE INTERFACE COMPOSITIONS

The growth rate of pearlite as discussed in the previous section depends upon the interface compositions of ferrite, cementite and austenite. In order to determine the full set of the interface compositions, we need to know the γ/α, γ/θ and α/θ interface compositions of carbon and the alloying element in Fe-C-X ternary alloys (X denotes the third substitutional element in the alloy). If the heterogeneity of the chemical concentration in ferrite and cementite is ignored, the eight interface compositions $x_1^{\gamma\alpha}$, $x_2^{\gamma\alpha}$, $x_1^{\alpha\gamma}$, $x_2^{\alpha\gamma}$, $x_1^{\gamma\theta}$, $x_2^{\gamma\theta}$, $x_1^{\theta\gamma}$ and $x_2^{\theta\gamma}$ are to be determined.

An approximate method which has been reported by Kirkaldy and his coworkers [25-27] will be used for the calculation of the interface compositions under either paraequilibrium or local equilibrium. The equilibrium condition can be expressed by the equality of the chemical potentials of each element in both phases at the interface. The chemical potentials of carbon, X and iron in ferrite, austenite and cementite are expressed as follows; the numbers 0, 1 and 2 denote, respectively, iron, carbon and the substitutional alloying element X.

In austenite and ferrite;

$$\mu_0 = G_0 + RT \ln x_0 - \frac{RT}{2} \sum \epsilon_{ii} x_i^2 - RT \epsilon_{12} x_1 x_2 \tag{5.13}$$

$$\mu_1 = G_1 + RT \ln x_1 + RT \sum \epsilon_{1i} x_i \tag{5.14}$$

$$\mu_2 = G_2 + RT \ln x_2 + RT(\epsilon_{12} x_2 + \epsilon_{22} x_2) \tag{5.15}$$

and in cementite;

$$\mu_{\mathrm{Fe_3C}} = G_{\mathrm{Fe_3C}} + \frac{3}{4} RT \ln y_0^\theta + \frac{3}{4}(1 - y_0^\theta) w_{02} y_2^\theta \tag{5.16}$$

$$\mu_{\mathrm{M_3C}} = G_{\mathrm{M_3C}} + \frac{3}{4} RT \ln y_2^\theta + \frac{3}{4} y_0^\theta w_{02}(1 - y_2^\theta). \tag{5.17}$$

where $y_i^\theta = \frac{4}{3} x_i^{\gamma\theta}$ are the i-th element concentration in cementite, w's are Fe-X interaction coefficients and ϵ's are Wagner's interaction coefficients.

In the case of paraequilibrium, the interface compositions can be determined from the following equations.

$$\mu_1^\gamma = \mu_1^\alpha \tag{5.18}$$

$$x_0^{\gamma\alpha}(\mu_0^\gamma - \mu_0^\alpha) + x_2^{\gamma\alpha}(\mu_2^\gamma - \mu_2^\alpha) = 0 \tag{5.19}$$

$$x_0^{\gamma\theta}\left(\frac{4}{3}\mu_{\mathrm{Fe_3C}} - \mu_0^\gamma - \frac{1}{3}\mu_1^\gamma\right) + x_2^{\gamma\theta}\left(\frac{4}{3}\mu_{\mathrm{M_3C}} - \mu_2^\gamma - \frac{1}{3}\mu_1^\gamma\right) = 0 \tag{5.20}$$

with the relation expressing the definition of the paraequilibrium,

$$\frac{x_2^{\alpha\gamma}}{x_0^{\alpha\gamma}} = \frac{x_2^{\gamma\alpha}}{x_0^{\gamma\alpha}} = \frac{x_2^{\gamma\theta}}{x_0^{\gamma\theta}} = \frac{y_2^\theta}{y_0^\theta} = \frac{\bar{x}_2}{\bar{x}_0} = k_2 \tag{5.21}$$

and the constant carbon concentration in cementite, $x_1^{\theta\gamma} = 0.25$.

In the case of the local equilibrium at the interface, on the other hand, the equilibrium conditions can be expressed as follows.

$$\mu_i^\alpha = \mu_i^\gamma, (i = 0 \text{ to } 2) \tag{5.22}$$

$$4\mu_{\mathrm{Fe_3C}} = 3\mu_0^\gamma + \mu_1^\gamma \tag{5.23}$$

$$4\mu_{\mathrm{M_3C}} = 3\mu_2^\gamma + \mu_1^\gamma \tag{5.24}$$

As long as a dilute solution is concerned, the following expressions can be adopted for the calculation of the interface compositions under either the paraequilibrium or the local equilibrium. For the γ/α equilibrium:

$$x_1^{\alpha\gamma} = A_1 x_1^{\gamma\alpha} \tag{5.25}$$

134

$$x_2^{\alpha\gamma} = A_2 x_2^{\gamma\alpha} \tag{5.26}$$

and for the γ/θ equilibrium:

$$y_2^{\theta} = B_2 x_2^{\gamma\theta} \tag{5.27}$$

with

$$A_1 = \frac{\exp(\Delta G_1^{\alpha\gamma}/RT + \epsilon_{11}^{\gamma} x_1^{\gamma\alpha})}{1 + \epsilon_{11}^{\alpha} x_1^{\gamma\alpha} \exp(\Delta G_1^{\alpha\gamma}/RT)} \tag{5.28}$$

$$A_2 = \frac{\exp(\Delta G_2^{\alpha\gamma}/RT + \epsilon_{1i}^{\gamma} x_1^{\gamma\alpha})}{1 + \epsilon_{1i}^{\alpha} x_1^{\gamma\alpha} \exp(\Delta G_1^{\alpha\gamma}/RT)} \tag{5.29}$$

$$B_2 = \exp[\{(\frac{4}{3}G_{Fe_3C} - G_0^{\gamma} - \frac{1}{3}G_1^{\gamma}) - (\frac{4}{3}G_{M_3C} - G_2^{\gamma} - \frac{1}{3}G_1^{\gamma}) - w_{02}\}/RT + \epsilon_{1i} x_1^{\gamma\alpha}] \tag{5.30}$$

When the growth rate of pearlite is controlled by the diffusion of carbon in austenite ahead of the interface between pearlite and austenite, it is natural to assume that there is no redistribution of X between matrix and precipitate phases. Therefore, the interface composition may be determined by the paraequilibrium condition.

When the redistribution of the third element X can occur during the growth event of pearlite, on the other hand, the local equilibrium condition is maintained at the interfaces. Since the diffusion of X is the controlling process in this case, the flux of carbon in the parent phase should be negligible when it is compared with that of X in the interfaces. This condition is referred to as 'partitioning under local equilibrium' (PLE) as it is well established in the case of the formation of ferrite from austenite [28,29]. The diffusivity of X, in this case, is expected to be much faster than that in the matrix (i.e. austenite) [30]. The bulk diffusion coefficient of Cr in austenite at $600\,^{\circ}$C is calculated to be $2.5 \times 10^{-18}\,\mathrm{cm^2\,s^{-1}}$ whereas the boundary diffusivity is $9.6 \times 10^{-10}\,\mathrm{cm^2\,s^{-1}}$ [30], assuming that the thickness of the interface is $3 \times 10^{-8}\,\mathrm{cm^2\,s^{-1}}$, which is comparable to the diffusion coefficient of carbon in austenite calculated to be $1.7 \times 10^{-9}\,\mathrm{cm^2\,s^{-1}}$ [31]. When the growth rate of pearlite is controlled by the diffusion of X atoms within the interface region, the partitioning under local equilibrium (PLE) may exist at the interfaces, under which the activities of carbon in austenite at the γ/α and γ/θ interfaces are identical so that the flux of carbon ahead of the interfaces is negligible, thus allowing the diffusion of X atoms catch up with that of carbon. Therefore the interface compositions can be determined by two tie lines AB and CD in Fig. 5.11, where the line AC is the isoactivity line of carbon in austenite. The PLE condition maintains until the supersaturation becomes large enough to make the flux of X atom comparable to that of carbon by producing a sharp spike at the vicinity of the interface. This condition should be designated as 'negligible partitioning under local equilibrium' (NPLE). Since there are two interfaces, γ/α and γ/θ, four different combinations of equilibrium at the interfaces are possible to exist; (1) PLE at the both interfaces, (2) NPLE at the both interfaces, (3) PLE at the γ/α interface and NPLE at the γ/θ interface, and (4) the vice versa. The transition from the PLE to the NPLE condition occurs when $x_2^{\alpha\gamma} = \bar{x}_2^{\gamma}$ for the γ/α interface and under the PLE condition $x_2^{\theta\gamma} = \bar{x}_2^{\gamma}$ for the γ/θ interface (Fig. 5.12).

At the final stage of the reaction, ferrite and cementite should be in equilibrium such that the compositions are determined by the tie line passing through the bulk composition of the steel in the ferrite/cementite two phase region. In the real situation, however, the partitioning of the substitutional alloying element becomes small as the temperature decreases.

Calculated phase diagrams for a Fe-1.08Mn-C wt.% and a Fe-1.41Cr-C wt.% alloys at different temperatures are presented in Fig. 5.13.

5.6 CALCULATION OF THE GROWTH RATE OF PEARLITE

Using the method described in the previous section for the calculation of the interface compositions, the growth rates of pearlite in Fe-C-X (X = Mn and Cr) ternary alloys were calculated. The two alloying elements were selected because fine experimental results are available from the published literature.

Calculation of paraequilibrium growth rate of pearlite is straightforward; *i.e.* the interface compositions calculated as discussed in the previous section will be used in equation (5.7) with the expressions for s and s_C. The diffusion coefficient of carbon in austenite is calculated as discussed by Trivedi and Pound [32]. The growth rate under the local equilibrium, on the other hand, is not as simple as the paraequilibrium case. In order to calculate the growth rate of pearlite under the local equilibrium, the constants K, D_B and δ in equation (5.11) should be determined. It is, however, less clear how to derive the constants. Therefore an empirical method which was used by Sharma *et al.* [14] is adopted here.

As mentioned earlier, the diffusion of substitutional alloying elements plays an important role when the supersaturation is low. As a result, the growth rate of pearlite is considered to be controlled by the interface diffusion of the substitutional alloying element at higher temperatures, whereas by the bulk diffusion of carbon at lower temperatures. However, as it is well established, the partitioning of chromium is observed even at temperatures where bainite transformation takes place [21]. Therefore interface diffusion may play an important role on governing the growth rate of pearlite even at low temperatures. Although Sharma *et al.* [14] obtained equation (5.12) using the data of the growth rate of pearlite at low supersaturations, it may be possible to modify the equation to include the data at higher supersaturations. Therefore the factor $KD_B\delta$ is estimated using the calculated interface compositions and the interlamellar spacing for eutectoid steels containing Mn or Cr using the following equation.

$$KD_B\delta = v_B / \left[12 \frac{s^2}{s_\alpha s_\theta} \frac{(x_2^{\gamma\alpha} - x_2^{\gamma\theta})}{\overline{x}_2} \frac{1}{s^2} \left(1 - \frac{s_C}{s} \right) \right] \qquad (5.31)$$

where the ratio between s_α and s_θ is assumed to be 7. The values s_C and s are calculated using equations (5.8) and (5.9) respectively. The data used to obtain the equation are listed in Table 5.3.

Assuming the same expression of $K\delta D_B$ as equation (5.12), we now obtain a relation as follows (Fig. 5.14).

$$KD_B\delta = C_0 \exp\left(-\frac{Q_B}{RT}\right) \, , \mathrm{cm^3\,s^{-1}} \, . \qquad (5.32)$$

where constants C_0 and Q_B are 2.223×10^{-8} cm^3 s^{-1} and 140940 J mol^{-1} for the 1.1 wt.% Mn steel and 1.052×10^{-8} cm^3 s^{-1} and 148320 J mol^{-1} for the Cr steels with between 0.9 and 1.8 wt.% of Cr. Assuming that the boundary diffusivities of Mn and Cr are same as

136

T, °C	$\overline{x}_1$, wt.%	v_B, cm² s⁻¹	$1/s$, cm⁻¹	$x_2^{\gamma\alpha} - x_2^{\gamma\theta}$	$KD_B\delta$, cm³ s⁻¹
720	Cr=1.8	0.35E-04	0.78E+05	0.0102	8.90E-17
720	Cr=1.3	0.18E-04	0.58E+05	0.0074	8.94E-17
710	Cr=1.8	0.70E-04	0.97E+05	0.0186	7.94E-17
710	Cr=1.3	0.40E-04	0.76E+05	0.0157	7.00E-17
710	Cr=0.9	0.38E-04	0.58E+05	0.0133	9.41E-17
700	Cr=1.8	1.20E-04	1.07E+05	0.0269	7.87E-17
700	Cr=1.3	0.84E-04	0.94E+05	0.0238	6.35E-17
690	Cr=1.8	1.80E-04	1.36E+05	0.0353	5.67E-17
690	Cr=1.3	1.40E-04	1.12E+05	0.0316	5.65E-17
680	Cr=1.8	2.15E-04	1.55E+05	0.0441	4.22E-17
670	Cr=1.8	2.20E-04	1.75E+05	0.0530	2.78E-17
660	Cr=1.4	5.00E-04	1.94E+05	0.0504	3.94E-17
650	Cr=1.4	4.50E-04	2.14E+05	0.0504	2.56E-17
640	Cr=1.4	3.70E-04	2.33E+05	0.0592	1.57E-17
670	Mn=1.1	0.82E-04	0.56E+05	0.0220	1.16E-16
660	Mn=1.1	1.45E-04	0.72E+05	0.0266	1.01E-16
640	Mn=1.1	5.22E-04	1.04E+05	0.0378	1.21E-16
620	Mn=1.1	11.3E-04	1.36E+05	0.0529	1.09E-16
580	Mn=1.1	11.3E-04	2.01E+05	0.0827	3.25E-17
550	Mn=1.1	9.22E-04	2.49E+05	0.1050	1.37E-17
530	Mn=1.1	4.59E-04	2.81E+05	0.1200	4.73E-18

Table 5.3: Calculation of $KD_B\delta$ from published pearlite growth data in Fe-C-Cr and Fe-C-Mn alloys. The first eleven data are after Sharma $et\ al.$ [14], the next three data after Chance and Ridley [21] and the last seven data after Razik [16]. $x_2^{\gamma\alpha} - x_2^{\gamma\theta}$ is measured in mole fraction.

the self boundary diffusion coefficient of iron in austenite, $D_B\delta$ can be expressed as $5.4 \times 10^{-8}\exp(-155500/RT)$ cm² s⁻¹ [30]. This gives expressions for the boundary segregation coefficients $K = 0.41\exp(14560/RT)$ and $K = 0.20\exp(7180/RT)$ for Mn and Cr respectively. The boundary segregation coefficients of Mn and Cr are evaluated to be 3.0 and 0.54 at 600° C respectively.

Ridley [8] reported the growth rate of pearlite, interlamellar spacing and partition coefficient in 1.08 wt% Mn and 1.41 wt.% Cr eutectoid steels (Fig. 5.15). The growth rate of pearlite has a peak in both cases whereas the partition coefficient shows a monotonous decrease towards the unity at lower temperatures. It is worth noting, however, the change in the partition coefficient as a function of reaction temperature in the Cr steel is more moderate than that in the Mn steel (Fig. 5.15).

The calculation of the interface compositions under local equilibrium was carried out using the method described in the previous section. The calculated interface compositions $x_2^{\theta\gamma}$ and $x_2^{\alpha\gamma}$ were then used to derive the partition coefficient K_P of X using the following expression.

$$K_P = x_2^{\theta\gamma}/x_2^{\alpha\gamma} \tag{5.33}$$

At higher temperatures, the partition coefficient is expected to have a larger value since the supersaturation of austenite is small at those temperatures whereas the mobility of X atom is high. The value K_P decreases with temperature and reaches the unity when the NPLE condition maintains both at the γ/α and at the γ/θ interfaces. A change in the K_P value in eutectoid steels with either 1.08% Mn or 1.41% Cr as a function of the transformation temperature is plotted in Fig. 5.16 and Fig. 5.17. Experimentally observed partition coefficients [8] were

also plotted in the figures. The calculation was conducted for 0.8, 0.7 and 0.6 wt.% alloys to clarify the effect of supersaturation on the partition coefficient in the case of the Mn steel. As it can be seen from the figures, the calculation seems to express the change in the K_P value successfully except at higher temperatures where an effect of the level of supersaturation is large. The difference in the change in the K_P values between the Mn and Cr steels was also reproduced successfully by the present model. The K_P in the Fe-C-Cr alloy stays higher even at low temperatures when it is compared with the Fe-C-Mn alloy. The PLE condition maintains even at 600° C in the Fe-C-Cr alloy whereas the NPLE condition takes over at around 600° C in the Fe-C-Mn alloy.

The calculated growth rates of pearlite are compared with the experimental values reported by Ridley [8] in Fig. 5.18. The growth rate calculated assuming paraequilibrium diffusion of carbon in austenite shows a good agreement with the observed growth rates except at lower temperatures than the temperature at which the growth rate becomes the maximum. The growth rate of pearlite under local equilibrium also shows a peak which is consistent with the experimental results (Fig. 5.18). Since the constants in equation (5.11) were determined by fitting the equation to the data for the Fe-C-Mn alloy, the growth rate of pearlite calculated under the local equilibrium is naturally consistent to the experimental values.

The paraequilibrium growth rate is retarded by Mn additions as shown in Fig. 5.19. Since the Ae_1 temperature is affected strongly by Mn addition, the growth rate at higher temperature is more sensitive to Mn addition than the lower temperatures. In the case of the local equilibrium, the effect of the Mn addition is more substantial (Fig. 5.20). In the both cases, the growth rate and the peak temperature are reduced by the Mn addition.

The growth rate calculation was also carried out for the Fe-1.41 wt% Cr eutectoid alloy. Calculated growth rates of pearlite under paraequilibrium or local equilibrium conditions are compared against observations in [8] (Fig. 5.21). Although the agreement is not as good as for the Mn steel, the temperature dependence of the growth rate seems to be well expressed especially by the local equilibrium calculation.

Although the equations derived in this work can only be appropriate for the steels concerned above, the calculation was extended to a Fe-0.3C-4.08Cr wt.% in which the growth rate of pearlite at 478 °C was measured to be around 1.0×10^{-9} cm s^{-1}. The paraequilibrium growth rate of pearlite at 478 °C was calculated to be 1.9×10^{-3} cm s^{-1} which is far larger than the observed one. The local equilibrium calculation gave the growth rate of pearlite equal to 6.8×10^{-5} cm s^{-1} at 478 °C which is much smaller than the paraequilibrium growth rate but still orders of larger than the experimental value. However, it should be noted that the theory discussed here is for conventional pearlite whereas the pearlite observed in the Fe-0.3C-4.08Cr wt.% alloy is alloy pearlite. Although the theory of the growth of alloy pearlite has not been developed, this result may suggest, for the first approximation, that the growth of pearlite at very low temperatures is not a diffusion controlled reaction but rather an interface controlled process. As a movement of an interface is controlled both by diffusions of atoms, which provide the chemical concentration differences within each phase, and by a sluggish transfer of atoms across the interface, which therefore does not give rise to any large concentration differences. The former case is referred to as a diffusion-controlled process, and the latter as an interface-controlled process [33]. It is not difficult to imagine that transformations from austenite to ferrite are controlled by the interface process more strongly than the diffusion of atoms. The rate of reaction will then be smaller than that expected by the local equilibrium mechanism

[33].

The rate of reaction controlled by the interface process is given by the following equation [1]:

$$v_I = \delta\nu \exp(\frac{-\Delta_a g^*}{RT})[1 - \exp(\frac{-\Delta g^{\beta\alpha}}{RT})] \tag{5.34}$$

where δ is the width of the interface, $\Delta_a g^*$ and $\Delta g^{\beta\alpha}$ are the activation energy and the driving force for the transformation per atom, ν is a characteristic frequency which is given by the value kT/h where k and h are Boltzmann's and Plank's constants respectively.

$\Delta g^{\beta\alpha}$ is calculated as the free energy change due to the formation of pearlite from austenite as follows [34].

$$\Delta g^{\beta\alpha} = (1 - x_1^\gamma)\Delta G_{Fe}^{\gamma\to\alpha} + x(\Delta G^\theta + 4.01T - 10580)$$
$$- RT[\frac{1 - x_1^\gamma}{5}\ln(\frac{1 - 6x_1^\gamma}{1 - x_1^\gamma}) + \ln(\frac{x_1^\gamma}{1 - 6x_1^\gamma})] \tag{5.35}$$

where

$$\Delta G^\theta = 29325 - 28.74T \text{ J mol}^{-1}$$
$$\Delta G_{Fe}^{\gamma\to\alpha} = -5024 + 9.86 \times 10^{-3}T^2 - 6.44 \times 10^{-6}T^3 \text{ J mol}^{-1}$$

Assuming that δ being the lattice parameter of austenite, ν being $kT/h = 1.57 \times 10^{13}$ s^{-1}, the growth rate controlled by the interface process can be calculated using equation (5.34) as a function of the activation energy $\Delta_a g^*$. Since the growth rate of pearlite at 478° C was measured to be 1.0×10^{-9} cm s^{-1}, the activation energy $\Delta_a g^*$ can be calculated from the equation. $\Delta G^\theta, \Delta G_{Fe}^{\gamma\to\alpha}$ are 7743.5 and -1551 J mol^{-1}, hence $\Delta g^{\beta\alpha} = -1496$ J mol^{-1}. Using the data $\delta = 3.573 \times 10^{-10}$ m and $\nu = kt/h = 1.57 \times 10^{13}$ s^{-1}, $\Delta_a g^*$ is calculated to be 202 kJ mol^{-1}, which is close to the activation energies of the self diffusion of iron in austenite and ferrite; i.e. 286 and 240 kJ mol^{-1}. Although the activation energy calculated from the observed growth rate at 478 °C is close to that of the self diffusion of iron, it is still uncertain if the reaction is controlled by the interface process. Further work is necessary together with the study of the growth rate of alloy pearlite instead of conventional pearlite to reach a decisive conclusion.

5.7 CONCLUSIONS

Although the bainite transformation terminates when the carbon concentration of the untransformed austenite reaches the T_0 or T_0' curve, the austenite can nevertheless decompose to ferrite and cementite by reconstructive transformation. A case is the formation of pearlite after the cessation of the bainite transformation. In this chapter, pearlite transformation kinetics at low temperatures and the formation of pearlite during heating after the termination of bainite transformation were studied and following conclusions were obtained.

1) The formation of pearlite during heating from a bainite transformation temperature after the cessation of the bainite reaction can be understood by the TTT curve for untransformed austenite with the carbon concentration of $x_{T_0'}$ at the bainite transformation temperature, and by Scheil's rule.

2) The result of the analysis is evidence for the incomplete reaction phenomenon during the bainite transformation.

3) The incubation period for pearlite transformation observed at 478 °C is reproducible by the upper C-curve of the TTT curve for the alloy.

4) The growth rate of pearlite was studied theoretically and the local equilibrium calculation of the interface compositions gave the partition coefficient of the substitutional alloying element which agrees reasonably well with the published results.

5) The growth rate of pearlite observed at 478 °C (1.0×10^{-9} cm s^{-1}) is far smaller than the calculated diffusion controlled growth rate. Although the pearlite observed in this work is alloy pearlite, this discrepancy in the growth rate may mean that the formation of pearlite at very low temperatures is controlled by the interface process instead of the long range diffusion of atoms.

REFERENCES

1. J. W. Christian: *"The Theory of Transformations in Metals and Alloys Part 1"*, Pergamon Press, Oxford, 1975.

2. H. K. D. H. Bhadeshia: *Metal Science*, 1982, **16**, 159.

3. K. C. Russell: *Acta Metall.*, 1969, **17**, 1123.

4. H. K. D. H. Bhadeshia: *Acta Metall.*, 1980, **28**, 1103.

5. H. K. D. H. Bhadeshia: *Proc. Int. Conf. "Solid-Solid Phase Transformations"*, 1981, 1041.

6. H. K. D. H. Bhadeshia and D. V. Edmonds: *Metall. Trans. A*, 1979, **10A**, 895.

7. M. P. Puls and J. S. Kirkaldy: *Metal. Trans.*, 1972, **3**, 2777.

8. N. Ridley: *Metal. Trans.*, 1984, **15A**, 1019.

9. C. Zener: *Trans. AIME*, 1946, **167**, 550.

10. M. Hillert: *Jernkont Ann.*, 1957, **141**, 757.

11. J. M. Shapio and J. S. Kirkaldy: *Acta Metall.*, 1968, **16**, 579.

12. B. E. Sandquist: *Acta Metall.*, 1968, **16**, 1413.

13. M. Hillert: *"The Mechanism of Phase Transformations in Crystalline Solids"*, Institute of Metals, London, 1969, 231.

14. R. C. Sharma, G. R. Purdy and J. S. Kirkaldy: *Metall. Trans.*, 1979, **10A**, 1129.

15. D. Brown and N. Ridley: *JISI*, 1966, **204**, 811.

16. N. A. Razik, W. Lorimer and N. Ridley: *Acta Metall.*, 1974, **22**, 1249.

17. J. W. Cahn and W. C. Hagel: *"Decomposition of Austenite by Diffusional Processes"*, ed. by V. F. Zackay and H. I. Aaronson, Interscience Publishers, New York, NY, 1962, 131.

18. S. A. Al-Salman, G. W. Lorimer and N. Ridley: *Acta Metall.*, 1979, **27**, 1391.

19. K. Hashiguchi and J. S. Kirkaldy: *Scandinavian Journal of Metall.*, 1984, **13**, 240.

20. B. E. Sandquist: *Acta Metall.*, 1969, **17**, 967.

21. J. Chance and N. Ridley: *Metall. Trans.*, 1981, **12A**, 1205.

22. M. Hillert: *Proc. Int. Conf. on "Solid-Solid Phase Transformations"*, 1981, 789.

23. M. L. Picklesimer, D. L. McElroy, T. M. Kegley, Jr., E. E. Stansbury and J. H. Frye, Jr.: *Trans. AIME*, 1960, **218**, 473.

24. J. H. Frye, Jr, E. E. Stansbury and D. L. McElroy: *Trans. AIME*, 1953, **February**, 219.

25. J. S. Kirkaldy, B. A. Thomson and E. A. Baganis: *"Hardenability Concepts with Applications to Steel"*, ed D. V. Doane and J. S. Kirkaldy, AIME, 1978, 82.

26. J. G. Gilmour, G. R. Purdy and J. S. Kirkaldy: *Metall. Trans.*, 1972, **3**, 1455.

27. K. Hashiguchi and J. S. Kirkaldy: *CALPHAD*, 1984, **8,** 173.

28. M. Hillert: *Internal Report, Swedish Institute of Metals Research,* 1953.

29. J. S. Kirkaldy: *Canadian J. Phys.,* 1958, **36,** 907.

30. J. Fridberg, L-E. Törndahl and M. Hillert: *Jernkont. Ann.,* 1969, **153,** 263.

31. J. Ågren: *Acta Metall.,* 1982, **30,** 841.

32. R. Trivedi and G. M. Pound: *J. Appl. Phys.,* 1969, **38,** 3569.

33. M. Hillert: *Metall. Trans. A,* 1975, **6A,** 5.

34. L. Kaufman and S. V. Radcliffe: *"Decomposition of Austenite by Diffusional Processes",* ed. by *V. F. Zackay and H. I. Aaronson, Interscience Publishers, New York, NY,* 1962, 313.
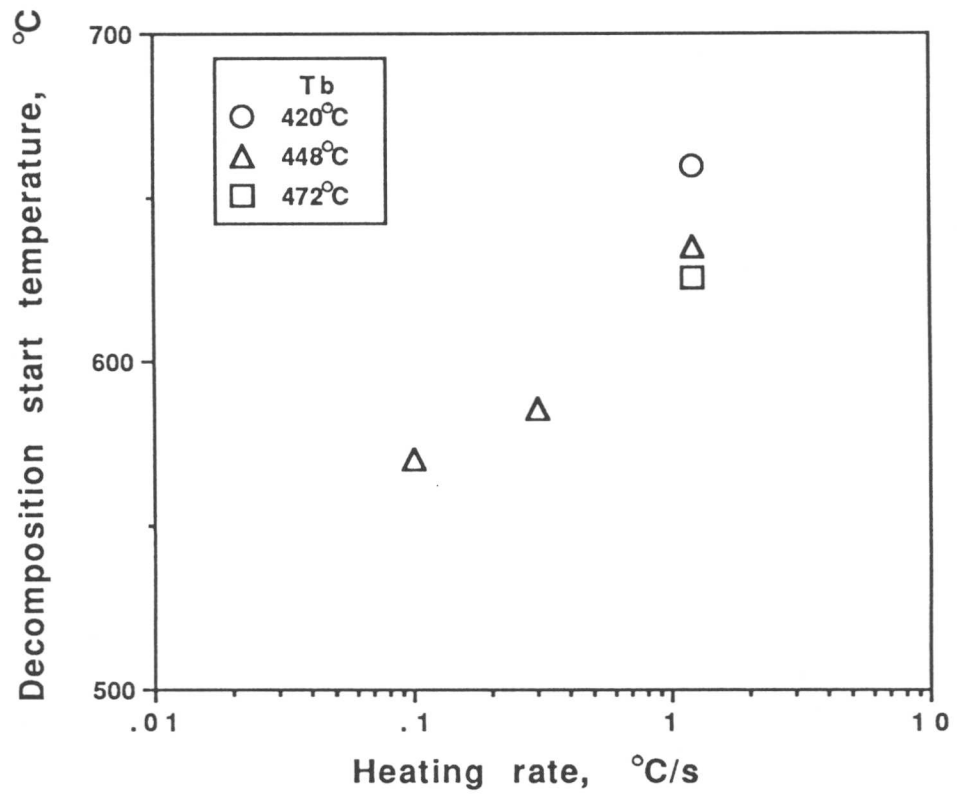
Fig. 5.1 Effect of heating rate on decomposition-start temperature of austenite remaining untransformed after the completion of the bainite transformation.
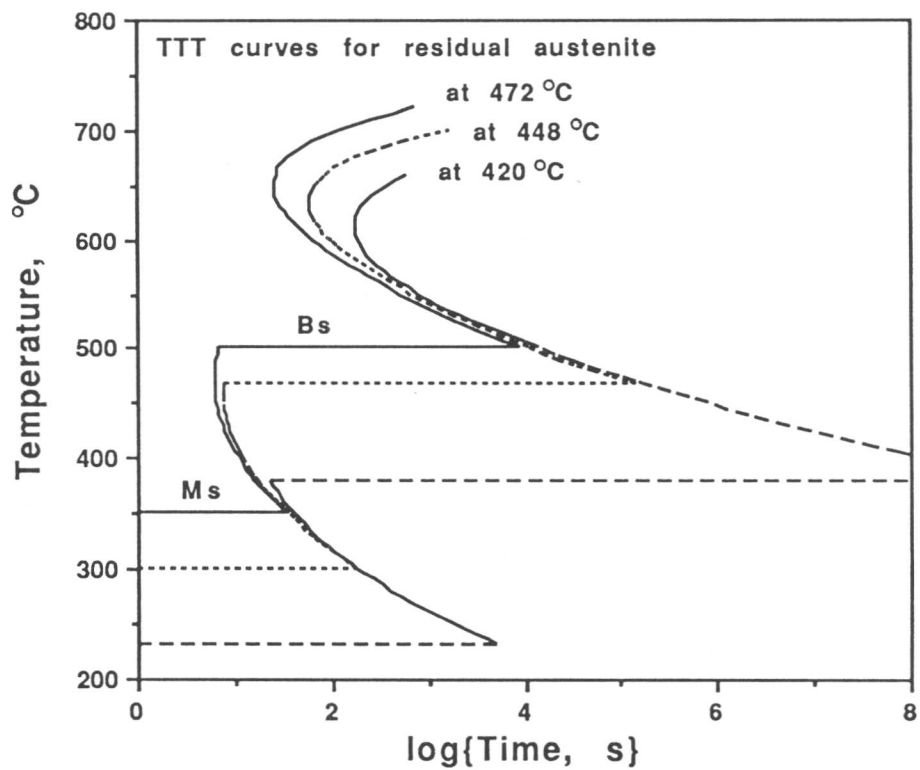
Fig. 5.2 Calculated TTT curves of austenite with chemical composition identical to the residual austenite after the formation of bainitic ferrite at 420 °C, 448 °C and 472 °C respectively.
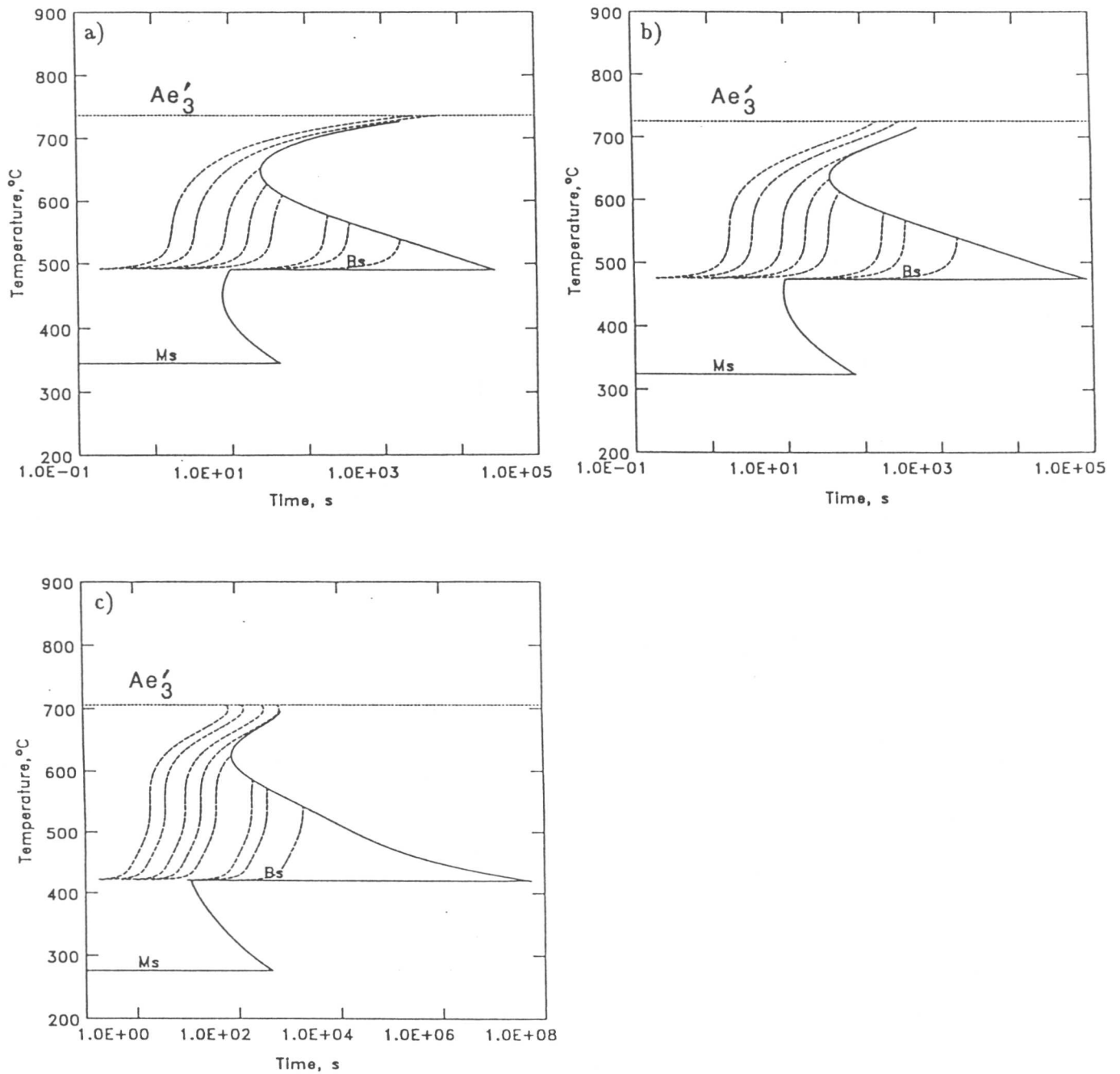
Fig. 5.3 Calculated TTT curves of residual austenite at (a) $420\,^\circ$C ($x_{\gamma 0} = 2.4$ at.%), (b) $448\,^\circ$C ($x_{\gamma 0} = 1.8$ at.%) and (c) $472\,^\circ$C ($x_{\gamma 0} = 1.4$ at.%) (solid line), and the position of austenite in the TTT curves during continuous heating at constant heating rates between 0.01 and $10\,^\circ$C s^{-1}(dashed lines).

143
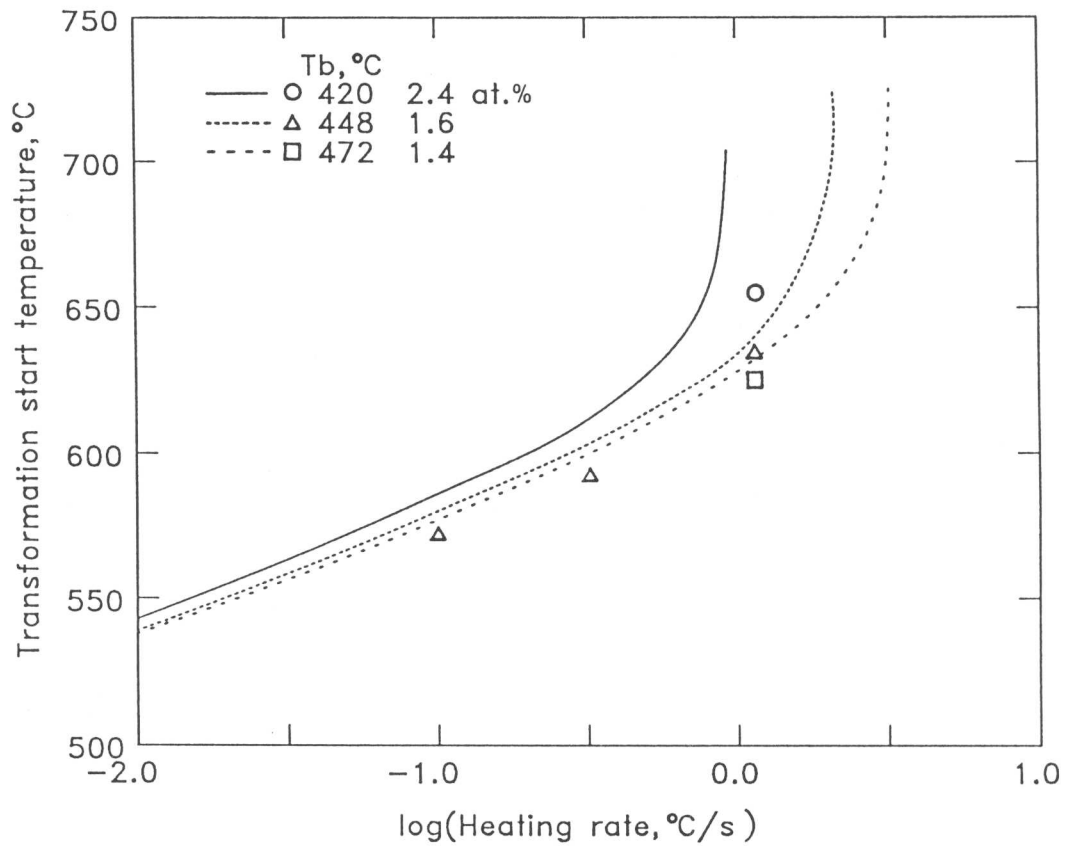
Fig. 5.4 Comparison between observed and calculated decomposition-start temperatures during the heating of austenite which is left untransformed after the bainite transformation steps.

144
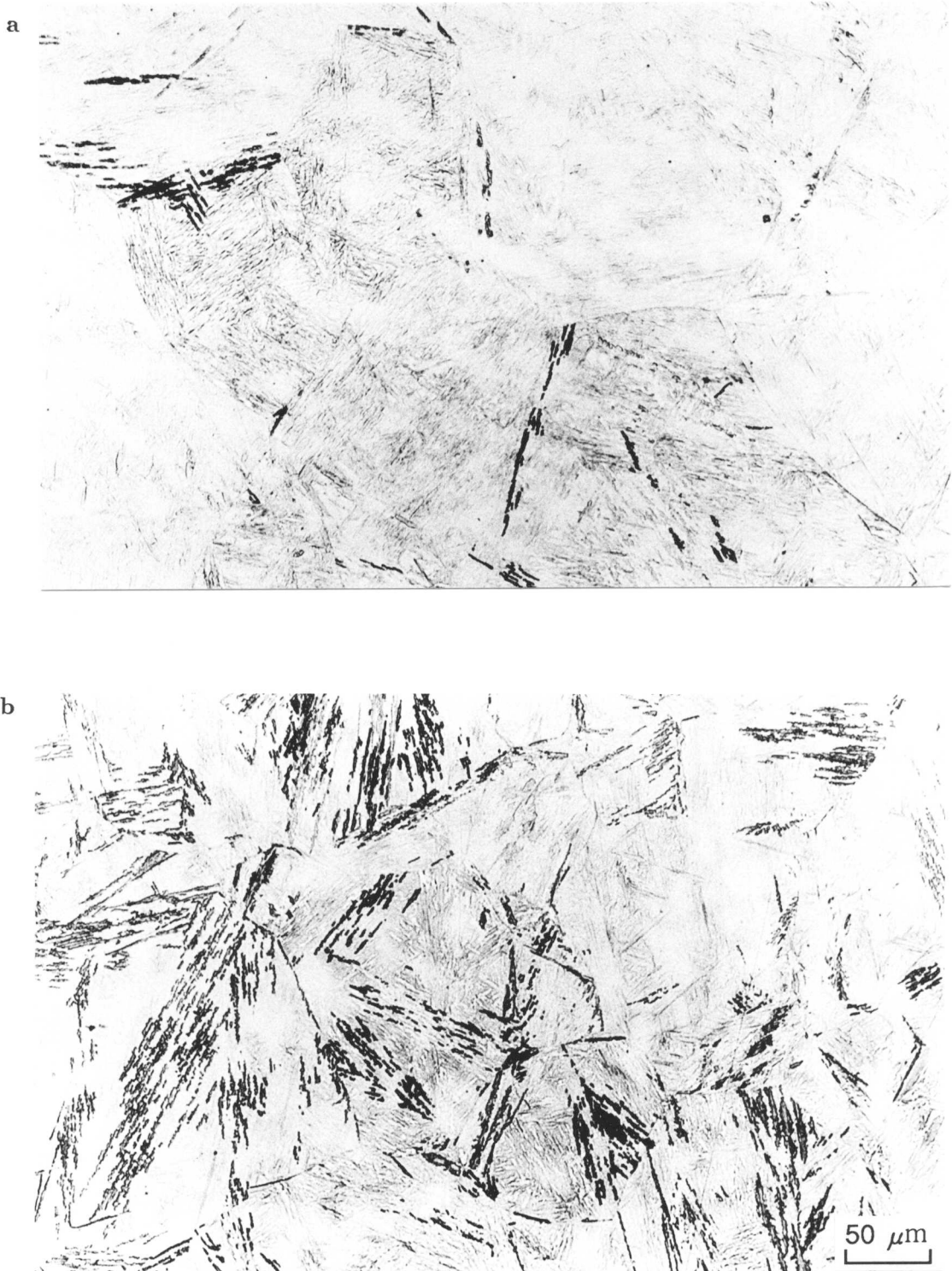
Fig. 5.5 Optical micrographs of specimens isothermally held at 478 °C for (a) 300 sec, (b) 600 sec, (c) 67 hours, (d) 160 hours, (e) 23 days and (f) 43 days.

145

c

d

50 μm

Fig. 5.5 (continued)

146

e

f

50 μm

Fig. 5.5 (continued)

147
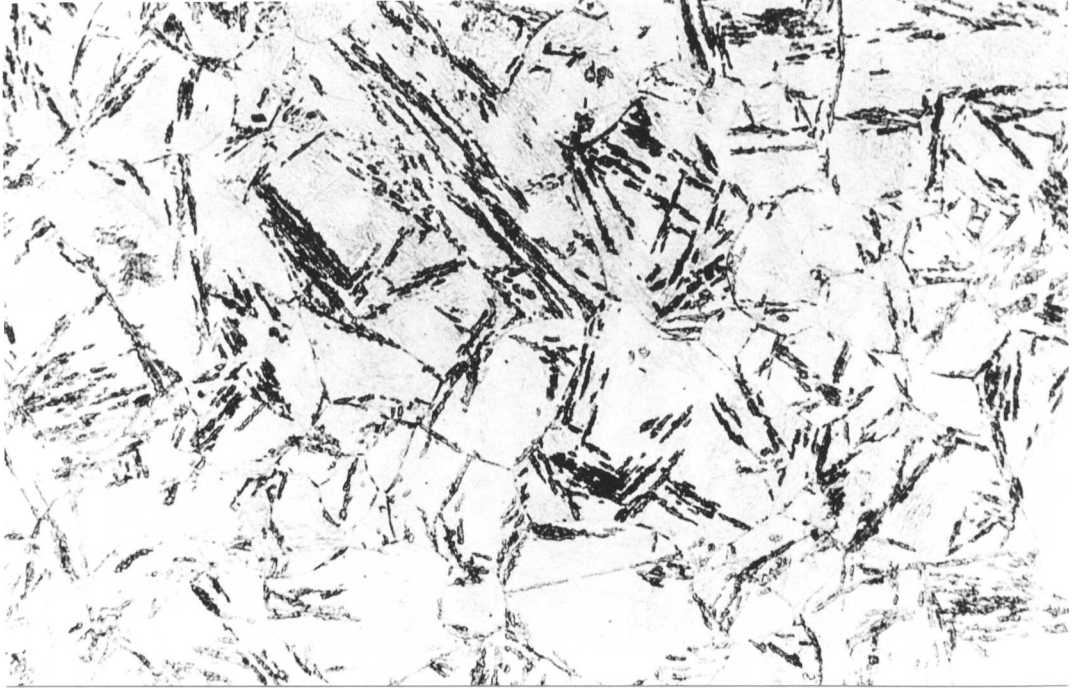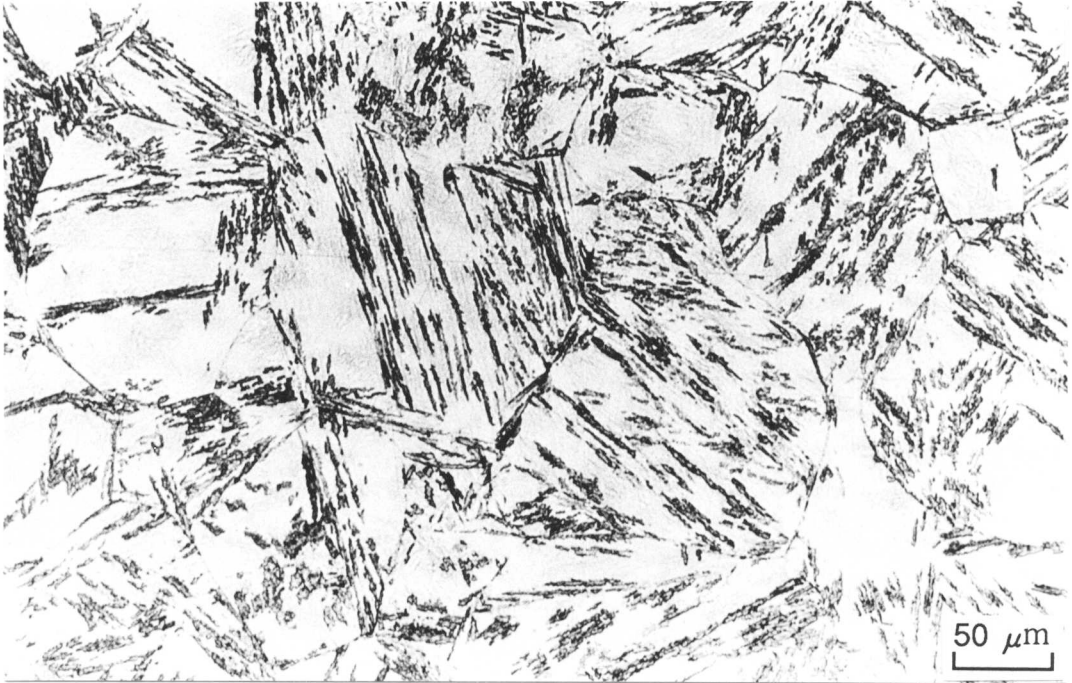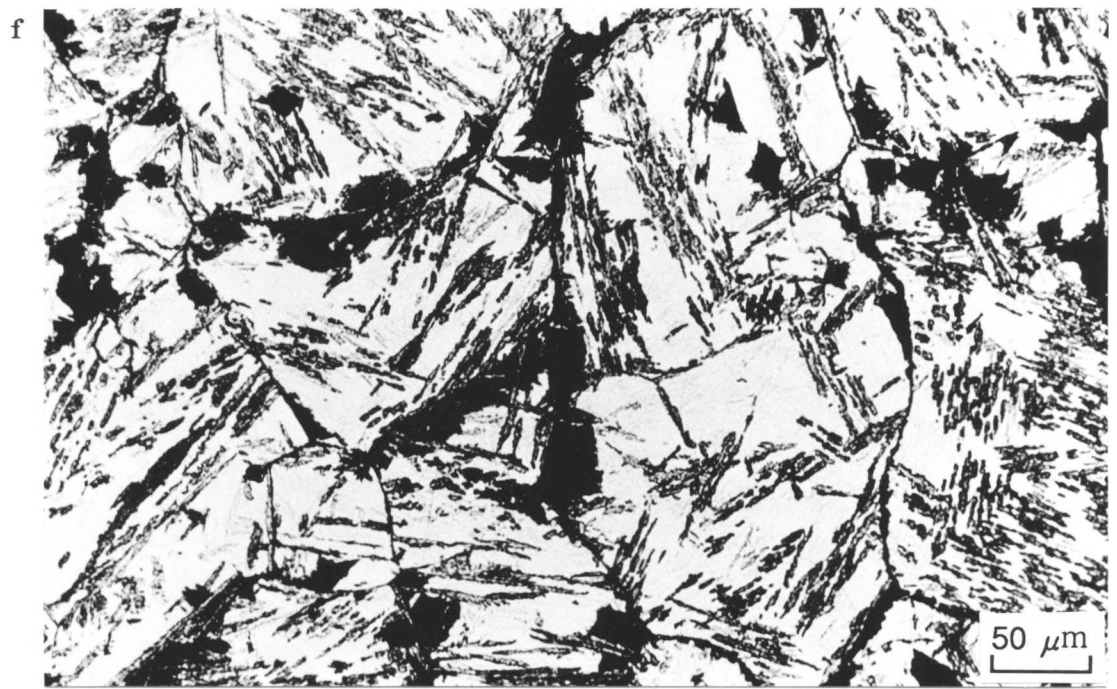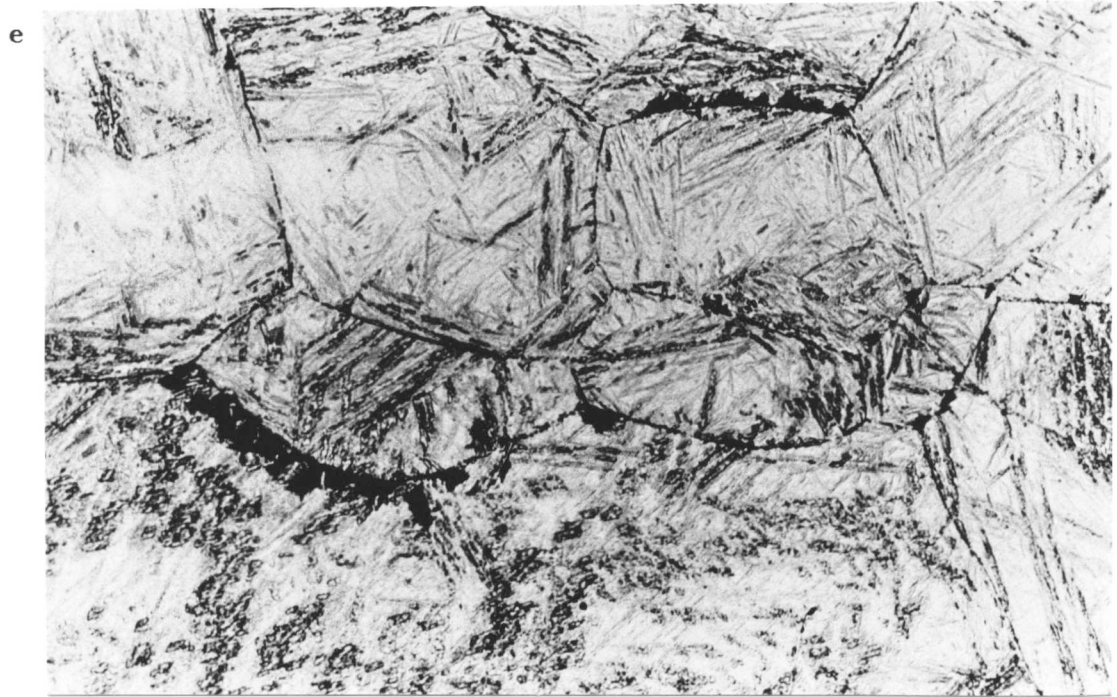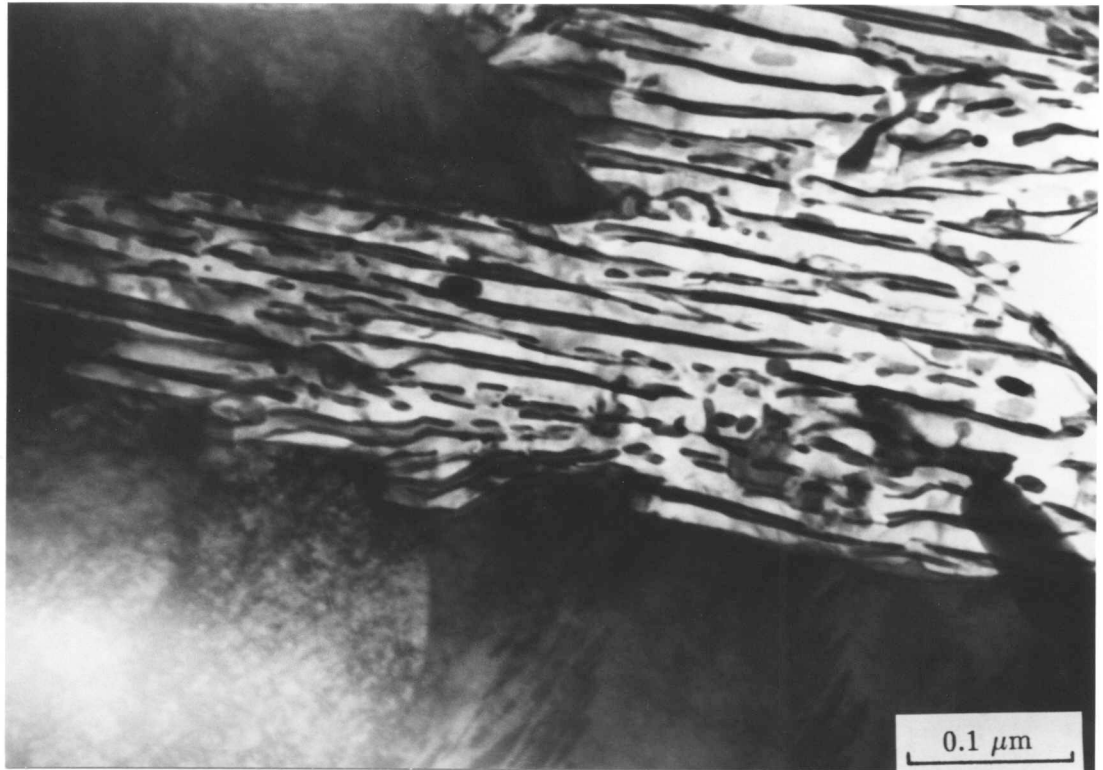
Fig. 5.6 TEM bright field image of alloy pearlite.
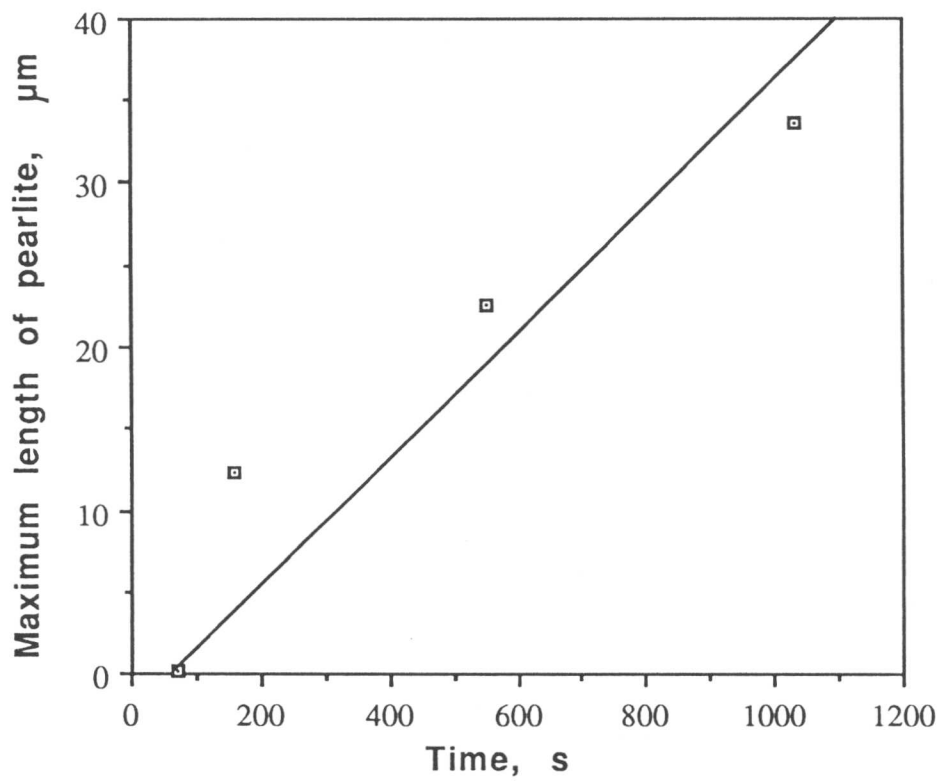
Fig. 5.7 Change in the maximum thickness of pearlite with isothermal holding time at 478 °C.
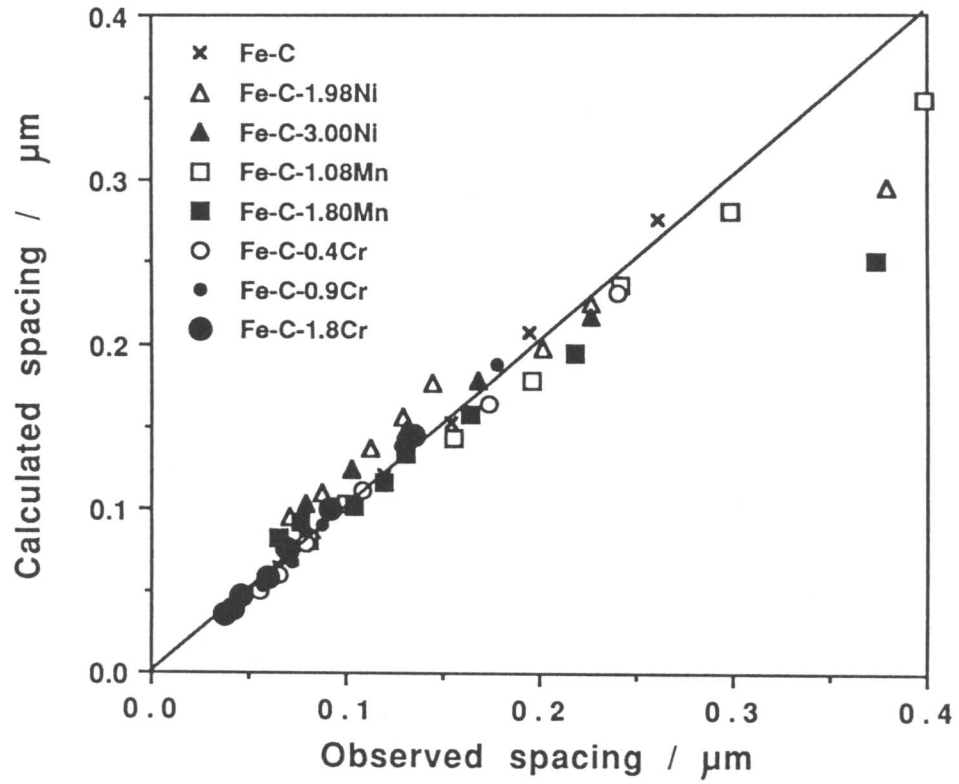
Fig. 5.8 Comparison between observed and calculated interlamellar spacing in Fe-C-Mn, F-C-Ni and Fe-C-Cr alloys.
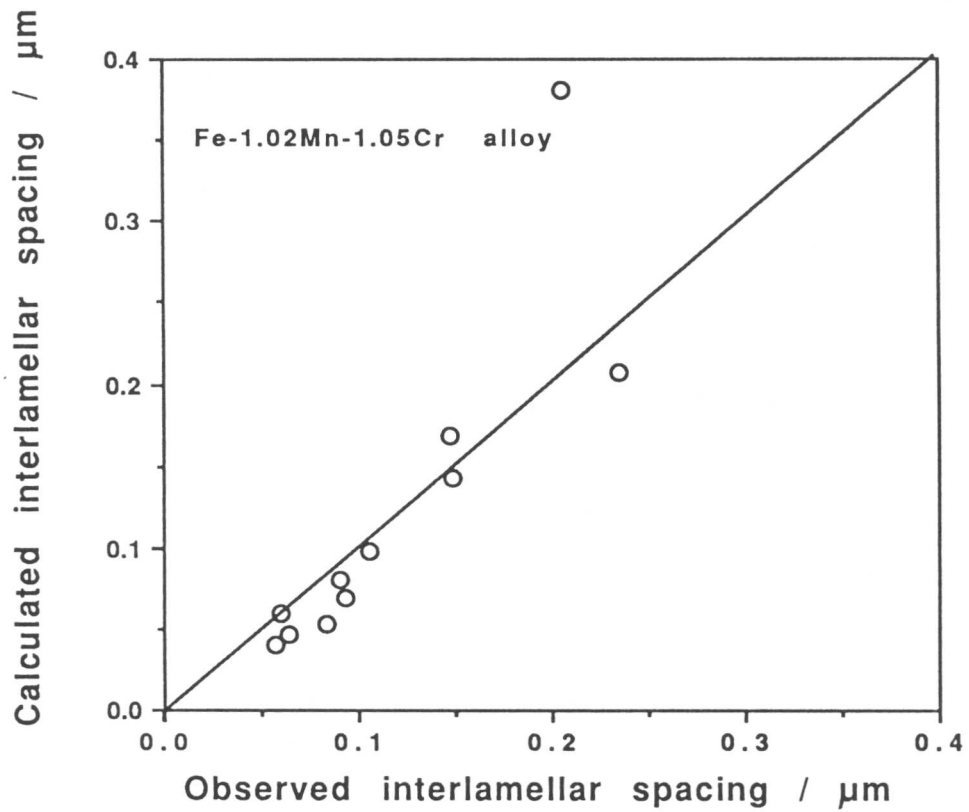
Fig. 5.9 Comparison between observed [18] and calculated interlamellar spacing in a Fe-1.02Mn-1.05Cr alloy.

149
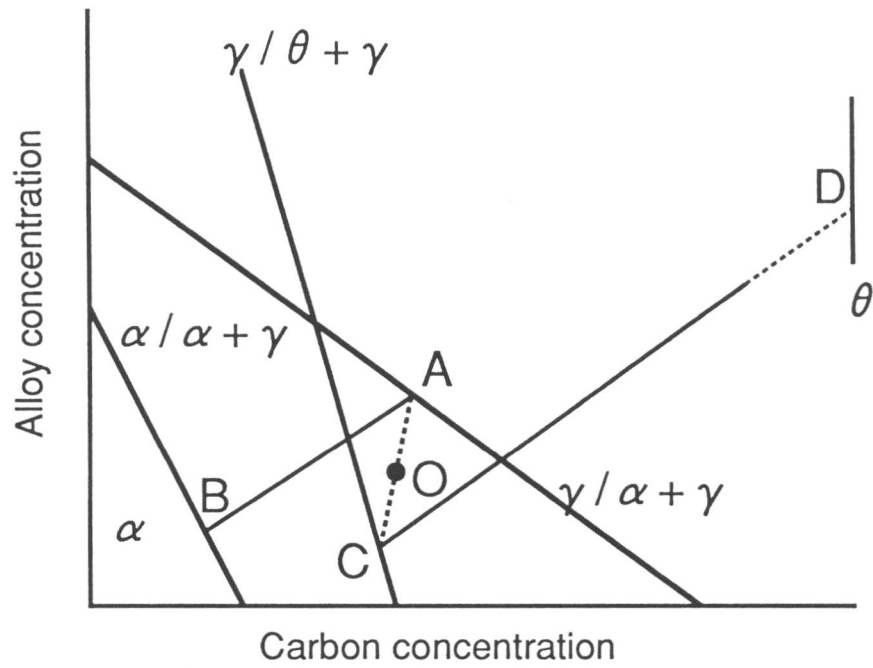
Fig. 5.10 Schematic illustration of the phase diagram showing the interface compositions during the growth of pearlite under local equilibrium.
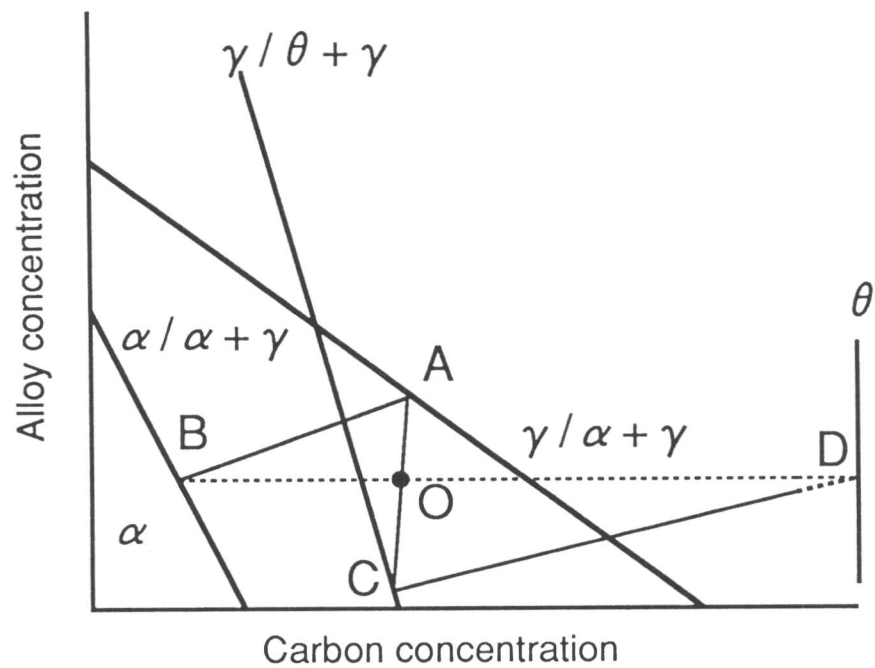
Fig. 5.11 Schematic illustration of the phase diagram showing the interface compositions during the growth of pearlite under the negligible partitioning under local equilibrium.
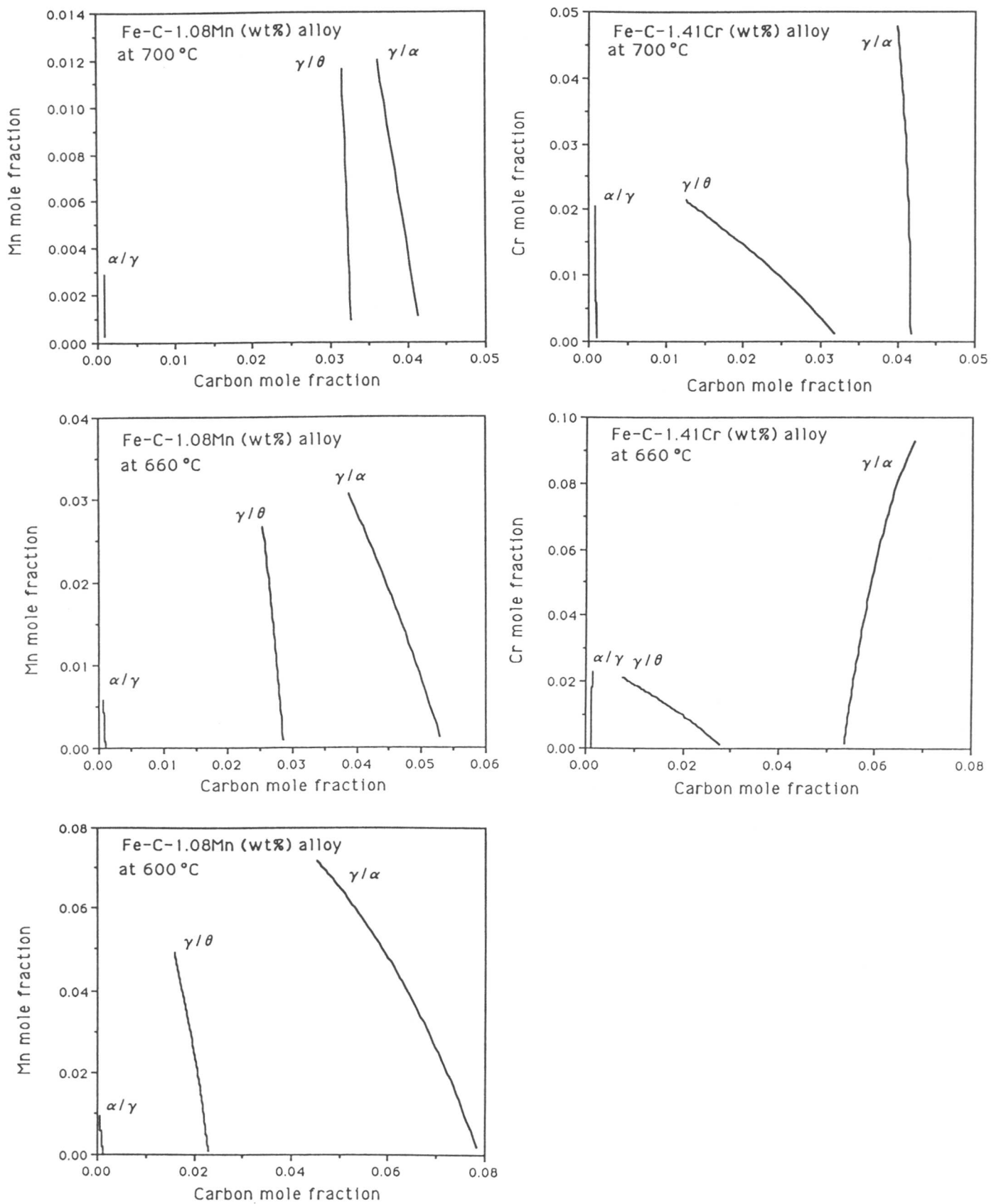
Fig. 5.12 Calculated phase diagrams for a Fe-1.08Mn-C wt.% and a Fe-1.41-C wt.% alloys.
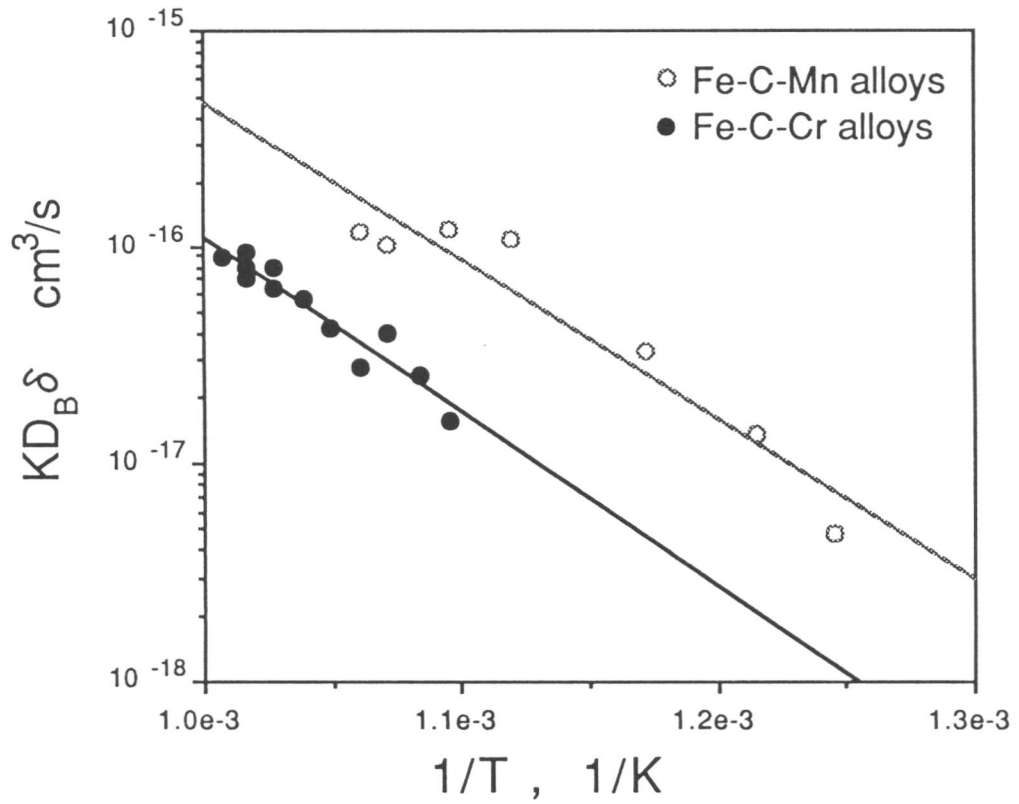
Fig. 5.13 Comparison between observed and calculated $K D_B \delta$ values in Fe-C-Cr and Fe-C-Mn alloys.
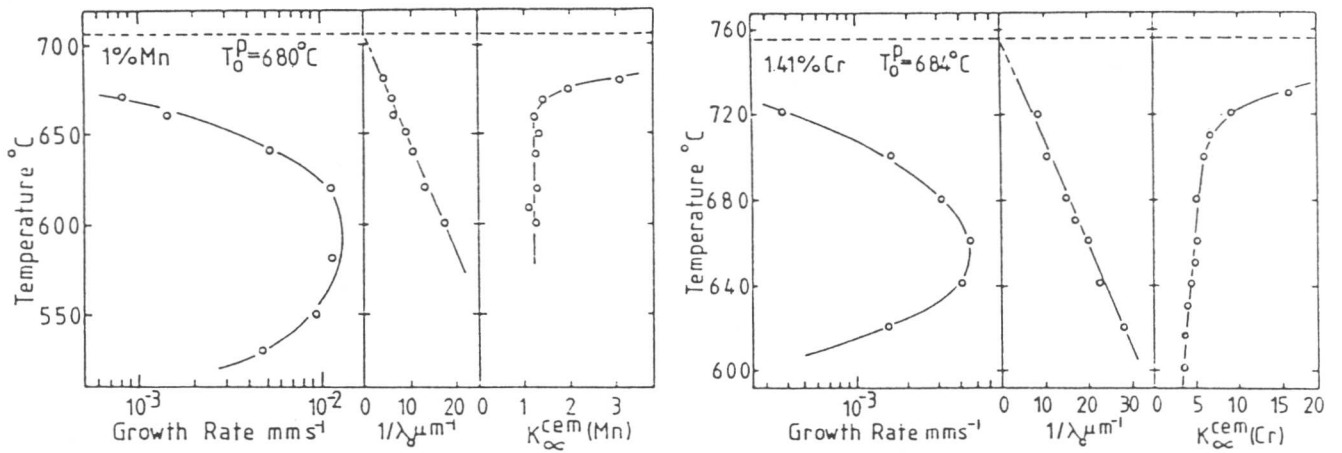
Fig. 5.14 Growth rate of pearlite and the partitioning coefficient of substitutional alloying element as a function of the reaction temperature in (a) a Fe-1.08Mn-C wt.% and (b) a Fe-1.41Cr-C wt.% alloys [8].
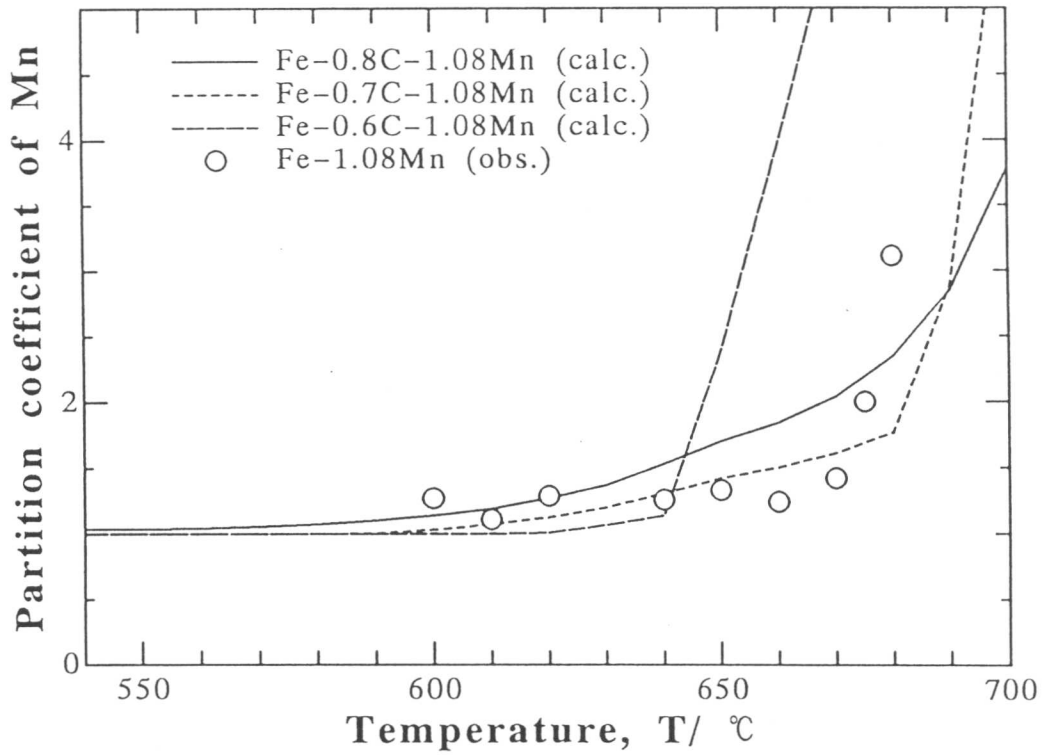
Fig. 5.15 Calculated partition coefficient of Mn in a Fe-1.08Mn-C wt.% alloy. Plots are after Ridley [8].
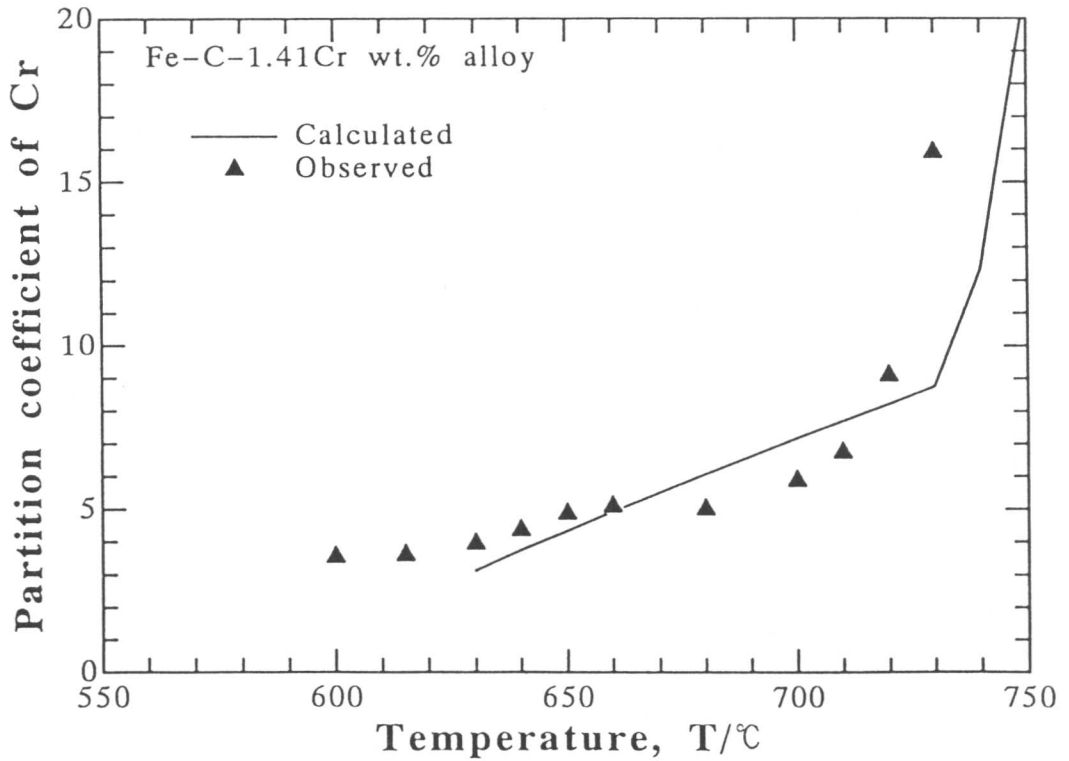
Fig. 5.16 Calculated partition coefficient of Cr in a Fe-1.41Cr-C wt.% alloy. Plots are after Ridley [8].

153
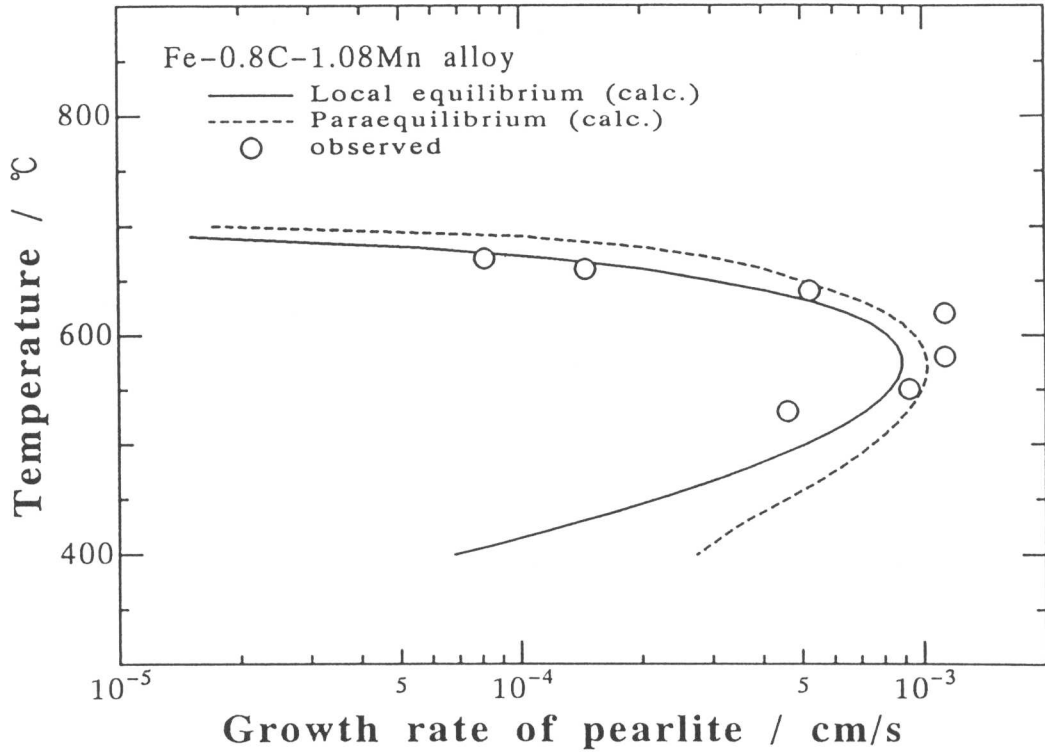
Fig. 5.17 Comparison between observed and calculated growth rate of pearlite in a Fe-1.08Mn-C wt.% alloy.
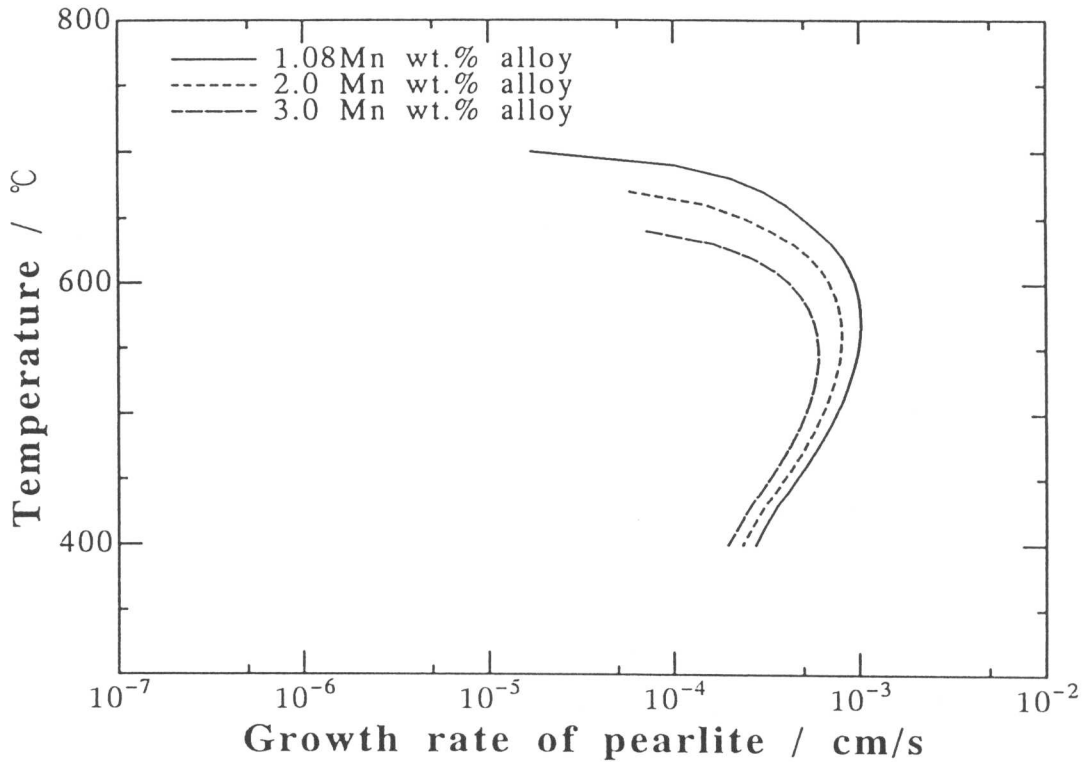
Fig. 5.18 Effect of the amount of Mn addition on the growth rate of pearlite under paraequilibrium.
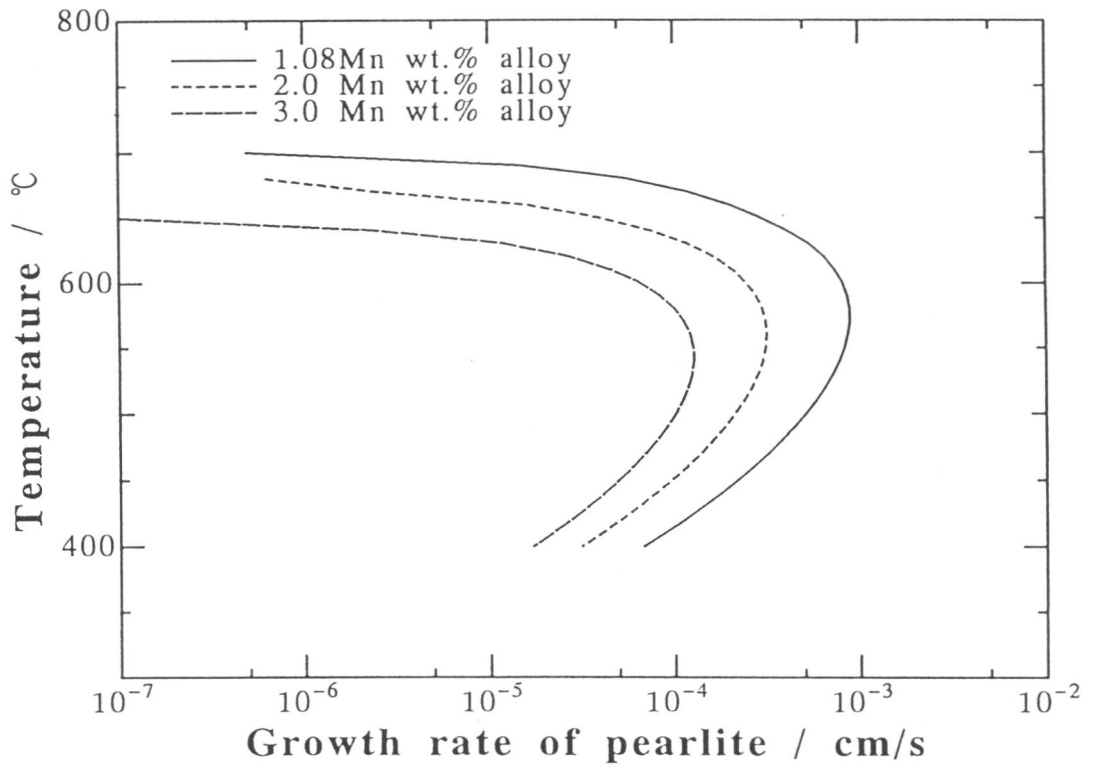
Fig. 5.19 Effect of the amount of Mn addition on the growth rate of pearlite under local equilibrium.
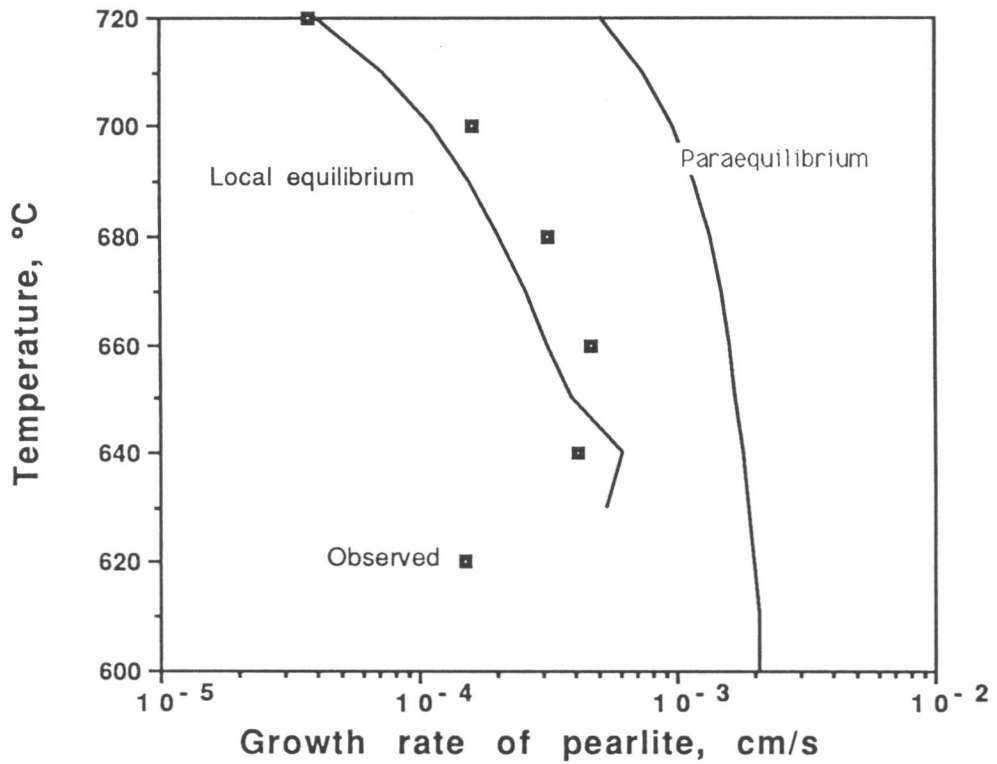
Fig. 5.20 Comparison between observed and calculated growth rate of pearlite in a Fe-1.41Cr-C alloy.

Table 5.2 Interlamellar spacing data for Fe-C, Fe-Mn-C, Fe-Ni-C and Fe-Cr-C alloys reported by (a) Brown and Ridley [15], (b) Razik *et al.* [16], (c) Ridley [8] and (d) Cahn and Hagel [17].

Temp. °C	Alloy wt%	S μm	ref.	Temp. °C	Alloy wt%	S μm	ref.
700		0.221	a)	672	1.98Ni	0.652	a)
680		0.130	a)	667	1.98Ni	0.379	a)
660		0.092	a)	660	1.98Ni	0.227	a)
640		0.071	a)	656	1.98Ni	0.201	a)
620		0.057	a)	652	1.98Ni	0.145	a)
690	1.08Mn	0.398	b)	647	1.98Ni	0.129	a)
685	1.08Mn	0.299	b)	641	1.98Ni	0.112	a)
680	1.08Mn	0.241	b)	629	1.98Ni	0.088	a)
670	1.08Mn	0.196	b)	620	1.98Ni	0.071	a)
660	1.08Mn	0.156	b)	648	3.00Ni	0.649	a)
640	1.08Mn	0.100	b)	644	3.00Ni	0.463	a)
620	1.08Mn	0.080	b)	640	3.00Ni	0.227	a)
670	1.80Mn	0.373	b)	633	3.00Ni	0.168	a)
660	1.80Mn	0.218	b)	625	3.00Ni	0.130	a)
650	1.80Mn	0.164	b)	616	3.00Ni	0.103	a)
640	1.80Mn	0.131	b)	605	3.00Ni	0.079	a)
630	1.80Mn	0.119	b)				
620	1.80Mn	0.104	b)				
610	1.80Mn	0.077	b)				
600	1.80Mn	0.065	b)				

Temp. °C	Alloy wt%	S μm	ref.	Temp. °C	Alloy wt%	S μm	ref.
720	1.80Cr	0.135	c)	706	0.40Cr	0.240	c)
705	1.80Cr	0.092	c)	696	0.40Cr	0.174	c)
690	1.80Cr	0.069	c)	680	0.40Cr	0.109	c)
670	1.80Cr	0.060	c)	660	0.40Cr	0.079	c)
650	1.80Cr	0.046	c)	637	0.40Cr	0.065	c)
630	1.80Cr	0.041	c)	620	0.40Cr	0.055	c)
620	1.80Cr	0.037	c)	790	9.00Cr	0.200	d)
710	0.90Cr	0.178	c)	750	9.00Cr	0.075	d)
700	0.90Cr	0.128	c)	700	9.00Cr	0.050	d)
680	0.90Cr	0.088	c)	675	9.00Cr	0.040	d)
660	0.90Cr	0.072	c)				
640	0.90Cr	0.057	c)				
618	0.90Cr	0.046	c)				

CHAPTER 6

REAUSTENITISATION ACCOMPANIED BY NUCLEATION OF AUSTENITE

6.1 INTRODUCTION

The aim of this chapter is to study the effect of the initial microstructure on reaustenitisation, in circumstances where the nucleation of austenite is required. Martensitic microstructures and mixtures of ferrite and carbide particles, are studied as the starting microstructures. It is essential for austenite to nucleate in these cases unlike the mixture of bainite and austenite which was discussed in Chapter 4. Differences in the overall transformation kinetics between reaustenitisations with and without the need to nucleate austenite may provide insight into the effect of nucleation on reaustenitisation.

6.2 EXPERIMENTAL PROCEDURE

All materials used in the experiments were homogenised at 1250°C for 3 days before the heat treatment to obtain the appropriate initial microstructures. A Fe-0.3C-4.08Cr wt.% and a Fe-0.12C-2.0Si-3.0Mn wt.% alloys were heated to either 1250°C or 1100°C and were quenched into iced water to give martensitic microstructures. Mixtures of carbide particles and ferrite were obtained by tempering specimens of the martensitic microstructure either at 500°C or at 700°C. After these heat treatments, the specimens were "up-quenched" to the reaustenitisation temperatures at the fastest heating rate available (about $500\,°C\,s^{-1}$) in order to investigate isothermal reaustenitisation, or were heated continuously at a variety of rates to study anisothermal reaustenitisation. The specimens were helium quenched in the dilatometer after the heat treatment. The cooling rate during quenching was about $30\,°C\,s^{-1}$ between 800 and 500°C. The same methods were used for the nickel plating to prevent surface degradation and for the sealing of specimens into a quartz tube while they were heat treated in a furnace as mentioned in Chapter 4. After the experiments, specimens were examined as discussed in Chapter 4.

6.3 ISOTHERMAL REAUSTENITISATION

The isothermal reaustenitisation behaviour of ferrite in which nucleation of austenite is required, is described in this section.

6.3.1 Reaustenitisation from a martensitic microstructure

Martensitic initial microstructure in the Fe − 0.3C − 4.08Cr wt.% alloy

First, reaustenitisation from martensite in the Fe-0.3C-4.08Cr wt.% alloy, obtained by quenching from 1100°C, was studied. An optical micrograph of the initial microstructure is shown in Fig. 6.1. A TEM micrograph of the specimen shows a lath martensitic microstructure (Fig. 6.2). The hardness of the initial microstructure was measured to be $H_V\{98.1N\} = 551$, which is very close to the value 582 calculated from the chemical composition and the cooling rate using the following equation (concentrations expressed in wt.%) [1].

$$H_V = 127 + 949C + 27Si + 11Mn + 8Ni + 16Cr + 21 \times \log\{\text{cooling rate}, (°C\,s^{-1})\} \qquad (6.1)$$

The martensitic samples were then up-quenched to elevated temperatures to study isothermal reaustenitisation. Optical micrographs of the specimens helium quenched after 30 min of isothermal reaustenitisation at each reaction temperature are shown in Fig. 6.3. Austenite was not observed after reaction at 750 °C (Fig. 6.3 a). When the reaction temperature was raised to 780 °C, isolated islands of austenite (white regions, Fig. 6.3 b) were found. The preferential nucleation site of austenite is the prior austenite grain boundaries. The austenite particles are globular in shape or slightly elongated along the prior austenite grain boundaries. The volume fraction of austenite increased with the reaction temperature (Fig. 6.3 b,c,d) and a fully austenitic microstructure (fully martensitic on quenching to ambient temperature) can be obtained above 805 °C (Fig. 6.3 e).

The austenite particles which nucleated at the prior austenite grain boundaries tended to grow only into one of the two adjacent prior austenite grains. At some grain boundaries, all of the austenite particles were found to grow into the same prior austenite grain (indicated by arrows in Fig. 6.3 c). A magnified micrograph shows detail of the structure of austenite nucleated at a prior austenite grain boundary (Fig. 6.4). Most of the austenite particles seem to grow into one prior austenite grain and a coalescence between adjacent austenite particles seems to occur at the later stage of transformation.

Similar results have been reported by Speich *et al.* [2] and Law and Edmonds [3] for the formation of austenite from a mixture of ferrite and spheroidised cementite particles. These austenite particles were found to grow into a grain to which the austenite particles are not orientation related.

At relatively high temperatures (790 °C for 20 seconds), the prior austenite grain boundaries first became covered completely with newly formed austenite particles (Fig. 6.5). The new austenite particles coalesced to form an allotriomorph of austenite at the prior austenite grain boundaries. After the occurrence of the site saturation at the prior austenite grain boundaries, nucleation of austenite within the prior austenite grains seems to become more prominent (Fig. 6.6; 790 °C for 50 seconds). The austenite particles are rather acicular in shape instead of the globular grains which form at the prior austenite grain boundaries. The austenite plates found within a given martensite block were parallel to each other. This suggests that the austenite plates are influenced by the ferrite/ferrite interfaces. They grew along these interfaces as discussed by Plichta and Aaronson [4].

These microstructural features of reaustenitisation from martensite were also obtained when the prior austenite grain size was large. Specimens heated to 1250 °C for three days and quenched in iced water were reaustenitised. The amount of austenite which forms at 778 °C was found to be very small (Fig. 6.7) with individual austenite grains separated at the prior austenite grain boundaries. Small particles of austenite appears at a prior austenite grain boundary at an early stage of the reaction, which seem to grow along the boundary and bulge into one of the grains which are separated by the boundary.

Martensitic initial microstructure in the Fe − 0.12C − 2.0Si − 3.0Mn wt.% alloy

When a martensitic starting microstructure in the Fe-0.12C-2.0Si-3.0Mn wt.% alloy was heated, intragranular austenite was found to form as discussed by Plichta and Aaronson [4]. The prior austenite grain boundaries are no longer the most preferred nucleation sites as shown in Fig. 6.8, which illustrates partially reaustenitised microstructures. The austenite particles are acicular and there is almost no nucleation observed at the prior austenite grain boundaries. The

is, therefore, expected to be higher in ferrite than in austenite causing the difference in particle sizes in the two phases.

In some part of tempered region, dislocation networks can be observed. Fig. 6.12 a) shows an example of this in a specimen isothermally held at 790°C for 20 seconds and quenched. Dislocations are found to be tied up by carbide particles in the tempered region. Interaction between the particles and dislocations can be clearly seen in another position of the specimen heat treated at 790°C (Fig. 6.12 b). Fig. 6.13 shows a bright field image of a recovered ferrite microstructure where ferrite grains whose interfaces seems to be pinned by particles, are found. However, a dark field image of the area shows that those grains have almost the same orientations, suggesting that those grains are subgrains separated by dislocation networks.

The particles observed in the tempered region show a similar orientation which can be seen in Fig. 6.14, together with a bright and a corresponding dark field images. This may indicate that these particles have precipitated in ferrite with a reproducible orientation relationship with that phase.

Twinned martensite is often observed in austenite regions (Fig. 6.15), which suggests that the carbon concentration there is high. Microhardness measurements near interfaces between tempered ferrite and austenite were conducted with the indentation load of 0.0981 N. Since the microstructure which is to be examined is martensite with more than 0.3 wt.% of carbon, the hardness measurement with the load smaller than 0.0981 N causes a substantial scatter. A decrease in hardness near the interfaces was observed (Fig. 6.16). This may correspond to the carbon profile in austenite which is considered to be maintained while austenite grows (Fig. 6.17). There is, however, the possibility of interference from surrounding soft ferrite phase near the interfaces.

Dilatometry

Typical relative length changes during isothermal reaustenitisation from martensitic initial microstructure obtained by water quenching from 1100°C and from 1250°C, are shown in Fig. 6.18 and Fig. 6.19. Since reaustenitisation happens during heating at high temperatures even at heating rates as high as $500°C\,s^{-1}$, the temperature correction which was discussed in Chapter 4 was used here again. The temperature corrected relative length changes are plotted in Fig. 6.20. The rate of the reaction increases with temperature. The maximum relative length change at each temperature increases with temperature and reaches a maximum value. These features of isothermal reaustenitisation are very similar to those in the case of reaustenitisation from a mixture of bainitic ferrite and austenite. The maximum relative length changes were plotted against the reaction temperature in Fig. 6.21. As was observed for the initial microstructure of bainitic ferrite and austenite, the maximum relative length change shows a maximum value at around 790°C which is identical to the value observed in the bainite + austenite initial microstructure within the accuracy of the experiments.

These two sets of the maximum relative length changes are compared in Fig. 6.22. The maximum relative length change at temperatures higher than 790°C (100% austenite) is larger for the martensitic initial microstructure since the amount of ferrite available for transformation is larger. The $\Delta L/L$ values at 790°C for the two different initial microstructures are consistent with the initial amount of ferrite which is 1.0 in the martensitic initial microstructure and 0.7 in the other. The maximum relative length change above the peak temperature shows a linear decrease which is parallel to that in the bainite + austenite starting microstructure. This

160

feature can be attributed to the difference in the thermal expansivities of ferrite and austenite as discussed in Chapter 4.

The thermal expansion coefficient during cooling after isothermal reaustenitisation at each reaction temperatures are plotted in Fig. 6.23 with the data obtained for reaustenitisation from the mixture of bainite and austenite in the Fe-0.3C-4.08Cr wt.% alloy. The thermal expansion coefficients during cooling depend on the microstructure at the end of isothermal holding and vary with the volume fraction of austenite and ferrite; *i.e.* $1.244 \times 10^{-5}\,{}^{\circ}C^{-1}$, when the volume fraction of austenite is zero, to that of austenite; *i.e.* $2.065 \times 10^{-5}\,{}^{\circ}C^{-1}$, when the microstructure is fully austenitic. It can be said that the fully austenitic microstructure is obtained above 790 °C, consistent with the results obtained from dilatometry and from optical micrographs.

When the microstructure at the end of isothermal reaustenitisation contains austenite, decomposition of that austenite can be observed during cooling. The relative length changes during helium quenching after 30 min of isothermal reaustenitisation at each temperatures can be seen in Fig. 6.24. The temperatures at which the decomposition of austenite is first observed were plotted against the reaustenitisation temperature (Fig. 6.25). The decomposition-start temperature decreases with increasing the reaustenitisation temperature independent of the initial microstructure. Since the average carbon concentration in austenite is higher at lower reaustenitisation temperatures, decomposition of austenite is expected to be retarded more when the reaustenitisation temperature is lowered. The experimental result contradicts this. To understand this, the phase equilibrium calculation was conducted using "Thermo-Calc" for the Fe-0.3C-4.08Cr wt.% alloy, although calculated equilibrium phase boundaries are not completely in agreement with the experimental results obtained in the present work. "Thermo-Calc" gives phase boundaries as shown in Fig. 6.26 a in which *fcc*, *bcc*, M_7C_3 and cementite were taken into account. As expected, the carbon concentration in austenite decreases with increasing temperature in the intercritical temperature range as shown in Fig. 6.26 b, but increases again with temperature when ferrite phase disappears. The chromium concentration, on the contrary, increases monotonically with temperature. This means that the kinetics of the formation of ferrite from austenite formed at an intercritical temperature can be retarded by higher concentration of chromium when the temperature is raised. Four temperatures, which are indicated as points **A**, **B**, **C** and **D** in Fig. 6.26 b,c, are selected to assess the effect of reaustenitisation temperature on the TTT curve for the formation of ferrite in this alloy. The TTT curve calculation method proposed by Bhadeshia [6] was used here. Using the equilibrium chemical compositions at these four temperatures, the TTT curves for these austenite compositions were calculated (Fig. 6.27). Both of the upper and lower C-curves are shifted to the right so the formation of ferrite is retarded by raising the reaustenitisation temperature. In addition to this, the lower the reaustenitisation temperature is, the smaller the austenite grain is expected, which also accelerates the reaction rate of ferrite formation.

6.3.2 Reaustenitisation from mixtures of ferrite and carbide particles

Two different mixtures of ferrite and carbide particles were studied. These initial microstructures were obtained by tempering the martensitic microstructure which was studied in the previous section at either $700\,^{\circ}$C or at $500\,^{\circ}$C.

Microstructure tempered at $500\,^{\circ}$C

An optical micrograph of a specimen tempered at $500\,^{\circ}$C for 17 hours is shown in Fig. 6.28. A TEM bright field image (Fig. 6.29) clearly shows a tempered microstructure. There are two types of carbides in this microstructure, one of which is rather small and elongated, and the other is larger and globular in shape. TEM diffraction patterns (Fig. 6.29) show that the former one is cementite and the latter M_7C_3 carbide. As shown in Chapter 4, cementite precipitation occurs from carbon supersaturated bainitic ferrite below the B_S temperature. Therefore cementite precipitation is expected to occur at $500\,^{\circ}$C (which is just above the B_S temperature) at least at the early stages of tempering. A prolonged holding at the temperature, however, may have allowed the M_7C_3 carbide, which is thermodynamically more stable than cementite, to form. The specimens were then up-quenched to intercritical temperatures to study isothermal reaustenitisation. A typical microstructure obtained by 30 min at $784\,^{\circ}$C is presented in Fig. 6.30. Austenite particles can be seen not only at the prior austenite grain boundaries but also within the grains, before all of the prior austenite grain boundaries are covered with newly formed austenite. The intragranular austenite as well as that nucleated at the grain boundaries were found to be globular in shape, in contrast to the formation of austenite from a martensitic microstructure. When the latter is heated, the prior austenite grain boundaries are first covered with austenite and intragranular transformation occurs afterwards. The shape of the austenite is acicular along the ferrite/ferrite interfaces in the tempered microstructure. Clearly, a nearly tempered microstructure contains ferrite/ferrite interfaces within the prior austenite grains, which are preferential nucleation sites for austenite. There are some prior austenite grain boundaries which are free from austenite formation as indicated by arrows in Fig. 6.30 even when austenite particles are found within the prior austenite grains.

Microstructure tempered at $700\,^{\circ}$C

When a martensitic specimen was tempered at $700\,^{\circ}$C for 51 hours, a slightly different microstructure was obtained. Fig. 6.31 shows carbide particles both at prior austenite grain boundaries and within the grains. The particles at the prior austenite grain boundaries are coarse and elongated along the boundaries, showing a "stitched" morphology. The particles at the boundaries appear disc shaped, of about 5 μm diameter. The particles within the grains are small in comparison. When this microstructure is heated to $785\,^{\circ}$C for 30 min, austenite particles nucleate both at the prior austenite grain boundaries and within the grains (Fig. 6.32). The preferred nucleation site is intragranular. Austenite particles can be found to grow across the boundaries as illustrated by the arrows in Fig. 6.32. In some regions, the growth of austenite is blocked by elongated carbide particles at the boundaries. This starting microstructure gives a more homogeneous dispersion of austenite than previously discussed.

During reaustenitisation from both the tempered martensitic microstructures, austenite nucleated within the prior austenite grains exhibited irregular (or wavy) interfaces. This may

be a result of a irregular substructure of the matrix which contains a lath martensitic microstructure, but is broken by prolonged isothermal holding at elevated temperatures. This substructure is not polygonal but acicular, and a sheaf like structure can also be seen which may provide various different direction of the growth of austenite causing wavy interfaces of the growing austenite.

A TEM micrograph of a specimen quenched after 30 min of isothermal reaustenitisation at 785 °C from the microstructure tempered at 700 °C is shown in Fig. 6.33. The micrograph contains an interface between tempered ferrite and austenite (now martensite). The carbide particles are found in both phases as discussed in the previous section. The particles are, however, almost of the same size in both phases. If the dissolution of carbide particles occurs in austenite after being engulfed, the particles found in austenite region are expected to be smaller than that in tempered ferrite region as shown in the starting microstructures of the bainite + austenite (Chapter 4) or martensite. This assumption, however, cannot explain the fact observed in the present case. The other possibility is due to the difference in the growth rate of carbide in each phase as discussed in the previous section. This assumption seems to be applicable for all of the cases. When the starting microstructure does not contain alloy carbide, the alloy carbide is required to nucleate and grow at the reaction temperature. The difference in the growth rate of carbide in each phase, as a result of the lower diffusivities of atoms in austenite than in ferrite, may play the most important role in determining the particle sizes in both phases; i.e. particles in austenite are smaller than those in ferrite. When the starting microstructure contains these carbide particles, these particles may grow or dissolve in both phases. The growth or dissolution of the particles may not be significant in the present case since the particles in the starting microstructure formed at 700 °C which is only 85 °C below the reaction temperature. As a result, the particles found in both phases are of almost the same size.

Dilatometry

Relative length changes during reaustenitisation from a microstructure tempered at 500 °C are presented in Fig. 6.34. The maximum relative length change which can be obtained from these data after the temperature correction (Chapter 4) can be seen in Fig. 6.35. The changes obtained in the present work; i.e. reaustenitisation from mixtures of bainite and austenite, martensitic microstructures and tempered martensitic microstructures, are compared in Fig. 6.36. No significant difference can be found for these different initial microstructures except for the bainite and austenite mixture where the maximum relative length change for 100% of reaustenitisation is smaller than others, as discussed in the previous section.

6.4 CONTINUOUS HEATING REAUSTENITISATION

6.4.1 Dilatometry

The relative length changes during continuous heating are shown in Fig. 6.37. The overall reaustenitisation behaviour can also be seen in Fig. 6.38. The transformation-start and -finish temperatures can be determined from the relative length change during continuous heating as points at which the relative length deviate from the constant thermal expansion of the initial and final microstructures. The transformation-start and -finish temperatures are plotted against heating rate in Fig. 6.39. Both temperatures increase with heating rate, consistent with the data on reaustenitisation from a mixture of bainite and austenite.

6.4.2 Tempering of martensite during heating

When the starting microstructure is supersaturated martensite, tempering can occur during heating to the austenitisation temperatures. The importance of this has been pointed out by Baeyertz [7]. When a specimen is heated at a slow heating rate, the tempering can be detected using dilatometry. The relative length changes obtained during continuous heating of a martensitic microstructure are presented in Fig. 6.37. A small deviation from the normal thermal expansion effect is seen to occur before the onset of reaustenitisation, at around 300 °C, which is designated as the "tempering-start temperature" (marked by arrows in Fig. 6.37), As expected, the tempering-start temperature increases with the heating rate (Fig. 6.40).

The expected relative length change during the tempering of martensite can be calculated from the difference in volume between carbon supersaturated martensite and a mixture of ferrite and cementite:

$$\frac{\Delta L}{L} = \frac{a_{\alpha'}^2 c_{\alpha'} - a_\alpha^3(1 - V_\theta) - \frac{1}{6}a_\theta^3 V_\theta}{a_{\alpha'}^2 c_{\alpha'}} \tag{6.2}$$

where $a_{\alpha'}$ and $c_{\alpha'}$ are lattice parameters of martensite, a_α is that of ferrite and a_θ^3 is the volume of cementite per unit cell, respectively. The volume fraction of cementite formed by tempering of carbon supersaturated martensite can be calculated from the total amount of carbon in the martensite. The thermal expansion coefficient of martensite was assumed to be identical to that of ferrite. The constants discussed in Chapter 4 were used here for the lattice parameters and the thermal expansion coefficients. The relative length change in equation 6.2 was calculated to be −0.00077. This decrease in relative length change is consistent with the experimentally observed one during heating and also during isothermal holding at 500° C for 30 min (Fig. 6.41). To compare this value with the experimentally observed contraction due to tempering, relative length changes at each heating rates were measured as differences between the two linear expansion lines before and after the tempering effect. The average of these values gives −0.00036. The smaller observed magnitude can be attributed to incomplete tempering.

6.5 CONCLUSIONS

Reaustenitisation from either martensite or mixtures of ferrite and carbide particles has been studied, in circumstances where new nucleation of austenite is necessary.

1) Prior austenite grain boundaries are the preferred nucleation sites for reaustenitisation from a martensitic initial microstructure, but are less prominent when the starting microstructure is tempered martensite in a Fe-0.3C-4.08Cr wt.% alloy. Almost no nucleation of austenite was observed at the prior austenite grain boundaries during reaustenitisation from martensite in a Fe-0.12C-2.0Si-3.0Mn wt.% alloy. The reason for this is not clear.

2) Formation of austenite within prior austenite grains became possible in the Fe-0.3C-4.08C wt.% alloy after the prior austenite grain boundary sites became saturated.

3) Austenite particles found at the prior austenite grain boundaries were globular whereas those formed within the grains are acicular in the case of reaustenitisation from martensitic initial microstructures. Globular austenite can, however, be found within the prior austenite grains when tempered martensite (a mixture of ferrite and carbide particles) is reaustenitised.

4) M_7C_3 particles observed in the untransformed ferrite matrix are larger than those in the austenite region when the starting microstructure is martensite, whereas no significant

difference in the particle size was observed for the starting microstructure tempered at 700 °C. This suggests that the difference in the particle size can be attributed to the difference in the growth rate of the particles in both phases.

5) When martensitic initial microstructure is heated slowly, tempering can occur on heating, and the starting temperature increases with heating rate. Even in the case of high heating rates carbide precipitation seems to occur at the very early stages of the reaction.

REFERENCES

1. R. Blondeau, Ph. Maynier, J. Dollet and B. Vieillard-Baron: *"Heat Treatment '76"*, *Metals Society, London,* 1976, 189.

2. G. R. Speich and A. Szirmae: *Trans. TMS-AIME,* 1969, **245,** 1063.

3. N. C. Law and D. V. Edmonds: *Metall. Trans.,* 1980, **11A,** 33.

4. M. R. Plichita and H. I. Aaronson: *Metall. Trans.,* 1974, **5,** 2611.

5. J. Fridberg, L-E. Törndahl and M. Hillert: *Jernkont. Ann.,* 1969, **153,** 263.

6. H. K. D. H. Bhadeshia: *Metal Sci.,* 1982, **16,** 159.

7. M. Baeyertz: *Trans. ASM,* 1942, **30,** 458.

Fig. 6.1 Optical micrograph of martensite obtained by water quenching from 1100° C in the Fe-0.3C-4.08Cr wt.% alloy.

Fig. 6.2 TEM bright field image of martensite obtained by water quenching from 1100°C in the Fe-0.3C-4.08Cr wt.% alloy.
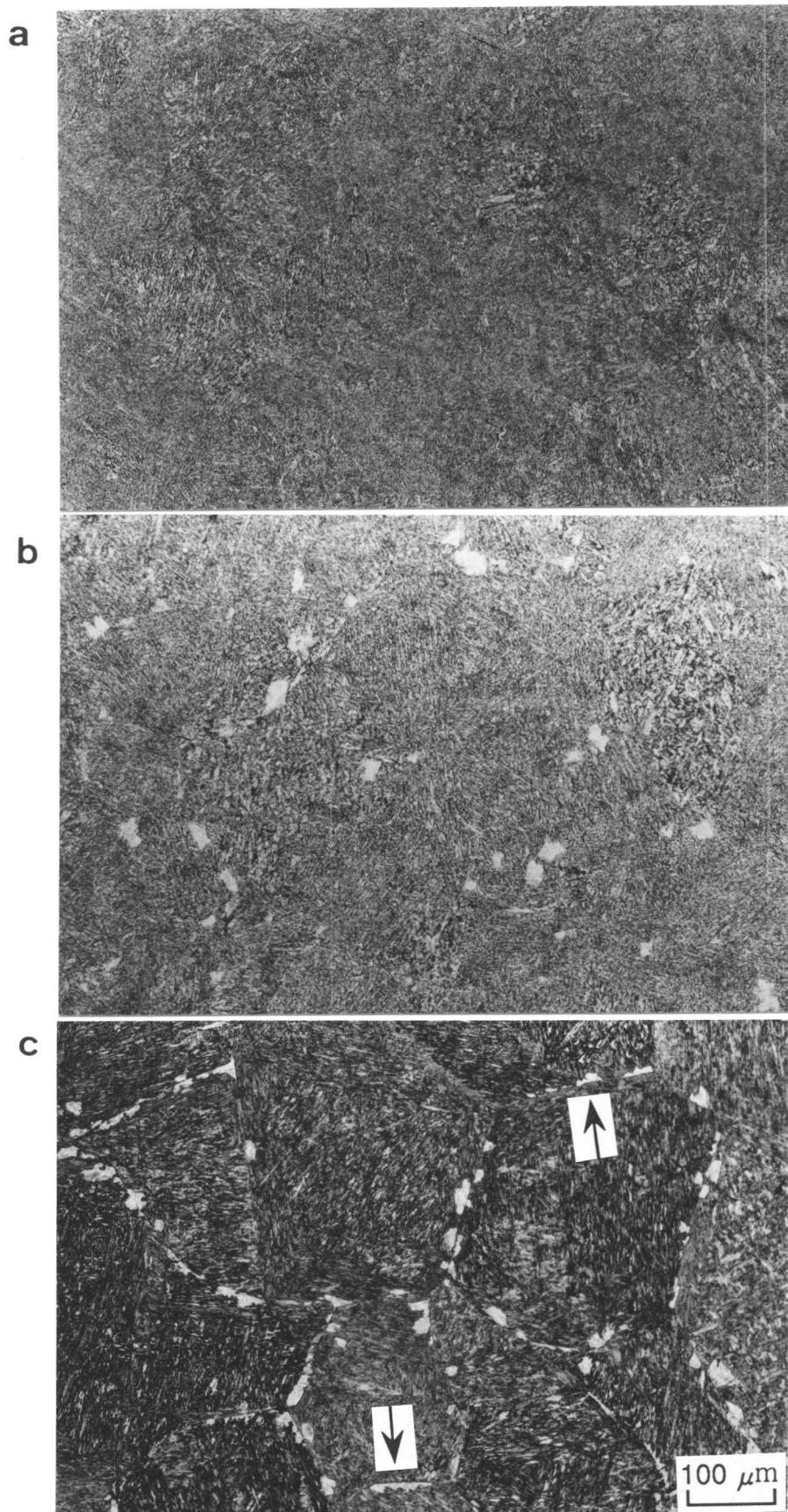
Fig. 6.3 Optical micrographs of specimens helium quenched after 30 min of isothermal reaustenitisation at a) 750 °C, b) 780 °C, c) 785 °C, d) 800 °C and e) 805 °C.

d

100 μm

e

25 μm

Fig. 6.3 (continued)

168
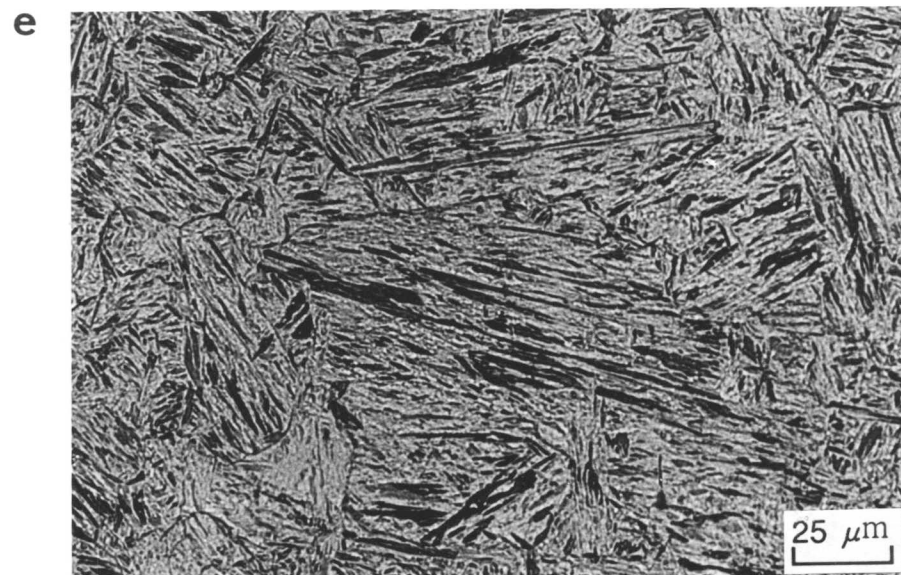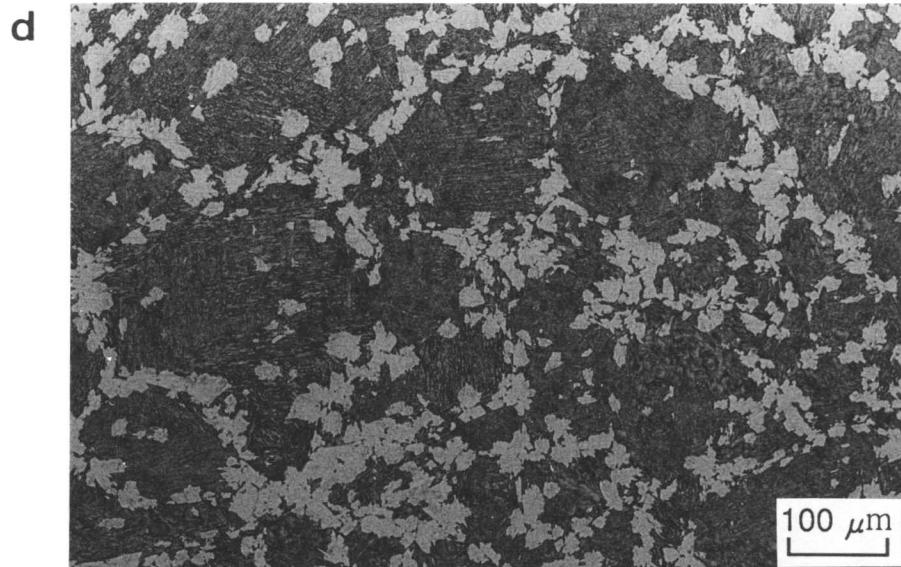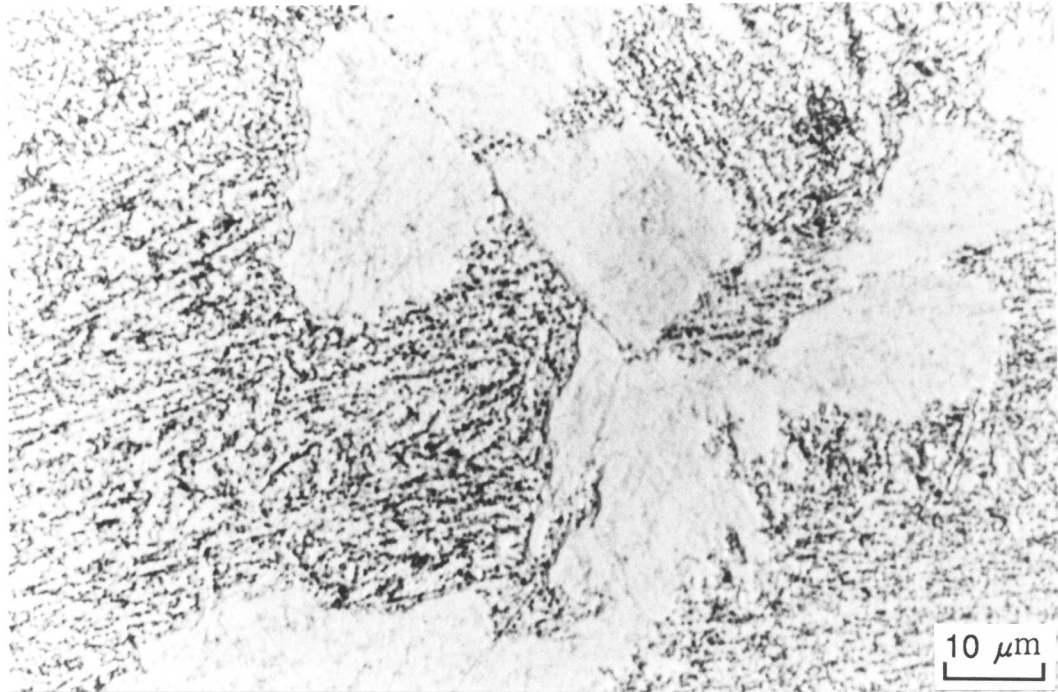
Fig. 6.4 Optical micrograph of a specimen helium quenched after 30 min of isothermal reaustenitisation at 800 °C.
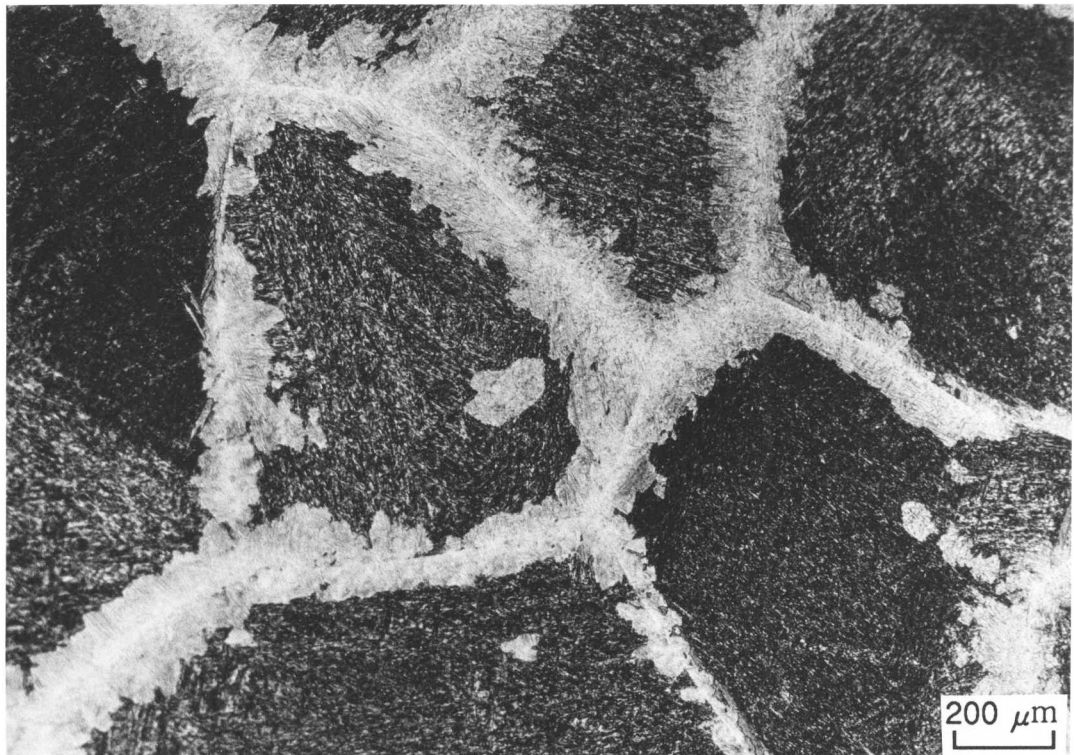
Fig. 6.5 Optical micrograph of a specimen helium quenched after 20 seconds of isothermal reaustenitisation at 790 °C showing a polycrystalline layer of austenite at the prior austenite grain boundaries.
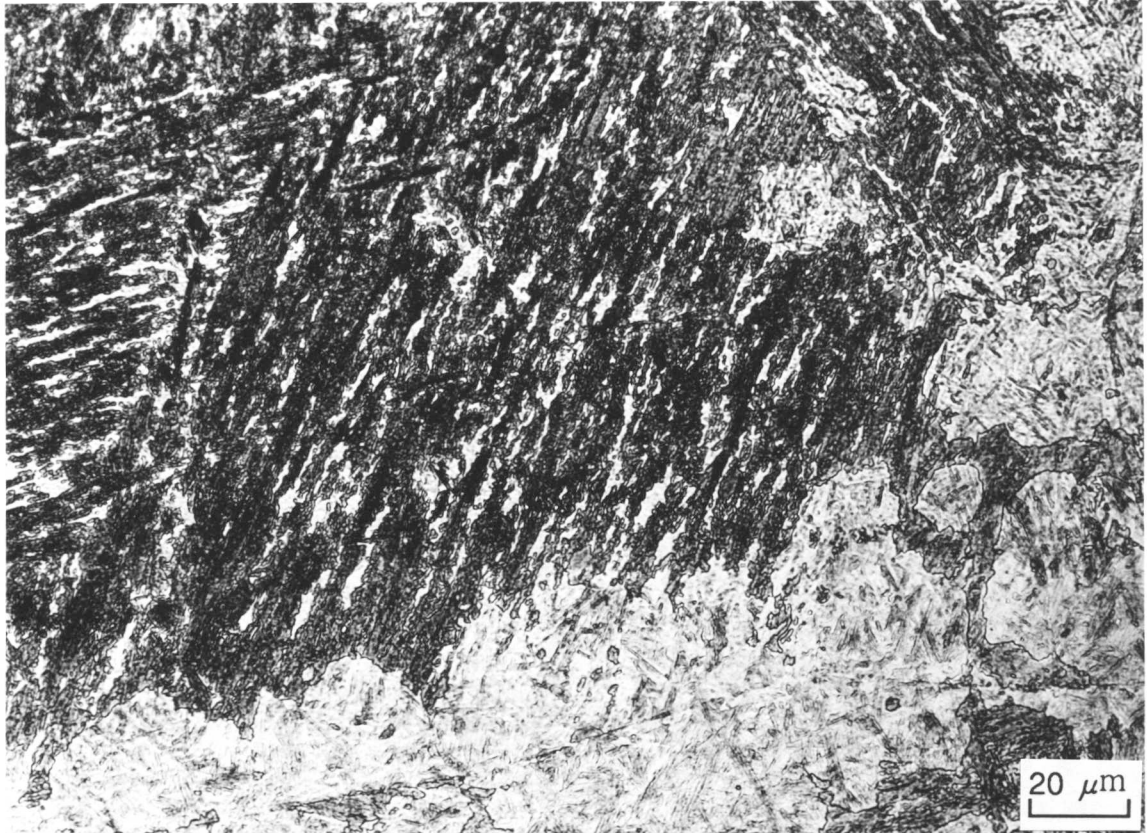
Fig. 6.6 Optical micrograph of a specimen helium quenched after 50 seconds of isothermal reausteni-
tisation at 790 °C.
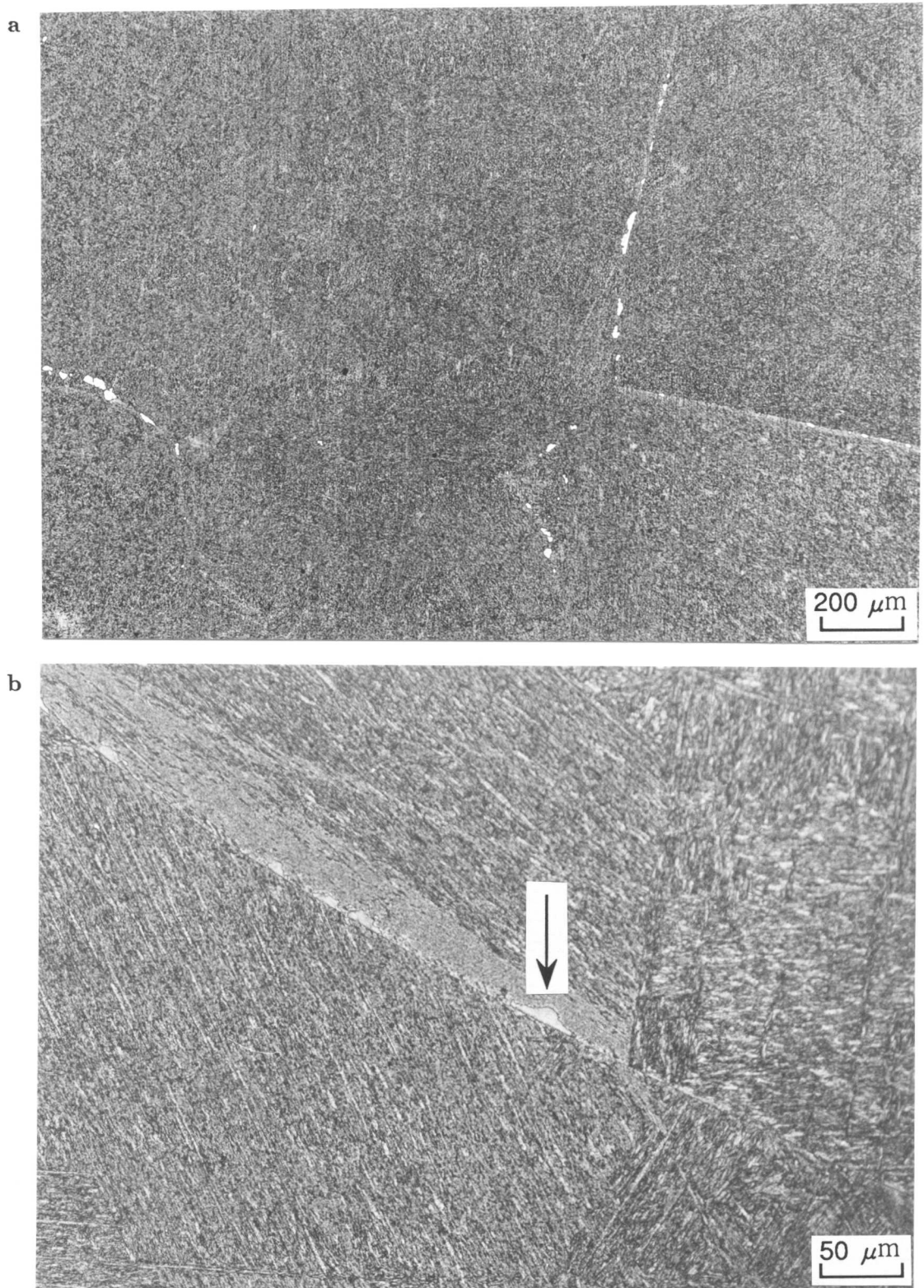
Fig. 6.7 Optical micrograph of a specimen helium quenched after 30 min of isothermal reausteni-
tisation at 778 °C. The initial microstructure is martensite obtained by water quenching
from 1250 °C.

171
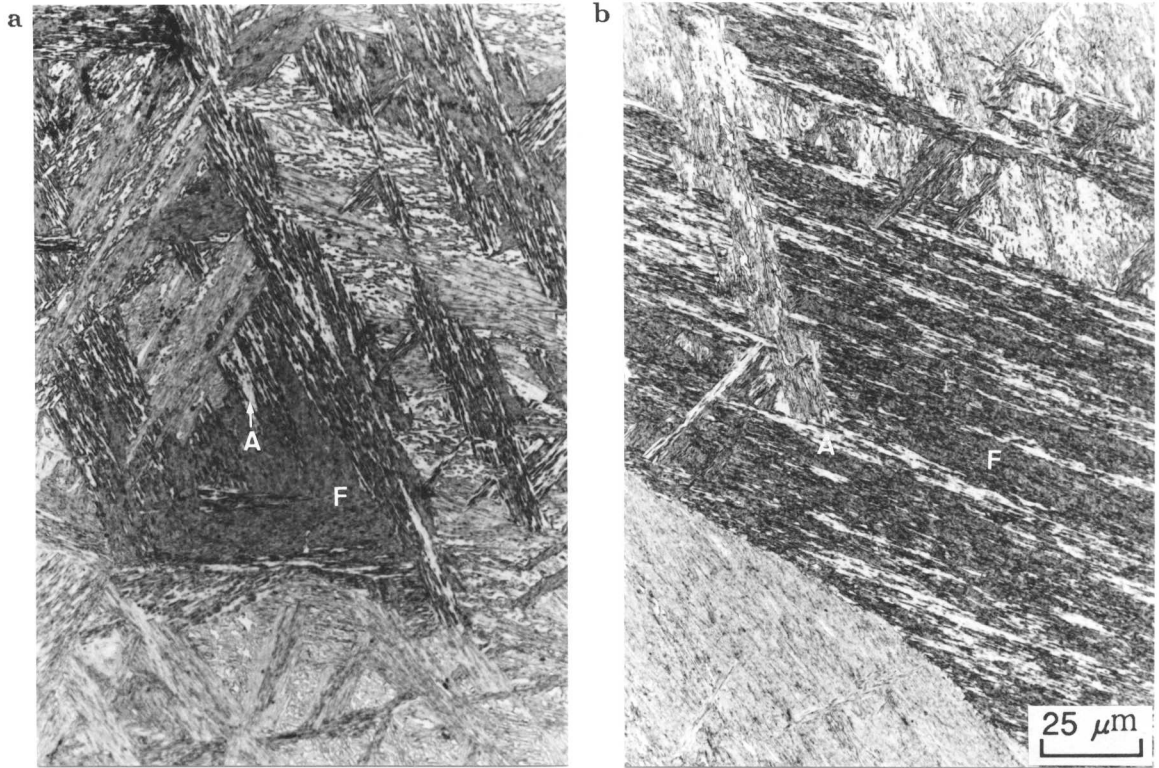
Fig. 6.8 Optical micrograph of a specimen helium quenched after 30 min of isothermal reausteni-
tisation at a) 770 °C and b) 790 °C. The initial microstructure is martensite obtained by
water quenching from 1250 °C in the Fe-0.12C-2.0Si-3.0Mn wt.% alloy. (A: austenite, F:
ferrite)

Fig. 6.9 TEM bright field image of a specimen helium quenched after 20 seconds of isothermal
reaustenitisation from martensite at 790 °C in the Fe-0.3C-4.08Cr wt.% alloy.

172
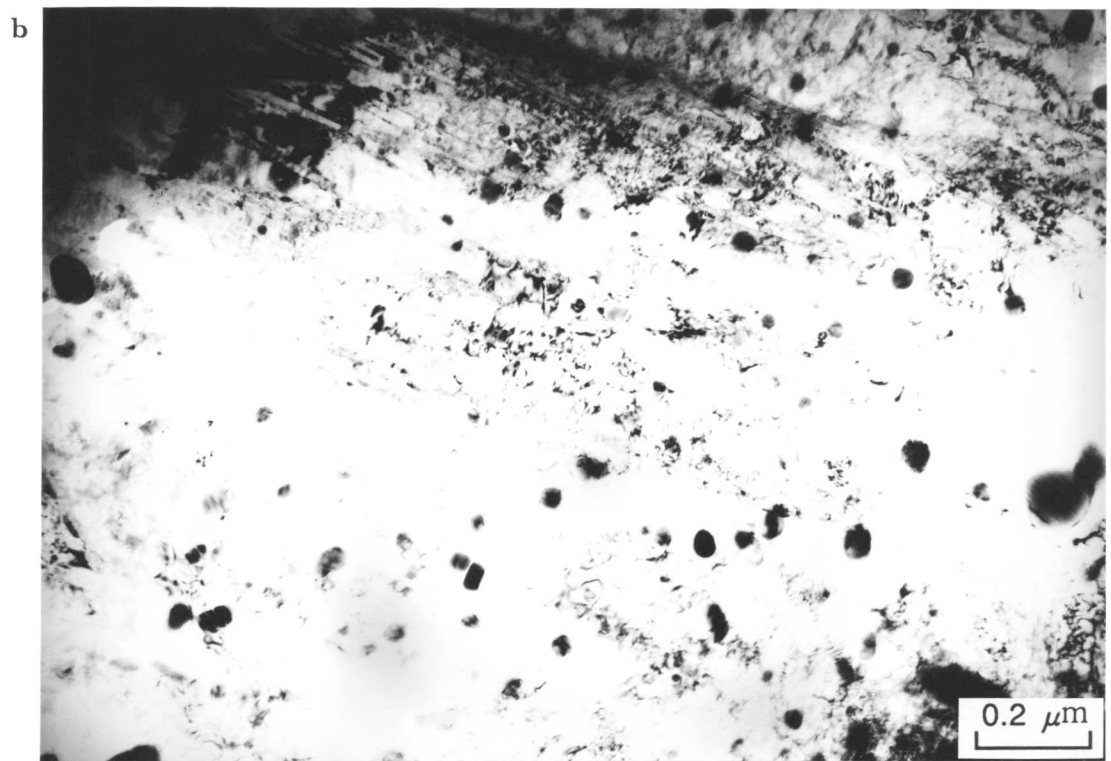
Fig. 6.10 TEM bright field images of a specimen helium quenched after 30 min of isothermal reausteni-
tisation from martensite at 800 °C. a) represents an untransformed part and b) an austeni-
tised area in the Fe-0.3C-4.08Cr wt.% alloy.
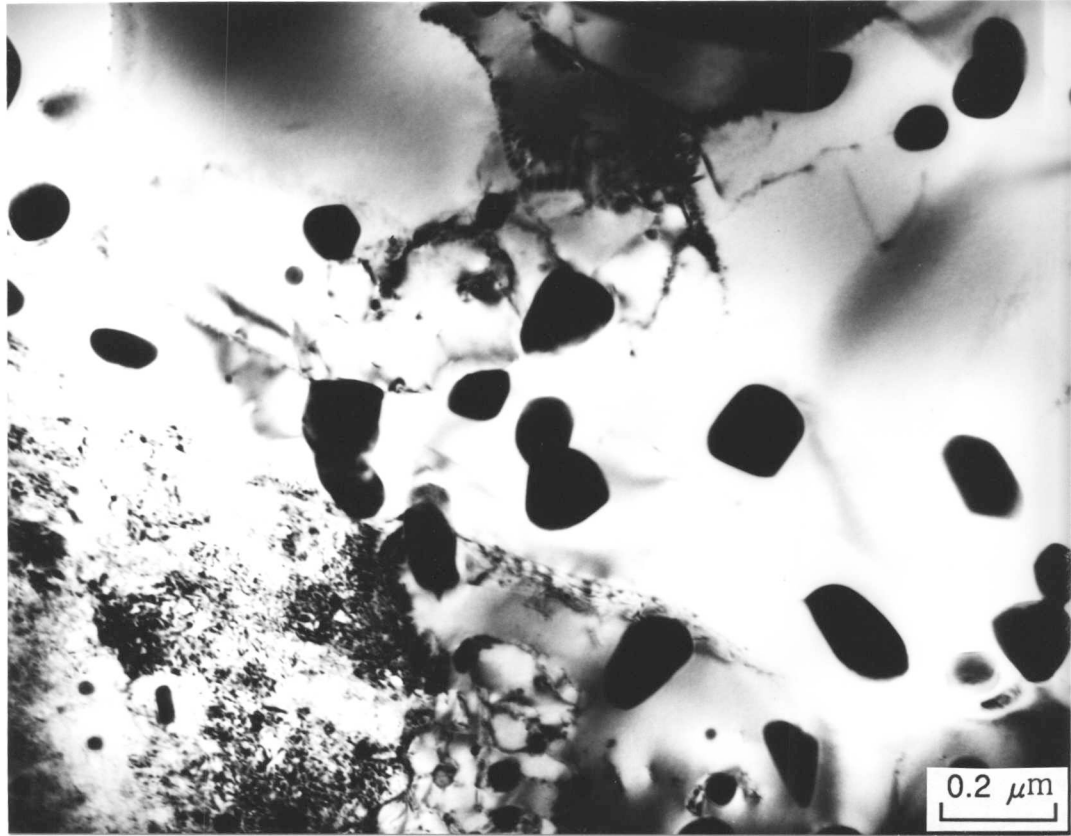
Fig. 6.11 TEM bright field image of a specimen helium quenched after 30 min of isothermal reausteni-tisation from martensite at 785 °C in the Fe-0.3C-4.08Cr wt.% alloy.

a
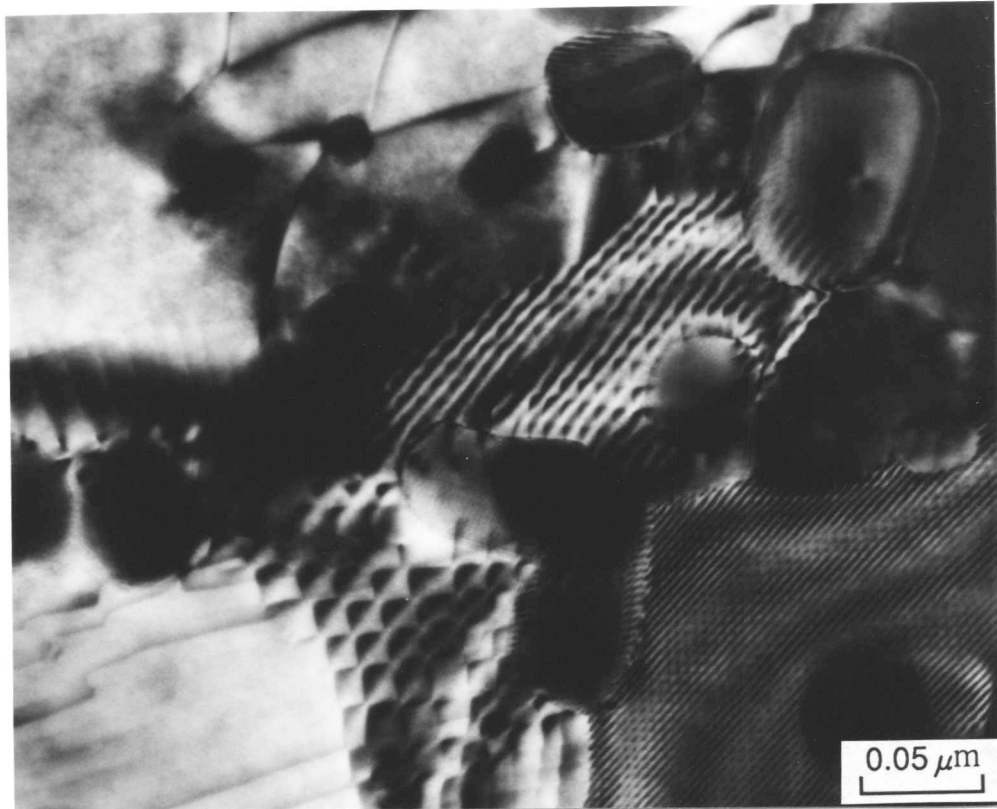
b
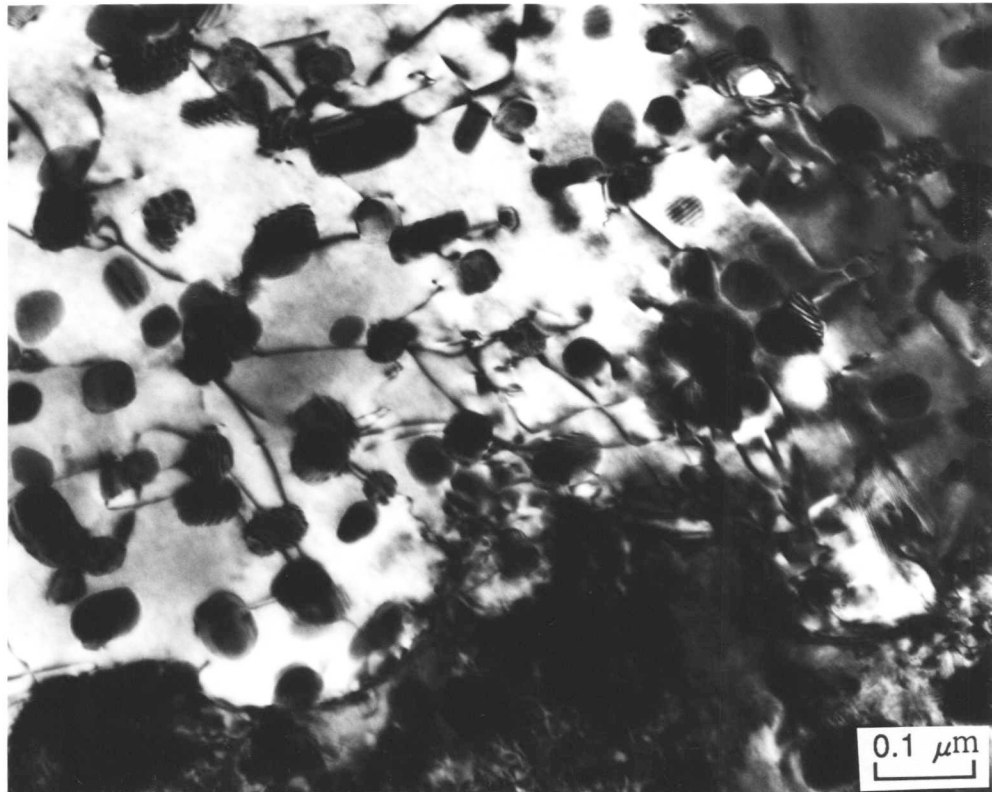
Fig. 6.12 Dislocation networks which are found in an untransformed region tempered during isothermal reaustenitisation for 20 seconds at 790°C in the Fe-0.3C-4.08Cr wt.% alloy.
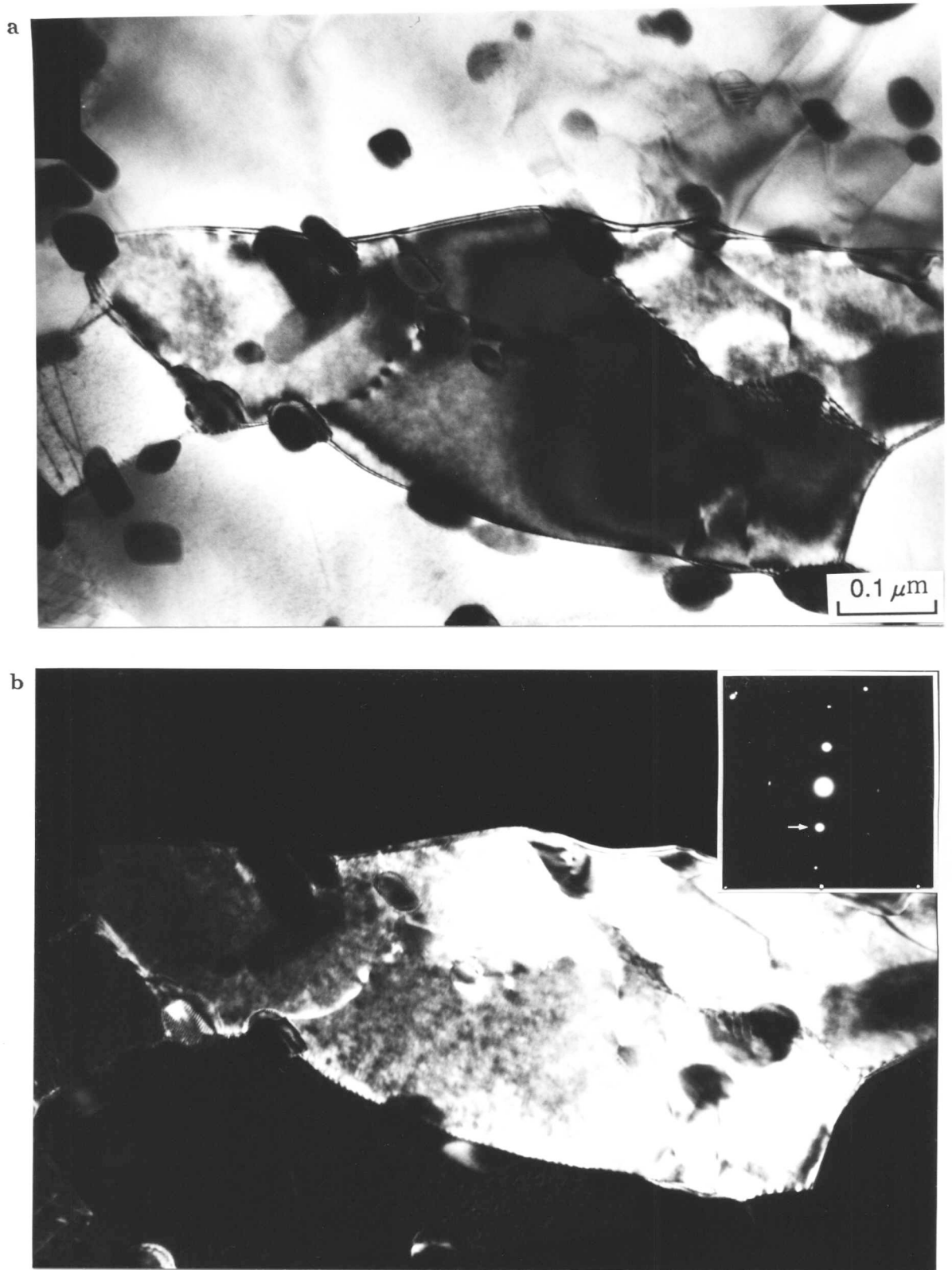
Fig. 6.13 TEM bright and dark field images showing a subgrain structure in a tempered martensite region after reaustenitisation at 790 °C in the Fe-0.3C-4.08Cr wt.% alloy.
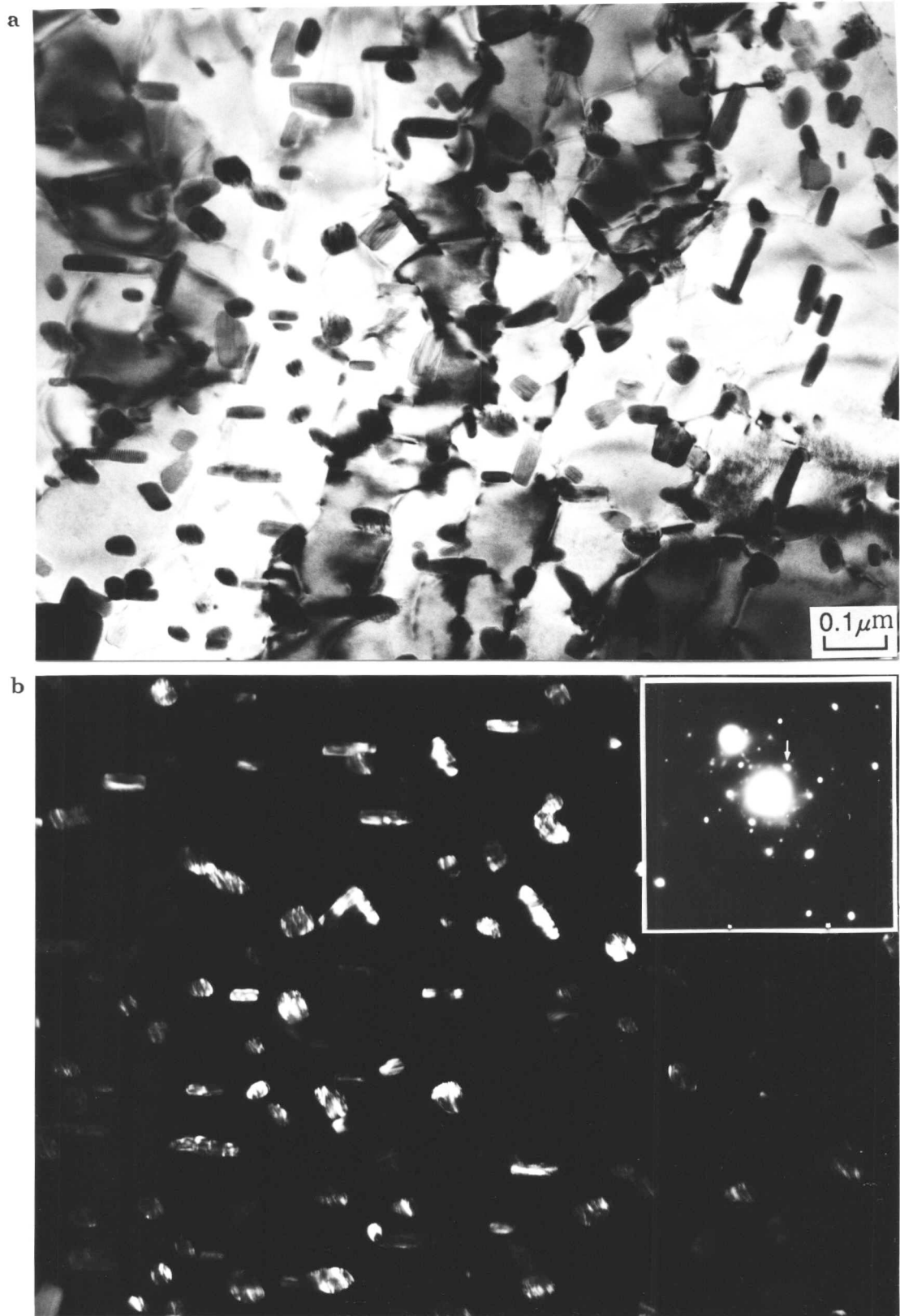
Fig. 6.14 TEM bright and dark field images of carbide particles found in the tempered martensite region in the Fe-0.3C-4.08Cr wt.% alloy.
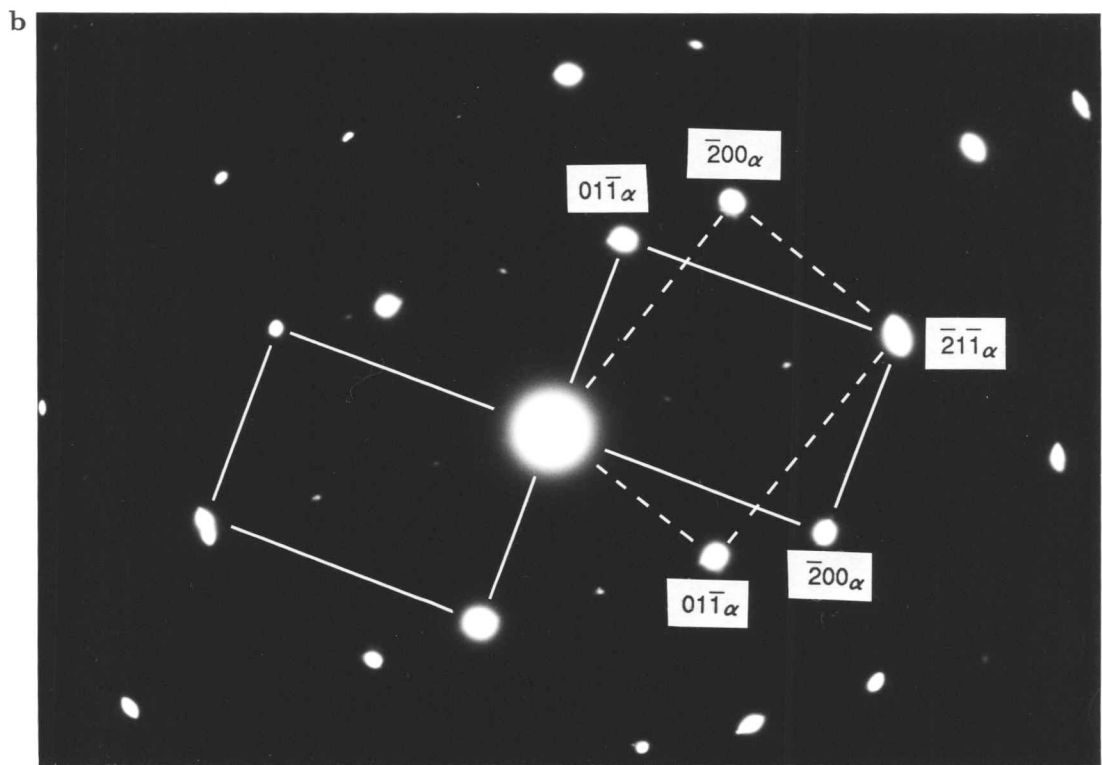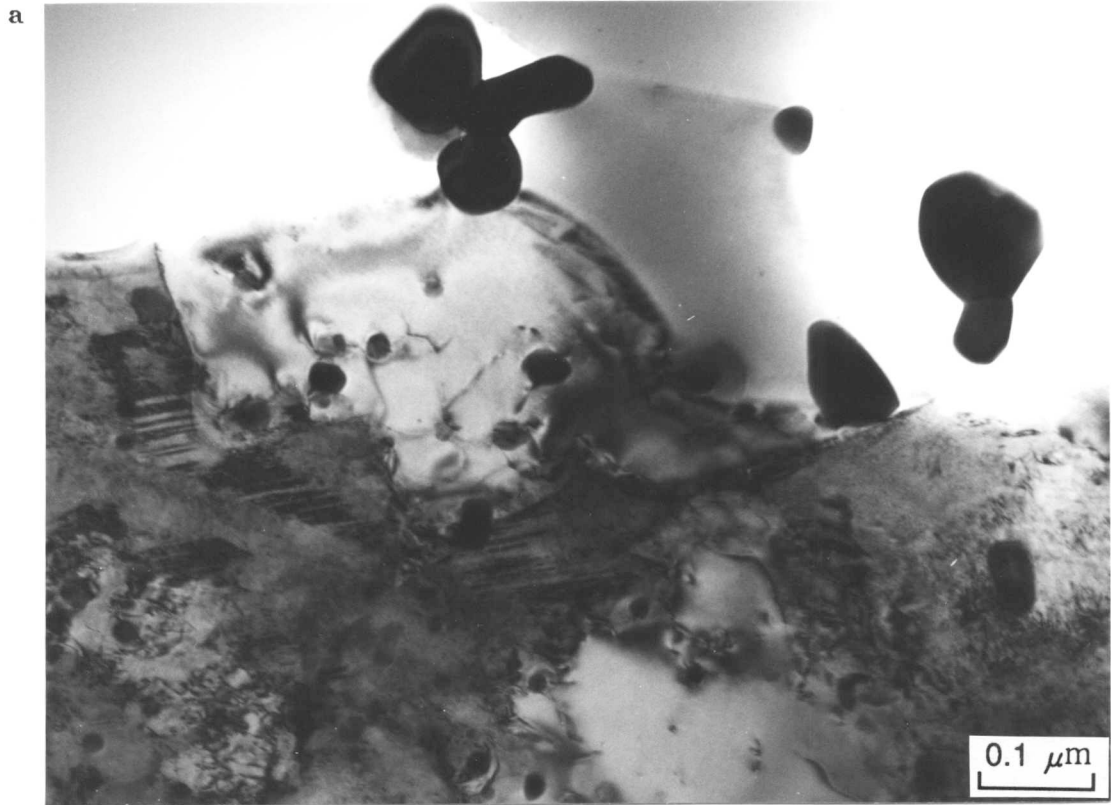
Fig. 6.15 Twinned martensite observed near the interface between austenite and untransformed ferritic matrix and a selected area electron diffraction pattern showing a twin relation.
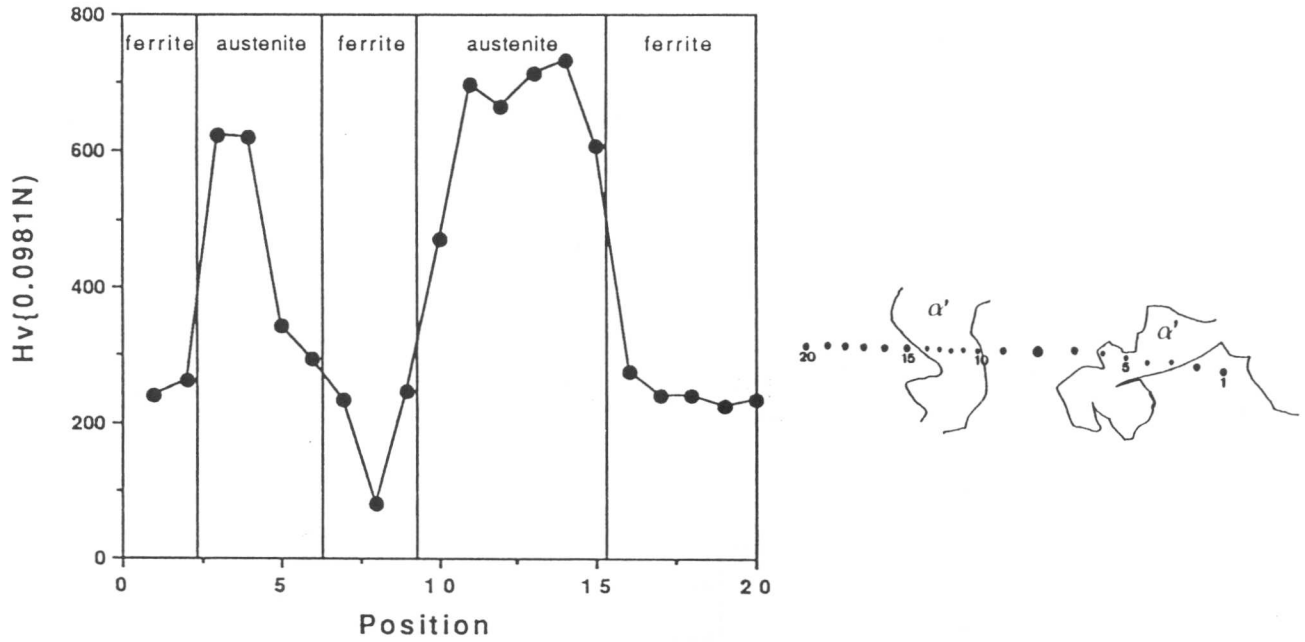
Fig. 6.16 Microhardness of phases measured by a 0.098N indentation across the austenite layer at prior austenite grain boundaries.
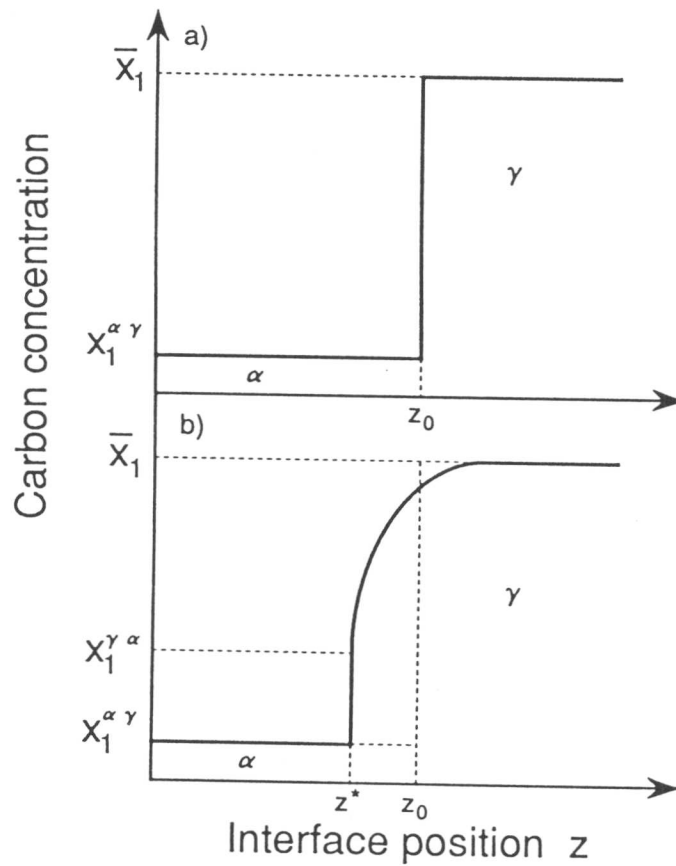
Fig. 6.17 Illustrative carbon profile in austenite near interface during the growth event of the austenite which exists in the initial microstructure of a mixture of bainite and austenite.
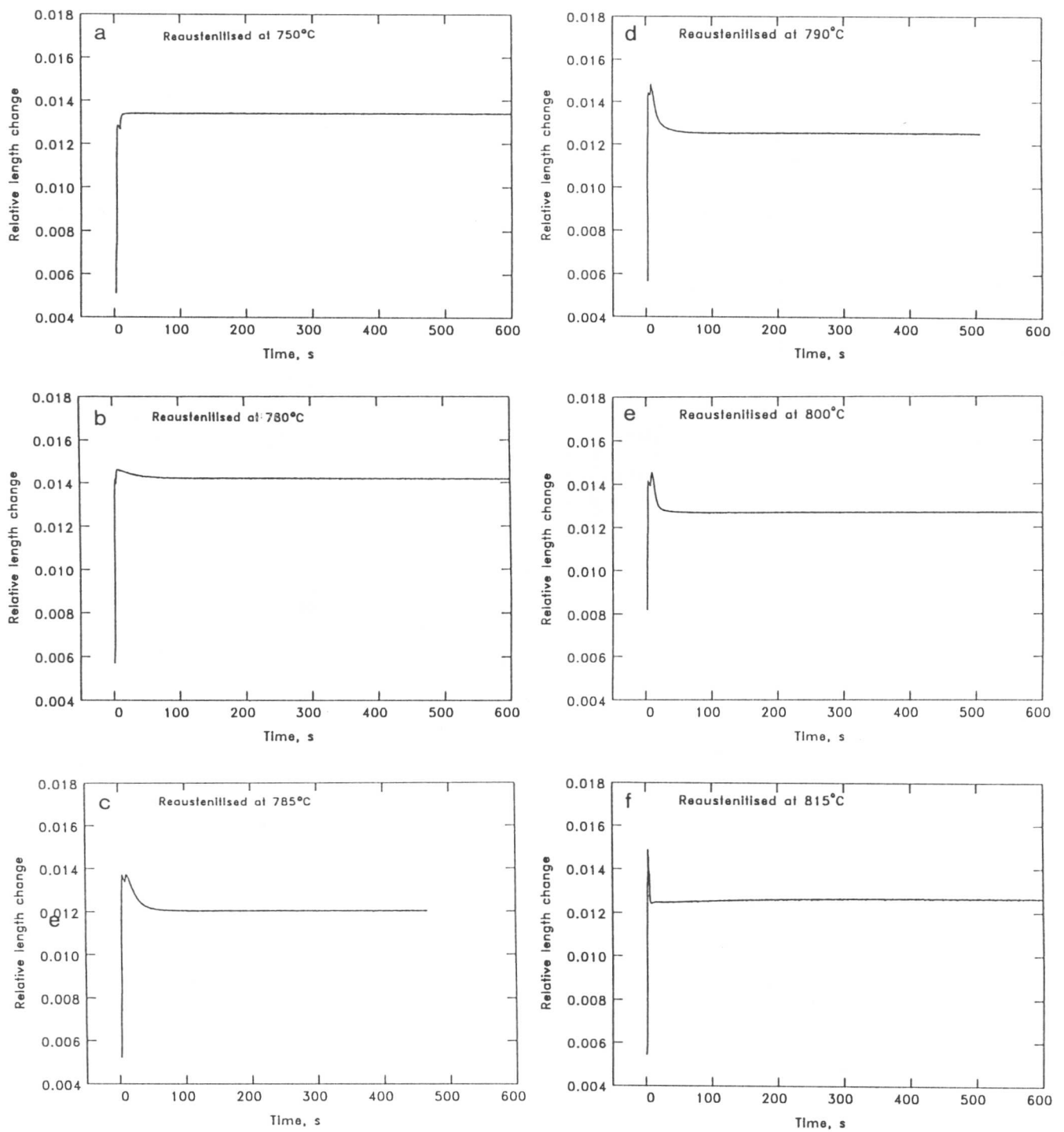
Fig. 6.18 Relative length changes obtained during isothermal reaustenitisation from martensite, which was obtained by quenching from 1100 °C, at a) 750 °C, b) 780 °C, c) 785 °C, d) 790 °C, e) 800 °C and f) 815 °C in the Fe-0.3C-4.08Cr wt.% alloy.
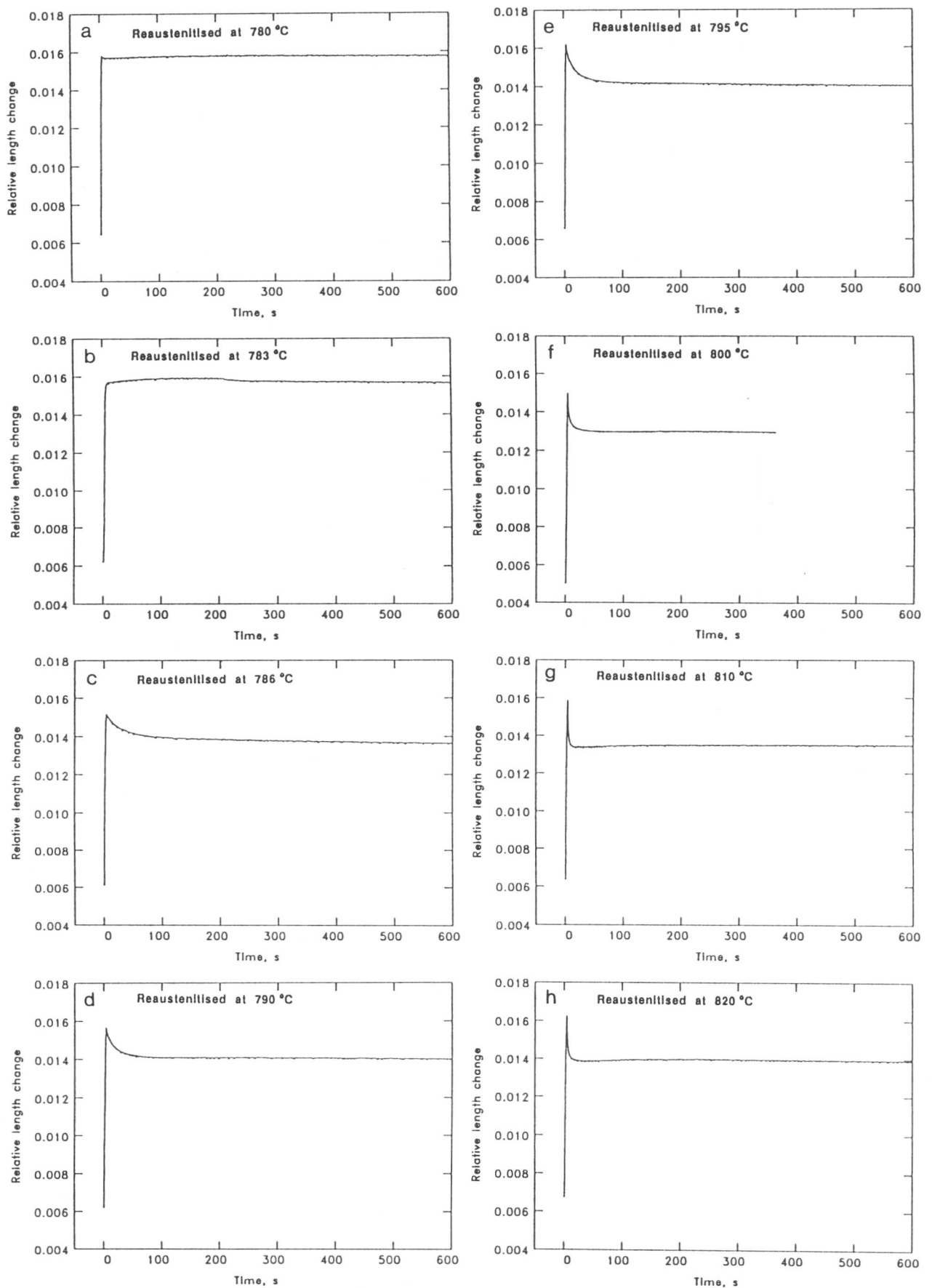
Fig. 6.19 Relative length changes obtained during isothermal reaustenitisation from martensite, which was obtained by quenching from 1250 °C, at a) 780 °C, b) 783 °C, c) 786 °C, d) 790 °C, e) 795 °C, f) 800 °C, g) 810 °C and h) 820 °C in the Fe-0.3C-4.08Cr wt.% alloy.

181
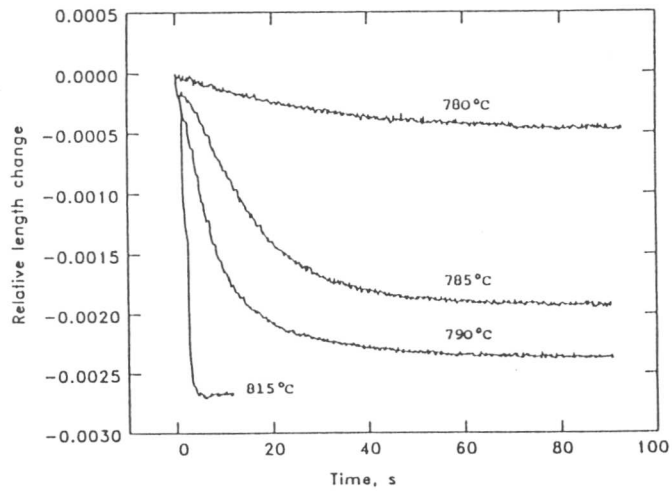
Fig. 6.20 Effect of the reaction temperature on the temperature corrected relative length change during the isothermal reaustenitisation from martensite.
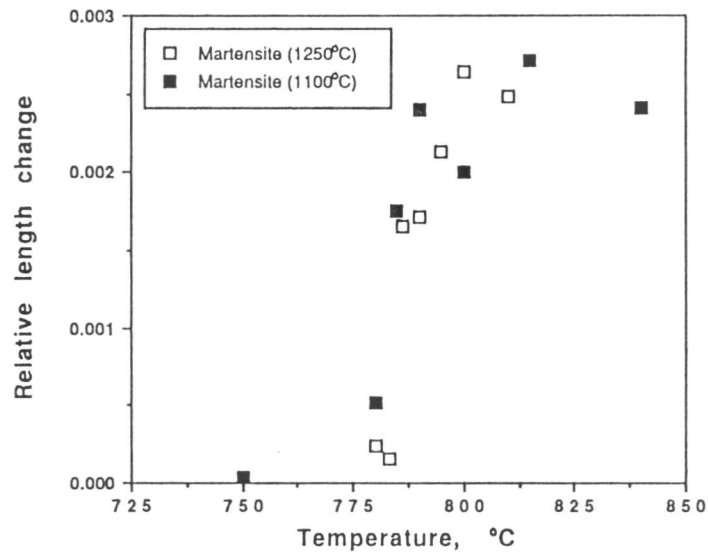
Fig. 6.21 Maximum relative length changes during 30 min of isothermal reaustenitisation from martensite which was obtained by quenching from either 1100 °C or 1250 °C in the Fe-0.3C-4.08Cr wt.% alloy.
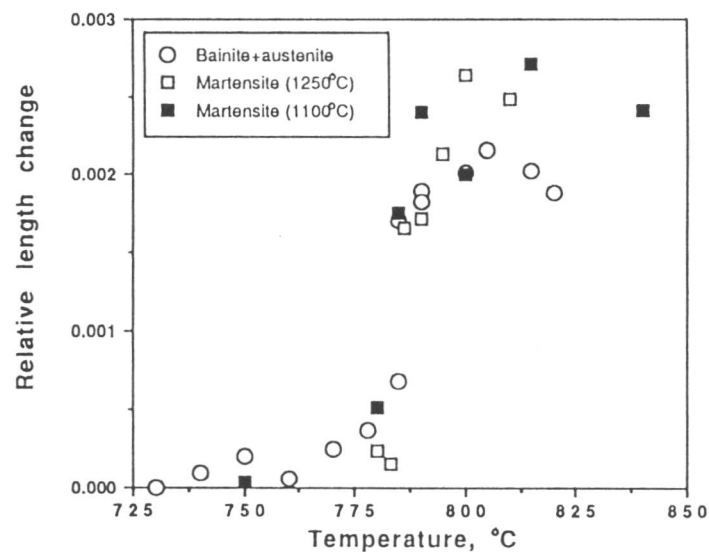
Fig. 6.22 Maximum relative length changes during 30 min of isothermal reaustenitisation from martensite and from the mixture of bainite and austenite in the Fe-0.3C-4.08Cr wt.% alloy.
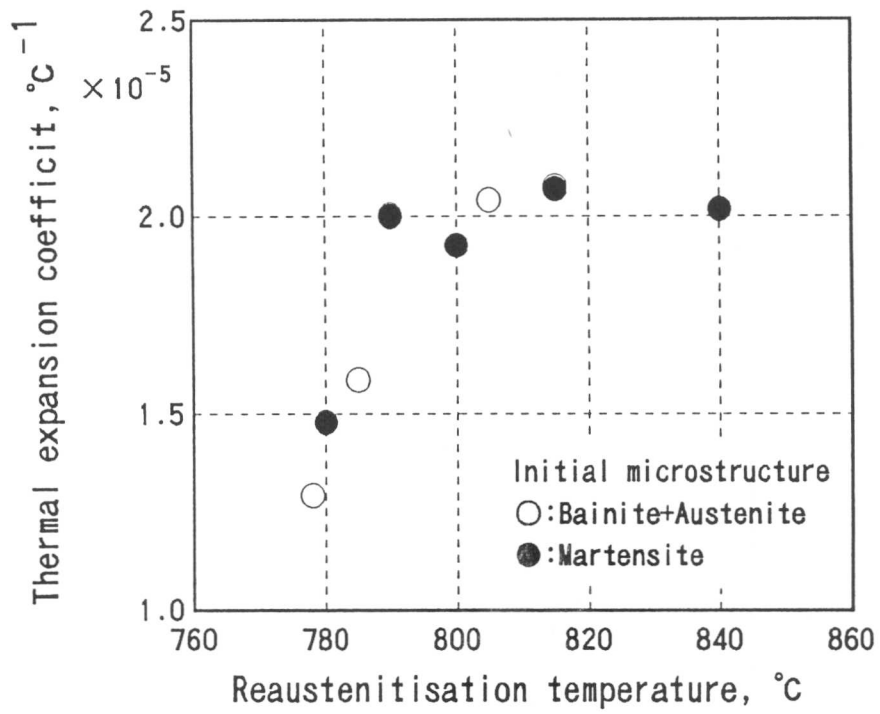
Fig. 6.23 Thermal expansion coefficient during cooling after 30 min of isothermal reaustenitisation from martensite as a function of reaction temperature.
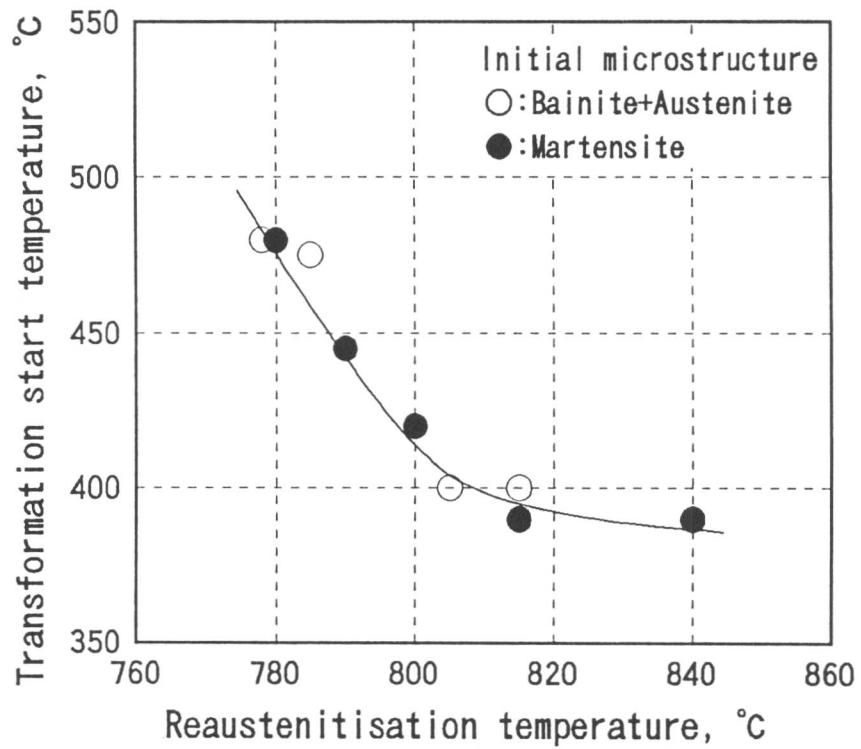
Fig. 6.25 Decomposition-start temperature during cooling after 30 min of isothermal reaustenitisation from martensite as a function of reaction temperature.
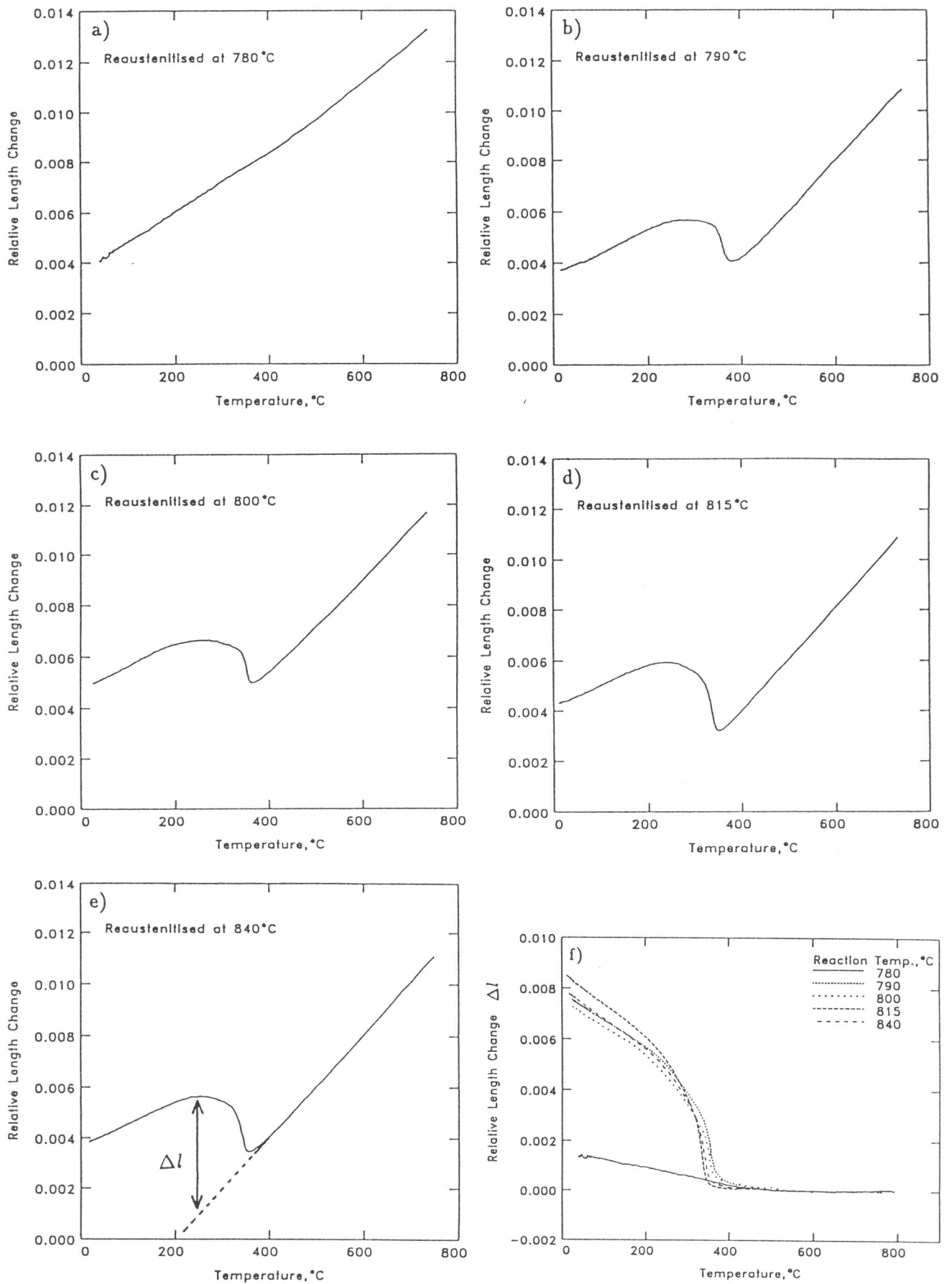
Fig. 6.24 Relative length change during helium quenching after 30 min of isothermal reaustenitisation at each temperatures.

184
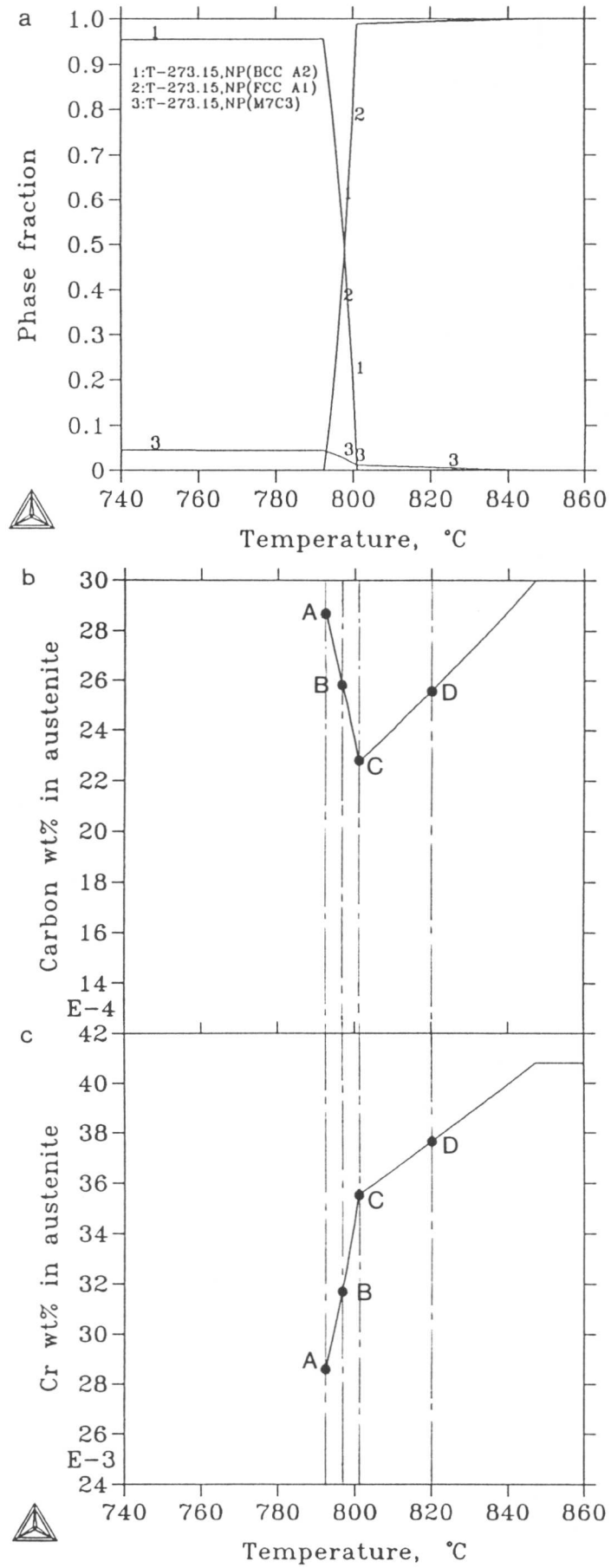
Fig. 6.26 Calculated phase boundaries and chemical compositions in austenite formed at intercritical temperatures. Calculation was carried out using "Thermo-Calc".
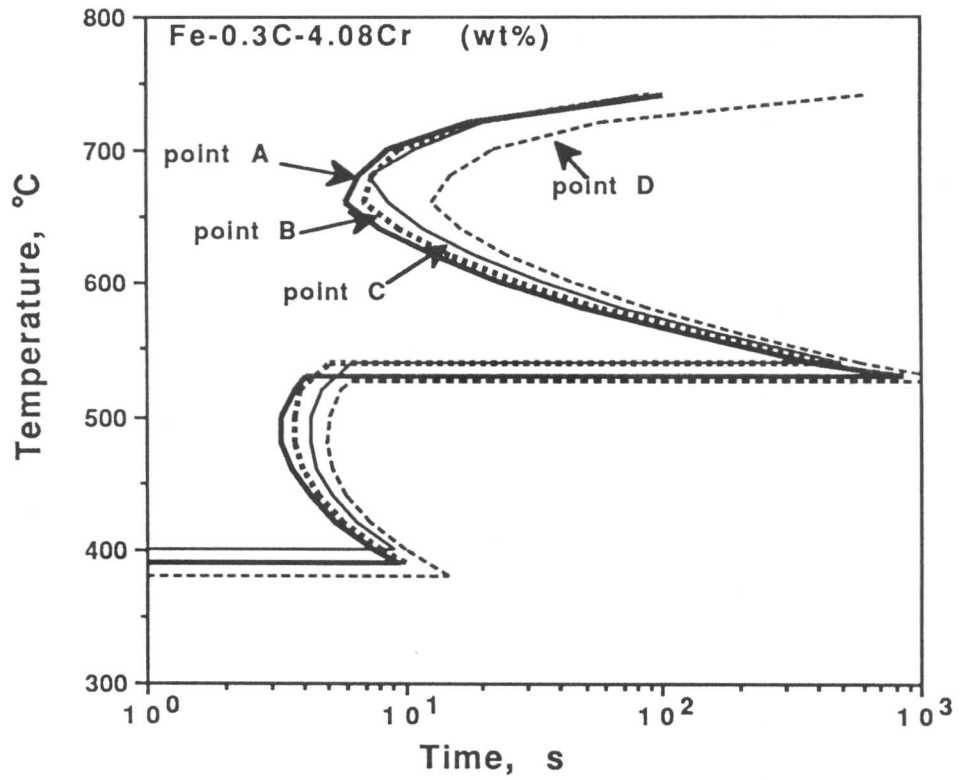
Fig. 6.27 Calculated TTT curves for austenite formed at points A, B, C and D in Fig. 6.28.
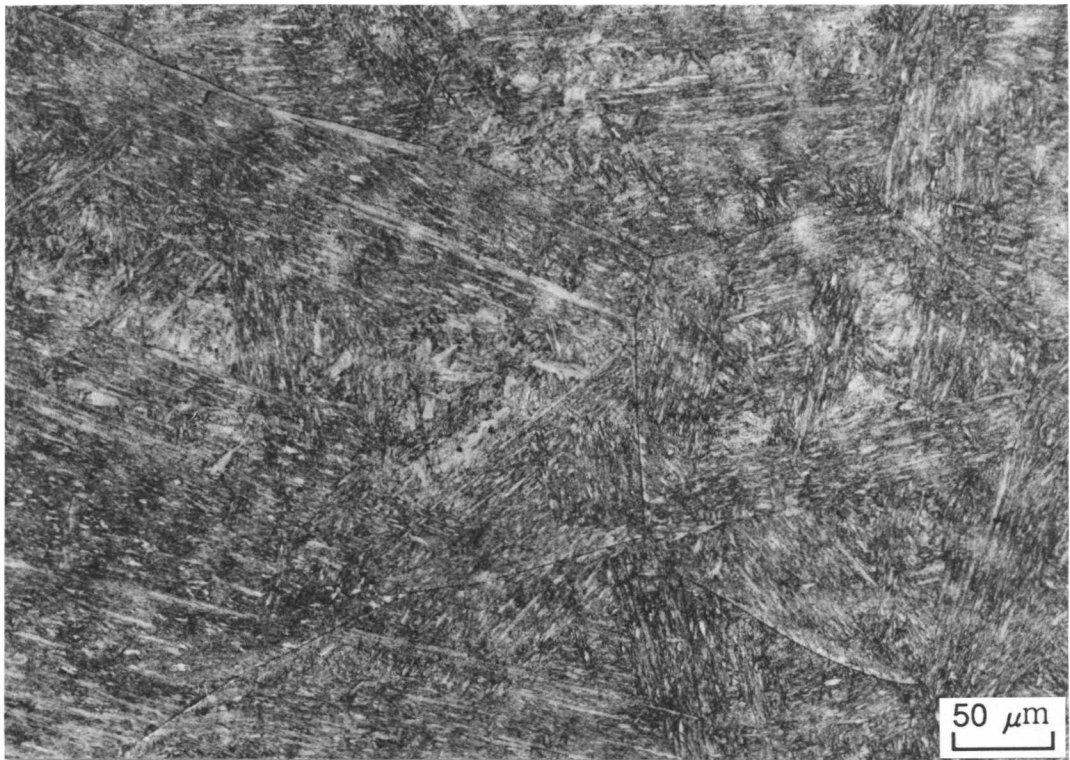
Fig. 6.28 Optical micrograph of a specimen water quenched after tempering of martensite at $500\,^\circ$C for 17 hours in the Fe-0.3C-4.08Cr wt.% alloy.
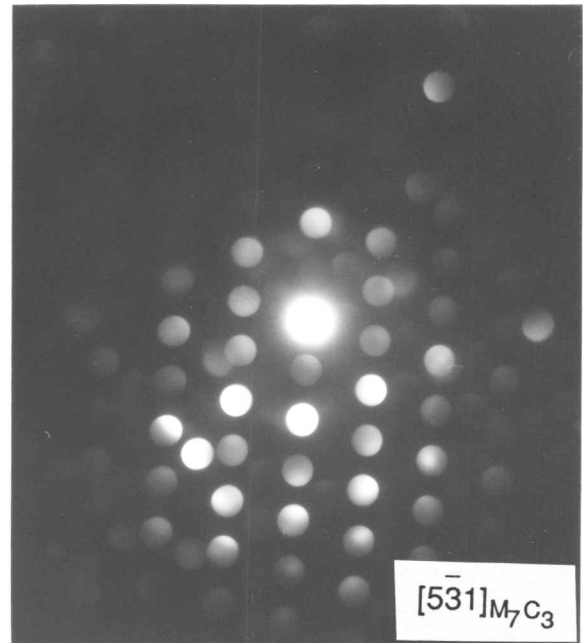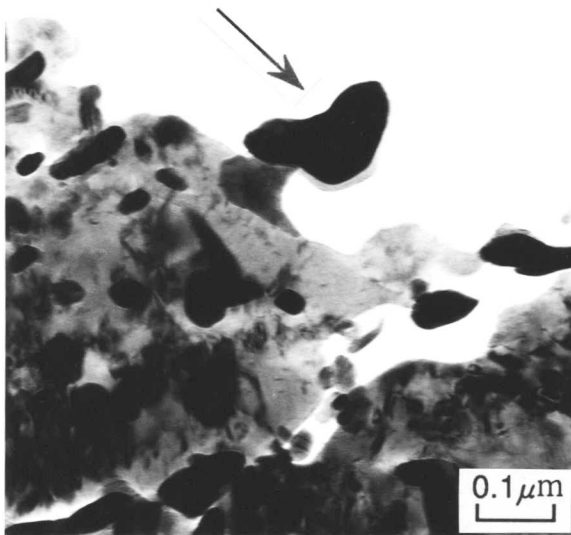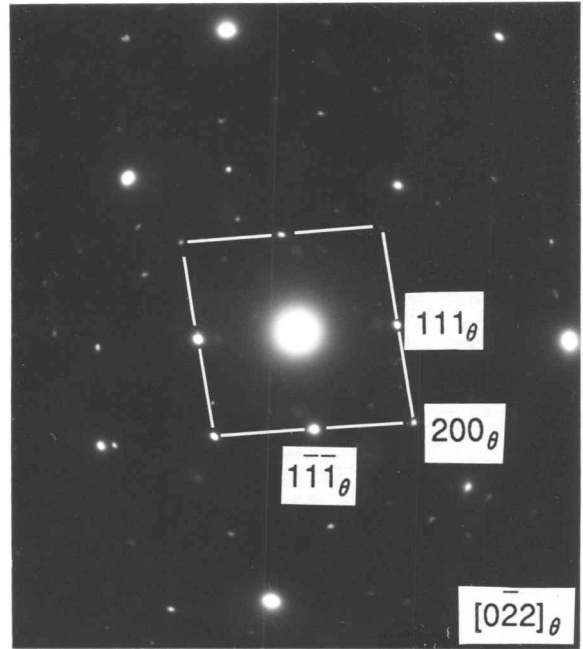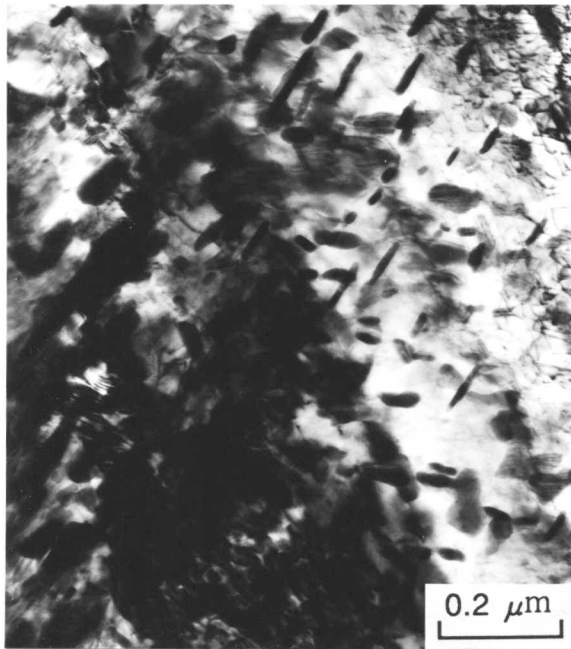
Fig. 6.29 TEM bright field images of a specimen water quenched after tempering of martensite at 500 °C for 17 hours in the Fe-0.3C-4.08Cr wt.% alloy.
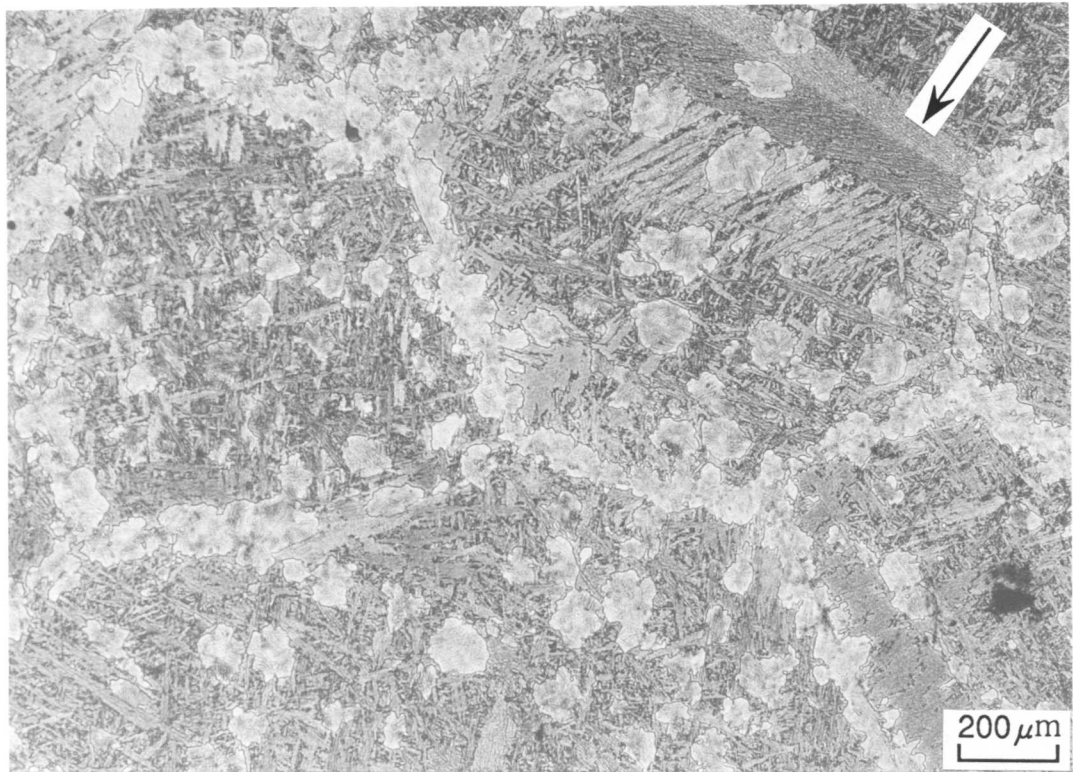
Fig. 6.30 Optical micrograph of a specimen helium quenched after 30 min of isothermal reausteniti-
sation from tempered martensite at 784 °C in the Fe-0.3C-4.08Cr wt.% alloy.

Fig. 6.31 Optical micrograph of a specimen water quenched after tempering of martensite at 700 °C
for 51 hours.
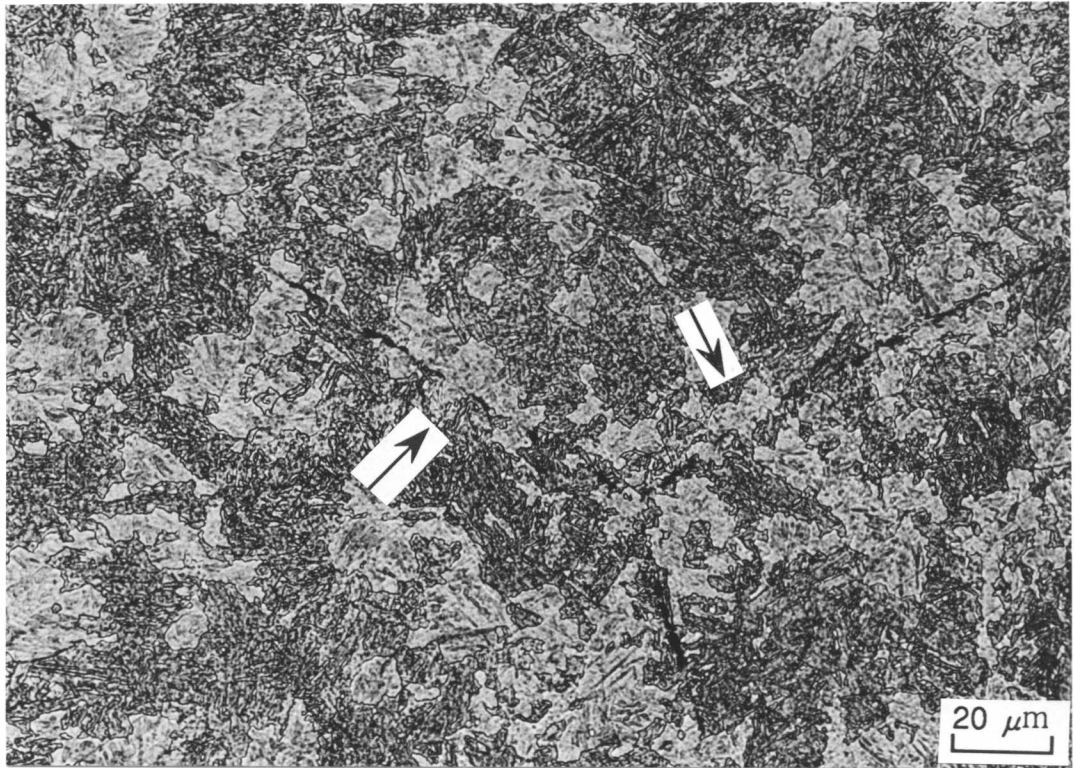
Fig. 6.32 Optical micrograph of a specimen helium quenches after 30 min of isothermal reaustenitisation from tempered martensite, which was obtained at 700 °C, at 785 °C.
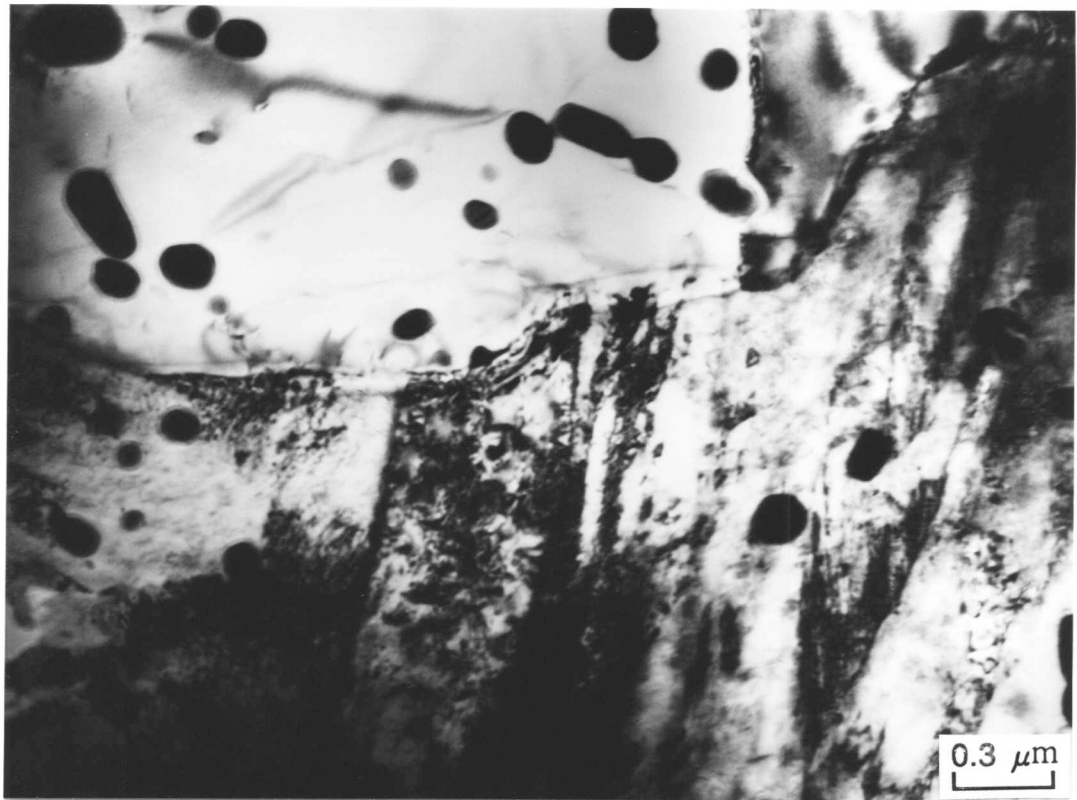
Fig. 6.33 TEM bright field image of a specimen helium quenches after 30 min of isothermal reaustenitisation from tempered martensite, which was obtained at 700 °C, at 785 °C.
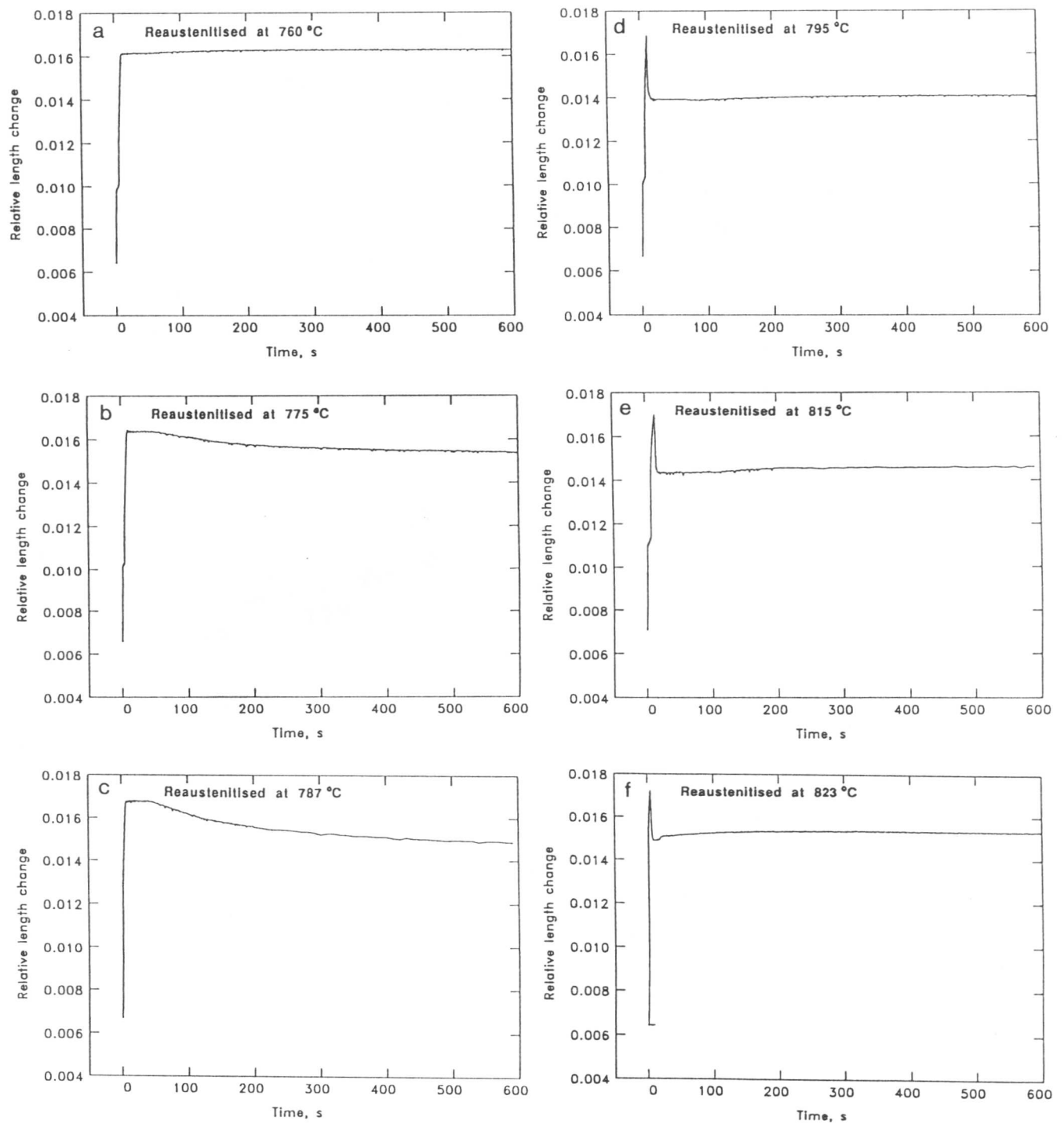
Fig. 6.34 Relative length change during 30 min of isothermal reaustenitisation from tempered marten-site which was obtained at 500°C.
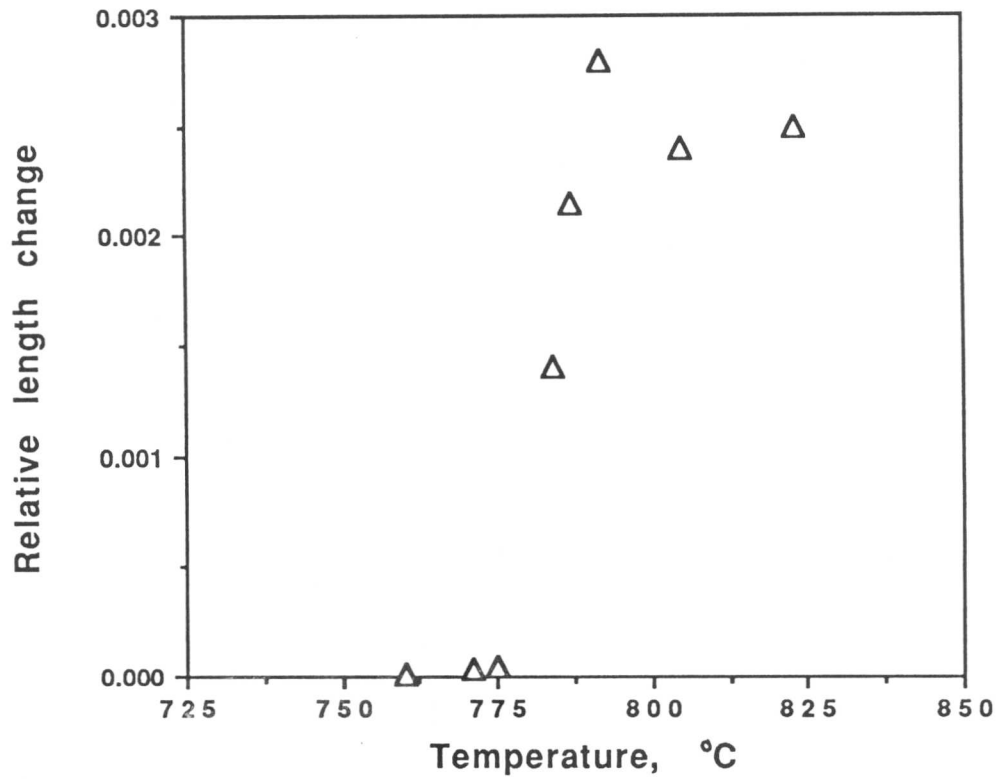
Fig. 6.35 Maximum relative length changes during 30 min of isothermal reaustenitisation from tempered martensite which was obtained at 500 °C.
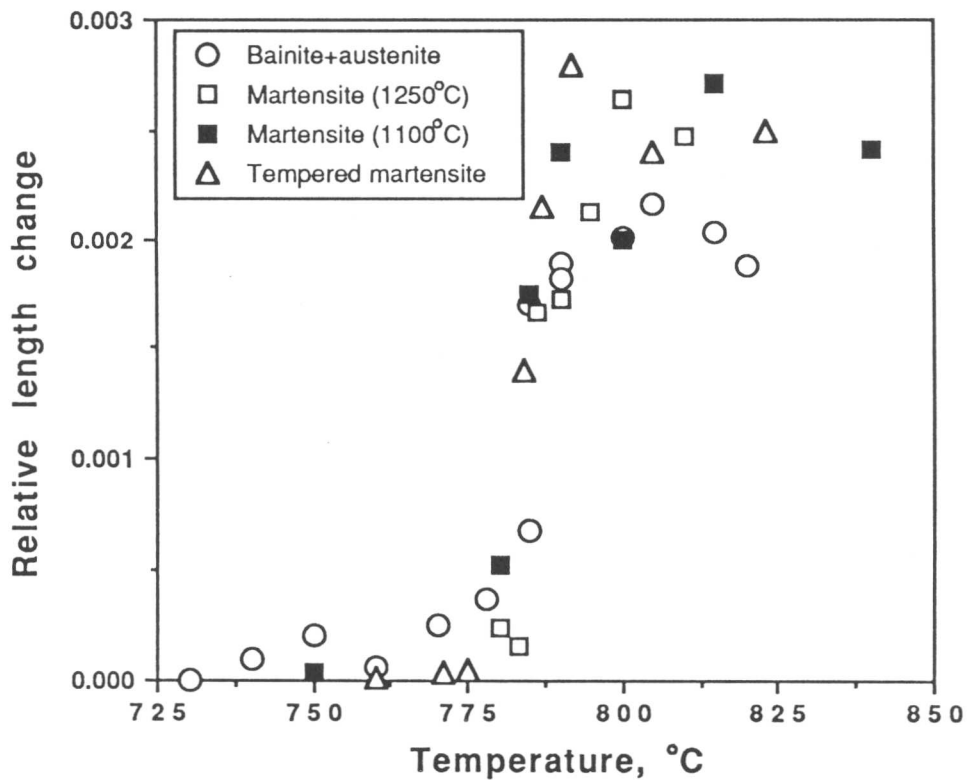
Fig. 6.36 Maximum relative length changes during 30 min of isothermal reaustenitisation from martensite, from the mixture of bainite and austenite, and from tempered martensite at 500 °C in the Fe-0.3C-4.08Cr wt.% alloy.

191
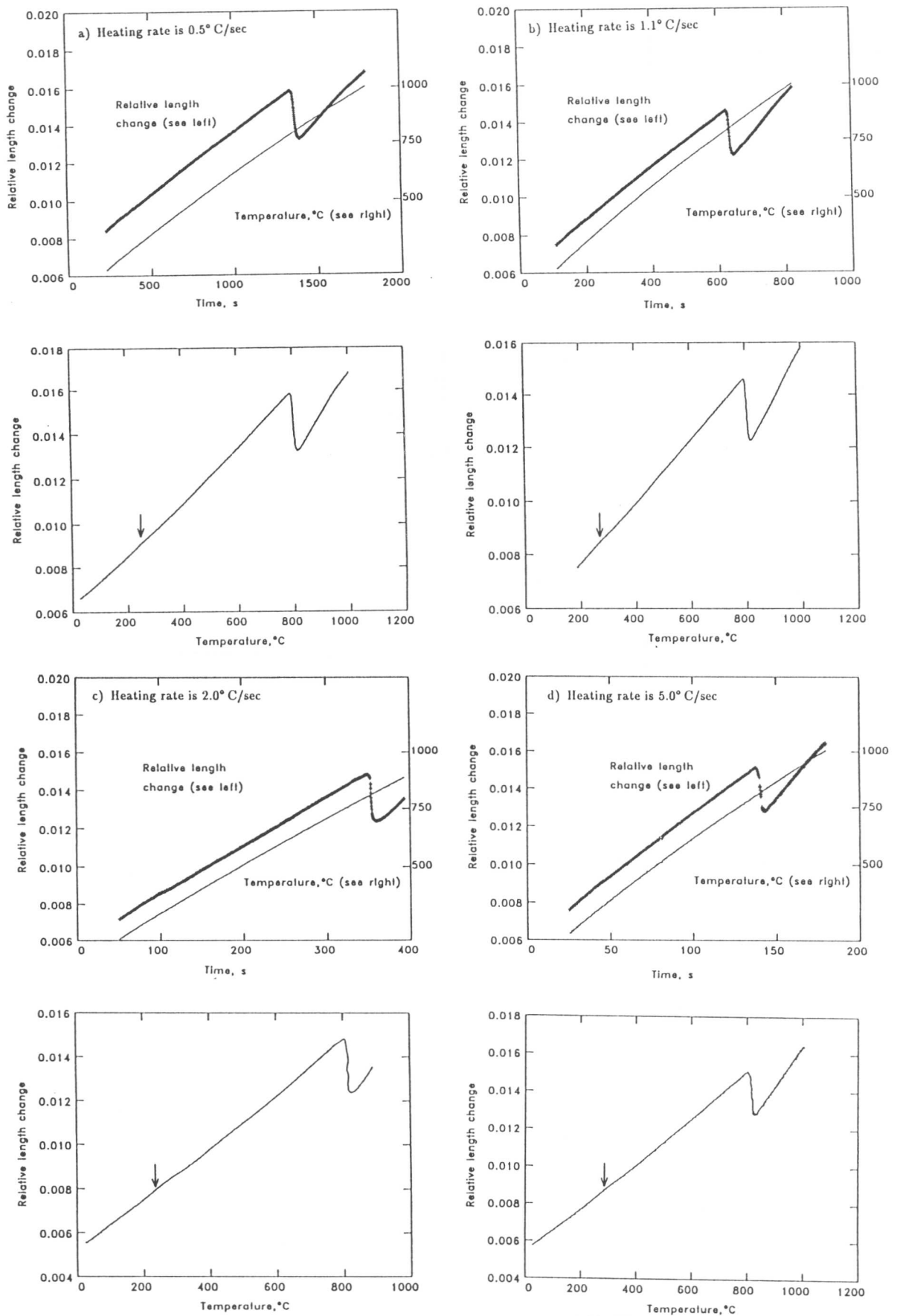
Fig. 6.37 Relative length changes during continuous heating at constant heating rates from the martensitic initial microstructure.

192
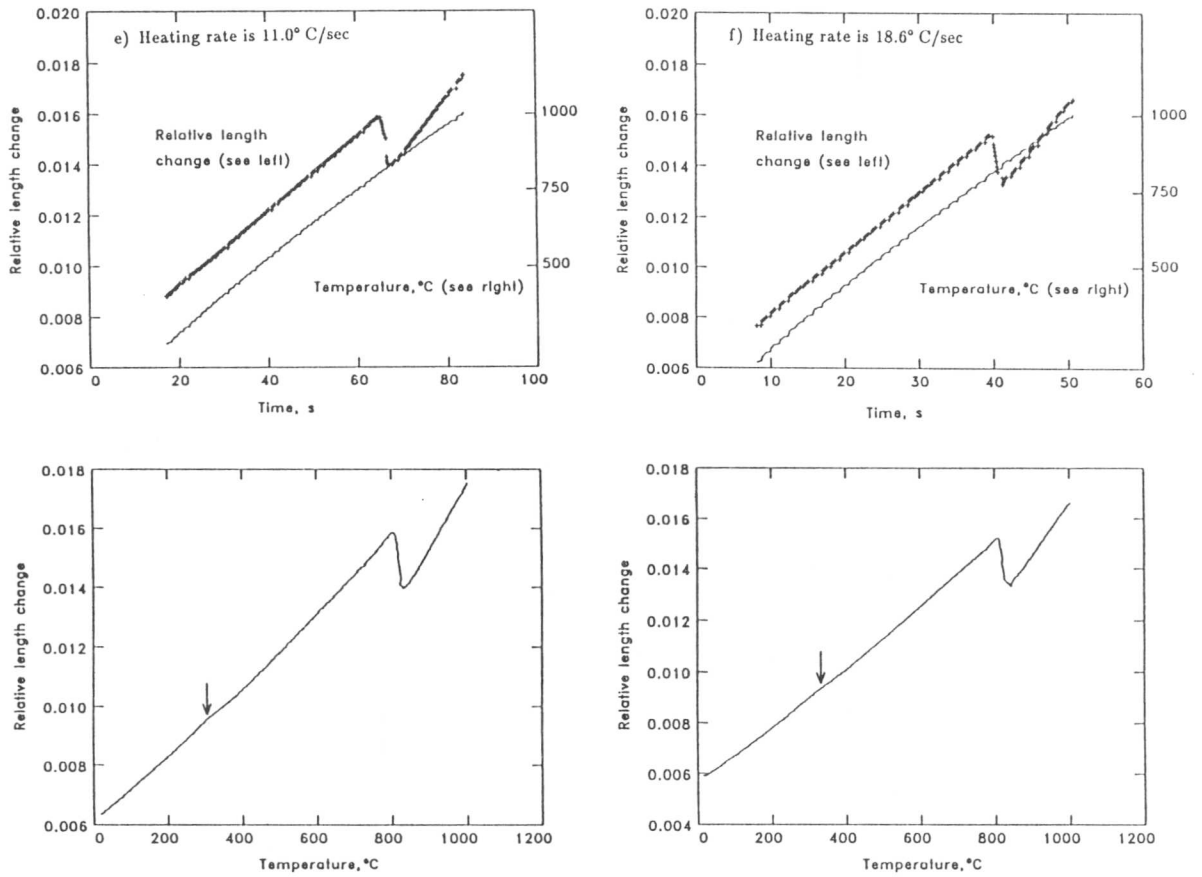
Fig. 6.37 (continued)
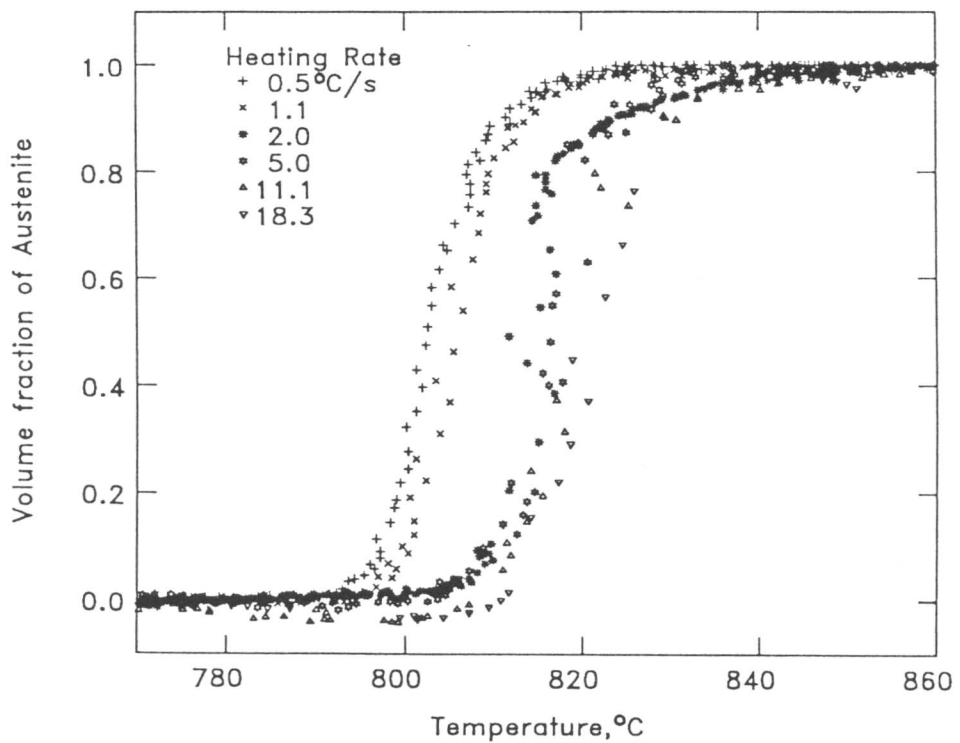
Fig. 6.38 Overall reaustenitisation behaviour during heating at constant heating rate from the martensitic initial microstructure.

193
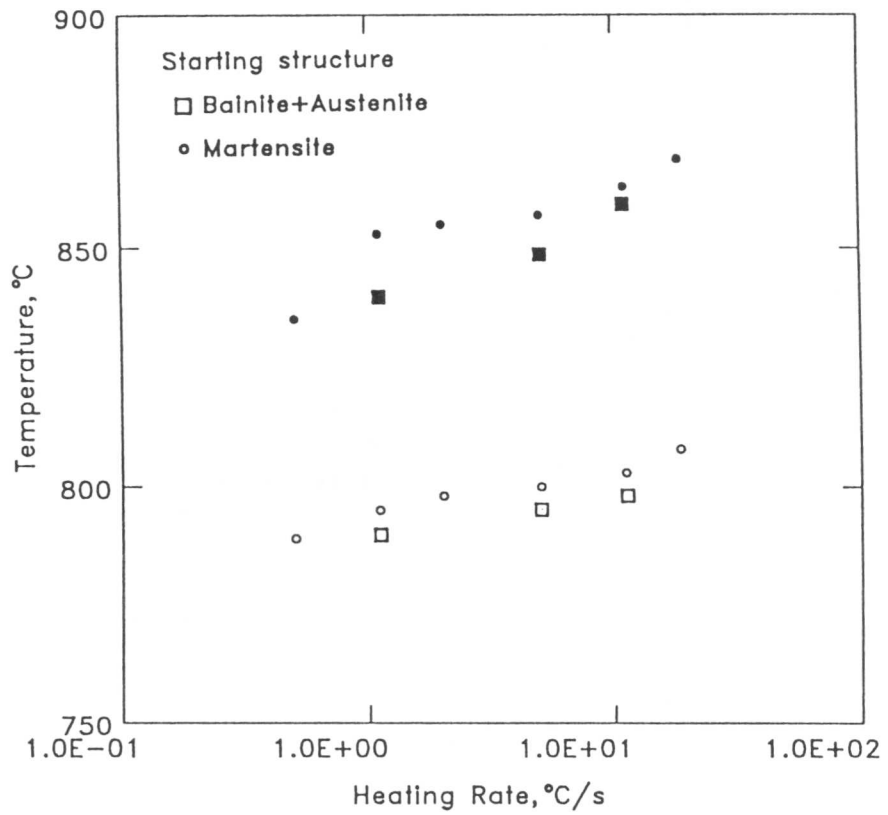
Fig. 6.39 Effect of heating rate on transformation-start and -finish temperatures during continuous heating at constant heating rates from the martensitic initial microstructure.
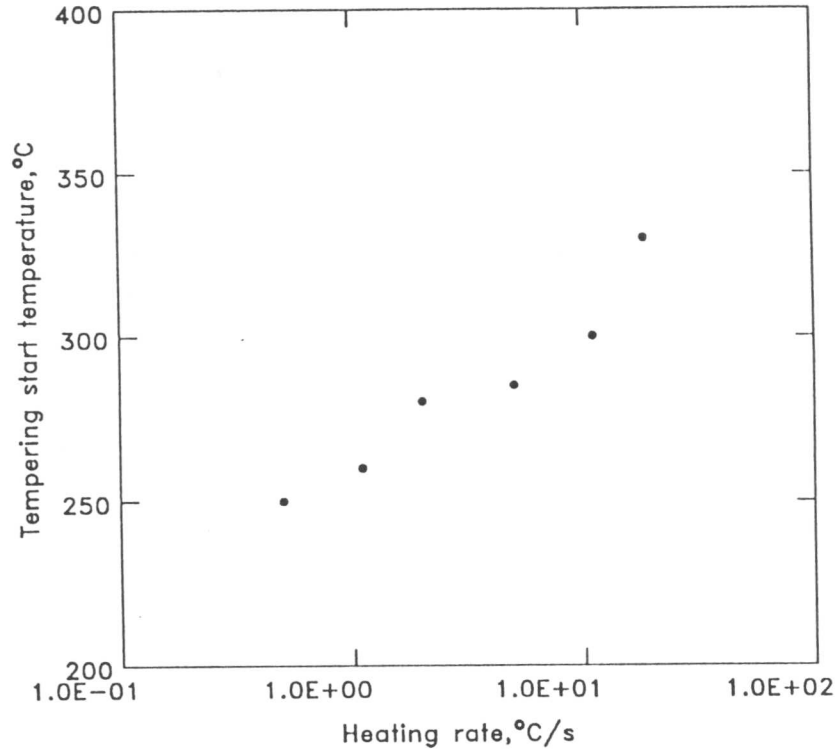
Fig. 6.40 Effect of heating rate on temperature at which tempering of martensite starts during continuous heating reaustenitisation from martensite.

194
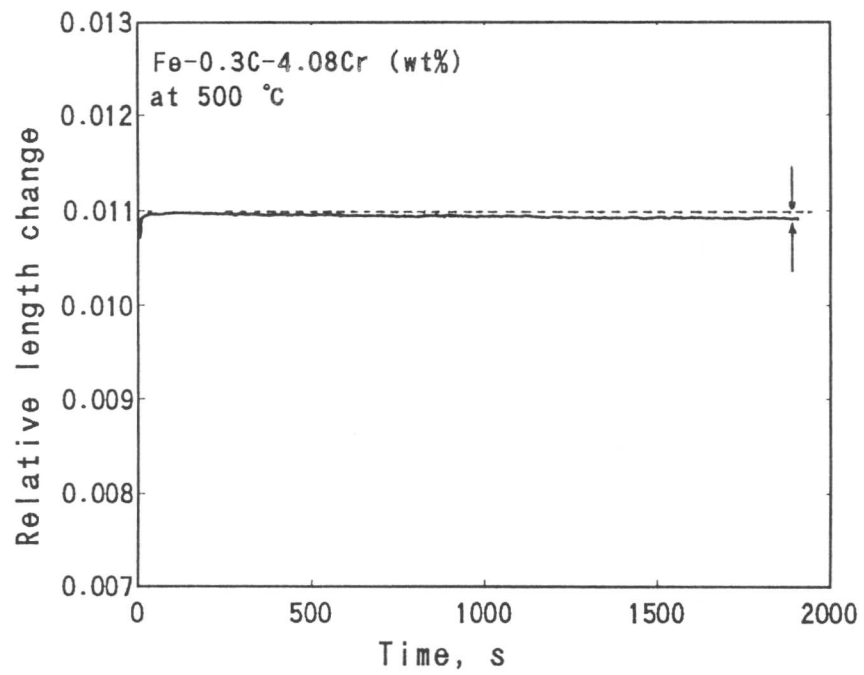
Fig. 6.41 Relative length change during 30 min of isothermal tempering of martensite at 500 °C.

CHAPTER 7

THERMODYNAMICS OF REAUSTENITISATION IN TERNARY ALLOYS

7.1 INTRODUCTION

The conditions which exist at the transformation interface during the growth of ferrite from austenite in steels have been discussed in much more detail than is the case for the reverse transformation from ferrite to austenite. The thermodynamic theory which has been developed for the decomposition of austenite should in principle be adaptable for the reverse transformation, but as will be seen later, there are some important differences which need to be taken into account.

The thermodynamics of the reconstructive formation of ferrite from austenite will be summarised first in order to summarise the techniques available for handling transformation in ternary steels, and an attempt will then be made to deduce a similar framework for the reverse transformation processes.

7.2 RECONSTRUCTIVE FORMATION OF FERRITE FROM AUSTENITE

Ferrite formation is expected to occur when austenite is cooled down below the equilibrium $\gamma/(\alpha + \gamma)$ transformation temperature Ae_3. It is well established that it is possible to obtain various kinds of transformation products, whose mechanism of transformation may be different, depending on a level of supercooling below the equilibrium transformation temperature. The key characteristics of these transformation products in steels have been summarised by Bhadeshia [1].

7.2.1 Reconstructive growth of ferrite in multi-component systems

Since the main interest here is the reconstructive formation of austenite, we begin with a summary of the thermodynamics dealing with the reconstructive transformation of austenite to ferrite in multi-component systems, with a view to using some of the principles for the reverse case.

In multi-component steels, a variety of different modes of equilibrium can be maintained locally at the moving transformation interface because of the existence of a remarkable difference in the diffusivities of interstitial atoms and substitutional alloying elements in iron [2-13] These modes can be classified into three categories; 1) partitioning local equilibrium (PLE) 2) negligible local equilibrium (NPLE) and 3) paraequilibrium (PE).

In a system such as Fe-C-X, the diffusion rate of carbon in the austenite may be as much as $10^7 - 10^9$ times greater than that of a substitutional atom in the temperature range of interest. These very different rates of atomic migration mean that true equilibrium segregation with regard to all components may not be produced at a migrating interface. It is, however, possible to envisage growth under diffusion control with local equilibrium at the interface in the sense that the compositions of two phases at the interface are related by a tie line of the equilibrium diagram, even though this tie line may not pass through the point representing the initial (or average) composition of the alloy. When these kinetic restrictions apply, the two phases may differ either significantly or negligibly in substitutional solute content. A qualitative analysis for ternary steels was first developed by Hillert [5], and a simplified quantitative theory in which diffusion cross terms are neglected was developed by Kirkaldy [6], Purdy *et al.* [7] and Coates

[10]; the effect of the cross terms was later examined by Coates [11,12]. The simple theory shows that for the diffusion-controlled growth of ferrite from austenite in an Fe-C-X alloy with initial composition near the $\gamma/(\alpha+\gamma)$ phase boundary (*i.e.* with a small supersaturation), the tie line selected will have the carbon composition of austenite at the interface almost equal to that of the bulk alloy so that the activity of carbon is nearly constant in the austenite, thus reducing the driving force for carbon diffusion almost to zero. There will be a concentration gradient of the substitutional solute ahead of the interface, resulting in appreciable partition, and the relatively slow growth rate will be determined by the diffusion rate of this solute (Fig. 7.1a). For large supersaturations, the tie line will have the Fe+X composition of the ferrite virtually identical with that of the bulk austenite, and partitioning of the substitutional solute will be extremely small, with a relatively fast growth rate (Fig. 7.1b). These are referred to as the partitioning local equilibrium (PLE) and negligible partitioning local equilibrium (NPLE) growth modes [7,11,12], and for a high ratio of the diffusivities, the theory predicts an abrupt transition from one to the other as the supersaturation increases.

In the NPLE mode, the concentration of the substitutional alloying element is uniform except for a small "spike" in the parent phase adjacent to the interface. As the ratio of interstitial and substitutional diffusion rates increases, the width of this spike decreases, and when it becomes of the order of atomic dimension, the concept of local equilibrium at the interface is invalid and has to be replaced (assuming the growth is nevertheless diffusion-controlled) by that of paraequilibrium [5,2,3,8,9]. In conditions of paraequilibrium, there is no redistribution of Fe + X atoms between the phases, the Fe/X ratio remaining uniform right up to the interface. One interpretation of the paraequilibrium limit is that reconstructive transformation occurs with all displacements of the Fe+X atoms taking place in the incoherent interface; another interpretation might be that only displacive transformation can occur. In either case, to quote from Coates [10], "the slow diffuser and the solvent participate only in the change of crystal structure". Paraequilibrium implies that the growth rate is controlled by the interstitial diffusivity, the interface compositions now being given by the tie lines of the pseudoequilibrium between the two phases under the constraint of a constant Fe/X ratio.

7.2.2 Calculation of tie lines for reconstructive formation of ferrite in ternary systems

For simplification, a ternary system Fe-C-X, where C and X denote respectively carbon and a substitutional alloying element, will be discussed in this section to demonstrate briefly the way to calculate tie lines and the growth rate of the product phase in different equilibrium modes. The bulk composition of austenite is designated $(\overline{x}_1^\gamma, \overline{x}_2^\gamma)$, and the interface compositions, which will be determined in the manner discussed below, are $x_1^{\gamma\alpha}$, $x_1^{\alpha\gamma}$, $x_2^{\gamma\alpha}$, and $x_2^{\alpha\gamma}$, where the subscripts denote carbon and the substitutional alloying element concentrations respectively, and the superscripts $\gamma\alpha$ and $\alpha\gamma$ represent respectively the interface compositions in austenite (γ) and in ferrite (α) which are in equilibrium.

Because the reaction is now controlled by the diffusion of both carbon and the substitutional alloying element, Fick's Law for both species has to be solved simultaneously. The one-dimensional diffusion equations in austenite are expressed as follows. (Note that the concept can easily be extended to two and three dimensional problems: see for example [11,12]):

$$\frac{\partial x_1^\gamma}{\partial t} = \frac{\partial}{\partial z}\left(D_{11}^\gamma \frac{\partial x_1^\gamma}{\partial z}\right) + \frac{\partial}{\partial z}\left(D_{12}^\gamma \frac{\partial x_2^\gamma}{\partial z}\right) \qquad (7.1)$$

197

$$\frac{\partial x_2^\gamma}{\partial t} = \frac{\partial}{\partial z}\left(D_{22}^\gamma \frac{\partial x_2^\gamma}{\partial z}\right) + \frac{\partial}{\partial z}\left(D_{21}^\gamma \frac{\partial x_1^\gamma}{\partial z}\right) \tag{7.2}$$

where z is the space co-ordinate normal to the transformation interface, D_{11}^γ and D_{22}^γ are the interdiffusion coefficients of carbon and X in austenite respectively, and D_{12}^γ and D_{21}^γ are the cross interdiffusion coefficients in the ternary system taking account of the dependence of the flux of one alloy element on the concentration gradient of another. Since the product phase is here assumed to grow with a constant composition, it is necessary only to consider the diffusion equations within the parent austenite phase.

The requirement of mass conservation at the interface is expressed by the following two equations

$$(x_1^{\gamma\alpha} - x_1^{\alpha\gamma})v = J_1|_{z=z^*} \tag{7.3}$$

$$(x_2^{\gamma\alpha} - x_2^{\alpha\gamma})v = J_2|_{z=z^*} \tag{7.4}$$

where v is the growth rate of the product phase, z^* is the position of the moving interface along the space co-ordinate z, and the fluxes of carbon and X at the moving interface, $J_1|_{z=z^*}$ and $J_2|_{z=z^*}$, are expressed by

$$J_1|_{z=z^*} = -D_{11}^\gamma \frac{\partial x_1^\gamma}{\partial z}\bigg|_{z=z^*} - D_{12}^\gamma \frac{\partial x_2^\gamma}{\partial z}\bigg|_{z=z^*} \tag{7.5}$$

$$J_2|_{z=z^*} = -D_{22}^\gamma \frac{\partial x_2^\gamma}{\partial z}\bigg|_{z=z^*} - D_{21}^\gamma \frac{\partial x_1^\gamma}{\partial z}\bigg|_{z=z^*} \tag{7.6}$$

where the differentiations should be taken at the interface.

The four interface compositions in the mass conservation equations are the components of two ends of the tie line in an isothermal section of the ternary equilibrium phase diagram at the reaction temperature of the system concerned. As has been discussed (for example see [11,12]), only one of them is independent given equilibrium since the chemical potentials of the species have to be identical in the phases concerned, giving the additional equations:

$$\mu_i^\alpha = \mu_i^\gamma \, ; i = 0, 1, 2 \tag{7.7}$$

where i's (i=0,1 and 2) correspond to iron, carbon and X respectively. Therefore the two mass conservation equations contain only two independent variables, one of which represents compositions at the interface, and the other the growth rate of the product phase. A unique solution can therefore be obtained from these equations.

When the supersaturation is low (*i.e.* at higher temperatures in the $\alpha + \gamma$ two phase field where the bulk concentration is close to the γ phase field), the PLE condition will be maintained at the interface (see Fig. 7.1a). In order to get a reduced driving force for carbon diffusion in austenite, the interface compositions in austenite are determined by the intersection between the carbon isoactivity line passing through the bulk composition (point **A** in Fig. 7.1a) and the $\gamma/(\gamma + \alpha)$ phase boundary. The other end of the tie line is then obtained via equations 7.7.

On the other hand at relatively higher supersaturations (NPLE) where the bulk alloy composition is close to the α phase field, the tie line is fixed by the intersection between a horizontal line ($x = \bar{x}_2^\gamma$) which passes through the bulk composition (point **B** in Fig. 7.1b) and

the $\alpha/(\alpha + \gamma)$ phase boundary, making the extent of partitioning of X effectively negligible and hence increasing its gradient in the austenite and allowing its flux to keep up with that of carbon. The other end of the tie line is again obtained from equations 7.7.

The intersection of two lines, one of which is the horizontal line passing through the ferrite end of the tie line, and the other is the carbon isoactivity line in austenite passing through the austenite end of the tie line, form the transition line between the PLE to the NPLE modes of growth. When the bulk composition is on the left hand side of the transition line, the NPLE condition will be maintained, whereas the PLE condition will otherwise be achieved (Fig. 7.1a,b).

Although the method discussed above is convenient for discussion, the required rigorous solution (*i.e.* the interface compositions and the growth rate) can be obtained only when the five equations, two of which are the mass conservation conditions at the moving interface and the others the equilibrium equations, are solved simultaneously.

7.3 THERMODYNAMICS OF REAUSTENITISATION

Austenite can be expected to form when steels which contain ferrite, carbide, austenite and their combinations, are heated to a temperature in the $\alpha + \gamma$ two phase region or into the austenite single phase field. When the reaction temperature is raised; *i.e.* the supersaturation is increased, the mobility of atoms also increases. This contrasts with transformation to ferrite from austenite, in which atomic mobility decreases as supercooling increases. Consequently, during austenite formation, the mechanism of transformation is likely to be reconstructive, especially for low alloy steels, whereas the tendency to form ferrite by displacive transformation increases as the undercooling is increased.

7.3.1 Local equilibrium conditions during reaustenitisation

In the case of reaustenitisation in steels, local equilibrium has been usually assumed to exist at the interface between austenite precipitate and ferrite matrix (see for example [14-16]), although Ågren suggested the possibility of partitionless transformation of ferrite to austenite at very high temperatures (higher than 847° C) in Fe-1.5 wt.% Mn system [16].

Assuming local equilibrium, when the reaction temperature is low (low supersaturation), the growth of austenite may be expected to occur by a PLE mechanism, and by the NPLE mechanism at relatively higher supersaturations. The procedure has been discussed qualitatively by Hillert [17]; to calculate the operative tie lines requires a model for the ferrite and austenite solid solution and the dilute solution, the Wagner interaction parameter method is adopted below. The transition line from the PLE to the NPLE condition in an isothermal section of the ternary equilibrium phase diagram is expressed by the line **RQ** instead of **PS** (Fig. 7.2), which is the transition line for the *decomposition* process of austenite [17].

When a steel, which is initially fully ferritic (*i.e.* a low carbon steel), is superheated to an intercritical temperature, it might be a good assumption that local equilibrium will be maintained at the interfaces between austenite and ferrite matrix, because of the high mobility of alloying elements at that temperature. In order to simplify the discussion, attention is focused initially on the reconstructive formation of austenite under conditions of local equilibrium, in a ternary alloy Fe-C-X. When the bulk composition of the steel (see point $\mathbf{I}\{\overline{x}_1, \overline{x}_2\}$ in Fig. 7.3) at the temperature T is in the NPLE condition (region **RQS** in Fig. 7.3), the operative tie line can be obtained as follows. In the NPLE mode, the gradient of X in the parent phase must be large: this can be achieved by allowing $x_2^{\gamma\alpha} \to \overline{x}_2$. One end of the tie line is, therefore,

obtained as the intersection of the $\gamma/(\alpha + \gamma)$ phase boundary and a horizontal $x_2 = \bar{x}_2$ line, which gives the point $\{x_1^{\gamma\alpha}, x_2^{\gamma\alpha}\}$ designated "A" in Fig. 7.3. The other end of the tie line follows automatically as the point $\mathbf{B}\{x_1^{\alpha\gamma}, x_2^{\alpha\gamma}\}$ (Fig. 7.3), from the fact that for a tie line,

$$\mu_i^{\alpha\gamma} = \mu_i^{\gamma\alpha} \; ; i = 0, 1, 2 \; . \tag{7.8}$$

Kirkaldy and his co-workers [18-20] have used dilute solution methods to calculate the tie lines in multi-component systems. The requirement of identical chemical potentials both in austenite and in ferrite at the interface, leads to the approximation [18].

$$\frac{\Delta G_i^{0\alpha \to \gamma}}{RT} = \ln \frac{x_i^\alpha}{x_i^\gamma} + \ln \frac{\Gamma_i^\alpha}{\Gamma_i^\gamma} \; ; i = 0, 1, 2 \tag{7.9}$$

where $\Delta G_i^{0\alpha \to \gamma}$ is the standard free energy change between α and γ for each element, and Γ_i are the activity coefficients for each of the elements, given by,

$$\ln \Gamma_1 = \epsilon_{11} x_1 + \epsilon_{12} x_2 \tag{7.10}$$

$$\ln \Gamma_2 = \epsilon_{12} x_1 + \epsilon_{22} x_2 \tag{7.11}$$

$$\ln \Gamma_0 = -\frac{\epsilon_{11}}{2} x_1^2 - \epsilon_{12} x_1 x_2 - \frac{\epsilon_{22}}{2} x_2^2 \; . \tag{7.12}$$

where ϵ_{ij} are empirical coefficients known as the Wagner interaction parameters. Therefore, from the fact that the alloying element concentration in austenite at the interface is identical to that of the bulk, it is possible to calculate the interfacial compositions (points A and B in Fig. 7.3) which satisfy the thermodynamic equations listed above, simultaneously. Then one can obtain the point $\mathbf{M}\{x_1^T, x_2^T\}$ on the transition line $\mathbf{RQ}$ (Fig. 7.3), which is the intersection of the isoactivity line of carbon in ferrite passing through the point B, and the constant substitutional alloying element line IA. † The activity of carbon at the points B and M (a_B and a_M respectively) in a dilute ternary system are given as follows, ignoring the higher-order terms of the expansion [21]:

$$\ln a_B^c = \ln x_1^{\alpha\gamma} + \epsilon_{11} x_1^{\alpha\gamma} + \epsilon_{12} x_2^{\alpha\gamma}$$

$$\ln a_M^c = \ln x_1^T + \epsilon_{11} x_1^T + \epsilon_{12} x_2^T \; .$$

Using these two equations, and by ignoring the small difference between the products $\epsilon_{11} x_1^{\alpha\gamma}$ and $\epsilon_{11} x_1^T$, we obtain

$$\ln x_1^T = \ln x_1^{\alpha\gamma} + \epsilon_{12} x_2^{\alpha\gamma} - \epsilon_{12} x_2^T \; . \tag{7.13}$$

On replacing x_2^T by $\bar{x}_2$, x_1^T can be calculated given the interface compositions $x_1^{\gamma\alpha}$ and $x_2^{\alpha\gamma}$. Because the bulk composition is now in the NPLE region, it should be noted that $x_1^T < \bar{x}_1$.

In the case of the PLE condition, in contrast, it is expected that $x_1^T > \bar{x}_1$. The following method is used in order to determine the tie line in this situation. When the bulk composition of ferrite is in the PLE region (see point $\mathbf{K}\{\bar{x}_1, \bar{x}_2\}$ in Fig. 7.4), it is necessary to ensure that the gradient of carbon in the parent phase is reduced to a level consistent with the sluggishness of X element diffusion. This can be done by ensuring that the carbon isoactivity line in ferrite passes

---

† Note that IA is not strictly parallel to the carbon axis since it is really the ratio of Fe/X atoms is constant along IA.

through the bulk composition $\mathbf{K}$; the intersection of that isoactivity line with the $\alpha/(\alpha + \gamma)$ phase boundary (see point $\mathbf{B}\{x_1^{\alpha\gamma}, x_2^{\alpha\gamma}\}$ in Fig. 7.4), then defines the operative tie line.

However, when the phase boundary is to be determined simultaneously with the tie line, it is possible to use a more convenient method to calculate these values. It is noted that the operative tie line AB for the bulk composition $\mathbf{K}$ is the NPLE tie line for an alloy whose bulk composition is same as the point $\mathbf{M}$ in Fig. 7.4, which is an intersection between the transition line and the isoactivity line of carbon in ferrite passing through the bulk composition $\mathbf{K}$. Therefore the operative tie line $\mathbf{AB}$ can be obtained by finding the point $\mathbf{M}$ and then calculating the NPLE tie line for the point.

First, one can calculate the point $\mathbf{G}\{x_1^T, x_2^{\alpha\gamma}\}$ corresponding to the point $\mathbf{K}$ using equation 7.13 and the NPLE interface compositions determined for the bulk composition $\mathbf{K}$; *i.e.* under the condition of $x_2^{\gamma\alpha} = \overline{x}_2$. Since the bulk composition is now in the PLE region, it is expected that $x_1^T > \overline{x}_1$. We now rename these points for simplicity: the bulk composition and the corresponding point $\mathbf{G}$ are now called $\mathbf{K}_0\{\overline{x}_{1,0}, \overline{x}_{2,0}\}$ and $\mathbf{G}_0\{x_{1,0}^T, x_{2,0}^T\}$ respectively (Fig. 7.4b). In order to find the point $\mathbf{M}$ effectively, a point $\mathbf{K}_1\{\overline{x}_{1,1}, \overline{x}_{2,1}\}$ on the isoactivity line of carbon in ferrite (*i.e.* , line $\mathbf{BK}$), which has a slightly higher alloying element composition than that of the bulk; *i.e.* $\overline{x}_{2,1} > \overline{x}_{2,0}$, is selected. And the corresponding point $\mathbf{G}_1(x_{1,1}^T, x_{2,1}^T)$ on the transition line is determined as mentioned above. Now one can estimate the point $\mathbf{G}_2(x_{1,2}^T, x_{2,2}^T)$ which may be close to the point $\mathbf{M}$ using points $\mathbf{K}_0$, $\mathbf{K}_1$, $\mathbf{G}_0$ and $\mathbf{G}_1$ by the following equations:

$$\overline{x}_{2,i+1} = \frac{\overline{x}_{2,i-1}(x_{1,i}^T - \overline{x}_{1,i}) - \overline{x}_{2,i}(x_{1,i-1}^T - \overline{x}_{1,i-1})}{(x_{1,i}^T - \overline{x}_{1,i}) - (x_{1,i-1}^T - \overline{x}_{1,i-1})} \tag{7.14}$$

and

$$\overline{x}_{1,i+1} = \exp\{\ln \overline{x}_{1,1} + \epsilon_{12}\overline{x}_{2,1} - \epsilon_{12}\overline{x}_{2,i+1}\} . \tag{7.15}$$

The point $\mathbf{M}$ is obtained by repeating this calculation until the difference between $\overline{x}_{1,i+1}$ and $x_{1,i+1}^T$ becomes smaller than the accuracy required. Then one can use exactly the same method to determine the tie line corresponding the point $\mathbf{M}$ as was used for the determination of the tie line for the NPLE condition. This tie line is, in fact, the operative tie line for the bulk composition $\mathbf{K}$ in Fig. 7.4.

7.3.2 Reconstructive growth of austenite under the local equilibrium

- starting from a mixture of ferrite and austenite of compositions $\overline{x}_i^\alpha$ and $\overline{x}_i^\gamma$

When the initial microstructure is a mixture of bainitic ferrite and austenite whose carbon concentration was determined by the T_0' curve at the bainite transformation temperature, tie lines for the local equilibrium mode can, in this case, also be determined using the method discussed above. The chemical distributions in both phases are, however, different from those in the case of reaustenitisation from a fully ferritic sample. Since the initial carbon and X concentrations in austenite are different from those at the interface, fluxes of carbon and X in austenite are also expected to exist. Illustrative chemical distributions are shown with an isothermal section of the equilibrium phase diagram in Fig. 7.5 and Fig. 7.6.

As mentioned in the previous section, rigorous solutions of the interface compositions and the growth rate of the product phase (*i.e.* austenite), can be obtained only when the mass conservation equations are solved giving the growth rate of the product phase which satisfies the equilibrium conditions at the interface.

201

Because there are now diffusional fields both in the matrix (*i.e.* ferrite) and in the product (*i.e.* austenite) phases, it is necessary to handle the diffusion equations in both phases, in a way which satisfies the mass conservation conditions at the interface. The one-dimensional diffusion equations in the ferrite matrix and austenite precipitate phase are expressed as follows.

$$\frac{\partial x_1^\gamma}{\partial t} = \frac{\partial}{\partial z}\left(D_{11}^\gamma \frac{\partial x_1^\gamma}{\partial z}\right) + \frac{\partial}{\partial z}\left(D_{12}^\gamma \frac{\partial x_2^\gamma}{\partial z}\right) \tag{7.16}$$

$$\frac{\partial x_2^\gamma}{\partial t} = \frac{\partial}{\partial z}\left(D_{22}^\gamma \frac{\partial x_2^\gamma}{\partial z}\right) + \frac{\partial}{\partial z}\left(D_{21}^\gamma \frac{\partial x_1^\gamma}{\partial z}\right) \tag{7.17}$$

$$\frac{\partial x_1^\alpha}{\partial t} = \frac{\partial}{\partial z}\left(D_{11}^\alpha \frac{\partial x_1^\alpha}{\partial z}\right) + \frac{\partial}{\partial z}\left(D_{12}^\alpha \frac{\partial x_2^\alpha}{\partial z}\right) \tag{7.18}$$

$$\frac{\partial x_2^\alpha}{\partial t} = \frac{\partial}{\partial z}\left(D_{22}^\alpha \frac{\partial x_2^\alpha}{\partial z}\right) + \frac{\partial}{\partial z}\left(D_{21}^\alpha \frac{\partial x_1^\alpha}{\partial z}\right) \tag{7.19}$$

The requirement for conservation of mass at the interface gives the following two equations:

$$(x_1^{\gamma\alpha} - x_1^{\alpha\gamma})v = -J_1^\alpha|_{z=z^*} + J_1^\gamma|_{z=z^*} \tag{7.20}$$

$$(x_2^{\gamma\alpha} - x_2^{\alpha\gamma})v = -J_2^\alpha|_{z=z^*} + J_2^\gamma|_{z=z^*} \tag{7.21}$$

where v is the growth rate of the product phase. We emphasise again that the fluxes in both the matrix and product phases contribute to mass conservation at the interface, and thus, to the growth rate of the product phase. The fluxes of carbon and the substitutional alloying element at the moving interface are given by,

$$J_1^\gamma|_{z=z^*} = -D_{11}^\gamma \frac{\partial x_1^\gamma}{\partial z}\bigg|_{z=z^*} - D_{12}^\gamma \frac{\partial x_2^\gamma}{\partial z}\bigg|_{z=z^*} \tag{7.22}$$

$$J_2^\gamma|_{z=z^*} = -D_{22}^\gamma \frac{\partial x_2^\gamma}{\partial z}\bigg|_{z=z^*} - D_{21}^\gamma \frac{\partial x_1^\gamma}{\partial z}\bigg|_{z=z^*} \tag{7.23}$$

$$J_1^\alpha|_{z=z^*} = -D_{11}^\alpha \frac{\partial x_1^\alpha}{\partial z}\bigg|_{z=z^*} - D_{12}^\alpha \frac{\partial x_2^\alpha}{\partial z}\bigg|_{z=z^*} \tag{7.24}$$

$$J_2^\alpha|_{z=z^*} = -D_{22}^\alpha \frac{\partial x_2^\alpha}{\partial z}\bigg|_{z=z^*} - D_{21}^\alpha \frac{\partial x_1^\alpha}{\partial z}\bigg|_{z=z^*} \tag{7.25}$$

where the differentials are taken in the respective phases at the interface.

Because analytical equations of the concentration distributions in both matrix and product phases (for the cases where diffusion fields in both phases should be considered simultaneously) are not available, linear chemical concentration gradients are assumed in both phases for the calculation of the growth rate of the product phase; this is the so-called Zener approximation.

As it is illustrated in Fig. 7.7, the diffusion distances of carbon and the substitutional alloying element in ferrite and in austenite are respectively, L_γ, L_α, l_γ and l_α. The fluxes of carbon and the substitutional alloying element at the moving boundary are then given by,

$$J_1^\gamma|_{z=z^*} = -D_{11}^\gamma \frac{\overline{x}_1^\gamma - x_1^{\gamma\alpha}}{L_\gamma} - D_{12}^\gamma \frac{\overline{x}_2^\gamma - x_2^{\gamma\alpha}}{l_\gamma} \tag{7.26}$$

$$J_2^\gamma|_{z=z^*} = -D_{22}^\gamma \frac{\overline{x}_2^\gamma - x_2^{\gamma\alpha}}{l_\gamma} - D_{21}^\gamma \frac{\overline{x}_1^\gamma - x_1^{\gamma\alpha}}{L_\gamma} \tag{7.27}$$

$$J_1^\alpha\big|_{z=z^*} = -D_{11}^\alpha \frac{\overline{x}_1^\alpha - x_1^{\alpha\gamma}}{L_\alpha} - D_{12}^\alpha \frac{\overline{x}_2^\alpha - x_2^{\alpha\gamma}}{l_\alpha} \tag{7.28}$$

$$J_2^\alpha\big|_{z=z^*} = -D_{22}^\alpha \frac{\overline{x}_2^\alpha - x_2^{\alpha\gamma}}{l_\alpha} - D_{21}^\alpha \frac{\overline{x}_1^\alpha - x_1^{\alpha\gamma}}{L_\alpha} \tag{7.29}$$

where $\overline{x}_1^{\alpha,\gamma}$ and $\overline{x}_2^{\alpha,\gamma}$ are average concentrations of carbon and the substitutional alloying element in each phase, and z^* is the position of the moving interface. The conservation conditions for carbon and the substitutional alloying element in the system as a whole provide the following equations:

$$(L_\gamma - z^*)(\overline{x}_1^\gamma - \overline{x}_1^\alpha) = \frac{L_\gamma}{2}[(x_1^{\gamma\alpha} - \overline{x}_1^\alpha) + (\overline{x}_1^\gamma - \overline{x}_1^\alpha)] - \frac{L_\alpha}{2}(\overline{x}_1^\alpha - x_1^{\alpha\gamma}) \tag{7.30}$$

$$\frac{l_\alpha}{2}(\overline{x}_2^\alpha - x_2^{\alpha\gamma}) = \frac{l_\gamma}{2}(x_2^{\gamma\alpha} - \overline{x}_2^\gamma) . \tag{7.31}$$

In addition to these equations, because the decrease in the amount of carbon (or X) in ferrite is equal to the integrated flux of carbon (or X) at the interface from $t = 0$ to $t = t$, one can introduce two further equations given below:

$$\int_0^t \left(\frac{D_{11}^\alpha(\overline{x}_1^\alpha - x_1^{\alpha\gamma})}{L_\alpha} + \frac{D_{12}^\alpha(\overline{x}_2^\alpha - x_2^{\alpha\gamma})}{l_\alpha} \right) dt = \frac{1}{2}(L_\alpha + 2z^*)(\overline{x}_1^\alpha - x_1^{\alpha\gamma}) \tag{7.32}$$

$$\int_0^t \frac{D_{22}^\alpha(\overline{x}_2^\alpha - x_2^{\alpha\gamma})}{l_\alpha} dt = \frac{1}{2}(l_\alpha + 2z^*)(\overline{x}_2^\alpha - x_2^{\alpha\gamma}) . \tag{7.33}$$

As discussed in Appendix, the interface position z^* and the diffusion distances L_γ, L_α, l_γ, and l_α are proportional to $t^{1/2}$:

$$z^* = \alpha_1 t^{1/2}$$
$$L_\gamma = k_{C\gamma} t^{1/2}$$
$$L_\alpha = k_{C\alpha} t^{1/2} ,$$
$$l_\gamma = k_{X\gamma} t^{1/2}$$
$$l_\alpha = k_{X\alpha} t^{1/2}$$

and, therefore, the growth rate of the product phase is given by:

$$v = \frac{dz^*}{dt} = \frac{1}{2}\alpha_1 t^{-1/2} , \tag{7.34}$$

where α_1 is one-dimensional parabolic thickening rate constant. Equations (7.32) and (7.33) give the following relations for the proportionality constants for the diffusion distances in ferrite:

$$k_{X\alpha} = -\alpha_1 + \sqrt{\alpha_1^2 + 4D_{22}^\alpha}$$
$$k_{C\alpha} = -k_\alpha + \sqrt{k_\alpha^2 + 4D_{11}^\alpha}$$

with

$$k_\alpha = \alpha_1 - \frac{2D_{12}^\alpha(\overline{x}_2^\alpha - x_2^{\alpha\gamma})}{\overline{x}_1^\alpha - x_1^{\alpha\gamma}} \frac{1}{k_{X\alpha}} .$$

From equations 7.30 and 7.31, $k_{C\gamma}$ and $k_{X\gamma}$ are expressed by α_1, $k_{C\alpha}$, and $k_{X\alpha}$, giving,

$$k_{X\gamma} = k_{X\alpha} \frac{\overline{x}_2^{\alpha} - x_2^{\alpha\gamma}}{x_2^{\gamma\alpha} - \overline{x}_2^{\gamma}}$$

$$k_{C\gamma} = 2\alpha_1 \frac{\overline{x}_1^{\gamma} - \overline{x}_1^{\alpha}}{\overline{x}_1^{\gamma} - x_1^{\gamma\alpha}} - k_{C\alpha} \frac{\overline{x}_1^{\alpha} - x_1^{\alpha\gamma}}{\overline{x}_1^{\alpha} - x_1^{\gamma\alpha}}$$

Now, these four diffusion distances and the interface position can be substituted into the mass conservation equations 7.30 and 7.31 to obtain the interface compositions and the growth rate of the product phase, assuming that the cross interdiffusion coefficient D_{21} is negligible [21]:

$$\alpha_1^2 - C_1\alpha_1 - C_2 = 0 \qquad (7.35)$$

$$\alpha_1^2 - C_3 = 0 \qquad (7.36)$$

with

$$C_1 = \frac{k_{C\alpha}}{2} \frac{\overline{x}_1^{\alpha} - x_1^{\alpha\gamma}}{\overline{x}_1^{\gamma} - \overline{x}_1^{\alpha}} + \frac{2D_{11}^{\alpha}}{k_{C\alpha}} \frac{\overline{x}_1^{\alpha} - x_1^{\alpha\gamma}}{x_1^{\gamma\alpha} - x_1^{\alpha\gamma}}$$

$$+ \frac{2D_{12}^{\alpha}}{k_{X\alpha}} \frac{\overline{x}_2^{\alpha} - x_2^{\alpha\gamma}}{x_1^{\gamma\alpha} - x_1^{\alpha\gamma}} - \frac{2D_{12}^{\gamma}}{k_{X\alpha}} \frac{(x_2^{\gamma\alpha} - \overline{x}_2^{\gamma})^2}{(x_1^{\gamma\alpha} - x_1^{\alpha\gamma})(\overline{x}_2^{\alpha} - x_2^{\alpha\gamma})}$$

$$C_2 = D_{11}^{\gamma} \frac{(\overline{x}_1^{\gamma} - x_1^{\gamma\alpha})^2}{(x_1^{\gamma\alpha} - x_1^{\alpha\gamma})(\overline{x}_1^{\gamma} - \overline{x}_1^{\alpha})} + \frac{k_{C\alpha}}{k_{X\alpha}} D_{12}^{\gamma} \frac{\overline{x}_1^{\alpha} - x_1^{\alpha\gamma}}{(x_1^{\gamma\alpha} - x_1^{\alpha\gamma})(\overline{x}_1^{\gamma} - \overline{x}_1^{\alpha})} \frac{(x_2^{\gamma\alpha} - \overline{x}_2^{\gamma})^2}{\overline{x}_2^{\alpha} - x_2^{\alpha\gamma}}$$

$$- D_{11}^{\alpha} \frac{(\overline{x}_1^{\alpha} - x_1^{\alpha\gamma})^2}{(x_1^{\gamma\alpha} - x_1^{\alpha\gamma})(\overline{x}_1^{\gamma} - \overline{x}_1^{\alpha})} - \frac{k_{C\alpha}}{k_{X\alpha}} D_{12}^{\alpha} \frac{(\overline{x}_1^{\alpha} - x_1^{\alpha\gamma})(\overline{x}_2^{\alpha} - x_2^{\alpha\gamma})}{(x_1^{\gamma\alpha} - x_1^{\alpha\gamma})(\overline{x}_1^{\gamma} - \overline{x}_1^{\alpha})}$$

$$C_3 = \frac{2D_{22}^{\alpha}}{k_{X\alpha}} \frac{\overline{x}_2^{\alpha} - x_2^{\alpha\gamma}}{x_2^{\gamma\alpha} - x_2^{\alpha\gamma}} - \frac{2D_{22}^{\gamma}}{k_{X\alpha}} \frac{(x_2^{\gamma\alpha} - \overline{x}_2^{\gamma})^2}{(x_2^{\gamma\alpha} - x_2^{\alpha\gamma})(\overline{x}_2^{\alpha} - x_2^{\alpha\gamma})}$$

One can then calculate the interface compositions and the growth rate of austenite by solving equations 7.35 and 7.36 and three thermodynamic equations 7.8 simultaneously.

It is worth noting that the flux in austenite may be negligible in the case of the formation of austenite from a fully ferritic initial microstructure by analogy with the reconstructive ferrite formation from austenite in which the ferrite is usually assumed to grow with a constant composition. Therefore the growth of austenite, in this case, is controlled only by diffusion of atoms in ferrite instead of in austenite. This is the same situation as the formation of ferrite from austenite despite the fact that the growth of ferrite is in later case controlled by diffusion in austenite. For the formation of austenite either from a mixture of ferrite and carbide particles, or from a mixture of bainitic ferrite and austenite, on the other hand, concentration gradients of carbon and X in austenite are expected to exist, and therefore, the growth of austenite will depend on diffusion in austenite as well as that in ferrite.

7.3.3 Reconstructive growth of austenite under paraequilibrium

When the supersaturation of ferrite is very high; *i.e.* at very high temperatures, paraequilibrium might be the condition which governs the growth of austenite.

According to the definition of the paraequilibrium, an identical X/Fe atoms ratio is now expected both in the matrix and product phases:

$$\frac{x_2^{\gamma}}{x_0^{\gamma}} = \frac{x_2^{\alpha}}{x_0^{\alpha}} = \frac{\overline{x}_2^{\alpha}}{\overline{x}_0^{\alpha}} = k_2 . \qquad (7.37)$$

204

Although the chemical potential of the substitutional alloying element or iron are no longer identical in the two phases at the interface, subject to that constraint, the carbon at the interface achieves equality of chemical potentials in both phases [18], giving

$$\frac{\Delta G_1^{0\alpha \to \gamma}}{RT} = \ln \frac{x_1^\alpha}{x_1^\gamma} + \ln \frac{\Gamma_1^\alpha}{\Gamma_1^\gamma} \, . \tag{7.38}$$

The following equation is used in order to define the paraequilibrium tie line [18].

$$\frac{\Delta G_2^{0\alpha \to \gamma}}{RT} - \ln \frac{x_2^\alpha}{x_2^\gamma} - \ln \frac{\Gamma_2^\alpha}{\Gamma_2^\gamma} = -\frac{1}{k_2} \frac{\Delta G_0^{0\alpha \to \gamma}}{RT} - \ln \frac{x_0^\alpha}{x_0^\gamma} - \ln \frac{\Gamma_0^\alpha}{\Gamma_0^\gamma} \tag{7.39}$$

These three equations allow the interface compositions to be calculated independently from the mass conservation equation at the moving interface. Therefore one can calculate the interface compositions first, and then put them into the mass conservation equation to obtain the growth rate of the product phase at the moving interface. Because of the definition of paraequilibrium, no flux of X atoms needs to be considered in this case. As a result, it is necessary only to set the mass conservation for carbon at the interface. The growth of the product phase is, therefore, controlled by carbon diffusion in both ferrite and austenite phases. The mass conservation equation for carbon, in this case, can be simplified as follows:

$$\alpha_1^2 - \alpha_1 \left[\frac{k_{C\alpha}}{2} \frac{\overline{x}_1^\alpha - x_1^{\alpha\gamma}}{\overline{x}_1^\gamma - \overline{x}_1^\alpha} + \frac{2D_{11}^\alpha}{k_{C\alpha}} \frac{\overline{x}_1^\alpha - x_1^{\alpha\gamma}}{x_1^{\gamma\alpha} - x_1^{\alpha\gamma}} \right]$$
$$= D_{11}^\gamma \frac{(\overline{x}_1^\gamma - x_1^{\gamma\alpha})^2}{(x_1^{\gamma\alpha} - x_1^{\alpha\gamma})(\overline{x}_1^\gamma - \overline{x}_1^\alpha)} - D_{11}^\alpha \frac{(\overline{x}_1^\alpha - x_1^{\alpha\gamma})^2}{(x_1^{\gamma\alpha} - x_1^{\alpha\gamma})(\overline{x}_1^\gamma - \overline{x}_1^\alpha)} \tag{7.40}$$

Fig. 7.8 and Fig. 7.9 represent illustrative phase diagrams for reaustenitisation from a ferritic initial microstructure, and from an initial microstructure which is a mixture of bainitic ferrite and austenite respectively.

7.3.4 Special cases

As mentioned earlier, with some exceptions, it is necessary to consider diffusion in both the ferrite matrix and austenite precipitate during reaustenitisation. However, there might exist circumstances where diffusion in just one of the two phases largely controls the growth of the product phase. The mass conservation equations derived in the previous section can then be simplified and also, more rigorous solutions for the chemical distributions in the phase are then available [6,11,12].

When a fully ferritic initial microstructure is heated into the $\alpha + \gamma$ two phase region, it may be a good approximation that there is no flux in the precipitate phase (*i.e.* austenite). For ferrite growth from austenite, the approximation is often very good because of the low solubility of carbon and in ferrite. On the other hand, in the case of the austenite growth from ferrite, the product phase usually has a high solubility for carbon and the substitutional alloying element. Therefore the assumption of no flux in austenite should be examined experimentally. In addition to this, fluxes in austenite may exist when soft impingement occurs: overlapping of diffusion fields can lead to a change in the boundary conditions.

Reaustenitisation from a mixture of bainitic ferrite and austenite or from a mixture of ferrite and carbides shows rather different features. The carbon concentration of the initial austenite at the reaustenitisation temperature is usually expected to be higher than the equilibrium

concentration at the interface at the reaction temperature [22-25], leading to the fact that the supersaturation level in carbon could be larger in austenite than that in ferrite. As a consequence, the contribution of fluxes in ferrite may be negligible [25] to the overall problem.

In the case of reaustenitisation from an initial microstructure of ferrite and cementite, the austenite is found to nucleate preferentially at the junctions between ferrite/ferrite grain boundaries and carbide particles [14,26-29]. The dissolution of carbide particles happens essentially happens after becoming engulfed by austenite. The early stages of the growth of austenite is then controlled by carbon diffusion through the austenite envelope [14,15]. Because the equilibrium carbon concentration in austenite at the interface between austenite and cementite is much larger than that at the interface between austenite and ferrite, the carbon concentration gradient in austenite is expected to be correspondingly larger than that in ferrite. Hence any flux in the ferrite may be considered negligible [14,15].

Under the circumstances where one of the two phases is not important in terms of the diffusion field which controls the growth of the product phase, the mass conservation equations relate to the first one of the two phases, giving:

$$(x_1^{\gamma\alpha} - x_1^{\alpha\gamma})v = J_1|_{z=z^*} \tag{7.41}$$

$$(x_2^{\gamma\alpha} - x_2^{\alpha\gamma})v = J_2|_{z=z^*} \tag{7.42}$$

where $J_1|_{z=z^*}$ and $J_2|_{z=z^*}$ are fluxes either in ferrite or in austenite depending on the phase which dominates as far as diffusion is concerned.

Growth of austenite from a ferritic sample

When the initial microstructure is ferritic, the growth of austenite might be controlled by fluxes of carbon and X in ferrite instead of in austenite as mentioned earlier. Assuming the approximation of the linear gradients of chemical compositions, the following equations for the conservation of mass at the interface (see Fig. 7.10) are obtained:

$$v(x_1^{\gamma\alpha} - x_1^{\alpha\gamma}) = \frac{D_{11}^\alpha}{L_\alpha}(\overline{x}_1^\alpha - x_1^{\alpha\gamma}) + \frac{D_{12}^\alpha}{l_\alpha}(\overline{x}_2^\alpha - x_2^{\alpha\gamma}) \tag{7.43}$$

$$v(x_2^{\gamma\alpha} - x_2^{\alpha\gamma}) = \frac{D_{22}^\alpha}{l_\alpha}(\overline{x}_2^\alpha - x_2^{\alpha\gamma}) . \tag{7.44}$$

The mass conservation conditions for carbon and X for the whole system give the following two equations (Fig. 7.10):

$$z^*(x_1^{\gamma\alpha} - \overline{x}_1^\alpha) = \frac{L_\alpha}{2}(\overline{x}_1^\alpha - x_1^{\alpha\gamma}) \tag{7.45}$$

$$z^*(x_2^{\gamma\alpha} - \overline{x}_2^\alpha) = \frac{l_\alpha}{2}(\overline{x}_2^\alpha - x_2^{\alpha\gamma}) . \tag{7.46}$$

The one-dimensional parabolic thickening rate constant for the growth of austenite is therefore given by the simultaneous solution of:

$$\alpha_1^2 = D_{11}^\alpha \frac{(\overline{x}_1^\alpha - x_1^{\alpha\gamma})^2}{(x_1^{\gamma\alpha} - x_1^{\alpha\gamma})(x_1^{\gamma\alpha} - \overline{x}_1^\alpha)} + D_{12}^\alpha \frac{(\overline{x}_2^\alpha - x_2^{\alpha\gamma})^2}{(x_2^{\gamma\alpha} - x_2^{\alpha\gamma})(x_2^{\gamma\alpha} - \overline{x}_2^\alpha)} \tag{7.47}$$

$$\alpha_1^2 = D_{22}^\alpha \frac{(\overline{x}_2^\alpha - x_2^{\alpha\gamma})^2}{(x_2^{\gamma\alpha} - x_2^{\alpha\gamma})(x_2^{\gamma\alpha} - \overline{x}_2^\alpha)} . \tag{7.48}$$

For paraequilibrium austenite growth, the interface compositions are calculated independently from the thermodynamic equations as discussed earlier. The parabolic rate constant of austenite in that case is given by:

$$\alpha_1^2 = D_{11}^\alpha \frac{(\bar{x}_1^\alpha - x_1^{\alpha\gamma})^2}{(x_1^{\gamma\alpha} - x_1^{\alpha\gamma})(x_1^{\gamma\alpha} - \bar{x}_1^\alpha)} \cdot \tag{7.49}$$

Growth of austenite from a mixture of ferrite and austenite

When the initial microstructure contains ferrite and austenite of equilibrium chemical composition, the growth of the pre-existing austenite into ferrite is mainly controlled by the diffusion fields in austenite if the superheating is high (Fig. 7.11). For that case, the mass conservation of carbon and the substitutional alloying element at the interface, and in the whole system give the following equations (see Fig. 7.11):

$$v(x_1^{\gamma\alpha} - x_1^{\alpha\gamma}) = \frac{D_{11}^\gamma}{L_\gamma}(\bar{x}_1^\gamma - x_1^{\gamma\alpha}) + \frac{D_{12}^\gamma}{l_\gamma}(\bar{x}_2^\gamma - x_2^{\gamma\alpha}) \tag{7.50}$$

$$v(x_2^{\gamma\alpha} - x_2^{\alpha\gamma}) = \frac{D_{22}^\gamma}{l_\gamma}(\bar{x}_2^\gamma - x_2^{\gamma\alpha}) \tag{7.51}$$

$$(L_\gamma - z^*)(\bar{x}_1^\gamma - x_1^{\alpha\gamma}) = \frac{L_\gamma}{2}[(\bar{x}_1^\gamma - x_1^{\alpha\gamma}) + (x_1^{\gamma\alpha} - x_1^{\alpha\gamma})] \tag{7.52}$$

$$(l_\gamma - z^*)(\bar{x}_2^\gamma - x_2^{\alpha\gamma}) = \frac{l_\alpha}{2}[(\bar{x}_2^\gamma - x_2^{\alpha\gamma}) + (x_2^{\gamma\alpha} - x_2^{\alpha\gamma})] \cdot \tag{7.53}$$

The one-dimensional parabolic thickening rate constant of austenite is therefore given by the simultaneous solution of:

$$\alpha_1^2 = D_{11}^\gamma \frac{(\bar{x}_1^\gamma - x_1^{\gamma\alpha})^2}{(x_1^{\gamma\alpha} - x_1^{\alpha\gamma})(\bar{x}_1^\gamma - x_1^{\alpha\gamma})} + D_{12}^\gamma \frac{(\bar{x}_2^\gamma - x_2^{\gamma\alpha})^2}{(x_2^{\gamma\alpha} - x_2^{\alpha\gamma})(\bar{x}_2^\gamma - x_2^{\alpha\gamma})} \tag{7.54}$$

$$\alpha_1^2 = D_{22}^\gamma \frac{(\bar{x}_2^\gamma - x_2^{\gamma\alpha})^2}{(x_2^{\gamma\alpha} - x_2^{\alpha\gamma})(\bar{x}_2^\gamma - x_2^{\alpha\gamma})} \cdot \tag{7.55}$$

For the case of paraequilibrium, the rate constant is given by:

$$\alpha_1^2 = D_{11}^\gamma \frac{(\bar{x}_1^\gamma - x_1^{\gamma\alpha})^2}{(x_1^{\gamma\alpha} - x_1^{\alpha\gamma})(\bar{x}_1^\gamma - x_1^{\alpha\gamma})} \cdot \tag{7.56}$$

Growth of austenite controlled by dissolution of cementite

In the case of reaustenitisation from a mixture of ferrite and cementite particles, the nucleation of austenite occurs preferentially at the junctions between ferrite/ferrite grain boundaries and cementite particles which locate on the grain boundaries. The austenite particles, then, engulf the cementite particles. The growth of austenite particles after this stage is mainly controlled by the dissolution of cementite particles within the austenite, if the supersaturation is reasonably low, and the effect of the dissolution of cementite particles within the ferrite matrix is small (see for example [15]). Assuming linear gradients of chemical composition in austenite (Fig. 7.12), we can obtain the following equations to satisfy the mass conservation at the interface and for the whole system:

$$v(x_1^{\gamma\alpha} - x_1^{\alpha\gamma}) = \frac{D_{11}^\gamma}{l_\theta + z^*}(x_1^{\gamma\theta} - x_1^{\gamma\alpha}) + \frac{D_{12}^\gamma}{l_\theta + z^*}(x_2^{\gamma\theta} - x_2^{\gamma\alpha}) \qquad (7.57)$$

$$v(x_2^{\gamma\alpha} - x_2^{\alpha\gamma}) = \frac{D_{22}^\gamma}{l_\theta + z^*}(x_2^{\gamma\theta} - x_2^{\gamma\alpha}) \qquad (7.58)$$

$$l_\theta(x_1^{\theta\gamma} - x_1^{\alpha\gamma}) = \frac{l_\theta + z^*}{2}[(x_1^{\gamma\theta} - x_1^{\alpha\gamma}) + (x_1^{\gamma\alpha} - x_1^{\alpha\gamma})] \qquad (7.59)$$

$$l_\theta(x_2^{\theta\gamma} - x_2^{\alpha\gamma}) = \frac{l_\theta - z^*}{2}[(x_2^{\gamma\theta} - x_2^{\alpha\gamma}) + (x_2^{\gamma\alpha} - x_2^{\alpha\gamma})] \, . \qquad (7.60)$$

where l_θ is the dissolution thickness of cementite (see Fig. 7.12), $x^{\theta\gamma}$, $x^{\gamma\theta}$ are respectively carbon (or X) concentrations at the interface in cementite and in austenite. From these equations, we can obtain the following two expressions which on simultaneous solution can yield the one-dimensional parabolic thickening rate constant:

$$\alpha_1^2 = D_{11}^\gamma \frac{(x_1^{\gamma\theta} - x_1^{\gamma\alpha})(2x_1^{\theta\gamma} - x_1^{\gamma\theta} - x_1^{\gamma\alpha})}{(x_1^{\gamma\alpha} - x_1^{\alpha\gamma})(x_1^{\theta\gamma} - x_1^{\alpha\gamma})} + D_{12}^\gamma \frac{(x_2^{\gamma\theta} - x_2^{\gamma\alpha})(2x_1^{\theta\gamma} - x_1^{\gamma\theta} - x_1^{\gamma\alpha})}{(x_2^{\gamma\alpha} - x_2^{\alpha\gamma})(x_2^{\theta\gamma} - x_2^{\alpha\gamma})} \qquad (7.61)$$

$$\alpha_1^2 = D_{22}^\gamma \frac{(x_2^{\gamma\theta} - x_2^{\gamma\alpha})(2x_2^{\theta\gamma} - x_2^{\gamma\theta} - x_2^{\gamma\alpha})}{(x_2^{\gamma\alpha} - x_2^{\alpha\gamma})(x_2^{\theta\gamma} - x_2^{\alpha\gamma})} \, . \qquad (7.62)$$

For the paraequilibrium growth of austenite, it follows that:

$$\alpha_1^2 = D_{11}^\gamma \frac{(x_1^{\gamma\theta} - x_1^{\gamma\alpha})(2x_1^{\theta\gamma} - x_1^{\gamma\theta} - x_1^{\gamma\alpha})}{(x_1^{\gamma\alpha} - x_1^{\alpha\gamma})(x_1^{\theta\gamma} - x_1^{\alpha\gamma})} \, . \qquad (7.63)$$

The chemical compositions at the interface between austenite and cementite also need to be determined. A method of this has been discussed by Hashiguchi and Kirkaldy [20].

Analytical solutions

When only one of the two phases is important in terms of the control of the growth of the product phase, analytical expressions for chemical distributions are available. The equations for the concentration distributions in each phase (i.e. ferrite and austenite) can be obtained from the diffusion equations [6] independently when no interaction between the fluxes in two phases exists. If the cross interdiffusion coefficient D_{21} is negligible [21], it is possible to simplify the general equation [6] as follows [10]:

$$x_1^\alpha = \overline{x}_1^\alpha + \frac{D_{12}^\alpha(x_2^{\alpha\gamma} - \overline{x}_2^\alpha)}{D_{11}^\alpha - D_{22}^\alpha} \frac{\text{erfc}\{\frac{z}{2\sqrt{D_{22}^\alpha t}}\}}{\text{erfc}\{\frac{z^*}{2\sqrt{D_{22}^\alpha t}}\}}$$

$$+ \left[(x_1^{\alpha\gamma} - \overline{x}_1^\alpha) - \frac{D_{12}^\alpha(x_2^{\alpha\gamma} - \overline{x}_2^\alpha)}{D_{11}^\alpha - D_{22}^\alpha}\right] \frac{\text{erfc}\{\frac{z}{2\sqrt{D_{11}^\alpha t}}\}}{\text{erfc}\{\frac{z^*}{2\sqrt{D_{11}^\alpha t}}\}} \qquad (7.64)$$

$$x_1^\gamma = \overline{x}_1^\gamma + \frac{D_{12}^\gamma(x_2^{\gamma\alpha} - \overline{x}_2^\gamma)}{D_{11}^\gamma - D_{22}^\gamma} \frac{\text{erfc}\{\frac{z}{2\sqrt{D_{22}^\gamma t}}\}}{\text{erfc}\{\frac{z^*}{2\sqrt{D_{22}^\gamma t}}\}}$$

$$+ \left[(x_1^{\gamma\alpha} - \overline{x}_1^{\gamma}) - \frac{D_{12}^{\gamma}(x_2^{\gamma\alpha} - \overline{x}_2^{\gamma})}{D_{11}^{\gamma} - D_{22}^{\gamma}} \right] \frac{\text{erfc}\{\frac{z}{2\sqrt{D_{11}^{\gamma}t}}\}}{\text{erfc}\{\frac{z^*}{2\sqrt{D_{11}^{\gamma}t}}\}} \tag{7.65}$$

$$x_2^{\alpha} = \overline{x}_2^{\alpha} + (x_2^{\alpha\gamma} - \overline{x}_2^{\alpha}) \frac{\text{erfc}\{\frac{z}{2\sqrt{D_{22}^{\alpha}t}}\}}{\text{erfc}\{\frac{z^*}{2\sqrt{D_{22}^{\alpha}t}}\}} \tag{7.66}$$

$$x_2^{\gamma} = \overline{x}_2^{\gamma} + (x_2^{\gamma\alpha} - \overline{x}_2^{\gamma}) \frac{\text{erfc}\{\frac{z}{2\sqrt{D_{22}^{\gamma}t}}\}}{\text{erfc}\{\frac{z^*}{2\sqrt{D_{22}^{\gamma}t}}\}} \cdot \tag{7.67}$$

It should be noted that these equations are not applicable if the diffusion fields in the two phases interact with each other; this is expected to happen in most real circumstances. The interface position is expressed by the diffusion coefficients and growth rate constants η_i (see for example [10]):

$$z^* = \eta_1^{\gamma}\sqrt{D_{11}^{\gamma}t} = \eta_2^{\gamma}\sqrt{D_{22}^{\gamma}t} = \eta_1^{\alpha}\sqrt{D_{11}^{\alpha}t} = \eta_2^{\alpha}\sqrt{D_{22}^{\alpha}t} \tag{7.68}$$

or,

$$z^* = \alpha_1 t^{1/2} \tag{7.69}$$

where α_1 is an one-dimensional parabolic thickening rate constant. The growth rate v is then given by:

$$v = \frac{dz^*}{dt} = \frac{\eta_i D_{ii}}{2\sqrt{D_{ii}t}} = \frac{1}{2}\alpha_1 t^{-1/2} \cdot \tag{7.70}$$

Substituting the derivatives of the distributions of chemical composition and the growth rate of the product phase into the mass conservation equations at the interface, one can obtain the relations between the interface compositions and the growth rate of the product phase.

When the growth of austenite is controlled by the diffusion field in austenite, the relations are given as follows [10]:

$$\frac{x_1^{\gamma\alpha} - \overline{x}_1^{\gamma}}{x_1^{\gamma\alpha} - x_1^{\alpha\gamma}} = H\{D_{11}^{\gamma}\} - \frac{B_1 D_{12}^{\gamma}}{D_{11}^{\gamma} - D_{22}^{\gamma}}[H\{D_{22}^{\gamma}\} - H\{D_{11}^{\gamma}\}] \tag{7.71}$$

$$\frac{x_2^{\gamma\alpha} - \overline{x}_2^{\gamma}}{x_2^{\gamma\alpha} - x_2^{\alpha\gamma}} = H\{D_{22}^{\gamma}\} \tag{7.72}$$

where

$$H\{D_{ii}\} = \sqrt{\frac{\pi}{4D_{11}}}\alpha_1[\text{erfc}\{\frac{\alpha_1}{\sqrt{4D_{ii}}}\}]\exp\{\frac{\alpha_1^2}{4D_{ii}}\}$$

$$B_1 = \frac{x_2^{\gamma\alpha} - x_2^{\alpha\gamma}}{x_1^{\gamma\alpha} - x_1^{\alpha\gamma}} \cdot$$

On the other hand, when the growth of austenite is controlled by diffusion in ferrite only, the following equation applies:

$$\frac{x_1^{\alpha\gamma} - \overline{x}_1^{\alpha}}{x_1^{\alpha\gamma} - x_1^{\gamma\alpha}} = H\{D_{11}^{\alpha}\} - \frac{B_1 D_{12}^{\alpha}}{D_{11}^{\alpha} - D_{22}^{\alpha}}[H\{D_{22}^{\alpha}\} - H\{D_{11}^{\alpha}\}] \tag{7.73}$$

$$\frac{x_2^{\alpha\gamma} - \overline{x}_2^{\alpha}}{x_2^{\alpha\gamma} - x_2^{\gamma\alpha}} = H\{D_{22}^{\alpha}\} \cdot \tag{7.74}$$

7.4 CALCULATED EXAMPLES

In order to demonstrate the calculation of tie lines under different equilibrium conditions as discussed in the previous section, reaustenitisation in a Fe-C-Cr ternary system will be discussed.

7.4.1 Thermodynamic parameters

The thermodynamic parameters for the system which are used for the calculation have represented by Kirkaldy and his co-workers [19,20]. Those parameters for the Fe-C-Cr system are listed below, with some correction of typographical errors.

$$\Delta G_0^{0\alpha \to \gamma} = 8933 - 14.406T + 12.083 \times 10^{-3}T^2 - 11.51 \times 10^{-6}T^3$$
$$+ 5.23 \times 10^{-9}T^4 \text{ , J mol}^{-1} \text{ (T} < 1000\text{K)}$$
$$= 71659 - 216.84T + 24.773 \times 10^{-2}T^2 - 12.661 \times 10^{-5}T^3$$
$$+ 24.397 \times 10^{-9}T^4 \text{ , J mol}^{-1} \text{ (T} > 1000\text{K)}$$
$$\Delta G_1^{0\alpha \to \gamma} = -65562 + 32.949T \text{ , J mol}^{-1}$$
$$\Delta G_2^{0\alpha \to \gamma} = -1534 - 19.472T + 2.749T \ln T \text{ , J mol}^{-1}$$
$$\epsilon_{11}^{\alpha} = 1.3$$
$$\epsilon_{11}^{\gamma} = 4.786 + 5066/T$$
$$\epsilon_{22}^{\alpha} = 2.819 - 6039/T$$
$$\epsilon_{22}^{\gamma} = 7.655 - 3154/T - 0.661 \ln T$$
$$\epsilon_{12}^{\gamma} = 14.19 - 30210/T$$
$$\epsilon_{12}^{\alpha} = \epsilon_{12}^{\gamma}$$

In order to calculate the growth rate of product phase and interface compositions satisfying the mass conservations at the moving interface and the diffusion equations in both phases, it is essential to know the diffusion coefficients of carbon and alloying elements both in ferrite and in austenite.

The diffusivity of carbon in austenite is known to vary significantly with carbon concentration. Therefore the diffusion equations should be solved with a diffusion coefficient which is a function of carbon concentration; thus it varies from place to place in austenite. However, it has also been shown that a weighted average diffusion coefficient of carbon in austenite, in which the average is taken between the minimum and maximum carbon concentrations in austenite, can be used in the calculation giving reasonable accuracy. Hence, in the present work, a weighted average diffusion coefficient of carbon in austenite will be used for further calculations. The average diffusion coefficient is expressed as follows [30]:

$$\overline{D} = \int_{\overline{x}_1^{\gamma}}^{x^{\gamma \alpha}} \frac{D \, dx}{(x^{\gamma \alpha} - \overline{x}_1^{\gamma})} \ . \tag{7.75}$$

This procedure is valid strictly for the situation where the concentration profile does not change with time, but is recognised to be a good approximation for non-steady state conditions, as exist during the growth of austenite into ferrite. For simplicity and consistency, we use a symbol D_{11}^{γ} as $\overline{D}$. As discussed by Brown and Kirkaldy [21], the cross coefficients are expressed by,

$$D_{12}^{\alpha,\gamma} = D_{11}^{\alpha,\gamma} \frac{\epsilon_{12}^{\alpha,\gamma} x_1^{\alpha,\gamma}}{1 + \epsilon_{11}^{\alpha,\gamma} x_1^{\alpha,\gamma}}. \tag{7.76}$$

The diffusion coefficient of carbon in ferrite is expressed as a function of temperature [16], giving,

$$D_{11}^{\alpha} = 0.02 \exp\left\{-\frac{10115}{T}\right\} \exp\left\{0.5898\left[1 + \frac{2}{\pi}\arctan(1.4985 - \frac{15309}{T})\right]\right\} \quad, \mathrm{cm^2\,s^{-1}}. \tag{7.77}$$

The diffusivities of alloying element in ferrite and austenite were discussed by Fridberg *et al.* [17]. On reproducing the data for Cr of figure 14 in their paper [17], the diffusion coefficients of Cr in ferrite and austenite are expressed as follows:

$$D_{22}^{\gamma} = 3.325 \exp\left\{-\frac{286000}{RT}\right\}, \quad \mathrm{cm^2\,s^{-1}} \tag{7.78}$$

$$D_{22}^{\alpha} = 4.288 \exp\left\{-\frac{240000}{RT}\right\}, \quad \mathrm{cm^2\,s^{-1}} \text{ (paramagnetic ferrite)}$$

$$= 1.340 \exp\left\{-\frac{240000}{RT}\right\}, \quad \mathrm{cm^2\,s^{-1}} \text{ (ferromagnetic ferrite)} \tag{7.79}$$

Calculated isothermal sections of the phase diagram of a Fe-0.3C-4.08 wt.% alloy are presented in Fig. 7.13.

7.4.2 Growth of austenite from a mixture of bainite and austenite

When the initial microstructure contains a certain amount of austenite, nucleation of austenite might be unnecessary during reaustenitisation. Especially when the initial micro structure is a mixture of bainitic ferrite and residual austenite, the plate shape of the two phases may allow us to treat reaustenitisation process as an one-dimensional parabolic growth of the residual austenite plates.

Specimens are assumed to be heated up to the austenite phase field, and then quenched to and held at a bainite transformation temperature for a sufficient length of time to allow the specimens to complete the bainite transformation. Because of the nature of bainite transformation, the reaction stops when the carbon concentration in residual austenite reaches the point where the diffusionless formation of ferrite from austenite becomes thermodynamically impossible: this if referred to as the incomplete reaction phenomenon. Therefore, if the other reactions such as carbide precipitations and reconstructive formations of ferrite are sluggish, one can obtain a mixture of bainitic ferrite plates and residual austenite trapped in between those bainitic ferrite plates. The carbon concentration in the residual austenite has been reported to be in a good agreement with T_0' curve in the phase diagram of the system, where ferrite, whose free energy has been raised by a stored energy term (*i.e.* 400 J mol^{-1}, after Bhadeshia and Edmonds [31]) associated with the transformation strain, and austenite of identical composition have the same free energy. Since the decarburisation of bainitic ferrite occurs soon after the reaction, the carbon concentration in ferrite may be close to its equilibrium level. There is no partitioning of substitutional alloying elements during bainite transformation [32-35], the alloying element compositions in the two phases are identical as long as there is no reconstructive formation of ferrite. Thus, if one chooses a bainite reaction temperature, one can obtain the average chemical compositions in ferrite and residual austenite.

The specimens are then heated directly to a reaustenitisation temperature without being cooled below the bainite transformation temperature T_b. So the initial microstructure is a mixture of bainitic ferrite with the equilibrium carbon concentration at the bainite reaction temperature; $\overline{x}_1^\alpha = x_1^{\alpha\gamma}\{T_b\}$, and residual austenite with carbon concentration at T_0' at the bainite transformation temperature; $\overline{x}_1^\gamma = x_{T_0'}\{T_b\}$.

One-dimensional parabolic thickening rate constants in the Fe-0.3C-4.08Cr wt.% alloy calculated for the paraequilibrium and the local equilibrium conditions are shown in Fig. 7.14. In order to show the effect of the initial carbon concentration on the rate constant, three different bainite transformation temperatures; 360, 420 and 480 °C, were selected. The calculated initial carbon concentrations in residual austenite and in ferrite are listed below [37,38].

T_b, °C	$x_{1,eq}^\alpha\{T_b\}$, mole fraction	$x_{T_0'}\{T_b\}$, mole fraction
360	0.000553	0.0265
420	0.000623	0.0228
480	0.000692	0.0163

Table 7.1: Carbon concentrations in bainitic ferrite and residual austenite at the end of bainite transformation at each temperature in Fe-0.3C-4.08Cr wt.% alloy.

It can be seen that the growth rate of austenite increases monotonically with temperature. It should be noted that the rate constant under local equilibrium is always larger than that under paraequilibrium. When the one dimensional parabolic rate constant for the growth of ferrite from austenite is calculated, it has been found that the rate constant under paraequilibrium is larger than that under local equilibrium at lower temperatures whereas the order swaps at higher temperatures. This could be understood as follows. Although the driving force for the formation of ferrite is always higher in local equilibrium than that under paraequilibrium, the diffusivity of the substitutional alloying element is remarkably low at low temperatures; this causes the retardation of the growth of austenite. Therefore the rate constant for the growth of ferrite under local equilibrium at lower temperatures is smaller than that under paraequilibrium (for example see [40]). At higher temperatures, on the other hand, the diffusivity of the substitutional alloying element becomes high and the driving force for the transformation under paraequilibrium decreases rapidly: in fact the driving force for the growth of ferrite under paraequilibrium becomes zero at the Ae_3' temperature. As a consequence, the rate constant under local equilibrium becomes greater than that under paraequilibrium [40]. However it should be noted that a spike of the substitutional alloying element in austenite adjacent to the transformation interface, which is under local equilibrium, becomes sharper with decreasing temperature, and little difference will be expected for the rate constants calculated from local equilibrium and paraequilibrium conditions as can be seen in Enomoto's calculations [40].

In the case of reaustenitisation, however, the diffusivity of the substitutional alloying element is very high because of the elevated temperatures for reaustenitisation, leading to the fact that the rate constant for the growth of austenite under local equilibrium always remains higher than that under paraequilibrium.

The rate constants for the growth of austenite under paraequilibrium for the three different mixtures of bainitic ferrite and residual austenite are compared in Fig. 7.15. The rate constants decrease gently with temperature at higher temperatures, but fall down steeply to zero at lower

temperature showing the lowest possible temperature where austenite can actually grow. It can also be seen that the rate constant at a temperature is larger when the bainite transformation temperature is lower. This can be understood qualitatively from the fact that $x_{T_0'}\{T_b\}$ is larger in lower bainite transformation temperature, which provides larger supersaturation of carbon in austenite at a reaction temperature and hence a larger growth rate of austenite. The reaustenitisation-start temperature under paraequilibrium; *i.e.* the lowest temperature where the growth of austenite can occur, also varies with the bainite transformation temperature. The reaustenitisation-start temperature from a mixture of bainitic ferrite and austenite can be understood in terms of the carbon concentration in residual austenite and the negative slope of the Ae_3 (or Ae_3') curve [22-25].

However it should be noted that Yang and Bhadeshia ignored the effect of diffusion of carbon in ferrite [22-25], which might have a substantial effect on the reaustenitisation-start temperature. This was examined by comparing the rate constant for the growth of austenite under paraequilibrium calculated by equation 7.40; in which the diffusion of carbon in both phases are taken into account, or equation 7.56; where the diffusion field exists only in austenite. Calculated rate constants for the growth of austenite from two different mixtures of bainitic ferrite and austenite are shown in Fig. 7.16. The calculated rate constant assuming the diffusion field only in austenite is larger than that calculated for the case where the diffusion fields exist in both phases at lower temperatures, whereas the order changes at higher temperatures. This crossover in the rate constants can be interpreted as follows. At a temperature where carbon concentration in residual austenite reaches the Ae_3' (note that this is not Ae_3) (see Fig. 7.17a), the growth of austenite can start if the diffusion of carbon in ferrite can be ignored. However, the growth of austenite is not yet possible in the case where the diffusion of carbon in both phases should be taken into account, since the negative gradient of carbon exists at the transformation interface in ferrite. This circumstance remains until the temperature is raised to a point at which the fluxes of carbon in ferrite and in austenite cancel each other out (Fig. 7.17b). Above this temperature, the growth of austenite can proceed even in the case where the diffusion of carbon in both phases is considered. In this circumstance, the growth rate of austenite calculated with carbon fluxes in both phases is smaller than that with the carbon diffusion only in austenite because of the negative slope of carbon in ferrite at the transformation interface. When the temperature reaches a point where the carbon concentration in the ferrite matrix is equal to that on the $\alpha/(\alpha + \gamma)$ phase boundary (see Fig. 7.17c), the rate constant calculated by the two different methods becomes identical since there is no flux of carbon in ferrite at the temperature. Above this temperature, the rate constant calculated with diffusion of the carbon in both phases becomes higher than that with the diffusion of carbon only in austenite since the positive flux of carbon in ferrite accelerates the movement of the transformation interface (Fig. 7.17d).

It is also suggested that the smaller the initial carbon concentration in ferrite the larger the difference in reaustenitisation temperatures calculated by the two different methods since more superheating is required to reach the temperature shown in Fig. 7.17b. In fact the difference in reaustenitisation-start temperatures calculated by the two different methods for the case of the bainite transformation at 360 °C was larger than the case of the 420 °C bainite transformation temperature, since in the former case the carbon concentration in the initial ferrite is lower than that of the later (see Table 7.1).

The calculated interface carbon concentrations during reaustenitisation under local equi-

The theory was applied to reaustenitisation from a mixture of bainitic ferrite and austenite, where nucleation of austenite may not be necessary since the initial microstructure contains austenite.

REFERENCES

1. H. K. D. H. Bhadeshia: *"Phase Transformations '87", Institute of Metals, London, ed. G. W. Lorimer,* 1987, 309.

2. A. Hultgren: *Jernkontorets Ann.,* 1951, **135,** 403.

3. E. Rudberg: *Jernkontorets Ann.,* 1952, **136,** 91.

4. M. Hillert: *Jernkontorets Ann.,* 1952, **136,** 25.

5. M. Hillert: *Internal Report, Swedish Institute of Metals Research.* 1953.

6. J. S. Kirkaldy: *Can. J. Phys.,* 1958, **36,** 907.

7. G. R. Purdy, D. H. Weichert and J. S. Kirkaldy: *TMS-AIME,* 1964, **230,** 1025.

8. H. I. Aaronson, H. A. Domian and G. M. Pound: *TMS-AIME,* 1966 **236,** 753.

9. H. I. Aaronson, H. A. Domian and G. M. Pound: *TMS-AIME,* 1966 **236,** 768.

10. D. E. Coates: *Metall. Trans.,* 1972, **3,** 1203.

11. D. E. Coates: *Metall. Trans.,* 1973, **4,** 1077.

12. D. E. Coates: *Metall. Trans.,* 1973, **4,** 2313.

13. H. K. D. H. Bhadeshia: *Progress in Materials Science,* 1985, **29,** 321.

14. R. R. Judd and H. W. Paxton: *TMS-AIME,* 1968, **242,** 206.

15. M. Hillert, K. Nilsson and L-E. Törndahl: *JISI,* 1971 **209,** 49.

16. J. Ågren: *Mat. Sci. and Eng.,* 1982, **55,** 135.

17. M. Hillert: *"Mechanism of Phase Transformations in Crystalline Solid", Monograph 13, Institute of Metals, London,* 1969, 231.

18. J. B. Gilmour, G. R. Purdy and J. S. Kirkaldy: *Metall. Trans.,* 1972, **3,** 1455.

19. J. S. Kirkaldy, B. A. Thomson and E. A. Baganis: *"Hardenability Concepts with Applications to Steel", ed. D. V. Doane and J. S. Kirkaldy, AIME,* 1978, 82.

20. K. Hashiguchi and J. S. Kirkaldy: *CALPHAD,* 1984, **8,** 173.

21. L. C. Brown and J. S. Kirkaldy: *Trans. AIME,* 1964, **230,** 223.

22. J-R. Yang and H. K. D. H. Bhadeshia: *"Welding Metallurgy of Structural Steels", TMS-AIME, Warrendate, Ohio, ed. J. Y. Koo,* 1987, 549.

23. J-R. Yang and H. K. D. H. Bhadeshia: *"Phase Transformations '87", The Institute of Metals, London, ed. G. W. Lorimer,* 1988, 203.

24. J-R. Yang and H. K. D. H. Bhadeshia: *Mat. Sci. and Eng.,* 1989, in press.

25. J-R. Yang: *Ph.D. Thesis, University of Cambridge,* 1988.

26. G. R. Speich and A. Szirmae: *TMS-AIME,* 1969, **245,** 1063.

27. C. I. Garcia and A. J. DeArdo: *Metall. Trans.,* 1981, **12A,** 521.

28. U. R. Lenel and R .W. K. Honeycombe: *Metal Science,* 1984, **18,** 201.

29. U. R. Lenel and R .W. K. Honeycombe: *Metal Science,* 1984, **18,** 503.

30. R. Trivedi and G. M. Pound: *J. Appl. Phys.,* 1967, **38,** 3569.

31. H. K. D. H. Bhadeshia: *Acta Metall.,* 1981, **29,** 1117.

32. H. K. D. H. Bhadeshia and A. R. Waugh: *Proc. of Int. Conf. on "Solid/Solid Phase Transformations", Pittsburgh, ASM, Ohio, U.S.A.,* 1981, 1041.

33. H. K. D. H. Bhadeshia and A. R. Waugh: *Acta Metall.*, 1982, **30,** 775.

34. I. Stark, G. D. W. Smith and H. K. D. H. Bhadeshia: *Proc. of Int. Conf. on "Solid/Solid Phase Transformations", Institute of Metals, London,* 1989, in press.

35. I. Stark, G. D. W. Smith and H. K. D. H. Bhadeshia: *Proc. of Int. Conf. on "The Bainite Transformation", Chicago, U.S.A, A.S.M.,* 1988, in press.

36. B. Josefsson and H. O. Andren: *Proc. of the 35th Int. Conf. on "Field Emission Symp.", Oak Ridge, Tennessee, U.S.A. 18-22 July,* 1988.

37. H. K. D. H. Bhadeshia and D. V. Edmonds: *Acta Metall.*, 1980, **28,** 1265.

38. H. K. D. H. Bhadeshia: *Metal Science,* 1982, **16,** 167.

39. J. W. Christian: *"The Theory of Transformation in Metals and Alloys", second ed. Part 1, Pergamon, Oxford,* 1975.

40. M. Enomoto: *1988,* Trans. ISIJ, **28,** 826.

41. K. R. Kinsman and H. I. Aaronson: *Metall. Trans.,* 1973, **4,** 959.

APPENDIX

The conservation of mass for the substitutional alloying element in a ternary system is expressed by the following three equations as discussed in the text:

$$v(x_2^{\gamma\alpha} - x_2^{\alpha\gamma}) = -\frac{D_{22}^\gamma}{l_\gamma}(x_2^{\gamma\alpha} - \overline{x}_2) + \frac{D_{22}^\alpha}{l_\alpha}(\overline{x}_2 - x_2^{\alpha\gamma}) \tag{7.81}$$

$$\frac{l_\alpha}{2}(\overline{x}_2^\alpha - x_2^{\alpha\gamma}) = \frac{l_\gamma}{2}(x_2^{\gamma\alpha} - \overline{x}_2^\gamma) \tag{7.82}$$

$$\int_0^t \frac{D_{22}^\alpha(\overline{x}_2^\alpha - x_2^{\alpha\gamma})}{l_\alpha} \, dt = \frac{1}{2}(l_\alpha + 2z^*)(\overline{x}_2^\alpha - x_2^{\alpha\gamma}) \, . \tag{7.83}$$

On eliminating l_γ from equations 7.81 and 7.82, a relation between v and l_α can be obtained:

$$vl_\alpha = -\frac{D_{22}^\gamma(x_2^{\gamma\alpha} - \overline{x}_2)^2}{(x_2^{\gamma\alpha} - x_2^{\alpha\gamma})(\overline{x}_2 - x_2^{\alpha\gamma})} + \frac{D_{22}^\alpha(\overline{x}_2 - x_2^{\alpha\gamma})}{x_2^{\gamma\alpha} - x_2^{\alpha\gamma}} \tag{7.84}$$

The right hand side of equation 7.84 is independent on time as long as soft impingement does not occur. Equation 7.84 can therefore be rewritten as follows regarding the fact that $v = dz/dt$:

$$l_\alpha \frac{dz}{dt} = C_1 \tag{7.85}$$

where C_1 is a constant which is equal to the right hand side of equation 7.84. In equation 7.85 l_α and z are both functions of time. Since $l_\alpha = 0$ at $t = 0$, it might be reasonable to assume the expression for l_α as follows:

$$l_\alpha = C_2 t^a \tag{7.86}$$

where C_1 and a are constants. Thus equation 7.85 becomes:

$$\frac{dz}{dt} = \frac{C_1}{C_2} t^{-a} \tag{7.87}$$

leading the expression for z:

$$z = C_3 t^{-a+1} \tag{7.88}$$

where $C_3 = \frac{C_1}{C_2(-a+1)}$ is a constant. On substituting equations 7.86 and 7.88 into 7.83, one can obtain the following expression:

$$\left(\frac{2D_{22}^\alpha}{C_2^2(-a+1)} - \frac{2C_3}{C_2}\right) t^{-2a+1} = 1 \tag{7.89}$$

Since equation 7.89 should be satisfied for any value of time t, the time exponent have to be equal to zero:

$$-2a + 1 = 0 \tag{7.90}$$

As a result, $a = 1/2$ is obtained.
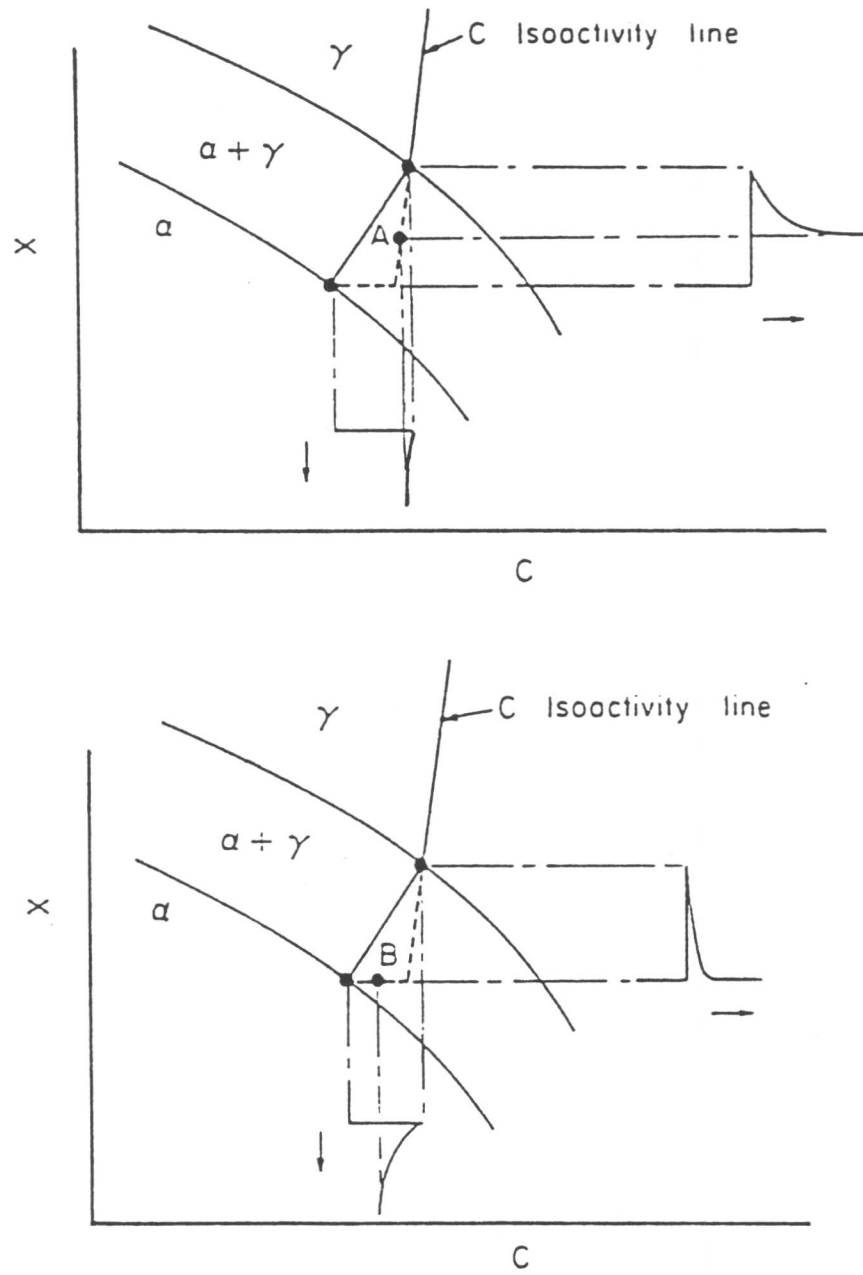
Fig. 7.1 Schematic isothermal section of a Fe-C-X ternary system, illustrating ferrite growth occurring with local equilibrium at the α/γ interface. (a) Growth at low supersaturations (PLE) with bulk composition of X, and (b) growth at high supersaturations (NPLE) with negligible partitioning of X during transformation. The bulk alloy compositions are designated "A" and "B" respectively.
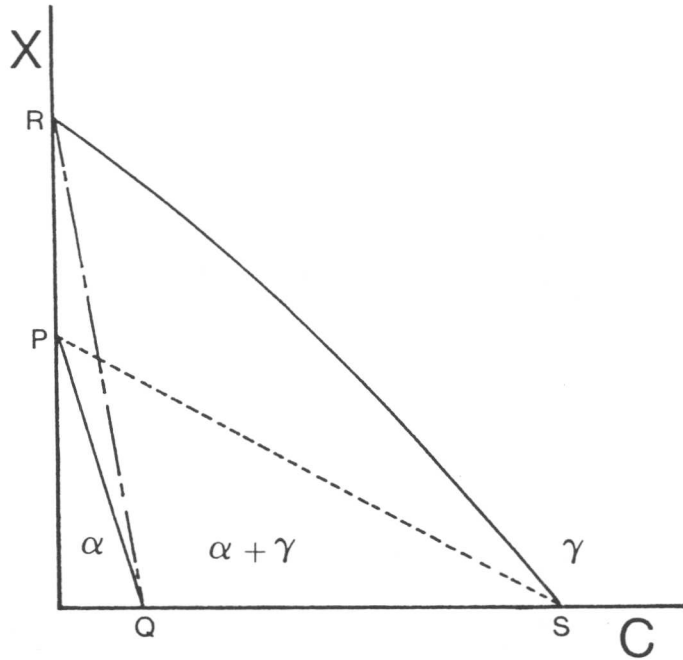
Fig. 7.2 Isothermal section of a ternary Fe-C-X phase diagram, with the $(\alpha + \gamma)$ phase field lying within the region **PQSR**. The decomposition of austenite by the NPLE mechanism can occur if the bulk composition lies in the region **QPS**, whereas the growth of austenite by the NPLE mechanism can only occur if the ferrite is superheated into the region **QRS**.

Fig. 7.3 The NPLE growth of austenite as a consequence of the superheating of a fully ferritic sample of bulk composition "I" to a temperature T.

Fig. 7.4 The PLE growth of austenite as a consequence of the superheating of a fully ferritic sample of bulk composition "K" to a temperature T.

Fig. 7.5 The NPLE growth of austenite as a consequence of the superheating of a sample with a mixture of bainitic ferrite and residual austenite initial microstructure of bulk composition "I" to a temperature T.

Fig. 7.6 The PLE growth of austenite as a consequence of the superheating of a sample with a mixture of bainitic ferrite and residual austenite initial microstructure of bulk composition "K" to a temperature T.

Fig. 7.7 Schematic diagram of carbon and X profiles during reconstructive growth of austenite from a mixture of bainitic ferrite and austenite assuming linear gradients. z^* designate the position of the transformation interface along a space coordinate normal to the interface.

Fig. 7.8 The paraequilibrium growth of austenite as a consequence of the superheating of a fully ferritic sample of bulk composition "L" to a temperature T.

Fig. 7.9 The paraequilibrium growth of austenite as a consequence of the superheating of a sample with a mixture of bainitic ferrite and residual austenite initial microstructure of bulk composition "L" to a temperature T.
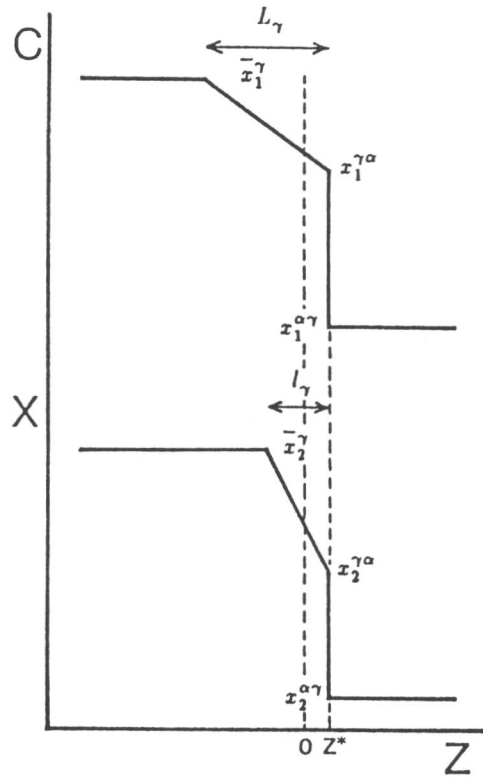
Fig. 7.10 Schematic diagram of carbon and X profiles during the growth of austenite from a fully ferritic initial microstructure assuming linear gradients which exist only in ferrite matrix. z^* designate the position of the transformation interface along a space coordinate normal to the interface.
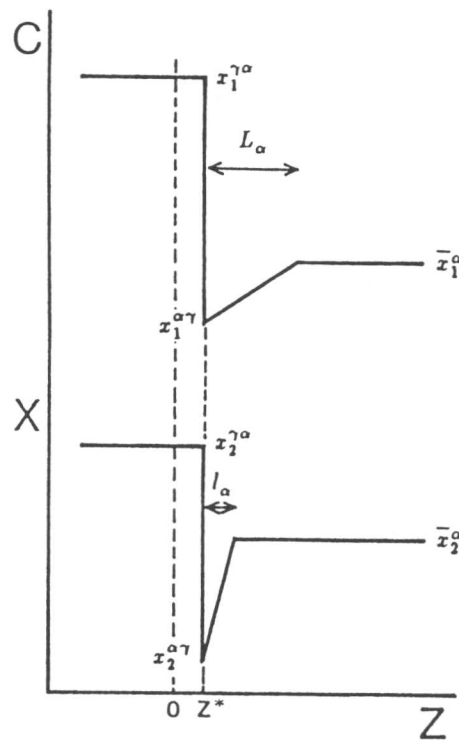
Fig. 7.11 Schematic diagram of carbon and X profiles during the growth of austenite from a mixture of ferrite and austenite assuming linear gradients which exist only in austenite. z^* designate position of the transformation interface along a space coordinate normal to the interface.

223
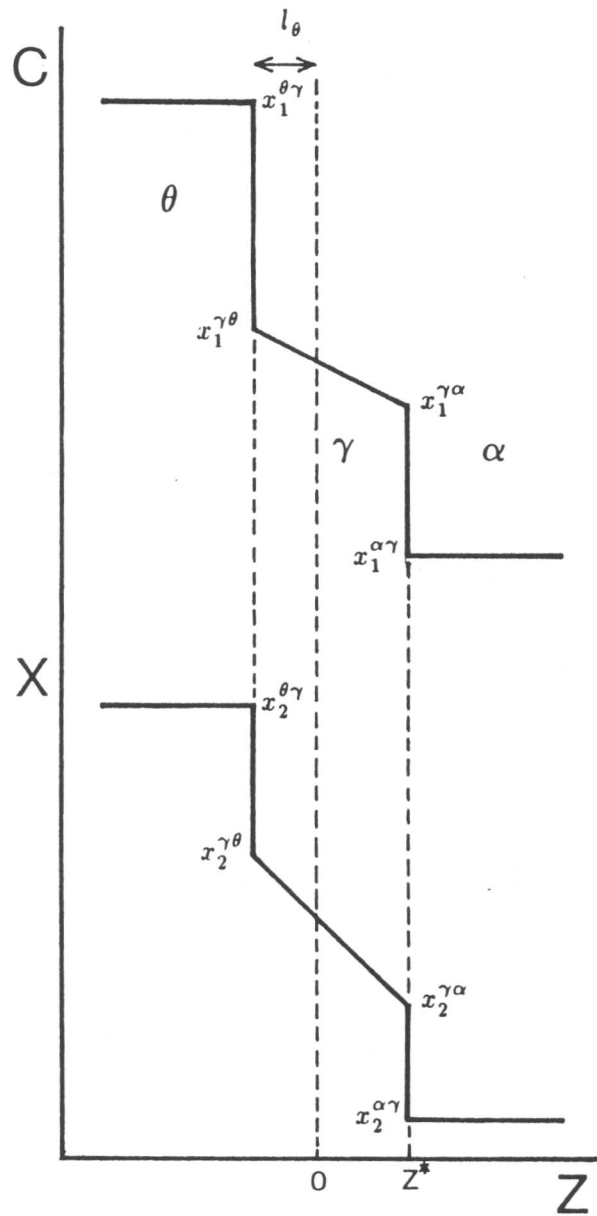
Fig. 7.12 Schematic diagram of carbon and X profiles during the growth of austenite from a mixture of ferrite and cementite particles assuming linear gradients which exist only in austenite. z^* designates the position of the transformation interface along a space coordinate normal to the interface.
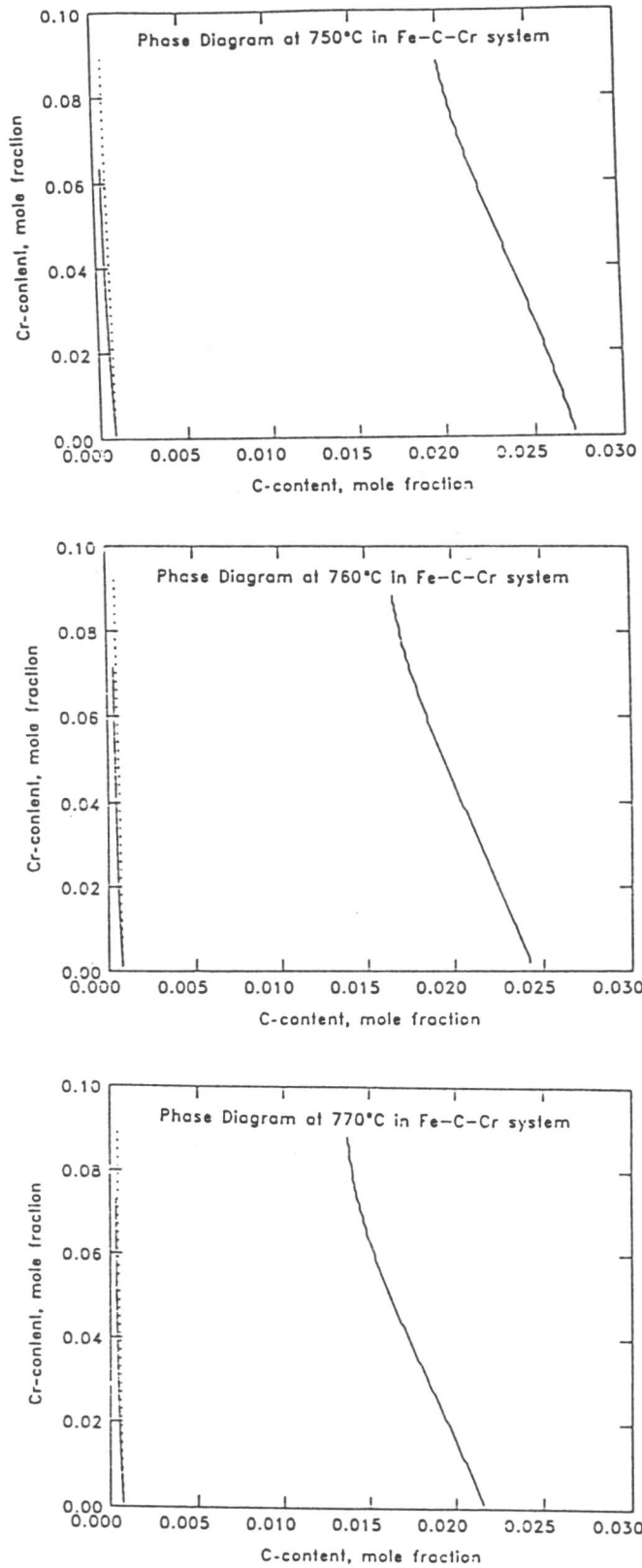
Fig. 7.13 Calculated isothermal sections of the phase diagram in the Fe-0.3C-4.08Cr wt.% alloy at 750, 760 and 770 °C respectively. Dashed lines represent the transition lines from NPLE to PLE condition.

225
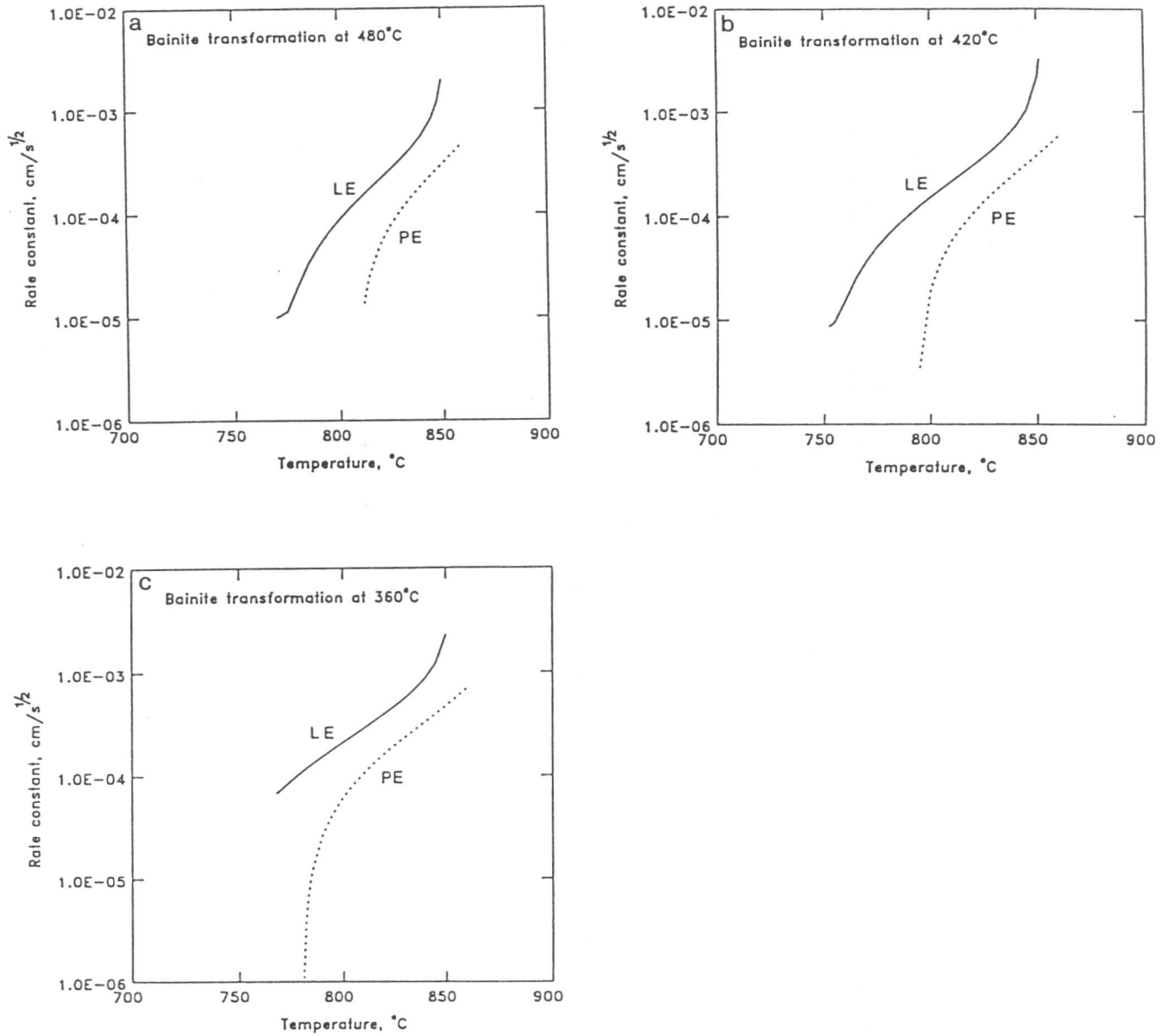
Fig. 7.14 Calculated one dimensional parabolic thickening rate constant of austenite as a function of the reaction temperature during reaustenitisation from a mixture of bainitic ferrite and residual austenite. The bainite transformation treatment was carried out at (a) 480 °C, (b) 420 °C and (c) 360 °C. Solid lines are the rate constant for the local equilibrium growth of austenite and dashed lines for the paraequilibrium growth of austenite.
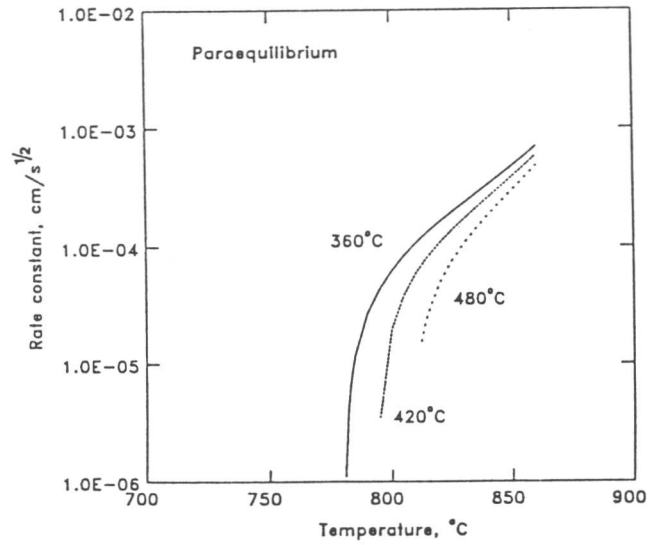
Fig. 7.15 Calculated one dimensional parabolic thickening rate constant of austenite as a function of the reaction temperature during reaustenitisation under paraequilibrium from mixtures of bainitic ferrite and residual austenite obtained at three different bainite transformation temperatures.
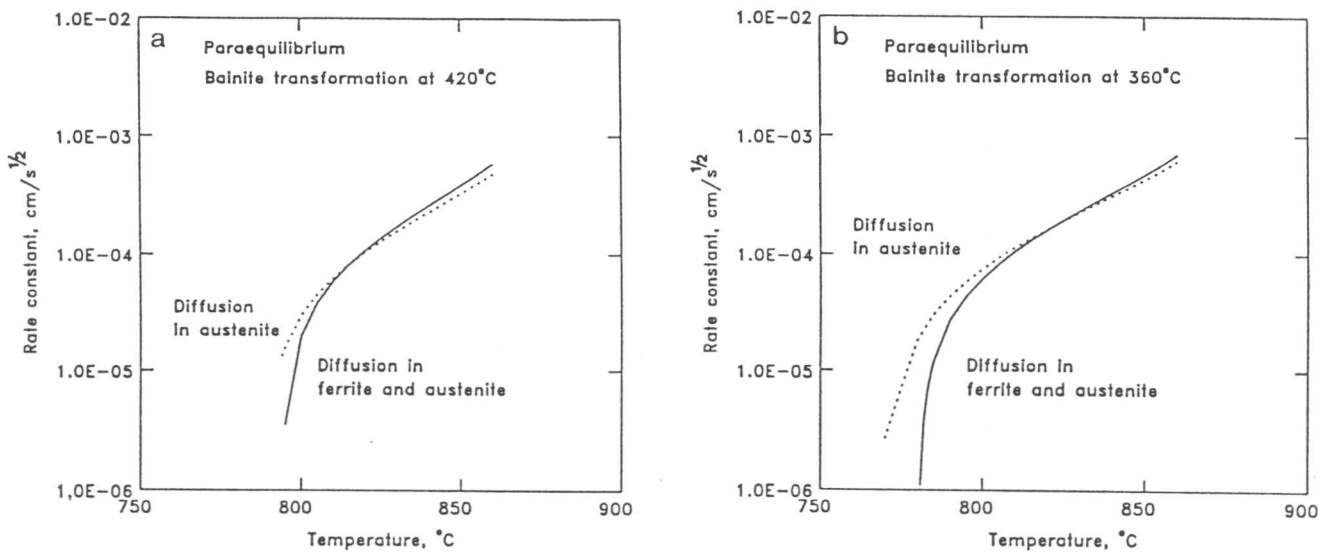
Fig. 7.16 Calculated one-dimensional parabolic thickening rate constant of austenite during reaustenitisation under paraequilibrium from a mixture of bainitic ferrite and residual austenite obtained at (a) 420 °C and (b) 360 °C. Solid line shows the rate constant as a function of the reaction temperature for the case where diffusion fields exist both in ferrite and austenite, whereas dashed line is for the case with diffusion fields only in austenite.

227
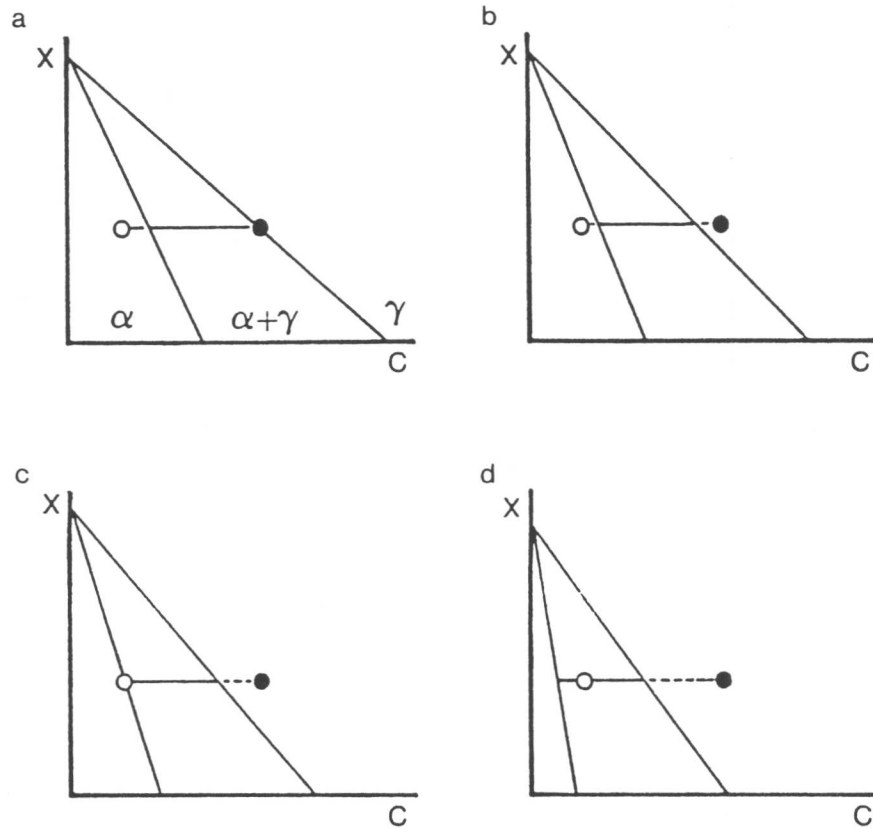
Fig. 7.17 Schematic isothermal sections of the phase diagrams at different temperatures with the paraequilibrium $\alpha/\alpha + \gamma$ and $\gamma/\alpha + \gamma$ phase boundaries, in which the initial carbon concentrations of ferrite and austenite are indicated by open and solid circles respectively.
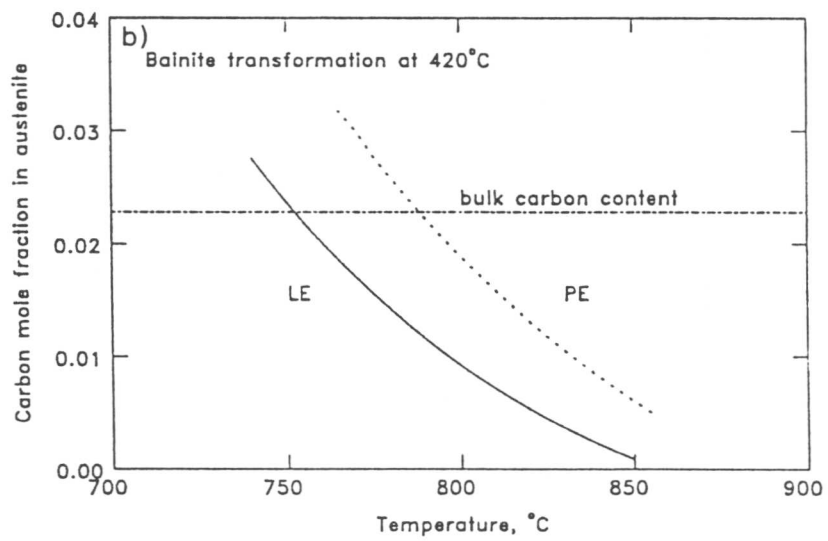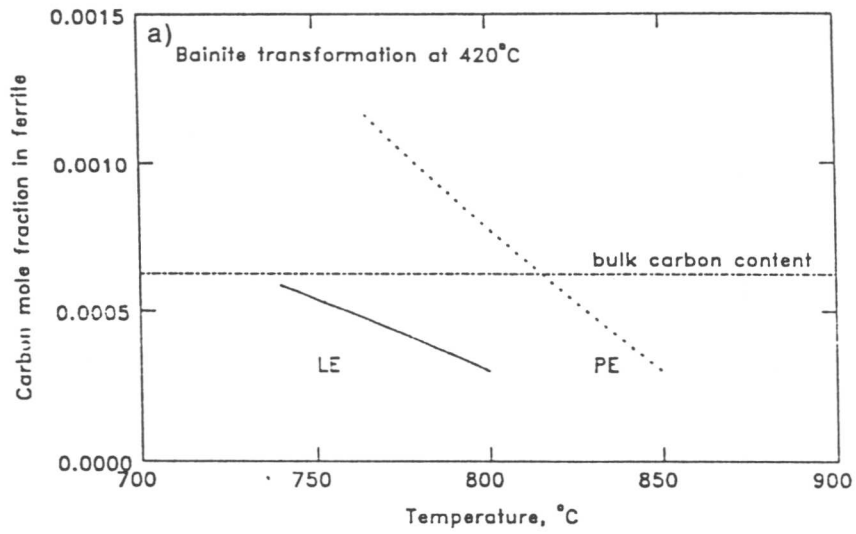
Fig. 7.18 Calculated interface carbon concentrations in ferrite (a) and austenite (b) for the parae-quilibrium (solid line) and the local equilibrium (dashed line) growth of austenite from a mixture of bainitic ferrite and austenite formed at 420 °C. Initial carbon concentration in the both phases are also shown.
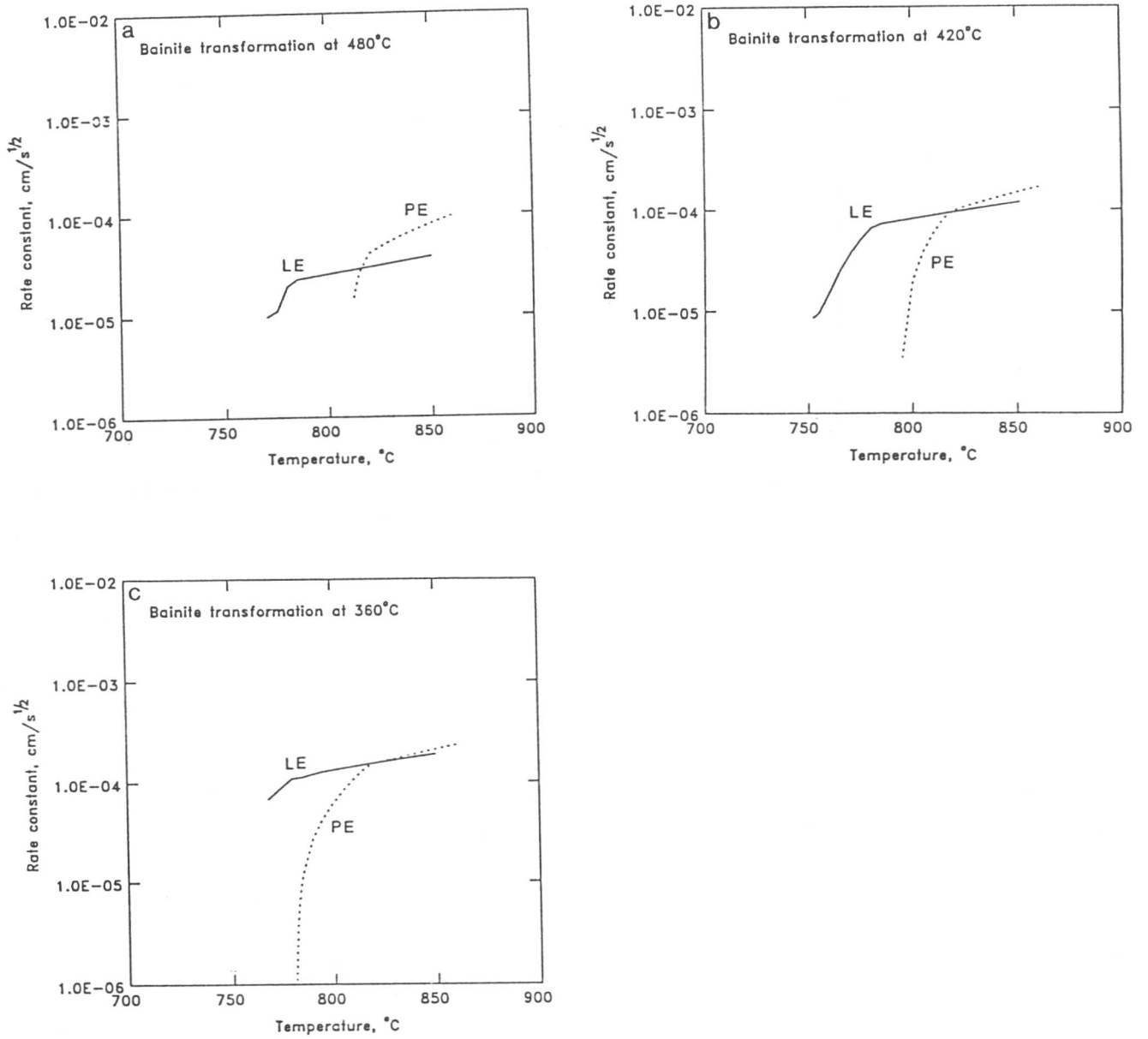
Fig. 7.19 Calculated one dimensional parabolic thickening rate constant of austenite as a function of the reaction temperature during reaustenitisation from a mixture of bainitic ferrite and residual austenite. The bainite transformation treatment was carried out at (a) 480 °C, (b) 420 °C and (c) 360 °C. Solid lines are the rate constant for the local equilibrium growth of austenite and dashed lines for the paraequilibrium growth of austenite. The carbon concentration at the interface in austenite was replaced by the bulk carbon content when the calculated $x_1^{\gamma\alpha}$ becomes smaller than the bulk carbon content.
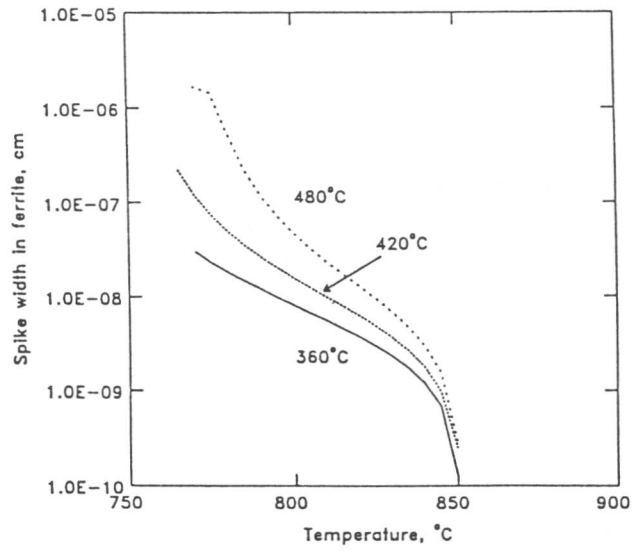
Fig. 7.20 Spike width of the substitutional alloying element calculated by equation 7.80 in the text, as a function of temperature and the initial condition.
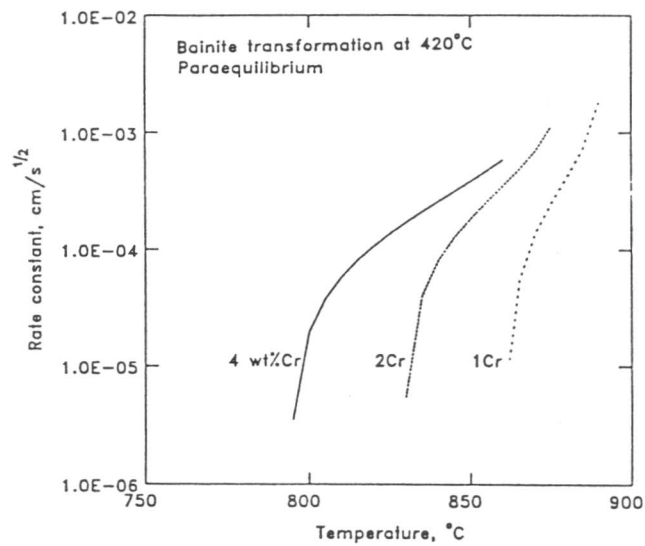
Fig. 7.21 Effect of Cr content on the one dimensional parabolic thickening rate constant of the paraequilibrium growth of austenite. The bainite transformation was carried out at 420 °C.

CHAPTER 8

TIME-TEMPERATURE-TRANSFORMATION CURVES AND OVERALL REAUSTENITISATION IN STEELS

8.1 INTRODUCTION

As mentioned in Chapter 1, the prediction of the microstructural development during cooling can be carried out using calculated time-temperature-transformation (TTT) curves for ferrite formation and an assumption of the additivity rule. For many applications, it is just as important to determine TTT curves for reaustenitisation from the initial microstructure of interest. Once TTT curves for various degrees of reaustenitisation are obtained, reaustenitisation during continuous heating, can be calculated adopting Scheil's rule [1] along any heat cycle. This is the major goal of the present work.

8.2 ASSESSMENT OF SCHEIL'S RULE IN REAUSTENITISATION

If the incubation period τ is obtained as a function of temperature, reaustenitisation will start when an integration of τ along a heating pass reaches unity (*i.e.* Scheil's rule)

$$\int_0^{t_s} \tau\{T\}^{-1} dt = 1 \qquad (8.1)$$

where the reaction temperature T is now a function of time t, and reaustenitisation starts at time t_s on heating.

The TTT curve for reaustenitisation in a Fe-C-Mn-Ni-Mo alloy reported by Yang [2] (Fig. 8.1) is reanalysed and continuous heating reaustenitisation experiments were conducted on the same alloy as Yang in order to assess the application of Scheil's rule.

Specimens were heated to 1000 °C for 10 min followed by quenching to 460 °C for 30 min allowing the bainite transformation completed. The specimens were then heated directly from the temperature at four different constant heating rates, 5, 10, 20 and 50 °C s^{-1}. Reaustenitisation-start temperatures were determined by deviations of the relative length change from a linear thermal expansion curve. The observed results were plotted against heating rate in Fig. 8.2.

An empirical expression for τ was obtained by regression analysis using Yang's isothermal data for the smallest detectable reaustenitisation from the mixture of bainite and residual austenite:

$$\log \tau = -57.737 \log T + 173.42 \qquad (8.2)$$

where τ and T are measured in s and K respectively.

The reaustenitisation start temperatures during continuous heating were calculated using equation 8.2 and are presented in Fig. 8.2. The agreement between experiment and calculation is reasonably good.

8.3 GROWTH OF AUSTENITE

Reaustenitisation in steels proceeds by a nucleation and growth mechanism. When the retained austenite is present in the initial microstructure, it may not be necessary to nucleate new austenite since the reaction can proceed by the growth of the retained austenite.

232

Assuming one-dimensional growth, and if the austenite/ferrite interfacial area per unit volume is S_V, the increase in volume fraction of austenite ΔV_γ during heat treatment is given by:

$$\Delta V_\gamma = S_V \alpha_1 t^{1/2}. \tag{8.3}$$

Adopting the extended volume concept (see Appendix), ξ the volume fraction of newly transformed austenite normalised by the maximum degree of reaction $\theta = V_\gamma^e - V_{\gamma 0}$ (V_γ^e and $V_{\gamma 0}$ are the equilibrium and initial volume fractions of austenite), is expressed as follows:

$$\xi\{t\} = 1 - \exp[-\frac{S_V \alpha_1}{\theta} t^{1/2}]. \tag{8.4}$$

When reaustenitisation proceeds not only by the one-dimensional thickening of austenite plates but also by lengthening of the plates, $\xi\{t\}$ should be then expressed by the parabolic thickening rate constants in two directions. Assuming that the initial volume of an austenite plate in the starting microstructure is $a_0 c_0^2$, and that at time t is ac^2, the volume fraction change ΔV_γ at time t during isothermal reaustenitisation can be expressed as follows:

$$\begin{aligned}
\Delta V_\gamma &= n(ac^2 - a_0 c_0^2) \\
&= n\{(a_0 + \alpha_1 t^{1/2})(c_0 + \beta t^{1/2})^2 - a_0 c_0^2\} \\
&= n\{(6a_0 c_0 + c_0^2)\alpha_1 t^{1/2} + (9a_0 + 6c_0)\alpha_1^2 t + 9\alpha_1^3 t^{3/2}\}
\end{aligned} \tag{8.5}$$

where β is the parabolic lengthening rate constant which was assumed to be $3\alpha_1$ after [3], and n is the number of growing austenite plates per unit volume. The volume fraction of newly transformed austenite normalised by the maximum degree of reaction θ is thus given by:

$$\xi\{t\} = 1 - \exp[-\frac{n}{\theta}\{(6a_0 c_0 + c_0^2)\alpha_1 t^{1/2} + (9a_0 + 6c_0)\alpha_1^2 t + 9\alpha_1^3 t^{3/2}\}]. \tag{8.6}$$

Yang and Bhadeshia [4] derived the time required to obtain a small increase in the volume fraction of austenite τ using equation 8.4 as follows:

$$\begin{aligned}
\tau &\simeq [\frac{\Delta \xi \theta}{S_V \alpha_1}]^2 \\
&= [\frac{\Delta V_\gamma}{S_V \alpha_1}]^2.
\end{aligned} \tag{8.7}$$

Therefore the incubation period τ is proportional to α_1^{-2}. If this theory is acceptable, the plot of $\log\{\tau\}$ against $\log\{\alpha_1^{-2}\}$ should show a linear correlation as shown by Yang [2]. It should be noted, however, that there are poor linear correlations between τ and α_1^{-2} as shown in Fig. 8.3 a. The slopes of the *log-log* plot are 1.56 for the smallest detectable reaustenitisation and 1.80 for the 0.05 of increase in the volume fraction of austenite (Fig. 8.3 b), which are expected to be unity from the theory. When $\log\{-\ln\{1 - \xi\}\}$ is plotted against $\log\{t\}$, the slope of the plot should be 1/2 in Yang's theory at the early stage of reaustenitisation. The slope of the plot is, however, not always 1/2 as shown in Fig. 8.4. These results may indicate that equation 8.6 could be more appropriate for an expression of the kinetics of reaustenitisation from a mixture of bainitic ferrite and austenite than equation 8.4. For simplification, the initial dimension of the retained austenite is assumed here to be $a_0 = 0.2 \ \mu$m and $c_0 = 5 \ \mu$m . Equation 8.6 becomes as follows:

$$\xi\{t\} = 1 - \exp[-\frac{31n\alpha_1}{\theta}t^{1/2}\{1 + 1.03\alpha_1 t^{1/2} + 0.29\alpha_1^2 t\}].\qquad(8.8)$$

The slope of the plot of $\log\{-\ln\{1 - \xi\}\}$ against $\log\{t\}$ varies with α_1 as shown in Fig. 8.5. The slope should then vary with temperature since α_1 depends on the reaction temperature. The slope of the plot of $\log\{-\ln\{1 - \xi\}\}$ against $\log\{t\}$ varies from 0.51 to 1.42 when α_1 is altered between 0.01 and 10 μm s$^{-1/2}$. When α_1 becomes 1.0 μm s$^{-1/2}$ (1×10^{-4} cm s$^{-1/2}$), the slope reaches around unity.

Using calculated parabolic thickening rate constants for Yang's alloy [2] and for the Fe-0.3C-4.08Cr wt.% alloy, the slopes of the plot of $\log\{-\ln\{1 - \xi\}\}$ against $\log\{t\}$ calculated as discussed above were compared with the observed slopes at 680, 700 and 710 °C for Yang's alloy [2] and at 778, 785 and 805 °C for the Fe-0.3C-4.08Cr wt.% alloy (Fig. 8.6). A reasonable agreement between experiment and calculated results was obtained. This suggests that equation 8.6 is applicable to the kinetic calculation of reaustenitisation from mixtures of bainitic ferrite and austenite where the initial austenite is plate in shape and grows in two directions; *i.e.* lengthening and thickening.

The effective number of austenite plates per unit volume which can grow during reaustenitisation; *i.e.* the number n in equation 8.6, can be evaluated from the observed data discussed above. The 50% reaustenitisation time (*i.e.* the time for $\xi = 0.5$) was used. The calculated n values are 1.30×10^{-4} at 680 °C, 2.91×10^{-5} at 700 °C and 5.49×10^{-4} at 710 °C for Yang's alloy, and 4.30×10^{-4} at 778 °C, 8.31×10^{-4} at 785 °C and 5.33×10^{-4} at 805 °C for the Fe-0.3C-4.08Cr wt.% alloy. Although there are significant scatter in the calculated n values, especially in Yang's alloy, the average value for each alloy is used for further analysis since the same starting microstructure was used for each alloy.

The TTT curve for a 0.05 increase in the volume fraction of austenite (*i.e.* $\Delta V_\gamma = 0.05$) was calculated and compared with the observed data [2] in Fig. 8.7. A reasonable agreement was obtained at high temperatures but not at temperatures below 690 °C. This may because the theory does not take into account of the effect of soft impingement. Since the maximum degree of reaction at low temperatures is not very large in comparison with 0.05, the growth rate of austenite may decrease significantly by soft impingement before ΔV_γ reaches 0.05.

The effect of reaction temperature on the increase in the volume fraction of austenite was calculated using equation 8.6 for the Fe-0.3C-4.08Cr wt.% alloy with bainite + 0.3 of retained austenite starting microstructure (Fig. 8.8). The calculated results were rearranged to show the TTT curves for different degrees of ΔV_γ (Fig. 8.9). The calculated TTT curve for $\Delta V_\gamma = 0.05$ was compared with the observed values in the present experiments (Fig. 8.10). The agreement is reasonably good. It should, however, noted that the formation of austenite was observed *during* heating when the reaction temperature is higher than 785 °C. The observed values in Fig. 8.10 may represent overestimates.

8.4 AUSTENITE FORMATION INCLUDING NUCLEATION AND GROWTH

Examples of the nucleation and growth reaustenitisation processes include the reheating of martensite or mixtures of ferrite and carbides. Although the morphology of the austenite formed depends strongly on the initial microstructure (Chapter 6), the simplest assumption is the spherical austenite model. The growth is then three-dimensional and the appropriate parabolic rate constant α_3 is used. The formation of austenite is assumed to occur from a carbon supersaturated ferrite matrix. The paraequilibrium carbon concentration at 500 °C was

used, without any proof, as the matrix carbon concentration after tempering during heating, since there is no knowledge about the amount of carbon left in the matrix before the reaction. The rate constant α_3 is given by [5]:

$$\frac{x_1^{\alpha\gamma} - \overline{x}_1^{\alpha}}{x_1^{\alpha\gamma} - x_1^{\gamma\alpha}} = H_3\{D_{11}^{\alpha}\} - \frac{B_1 D_{12}^{\alpha}}{D_{11}^{\alpha} - D_{22}^{\alpha}}[H_3\{D_{22}^{\alpha}\} - H_3\{D_{11}^{\alpha}\}]$$

$$\frac{x_2^{\alpha\gamma} - \overline{x}_2^{\alpha}}{x_2^{\alpha\gamma} - x_2^{\gamma\alpha}} = H_3\{D_{22}^{\alpha}\}$$

(8.9)

where

$$H_3\{D_{ii}^{\alpha}\} = \frac{\alpha_3^2}{2D_{ii}^{\alpha}}[1 - (\frac{\pi}{4D_{ii}^{\alpha}})^{0.5}\alpha_3 \exp\{\frac{\alpha_3^2}{4D_{ii}^{\alpha}}\}\mathrm{erfc}\{(\frac{\alpha_3^2}{4D_{ii}^{\alpha}})^{0.5}\}]$$

$$B_1 = \frac{x_2^{\alpha\gamma} - x_2^{\gamma\alpha}}{x_1^{\alpha\gamma} - x_1^{\gamma\alpha}}$$

where D_{11}^{α} and D_{22}^{α} are diffusivities of carbon and substitutional alloying element in ferrite, and the x's are chemical compositions at the interface.

Using the extended volume concept with the nucleation rate I and the growth rate α_3, the volume fraction of austenite ξ at time t normalised by the maximum degree of reaction θ (note that θ here is equal to V_γ^e) is given by:

$$\xi\{t\} = 1 - \exp[-\int_0^t I\frac{4}{3\theta}\pi\alpha_3^3(t - t')^{3/2}dt']$$

$$= 1 - \exp[-\frac{4\pi\alpha_3^3}{3\theta}\int_0^t I(t - t')^{3/2}dt'].$$

(8.10)

The nucleation rate I is a function of temperature, driving force for nucleation, site density and time. To simplify the calculation, I is assumed to have the following form:

$$I\{t\} = N_0\nu_1 \exp(-\nu_1 t)$$

(8.11)

where N_0 is the initial nucleation site density and ν_1 is the rate constant for nucleation. Substituting the expression of I into equation 8.10, the following relation is obtained:

$$\xi\{t\} = 1 - \exp[-\frac{4\pi\alpha_3^3 N_0\nu_1}{3\theta}\int_0^t \exp\{-\nu_1 t'\}(t - t')^{3/2}dt'].$$

(8.12)

The total number of particles N at time t can be calculated from equation 8.11, namely;

$$N\{t\} = \int_0^t I dt' = \int_0^t N_0\nu_1 e^{-\nu_1 t}dt' = N_0(1 - e^{-\nu_1 t}).$$

(8.13)

Therefore, the time required to exhaust 95% of the nucleation sites is roughly equal to $3/\nu_1$.

At a temperature T, the following relation can be obtained from equation 8.12 and be used to determine the values ν_1 and N_0.

$$\log\{-\ln\{1 - \xi\}\} = \log K_T + \log[\int_0^t e^{-\nu_1 t'}(t - t')^{3/2}dt']$$

(8.14)

where $K_T = 4\pi\alpha_3^3 N_0\nu_1/3\theta$. By altering the value ν_1 in the second term, the slope of the plot of the both sides of the equation against $\log t$ can be made identical. Then the value ν_1 obtained here will be substituted into the expression of K_T giving the value N_0 at temperature

T using the calculated α_3 from thermodynamic knowledge as discussed earlier. Once the values in equation 8.12 are obtained, the time required to obtain the increase in the volume fraction of austenite ΔV_γ can be obtained.

When the rate constant ν_1 in the nucleation function is altered, the slope of the plot of $\log\{-\ln\{1-\xi\}\}$ against $\log\{t\}$ decreases with ν_1 as it can be seen in Fig. 8.11. Since the slopes of the plot which were obtained in the present experiments (Fig. 8.12) were close to unity between 778 and 805 °C, the rate constant ν_1 is said to be about $2.0\,\mathrm{s}^{-1}$ in this temperature range. Using the normalised volume fraction, $\nu_1 = 2.0\,\mathrm{s}^{-1}$ and α_3 (Fig. 8.13) which was calculated using equation 8.9 with the thermodynamic equations discussed in Chapter 7, the initial nucleation site density N_0 was obtained as a function of the reaction temperature (Fig. 8.14). N_0 increases slightly with reaction temperature, which may assist in increasing the rate of reaustenitisation with reaction temperature. Using N_0, ν_1 and α_3, the effect of temperature on the kinetics of reaustenitisation was calculated (Fig. 8.15).

8.5 CONCLUSIONS

The diffusional growth theory discussed in the previous chapter was applied to overall reaustenitisation either from mixtures of bainite and austenite where growth of the pre-existing austenite dominates the reaction, or from a martensitic initial microstructure where the nucleation of austenite is necessary. The analysis leads the following concluding remarks.

1) Reaustenitisation from mixtures of bainite and austenite can be expressed by the parabolic growth theory of the pre-existing austenite films.
2) Reaustenitisation from the mixture of bainite and austenite seems to proceed by the growth of the pre-existing austenite films in two directions; lengthening and thickening.
3) Observed time-temperature-transformation curves for reaustenitisation from the mixtures of bainite and austenite can be reproduced successfully by the growth theory.
4) The formation of austenite including nucleation and growth was modelled using a simple expression for nucleation and the three-dimensional parabolic rate constant.
5) This analysis showed that the initial nucleation site density of austenite from the martensitic initial microstructure increases with reaction temperature.

REFERENCES

1. J. W. Christian: *"The Theory of Transformation in Metals and Alloys"*, 2nd ed. *Part 1, Pergamon, Oxford*, 1981.
2. J-R. Yang: *Ph. D. Thesis, University of Cambridge* 1988.
3. J. R. Bradley, J. M. Rigsbee and H. I. Aaronson: *Metall. Trans. A*, 1977, **8A,** 323.
4. J-R. Yang and H. K. D. H. Bhadeshia: *"Welding Metallurgy of Structural Steels"*, *TMS-AIME, Warrendale, Ohio, ed. J. Y. Koo*, 1987, 549.
5. D. E. Coates: *Metall. Trans.*, 1973, **4,** 1077.

8.6 APPENDIX

When there are n^e interfaces between α and γ per unit volume at the beginning of the reaction, and these thicken parabolically, the actual volume fraction of newly formed austenite is V_γ and the volume fraction of newly formed austenite assuming that there is no impingement is V_γ^e, the increase in V_γ and V_γ^e; *i.e.* dV_γ and dV_γ^e, can be expressed by the increase in the thickness of austenite dq as follows:

$$dV_\gamma = n\, dq$$

$$dV_\gamma^e = n^e\, dq$$

where n is the number of interfaces per unit volume which can grow at time t. Since the thickness of ferrite plates has a distribution, a thinner ferrite plate can be exhausted by growing austenite earlier than a thicker one. So the number of interfaces which has already been encountered by the adjacent interface is $\Delta n = n^e - n$. Although the distribution function of the thickness of ferrite plates is not known, the simplest assumption is $\Delta n = \frac{V_\gamma}{\theta} n^e$, where $\theta = 1 - V_{\gamma 0}$ with the initial volume fraction of austenite given by $V_{\gamma 0}$. Therefore the relation between dV_γ and dV_γ^e is as follows:

$$dV_\gamma = \frac{n}{n^e} dV_\gamma^e$$
$$= \frac{n^e - (V_\gamma/\theta)n^e}{n^e} dV_\gamma^e$$
$$= (1 - \frac{V_\gamma}{\theta}) dV_\gamma^e$$

which leads to the relation:

$$-\theta \ln\{1 - \frac{V_\gamma}{\theta}\} = V_\gamma^e.$$

Therefore,

$$\frac{V_\gamma}{\theta} = 1 - \exp\{-\frac{V_\gamma^e}{\theta}\}$$

which is the same as the extended volume concept.
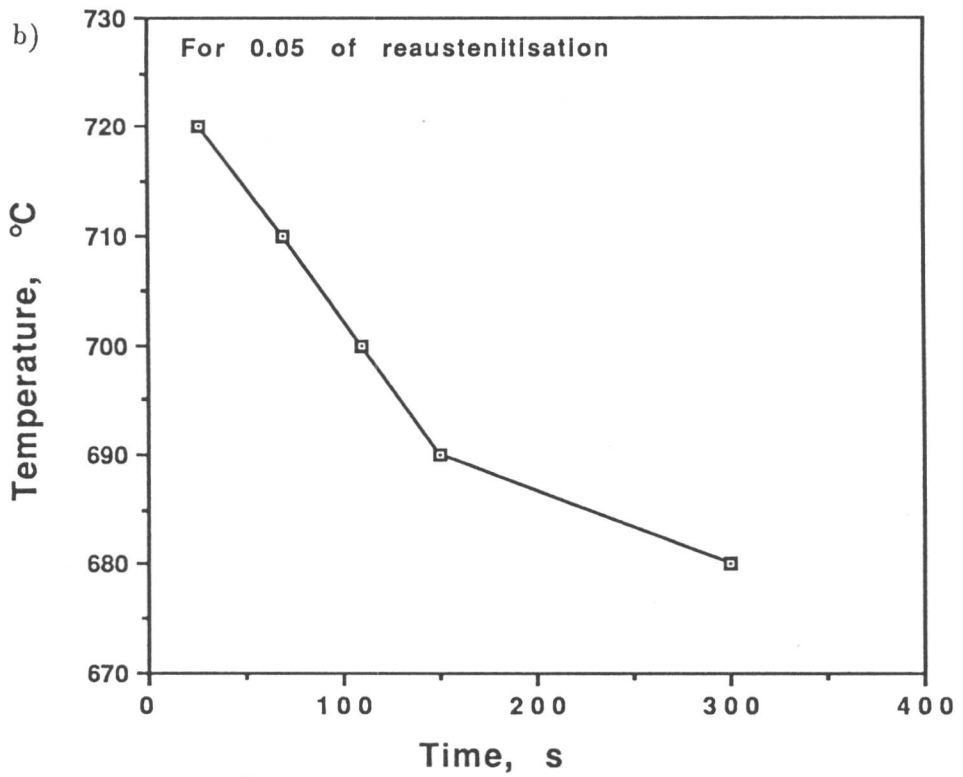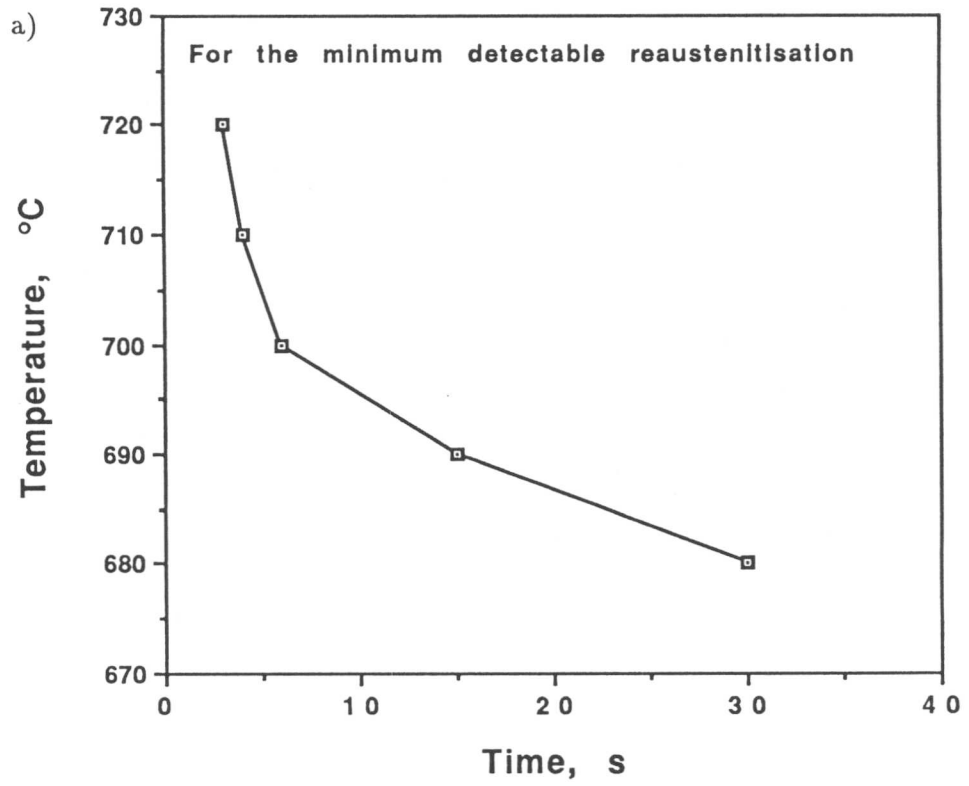
Fig. 8.1 TTT curves for reaustenitisation from a mixture of bainite and austenite in a Fe-C-Mn-Ni-Mo alloy (after Yang [2]). a) is for the minimum detectable reaustenitisation and b) for 0.05 of increase in the volume fraction of austenite.
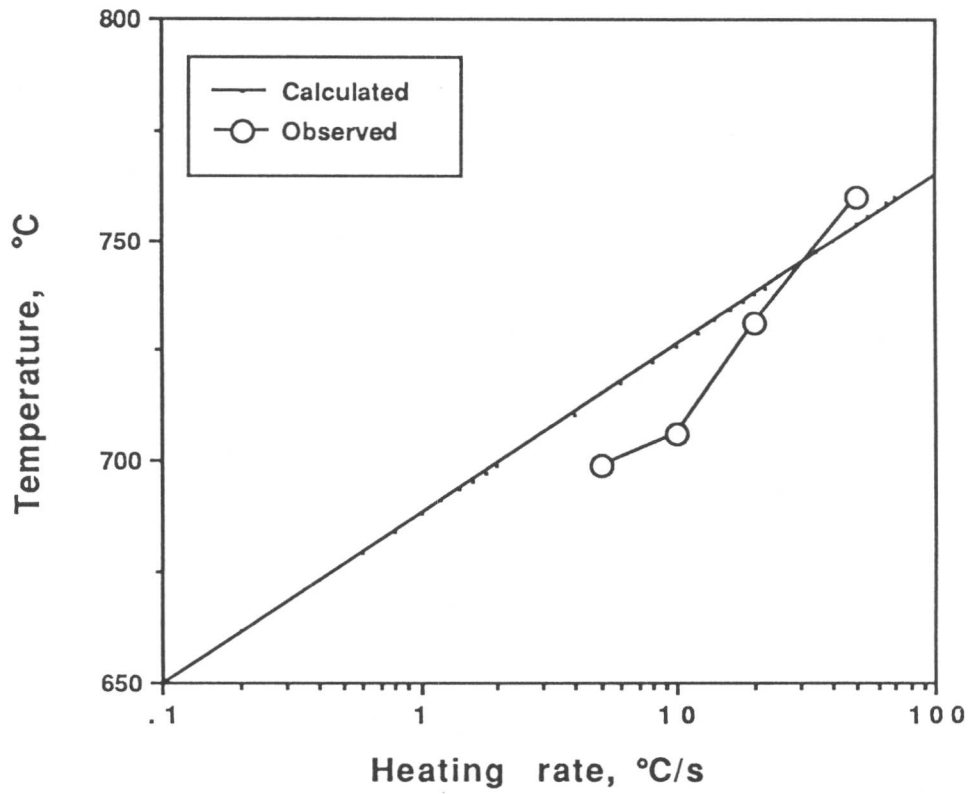
Fig. 8.2 Calculated (line) and observed (plots) reaustenitisation-start temperatures during continuous heating at constant heating rates from a mixture of bainite and austenite in the Fe-C-Mn-Ni-Mo alloy as a function of heating rate.
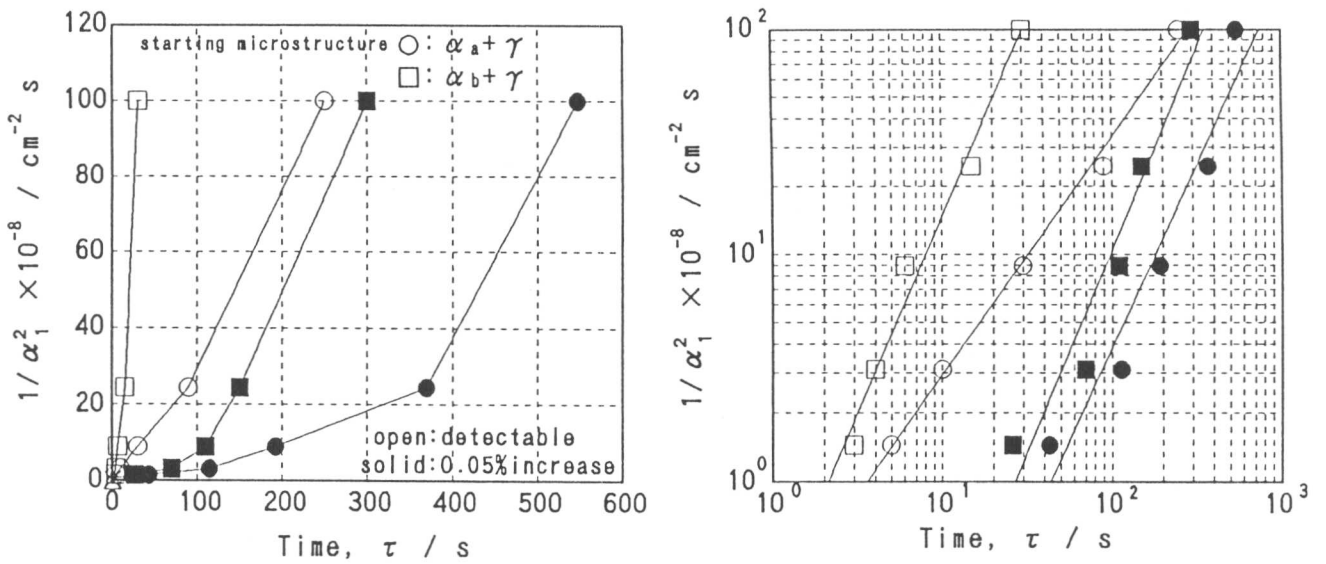
Fig. 8.3 Relation between τ and α_1^{-2} plotted (a) in linear scale and (b) in logarithmic scale.
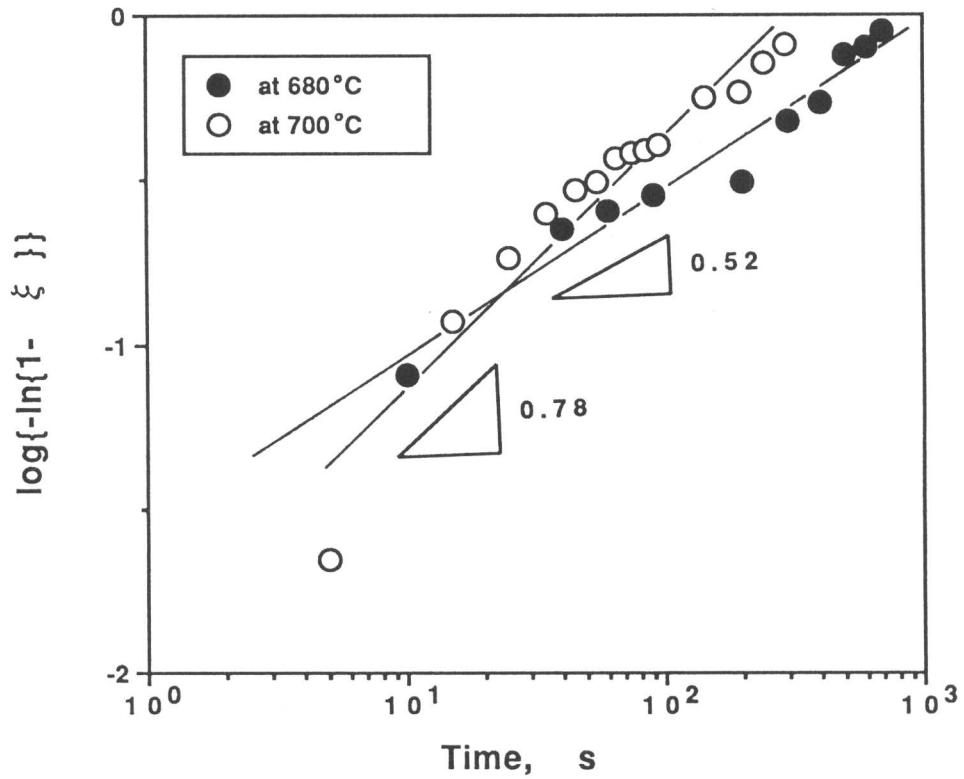
Fig. 8.4 $\log\{-\ln\{1 - \xi\}\}$ v.s. $\log\{t\}$ plots in the Fe-C-Mn-Ni-Mo alloy (after Yang [4]).
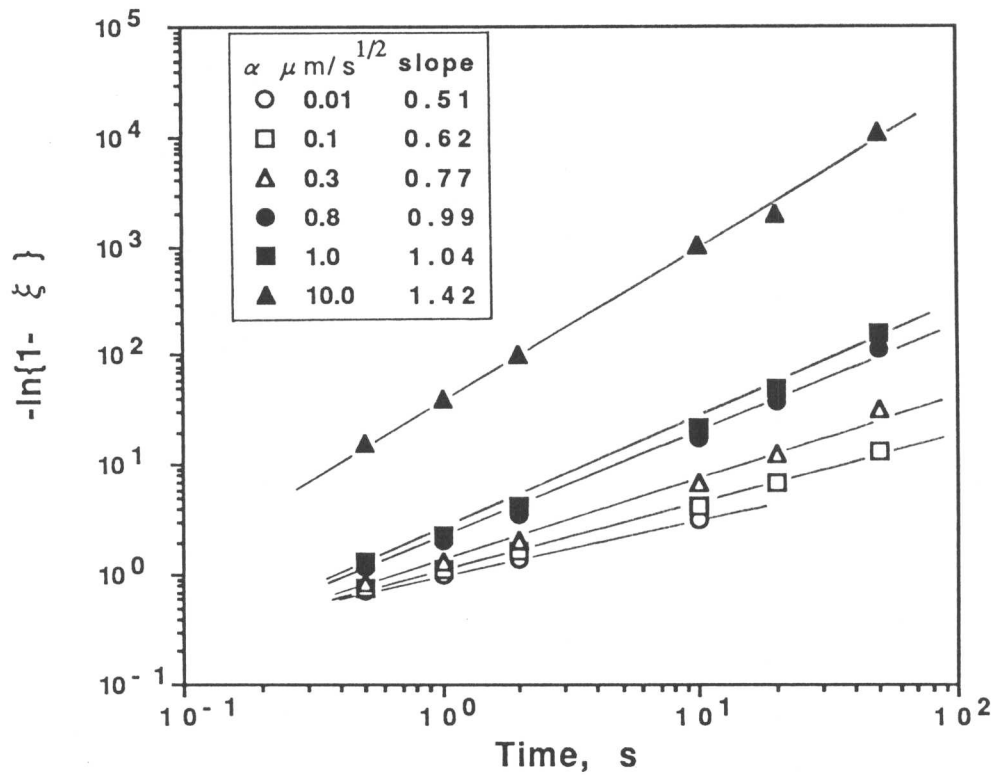
Fig. 8.5 Change in the slope of the plot of $\log\{-\ln\{1 - \xi\}\}$ against $\log\{t\}$ with the parabolic thickening rate constant α_1.
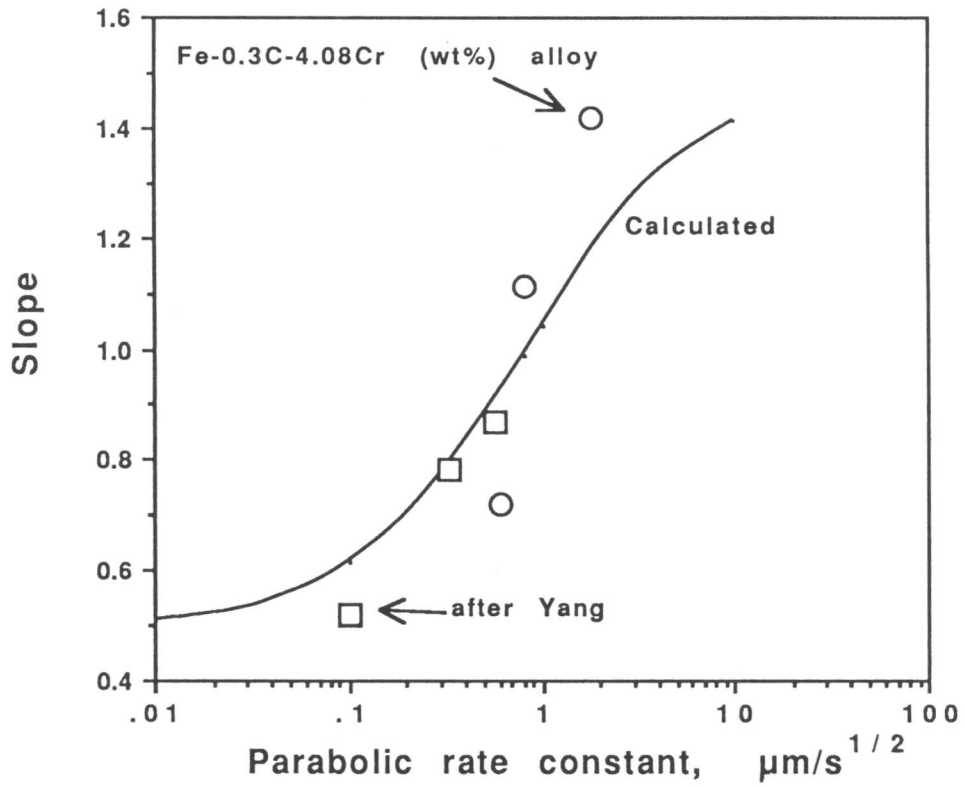
Fig. 8.6 Comparison between observed and calculated slopes of the plot of $\log\{-\ln\{1-\xi\}\}$ against $\log\{t\}$.
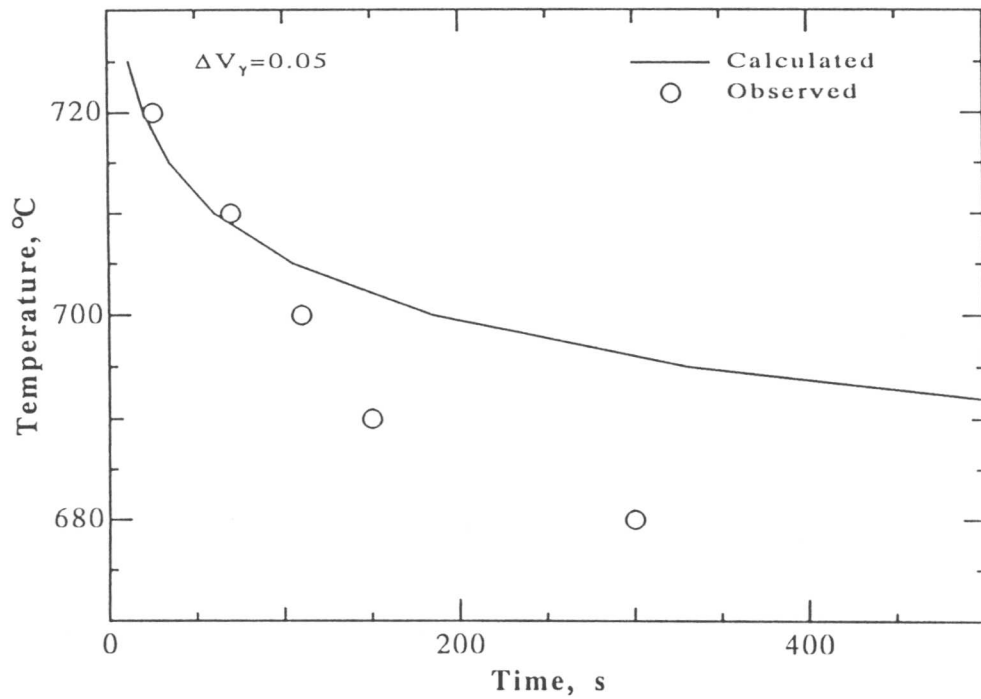
Fig. 8.7 Comparison between calculated (line) and observed (plots [4]) TTT curves for reausteniti-sation from the mixture of bainite and austenite in the Fe-C-Mn-Ni-Mo alloy.
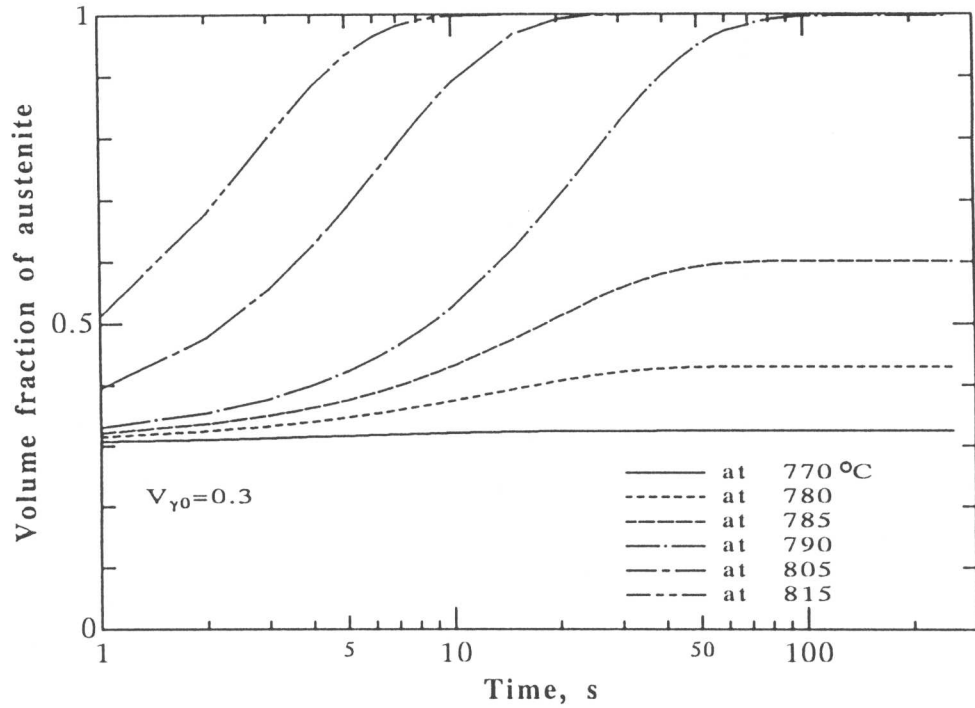
Fig. 8.8 Calculated reaustenitisation behaviour showing the effect of the reaction temperature on the kinetics of reaustenitisation.
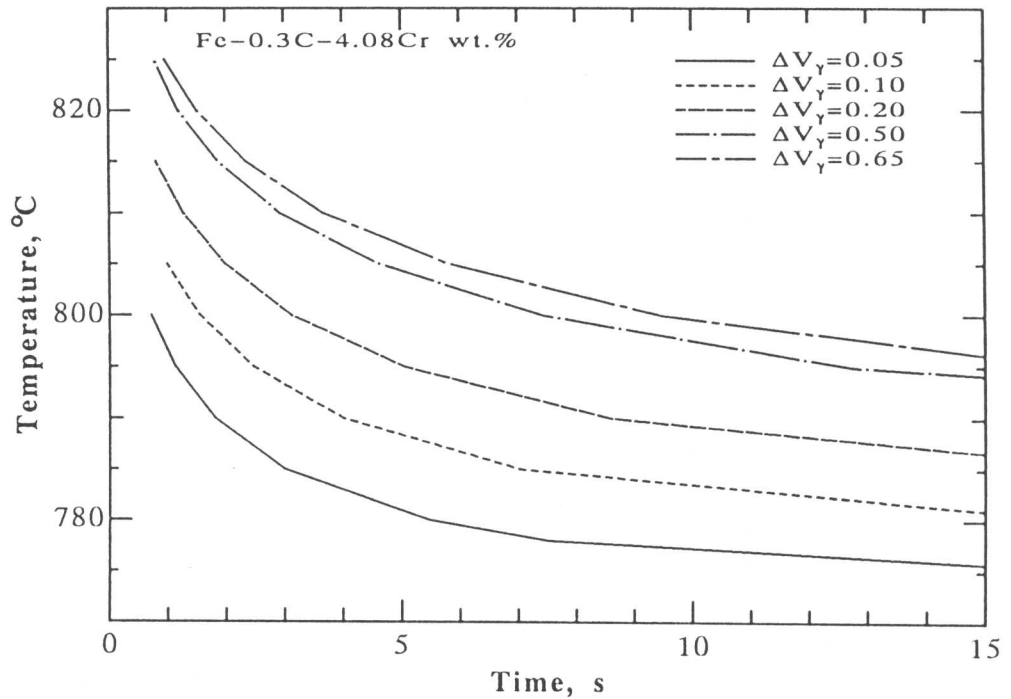
Fig. 8.9 Calculated TTT curves for $\Delta V_\gamma = 0.05$, 0.10, 0.20, 0.50 and 0.65 of reaustenitisation from the bainite + 30% of austenite obtained at 420 °C in the Fe-0.3C-4.08Cr wt.% alloy.
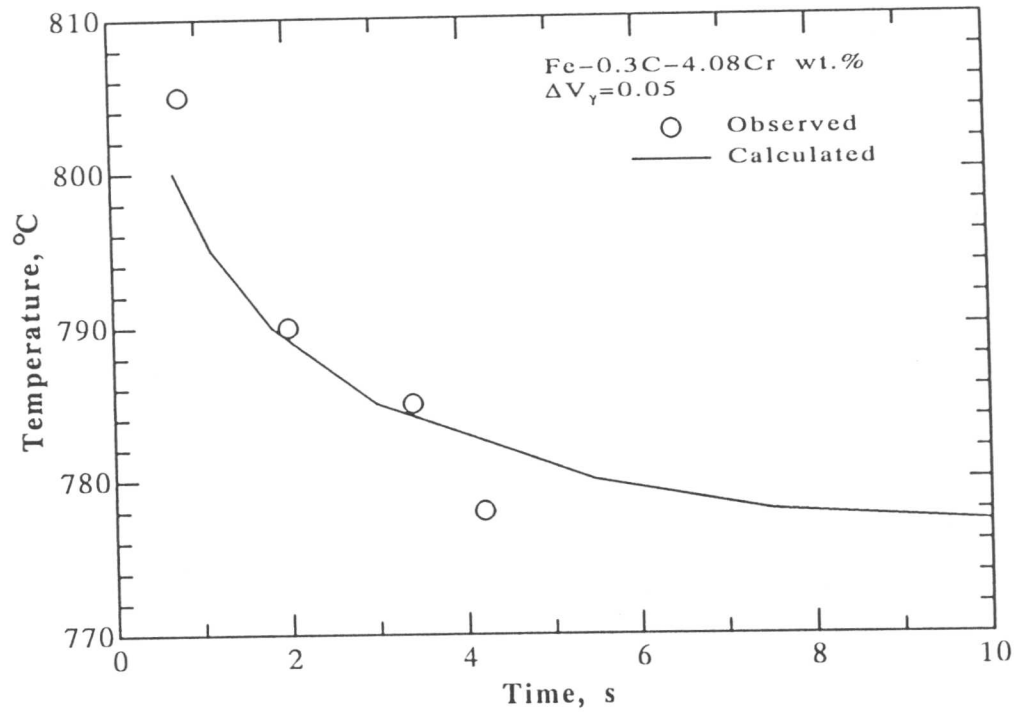
Fig. 8.10 Comparison between calculated (line) and observed (plots) TTT curves for $\Delta V_\gamma = 0.05$ from the mixture of bainite and austenite obtained at 420 °C in the Fe-0.3C-4.08Cr wt.% alloy.
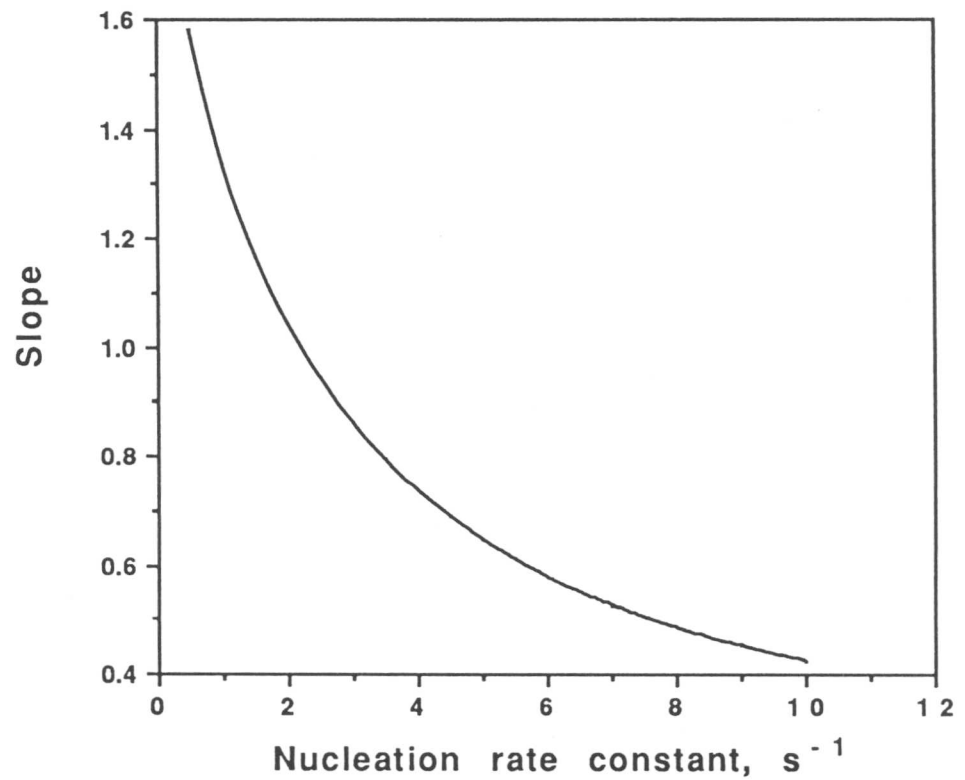
Fig. 8.11 Change in the slope of the plot of $\log\{-\ln\{1-\xi\}\}$ against $\log\{t\}$ with the nucleation rate constant ν_1.
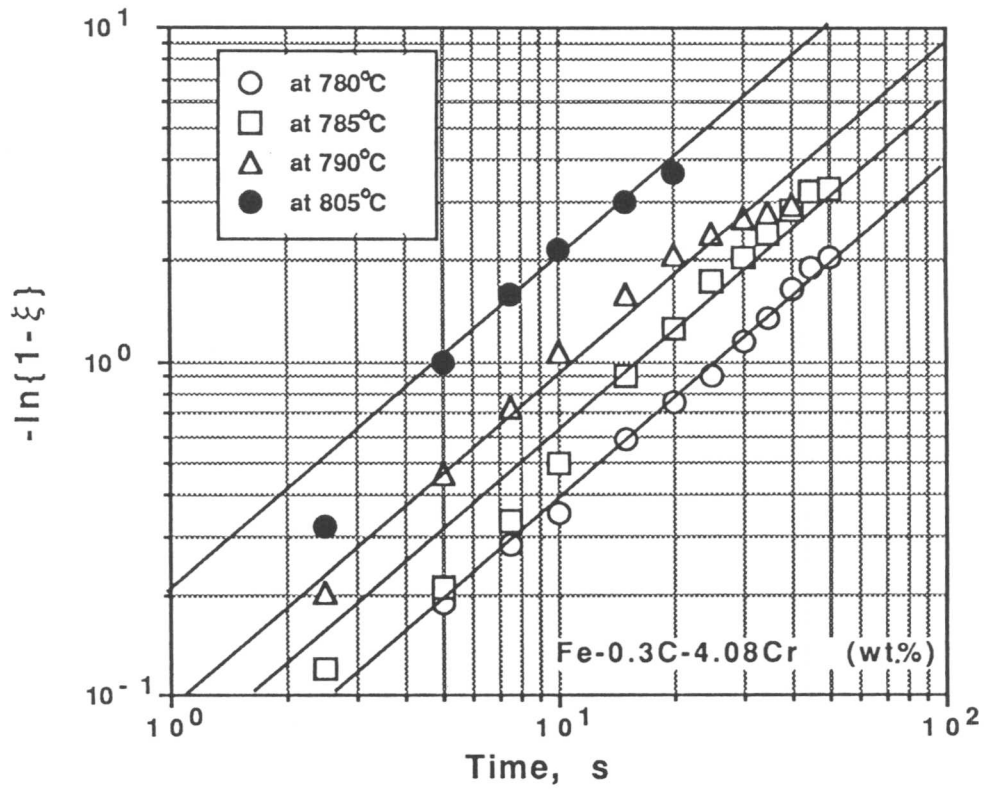
Fig. 8.12 $\log\{-\ln\{1-\xi\}\}$ v.s. $\log\{t\}$ plots for reaustenitisation from martensitic initial microstructure in the Fe-0.3C-4.08Cr wt.% alloy.
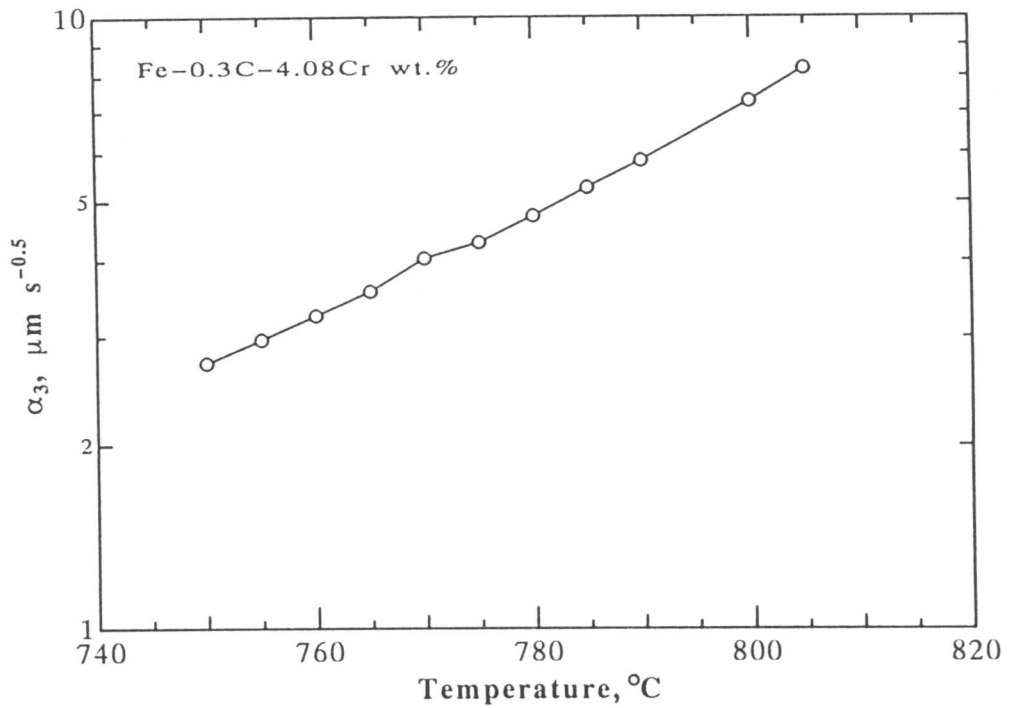
Fig. 8.13 Calculated three-dimensional parabolic rate constant α_3 of austenite formed in a carbon supersaturated ferrite matrix whose carbon concentration is the same as the paraequilibrium carbon concentration at 500°C.

Fe−0.3C−4.08Cr wt.%
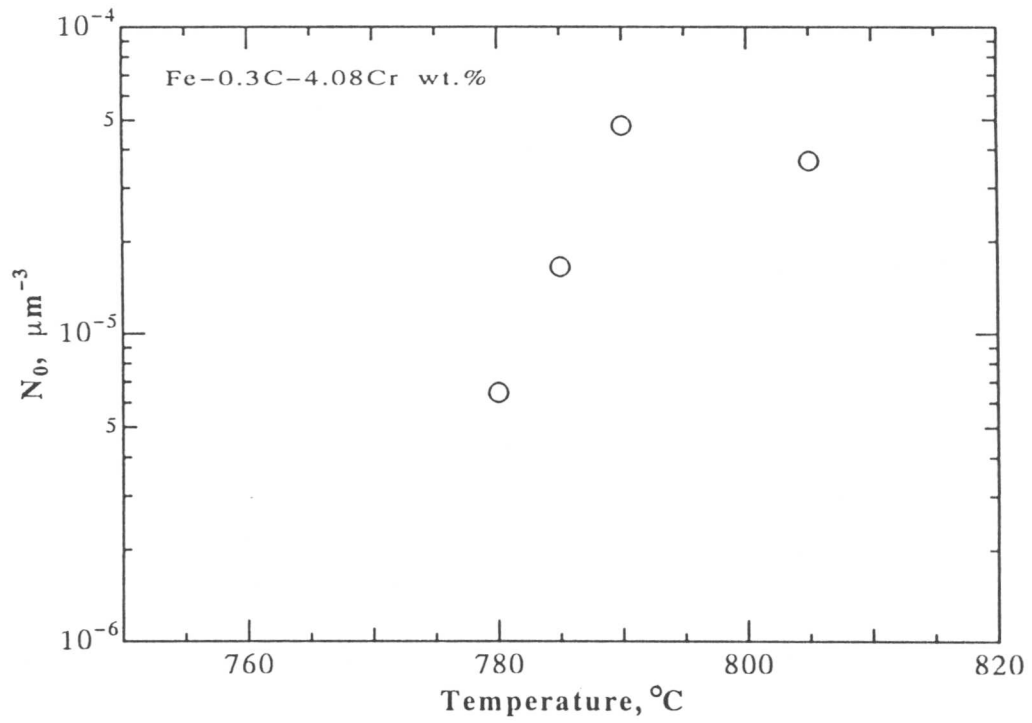
Fig. 8.14 Change in the initial nucleation site density for reaustenitisation N_0 from martensitic initial microstructure with temperature.
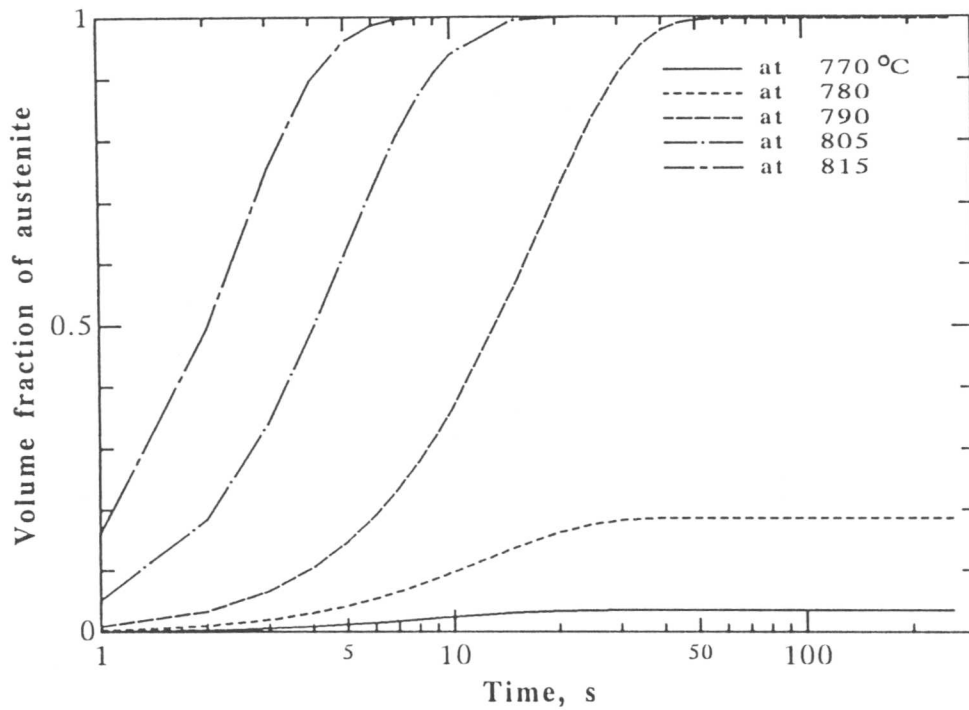
Fig. 8.15 Calculated isothermal reaustenitisation from martensitic initial microstructure.

CHAPTER 9

FURTHER WORK

The ultimate goal of this work is to develop a complete computer model which enables the calculation of microstructural development during austenitisation as a function of alloy chemistry and starting microstructure. Such a model would form a powerful combination with an appropriate computer model for the decomposition of austenite to transformation products such as allotriomorphic ferrite, pearlite, Widmanstätten ferrite, acicular ferrite, bainite and martensite. A grand scheme like this could be applied to a variety of engineering applications, and for the optimisation of material and process designs. Although this final goal is still out of reach, the work presented in this thesis shows that substantial progress can be made for the formation of austenite from well defined initial microstructures.

Since the general problem of austenite formation is strongly dependent on the initial microstructure, it is essential to understand the decomposition products of austenite in steels. The models developed in chapter 2, 3 and 5 illustrate how the details of the mechanism of the bainite and pearlite transformation allow the formation of austenite to be characterised theoretically. It is, however, important to take into account the effect of nucleation if these models are ever to be capable of generally useful application. The diffusional growth theory discussed in chapter 7 can be combined with any nucleation theories which may be developed in the future.

Apart from nucleation theory, the major problems highlighted by the present work, and which need further research are as follows:

1) It is necessary to be able to model the dissolution/precipitation of carbides during austenite formation and during heating to the test temperature.

2) It is convenient to assume that conditions of local equilibrium or paraequilibrium exist at the transformation interface. However, non-equilibrium growth in which none of the elements achieve equality of chemical potential, is also possible and needs to be investigated. In fact, it would be very useful to experimentally investigate the conditions at the transformation interface using an atom-probe.

COMPUTER PROGRAMS

```
C Program for the calculation of the time required to decarburise a plate of bainitic ferrite and time for
C a certain amount of cementite.
C
C Typical dataset:
C 1  No. of alloys,
C 0.2 (C) 0.2 (Si) 0.3 (Mn) 0.4(Ni) 0.5(Mo) 0.6 (Cr) 0.1 (V) wt.%
C
      IMPLICIT REAL*8(A-H,K-Y), INTEGER(I,J,Z)
      DOUBLE PRECISION DIFF(300),CARB(300),C(8),ATIME(40),ATEMP(40)
C HH=PLANCKS CONST.JOULES/SEC,KK=BOLTZMANNS CONST.JOULES/DEGREE KELVIN
C   D=DIFFUSIVITY OF CARBON IN AUSTENITE
C   Z=COORDINATION OF INTERSTIAL SITE
C   TIME=Time to decarburise a plate of ferrite, seconds
C   THICK= thickness of ferrite plate, meters
C   PSI=COMPOSITION DEPENDENCE OF DIFFUSION COEFFICIENT
C   THETA=NO. C ATOMS/ NO. FE ATOMS
C   ACTIV=ACTIVITY OF CARBON IN AUSTENITE
C   R=GAS CONSTANT
C   X=MOLE FRACTION OF CARBON
C   T=ABSOLUTE TEMPERATURE
C   SIGMA=SITE EXCLUSION PROBABLITY
C   W=CARBON CARBON INTERACTION ENERGY IN AUSTENITE
C   IJK1 gives the number of steels, I6 the number of data points
C
      HH=6.6262D-34
      KK=1.38062D-23
      READ(5,*) IJK1
      DO 1008 II22=1,IJK1
      CALL OMEGA0(W,XBAR,C)
      Z=12
      A5=1.0D+00
      R=8.31432D+00
      RADIUS=0.0
      VMAX=0.0
      M1=0.00
      I6=12
      DO 222 I7=1,I6
       T=50.0D+00*I7+50.0D+00
      THICK=0.2D-06
      CTEMP=T
      STRAIN=400.0D+00
      CALL AA3(C,CTEMP,XMAX,STRAIN)
       T=T+273.00D+00
      II2=0
      ICRIT=0
      XALPHA=XALPH(T)
      A6=(XMAX-XBAR)/290.0D+00
      IF(A6 .LT. 0.0D+00) GOTO 222
      DASH=(KK*T/HH)*DEXP(-(21230.0D+00/T))*DEXP(-31.84D+00)
      DO 999 II=1,300
      CARB(1)=XBAR
      IF (II .GT. 1)GOTO 1000
      GOTO 1001
1000  CARB(II)=CARB(II-1)+A6
      IF (CARB(II) .GT. XMAX) GOTO 1002
1001  X=CARB(II)
      II2=II2+1
      THETA=X/(A5-X)
      ACTIV=CG(X,T,W,R)
      ACTIV=DEXP(ACTIV)
      DACTIV=DCG(X,T,W,R)
      DACTIV=DACTIV*ACTIV
      DACTIV=DACTIV*A5/((A5+THETA)**2)
      SIGMA=A5-DEXP((-(W))/(R*T))
      PSI=ACTIV*(A5+Z*((A5+THETA)/(A5-(A5+Z/2)*THETA+(Z/2)*(A5+Z/2)*
     &(A5-SIGMA)*THETA*THETA)))+(A5+THETA)*DACTIV
      DIFF(II)=DASH*PSI
      IF(DIFF(II) .LE. 0.0D+00 .AND. ICRIT .EQ. 0) THEN
       ICRIT=II
      ENDIF
999   CONTINUE
1002  IF(ICRIT .EQ. 0) GOTO 1012
      DO 1333 I=1,II2
       IF(I .LT. ICRIT-10) GOTO 1333
```

```
        DIFF(I)=DIFF(ICRIT-10)
1333 CONTINUE
1012 II3=0
     CALL D01GAF(CARB,DIFF,II2,ANS,ERROR,II3)
     ANS=ANS*1.0D-04/(XMAX-XBAR)
     TIME=(THICK*(XBAR-XALPHA)*DSQRT(3.14159D+00)/(4.0D+00
    &*ANS**0.5*(XMAX-XBAR)))**2.0D+00
     ATIME(I7)=TIME
     ATEMP(I7)=CTEMP
222 CONTINUE
     WRITE(6,*)'  TEMP     td,s      t0.01',
    &'   t0.02    t0.05    t0.10    t0.50'
     DO 3 JJJ=1,40
     IF(ATEMP(JJJ) .EQ. 0) GOTO 3
     TC001=TC(ATEMP(JJJ),C,0.01D+00)
     TC002=TC(ATEMP(JJJ),C,0.02D+00)
     TC005=TC(ATEMP(JJJ),C,0.05D+00)
     TC010=TC(ATEMP(JJJ),C,0.10D+00)
     TC050=TC(ATEMP(JJJ),C,0.50D+00)
      WRITE(6,4) ATEMP(JJJ),ATIME(JJJ),TC001,TC002,TC005,TC010,TC050
     ATIME(JJJ)=0.0D+00
     ATEMP(JJJ)=0.0D+00
4    FORMAT(1H ,F8.2,6D12.4)
3    CONTINUE
1008 CONTINUE
     END
C
C----------------------------------------------------------------
     SUBROUTINE OMEGA0(W,XBAR,D)
C SUBROUTINE TO CALCULATE THE CARBON CARBON INTERACTION ENERGY IN
C AUSTENITE, AS A FUNCTION OF ALLOY COMPOSITION.  BASED ON .MUCG18
C THE ANSWER IS IN JOULES PER MOL.  **7 OCTOBER 1981**
     DOUBLE PRECISION C(8),D(8),W,P(8),B1,B2,Y(8),T10,T20,B3,XBAR
     INTEGER B5,I,U,B4
     READ (5,*) C(1),C(2),C(3),C(4),C(5),C(6),C(7)
     D(1)=C(1)
     D(2)=C(2)
     D(3)=C(3)
     D(4)=C(4)
     D(5)=C(5)
     D(6)=C(6)
     D(7)=C(7)
     D(8)=100.0-C(1)-C(2)-C(3)-C(4)-C(5)-C(6)-C(7)
     WRITE(6,*)''
     WRITE(6,261) (C(B4),B4=1,7)
     B3=0.0D+00
     C(8)=C(1)+C(2)+C(3)+C(4)+C(5)+C(6)+C(7)
     C(8)=100.0D+00-C(8)
     C(8)=C(8)/55.84D+00
     C(1)=C(1)/12.0115D+00
     C(2)=C(2)/28.09D+00
     C(3)=C(3)/54.94D+00
     C(4)=C(4)/58.71D+00
     C(5)=C(5)/95.94D+00
     C(6)=C(6)/52.0D+00
     C(7)=C(7)/50.94D+00
     B1=C(1)+C(2)+C(3)+C(4)+C(5)+C(6)+C(7)+C(8)
     DO 107 U=2,7
     Y(U)=C(U)/C(8)
107 CONTINUE
     DO 106 U=1,8
     C(U)=C(U)/B1
106 CONTINUE
     XBAR=C(1)
     XBAR=DINT(10000.0D+00*XBAR)
     XBAR=XBAR/10000
     B2=0.0D+00
     T10=Y(2)*(-3)+Y(3)*2+Y(4)*12+Y(5)*(-9)+Y(6)*(-1)+Y(7)*(-12)
     T20=-3*Y(2)-37.5*Y(3)-6*Y(4)-26*Y(5)-19*Y(6)-44*Y(7)
       P(2)=2013.0341+763.8167*C(2)+45802.87*C(2)**2-280061.63*C(2)**3
      &+3.864D+06*C(2)**4-2.4233D+07*C(2)**5+6.9547D+07*C(2)**6
       P(3)=2012.067-1764.095*C(3)+6287.52*C(3)**2-21647.96*C(3)**3-
      &2.0119D+06*C(3)**4+3.1716D+07*C(3)**5-1.3885D+08*C(3)**6
       P(4)=2006.8017+2330.2424*C(4)-54915.32*C(4)**2+1.6216D+06*C(4)**3
```

```fortran
     &-2.4968D+07*C(4)**4+1.8838D+08*C(4)**5-5.5531D+08*C(4)**6
      P(5)=2006.834-2997.314*C(5)-37906.61*C(5)**2+1.0328D+06*C(5)**3
     &-1.3306D+07*C(5)**4+8.411D+07*C(5)**5-2.0826D+08*C(5)**6
      P(6)=2012.367-9224.2655*C(6)+33657.8*C(6)**2-566827.83*C(6)**3
     &+8.5676D+06*C(6)**4-6.7482D+07*C(6)**5 +2.0837D+08*C(6)**6
      P(7)=2011.9996-6247.9118*C(7)+5411.7566*C(7)**2
     &+250118.1085*C(7)**3-4.1676D+06*C(7)**4
      DO 108 U=2,7
      B3=B3+P(U)*Y(U)
      B2=B2+Y(U)
108  CONTINUE
      IF (B2 .EQ. 0.0D+00) GOTO 455
      W=(B3/B2)*4.187
      GOTO 456
455   W=8054.0
456   WRITE (6,261)(C(B4),B4=1,7)
261   FORMAT (4H  C=,F6.4,4H SI=,F6.4,4H MN=,F6.4,
     &4H NI=,F6.4,4H MO=,F6.4,4H CR=,F6.4,4H  V=,F6.4)
      RETURN
      END
C
C-------------------------------------------------------------
      SUBROUTINE AA3(CW,AE3T,XEQ,STRAIN)
C AE3T is read in centigrade
C Matrix C represents chemical composition in weight percent
C STRAIN is in Joules per mole
C XEQ is the paraequilibrium carbon concentration in gamma at AE3T
C
      DOUBLE PRECISION X,X1,T,R,A,A1,AFE,A1FE,DA1,DA2,DA1FE,H,H1,S,S1
      INTEGER T1,I,NO,U,B4,J99,C99
      DOUBLE PRECISION D11,STRAIN
     1DEQ,ETEQ,T10,T20,XA,AFEQ,AEQ,ETEQ2,TEQ,
     1J,J1,D,D1,W,W1,F,TEST,ERROR,T4,XEQ,FPRO
     1,C(8),B1,B2,P(7),Y(7),B3,AE3T,CW(8),Z
      Z=0.0D+00
      DO 104 I=1,7
      C(I)=CW(I)
      Z=Z+CW(I)
104  CONTINUE
      CW(8)=100.0D+00-Z
      B3=0.0D+00
      C(8)=(100.0-C(1)-C(2)-C(3)-C(4)-C(5)-C(6)-(C7))/55.84
      C(1)=C(1)/12.0115
      C(2)=C(2)/28.09
      C(3)=C(3)/54.94
      C(4)=C(4)/58.71
      C(5)=C(5)/95.94
      C(6)=C(6)/52.0
      C(7)=C(7)/50.94
      B1=C(1)+C(2)+C(3)+C(4)+C(5)+C(6)+C(7)+C(8)
      DO 107 U=2,7
      Y(U)=C(U)/C(8)
107  CONTINUE
      DO 106 U=1,7
      C(U)=C(U)/B1
106  CONTINUE
      B2=0.0
      T10=Y(2)*(-3)+Y(3)*2+Y(4)*12+Y(5)*(-9)+Y(6)*(-1)+Y(7)*(-12)
      T20=-3*Y(2)-37.5*Y(3)-6*Y(4)-26*Y(5)-19*Y(6)-44*Y(7)
      P(2)=2013.0341+763.8167*C(2)+45802.87*C(2)**2-280061.63*C(2)**3
     1+3.864D+06*C(2)**4-2.4233D+07*C(2)**5+6.9547D+07*C(2)**6
      P(3)=2012.067-1764.095*C(3)+6287.52*C(3)**2-21647.96*C(3)**3-
     12.0119D+06*C(3)**4+3.1716D+07*C(3)**5-1.3885D+08*C(3)**6
      P(4)=2006.8017+2330.2424*C(4)-54915.32*C(4)**2+1.6216D+06*C(4)**3
     1-2.4968D+07*C(4)**4+1.8838D+08*C(4)**5-5.5531D+08*C(4)**6
      P(5)=2006.834-2997.314*C(5)-37906.61*C(5)**2+1.0328D+06*C(5)**3
     1-1.3306D+07*C(5)**4+8.411D+07*C(5)**5-2.0826D+08*C(5)**6
      P(6)=2012.367-9224.2655*C(6)+33657.8*C(6)**2-566827.83*C(6)**3
     1+8.5676D+06*C(6)**4-6.7482D+07*C(6)**5 +2.0837D+08*C(6)**6
      P(7)=2011.9996-6247.9118*C(7)+5411.7566*C(7)**2
     1+250118.1085*C(7)**3-4.1676D+06*C(7)**4
      DO 108 U=2,7
      B3=B3+P(U)*Y(U)
      B2=B2+Y(U)
```

```fortran
108  CONTINUE
     IF(B2 .EQ. 0.0) GOTO 455
     W=(B3/B2)*4.187
     GOTO 456
455  W=8054.0
456  CONTINUE
     X1=C(1)
     R=8.31432
     W1=48570.0
     H=38575.0
     S=13.48
201  XEQ=0.1
     T=AE3T+273.0
     IF (T .LE. 1000) GOTO 20
     H1=105525
     S1=45.34521
     GOTO 19
20   H1=111918
     S1=51.44
19   F=ENERGY(T,T10,T20)+STRAIN
     J=1-DEXP(-W/(R*T))
51   DEQ=DSQRT(1-2*(1+2*J)*XEQ+(1+8*J)*XEQ*XEQ)
     TEQ=5*DLOG((1-XEQ)/(1-2*XEQ))
     TEQ=TEQ+DLOG(((1-2*J+(4*J-1)*XEQ-DEQ)/(2*J*(2*XEQ-1)))**6)
     TEQ=TEQ*R*T-F
     IF (DABS(TEQ) .LT. 1.0) GOTO 50
     ETEQ=5*((1/(XEQ-1))+2/(1-2*XEQ))
     ETEQ2=6*((4*J-1-(0.5/DEQ)*(-2-4*J+2*XEQ+16*XEQ*J))/(1-2*J+(4*J
    1-1)*XEQ-DEQ))+6*(4*J/(2*J*(2*XEQ-1)))
     ETEQ=(ETEQ+ETEQ2)*R*T
     XEQ=XEQ-TEQ/ETEQ
     GOTO 51
50   IF (XEQ .LT. 0.001) GOTO 2444
2444 CONTINUE
802  RETURN
     END
C
C----------------------------------------------------------------
     DOUBLE PRECISION FUNCTION TC(T,C,X)
     DOUBLE PRECISION K, Q, R, T, K0, N, C, X, TT
     INTEGER I
     R=1.987D+00
     Q=8030.0D+00
     K0=36.2D+00*C**0.635
     N=0.62D+00
     TT=T+273.0D+00
     K=K0*DEXP(-Q/R/TT)
     TC=(-DLOG(1.0D+00-X)/K)**(1.0D+00/N)
     RETURN
     END
C----------------------------------------------------------------
```

```
C Program to calculate the parabolic thickening rate constants
C (1, 2, and 3 dimensional) and the time required to obtain a certain
C amount of cementite ignoring the effect of nucleation of cementite.
C
C 25 October 1988
C
C Typical data set
C  0.1 (C) 0.2 (Si) 0.2 (Mn) 0.2 (Ni) 0.2 (Mo) 0.2 (Cr) 0.1 (V)
C  420 --- temperature in deg. C
C  500
C
C
      IMPLICIT REAL*8(A-H,K-Y), INTEGER(I,J,Z)
      DOUBLE PRECISION S13AAF,CTEMP,T,XALPHA,XGAG,T5,DIFF,B0,B1,B2,A2,DIS
     &,DIFF0,T50
      EXTERNAL S13AAF
      CALL OMEGA(W,XONE)
1     READ (5,*, END=2) CTEMP
      T=CTEMP+273.0D0
      XALPHA=0.0D0
      XGAG=0.25
        B0=9.28480435985404817D+00
        B1=6880.73079777086696D+00
        B2=-1780359.64568034932D+00
        DIFF0=4.0D-3*DEXP(-19200.0D0/1.987D0/T)*1.0D-04
      DIFF=DF(T)
      CALL AL(XONE,XALPHA,XGAG,DIFF0,CTEMP,ALPHA)
      A2=1.0D+00/ALPHA**2
      DIS=B0+B1/T+B2/T/T
      DIS=10.0D0**DIS
      WRITE(6,*) 'DISLOCATION DENS., M**-2  = ',DIS
      WRITE(6,*) 'DIFFUSION COEFF.H, M**2/S = ',DIFF
      WRITE(6,*) 'DIFFUSION COEFF.E, M**2/S = ',DIFF0
      VE=1.037D-03*XONE
      DIS0=10.0D-06
      T5=(0.05D0*VE/(DIS/DIS0*9.0*ALPHA*ALPHA*ALPHA))**(2.0/3.0)
      T50=(0.5D0*VE/(DIS/DIS0*9.0*ALPHA*ALPHA*ALPHA))**(2.0/3.0)
      WRITE(6,*)' TEMP    ALPHA    1/ALPHA**2'
     &,'  t(0.05)    t(0.5)'
      WRITE(6,1229) CTEMP, ALPHA, A2, T5, T50
      WRITE(6,*) ''
1229  FORMAT(F8.1,4D12.4)
      GOTO 1
2     STOP
      END
C***********************************************************************
C FUNCTION GIVING V0
      DOUBLE PRECISION FUNCTION V0(T,ALPHA)
      HLEN=10.0D-04
      HWID=0.2D-04
      BETA=3.0D+00*ALPHA
      V0=0.05-(((2*BETA/HLEN)+(ALPHA/HWID))*T**0.5 -
     &((BETA/HLEN)**2 + 2*ALPHA*ALPHA/(HLEN*HWID))*T +
     & ALPHA*BETA*BETA*T**1.5/(HLEN*HLEN*HWID))
      RETURN
      END
C***********************************************************************
C FUNCTION GIVING LFG  LN(ACTIVITY) OF CARBON IN AUSTENITE
      DOUBLE PRECISION FUNCTION CG(X,T,W,R)
      DOUBLE PRECISION J,DG,DUMMY,T,R,W,X
      J=1-DEXP(-W/(R*T))
      DG=DSQRT(1-2*(1+2*J)*X+(1+8*J)*X*X)
      DUMMY=5*DLOG((1-2*X)/X)+6*W/(R*T)+((38575.0)-(
     &13.48)*T)/(R*T)
      CG=DUMMY+DLOG((((DG-1+3*X)/(DG+1-3*X))**6)
      RETURN
      END
C***********************************************************************
C FUNCTION GIVING DIFFERENTIAL OF LN(ACTIVITY) OF CARBON IN AUSTENITE, LFG
C DIFFERENTIAL IS WITH RESPECT TO X
      DOUBLE PRECISION FUNCTION DCG(X,T,W,R)
      DOUBLE PRECISION J,DG,DDG,X,T,W,R
      J=1-DEXP(-W/(R*T))
      DG=DSQRT(1-2*(1+2*J)*X+(1+8*J)*X*X)
```

```fortran
      DDG=(0.5/DG)*(-2-4*J+2*X+16*J*X)
      DCG=-((10/(1-2*X))+(5/X))+6*((DDG+3)/(DG-1+3*X
     &)-(DDG-3)/(DG+1-3*X))
      RETURN
      END
C*****************************************************************************
      SUBROUTINE OMEGA(W,XONE)
C SUBROUTINE TO CALCULATE THE CARBON CARBON INTERACTION ENERGY IN
C AUSTENITE, AS A FUNCTION OF ALLOY COMPOSITION.  BASED ON .MUCG18
C THE ANSWER IS IN JOULES PER MOL.  **7 OCTOBER 1981**
      DOUBLE PRECISION C(8),W,P(8),B1,B2,Y(8),T10,T20,B3,XONE
      INTEGER B5,I,U,B4
      READ (5,*) C(1),C(2),C(3),C(4),C(5),C(6),C(7)
      WRITE(6,261) (C(B4),B4=1,7)
      B3=0.0D+00
      C(8)=C(1)+C(2)+C(3)+C(4)+C(5)+C(6)+C(7)
      C(8)=100.0D+00-C(8)
      C(8)=C(8)/55.84D+00
      C(1)=C(1)/12.0115D+00
      C(2)=C(2)/28.09D+00
      C(3)=C(3)/54.94D+00
      C(4)=C(4)/58.71D+00
      C(5)=C(5)/95.94D+00
      C(6)=C(6)/52.0D+00
      C(7)=C(7)/50.94D+00
      B1=C(1)+C(2)+C(3)+C(4)+C(5)+C(6)+C(7)+C(8)
      DO 107 U=2,7
      Y(U)=C(U)/C(8)
107   CONTINUE
      DO 106 U=1,8
      C(U)=C(U)/B1
106   CONTINUE
      XONE=C(1)
      XONE=DINT(10000.0D+00*XONE)
      XONE=XONE/10000
      B2=0.0D+00
      T10=Y(2)*(-3)+Y(3)*2+Y(4)*12+Y(5)*(-9)+Y(6)*(-1)+Y(7)*(-12)
      T20=-3*Y(2)-37.5*Y(3)-6*Y(4)-26*Y(5)-19*Y(6)-44*Y(7)
      P(2)=2013.0341+763.8167*C(2)+45802.87*C(2)**2-280061.63*C(2)**3
     &+3.864D+06*C(2)**4-2.4233D+07*C(2)**5+6.9547D+07*C(2)**6
      P(3)=2012.067-1764.095*C(3)+6287.52*C(3)**2-21647.96*C(3)**3-
     &2.0119D+06*C(3)**4+3.1716D+07*C(3)**5-1.3885D+08*C(3)**6
      P(4)=2006.8017+2330.2424*C(4)-54915.32*C(4)**2+1.6216D+06*C(4)**3
     &-2.4968D+07*C(4)**4+1.8838D+08*C(4)**5-5.5531D+08*C(4)**6
      P(5)=2006.834-2997.314*C(5)-37906.61*C(5)**2+1.0328D+06*C(5)**3
     &-1.3306D+07*C(5)**4+8.411D+07*C(5)**5-2.0826D+08*C(5)**6
      P(6)=2012.367-9224.2655*C(6)+33657.8*C(6)**2-566827.83*C(6)**3
     &+8.5676D+06*C(6)**4-6.7482D+07*C(6)**5 +2.0837D+08*C(6)**6
      P(7)=2011.9996-6247.9118*C(7)+5411.7566*C(7)**2
     &+250118.1085*C(7)**3-4.1676D+06*C(7)**4
      DO 108 U=2,7
      B3=B3+P(U)*Y(U)
      B2=B2+Y(U)
108   CONTINUE
      IF (B2 .EQ. 0.0D+00) GOTO 455
      W=(B3/B2)*4.187
      GOTO 456
455   W=8054.0
456   WRITE (6,261)(C(B4),B4=1,7)
      WRITE(6,1006)W
1006  FORMAT(' CARBON-CARBON INTERACTION ENERGY IN GAMMA, J/MOL=',F9.4)
261   FORMAT (4H C=,F6.4,4H SI=,F6.4,4H MN=,F6.4,
     &4H NI=,F6.4,4H MO=,F6.4,4H CR=,F6.4,4H  V=,F6.4)
      RETURN
      END
C     *****************************************************************************
C FUNCTION GIVING THE EQUILIBRIUM MOL.FRAC. CARBON IN ALPHA
C BASED ON MY PAPER ON FIRST ORDER QUASICHEMICAL THEORY,METSCI
      DOUBLE PRECISION FUNCTION XALPH(T)
      DOUBLE PRECISION T,CTEMP
      CTEMP=(T-273.0D+00)/900.0D+00
      XALPH=0.1528D-02-0.8816D-02*CTEMP+0.2450D-01*CTEMP*CTEMP
     &-0.2417D-01*CTEMP*CTEMP*CTEMP+
     &0.6966D-02*CTEMP*CTEMP*CTEMP*CTEMP
```

```fortran
      RETURN
      END
C*************************************************************************
C********************************************************
      SUBROUTINE AL(XGAG,XAGA,XONE,DIFF,CTEMP,ALPHA)
      DOUBLE PRECISION DIFF,ALPHA,XAGA,XGAG,XONE,CTEMP,DUMMY1
     &,DER,FUN2,ALPH,DUMMY2,DUMMY3
      III=0
      ALPHA=DSQRT(DIFF)
      DUMMY2=ALPHA
C ABOVE IS A GUESSED VALUE OF ALPHA
4     CALL FUNN(DUMMY1,ALPHA,XGAG,XONE,XAGA,DIFF,CTEMP)
      III=III+1
C     WRITE(6,20)ALPHA,DUMMY1,DER
46    IF(III .GT. 100) GOTO 3
      IF (DABS(DUMMY1) .GT. 0.0001D-06) GOTO 2
      GOTO 3
20    FORMAT(3D12.4)
2     DUMMY2=DUMMY1
      ALPH=ALPHA*1.00000001D+00
      CALL FUNN(FUN2,ALPH,XGAG,XONE,XAGA,DIFF,CTEMP)
      DER=(DUMMY1-FUN2)/(ALPHA-ALPH)
      ALPHA=ALPHA-(DUMMY1/DER)*0.5D0
      GOTO 4
3     WRITE(6,23)CTEMP, ALPHA,DUMMY1
      WRITE(6,*) 'ALPHA/SQRT.DIFF = ',(ALPHA/DSQRT(DIFF))
23    FORMAT(' CTEMP=',F8.2,'   ALPHA (M PER SEC**.5)=',D12.5,
     &' DUMMY1=',D12.5)
      WRITE(6,*) 'Fi= ', ((XGAG-XAGA)/(XONE-XAGA))
      RETURN
      END
C*************************************************************************
      SUBROUTINE FUNN(FUN,ALPHA,XGAG,XONE,XAGA,DIFF,CTEMP)
C 'FUN' COMPUTES EQ.2 OF KINSMAN AND AARONSONS TRANSFORMATION AND
C HARDENABILITY PAPER.  DIFF=INTEGRATED AVERAGE DIFFUSIVITY OF C IN
C GAMMA, ALPHA = PARABOLIC RATE CONSTANT.
      DOUBLE PRECISION DIFF,ALPHA,XAGA,XGAG,XONE,FUN
      FUN=DSQRT(3.141593D+00/DIFF)/2.0D+00
      FUN=FUN*ALPHA*DEXP(ALPHA*ALPHA/(4.0D+00*DIFF))
      FUN=FUN*(1.0D+00-DERF(ALPHA/(2.0D+00*DSQRT(DIFF))))
      FUN=(XGAG-XAGA)/(XONE-XAGA)-FUN
      RETURN
      END
C*************************************************************************
      SUBROUTINE FUNN1(FUN,ALPHA,XGAG,XONE,XAGA,DIFF,CTEMP)
      DOUBLE PRECISION DIFF,ALPHA,XAGA,XGAG,XONE,FUN
     &,S13AAF
      EXTERNAL S13AAF
      FUN=ALPHA*ALPHA/4.0D+00/DIFF*DEXP(ALPHA*ALPHA/(4.0D+00*DIFF))
      FUN=FUN*S13AAF(ALPHA*ALPHA/(4.0D+00*DIFF), 0)
      FUN=(XGAG-XAGA)/(XONE-XAGA)-FUN
      RETURN
      END
C*************************************************************************
      SUBROUTINE FUNN2(FUN,ALPHA,XGAG,XONE,XAGA,DIFF,CTEMP)
      DOUBLE PRECISION DIFF,ALPHA,XAGA,XGAG,XONE,FUN
      FUN=ALPHA*ALPHA/(2.0D+00*DIFF)*(1.0D+00-DSQRT(3.141592D+00/DIFF)*
     &ALPHA/2.0D+00*DEXP(ALPHA*ALPHA/(4.0D+00*DIFF))
     &*(1.0D+00-DERF(ALPHA/(2.0D+00*DSQRT(DIFF)))))
      FUN=(XGAG-XAGA)/(XONE-XAGA)-FUN
      RETURN
      END
C*************************************************************************
      DOUBLE PRECISION FUNCTION DF(KTEMP)
      DOUBLE PRECISION R,KTEMP,PHI,DOTO,DTT,F
      R=8.3143D+00
      PHI=1.0D+00-1.0/(0.5D+00*DEXP(7.2D+03*4.184/(R*KTEMP))
     &*DEXP(4.4D+00)+1.0D+00)
      DOTO=3.3D-07*DEXP(-19.3D+03*4.184D+00/(R*KTEMP))
      DTT=3.0D-04*DEXP(-14.7D+03*4.184D+00/(R*KTEMP))
      F=0.86D+00
      DF=PHI*DOTO+(1.0D+00-PHI)*F*DTT+(1.0D+00-PHI)
     &*(1.0D+00-F)*DOTO
C DIFFUSION OF CARBON IN FERRITE, M*M/S
```

```
C MCLELLAN ET AL., TRANS. MET. SOC. AIME, VOL.233 (1965) 1938
C R = UNIVERSAL GAS CONSTANT, J/MOL/K
C KTEMP = ABSOLUTE TEMPERATURE
   RETURN
   END
C
C*************************************************************************
```

```fortran
C    FTVSCLR PROGRAM=%H% DATA=&D NAG
C Program to calculate cementite precipitation from a supersaturated
C ferrite based on a nucleation and growth theory. Nucleation occurs
C on the dislocation. The growth of cementite plate is calculated
C using the one-dimensional parabolic thickening rate constant (ALPHA).
C
      IMPLICIT REAL*8(A-H,K-Z), INTEGER(I,J)
      DOUBLE PRECISION X(200),Y(200)
C
C--------------------------------------------------------------
C Initial carbon mole fraction in ferrite (XMOL) and the maximum
C possible volume fraction of cementite (VE).
C
      XMOL=0.0183
        VE=1.00645D+00*4.0D+00*XMOL/(1.0D+00-4.0D+00*XMOL)
C
C--------------------------------------------------------------
C ALPHA : one demensional parabolic rate constant, m/sec**0.5
C DG : activation energy of the nucleation of cementite, J/mole
C
C Typical data set
C 450:Temperature deg.C,  0.1234D-06: Rate constant m/sec**5
C 500             0.3456D-06
C
1     READ(5,*,END=333) T,ALPHA
      DG=180000.0D+00
      WRITE(6,*) 'G* = ',DG
      R=8.314D+00
      TT=T+273.0D+00
C
C--------------------------------------------------------------
C Calculation of the dislocation density in ferrite.
C
        A1=9.28480435985404817D+00
        A2=6880.73079777086696D+00
        A3=-1780359.64568034932D+00
      ROU=A1+A2/TT+A3/TT/TT
      ROU=10.0D+00**ROU
       R0=((2.26D+00-6.4D-03*TT+4.6D-06*TT*TT)*VE/1000.0)
      &   **(1.0/3.0)*1.0D-06
C
C--------------------------------------------------------------
C N0 : Number of particles per unit volume
C
        N0=VE/(4.0/3.0*3.141593*R0*R0*R0)
C
C--------------------------------------------------------------
C Coefficients in the nucleation function.
C see Christian "The Theory of Transformations in Metals and Alloys"
C
        A=2.8664D-10*3.0D+00**0.5/2.0D+00
        K=(ROU/A)**(1.0/3.0)*2.08D+10*TT*DEXP(-DG/R/TT)*ROU
        VNC=(ROU/A)**(1.0/3.0)*ROU
C
C--------------------------------------------------------------
      WRITE(6,98) T,VE,RMAX,ALPHA,DG,ROU,N0,VNC,K
98    FORMAT(/
      &' TEMPERATURE, DEG          = ',F10.4/
      &' EQUILIBRIUM V-THETA       = ',D12.4/
      &' R-MAX (FROM V-THETA) , um  = ',D12.4/
      &' ALPHA, M/SEC**0.5         = ',D12.4/
      &' DELTA-G, J/MOLE           = ',D12.4/
      &' DISLOCATION DENSITY, 1/M**2 = ',D12.4/
      &' EATA (NO. OF PARTICLE),M**-3= ',D12.4/
      &' Nv= ROU*N               = ',D12.4/
      &' NUCLEATION RATE I,        = ',D12.4)
C
C--------------------------------------------------------------
C Calculation of time required for 0.05 cementite precipitation
C (TIME), and the total number of particles at the end of the
C reaction (NTOT).
C
      Z=-DLOG(1.0D+00-0.05D+00)
        TIME=(Z*5.0/18.0*VE/K/ALPHA**3.0)**(2.0/5.0)
```

```
30   WRITE(6,99) TIME
99   FORMAT(1H ,'TIME FOR 0.05 PRECIPITATION = ',D12.4)
     TC=(30.0*5.0/18.0*VE/K/ALPHA**3.0)**(2.0/5.0)
   DTC=TC/200.0
   DO 20 I=1,200
    X(I)=DTC*(I-1)
     Y(I)=DEXP(-18.0/5.0*K*ALPHA**3.0/VE*X(I)**(5.0/2.0))
20   CONTINUE
   II3=0
   CALL D01GAF(X,Y,200,ANS,ERROR,II3)
   NTOT=K*ANS
   WRITE(6,911) NTOT
911  FORMAT(1H ,'NUMBER OF PARTICLE, M**-3  = ',D12.4)
   GOTO 1
333  STOP
   END
C
C---------------------------------------------------------------
```

```
C    FTVSCLR PROGRAM=%H% NAG DATA=&DATA
C  H. K. D. H. Bhadeshia and M. Takahashi
C
C Program to calculate the growth rate based on a plate growth theory
C and the time required to obtain 0.05 cementite precipitation.
C
C Typical dataset:
C 1 40  No. of centigrade-mole fraction carbon pairs, No. of alloys
C 0.2 (C) 0.2 (Si) 0.3 (Mn) 0.4(Ni) 0.5(Mo) 0.6 (Cr) 0.1 (V) wt.%
C 600 -------- temperature in deg.C
C
     IMPLICIT REAL*8(A-H,K-Y), INTEGER(I,J,Z)
     DOUBLE PRECISION DIFF(300),CARB(300)
     &, B0,B1,B2,T5,DIS
C
C XMAXR IS THE EQUILIBRIUM CONC AT PLATE TIP OF RADIUS R, IN GAMMA
C HH=PLANCKS CONST.JOULES/SEC,KK=BOLTZMANNS CONST.JOULES/DEGREE KELVIN
C
     HH=6.6262D-34
     KK=1.38062D-23
     READ(5,*)I6,IJK1
     DO 1008 II22=1,IJK1
     CALL OMEGA(W,XBAR)
     Z=12
     A5=1.0D+00
     R=8.31432D+00
C
C    D=DIFFUSIVITY OF CARBON IN AUSTENITE
C    Z=COORDINATION OF INTERSTIAL SITE
C    R=GAS CONSTANT
C    X=MOLE FRACTION OF CARBON
C    T=ABSOLUTE TEMPERATURE
C    SIGMA=SITE EXCLUSION PROBABLITY
C    W=CARBON CARBON INTERACTION ENERGY IN AUSTENITE
C
     RADIUS=0.0
     VMAX=0.0
     M1=0.00
     WRITE(6,1009)
1009  FORMAT('*************************'/5H      )
     DO 222 I7=1,I6
     READ(5,*)T
     XTH=0.25
     XMAX=XTH
     CTEMP=T
     T=T+273.00D+00
     II2=0
     XALPHA=XALPH(T)
     WRITE(6,1005)T,CTEMP,XBAR,XALPHA
     CALL RRAD(RADIUS,XMAX,XALPHA,XBAR,T,R,XMAXR,W)
     A6=(XMAXR-XBAR)/290.0D+00
1005  FORMAT(' ABSOLUTE TEMPERATURE, DEGREES KELVIN =',F8.1/
     &'       TEMPERATURE IN DEGREES CENTIGRADE =',F8.1/
     &' MOL FRAC CARBON IN ALLOY = ',F8.4/
     &' EQUILIBRIUM MOL FRAC OF C IN FERRITE=',D12.4)
     DIFF0=DF(T)
     CALL VEL(VMAX,DIFF0,RADIUS,XMAX,XBAR,XALPHA)
     CALL VEL3(VMAX,DIFF0,RADIUS,XMAX,XBAR,XALPHA)
     CALL VEL2(VMAX,DIFF0,RADIUS,XMAX,XBAR,XALPHA)
     CALL VEL4(VMAX,DIFF0,RADIUS,XMAX,XBAR,XALPHA)
     B0=9.05839817855180618D0
     B1=7528.72136707062509D0
     B2=-2107436.07233760227D0
     DIS=B0+B1/T+B2/T/T
     DIS=10.0D0**DIS
     WRITE(6,902) DIS
902   FORMAT(1H ,'DISLOCATION DENS., M**-2  = ',D15.6)
     VE=1.00645D+00*4.0D+00*XBAR/(1.0D+00-4.0D+00*XBAR)
     R0=((2.26D+00-6.4D-03*T+4.6D-06*T*T)*VE/1000.0)
     &   **(1.0/3.0)*1.0D-06
     N0=VE/(4.0/3.0*3.14159265D+00*R0*R0*R0)/DIS
     NTOT=N0*DIS
     ASP=15.0D+00
     WRITE(6,903) VE
```

```fortran
903   FORMAT(1H ,'MAXIMUM VOLUME FRACTION OF CEMENTITE = ',D15.6)
      WRITE(6,904) ASP
904   FORMAT(1H ,'ASPECT RATIO OF CEMENTITE = ',F10.4)
      WRITE(6,905) R0
905   FORMAT(1H ,'AVERAGE PARTICLE SIZE, M  = ',D15.6)
      WRITE(6,906) NTOT
906   FORMAT(1H ,'NUMBER OF PARTICLES, M**-3= ',D15.6)
      T5=(VE*0.05D+00/(3.14159265D+00
     &      *VMAX*VMAX*VMAX*DIS/ASP*N0))**(1.0D+00/3.0D+00)
      WRITE(6,901) VMAX,T5
      WRITE(6,*) ' '
      WRITE(6,*) ' '
901   FORMAT(1H ,'MAX. VELOCITY, M/SEC = ',D15.4/
     &' TIME FOR 0.05 PRECIPITATION OF CEMENTITE, SEC = ',D15.4)
222   CONTINUE
1008  CONTINUE
      END
C
C-------------------------------------------------------------
      SUBROUTINE OMEGA(W,XBAR)
C SUBROUTINE TO CALCULATE THE CARBON CARBON INTERACTION ENERGY IN
C AUSTENITE, AS A FUNCTION OF ALLOY COMPOSITION.  BASED ON .MUCG18
C THE ANSWER IS IN JOULES PER MOL.  **7 OCTOBER 1981**
      DOUBLE PRECISION C(8),W,P(8),B1,B2,Y(8),T10,T20,B3,XBAR
      INTEGER B5,I,U,B4
      READ (5,*) C(1),C(2),C(3),C(4),C(5),C(6),C(7)
      WRITE(6,261) (C(B4),B4=1,7)
      B3=0.0D+00
      C(8)=C(1)+C(2)+C(3)+C(4)+C(5)+C(6)+C(7)
      C(8)=100.0D+00-C(8)
      C(8)=C(8)/55.84D+00
      C(1)=C(1)/12.0115D+00
      C(2)=C(2)/28.09D+00
      C(3)=C(3)/54.94D+00
      C(4)=C(4)/58.71D+00
      C(5)=C(5)/95.94D+00
      C(6)=C(6)/52.0D+00
      C(7)=C(7)/50.94D+00
      B1=C(1)+C(2)+C(3)+C(4)+C(5)+C(6)+C(7)+C(8)
      DO 107 U=2,7
      Y(U)=C(U)/C(8)
107   CONTINUE
      DO 106 U=1,8
      C(U)=C(U)/B1
106   CONTINUE
      XBAR=C(1)
      XBAR=DINT(10000.0D+00*XBAR)
      XBAR=XBAR/10000
      B2=0.0D+00
      T10=Y(2)*(-3)+Y(3)*2+Y(4)*12+Y(5)*(-9)+Y(6)*(-1)+Y(7)*(-12)
      T20=-3*Y(2)-37.5*Y(3)-6*Y(4)-26*Y(5)-19*Y(6)-44*Y(7)
      P(2)=2013.0341+763.8167*C(2)+45802.87*C(2)**2-280061.63*C(2)**3
     &+3.864D+06*C(2)**4-2.4233D+07*C(2)**5+6.9547D+07*C(2)**6
      P(3)=2012.067-1764.095*C(3)+6287.52*C(3)**2-21647.96*C(3)**3-
     &2.0119D+06*C(3)**4+3.1716D+07*C(3)**5-1.3885D+08*C(3)**6
      P(4)=2006.8017+2330.2424*C(4)-54915.32*C(4)**2+1.6216D+06*C(4)**3
     &-2.4968D+07*C(4)**4+1.8838D+08*C(4)**5-5.5531D+08*C(4)**6
      P(5)=2006.834-2997.314*C(5)-37906.61*C(5)**2+1.0328D+06*C(5)**3
     &-1.3306D+07*C(5)**4+8.411D+07*C(5)**5-2.0826D+08*C(5)**6
      P(6)=2012.367-9224.2655*C(6)+33657.8*C(6)**2-566827.83*C(6)**3
     &+8.5676D+06*C(6)**4-6.7482D+07*C(6)**5 +2.0837D+08*C(6)**6
      P(7)=2011.9996-6247.9118*C(7)+5411.7566*C(7)**2
     &+250118.1085*C(7)**3-4.1676D+06*C(7)**4
      DO 108 U=2,7
      B3=B3+P(U)*Y(U)
      B2=B2+Y(U)
108   CONTINUE
      IF (B2 .EQ. 0.0D+00) GOTO 455
      W=(B3/B2)*4.187
      GOTO 456
455   W=8054.0
456   WRITE (6,261)(C(B4),B4=1,7)
      WRITE(6,1006)W
1006  FORMAT(' CARBON-CARBON INTERACTION ENERGY IN GAMMA, J/MOL=',F9.4)
```

```fortran
261   FORMAT (4H  C=,F7.4,4H SI=,F7.4,4H MN=,F7.4,
     &4H NI=,F7.4,4H MO=,F7.4,4H CR=,F7.4,4H  V=,F7.4)
      RETURN
      END
C
C-------------------------------------------------------
      SUBROUTINE RRAD(RADIUS,XMAX,XALPHA,XBAR,T,R,XMAXR,W)
      DOUBLE PRECISION RADIUS,XMAX,XBAR,T,R,SIG,MOLVOL,XMAXR
     &,XALPHA,RAD,OMEGA,CAPCON,EPSI
      SIG=0.7
C SIG=INTERFACIAL ENERGY, JOULES PER METRE SQUARED
      MOLVOL=5.8033D-06*(1.0D+00+3.549D-05*(T-298.0D+00))
C MOLVOL = MOLAR VOLUME OF FERRITE
C RADIUS IS THE CRITICAL RADIUS FOR ZERO GROWTH
C RAD IS THE RATIO OF THE ACTUAL RADIUS TO THE CRITICAL RADIUS
      EPSI=XALPHA*DF(T)
C     CAPCON=(SIG*MOLVOL/(R*T))*((1.0D+00-XALPHA)/(XMAX-XALPHA))
C     &/EPSI
      CAPCON=(SIG*MOLVOL/(R*T))/(XMAX-XALPHA)
      RADIUS=CAPCON*XALPHA/(XMAX-XALPHA)
      OMEGA=(XALPHA-XBAR)/(XALPHA-XMAX)
      RAD=0.2026D+01-0.1917D+01*OMEGA-0.8953D+00*OMEGA*OMEGA
     &+0.3670D+01*OMEGA*OMEGA*OMEGA-0.2519D+01*OMEGA*OMEGA*OMEGA*OMEGA
      RAD=10.00D+00**RAD
      RAD=RADIUS*RAD
      XMAXR=XMAX*(1.0D+00+(CAPCON/RAD))
      WRITE(6,1)SIG,MOLVOL,RADIUS,XMAXR,CAPCON,EPSI
1     FORMAT(' INTERFACIAL ENERGY=',F8.4,' JOULES/METERS SQUARED'/
     &' MOLAR VOLUME OF CEMENTITE(METERS CUBED PER MOL)=',D15.6/
     &' GIBBS THOMPSON CRITICAL RADIUS(METERS)=',D15.6/
     &' EQUILIBRIUM CONC AT PLATE TIP, MOL FRAC, XMAXR=',D15.6/
     &' CAPILLARITY CONSTANT CAPCON,=',D15.6/
     &' NON-IDEALITY PARAMETER EPSI=',D15.6)
      RETURN
      END
C
C---------------------------------------------------------------
      SUBROUTINE RRAD1(RADIUS,XMAX,XALPHA,XBAR,T,R,XMAXR,W)
      DOUBLE PRECISION RADIUS,XMAX,XBAR,T,R,SIG,MOLVOL,XMAXR
     &,XALPHA,RAD,OMEGA,CAPCON,EPSI
C RADIUS IS THE CRITICAL RADIUS FOR ZERO GROWTH
      XMAXR=XMAX
      RADIUS=6.5D-08
      WRITE(6,9) XMAX,RADIUS
9     FORMAT(1H ,'CARBON IN CEMENTITE, MOLE FRACTION = ',F10.4/
     &'CRITICAL RADIUS, M = ',D15.4)
      RETURN
      END
C
C---------------------------------------------------------------
      SUBROUTINE VEL(VMAX,ANS,RADIUS,XMAX,XBAR,XALPHA)
      DOUBLE PRECISION OMEGA,ANS,RADIUS,P,VMAX,XMAX,XBAR
     &,XALPHA
      OMEGA=(XALPHA-XBAR)/(XALPHA-XMAX)
      P=(1.0D+00/8.0D+00)*(OMEGA/(1.0D+00-OMEGA))
      VMAX=(ANS*1.0D-04)*P/RADIUS
      WRITE(6,1)VMAX
1     FORMAT(' MAXIMUM GROWTH RATE (EQ.9,MET.TRANS,V6A,1975,P7,=',
     &D10.4,'METERS PER SECOND')
      RETURN
      END
C
C---------------------------------------------------------------
      SUBROUTINE VEL2(VMAX,ANS,RADIUS,XMAX,XBAR,XALPHA)
      DOUBLE PRECISION OMEGA,ANS,RADIUS,P,VMAX,XMAX,XBAR
     &,XALPHA
      OMEGA=(XALPHA-XBAR)/(XALPHA-XMAX)
      P=(1.0D+00/4.0D+00)*(OMEGA/(1.0D+00-OMEGA))
      VMAX=((10.0D+00)**(-2.5D+00*(1.0D+00-OMEGA)))
     &*(ANS*1.0D-04)*P/RADIUS
      WRITE(6,1)VMAX
1     FORMAT(' MAXIMUM GROWTH RATE (EQ.14,MET.TRANS,V6A,1975,P7,=',
     &D10.4,'METERS PER SECOND')
      RETURN
```

```fortran
      END
C
C------------------------------------------------------------
      SUBROUTINE VEL3(VMAX,ANS,RADIUS,XMAX,XBAR,XALPHA)
      DOUBLE PRECISION OMEGA,ANS,RADIUS,P,VMAX,XMAX,XBAR
     &,XALPHA
      OMEGA=(XALPHA-XBAR)/(XALPHA-XMAX)
       P=((OMEGA/(1.0D+00-(2.0D+00/3.14159D+00)*OMEGA-
     &(1.0D+00/(2.0D+00*3.14159D+00))*(OMEGA*OMEGA)))**3)
       P=P*27.0D+00/(256.0D+00*3.14159D+00)
      VMAX=(ANS*1.0D-04)*P/RADIUS
      WRITE(6,1)VMAX
1     FORMAT(' MAXIMUM GROWTH RATE (EQ.13,MET.TRANS,V6A,1975,P7,=',
     &D10.4,'METERS PER SECOND')
      RETURN
      END
C
C------------------------------------------------------------
      SUBROUTINE VEL4(VMAX,ANS,RADIUS,XMAX,XBAR,XALPHA)
      DOUBLE PRECISION OMEGA,ANS,RADIUS,PECLET,XMAX,XBAR,XALPHA,PI
     &,VDUM,DUMMY,VMAX,DD,S2,RAD,DDD
      INTEGER I1,I2,I3
      WRITE(6,4)
4     FORMAT(/ DIFFUSION CONTROLLED GROWTH, TRIVEDI ANALYSIS')
      I2=100
      DD=0.01
      VDUM=DD*VMAX
      VMAX=0.5*VMAX
      ANS=ANS*1.0D-04
      WRITE(6,44)
44    FORMAT(' OMEGA  DUMMY   VMAX(M/S)   PECLET   RAD(M)')
      OMEGA=(XALPHA-XBAR)/(XALPHA-XMAX)
       RAD=0.2026D+01-0.1917D+01*OMEGA-0.8953D+00*OMEGA*OMEGA
     &+0.3670D+01*OMEGA*OMEGA*OMEGA-0.2519D+01*OMEGA*OMEGA*OMEGA*OMEGA
       RAD=10.0D+00**RAD
      RAD=RADIUS*RAD
      DO 1 I1=1,I2
      PECLET=VMAX*RAD/(2.0D+00*ANS)
       S2=-1.073019925D+00*(DLOG10(PECLET))-0.273767575D+00
       S2=10.0D+00**S2
      PI=3.14159D+00
      DUMMY=(DSQRT(PI*PECLET))*(DEXP(PECLET))*(DERFC(DSQRT(PECLET)))
     &*(1.0D+00+(RADIUS/RAD)*OMEGA*S2)
      DDD=DABS(100.0D+00*(DUMMY-OMEGA))
      IF (DDD .GT. 0.1D+00) GOTO 55
      WRITE(6,2)OMEGA,DUMMY,VMAX,PECLET,RAD
2     FORMAT(7D12.4)
      IF (DDD .LT. 0.01D+00) GOTO 56
55    VMAX=VMAX+VDUM
1     CONTINUE
56    RETURN
      END
C
C------------------------------------------------------------
C FUNCTION GIVING THE EQUILIBRIUM MOL.FRAC. CARBON IN ALPHA
C BASED ON THE PAPER ON FIRST ORDER QUASICHEMICAL THEROY,METSCI
      DOUBLE PRECISION FUNCTION XALPH(T)
      DOUBLE PRECISION T,CTEMP
       CTEMP=(T-273.0D+00)/900.0D+00
       XALPH=0.1528D-02-0.8816D-02*CTEMP+0.2450D-01*CTEMP*CTEMP
     &-0.2417D-01*CTEMP*CTEMP*CTEMP+
     &0.6966D-02*CTEMP*CTEMP*CTEMP*CTEMP
      RETURN
      END
C
C------------------------------------------------------------
      DOUBLE PRECISION FUNCTION DF(KTEMP)
      DOUBLE PRECISION R,KTEMP,PHI,DOTO,DTT,F
       R=8.3143D+00
       PHI=1.0D+00-1.0/(0.5D+00*DEXP(7.2D+03*4.184/(R*KTEMP))
     &*DEXP(4.4D+00)+1.0D+00)
       DOTO=3.3D-07*DEXP(-19.3D+03*4.184D+00/(R*KTEMP))
       DTT=3.0D-04*DEXP(-14.7D+03*4.184D+00/(R*KTEMP))
       F=0.86D+00
```

A-14

```
      DF=PHI*DOTO+(1.0D+00-PHI)*F*DTT+(1.0D+00-PHI)
     &*(1.0D+00-F)*DOTO
C DIFFUSION OF CARBON IN FERRITE, M*M/S
C MCLELLAN ET AL., TRANS. MET. SOC. AIME, VOL.233 (1965) 1938
C R = UNIVERSAL GAS CONSTANT, J/MOL/K
C KTEMP = ABSOLUTE TEMPERATURE
      RETURN
      END
C
C----------------------------------------------------------------
```

```
C PROGRAM TO CALCULATE THE GROWTH RATE OF CEMENTITE ASSUMING
C ONE DIMENSIONAL PARABOLIC THICKENING OF CEMENTITE FROM AUSTENITE.
C KIRKALDY'S METHOD IS USED TO CALCULATE EQUILIBRIUM CONDITIONS.
C
C SEE HASHIGUCHI ET AL., CALPHAD VOL.8 NO.2(1984) PP173-186
C
C THE LINEAR APPROXIMATION IS USED FOR THE CHEMICAL PROFILE IN
C AUSTENITE AHEAD OF THE INTERFACE.
C
C                    M. TAKAHASHI, 19.1.1990
C
      IMPLICIT REAL*8 (A-H,K-Z)
       DOUBLE PRECISION C(8),Y(8),K(8),X(8),C0(8),W0(8),CB(3),DUM(3)
      &,G(8),E(8,8),WW(8),G2(8),LFX(2,8),GM(8),AC(8)
      COMMON/TRANS/C0,W0
      COMMON/COEFF/G,E,WW,GFE3C
      COMMON/HILL/G2,LFX,LCV,GM,AC,DDG,GFEC
      READ(5,*) III
      IIII=0
27    IIII=IIII+1
      IF (IIII .GT. III) GOTO 26
      READ(5,*) (W0(I),I=1,7)
      READ(5,*) TI,DCT,TF
      READ(5,*) SECS,DSEC,SECF,IN
      CALL CONV(1,W0,C0)
      IM=0
      WRITE(6,*) 'INITIAL COMPOSITIONS'
      WRITE(6,198)
       WRITE(6,199) (W0(I),I=1,7)
       WRITE(6,199) (C0(I),I=1,7)
199   FORMAT(1H ,7F9.5)
198   FORMAT(1H ,'   C     SI     MN     NI'
      &,'    CR     MO     CU ')
      WRITE(6,*)
      CALL OMEGA(W)
      CC=0.0D+00
      DO 1 I=1,7
       CC=CC+C0(I)
1     CONTINUE
      C0(8)=1.0D+00-CC
      KK=0.0D+00
      DO 2 I=2,7
       K(I)=C0(I)/C0(8)
       KK=KK+K(I)
       IF (C0(I) .EQ. 0.0D+00) GOTO 2
       IM=I
2     CONTINUE
      YY=0.0D+00
      DO 3 I=2,7
       Y(I)=K(I)/(1.0D+00+KK)
       YY=YY+Y(I)
3     CONTINUE
      Y(8)=1.0D+00-YY
      CTEMP=TI
20    CTEMP=CTEMP+DCT
      T=CTEMP+273.0D+00
      IF (CTEMP .GT. TF) GOTO 25
C
C THERMODYNAMIC PARAMETERS
C IN ORDER OF SI,MN,NI,CR,MO,CU.
C
      DG=46150.0D+00/3.0-19.205D+00*T/3.0
      GFE3C=1.332D+04-64.718*T+7.481*T*DLOG(T)-DG
      G(2)=28535.0D+00-DG
      G(3)=-14263.0D+00+10.0D+00*T-DG
C     G(3)=-13532.0D+00-DG
      G(4)=20338.0D+00-2.368D+00*T-DG
      G(5)=-24418.0D+00+16.61D+00*T-2.749D+00*T*DLOG(T)-DG
      G(6)=-19644.0D+00-0.628*T-DG
      G(7)=28535.0D+00-DG
C
      E(1,1)=4.7859D+00+5066.0D+00/T
C     E(1,2)=4.84D+00-7370.0D+00/T
      E(1,2)=14795.0D+00/T
```

```
      E(1,3)=-4811.0D+00/T
      E(1,4)=-2.2D+00+7600.0D+00/T
      E(1,5)=24.4-38400.0D+00/T
      E(1,6)=3.855D+00-17870.0D+00/T
      E(1,7)=4200.0D+00/T
C
      E(2,2)=26048.0D+00/T
      E(3,3)=2.406D+00-175.6D+00/T
C     E(3,3)=0.2D+00
      E(4,4)=-721.7D+00/T
      E(5,5)=7.655D+00-3154.0D+00/T-0.661D+00*DLOG(T)
      E(6,6)=-2330.0D+00/T
      E(7,7)=-0.161D+00-7834.0D+00/T
C
      WW(2)=0.0D+00
      WW(3)=8351.0D+00-15.188D+00*T
      WW(4)=0.0D+00
      WW(5)=1791.0D+00
      WW(6)=0.0D+00
      WW(7)=0.0D+00
C----------------------------------------------------------------
      G2(2)=123000D+00
      G2(3)=-48500D+00
      G2(4)=46000D+00
      G2(5)=-251160D+00+118.0D+00*T
      G2(6)=-267200D+00
      G2(7)=-46000.0D+00+55.0D+00*T
      LFX(1,2)=-108280.0D+00
      LFX(1,3)=730.0D+00-10.0D+00*T
      LFX(1,4)=-14600.0D+00
      LFX(1,5)=13110.0D+00-31.82D+00*T+2.748D+00*T*DLOG(T)
      LFX(1,6)=9686.0D+00
      LFX(1,7)=49752.0D+00-9.431D+00*T
      LFX(2,2)=0.0D+00
      LFX(2,3)=0.0D+00
      LFX(2,4)=8800.0D+00
      LFX(2,5)=0.0D+00
      LFX(2,6)=0.0D+00
      LFX(2,7)=-8594.0D+00+5.05D+00*T
      LCV=-21058.0D+00-11.581D+00*T
C     GM(2)=28535.0D+00
      GM(2)=0.0D+00
      GM(3)=-13532.0D+00
      GM(4)=14540.0D+00-2.367D+00*T
      GM(5)=-850.0D+00-14.58D+00*T
      GM(6)=502.0D+00
      GM(7)=28535.0D+00
      AC(2)=0.0D+00
      AC(3)=8350.0D+00-15.2D+00*T
      AC(4)=0.0D+00
      AC(5)=1790.0D+00
      AC(6)=0.0D+00
      AC(7)=0.0D+00
      GFEC=1.332D+04-64.718*T+7.481*T*DLOG(T)
      DDG=46150.0D+00-19.221D+00*T
C----------------------------------------------------------------
C
C CALCULATION OF THE MAXIMUM FREE ENERGY CHANGE
      CALL GCM(T,GMAX,XCEM)
      WRITE(6,*) 'GMAX=',GMAX
C DIFFUSIVITY OF X IN GAMMA
      D22=DIFX(T)
      WRITE(6,*) 'D22=',D22
C FE-C CASE
C     CALL FUNCFC(T,XGA)
      CALL FUNCFC2(T,XGA)
      CALL ALP(T,ALPHA,XGA,D11,W)
      WRITE(6,195) CTEMP,XGA,ALPHA
195   FORMAT(1H ,'FE-C : AT TEMP =',F8.2,'   C-EQ=',F8.6,
     &     '  ALPHA=',D12.6)
C
      IF (IM .EQ. 0) GOTO 24
C PARAEQUILIBRIUM CASE
C     CALL FUNCP(T,XGA,IM)
```

A-17

```fortran
      CALL FUNCP2(T,XGA,IM)
      CALL ALP(T,ALPHA,XGA,D11,W)
      WRITE(6,194) CTEMP,XGA,ALPHA
194   FORMAT(1H ,'PARA : AT TEMP =',F8.2,'  C-EQ=',F8.6,
     &    '  ALPHA=',D12.6)
C
C DETERMINATION OF THE FINAL EQUILIBRIUM
      CALL FUNCO(T,C0,X,Y,IM)
C     CALL FUNCOR(T,C0,X,Y,IM)
      XEQ1=X(1)
      XEQ2=X(IM)
      YEQ1=Y(1)
      YEQ2=Y(IM)
      WRITE(6,196) CTEMP
196   FORMAT(1H ,'AT TEMPERATURE DEG C = ',F8.2)
      WRITE(6,*)' EQUILIBRIUM COMPOSITIONS'
      WRITE(6,91) XEQ1,XEQ2,YEQ1,YEQ2
91    FORMAT(1H ,'  CGC=',F9.5,'  MGC=',F9.5,'  CCG=',F9.5,
     &' MCG=',F9.5)
89    FORMAT(1H ,' C0(IM)-X(IM) = ',D12.5)
      IF (X(1) .GT. C0(1)) GOTO 25
C
C    IF(YEQ2 .GT. C0(IM)) THEN
C      DMAX=YEQ2
C      DMIN=C0(IM)
C    ELSE
C      DMAX=C0(IM)
C      DMIN=YEQ2
C    ENDIF
      DMAX=0.25D+00
      DMIN=C0(1)
C    DMIN=0.0D+00
C
C
C DETERMINATION OF A TIE LINE
C
C      CB(3)=(9.0*YEQ2+C0(IM))/10.0D+00
      CB(3)=C0(1)+1.0D-05
C      CB(3)=0.24D+00
C      CB(3)=CB(IM)
      DEL=CB(3)
      DCB=1.0D-10
C
10    CB(1)=CB(3)-DCB
      CB(2)=CB(3)+DCB
C    IF(CB(3) .LT. C0(IM)+2.0D-10) GOTO 30
      DO 5 II=1,3
      DO 23 I3=1,8
      C(I3)=0.0D+00
23    CONTINUE
C    C(IM)=CB(II)
C      C(1)=0.24D+00
      C(IM)=C0(IM)
      C(1)=CB(II)
      C(8)=1.0D+00-C(IM)-C(1)
C    WRITE(6,*)'C1,CIM=',C(1),C(IM)
      CALL FUNCO(T,C,X,Y,IM)
C    CALL FUNCOR(T,C,X,Y,IM)
C    WRITE(6,*) 'C1,CIM=',C(1),C(IM)
C    WRITE(6,*) 'C0,CGC=',C0(1),X(1)
C    WRITE(6,188) II,X(1),X(IM),Y(IM)
188    FORMAT(1H ,I2,'  X1=',F9.5,'  X2=',F9.5,'  Y2=',F9.5)
C
C CALCULATION OF THE GROWTH RATE, ALPHA CM/SEC**0.5
C
      CALL AL(T,X,Y,ALPHA,DUM(II),W,D11,IM)
5     CONTINUE
C    WRITE(6,*) 'DUM 1 2 3=',DUM(1),DUM(2),DUM(3)
      IF (ABS(DUM(3)) .LT. ALPHA/1.0D+02) GOTO 30
      IF (ABS(0.25D+00-CB(3)) .LT. 1.0D-04) THEN
       WRITE(6,*) 'ENTER THE NPLE REGIME'
       GOTO 30
      ENDIF
      DEL=CB(3)-2.0*DCB*DUM(3)/(DUM(2)-DUM(1))
```

A-18

```fortran
C    WRITE(6,*) 'CB3,DEL=',CB(3),DEL
     IF (DEL .LT. DMIN) THEN
       DEL=(CB(3)+DMIN)/2.0D+00
     ENDIF
     IF (DEL .GT. DMAX) THEN
       DEL=(CB(3)+DMAX)/2.0D+00
     ENDIF
C    WRITE(6,*) 'CB3,DEL=',CB(3),DEL
C    WRITE(6,*) 'ALPHA,DUM=',ALPHA,DUM(3)
     IF (DUM(3) .GT. 0.0D+00) THEN
       CBUL=CB(3)
       CB(3)=DEL
     ELSE
       CB(3)=(CB(3)+CBUL)/2.0
     ENDIF
     GOTO 10
30   WRITE(6,*) 'LOCAL EQUILIBRIUM'
     WRITE(6,*) ' IN AUSTENITE'
     WRITE(6,198)
     WRITE(6,199) (X(I),I=1,7)
     WRITE(6,*) ' IN CEMENTITE'
     WRITE(6,199) (Y(I),I=1,7)
     WRITE(6,193) CTEMP,X(1),ALPHA
193  FORMAT(1H ,'L-EQ : AT TEMP =',F8.2,'   C-EQ=',F8.6,
     &    ' ALPHA=',D12.6)
     WRITE(6,*) ''
C
C    CALCULATION OF NUCLEATION
     IF (IN .EQ. 1) GOTO 24
       CALL NUC(C0,D11,T)
C
C
24   GOTO 20
25   GOTO 27
26   STOP
     END
C
C----------------------------------------------------------------
C CALCULATION OF NUCLEATION RATE AND VOLUME FRACTION OF
C CEMENTITE ASSUMING A PILLBOX TYPE NUCLEUS
C
C----------------------------------------------------------------
C CONSTANTS IN NUCLEATION FUNCTION
     SUBROUTINE NUC(C0,D11,T)
     IMPLICIT REAL*8 (A-H,K-Z)
     DOUBLE PRECISION C0(8)
     CTEMP=T-273.0D+00
     N=1.0D+15
     SV=5.0D+08
     NA=6.022D+23
     V=1.285D-23
     A4=8.268D-30
     KK=8.314D+00*1.0D+07/NA/V
     PAI=3.141592654D+00
     EP=1.0D+00
     SIGE=1.0D+00
     AR=3.0D+00
     PHAI=GMAX*1.0D+07/NA/V
     CJ=SV*N*(2.0D+00*C0(1)*D11*V*EP**0.5)
     &/(A4*(3.0D+00*KK*T)**0.5)
     CJ=CJ*DEXP(-4.0D+00*PAI*SIGE*SIGE*EP
     &/(PHAI*PHAI*KK*T))
     CJ1=12.0D+00*KK*T*A4*SIGE/(D11*C0(1)*V*PHAI*PHAI)
     VTETA=4.0D+00*C0(1)
     CJ0=AR*AR*ALPHA*ALPHA*ALPHA/VTETA*CJ
     WRITE(6,*) 'CJ0=',CJ0
     WRITE(6,*) 'CJ1=',CJ1
     WRITE(6,*) 'D11=',D11
C----------------------------------------------------------------
C CALCULATION OF VOLUME FRACTION OF CEMENTITE
     SEC=SECS
     YE=0.0D+00
     YO=0.0D+00
200  SEC=SEC+DSEC
```

```
      IF(SEC .GT. SECF) GOTO 202
      XMIN=0.0D+00
      XMAX=SEC
      XX=XMAX-XMIN
      DO 201 II=1,150
        IO=II*2.0D+00-1.0D+00
        IE=II*2.0D+00
        XO=XX/300.0D+00*IO+XMIN
        XE=XX/300.0D+00*IE+XMIN
        IF (LOG(CJ1/XO) .GT. 3.5D+00) GOTO 201
          YO=YO+(XMAX-XO)**1.5*DEXP(-CJ1/XO)
          IF (XMAX .LE. XE) GOTO 201
          YE=YE+(XMAX-XE)**1.5*DEXP(-CJ1/XE)
201   CONTINUE
      XE=CJ0*XX/300.0D+00*(4.0/3.0*YE+2.0/3.0*YO)
      XXE=1.0D+00-DEXP(-XE)
      WRITE(6,299) CTEMP,SEC,XXE
      IF (XXE .GT. 0.95D+00) GOTO 202
299   FORMAT(1H ,'TEMP=',F6.1,'  TIME=',D12.4,'  V-TETA=',D12.4)
      GOTO 200
202   RETURN
      END
C
C----------------------------------------------------------------
C SUBROUTINE TO CALCULATE ONE DIMENSIONAL RATE CONSTANT
C ASSUMING THE LINEAR GRADIENT OF CHEMISTRY
C ALPHA = CM/SEC **0.5
C----------------------------------------------------------------
C
      SUBROUTINE AL(T,X,Y,ALPHA,DUM,W,D11,IM)
      IMPLICIT REAL*8(A-H,K-Z)
      DOUBLE PRECISION C0(8),W0(8),X(8),Y(8),G(8),E(8,8),WW(8)
      COMMON/TRANS/C0,W0
      COMMON/COEFF/G,E,WW,GFE3C
      CCG=0.25D+00
      D22=DIFX(T)
      D11=DIFFG(T,C0(1),X(1),W)
C     WRITE(6,*) 'D11=',D11
C     WRITE(6,*) 'D22=',D22
      D12=D11*E(1,IM)*C0(1)/(1.0D+00+E(1,1)*C0(1))
C     D12=0.0D+00
      ALPHAC=D11*(C0(1)-X(1))*(C0(1)-X(1))
     &/(CCG-C0(1))/(CCG-X(1))
      ALPHAC=ALPHAC+D12*(C0(IM)-X(IM))*(C0(IM)-X(IM))
     &/(Y(IM)-C0(IM))/(CCG-X(1))
      IF(ALPHAC .LT. 0.0D+00) THEN
        ALPHAC=0.0D+00
        GOTO 330
      ENDIF
      ALPHAC=ALPHAC**0.5D+00
330   ALPHAX=D22*(C0(IM)-X(IM))*(C0(IM)-X(IM))
     &/(Y(IM)-C0(IM))/(Y(IM)-X(IM))
      IF(ALPHAX .LT. 0.0D+00) THEN
        DUM=0.0D+00
        GOTO 333
      ENDIF
      ALPHAX=ALPHAX**0.5D+00
C
      DUM=ALPHAC-ALPHAX
      IF (DUM .GT. 0.0D+00) THEN
        ALPHA=ALPHAC
      ELSE
        ALPHA=ALPHAX
      ENDIF
C     WRITE (6,*) 'ALPHA,DUM=',ALPHA,DUM
333   RETURN
      END
C
C----------------------------------------------------------------
C SUBROUTINE TO CALCULATE ONE DIMENSIONAL RATE CONSTANT
C ASSUMING THE LINEAR GRADIENT OF CHEMISTRY
C ALPHA = CM/SEC **0.5   ****PARAEQUILIBRIUM CONDITION****
C----------------------------------------------------------------
C
```

```fortran
      SUBROUTINE ALP(T,ALPHA,XGA,D11,W)
      IMPLICIT REAL*8(A-H,K-Z)
      DOUBLE PRECISION C0(8),W0(8),G(8),E(8,8),WW(8)
      COMMON/TRANS/C0,W0
      COMMON/COEFF/G,E,WW,GFE3C
      CCG=0.25D+00
      D11=DIFFG(T,C0(1),XGA,W)
      ALPHAC=D11*(C0(1)-XGA)*(C0(1)-XGA)
     &/(CCG-C0(1))/(CCG-XGA)
      ALPHAC=ALPHAC**0.5D+00
      ALPHA=ALPHAC
C     WRITE (6,*) 'ALPHA,DUM=',ALPHA,DUM
333   RETURN
      END
C
C----------------------------------------------------------------
C SUBROUTINE TO CALCULATE THE EQUILIBRIUM INTERFACE CHEMISTRY
C----------------------------------------------------------------
C
      SUBROUTINE FUNCOR(T,C,X,Y,IM)
      IMPLICIT REAL*8 (A-H,K-Z)
      DOUBLE PRECISION X(8),Y(8),E(7,7),WW(7),C0(8),C(8),G(7)
     &,YY(3),FUN(3)
      COMMON/TRANS/C0,W0
C
C INITIAL GUESS OF X2 AND Y2
C
      X1=X(1)
      X2=X(IM)
      Y2=Y(IM)*4.0/3.0
C
      DELTA=1.0D-10
C
499   YY(1)=Y2-DELTA
      YY(2)=Y2+DELTA
      YY(3)=Y2
      DO 10 I=1,3
      Y2=YY(I)
C
500   FF=FXY(T,C,X1,X2,Y2,IM,1)
      MM=FXY(T,C,X1,X2,Y2,IM,0)
      DFX=(FXY(T,C,X1+DELTA,X2,Y2,IM,1)-FXY(T,C,X1-DELTA,X2,Y2,IM,1))
     &  /2.0/DELTA
      DFY=(FXY(T,C,X1,X2+DELTA,Y2,IM,1)-FXY(T,C,X1,X2-DELTA,Y2,IM,1))
     &  /2.0/DELTA
      DMX=(FXY(T,C,X1+DELTA,X2,Y2,IM,0)-FXY(T,C,X1-DELTA,X2,Y2,IM,0))
     &  /2.0/DELTA
      DMY=(FXY(T,C,X1,X2+DELTA,Y2,IM,0)-FXY(T,C,X1,X2-DELTA,Y2,IM,0))
     &  /2.0/DELTA
C
      IF (ABS(FF) .LT. 1.0D-06 .AND.
     &   ABS(MM) .LT. 1.0D-06) GOTO 502
      DENO=1.0D+00
      DET=DFX*DMY-DMX*DFY
      DX1=(-FF*DMY+MM*DFY)/DET
      DX2=(-MM*DFX+FF*DMX)/DET
      IF (X1/DENO+DX1 .LT. 0.0D+00) THEN
       X1=X1/2.0/DENO
      ELSE
       X1=X1/DENO+DX1
      ENDIF
      IF (X2/DENO+DX2 .LT. 0.0D+00) THEN
       X2=X2/2.0/DENO
      ELSE
       X2=X2/DENO+DX2
      ENDIF
C
C     WRITE(6,*) X2,Y2,FF
      GOTO 500
502   FUN(I)=1.0D+00-(C(IM)-X2)/(C(1)-X1)
     &        /(3.0*Y2-4.0*X2)*(1.0D+00-4.0*X1)
10    CONTINUE
      COEFF=(C(IM)-X2)/(C(1)-X1)
      IF (ABS(FUN(3)) .LT. 1.0D-02) GOTO 503
```

A-21

```
        DUMMY=Y2-2.0*DELTA*FUN(3)/(FUN(2)-FUN(1))
        IF (DUMMY .LT. 0.0D+00) THEN
         DUMMY=Y2/2.0D+00
       ENDIF
       Y2=DUMMY
       GOTO 499
503   X(1)=X1
      X(IM)=X2
      Y(IM)=Y2*3.0/4.0
      RETURN
      END
C
C
C-----------------------------------------------------------
C FUNCTION TO CALCULATE EQUILIBRIUM FUNCTION F AND M
C  IMF=1: F(X,Y)   IMF=0: M(X,Y)
C
      DOUBLE PRECISION FUNCTION FXY0(T,C,X1,X2,Y2,IM,IMF)
      IMPLICIT REAL*8 (A-H,K-Z)
      DOUBLE PRECISION E(8,8),WW(8),G(8),C0(8),C(8)
      COMMON/TRANS/C0,W0
      COMMON/COEFF/G,E,WW,GFE3C
      R=8.314D+00
C
C
      CG=X1
       X1=(C(1)*(3.0*Y2-4.0*X2)-(C(IM)-X2))/(3.0*Y2-4.0*C(IM))
      X8=1.0D+00-X1-X2
      Y8=1.0D+00-Y2
C
      MFE3C=R*T*DLOG(Y8)
      MFE=R*T*DLOG(X8)-R*T/2.0*E(1,1)*X1*X1
       MC=R*T/3.0*DLOG(X1)+R*T/3.0*E(1,1)*X1
      MFE3C=MFE3C+(1-Y8)*WW(IM)*Y2
       MFE=MFE-R*T/2.0*E(IM,IM)*X2*X2-R*T*X1*E(1,IM)*X2
       MC=MC+R*T/3.0*E(1,IM)*X2
      MX= R*T*DLOG(X2)
      &      +R*T*(E(1,IM)*X1+E(IM,IM)*X2)
      MM3C= R*T*DLOG(Y2)
      &      +Y8*WW(IM)
       MM3C=MM3C-Y8*WW(IM)*Y2
C
      IF (IMF .EQ. 1) THEN
       FXY0=GFE3C+MFE3C-MFE-MC
      ELSE
       FXY0=G(IM)+MM3C-MX-MC
      ENDIF
C
      RETURN
      END
C
C
C-----------------------------------------------------------
C SUBROUTINE TO CALCULATE THE EQUILIBRIUM INTERFACE CHEMISTRY
C-----------------------------------------------------------
C
      SUBROUTINE FUNC0(T,C,X,Y,IM)
      IMPLICIT REAL*8 (A-H,K-Z)
      DOUBLE PRECISION X(8),Y(8),E(8,8),WW(8),X1(3),K(8)
      &,FUN(3),G(8),MM3C(8),MX(8),C0(8),C(8)
      COMMON/TRANS/C0,W0
      COMMON/COEFF/G,E,WW,GFE3C
      R=8.314D+00
C
C
      XGA=1.0D-10
      DUMMY=1.0D-12
100   X1(1)=XGA-DUMMY
      X1(2)=XGA+DUMMY
      X1(3)=XGA
      DO 10 I=1,3
       XX=0.0D+00
       YY=0.0D+00
       FUN(I)=0.0D+00
```

```fortran
      B=DEXP((GFE3C-G(IM)-WW(IM))/R/T+E(1,IM)*X1(I))
       X(IM)=C(IM)*(4.0*X1(I)-1.0D+00)/
     &      (3.0*B*(X1(I)-C(1))+4.0*C(1)-1.0D+00)
       Y(IM)=B*X(IM)
      XX=XX+X(IM)
      YY=YY+Y(IM)
       X(1)=X1(I)
       X(8)=1.0D+00-X(1)-XX
       IF (X(8) .LT. 0.0D+00) THEN
         WRITE(6,*) 'X(8),X(1),XX=',X(8),X(1),XX
       ENDIF
        Y(8)=1.0D+00-YY
C
C
       MFE3C=R*T*DLOG(Y(8))
       MFE=R*T*DLOG(X(8))-R*T/2.0*E(1,1)*X(1)*X(1)
        MC=R*T/3.0*DLOG(X(1))+R*T/3.0*E(1,1)*X(1)
       MFE3C=MFE3C+(1-Y(8))*WW(IM)*Y(IM)
       MFE=MFE-R*T/2.0*E(IM,IM)*X(IM)*X(IM)-R*T*X(1)*E(1,IM)*X(IM)
       MC=MC+R*T/3.0*E(1,IM)*X(IM)
       MX(IM)= R*T*DLOG(X(IM))
     &      +R*T*(E(1,IM)*X(1)+E(IM,IM)*X(IM))
       MM3C(IM)= R*T*DLOG(Y(IM))
     &      +Y(8)*WW(IM)
       MM3C(IM)=MM3C(IM)-Y(8)*WW(IM)*Y(IM)
C
       FUN(I)=GFE3C+MFE3C-MFE-MC
C
10    CONTINUE
       IF(ABS(FUN(3)) .LT. 1.0D-06) GOTO 20
       XGA=X1(3)-2.0*DUMMY*FUN(3)/(FUN(2)-FUN(1))
       IF(XGA .LE. 0.0D+00) THEN
         XGA=X1(3)/2.0D+00
       ENDIF
       GOTO 100
20     DO 30 I=1,8
        X(I)=X(I)
         Y(I)=3.0D+00/4.0D+00*Y(I)
30    CONTINUE
       Y(1)=0.25D+00
       RETURN
       END
C
C-------------------------------------------------------------------
C SUBROUTINE TO CALCULATE THE PARAEQUILIBRIUM INTERFACE CHEMISTRY
C-------------------------------------------------------------------
C
       SUBROUTINE FUNCP(T,XGA,IM)
       IMPLICIT REAL*8 (A-H,K-Z)
       DOUBLE PRECISION X(8),Y(8),E(8,8),WW(8),X1(3)
     &,FUN(3),G(8),C0(8),W0(8)
       COMMON/TRANS/C0,W0
       COMMON/COEFF/G,E,WW,GFE3C
       R=8.314D+00
       XGA=0.005D+00
C
C
       DUMMY=1.0D-08
100    X1(1)=XGA-DUMMY
       X1(2)=XGA+DUMMY
       X1(3)=XGA
       DO 10 I=1,3
        XX=0.0D+00
        FUN(I)=0.0D+00
        K=C0(IM)/C0(8)
        Y(IM)=K/(1+K)
        X(IM)=(1-X1(I))*Y(IM)
        X(1)=X1(I)
        X(8)=1.0D+00-X(1)-X(IM)
        Y(8)=1.0D+00-Y(IM)
C
       DENO=1.0D+00
C
       MFE3C=R*T*DLOG(Y(8))
```

A-23

```fortran
      MFE=R*T*DLOG(X(8)/DENO)-R*T/2.0*E(1,1)*X(1)*X(1)/DENO/DENO
      MC=R*T/3.0*DLOG(X(1)/DENO)+R*T/3.0*E(1,1)*X(1)/DENO
      MFE3C=MFE3C+(1-Y(8))*WW(IM)*Y(IM)
      MFE=MFE-R*T/2.0*E(IM,IM)*X(IM)*X(IM)/DENO/DENO
      MFE=MFE-R*T*X(1)*E(1,IM)*X(IM)/DENO/DENO
      MC=MC+R*T/3.0*E(1,IM)*X(IM)/DENO
      MX= R*T*DLOG(X(IM)/DENO)
     &      +R*T*(E(1,IM)*X(1)+E(IM,IM)*X(IM))/DENO
      MM3C= R*T*DLOG(Y(IM))
     &        +Y(8)*WW(IM)-Y(8)*WW(IM)*Y(IM)
C
      FUN(I)=X(8)*(GFE3C+MFE3C-MFE-MC)
      FUN(I)=FUN(I)+X(IM)*(G(IM)+MM3C-MX-MC)
C
C     WRITE(6,*) IM,E(1,1),E(1,IM),E(IM,IM)
C
10    CONTINUE
      IF(ABS(FUN(3)) .LT. 1.0D-10) GOTO 20
      XGA=X1(3)-2.0*DUMMY*FUN(3)/(FUN(2)-FUN(1))
      GOTO 100
20    XGA=X1(3)
      RETURN
      END
C
C------------------------------------------------------------
C SUBROUTINE TO CALCULATE THE EQUILIBRIUM INTERFACE CONPOSITION
C IN FE-C SYSTEMS
C------------------------------------------------------------
C
      SUBROUTINE FUNCFC(T,XGA)
      IMPLICIT REAL*8 (A-H,K-Z)
      DOUBLE PRECISION FUN(3),X(3),G(8),E(8,8),WW(8)
      COMMON/COEFF/G,E,WW,GFE3C
      R=8.314D+00
      XGA=0.005D+00
      DUMMY=1.0D-08
10    X(1)=XGA-DUMMY
      X(2)=XGA+DUMMY
      X(3)=XGA
      DO 20 I=1,3
        X8=1.0D+00-X(I)
        MFE=R*T*DLOG(X8)-R*T/2.0*E(1,1)*X(I)*X(I)
        MC=R*T/3.0*DLOG(X(I))+R*T/3.0*E(1,1)*X(I)
        FUN(I)=GFE3C-MFE-MC
20    CONTINUE
      IF(ABS(FUN(3)) .LT. 1.0D-06) GOTO 30
      XGA=X(3)-2.0*DUMMY*FUN(3)/(FUN(2)-FUN(1))
      GOTO 10
30    XGA=X(3)
      RETURN
      END
C
C
C------------------------------------------------------------
C SUBROUTINE TO CONVERT WT% TO MOLE FRACTION
C            OR MOLE FRACTION TO WT%.
C------------------------------------------------------------
C
      SUBROUTINE CONV(N,WT,C)
      IMPLICIT REAL*8 (A-H,O-Z)
      DOUBLE PRECISION AN(8), WT(8), C(8), A(8)
      AN(1)=12.0115D+00
      AN(2)=28.09D+00
      AN(3)=54.94D+00
      AN(4)=58.71D+00
      AN(6)=95.94D+00
      AN(5)=52.00D+00
      AN(7)=63.55D+00
      AN(8)=55.84D+00
      IF (N .EQ. 0) GOTO 1
      WT(8)=100.0D+00-WT(1)-WT(2)-WT(3)-WT(4)-WT(5)-WT(6)-WT(7)
      AT=0.0D+00
      DO 2 I=1,8
        A(I)=WT(I)/AN(I)
```

```fortran
      AT=AT+A(I)
2     CONTINUE
      DO 3 I=1,8
       C(I)=WT(I)/AN(I)/AT
3     CONTINUE
      GOTO 4
1     C(8)=1.0D+00-C(1)-C(2)-C(3)-C(4)-C(5)-C(6)-C(7)
      AT=0.0D+00
      DO 5 I=1,8
       A(I)=C(I)*AN(I)
       AT=AT+A(I)
5     CONTINUE
      DO 6 I=1,8
       WT(I)=C(I)*AN(I)/AT*100.0D+00
6     CONTINUE
4     RETURN
      END
C
C-----------------------------------------------------------------
C FUNCTION GIVING THE CARBON DIFFUSIVITY IN FERRITE BASED ON
C AGREN'S WORK
C DCA : CM**2/SEC
C
      DOUBLE PRECISION FUNCTION DCA(T)
      DOUBLE PRECISION T,PAI
       PAI=3.141592654D+00
       DCA=0.02D+00*DEXP(-10115.0D+00/T)
       DCA=DCA*DEXP(0.5898D+00*(1.0D+00+2.0/PAI
      &*DATAN(1.4985D+00-15309.0D+00/T)))
      RETURN
      END
C
C-----------------------------------------------------------------
C FUNCTION GIVING THE CARBON DIFFUSIVITY IN AUSTENITE
C
      DOUBLE PRECISION FUNCTION DIFFG(T,X1,X2,W)
      IMPLICIT REAL*8(A-H,K-Y), INTEGER(I,J,Z)
      DOUBLE PRECISION DIFF(300),CARB(300)
C HH=PLANCK CONST.J/S, KK=BOLTZMAN CONST. J/K
       HH=6.6262D-34
       KK=1.38062D-23
       Z=12
       A5=1.0D+00
       R=8.31432D+00
C
C    DIFF=DIFFUSIVITY OF CARBON IN AUSTENITE, CM**/SEC
C    Z=COORDINATION OF INTERSTIAL SITE
C    PSI=COMPOSITION DEPENDENCE OF DIFFUSION COEFFICIENT
C    THETA=NO. C ATOMS/ NO. FE ATOMS
C    ACTIV=ACTIVITY OF CARBON IN AUSTENITE
C    R=GAS CONSTANT
C    X=MOLE FRACTION OF CARBON
C    T=ABSOLUTE TEMPERATURE
C    SIGMA=SITE EXCLUSION PROBABLITY
C    W=CARBON CARBON INTERACTION ENERGY IN AUSTENITE
C
       DASH=(KK*T/HH)*DEXP(-(21230.0D+00/T))*DEXP(-31.84D+00)
       XINCR=(X1-X2)/300.0D+00
       DO 1 I=1,300
       CARB(I)=X2+(I-1)*XINCR
       X=CARB(I)
       THETA=X/(A5-X)
       ACTIV=CG(X,T,W,R)
       ACTIV=DEXP(ACTIV)
       DACTIV=DCG(X,T,W,R)
       DACTIV=DACTIV*ACTIV
       DACTIV=DACTIV*A5/((A5+THETA)**2)
       SIGMA=A5-DEXP((-(W))/(R*T))
       PSI=ACTIV*(A5+Z*((A5+THETA)/(A5-(A5+Z/2)*THETA+(Z/2)*(A5+Z/2)*
      &(A5-SIGMA)*THETA*THETA)))+(A5+THETA)*DACTIV
       DIFF(I)=DASH*PSI
1      CONTINUE
       II3=0
       CALL DQSES(XINCR,DIFF,300,ANS,ERROR)
```

```fortran
      DIFFG=ANS/(X1-X2)
      RETURN
      END
C
C----------------------------------------------------------------
C FUNCTION GIVING THE CARBON DIFFUSIVITY IN AUSTENITE.
C
      DOUBLE PRECISION FUNCTION DIFFG1(T,X,W)
      IMPLICIT REAL*8(A-H,K-Y), INTEGER(I,J,Z)
C HH=PLANCK CONST.J/S, KK=BOLTZMAN CONST. J/K
      HH=6.6262D-34
      KK=1.38062D-23
      Z=12
      A5=1.0D+00
      R=8.31432D+00
C
C    DIFF=DIFFUSIVITY OF CARBON IN AUSTENITE, CM**2/SEC
C    Z=COORDINATION OF INTERSTIAL SITE
C    PSI=COMPOSITION DEPENDENCE OF DIFFUSION COEFFICIENT
C    THETA=NO. C ATOMS/ NO. FE ATOMS
C    ACTIV=ACTIVITY OF CARBON IN AUSTENITE
C    R=GAS CONSTANT
C    X=MOLE FRACTION OF CARBON
C    T=ABSOLUTE TEMPERATURE
C    SIGMA=SITE EXCLUSION PROBABLITY
C    W=CARBON CARBON INTERACTION ENERGY IN AUSTENITE
C
      DASH=(KK*T/HH)*DEXP(-(21230.0D+00/T))*DEXP(-31.84D+00)
      THETA=X/(A5-X)
      ACTIV=CG(X,T,W,R)
      ACTIV=DEXP(ACTIV)
      DACTIV=DCG(X,T,W,R)
      DACTIV=DACTIV*ACTIV
      DACTIV=DACTIV*A5/((A5+THETA)**2)
      SIGMA=A5-DEXP((-(W))/(R*T))
      PSI=ACTIV*(A5+Z*((A5+THETA)/(A5-(A5+Z/2)*THETA+(Z/2)*(A5+Z/2)*
     &(A5-SIGMA)*THETA*THETA)))+(A5+THETA)*DACTIV
      DIFFG1=DASH*PSI
      RETURN
      END
C
C----------------------------------------------------------------
C FUNCTION GIVING LFG LN(ACTIVITY) OF CARBON IN AUSTENITE.
C
      DOUBLE PRECISION FUNCTION CG(X,T,W,R)
      DOUBLE PRECISION J,DG,DUMMY,T,R,W,X
      J=1-DEXP(-W/(R*T))
      DG=DSQRT(1-2*(1+2*J)*X+(1+8*J)*X*X)
      DUMMY=5*DLOG((1-2*X)/X)+6*W/(R*T)+((38575.0)-(
     &13.48)*T)/(R*T)
      CG=DUMMY+DLOG(((DG-1+3*X)/(DG+1-3*X))**6)
      RETURN
      END
C
C----------------------------------------------------------------
C FUNCTION GIVING DIFFERENTIAL OF LN(ACTIVITY) OF CARBON
C IN AUSTENITE.
C DIFFERENTIAL IS WITH RESPECT TO X.
C
      DOUBLE PRECISION FUNCTION DCG(X,T,W,R)
      DOUBLE PRECISION J,DG,DDG,X,T,W,R
      J=1-DEXP(-W/(R*T))
      DG=DSQRT(1-2*(1+2*J)*X+(1+8*J)*X*X)
      DDG=(0.5/DG)*(-2-4*J+2*X+16*J*X)
      DCG=-((10/(1-2*X))+(5/X))+6*((DDG+3)/(DG-1+3*X
     &)-(DDG-3)/(DG+1-3*X))
      RETURN
      END
C
C----------------------------------------------------------------
      SUBROUTINE OMEGA(W)
C SUBROUTINE TO CALCULATE THE CARBON CARBON INTERACTION ENERGY IN
C AUSTENITE, AS A FUNCTION OF ALLOY COMPOSITION.  BASED ON .MUCG18
C THE ANSWER IS IN JOULES PER MOL.  **7 OCTOBER 1981**
```

```fortran
      COMMON/TRANS/C0,W0
      DOUBLE PRECISION C(8),W,P(8),B1,B2,Y(8),T10,T20,B3,XONE
     &,C0(8),W0(8)
      INTEGER B5,I,U,B4
      DO 1 I=1,8
      C(I)=W0(I)
1     CONTINUE
      B3=0.0D+00
      C(8)=C(1)+C(2)+C(3)+C(4)+C(5)+C(6)+C(7)
      C(8)=100.0D+00-C(8)
      C(8)=C(8)/55.84D+00
      C(1)=C(1)/12.0115D+00
      C(2)=C(2)/28.09D+00
      C(3)=C(3)/54.94D+00
      C(4)=C(4)/58.71D+00
      C(5)=C(5)/95.94D+00
      C(6)=C(6)/52.0D+00
      C(7)=C(7)/50.94D+00
      B1=C(1)+C(2)+C(3)+C(4)+C(5)+C(6)+C(7)+C(8)
      DO 107 U=2,7
      Y(U)=C(U)/C(8)
107   CONTINUE
      DO 106 U=1,8
      C(U)=C(U)/B1
106   CONTINUE
      XONE=C(1)
C     XONE=DINT(10000.0D+00*XONE)
C     XONE=XONE/10000
      B2=0.0D+00
      T10=Y(2)*(-3)+Y(3)*2+Y(4)*12+Y(5)*(-9)+Y(6)*(-1)+Y(7)*(-12)
      T20=-3*Y(2)-37.5*Y(3)-6*Y(4)-26*Y(5)-19*Y(6)-44*Y(7)
      P(2)=2013.0341+763.8167*C(2)+45802.87*C(2)**2-280061.63*C(2)**3
     &+3.864D+06*C(2)**4-2.4233D+07*C(2)**5+6.9547D+07*C(2)**6
      P(3)=2012.067-1764.095*C(3)+6287.52*C(3)**2-21647.96*C(3)**3-
     &2.0119D+06*C(3)**4+3.1716D+07*C(3)**5-1.3885D+08*C(3)**6
      P(4)=2006.8017+2330.2424*C(4)-54915.32*C(4)**2+1.6216D+06*C(4)**3
     &-2.4968D+07*C(4)**4+1.8838D+08*C(4)**5-5.5531D+08*C(4)**6
      P(5)=2006.834-2997.314*C(5)-37906.61*C(5)**2+1.0328D+06*C(5)**3
     &-1.3306D+07*C(5)**4+8.411D+07*C(5)**5-2.0826D+08*C(5)**6
      P(6)=2012.367-9224.2655*C(6)+33657.8*C(6)**2-566827.83*C(6)**3
     &+8.5676D+06*C(6)**4-6.7482D+07*C(6)**5 +2.0837D+08*C(6)**6
      P(7)=2011.9996-6247.9118*C(7)+5411.7566*C(7)**2
     &+250118.1085*C(7)**3-4.1676D+06*C(7)**4
      DO 108 U=2,7
      B3=B3+P(U)*Y(U)
      B2=B2+Y(U)
108   CONTINUE
      IF (B2 .EQ. 0.0D+00) GOTO 455
      W=(B3/B2)*4.187
      GOTO 456
455   W=8054.0
456   RETURN
      END
C
C-----------------------------------------------------------------
C FUNCTION GIVING THE EQUILIBRIUM MOLE FRACTION OF CARBON IN FERRITE.
C
      DOUBLE PRECISION FUNCTION XALPH(T)
      DOUBLE PRECISION T,CTEMP
      CTEMP=(T-273.0D+00)/900.0D+00
      XALPH=0.1528D-02-0.8816D-02*CTEMP+0.2450D-01*CTEMP*CTEMP
     &-0.2417D-01*CTEMP*CTEMP*CTEMP+
     &0.6966D-02*CTEMP*CTEMP*CTEMP*CTEMP
      RETURN
      END
C-----------------------------------------------------------------
C DATA FOR DIFFUSIVITIES OF THE THIRD ELEMENT IN AUSTENITE
C IN ORDER OF SI,MN,NI,CR,MO,CU
      BLOCK DATA COEF
      COMMON/DIFFUS/D22
      DOUBLE PRECISION D22(7)
      DATA (D22(J),J=2,7)/
     & 6.4D+00,2.41D+00,0.475D+00,4.75D+00,2.73D+00,1.0D+00/
      END
```

```
C------------------------------------------------------------------
C FUNCTION TO CALCULATE DIFFUSIVITY OF THE THIRD ELEMENT
C  CM**2/SEC
C
      DOUBLE PRECISION FUNCTION DIFX(T)
      IMPLICIT REAL*8(A-H,K-Z)
      DOUBLE PRECISION C0(8),W0(8),D22(7)
      COMMON/TRANS/C0,W0
      COMMON/DIFFUS/D22
      Q=286000.0D+00
      K=8.314D+00
      D0=0.7D+00
      I=1
10    I=I+1
      IF(I .GT. 8) GOTO 20
      IF(C0(I) .NE. 0) GOTO 20
      GOTO 10
20    DIFX=D22(I)*D0*DEXP(-Q/K/T)
      RETURN
      END
C ------------------------------------------------------------------
C SUBROUTINE TO CALCULATE THE MAXIMUM FREE ENERGY CHANGE AVAILABLE
C FOR NUCLEATION OF CEMENTITE FROM AUSTENITE.
C KIRKALDY'S METHOD IS USED.
C SEE HASHIGUCHI ET AL., CALPHAD VOL.8 NO.2(1984) PP173-186
C
C                 M. TAKAHASHI, 20.11.1989
C
C
      SUBROUTINE GCM(T,GMAX,XCEM)
      IMPLICIT REAL*8 (A-H,K-Z)
      COMMON/TRANS/C0,W0
      DOUBLE PRECISION X(8),Y(8),E(8,8),WW(8),X1(3),K(8)
     &,FUN(3),G(8),C0(8),Y2(3)
      COMMON/COEFF/G,E,WW,GFE3C
      R=8.314D+00
      XGA=0.01D+00
C
C
      DUMMY=1.0D-06
      DO 1 I=1,7
        X(I)=C0(I)
        IF(X(I) .EQ. 0.0D+00) GOTO 1
        IFLAG=I
1     CONTINUE
      X(8)=C0(8)
      YINIT=4.0D+00/3.0D+00*X(IFLAG)
100   Y2(1)=YINIT-DUMMY
      Y2(2)=YINIT+DUMMY
      Y2(3)=YINIT
      DO 10 I=1,3
      FUN(I)=0.0D+00
      DO 2 II=2,7
      IF(II .NE. IFLAG) THEN
        Y(II)=0.0D+00
      ELSE
        Y(II)=Y2(I)
      ENDIF
2     CONTINUE
      Y(8)=1.0D+00-Y(IFLAG)
C
C
      MFE3C=R*T*DLOG(Y(8))+(1.0D+00-Y(8))*WW(IFLAG)*Y(IFLAG)
      MFE=R*T*DLOG(X(8))-R*T/2.0*(E(1,1)*X(1)*X(1)+E(IFLAG,IFLAG)
     &*X(IFLAG)*X(IFLAG))-R*T*X(1)*E(1,IFLAG)*X(IFLAG)
      MC=R*T/3.0*DLOG(X(1))+R*T/3.0*(E(1,1)*X(1)+E(1,IFLAG)
     &*X(IFLAG))
      MX=R*T*DLOG(X(IFLAG))+R*T*(E(1,IFLAG)*X(1)
     &+E(IFLAG,IFLAG)*X(IFLAG))
      MM3C=R*T*DLOG(Y(IFLAG))+Y(8)*WW(IFLAG)*(1.0D+00-Y(IFLAG))
C
      FFC=GFE3C+MFE3C-MFE-MC
      FMC=G(IFLAG)+MM3C-MX-MC
      FUN(I)=FFC-FMC
```

```
      MUFEC=MFE3C*3.0D+00/4.0D+00+GFE3C
C
10    CONTINUE
      IF(ABS(FUN(3)) .LT. 1.0D-06) GOTO 20
      YINIT=YINIT-2.0*DUMMY*FUN(3)/(FUN(2)-FUN(1))
      IF (YINIT .LT. 0.0D+00) THEN
        YINIT=1.0D-04
      ENDIF
      GOTO 100
20    GMAX=(FMC+FFC)/2.0D+00*3.0D+00/4.0D+00
      XCEM=YINIT*3.0/4.0
      RETURN
      END
C ----------------------------------------------------------------
C SUBROUTINE TO CALCULATE PARAEQUILIBRIUM BAOUNDARY COMPOSITIONS
C HILLERT-STAFFANSON SUB-REGULAR SOLUTION MODEL IS USED
C     1991.1.8   M.TAKAHASHI
C
      SUBROUTINE FUNCP2(T,XGA,IM)
      IMPLICIT REAL*8 (A-H,K-Z)
      DOUBLE PRECISION X(8),Y(8),G2(8),LFX(2,8),GM(8),AC(8)
     &,C0(8),W0(8),X1(3),FUN(3)
      COMMON/TRANS/C0,W0
      COMMON/HILL/G2,LFX,LCV,GM,AC,DDG,GFEC
      R=8.314D+00
      XGA=0.005D+00
C
      DUMMY=1.0D-08
100   X1(1)=XGA-DUMMY
      X1(2)=XGA+DUMMY
      X1(3)=XGA
      DO 10 I=1,3
      K=C0(IM)/C0(8)
      Y(IM)=K/(1.0D+00+K)
      X(IM)=(1.0D+00-X1(I))*Y(IM)
      X(1)=X1(I)
      DENO=1.0D+00-X(1)
      Y(8)=1.0D+00-Y(IM)
      X(8)=1.0D+00-X(1)-X(IM)
      X(1)=X(1)/DENO
      X(IM)=X(IM)/DENO
      X(8)=X(8)/DENO
C
      EG0=-X(IM)*X(1)*G2(IM)+X(IM)*X(IM)*
     &    (LFX(1,IM)+(3.0D+00-4.0*X(IM))*LFX(2,IM))+X(1)*X(1)*LCV
      EG1=-2.0*X(1)*LCV+X(IM)*G2(IM)
      EG2=X(8)*X(1)*G2(IM)+X(8)*X(8)*
     &    (LFX(1,IM)+(1.0D+00-4.0*X(IM))*LFX(2,IM))+X(1)*X(1)*LCV
C
C
      FUN(I)=X(8)*(
     &    GFEC-DDG/3  + R*T*DLOG(Y(8))+AC(IM)*Y(IM)*Y(IM)
     &        - R*T*DLOG(X(8))-R*T*DLOG(1.0D+00-X(1))
     &        - R*T/3*DLOG(X(1)/(1.0D+00-X(1)))
     &        - EG0-EG1/3 )
      FUN(I)=FUN(I)+X(IM)*(
     &    GM(2)-DDG/3  + R*T*DLOG(Y(IM))+AC(IM)*Y(8)*Y(8)
     &        - R*T*DLOG(X(IM))-R*T*DLOG(1.0D+00-X(1))
     &        - R*T/3*DLOG(X(1)/(1.0D+00-X(1)))
     &        - EG2-EG1/3 )
C
10    CONTINUE
      IF(ABS(FUN(3)) .LT. 1.0D-06) GOTO 20
      XGA=X(1)-2.0*DUMMY*FUN(3)/(FUN(2)-FUN(1))
      IF (XGA .LT. DUMMY) THEN
        XGA=X(1)/2.0D+00
      ENDIF
      IF (XGA .GT. 1.0D+00) THEN
        XGA=(1.0D+00+X(1))/2.0
      ENDIF
      XGA=XGA*DENO
      GOTO 100
20    XGA=X1(3)
      RETURN
```

```
      END
C
C -----------------------------------------------------
C SUBROUTINE TO CALCULATE EQUILIBRIUM BAOUNDARY COMPOSITIONS
C IN FE-C-X TERNARY SYSTEM.
C HILLERT-STAFFANSON SUB-REGULAR SOLUTION MODEL IS USED.
C     1991.1.8   M.TAKAHASHI
C
      SUBROUTINE FUNCFC2(T,XGA)
      IMPLICIT REAL*8 (A-H,K-Z)
      DOUBLE PRECISION X(8),Y(8),G2(8),LFX(2,8),GM(8),AC(8)
     &,C0(8),W0(8),X1(3),FUN(3)
      COMMON/TRANS/C0,W0
      COMMON/HILL/G2,LFX,LCV,GM,AC,DDG,GFEC
      R=8.314D+00
      XGA=0.005D+00
C
      DUMMY=1.0D-08
100   X1(1)=XGA-DUMMY
      X1(2)=XGA+DUMMY
      X1(3)=XGA
      DO 10 I=1,3
      X(1)=X1(I)
      DENO=1.0D+00-X(1)
      X(8)=1.0D+00-X(1)
      X(1)=X(1)/DENO
      X(8)=X(8)/DENO
C
      EG0=X(1)*X(1)*LCV
      EG1=-2.0*X(1)*LCV
C
C
      FUN(I)=GFEC-DDG/3
     &          - R*T*DLOG(1.0D+00-X(1))
     &          - R*T/3*DLOG(X(1)/(1.0D+00-X(1)))
     &          - EG0-EG1/3
C
10    CONTINUE
      IF(ABS(FUN(3)) .LT. 1.0D-06) GOTO 20
      XGA=X(1)-2.0*DUMMY*FUN(3)/(FUN(2)-FUN(1))
      IF (XGA .LT. DUMMY) THEN
        XGA=X(1)/2.0D+00
      ENDIF
      IF (XGA .GT. 1.0D+00) THEN
        XGA=(1.0D+00+X(1))/2.0
      ENDIF
      XGA=XGA*DENO
      GOTO 100
20    XGA=X1(3)
      RETURN
      END
C
C -----------------------------------------------------
C HILLERT-STAFFANSON SUB-REGULAR SOLUTION MODEL IS USED
C     1991.1.8   M.TAKAHASHI
C IMF=1: F(X,Y)   IMF=0: M(X,Y)
C
      DOUBLE PRECISION FUNCTION FXY(T,C,X1,X2,Y2,IM,IMF)
      IMPLICIT REAL*8 (A-H,K-Z)
      DOUBLE PRECISION X(8),Y(8),G2(8),LFX(2,8),GM(8),AC(8)
     &,C0(8),W0(8),FUN(3),C(8)
      COMMON/TRANS/C0,W0
      COMMON/HILL/G2,LFX,LCV,GM,AC,DDG,GFEC
      R=8.314D+00
C
C     X(1)=(C(1)*(3.0*Y2-4.0*X2)-(C(IM)-X2))/(3.0*Y2-4.0*C(IM))
      X(1)=X1
      X(IM)=X2
      X(8)=1.0D+00-X(1)-X(IM)
      Y(IM)=Y2
      Y(8)=1.0D+00-Y(IM)
      DENO=1.0D+00-X(1)
      X(1)=X(1)/DENO
      X(IM)=X(IM)/DENO
```

```fortran
      X(8)=X(8)/DENO
C
      EG0=-X(IM)*X(1)*G2(IM)+X(IM)*X(IM)*
     &    (LFX(1,IM)+(3.0D+00-4.0*X(IM))*LFX(2,IM))+X(1)*X(1)*LCV
      EG1=-2.0*X(1)*LCV+X(IM)*G2(IM)
      EG2=X(8)*X(1)*G2(IM)+X(8)*X(8)*
     &    (LFX(1,IM)+(1.0D+00-4.0*X(IM))*LFX(2,IM))+X(1)*X(1)*LCV
C
      IF (IMF .EQ. 1) THEN
        FXY =GFEC-DDG/3  + R*T*DLOG(Y(8))+AC(IM)*Y(IM)*Y(IM)
     &            - R*T*DLOG(X(8))-R*T*DLOG(1.0D+00-X(1))
     &            - R*T/3*DLOG(X(1)/(1.0D+00-X(1)))
     &            - EG0-EG1/3
      ELSE
        FXY =GM(2)-DDG/3  + R*T*DLOG(Y(IM))+AC(IM)*Y(8)*Y(8)
     &            - R*T*DLOG(X(IM))-R*T*DLOG(1.0D+00-X(1))
     &            - R*T/3*DLOG(X(1)/(1.0D+00-X(1)))
     &            - EG2-EG1/3
      ENDIF
C
      RETURN
      END
C
C---------------------------------------------------------------
```

```fortran
C PROGRAM TO CALCULATE THE CARBON CONCENTRATION IN AUSTENITE WHICH
C IS IN EITHER PARA- OR ORTHO- EQUILIBRIUM WITH CEMENTITE.
C KIRKALDY'S METHOD IS USED.
C SEE HASHIGUCHI ET AL., CALPHAD VOL.8 NO.2(1984) PP173-186
C
C                M. TAKAHASHI, 22.8.1989
C
      IMPLICIT REAL*8 (A-H,K-Z)
      DOUBLE PRECISION C(8),Y(8),K(8),X(8)
     &,C0(8),W0(8),CORTHO(8),WORTHO(8),CPARA(8),WPARA(8)
      COMMON/TRANS/C0
      READ(5,*) IALLOY
      READ(5,*)(W0(I),I=1,7)
      READ(5,*) CTEMPU,DTEMP,CTEMPL
      CALL CONV(1,W0,C0)
      WRITE(6,199) (W0(I),I=1,7)
      WRITE(6,199) (C0(I),I=1,7)
199   FORMAT(4H  C=,F7.4,4H SI=,F7.4,4H MN=,F7.4,
     &4H NI=,F7.4,4H MO=,F7.4,4H CR=,F7.4,4H  V=,F7.4)
      WRITE(6,*)
      CC=0.0D+00
      DO 1 I=1,7
      CC=CC+C0(I)
1     CONTINUE
      C0(8)=1.0D+00-CC
      KK=0.0D+00
      DO 2 I=2,7
      K(I)=C0(I)/C0(8)
      KK=KK+K(I)
2     CONTINUE
      YY=0.0D+00
      DO 3 I=2,7
      Y(I)=K(I)/(1.0D+00+KK)
      YY=YY+Y(I)
3     CONTINUE
      Y(8)=1.0D+00-YY
C
C
      WRITE(6,*) 'T-ACM, C  P-WT%C    P-M.F.C   O-WT%C'
     &,'  O-M.F.C    O-WT%X    O-M.F.X'
      CTEMP=CTEMPU+DTEMP
200   CTEMP=CTEMP-DTEMP
      IF (CTEMP .LT. CTEMPL) GOTO 300
      T=CTEMP+273.0D+00
      CALL FUNCP(T,Y,K,CPARA)
      CALL CONV(0,WPARA,CPARA)
      CALL FUNCO(T,CORTHO)
      CALL CONV(0,WORTHO,CORTHO)
      WRITE(6,98) T-273.0D+00,WPARA(1),CPARA(1),WORTHO(1),CORTHO(1)
     &,WORTHO(IALLOY),CORTHO(IALLOY)
98    FORMAT(1H ,F8.2, 6D12.4)
      GOTO 200
C
C
300   STOP
      END
C
C-------------------------------------------------------------
C SUBROUTINE TO CALCULATE THE PARAEQUILIBRIUM ACM TEMP.
C-------------------------------------------------------------
C
      SUBROUTINE FUNCP(T,Y,K,X)
      IMPLICIT REAL*8 (A-H,K-Z)
      DOUBLE PRECISION X(8),Y(8),E(7,7),W(7),X1(3),K(8)
     &,FUN(3),G(7),MM3C(8),MX(8)
      R=8.314D+00
      XGA=0.005D+00
C
C THERMODYNAMIC PARAMETERS
C IN ORDER OF SI,MN,NI,CR,MO,CU.
C
      DG=46150.0D+00/3.0-19.205D+00*T/3.0
      GFE3C=1.332D+04-64.718*T+7.481*T*DLOG(T)-DG
      G(2)=28535.0D+00-DG
```

A-32

```fortran
      G(3)=-14263.0D+00+10.0D+00*T-DG
C     G(3)=-13532.0D+00-DG
      G(4)=20338.0D+00-2.368D+00*T-DG
      G(5)=-24418.0D+00+16.61D+00*T-2.749D+00*T*DLOG(T)-DG
      G(6)=-19644.0D+00-0.628*T-DG
      G(7)=28535.0D+00-DG
C
      E(1,1)=8910.0D+00/T
      E(1,2)=4.84D+00-7370.0D+00/T
      E(1,3)=-4811.0D+00/T
      E(1,4)=-2.2D+00+7600.0D+00/T
      E(1,5)=24.4-38400.0D+00/T
      E(1,6)=3.855D+00-17870.0D+00/T
      E(1,7)=4200.0D+00/T
C
      E(2,2)=26048.0D+00/T
      E(3,3)=2.406D+00-175.6D+00/T
C     E(3,3)=0.2D+00
      E(4,4)=-721.7D+00/T
      E(5,5)=7.655D+00-3154.0D+00/T-0.661D+00*DLOG(T)
      E(6,6)=-2330.0D+00/T
      E(7,7)=-0.161D+00-7834.0D+00/T
C
      W(2)=0.0D+00
      W(3)=8351.0D+00-15.188D+00*T
      W(4)=0.0D+00
      W(5)=1791.0D+00
      W(6)=0.0D+00
      W(7)=0.0D+00
C
C
      DUMMY=1.0D-06
100   X1(1)=XGA-DUMMY
      X1(2)=XGA+DUMMY
      X1(3)=XGA
      DO 10 I=1,3
      XX=0.0D+00
      FUN(I)=0.0D+00
      DO 1 II=2,7
       X(II)=(1.0D+00-X1(I))*Y(II)
       XX=XX+X(II)
1     CONTINUE
      X(1)=X1(I)
      X(8)=1.0D+00-X(1)-XX
C
C
      MFE3C=R*T*DLOG(Y(8))
      MFE=R*T*DLOG(X(8))-R*T/2.0*E(1,1)*X(1)*X(1)
      MC=R*T/3.0*DLOG(X(1))+R*T/3.0*E(1,1)*X(1)
      DO 2 J1=2,7
       IF (X(J1) .EQ. 0.0D+00) GOTO 2
       MFE3C=MFE3C+(1-Y(8))*W(J1)*Y(J1)
        MFE=MFE-R*T/2.0*E(J1,J1)*X(J1)*X(J1)-R*T*X(1)*E(1,J1)*X(J1)
       MC=MC+R*T/3.0*E(1,J1)*X(J1)
       MX(J1)= R*T*DLOG(X(J1))
     &     +R*T*(E(1,J1)*X(1)+E(J1,J1)*X(J1))
       MM3C(J1)= R*T*DLOG(Y(J1))
     &     +Y(8)*W(J1)
        DO 3 J2=2,7
         MM3C(J1)=MM3C(J1)-Y(8)*W(J2)*Y(J2)
3     CONTINUE
2     CONTINUE
C
      FUN(I)=FUN(I)+X(8)*(GFE3C+MFE3C-MFE-MC)
      DO 15 J3=2,7
       FUN(I)=FUN(I)+X(J3)*(G(J3)+MM3C(J3)-MX(J3)-MC)
15    CONTINUE
C
10    CONTINUE
      IF(ABS(FUN(3)) .LT. 1.0D-06) GOTO 20
      XGA=X1(3)-2.0*DUMMY*FUN(3)/(FUN(2)-FUN(1))
      GOTO 100
20    XGA=X1(3)
      RETURN
```

```
      END
C
C-----------------------------------------------------------
C SUBROUTINE TO CALCULATE THE EQUILIBRIUM ACM TEMP.
C-----------------------------------------------------------
C
      SUBROUTINE FUNCO(T,X)
      IMPLICIT REAL*8 (A-H,K-Z)
      COMMON/TRANS/C0
      DOUBLE PRECISION X(8),Y(8),E(7,7),W(7),X1(3),K(8)
     &,FUN(3),G(7),MM3C(8),MX(8),C0(8)
      R=8.314D+00
      XGA=0.01D+00
C
C THERMODYNAMIC PARAMETERS
C IN ORDER OF SI,MN,NI,CR,MO,CU.
C
      DG=46150.0D+00/3.0-19.205D+00*T/3.0
      GFE3C=1.332D+04-64.718*T+7.481*T*DLOG(T)-DG
      G(2)=28535.0D+00-DG
      G(3)=-14263.0D+00+10.0D+00*T-DG
C     G(3)=-13532.0D+00-DG
      G(4)=20338.0D+00-2.368D+00*T-DG
      G(5)=-24418.0D+00+16.61D+00*T-2.749D+00*T*DLOG(T)-DG
      G(6)=-19644.0D+00-0.628*T-DG
      G(7)=28535.0D+00-DG
C
      E(1,1)=8910.0D+00/T
      E(1,2)=4.84D+00-7370.0D+00/T
      E(1,3)=-4811.0D+00/T
      E(1,4)=-2.2D+00+7600.0D+00/T
      E(1,5)=24.4-38400.0D+00/T
      E(1,6)=3.855D+00-17870.0D+00/T
      E(1,7)=4200.0D+00/T
C
      E(2,2)=26048.0D+00/T
      E(3,3)=2.406D+00-175.6D+00/T
C     E(3,3)=0.2D+00
      E(4,4)=-721.7D+00/T
      E(5,5)=7.655D+00-3154.0D+00/T-0.661D+00*DLOG(T)
      E(6,6)=-2330.0D+00/T
      E(7,7)=-0.161D+00-7834.0D+00/T
C
      W(2)=0.0D+00
      W(3)=8351.0D+00-15.188D+00*T
      W(4)=0.0D+00
      W(5)=1791.0D+00
      W(6)=0.0D+00
      W(7)=0.0D+00
C
C
      DUMMY=1.0D-06
100   X1(1)=XGA-DUMMY
      X1(2)=XGA+DUMMY
      X1(3)=XGA
      DO 10 I=1,3
       XX=0.0D+00
       YY=0.0D+00
       FUN(I)=0.0D+00
       DO 1 II=2,7
        B=DEXP((GFE3C-G(II)-W(II))/R/T+E(1,II)*X1(I))
        X(II)=C0(II)*(4.0*X1(I)-1.0D+00)/
     &        (3.0*B*(X1(I)-C0(1))+4.0*C0(1)-1.0D+00)
        Y(II)=B*X(II)
        XX=XX+X(II)
        YY=YY+Y(II)
1      CONTINUE
       X(1)=X1(I)
       X(8)=1.0D+00-X(1)-XX
       Y(8)=1.0D+00-YY
C
C
      MFE3C=R*T*DLOG(Y(8))
      MFE=R*T*DLOG(X(8))-R*T/2.0*E(1,1)*X(1)*X(1)
```

```fortran
      MC=R*T/3.0*DLOG(X(1))+R*T/3.0*E(1,1)*X(1)
      DO 2 J1=2,7
       IF (X(J1) .EQ. 0.0D+00) GOTO 2
       MFE3C=MFE3C+(1-Y(8))*W(J1)*Y(J1)
        MFE=MFE-R*T/2.0*E(J1,J1)*X(J1)*X(J1)-R*T*X(1)*E(1,J1)*X(J1)
       MC=MC+R*T/3.0*E(1,J1)*X(J1)
       MX(J1)= R*T*DLOG(X(J1))
     &       +R*T*(E(1,J1)*X(1)+E(J1,J1)*X(J1))
       MM3C(J1)= R*T*DLOG(Y(J1))
     &       +Y(8)*W(J1)
        DO 3 J2=2,7
         MM3C(J1)=MM3C(J1)-Y(8)*W(J2)*Y(J2)
3     CONTINUE
2     CONTINUE
C
      FUN(I)=GFE3C+MFE3C-MFE-MC
C
10    CONTINUE
      IF(ABS(FUN(3)) .LT. 1.0D-06) GOTO 20
      XGA=X1(3)-2.0*DUMMY*FUN(3)/(FUN(2)-FUN(1))
      GOTO 100
20    XGA=X1(3)
      RETURN
      END
C
C-------------------------------------------------------------
C SUBROUTINE TO CONVERT WT% TO MOLE FRACTION
C            OR MOLE FRACTION TO WT%.
C-------------------------------------------------------------
C
      SUBROUTINE CONV(N,W,C)
      IMPLICIT REAL*8 (A-H,O-Z)
      DOUBLE PRECISION AN(8), W(8), C(8), A(8)
      AN(1)=12.0115D+00
      AN(2)=28.09D+00
      AN(3)=54.94D+00
      AN(4)=58.71D+00
      AN(5)=95.94D+00
      AN(6)=52.00D+00
      AN(7)=50.94D+00
      AN(8)=55.84D+00
      IF (N .EQ. 0) GOTO 1
      W(8)=100.0D+00-W(1)-W(2)-W(3)-W(4)-W(5)-W(6)-W(7)
      AT=0.0D+00
      DO 2 I=1,8
       A(I)=W(I)/AN(I)
       AT=AT+A(I)
2     CONTINUE
      DO 3 I=1,8
       C(I)=W(I)/AN(I)/AT
3     CONTINUE
      GOTO 4
1     C(8)=1.0D+00-C(1)-C(2)-C(3)-C(4)-C(5)-C(6)-C(7)
      AT=0.0D+00
      DO 5 I=1,8
       A(I)=C(I)*AN(I)
       AT=AT+A(I)
5     CONTINUE
      DO 6 I=1,8
       W(I)=C(I)*AN(I)/AT*100.0D+00
6     CONTINUE
4     RETURN
      END
C-------------------------------------------------------------
```

```
C PROGRAM TO CALCULATE THE GROWTH RATE OF PEARLITE ASSUMING THE BULK OR
C INTERFACE DIFFUSION CONTROL.
C
C GAMMA/GAMMA+ALPHA AND GAMMA/GAMMA+THETA INTERFACE COMPOSITIONS
C ARE CALCULATED USING KIRKALDY'S APPROXIMATE METHOD.
C
C                        1991.5.12 M.TAKAHASHI
C
      IMPLICIT REAL*8 (A-H,K-Z)
      DOUBLE PRECISION X(8),Y(8),C0(8),W0(8),WW(8),K(8),G0(8)
     &,G(8),G2(8),G3(8),G4(8),GM(8),LFX(4,8),AC(8),E(8,8),EA(8,8)
      COMMON/TRANS/C0,W0,K
      COMMON/HILL/G2,LFX,LCV,GM,AC,DDG,GFEC
     &        ,GFE3C,G3,G4,WW,E,EA,G,G0
      READ(5,*) ISAMPLE
      IS=0
10    IS=IS+1
      IF (IS .GT. ISAMPLE) GOTO 100
      READ(5,*) (W0(I),I=1,7)
      READ(5,*) TI,DT,TF
C
      CALL CONV(1,W0,C0)
C
      WRITE(6,*) 'INITIAL COMPOSITION'
      WRITE(6,199)
      WRITE(6,198) (W0(I),I=1,7)
      WRITE(6,198) (C0(I),I=1,7)
199   FORMAT(1H ,'   C    SI    MN    NI'
     &,'   CR    MO    CU ')
198   FORMAT(1H ,7F9.5)
      WRITE(6,*)
C
      CALL OMEGA(W)
C
      CC=0.0D+00
      DO 11 I=1,7
      CC=CC+C0(I)
11    CONTINUE
      C0(8)=1.0D+00-CC
      KK=0.0D+00
      DO 12 I=2,7
      K(I)=C0(I)/C0(8)
      KK=KK+K(I)
      IF (C0(I) .EQ. 0.0D+99) GOTO 12
      IM=I
12    CONTINUE
      YY=0.0D+00
      DO 13 I=2,7
      Y(I)=K(I)/(1.0D+00+KK)
      YY=YY+Y(I)
13    CONTINUE
      Y(8)=1.0D+00-YY
C
C
      CTEMP=TI+DT
20    CTEMP=CTEMP-DT
      T=CTEMP+273.0D+00
      IF (CTEMP .LT. TF) GOTO 100
      IFLAGF=0
      IFLAGC=0
C
C
C THERMODYNAMIC PARAMETERS IN ORDER OF SI,MN,NI,CR,MO,CU
C----------------------------------------------------------------
C THERMODYNAMIC PARAMETERS
C IN ORDER OF SI,MN,NI,CR,MO,CU.
C
      DG=46150.0D+00/3.0-19.205D+00*T/3.0
      GFE3C=1.332D+04-64.718*T+7.481*T*DLOG(T)-DG
      SFG=-11.906D-04*T+8.272D-06*T*T-15.079D-09*T*T*T
     &  +12.857D-12*T*T*T*T
      G0(1)=-65562.0D+00+32.949*T
      G0(3)=-20520.0D+00+4.086D+00*T+1500.0D+00*SFG
      G0(5)=-1534.0D+00-19.472*T+2.749*T*DLOG(T)
```

```
      G(2)=28535.0D+00-DG
      G(3)=-14263.0D+00+10.0D+00*T-DG
C     G(3)=-13532.0D+00-DG
      G(4)=20338.0D+00-2.368D+00*T-DG
      G(5)=-24418.0D+00+16.61D+00*T-2.749D+00*T*DLOG(T)-DG
      G(6)=-19644.0D+00-0.628*T-DG
      G(7)=28535.0D+00-DG
C
C     E(1,1)=4.7859D+00+5066.0D+00/T
      E(1,1)=8910.0D+00/T
C     E(1,2)=4.84D+00-7370.0D+00/T
      E(1,2)=14795.0D+00/T
      E(1,3)=-4811.0D+00/T
      E(1,4)=-2.2D+00+7600.0D+00/T
      E(1,5)=24.4-38400.0D+00/T
      E(1,6)=3.855D+00-17870.0D+00/T
      E(1,7)=4200.0D+00/T
C
      E(2,2)=26048.0D+00/T
      E(3,3)=2.406D+00-175.6D+00/T
C     E(3,3)=0.2D+00
      E(4,4)=-721.7D+00/T
      E(5,5)=7.655D+00-3154.0D+00/T-0.661D+00*DLOG(T)
      E(6,6)=-2330.0D+00/T
      E(7,7)=-0.161D+00-7834.0D+00/T
C
      EA(1,1)=1.3D+00
      EA(2,2)=-13.31D+00+44088.0/T
      EA(3,3)=3.082D+00-4679.0/T+1509.8*SFG/T
      EA(4,4)=2.041D+00-2478.0/T+385.5*SFG/T
      EA(5,5)=2.819D+00-6039.0/T
      EA(6,6)=-0.219D+00-4772.0/T+402.6*SFG/T
      EA(7,7)=0.634D+00-11270.0/T+1006.5*SFG/T
C
      WW(2)=0.0D+00
      WW(3)=8351.0D+00-15.188D+00*T
      WW(4)=0.0D+00
      WW(5)=1791.0D+00
      WW(6)=0.0D+00
      WW(7)=0.0D+00
C----------------------------------------------------------------
      G2(2)=123000D+00
      G2(3)=-48500D+00
      G2(4)=46000D+00
      G2(5)=-251160D+00+118.0D+00*T
      G2(6)=-267200D+00
      G2(7)=-46000.0D+00+55.0D+00*T
      G3(2)=404180.0D+00
      G3(3)=-145500.0D+00
      G3(4)=138000.0D+00
      G3(5)=-153640.0D+00+38.860*T
      G3(6)=-267200.0D+00
      G3(7)=-46000.0D+00+55.0*T
      G4(1)=-65563.0D+00+23.815*T
      G4(2)=-64818.0D+00+38.543*T
      G4(3)=-1800.0D+00+1.276*T
      G4(4)=-5650.0D+00-3.35*T
      G4(5)=10460.0D+00+0.628*T
      G4(6)=10460.0D+00+0.628*T
      G4(7)=-6276.0D+00+3.347*T
      G4(8)=(-1.0D+00)*ENERGY(T,T10,T20)
C     IF (T .LT. 1000.0D+00) THEN
C        G4(8)=8933.0D+00-14.406*T+12.083D-03*T*T-11.51D-06*T*T*T
C     &       +5.23D-09*T*T*T*T
C     ELSE
C        G4(8)=71659.0D+00-216.84*T+24.773D-02*T*T-12.661D-05*T*T*T
C     &       +24.397D-09*T*T*T*T
C     ENDIF
C----------------------------------------------------------------
C
C CALCULATION OF PARAEQUILIBRIUM COMPOSITIONS (GAMMA/GAMMA+ALPHA)
C
C
      CALL PEQGA0(T,X,Y,IM)
```

```
C     CALL PEQGA(T,X,Y,IM)
C
      PX1GA=X(1)
      PX2GA=X(IM)
      PX1AG=Y(1)
      PX2AG=Y(IM)
C
C
C CALCULATION OF PARAEQUILIBRIUM COMPOSITIONS (GAMMA/GAMMA+THETA)
C
C
      CALL PEQGC0(T,X,Y,IM)
C
      PX1GC=X(1)
      PX2GC=X(IM)
      PX1CG=0.25D+00
      PX2CG=Y(IM)
C
C
C CALCULATION OF VOLUME DIFFUSION CONTROLLED GROWTH RATE OF PEARLITE
C
C     SC=5.9D-04/(1000.0D+00-T)/2
C       SC=1.0D-04/2.0D+00/(131.12D+00-0.1783*CTEMP
C     &   +4.238D+00*W0(IM))
      SC=2.0*600.0*1000.0/6.09D09/(1000.0D+00-CTEMP)
      S=1.0D-04/(127.351D+00-0.17368D+00*CTEMP-4.9195*W0(3)
     &     +1.7868*W0(5))
      CCC=(PX1GA+PX1GC)/2.0
      D=DIFF(T,CCC,CCC*1.001,W)
C
      VEL1=VD(PX1GA,PX1GC,PX1AG,SC,D,S)
C
      WRITE(6,*) ' '
      WRITE(6,*) 'Paraequilibrium carbon diffusion control'
      WRITE(6,99) CTEMP,PX1GC,PX2GC,PX1CG,PX2CG
      WRITE(6,69) PX1GA,PX2GA,PX1AG,PX2AG
      WRITE(6,68) VEL1,D
99    FORMAT(1H ,'AT Temp=',F6.1,' CGC=',F8.6,' XGC=',
     &F8.6,' CCG=',F8.6,' XCG=',F8.6)
69    FORMAT(1H ,'          CGA=',F8.6,' XGA=',
     &F8.6,' CAG=',F8.6,' XAG=',F8.6)
68    FORMAT(1H ,' V(bulk diff of C) / cm/sec=',D12.5
     &,'   Diff. Coef=',D10.4)
C
C
C CALCULATION OF THE INTEFACE COMPOSITIONS (GAMMA/GAMMA+ALPHA)
C IDENTICAL ISOACTIVITY OF CARBON IN GAMMA IS ASSUMED
C
C CALCULATION OF ACTIVITY OF CARBON IN GAMMA
C
      ACTIV=ACG0(T,C0(1),C0(IM),E(1,1),E(1,IM))
      write(6,*) 'ACTIV=',ACTIV
C
      CALL NPGA0(T,X,Y,IM)
      X1GANP=X(1)
      X2GANP=X(IM)
      X1AGNP=Y(1)
      X2AGNP=Y(IM)
C
      X2TRANS=X2AC0(T,X1GANP,ACTIV,E(1,1),E(1,IM))
      write(6,*) 'X2GANP,X2TRANS = ',X2GANP,X2TRANS
      IF (X2GANP .LT. X2TRANS) THEN
       WRITE(6,*) 'ENTERING NPLE REGIME FOR FERRITE.....'
       IFLAGF=1
       X1GA=X1GANP
       X2GA=X2GANP
       X1AG=X1AGNP
       X2AG=X2AGNP
      ELSE
       CALL EQGA0(T,X,Y,ACTIV,IM)
       X1GA=X(1)
       X2GA=X(IM)
       X1AG=Y(1)
       X2AG=Y(IM)
```

A-38

```
      ENDIF
C
C CALCULATION OF THE INTERFACE COMPOSITIONS (GAMMA/GAMMA+THETA)
C IDENTICAL ISOACTIVITY OF CARBON IN GAMMAAT THE INTERFACES IS ASSUMED
C
      CALL NPGC0(T,X,Y,IM)
      X1GCNP=X(1)
      X2GCNP=X(IM)
      X1CGNP=0.25D+00
      X2CGNP=Y(IM)
C
      X2TRANS=X2AC0(T,X1GCNP,ACTIV,E(1,1),E(1,IM))
      IF(X2GCNP .GT. X2TRANS) THEN
      WRITE(6,*) 'ENTERING NPLE REGIME FOR CEMENTITE......'
      IFLAGC=1
      X1GC=X1GCNP
      X2GC=X2GCNP
      X1CG=X1CGNP
      X2CG=X2CGNP
      ELSE
      CALL EQGC0(T,X,Y,ACTIV,IM)
      X1GC=X(1)
      X2GC=X(IM)
      X1CG=0.25D+00
      X2CG=Y(IM)
      ENDIF
C
C CALCULATION OF BOUNDARY DIFFUSION CONTROLLED GROWTH RATE OF PEARLITE
C
      VEL2=VBD(T,X2GA,X2GC,SC,C0(IM),S,IM)
C
50    WRITE(6,*) 'Boundary diffusion controlled growth'
      WRITE(6,98) CTEMP,X1GC,X2GC,X1CG,X2CG
      WRITE(6,67) X1GA,X2GA,X1AG,X2AG
      WRITE(6,66) VEL2
98    FORMAT(1H ,'AT Temp=',F6.1,' CGC=',F8.6,' XGC=',
     &F8.6,' CCG=',F8.6,' XCG=',F8.6)
67    FORMAT(1H ,'          CGA=',F8.6,' XGA=',
     &F8.6,' CAG=',F8.6,' XAG=',F8.6)
66    FORMAT(1H ,' V(boundary diff of X) /cm/sec=',D12.5)
C
C
      GOTO 20
C
100   END
C
C----------------------------------------------------------------
C SUBROUTINE TO CALCULATE INTERFACE COMPOSITIONS (GAMMA/GAMMA+ALPHA)
C Kirkaldy's approximate method is used to obtain the first
C guess value of NPLE calculation
C
      SUBROUTINE NPGA0(T,X,Y,IM)
      IMPLICIT REAL*8 (A-H,K-Z)
      DOUBLE PRECISION X(8),Y(8),C0(8),W0(8),WW(8),K(8)
     &,XX(3),G(8),G2(8),G3(8),G4(8),GM(8),G0(8)
     &,LFX(4,8),AC(8),E(8,8),EA(8,8),FUN(3)
      COMMON/TRANS/C0,W0,K
      COMMON/HILL/G2,LFX,LCV,GM,AC,DDG,GFEC,
     &      GFE3C,G3,G4,WW,E,EA,G,G0
C
C     write(6,*) 'IM=',IM
      R=8.314D+00
      XGA=C0(1)+0.01D+00
      ITER=0
      ACC=1.0D-05
      DX1=1.0D-10
200   XX(1)=XGA-DX1
      XX(2)=XGA+DX1
      XX(3)=XGA
      ITER=ITER+1
      IF(ITER .GT. 10) THEN
        ACC=ACC*10
        ITER=0
      ENDIF
```

A-39

```
      DO 220 I=1,3
      X1=XX(I)
C
      A1=DEXP(G0(1)/R/T+E(1,1)*X1)/
     &     (1.0D+00+EA(1,1)*X1*DEXP(G0(1)/R/T))
      A2=DEXP(G0(IM)/R/T+E(1,IM)*X1)/
     &     (1.0D+00+E(1,IM)*X1*DEXP(G0(1)/R/T))
C     write(6,*) 'A1,A2=',A1,A2
      Y1=A1*X1
C
      Y2=C0(IM)
      X2=Y2/A2
C     write(6,*) 'X2AC=',X2
      X0=1.0D+00-X1-X2
      Y0=1.0D+00-Y1-Y2
C
      FFG=DLOG(X0)-1.0/2.0*E(1,1)*X1*X1-1.0/2.0*E(IM,IM)*X2*X2
     &     -E(1,IM)*X1*X2
      FFA=DLOG(Y0)-1.0/2.0*EA(1,1)*Y1*Y1-1.0/2.0*EA(IM,IM)*Y2*Y2
     &     -E(1,IM)*Y1*Y2
C
      FUN(I)=G4(8)/R/T+FFG-FFA
C     FUN(I)=Y0-X0*DEXP(G4(8)/R/T
C    &        +EA(1,1)/2.0*Y1*Y1+E(1,IM)*Y1*Y2
C    &           +EA(IM,IM)/2.0*Y2*Y2
C    &        -E(1,1)/2.0*X1*X1-E(1,IM)*X1*X2
C    &           -E(IM,IM)/2.0*X2*X2)
220   CONTINUE
      IF (ABS(FUN(3)) .LT. ACC) GOTO 100
      DUMMY=XGA-2.0*DX1*FUN(3)/(FUN(2)-FUN(1))
C     write(6,*) 'DUMMY=',DUMMY
C     write(6,*) 'FUN1,2,3=',(FUN(III),III=1,3)
      IF (DUMMY .LT. 0.0D+00) THEN
       DUMMY=XGA/2.0D+00
      ENDIF
      IF (DUMMY .GT. 0.25D+00) THEN
       DUMMY=(0.25D+00+XGA)/2.0
      ENDIF
      XGA=DUMMY
C     write(6,*) 'FUN3,X1=',FUN(3),XGA
      GOTO 200
100   X(1)=X1
      X(IM)=X2
      Y(1)=Y1
      Y(IM)=Y2
C
      RETURN
      END
C
C---------------------------------------------------------------
C SUBROUTINE TO CALCULATE INTERFACE COMPOSITIONS (GAMMA/GAMMA+ALPHA)
C Kirkaldy's approximate method is used to obtain the first
C guess value.
C
      SUBROUTINE EQGA0(T,X,Y,ACTIV,IM)
      IMPLICIT REAL*8 (A-H,K-Z)
      DOUBLE PRECISION X(8),Y(8),C0(8),W0(8),WW(8),K(8)
     &,XX(3),G(8),G2(8),G3(8),G4(8),GM(8),G0(8)
     &,LFX(4,8),AC(8),E(8,8),EA(8,8),FUN(3)
      COMMON/TRANS/C0,W0,K
      COMMON/HILL/G2,LFX,LCV,GM,AC,DDG,GFEC,
     &        GFE3C,G3,G4,WW,E,EA,G,G0
C
      R=8.314D+00
      XGA=C0(1)*1.1D+00
      DX1=1.0D-06
200   XX(1)=XGA-DX1
      XX(2)=XGA+DX1
      XX(3)=XGA
      DO 220 I=1,3
      X1=XX(I)
C
      A1=DEXP(G0(1)/R/T+E(1,1)*X1)/
     &     (1.0D+00+EA(1,1)*X1*DEXP(G0(1)/R/T))
```

```fortran
      A2=DEXP(G0(IM)/R/T+E(1,IM)*X1)/
     &     (1.0D+00+E(1,IM)*X1*DEXP(G0(1)/R/T))
      Y1=A1*X1
C
      X2=X2AC0(T,X1,ACTIV,E(1,1),E(1,IM))
C     X2=X2AC(T,X1,ACTIV,LCV,G2(IM))
C     X2=C0(IM)*(1.0D+00-A1)*X1/
C     &    ((1.0D+00-A2)*C0(1)+(A2-A1)*X1)
      Y2=A2*X2
      X0=1.0D+00-X1-X2
      Y0=1.0D+00-Y1-Y2
C
      FFG=DLOG(X0)-1.0/2.0*E(1,1)*X1*X1-1.0/2.0*E(IM,IM)*X2*X2
     &    -E(1,IM)*X1*X2
      FFA=DLOG(Y0)-1.0/2.0*EA(1,1)*Y1*Y1-1.0/2.0*EA(IM,IM)*Y2*Y2
     &    -E(1,IM)*Y1*Y2
C
      FUN(I)=G4(8)/R/T+FFG-FFA
C     FUN(I)=Y0-X0*DEXP(G4(8)/R/T
C     &        +EA(1,1)/2.0*Y1*Y1+E(1,IM)*Y1*Y2
C     &           +EA(IM,IM)/2.0*Y2*Y2
C     &        -E(1,1)/2.0*X1*X1-E(1,IM)*X1*X2
C     &            -E(IM,IM)/2.0*X2*X2)
220   CONTINUE
      IF (ABS(FUN(3)) .LT. 1.0D-06) GOTO 100
      DUMMY=XGA-2.0*DX1*FUN(3)/(FUN(2)-FUN(1))
      IF (DUMMY .LT. 0.0D+00) THEN
       DUMMY=XGA/2.0D+00
      ENDIF
      IF (DUMMY .GT. 1.0D+00) THEN
       DUMMY=(1.0D+00+XGA)/2.0
      ENDIF
      XGA=DUMMY
      GOTO 200
100   X(1)=X1
      X(IM)=X2
      Y(1)=Y1
      Y(IM)=Y2
C
      RETURN
      END
C
C----------------------------------------------------------------
C SUBROUTINE TO CALCULATE INTERFACE COMPOSITIONS (GAMMA/GAMMA+ALPHA)
C Kirkaldy's approximate method is used to obtain the first
C guess value.      -paraequilibrium-
C
      SUBROUTINE PEQGA0(T,X,Y,IM)
      IMPLICIT REAL*8 (A-H,K-Z)
      DOUBLE PRECISION X(8),Y(8),C0(8),W0(8),WW(8)
     &,K(8),XXX(3),FUN1(3),G(8),G2(8),G3(8),G4(8),GM(8)
     &,LFX(4,8),AC(8),E(8,8),EA(8,8),G0(8)
      COMMON/TRANS/C0,W0,K
      COMMON/HILL/G2,LFX,LCV,GM,AC,DDG,GFEC
     &        ,GFE3C,G3,G4,WW,E,EA,G,G0
C
      R=8.314D+00
C
      X1=0.01D+00
      DX1=1.0D-06
200   XXX(1)=X1-DX1
      XXX(2)=X1+DX1
      XXX(3)=X1
      DO 220 I=1,3
      X1=XXX(I)
C
      A1=DEXP(G4(1)/R/T+E(1,1)*X1)/
     &     (1.0D+00+EA(1,1)*X1*DEXP(G4(1)/R/T))
      Y1=A1*X1
      X2=(1.0D+00-X1)*K(IM)/(1.0D+00+K(IM))
      Y2=(1.0D+00-Y1)*K(IM)/(1.0D+00+K(IM))
      X0=1.0D+00-X1-X2
      Y0=1.0D+00-Y1-Y2
C
```

```fortran
      FFG=R*T*DLOG(X0)-R*T/2.0*E(1,1)*X1*X1
     &    -R*T/2.0*E(IM,IM)*X2*X2
     &    -R*T*E(1,IM)*X1*X2
      FFA=R*T*DLOG(Y0)-R*T/2.0*EA(1,1)*Y1*Y1
     &    -R*T/2.0*EA(IM,IM)*Y2*Y2
     &    -R*T*E(1,IM)*Y1*Y2
      F2G=R*T*DLOG(X2)+R*T*(E(1,IM)*X1+E(IM,IM)*X2)
      F2A=R*T*DLOG(Y2)+R*T*(E(1,IM)*Y1+EA(IM,IM)*Y2)
      FUN1(I)=X0*(G4(8)+FFG-FFA)+X2*(G4(IM)+F2G-F2A)
C
220   CONTINUE
      IF (FUN1(3) .LT. 1.0D-06) GOTO 300
       DUMMY1=X1-2.0*DX1*FUN1(3)/(FUN1(2)-FUN1(1))
       IF (DUMMY1 .LT. 0.0D+00) THEN
        DUMMY1=X1/2.0D+00
      ENDIF
       X1=DUMMY1
       GOTO 200
300   X(1)=X1
      X(IM)=X2
      Y(1)=Y1
      Y(IM)=Y2
C
      RETURN
      END
C
C----------------------------------------------------------------
      DOUBLE PRECISION FUNCTION ACG0(T,X1,X2,E11,E12)
      IMPLICIT REAL*8 (A-H,K-Z)
C
      ACG0=DEXP(DLOG(X1)+E11*X1+E12*X2)
C
      RETURN
      END
C
C----------------------------------------------------------------
      DOUBLE PRECISION FUNCTION X2AC0(T,X1,A,E11,E12)
      IMPLICIT REAL*8 (A-H,K-Z)
C
      X2AC0=(DLOG(A)-DLOG(X1)-E11*X1)/E12
C
      RETURN
      END
C
C----------------------------------------------------------------
      DOUBLE PRECISION FUNCTION ENERGY(T,T10,T20)
      DOUBLE PRECISION T,T10,T20,F,T7
      T7=T-1.0D+02*T20
      IF (T7 .LT. 3.0D+02) GOTO 1
      IF (T7 .LT. 7.0D+02) GOTO 2
      IF (T7 .LT. 9.21D+02) GOTO 3
      IF (T7 .LT. 1.0D+03) GOTO 5
        F=(3.381D+02-3.31D+00*(T7-1.0D+03)+9.83D-03*(T7-9.9999999D+02
     &)**1.96D+00-7.11D+00*DSIN(0.034*(T7-1.0D+03)))/(-4.187D+00)
      GOTO 4
1       F=1.38D+00*T7-1.499D+03
      GOTO 4
2       F=1.65786D+00*T7-1.581D+03
      GOTO 4
3       F=1.30089D+00*T7-1.331D+03
      GOTO 4
5       F=-1.0D+00*(1.20D+02-(T7-9.4D+02)*(0.73333333333D+00))
4     ENERGY=(1.41D+02*T10 + F)*4.187D+00
      RETURN
      END
C
C----------------------------------------------------------------
C FUNCTION TO CALCULATE PARAEQUILIBRIUM CARBON DIFFUSION
C CONTROLLED GROWTH RATE OF PEARLITE
C
      DOUBLE PRECISION FUNCTION VD(XGA,XGC,XAG,SC,D,S)
      IMPLICIT REAL*8 (A-H,K-Z)
      A=0.72D+00
      SA=S*7.0D+00/8.0D+00
```

```
      SCEM=S/8.0D+00
      CCEM=0.25D+00
      VD=D/A*S**2/SA/SCEM*(XGA-XGC)/
     &          (CCEM-XAG)/S*(1.0D+00-SC/S)
      RETURN
      END
C
C--------------------------------------------------------------
C FUNCTION TO CALCULATE BOUNDARY DIFFUSION CONTROLLED GROWTH RATE
C OF PEARLITE
C
      DOUBLE PRECISION FUNCTION VBD(T,XGA,XGC,SC,XBAR,S,IM)
      IMPLICIT REAL*8 (A-H,K-Z)
      DOUBLE PRECISION CK(8),Q(8)
      CK(3)=1.126D-08
      CK(5)=2.455D-09
      Q(3)=141178.0D+00
      Q(5)=138516.0D+00
      R=8.314D+00
      SA=S*7.0D+00/8.0D+00
      SCEM=S/8.0D+00
      KDD=CK(IM)*DEXP(-Q(IM)/R/T)
      VBD=12.0D+00*KDD/SA/SCEM*(XGA-XGC)/
     &            XBAR*(1.0D+00-SC/S)
      RETURN
      END
C
C--------------------------------------------------------------
C SUBROUTINE TO CONVERT WT% TO MOLE FRACTION
C          OR MOLE FRACTION TO WT%.
C
      SUBROUTINE CONV(N,WT,C)
      IMPLICIT REAL*8 (A-H,O-Z)
      DOUBLE PRECISION AN(8), WT(8), C(8), A(8)
      AN(1)=12.0115D+00
      AN(2)=28.09D+00
      AN(3)=54.94D+00
      AN(4)=58.71D+00
      AN(6)=95.94D+00
      AN(5)=52.00D+00
      AN(7)=63.55D+00
      AN(8)=55.84D+00
      IF (N .EQ. 0) GOTO 1
      WT(8)=100.0D+00-WT(1)-WT(2)-WT(3)-WT(4)-WT(5)-WT(6)-WT(7)
      AT=0.0D+00
      DO 2 I=1,8
        A(I)=WT(I)/AN(I)
        AT=AT+A(I)
2     CONTINUE
      DO 3 I=1,8
        C(I)=WT(I)/AN(I)/AT
3     CONTINUE
      GOTO 4
1     C(8)=1.0D+00-C(1)-C(2)-C(3)-C(4)-C(5)-C(6)-C(7)
      AT=0.0D+00
      DO 5 I=1,8
        A(I)=C(I)*AN(I)
        AT=AT+A(I)
5     CONTINUE
      DO 6 I=1,8
        WT(I)=C(I)*AN(I)/AT*100.0D+00
6     CONTINUE
4     RETURN
      END
C
C--------------------------------------------------------------
C FUNCTION GIVING LFG LN(ACTIVITY) OF CARBON IN AUSTENITE.
C
      DOUBLE PRECISION FUNCTION CG(X,T,W,R)
      DOUBLE PRECISION J,DG,DUMMY,T,R,W,X
      J=1-DEXP(-W/(R*T))
      DG=DSQRT(1-2*(1+2*J)*X+(1+8*J)*X*X)
      DUMMY=5*DLOG((1-2*X)/X)+6*W/(R*T)+((38575.0)-(
     &13.48)*T)/(R*T)
```

```fortran
      CG=DUMMY+DLOG(((DG-1+3*X)/(DG+1-3*X))**6)
      RETURN
      END
C
C-------------------------------------------------------------
C FUNCTION GIVING DIFFERENTIAL OF LN(ACTIVITY) OF CARBON IN
C AUSTENITE. DIFFERENTIAL IS WITH RESPECT TO X.
C
      DOUBLE PRECISION FUNCTION DCG(X,T,W,R)
      DOUBLE PRECISION J,DG,DDG,X,T,W,R
      J=1-DEXP(-W/(R*T))
      DG=DSQRT(1-2*(1+2*J)*X+(1+8*J)*X*X)
      DDG=(0.5/DG)*(-2-4*J+2*X+16*J*X)
      DCG=-((10/(1-2*X))+(5/X))+6*((DDG+3)/(DG-1+3*X
     &)-(DDG-3)/(DG+1-3*X))
      RETURN
      END
C
C-------------------------------------------------------------
      SUBROUTINE OMEGA(W)
C SUBROUTINE TO CALCULATE THE CARBON CARBON INTERACTION ENERGY IN
C AUSTENITE, AS A FUNCTION OF ALLOY COMPOSITION.  BASED ON .MUCG18
C THE ANSWER IS IN JOULES PER MOL.  **7 OCTOBER 1981**
      COMMON/TRANS/C0,W0,K
      DOUBLE PRECISION C(8),W,P(8),B1,B2,Y(8),T10,T20,B3,XONE
     &,C0(8),W0(8),K(8)
      INTEGER I,U
      DO 1 I=1,8
      C(I)=W0(I)
1     CONTINUE
      B3=0.0D+00
      C(8)=C(1)+C(2)+C(3)+C(4)+C(5)+C(6)+C(7)
      C(8)=100.0D+00-C(8)
      C(8)=C(8)/55.84D+00
      C(1)=C(1)/12.0115D+00
      C(2)=C(2)/28.09D+00
      C(3)=C(3)/54.94D+00
      C(4)=C(4)/58.71D+00
      C(5)=C(5)/95.94D+00
      C(6)=C(6)/52.0D+00
      C(7)=C(7)/50.94D+00
      B1=C(1)+C(2)+C(3)+C(4)+C(5)+C(6)+C(7)+C(8)
      DO 107 U=2,7
      Y(U)=C(U)/C(8)
107   CONTINUE
      DO 106 U=1,8
      C(U)=C(U)/B1
106   CONTINUE
      XONE=C(1)
C     XONE=DINT(10000.0D+00*XONE)
C     XONE=XONE/10000
      B2=0.0D+00
      T10=Y(2)*(-3)+Y(3)*2+Y(4)*12+Y(5)*(-9)+Y(6)*(-1)+Y(7)*(-12)
      T20=-3*Y(2)-37.5*Y(3)-6*Y(4)-26*Y(5)-19*Y(6)-44*Y(7)
      P(2)=2013.0341+763.8167*C(2)+45802.87*C(2)**2-280061.63*C(2)**3
     &+3.864D+06*C(2)**4-2.4233D+07*C(2)**5+6.9547D+07*C(2)**6
      P(3)=2012.067-1764.095*C(3)+6287.52*C(3)**2-21647.96*C(3)**3-
     &2.0119D+06*C(3)**4+3.1716D+07*C(3)**5-1.3885D+08*C(3)**6
      P(4)=2006.8017+2330.2424*C(4)-54915.32*C(4)**2+1.6216D+06*C(4)**3
     &-2.4968D+07*C(4)**4+1.8838D+08*C(4)**5-5.5531D+08*C(4)**6
      P(5)=2006.834-2997.314*C(5)-37906.61*C(5)**2+1.0328D+06*C(5)**3
     &-1.3306D+07*C(5)**4+8.411D+07*C(5)**5-2.0826D+08*C(5)**6
      P(6)=2012.367-9224.2655*C(6)+33657.8*C(6)**2-566827.83*C(6)**3
     &+8.5676D+06*C(6)**4-6.7482D+07*C(6)**5 +2.0837D+08*C(6)**6
      P(7)=2011.9996-6247.9118*C(7)+5411.7566*C(7)**2
     &+250118.1085*C(7)**3-4.1676D+06*C(7)**4
      DO 108 U=2,7
      B3=B3+P(U)*Y(U)
      B2=B2+Y(U)
108   CONTINUE
      IF (B2 .EQ. 0.0D+00) GOTO 455
      W=(B3/B2)*4.187
      GOTO 456
455   W=8054.0
```

```fortran
456  RETURN
     END
C
C---------------------------------------------------------------
C FUNCTION GIVING THE EQUILIBRIUM MOLE FRACTION OF CARBON IN
C FERRITE.
C
     DOUBLE PRECISION FUNCTION XALPH(T)
     DOUBLE PRECISION T,CTEMP
      CTEMP=(T-273.0D+00)/900.0D+00
      XALPH=0.1528D-02-0.8816D-02*CTEMP+0.2450D-01*CTEMP*CTEMP
     &-0.2417D-01*CTEMP*CTEMP*CTEMP+
     &0.6966D-02*CTEMP*CTEMP*CTEMP*CTEMP
     RETURN
     END
C
C---------------------------------------------------------------
C SUBROUTINE TO CALCULATE THE PARAEQUILIBRIUM INTERFACE CHEMISTRY
C
     SUBROUTINE PEQGC0(T,X,Y,IM)
     IMPLICIT REAL*8 (A-H,K-Z)
     DOUBLE PRECISION X(8),Y(8),C0(8),W0(8),WW(8)
     &,K(8),X1(3),FUN(3),G(8),G2(8),G3(8),G4(8),GM(8)
     &,LFX(4,8),AC(8),E(8,8),EA(8,8),G0(8)
     COMMON/TRANS/C0,W0,K
     COMMON/HILL/G2,LFX,LCV,GM,AC,DDG,GFEC
     &       ,GFE3C,G3,G4,WW,E,EA,G,G0
     R=8.314D+00
     XGA=0.005D+00
C
C
     DUMMY=1.0D-08
100  X1(1)=XGA-DUMMY
     X1(2)=XGA+DUMMY
     X1(3)=XGA
     DO 10 I=1,3
      XX=0.0D+00
      FUN(I)=0.0D+00
      KK=K(IM)
      Y(IM)=KK/(1+KK)
      X(IM)=(1-X1(I))*Y(IM)
      X(1)=X1(I)
      X(8)=1.0D+00-X(1)-X(IM)
      Y(8)=1.0D+00-Y(IM)
C
     DENO=1.0D+00
C
     MFE3C=R*T*DLOG(Y(8))
     MFE=R*T*DLOG(X(8)/DENO)
     &        -R*T/2.0*E(1,1)*X(1)*X(1)/DENO/DENO
     MC=R*T/3.0*DLOG(X(1)/DENO)
     &        +R*T/3.0*E(1,1)*X(1)/DENO
     MFE3C=MFE3C+(1-Y(8))*WW(IM)*Y(IM)
     MFE=MFE-R*T/2.0*E(IM,IM)*X(IM)*X(IM)/DENO/DENO
     MFE=MFE-R*T*X(1)*E(1,IM)*X(IM)/DENO/DENO
     MC=MC+R*T/3.0*E(1,IM)*X(IM)/DENO
     MX= R*T*DLOG(X(IM)/DENO)
     &        +R*T*(E(1,IM)*X(1)+E(IM,IM)*X(IM))/DENO
     MM3C= R*T*DLOG(Y(IM))
     &        +Y(8)*WW(IM)-Y(8)*WW(IM)*Y(IM)
C
     FUN(I)=X(8)*(GFE3C+MFE3C-MFE-MC)
     FUN(I)=FUN(I)+X(IM)*(G(IM)+MM3C-MX-MC)
C
C    WRITE(6,*) IM,E(1,1),E(1,IM),E(IM,IM)
C
10   CONTINUE
     IF(ABS(FUN(3)) .LT. 1.0D-6) GOTO 20
     XGA=X1(3)-2.0*DUMMY*FUN(3)/(FUN(2)-FUN(1))
     GOTO 100
20   XGA=X1(3)
     RETURN
     END
C
```

```fortran
C-----------------------------------------------------------
C SUBROUTINE TO CALCULATE THE EQUILIBRIUM INTERFACE CHEMISTRY
C
      SUBROUTINE NPGC0(T,X,Y,IM)
      IMPLICIT REAL*8 (A-H,K-Z)
      DOUBLE PRECISION X(8),Y(8),C0(8),W0(8),WW(8)
     &,K(8),XX(3),FUN(3),G0(8)
     &,G(8),G2(8),G3(8),G4(8),GM(8),MX(8),MM3C(8)
     &,LFX(4,8),AC(8),E(8,8),EA(8,8)
      COMMON/TRANS/C0,W0,K
      COMMON/HILL/G2,LFX,LCV,GM,AC,DDG,GFEC
     &      ,GFE3C,G3,G4,WW,E,EA,G,G0
C
      R=8.314D+00
C
      XGC=C0(IM)*0.99D+00
      DUMMY=1.0D-6
100   XX(1)=XGC-DUMMY
      XX(2)=XGC+DUMMY
      XX(3)=XGC
      DO 10 I=1,3
      X1=XX(I)
      FUN(I)=0.0D+00
      B=DEXP((GFE3C-G(IM)-WW(IM))/R/T+E(1,IM)*X1)
       Y2=C0(IM)*4.0/3.0
      X2=Y2/B
      X8=1.0D+00-X1-X2
      Y8=1.0D+00-Y2
      IF (X(8) .LT. 0.0D+00) THEN
        WRITE(6,*) 'X8,X1=',X8,X1
      ENDIF
C
C
      MFE3C=R*T*DLOG(Y8)
       MFE=R*T*DLOG(X8)-R*T/2.0*E(1,1)*X1*X1
       MC=R*T/3.0*DLOG(X1)+R*T/3.0*E(1,1)*X1
      MFE3C=MFE3C+(1-Y8)*WW(IM)*Y2
       MFE=MFE-R*T/2.0*E(IM,IM)*X2*X2-R*T*X1*E(1,IM)*X2
       MC=MC+R*T/3.0*E(1,IM)*X2
      MX(IM)= R*T*DLOG(X2)
     &      +R*T*(E(1,IM)*X1+E(IM,IM)*X2)
      MM3C(IM)= R*T*DLOG(Y2)
     &      +Y8*WW(IM)
       MM3C(IM)=MM3C(IM)-Y8*WW(IM)*Y2
C
      FUN(I)=GFE3C+MFE3C-MFE-MC
C
10    CONTINUE
      IF(ABS(FUN(3)) .LT. 1.0D-02) GOTO 20
       DUMMY1=XGC-2.0*DUMMY*FUN(3)/(FUN(2)-FUN(1))
       IF (DUMMY1 .LT. 0.0D+00) THEN
        DUMMY1=XGC/2.0D+00
       ENDIF
       XGC=DUMMY1
      GOTO 100
20    X(1)=X1
      X(IM)=X2
       Y(1)=0.25D+00
       Y(IM)=3.0D+00/4.0D+00*Y2
      RETURN
      END
C
C-----------------------------------------------------------
C SUBROUTINE TO CALCULATE THE EQUILIBRIUM INTERFACE CHEMISTRY
C
      SUBROUTINE EQGC0(T,X,Y,ACTIV,IM)
      IMPLICIT REAL*8 (A-H,K-Z)
      DOUBLE PRECISION X(8),Y(8),C0(8),W0(8),WW(8)
     &,K(8),XX(3),FUN(3),G0(8)
     &,G(8),G2(8),G3(8),G4(8),GM(8),MX(8),MM3C(8)
     &,LFX(4,8),AC(8),E(8,8),EA(8,8)
      COMMON/TRANS/C0,W0,K
      COMMON/HILL/G2,LFX,LCV,GM,AC,DDG,GFEC
     &      ,GFE3C,G3,G4,WW,E,EA,G,G0
```

```fortran
C
      R=8.314D+00
C
      XGC=C0(IM)*0.99D+00
7     X2=X2AC0(T,XGC,ACTIV,E(1,1),E(1,IM))
C7    X2=X2AC(T,XGC,ACTIV,LCV,G2(IM))
      IF (X2 .LT. 0.0D+00) THEN
       XGC=(C0(1)+XGC)/2.0
       GOTO 7
      ENDIF
      DUMMY=1.0D-6
100   XX(1)=XGC-DUMMY
      XX(2)=XGC+DUMMY
      XX(3)=XGC
      DO 10 I=1,3
      X1=XX(I)
      FUN(I)=0.0D+00
      B=DEXP((GFE3C-G(IM)-WW(IM))/R/T+E(1,IM)*X1)
C       X2=C0(IM)*(4.0*X1-1.0D+00)/
C    &    (3.0*B*(X1-C0(1))+4.0*C0(1)-1.0D+00)
C       X2=X2AC(T,X1,ACTIV,LCV,G2(IM))
      X2=X2AC0(T,X1,ACTIV,E(1,1),E(1,IM))
      Y2=B*X2
      X8=1.0D+00-X1-X2
      Y8=1.0D+00-Y2
      IF (X(8) .LT. 0.0D+00) THEN
        WRITE(6,*) 'X8,X1=',X8,X1
      ENDIF
C
C
      MFE3C=R*T*DLOG(Y8)
      MFE=R*T*DLOG(X8)-R*T/2.0*E(1,1)*X1*X1
      MC=R*T/3.0*DLOG(X1)+R*T/3.0*E(1,1)*X1
      MFE3C=MFE3C+(1-Y8)*WW(IM)*Y2
      MFE=MFE-R*T/2.0*E(IM,IM)*X2*X2-R*T*X1*E(1,IM)*X2
      MC=MC+R*T/3.0*E(1,IM)*X2
      MX(IM)= R*T*DLOG(X2)
     &       +R*T*(E(1,IM)*X1+E(IM,IM)*X2)
      MM3C(IM)= R*T*DLOG(Y2)
     &       +Y8*WW(IM)
      MM3C(IM)=MM3C(IM)-Y8*WW(IM)*Y2
C
      FUN(I)=GFE3C+MFE3C-MFE-MC
C
10    CONTINUE
      IF(ABS(FUN(3)) .LT. 1.0D-02) GOTO 20
       DUMMY1=XGC-2.0*DUMMY*FUN(3)/(FUN(2)-FUN(1))
       IF (DUMMY1 .LT. 0.0D+00) THEN
        DUMMY1=XGC/2.0D+00
       ENDIF
       XGC=DUMMY1
      GOTO 100
20    X(1)=X1
      X(IM)=X2
       Y(1)=0.25D+00
       Y(IM)=3.0D+00/4.0D+00*Y2
      RETURN
      END
C
C------------------------------------------------------------
C FUNCTION TO CALCULATE EQUILIBRIUM FUNCTION F AND M
C  IMF=1: F(X,Y)   IMF=0: M(X,Y)
C
      DOUBLE PRECISION FUNCTION FXY0(T,C,X1,X2,Y2,IM,IMF)
      IMPLICIT REAL*8 (A-H,K-Z)
      DOUBLE PRECISION C(8),C0(8),W0(8),WW(8),K(8),G0(8)
     &,G(8),G2(8),G3(8),G4(8),GM(8),LFX(4,8),AC(8),E(8,8),EA(8,8)
      COMMON/TRANS/C0,W0,K
      COMMON/HILL/G2,LFX,LCV,GM,AC,DDG,GFEC
     &        ,GFE3C,G3,G4,WW,E,EA,G,G0
      R=8.314D+00
C
C
      CG=X1
```

```
      X1=(C(1)*(3.0*Y2-4.0*X2)-(C(IM)-X2))/(3.0*Y2-4.0*C(IM))
      X8=1.0D+00-X1-X2
      Y8=1.0D+00-Y2
C
      MFE3C=R*T*DLOG(Y8)
      MFE=R*T*DLOG(X8)-R*T/2.0*E(1,1)*X1*X1
      MC=R*T/3.0*DLOG(X1)+R*T/3.0*E(1,1)*X1
      MFE3C=MFE3C+(1-Y8)*WW(IM)*Y2
      MFE=MFE-R*T/2.0*E(IM,IM)*X2*X2-R*T*X1*E(1,IM)*X2
      MC=MC+R*T/3.0*E(1,IM)*X2
      MX= R*T*DLOG(X2)
     &      +R*T*(E(1,IM)*X1+E(IM,IM)*X2)
      MM3C= R*T*DLOG(Y2)
     &      +Y8*WW(IM)
      MM3C=MM3C-Y8*WW(IM)*Y2
C
      IF (IMF .EQ. 1) THEN
        FXY0=GFE3C+MFE3C-MFE-MC
      ELSE
        FXY0=G(IM)+MM3C-MX-MC
      ENDIF
C
      RETURN
      END
C
C----------------------------------------------------------------
C FUNCTION GIVING THE CARBON DIFFUSIVITY IN AUSTENITE
C
      DOUBLE PRECISION FUNCTION DIFF(T,X1,X2,W)
      IMPLICIT REAL*8(A-H,K-Y), INTEGER(I,J,Z)
      DOUBLE PRECISION D(300),CARB(300)
C HH=PLANCK CONST.J/S, KK=BOLTZMAN CONST. J/K
      HH=6.6262D-34
      KK=1.38062D-23
      Z=12
      A5=1.0D+00
      R=8.31432D+00
C
C    DIFF=DIFFUSIVITY OF CARBON IN AUSTENITE, CM**/SEC
C    Z=COORDINATION OF INTERSTIAL SITE
C    PSI=COMPOSITION DEPENDENCE OF DIFFUSION COEFFICIENT
C    THETA=NO. C ATOMS/ NO. FE ATOMS
C    ACTIV=ACTIVITY OF CARBON IN AUSTENITE
C    R=GAS CONSTANT
C    X=MOLE FRACTION OF CARBON
C    T=ABSOLUTE TEMPERATURE
C    SIGMA=SITE EXCLUSION PROBABLITY
C    W=CARBON CARBON INTERACTION ENERGY IN AUSTENITE
C
      DASH=(KK*T/HH)*DEXP(-(21230.0D+00/T))*DEXP(-31.84D+00)
      XINCR=(X1-X2)/300.0D+00
      DO 1 I=1,300
      CARB(I)=X2+(I-1)*XINCR
      X=CARB(I)
      THETA=X/(A5-X)
      ACTIV=CG(X,T,W,R)
      ACTIV=DEXP(ACTIV)
      DACTIV=DCG(X,T,W,R)
      DACTIV=DACTIV*ACTIV
      DACTIV=DACTIV*A5/((A5+THETA)**2)
      SIGMA=A5-DEXP((-(W))/(R*T))
      PSI=ACTIV*(A5+Z*((A5+THETA)/(A5-(A5+Z/2)*THETA+(Z/2)*(A5+Z/2)*
     &(A5-SIGMA)*THETA*THETA)))+(A5+THETA)*DACTIV
      D(I)=DASH*PSI
 1    CONTINUE
      II3=0
      CALL DQSES(XINCR,D,300,ANS,ERROR)
      DIFF=ANS/(X1-X2)
      RETURN
      END
C----------------------------------------------------------------
```